SKB

TECHNICAL REPORT 92-32

Äspö Hard Rock Laboratory: Evaluation of the combined longterm pumping and tracer test (LPT2) in borehole KAS06

Ingvar Rhén[1] (ed.), Urban Svensson[2] (ed.),
Jan-Erik Andersson[3], Peter Andersson[3], Carl-Olof Eriksson[3],
Erik Gustafsson[3], Thomas Ittner[3], Rune Nordqvist[3]

[1] VBB VIAK AB
[2] Computer-aided Fluid Engineering
[3] Geosigma AB

November 1992

SVENSK KÄRNBRÄNSLEHANTERING AB
SWEDISH NUCLEAR FUEL AND WASTE MANAGEMENT CO

BOX 5864 S-102 48 STOCKHOLM

TEL 08-665 28 00 TELEX 13108 SKB S
TELEFAX 08-661 57 19

ÄSPÖ HARD ROCK LABORATORY:
EVALUATION OF THE COMBINED LONGTERM PUMPING AND TRACER TEST (LPT2) IN BOREHOLE KAS06

Ingvar Rhén[1] (ed.), Urban Svensson[2] (ed.), Jan-Erik Andersson[3], Peter Andersson[3], Carl-Olof Eriksson[3], Erik Gustafsson[3], Thomas Ittner[3], Rune Nordqvist[3]

1 VBB VIAK AB
2 Computer-aided Fluid Engineering
3 Geosigma AB

November 1992

ÄSPÖ HARD ROCK LABORATORY

Evaluation of the combined longterm pumping and tracer test (LPT2) in borehole KAS06

by

Ingvar Rhén	VBB VIAK AB (editor)
Urban Svensson	Computer-aided Fluid (editor) Engineering
Jan Erik Andersson	GEOSIGMA AB
Peter Andersson	"-
Carl-Olof Eriksson	"-
Erik Gustafsson	"-
Thomas Ittner	"-
Rune Nordqvist	"-

November 1992

S1122.200 Gothenburg

ABSTRACT

This report summarizes the results from the LPT2 experiment. The field experiment had three major parts: a pumping test, a tracer experiment and a tracer dilution experiment. These are described in detail in the appendices of the report. Numerical simulations have been carried out both prior to and after the experiments. Results from these are also reported.

The longterm pumping test and tracer test performed in KAS06, called LPT2, was the first attempt to clarify the transport of solutes in the site scale of Äspö. The test was not intended to be complete regarding the transport parameters needed for nuclide transport modelling. In the operating phase of the Äspö Hard Rock Laboratory more detailed tracer tests and numerical modelling will be conducted

The main conclusion from the field experiment is that the present conceptual model of Äspö is sound, but some modifications may be required. These include both the extension and transmissivities of fracture zones.The field experiment has also produced additional information on the properties of the fracture zones like porosity and dispersivity. The cumulative aperture of all hydraulic fractures was estimated to $10 \cdot 10^{-3}$ - $30 \cdot 10^{-3}$ m for two different sets of zones. Considering the estimated width of the zones the flow porosities were estimated to 0.02 - 0.1 %. The dispersivities were estimated to 0.1 - 0.2 of the flow path distance and the Peclet number to 4-11.

The numerical simulations made prior to the experiment, dealing with the travel time of tracers, were found to be in reasonable agreement with the measurements. The data gathered in the field experiment will however make it possible to pursue the modelling efforts further.

CONTENTS

	ABSTRACT	i
1	INTRODUCTION	1
1.1	Background	1
1.2	This report	1
1.3	Introduction to LPT2	3
2	NUMERICAL SIMULATIONS, THE PREDICTION OF LPT2	7
2.1	Introduction	7
2.2	Method	7
2.3	Results	7
2.4	Conclusions	9
3	PUMPING TEST	11
3.1	Introduction	11
3.2	Method	11
3.3	Results	11
3.4	Conclusions	13
4	THE TRACER EXPERIMENT	15
4.1	Introduction	15
4.2	Method	15
4.3	Results	16
4.4	Conclusions	19
5	THE TRACER DILUTION MEASUREMENTS	20
5.1	Introduction	20
5.2	Method	20
5.3	Results	21
5.4	Conclusions	25
6	VALIDATION OF THE NUMERICAL MODEL	26
6.1	Introduction	26
6.2	Travel times	26
6.3	Drawdowns	27
6.4	Conclusions	28
7	DISCUSSION OF THE CONCEPTUAL MODEL	30
8	REFERENCES	32

APPENDIX A	Prediction of flow trajectories for the LPT2 test
APPENDIX B	Evaluation of pumping test LPT2 in KAS06 at Äspö
APPENDIX C	Large scale three-dimensional tracer test at Äspö
APPENDIX D	Groundwater flow measurements at Äspö with the dilution method
APPENDIX E	Comparison between calculated and measured drawdown

1 INTRODUCTION

1.1 Background

The Äspö Hard Rock Laboratory (HRL) project is a rehearsal before the construction of a final repository for high level waste in Sweden.

The plans for the Äspö Hard Rock Laboratory were initially presented in the R&D programme 1986 */SKB, 1986/*. In that report it was stated that the laboratory should be placed close to one of the nuclear power plants where existing services and the kind of infrastructure needed for research already existed. Therefore investigations were first carried out near the nuclear power facility at Simpevarp, Oskarsham, *figure 1.1*. SKB found the island of Äspö to be suitable. Permits pursuant to the Act on the Conversation of Natural Resources, The Planning and Building Code and the Act on water Preservation were obtained from the concerned authorities and excavation of the laboratory started in October 1990.

The Äspö Hard Rock Laboratory is a continuation of the R&D effort developed during the study-site investigations, at Finnsjön and in the international STRIPA project. The goals and objectives of the HRL are discussed in SKB's R&D Programme 89 */SKB 1989/*. It should be noted that the site of the HRL will not be considered as a site for the final repository.

The HRL project is basically divided into three main phases. The first phase comprises the pre-investigations. The second phase is the excavation and construction of the laboratory and the third the operating phase, *see SKB, /1989/*.

1.2 This report

The longterm pumping test and tracer test performed in KAS06, called LPT2, was the first attempt to clarify the transport of solutes in the site scale of Äspö. The test was not intended to be complete regarding the transport parameters needed for nuclide transport modelling. In the operating phase of the Äspö Hard Rock Laboratory more detailed tracer tests and numerical modelling will be conducted

This report compiles four different reports concerning the results of the LPT2 test. The detailed information is found in the reports listed in the *appendices*. The main text in this report gives a summary of these reports and discusses what impact the results may have on the conceptual model of Äspö. Two of the reports in the appendices, *A* and *D* , are also

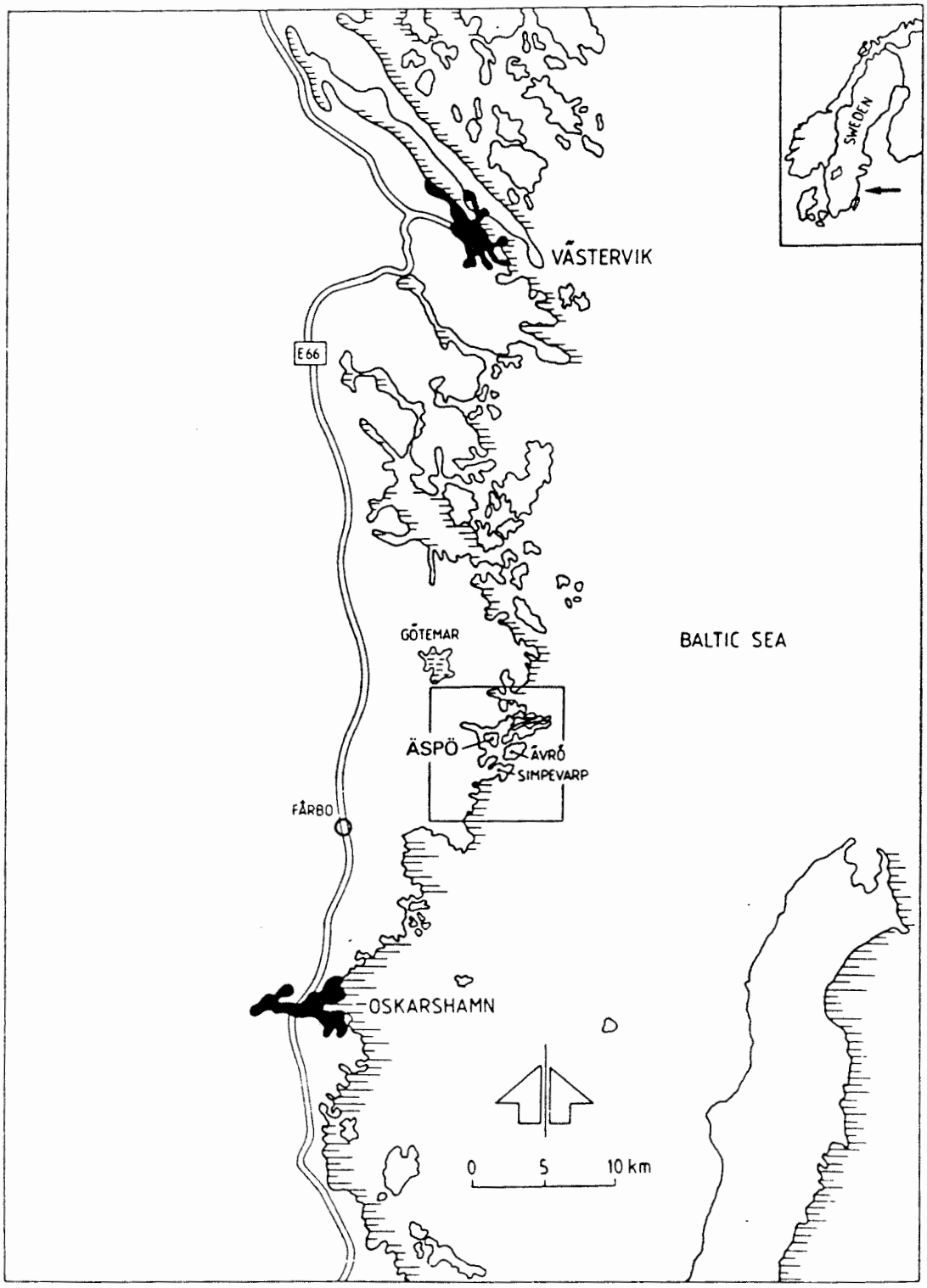

Fig 1.1 Overview of Äspö and environments.

published as separate progress reports (*PR 25-91-17 and PR 25-91-18*). Appendix *D* deals with point measurements of groundwater flow during LPT2 and also during natural gradient and another pumping test prior to the LPT2 test.

1.3 Introduction to LPT2

Within the extensive pre-investigations for the HRL, field experiments have been carried out in order to characterize the site geologically, hydrogeologically, and hydrochemically. One important part of these investigations has been to identify major conductive structures on Äspö, *see figures 1.2 and 1.3*, and pumping tests have been important for this identification. (The preinvestigations and the conceptual models based on these investigations are presented in *Wikberg et al, 1991).* In the autumn of 1990 the combined longterm pumping- and tracer test in borehole KAS06, LPT2, was carried out as one of the last pre-investigations for HRL, *see figure 1.4.*

The pumping began September 17, 1990. The drawdown phase continued until December 18 1990 and the recovery phase until January 18, 1991. During LPT2 observations of drawdowns were made in about 100 borehole sections. During the test tracers were injected in 6 packed-off borehole sections intersected by major hydraulic conductors and the arrivals in the pumped borehole were studied. Groundwater flow through 10 borehole sections was determined by means of the dilution method. The measurements were made at depths ranging from 140 to 800 meters in order to select sections for the tracer injections. Dilution measurements carried out prior to the LPT2 test were also utilized and are presented in this report.

Numerical simulations of the drawdowns and the tracer flow paths and travel times have also been performed. These were done in advance of the experiment in order to test the predictive capabilities of the model. Updated numerical simulations of the drawdowns are also presented in the report.

In *chapters 2-5* the basic information from the appendices is summarized. In *chapter 6* the results from the numerical model are discussed and in *chapter 7* the conceptual models, according to *Wikberg et al /1991/*, is discussed with respect to the results from LPT2.

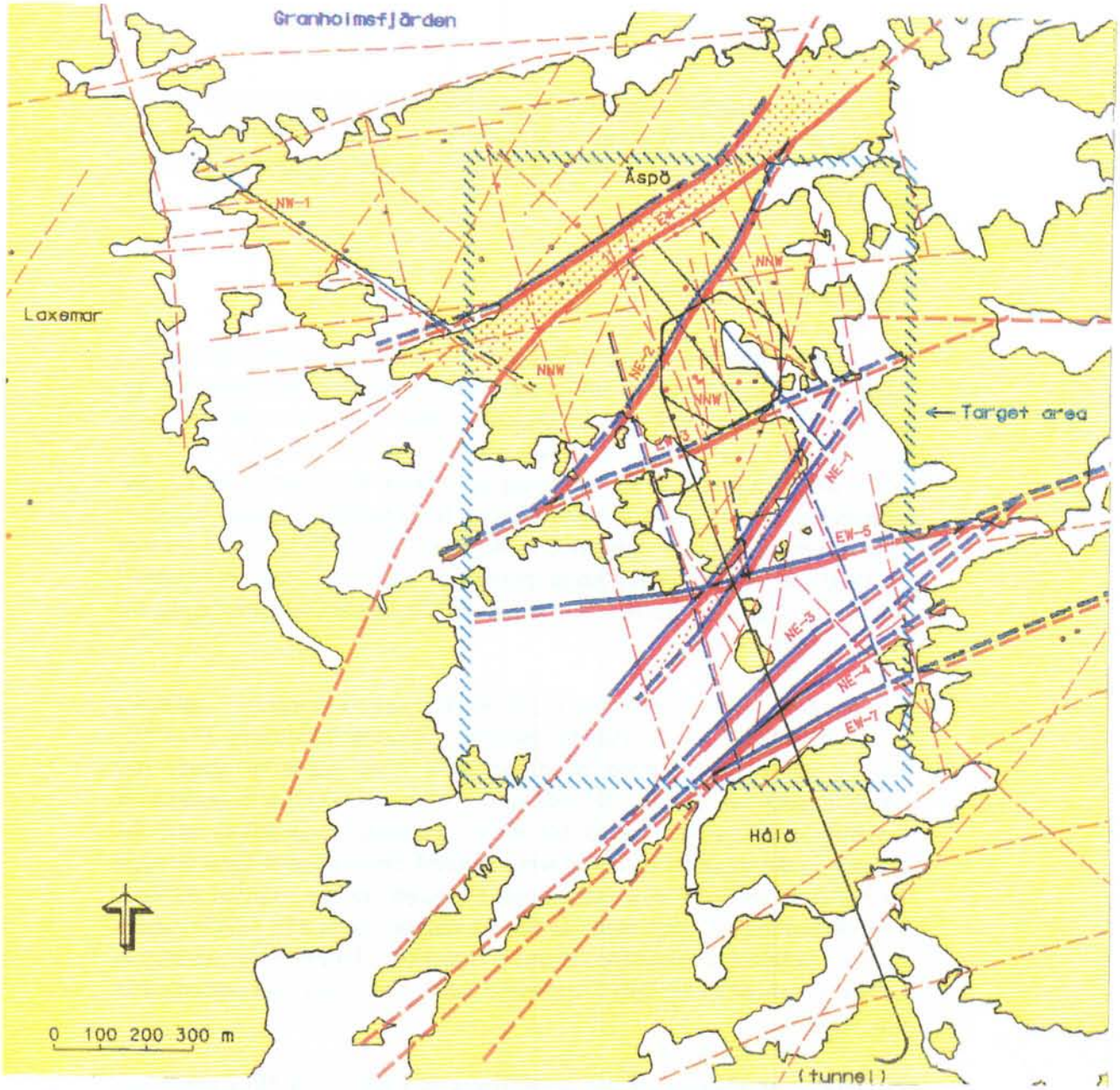

Fig 1.2 Conceptual model of the fracture zones on Äspö.

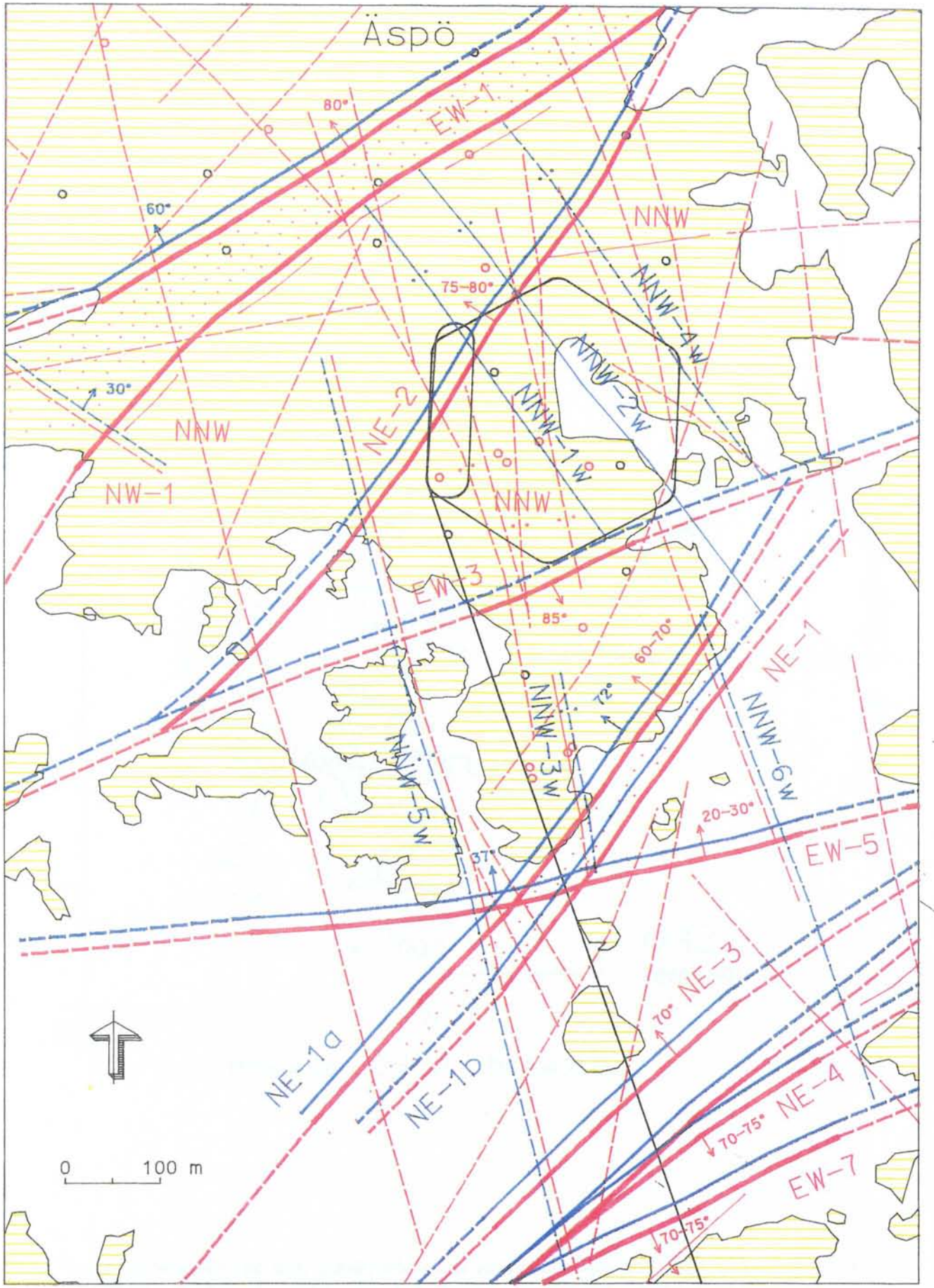

Fig 1.3 Structural model of the target area. For legend see figure 1.2.

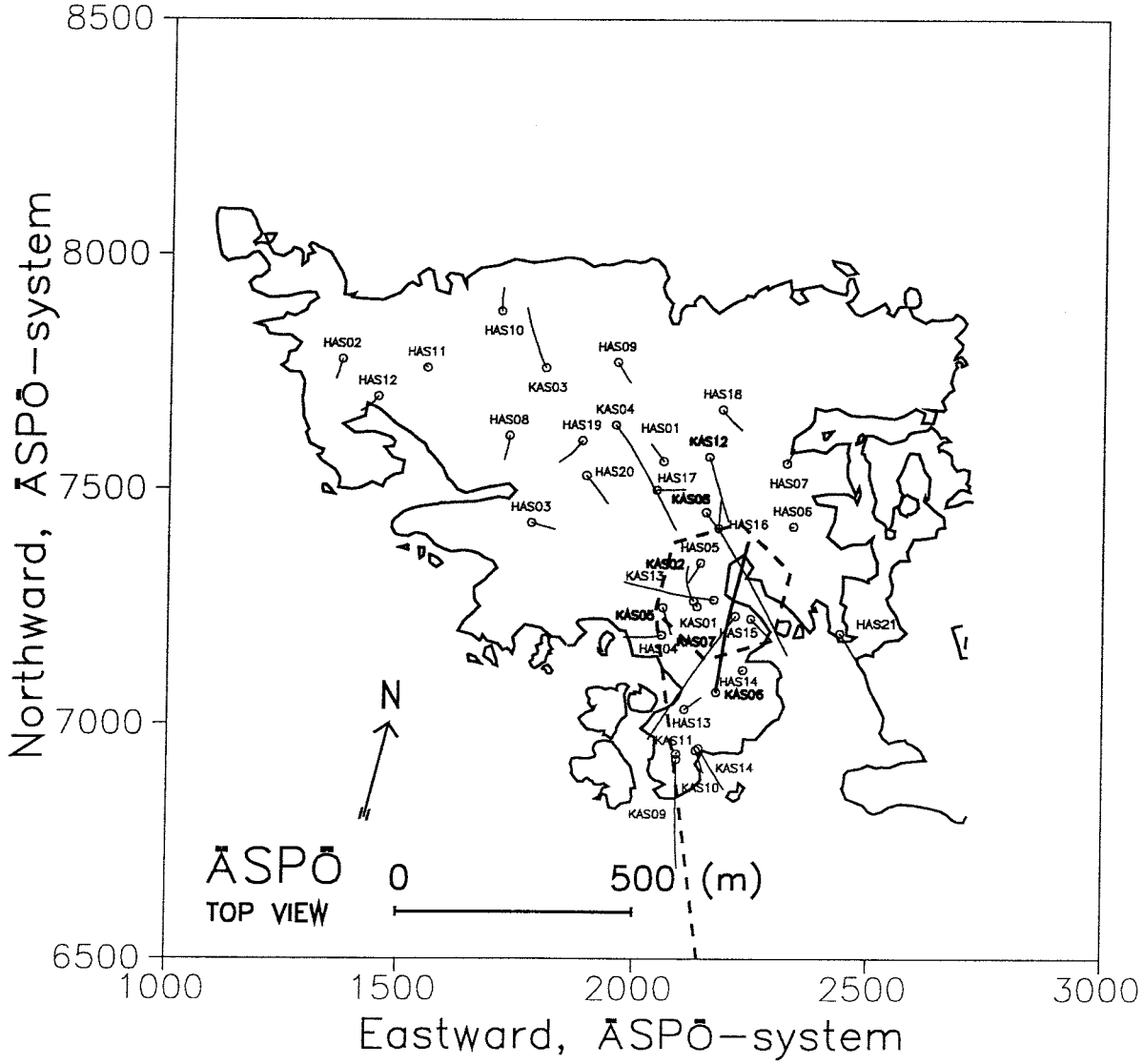

Fig 1.4 *The Island of Äspö. Location of the boreholes and the planned tunnel. The borehole KAS06 was pumped during LPT2. In KAS02, KAS05, KAS07, KAS08 and KAS12 tracers were injected during LPT2.*

2 NUMERICAL SIMULATIONS, THE PREDICTION OF LPT2

2.1 Introduction

Numerical simulations were carried out in advance of the field experiment. This was done for two reasons; firstly some guidance can be obtained from the numerical simulations when the field experiment is planned and, secondly, the evaluation of the predictive capabilities of the numerical model requires that the results from the model are documented prior to the experiment.

The numerical model is fully described in *Svensson /1991/* and the reader is referred to this report for a presentation of basic concepts, methods, calibration cases, etc. In *appendix A* the particle tracking method used is outlined and in *chapter 6* the drawdowns are presented and discussed. In *figure 2.1* the slightly simplified conceptual model of the conductive structures used in the numerical simulations is presented.

2.2 Method

The steady flow pattern when pumping in KAS06 is first predicted, using the above mentioned numerical model. Pumping, with a flow rate of 2.5 l/s, is assumed to be carried out in two sections in KAS06; the crossing with NNW1 (30%) and the crossing with NNW2 and EW5 (70%), *see figures 1.4 and 2.1*. As will be discussed later this is not in perfect agreement with the experimental conditions but was the best guess that could be done in advance.

The tracking of a marked fluid element is done in a Lagrangian manner, i e

$$\vec{ds} = \vec{u}\, dt$$

where $\vec{ds}$ denotes increment in space, $\vec{u}$ the local velocity vector and dt the timestep.

2.3 Results

Altogether nine trajectories, assumed to be of interest in the LPT2 experiment, were calculated and illustrated graphically. Details of the trajectories, including for example active fracture zones, were also listed in tables. All these results are fully described in *appendix A*. Here only one example will be discussed, namely injection in KAS02, section B4.

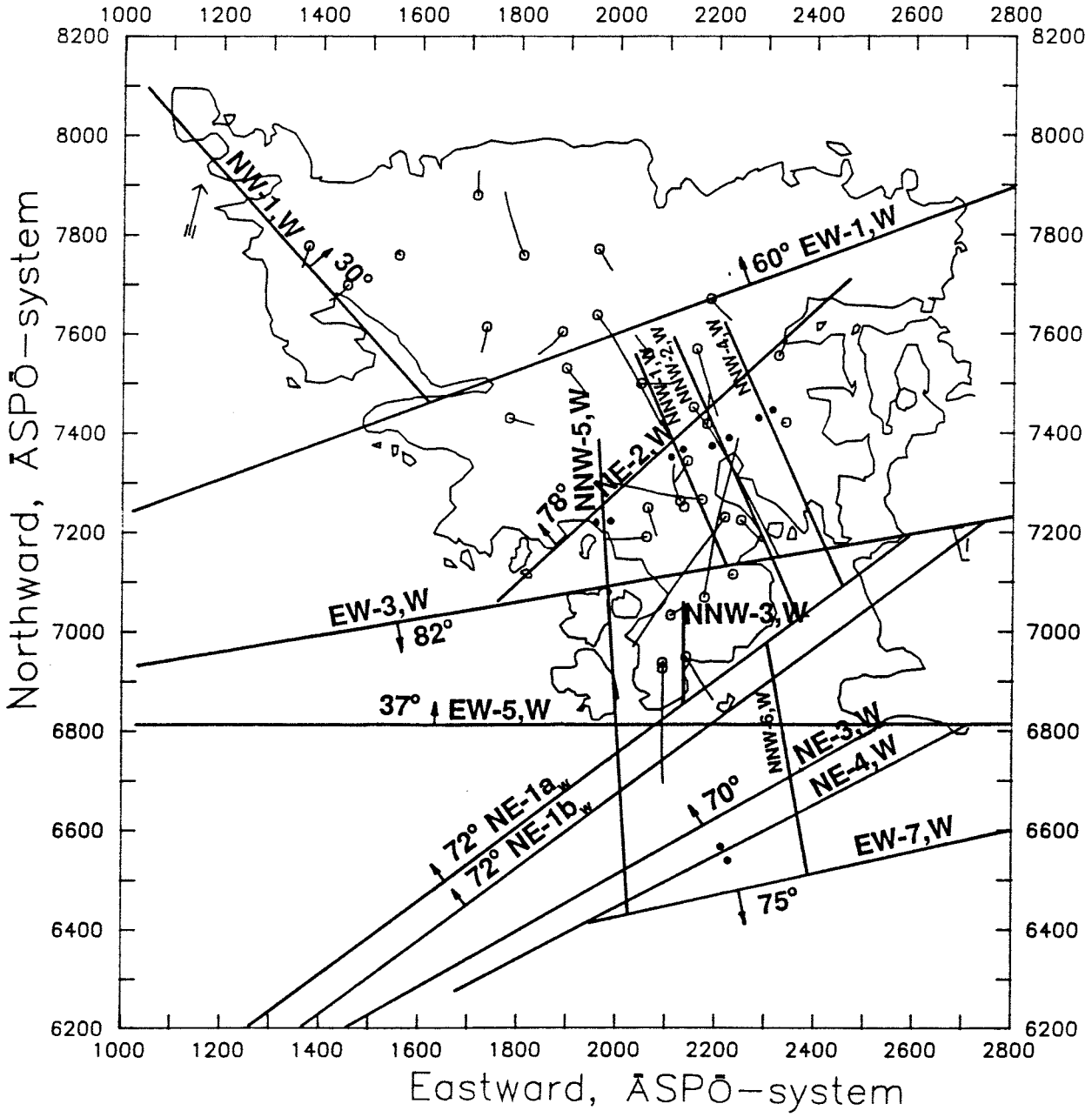

Fig 2.1 *Conceptual model of the conductive structures on Äspö used in the numerical simulation.*

A graphical presentation is given by *figure 2.2*. The tracer is injected at a section located about one third of the total length of KAS02. From the horizontal plane (z-y) one can see that the tracer ends up in the upper pump-section in KAS06, i e the crossing with NNW1.

One of the objectives of the numerical simulations is to estimate the travel times for the tracers. These can be found in *table 2.1*. Both the Darcian time in seconds and the time in days, assuming a porosity of n = 10^{-3}, are given in the table. One of the travel times, injection in KAS02 section B2, is significantly longer than the others; the explanation is that no fracture zone is present close to the injection point.

Table 2.1 Travel times for nine injection points (n = porosity, Darcian time for n=1)

Injection hole	Section* (m)	Time n=1 $\cdot 10^{10}$ (s)	Time n=10^{-3} (days)
KAS02, section B4	309-345	0.68	79
KAS02, section B2	800-854	204	23700
KAS04, section D2	332-392	11.5	1330
KAS05, section E3	320-380	1.1	128
KAS07, section J4	191-290	0.41	48
KAS08, section M3	140-200	0.20	23
KAS08, section M1	503-601	0.16	19
KAS11, section CE	47-64	3.5	406
KAS12, section DD	102-233	0.53	61

* Length along the borehole from top of casing.

2.4 Conclusions

The realism of the predictions presented depends on the accuracy of the hydrodynamical model which, in turn, is based on a conceptual model of Äspö. The trajectories do look plausible and some verification of the hydrodynamical model has been presented in *Svensson /1991/*. The tentative conclusion from the work presented in *appendix A* was therefore that the predicted trajectories do give an indication of the correct trajectories and that the typical Darcian flow time for the cases considered is 10^{10} s.

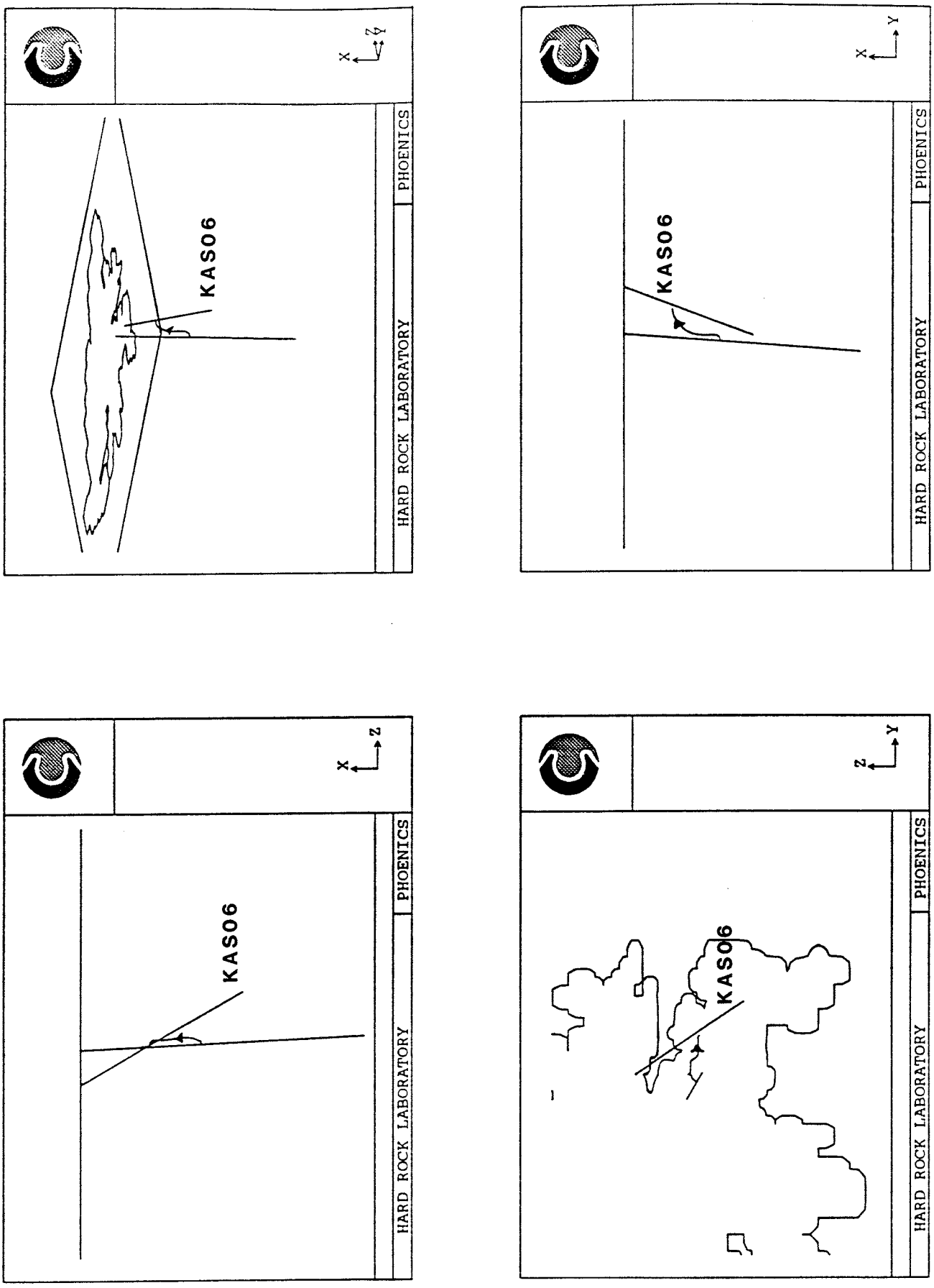

Fig 2.2. Trajectory when injecting in KAS02, section B4.

3 PUMPING TEST

3.1 Introduction

Observations of drawdown were generally performed in several sections in all boreholes during LPT2. An extensive data set is thus available. The data set for future numerical simulations was one of the objectives of the pumping test, and another one was to evaluate the consistence between the results from LPT2 and the current conceptual model of Äspö */Wikberg et al, 1991/*. The pumping test is reported in detail in *appendix B*.

3.2 Method

In all observation boreholes (except HAS01, KAS01 and KAS10) between two and six sections were isolated by packers. Automatic registrations of drawdown were made in most sections.

In the cored boreholes KAS02-05 and KAS07-14 the electric conductivity of the groundwater was measured at two different levels in each borehole. Also the precipitation and the barometric pressure during the pumping test were recorded and documented. In addition, the flowrate, electric conductivity and redox potential of the pumped water were registered.

3.3 Results

The inflow to KAS06 during pumping has mainly been estimated from spinner measurements (the flowrate along the borehole can be measured with a spinner during pumping), except for inflow from EW-3 which is estimated from tracer measurements. The total inflow, 2.25 l/s, is estimated to be distributed as follows: EW-3 (15%), NNW-1 (21%), EW-5 (33%), NNW-2 (26%) and EW-X (5%).

In order to assess the hydraulic connections between the different observation sections and the pumping borehole, the response times were estimated for each section in the observation boreholes. The response time chosen corresponds to the approximate time from start of pumping until a drawdown of 0.1 m was observed in a section. A response time ratio was then calculated for each section by dividing the response time with the squared distance to the pumping borehole. This ratio is inversely proportional to the hydraulic diffusivity of the rock. Low ratios can be expected for borehole sections in fracture zones while higher ratios can be expected for borehole sections with less good contact with the pumped borehole.

A distance-drawdown plot was also prepared, *see figure 3.1*. In this plot the total drawdown in each observation section at stop of pumping versus the squared distance to the pumping borehole is shown. For comparison, the Theis type curve is also included in the figure. The drawdowns at stop of pumping are also listed in *appendix B, table 4.1*, together with calculated flow through some borehole sections, electric conductivity and a classification of hydraulic connectivity based on the above discussed response time ratio.

The transmissivities of the fracture zones have been estimated by analyzing the drawdown responses in borehole sections, assumed to be intersected by fracture zones. The results are compared with what can be expected from the current conceptual model. Deviations are found, both with respect to extensions and transmissivities of fracture zones, but the general conclusion is that the results from LPT2 support the current conceptual model */Wikberg et al, 1991/*. The observed drawdown response in KAS03 indicates that there is a hydraulic communication between the northern and southern parts of Äspö, possibly via zone EW-5. This zone may also extend further towards northeast.

LPT2 also indicates that zone EW-3 may be more transmissive than assumed in the conceptual model.

Another important result from LPT2 is that zone NE-1 seems to be a major recharge boundary, effectively attenuating the drawdown in boreholes close to NE-1 (KAS09, KAS11 and KAS14).

In *table 3.1* the estimated ranges of transmissivities from LPT2 and the conceptual model are compared for some of the conductive structures.

Table 3.1 Estimated range of transmissivity of the dominating fracture zones according to the LPT-2 test and according to the conceptual model */Wikberg el al, 1991/*

Fracture zone	LPT2 T $\cdot 10^{-5}$ (m^2/s)	Conceptual model T $\cdot 10^{-5}$ (m^2/s)
EW-5W	3.3 - 5.6	1 - 4
NNW-1W	0.84 - 4.0	0.5 - 2
NNW-2W	2.6 - 3.6	2 - 6
EW - 3W	0.91 ?	0.01 - 0.1
EW-X	0.95	-

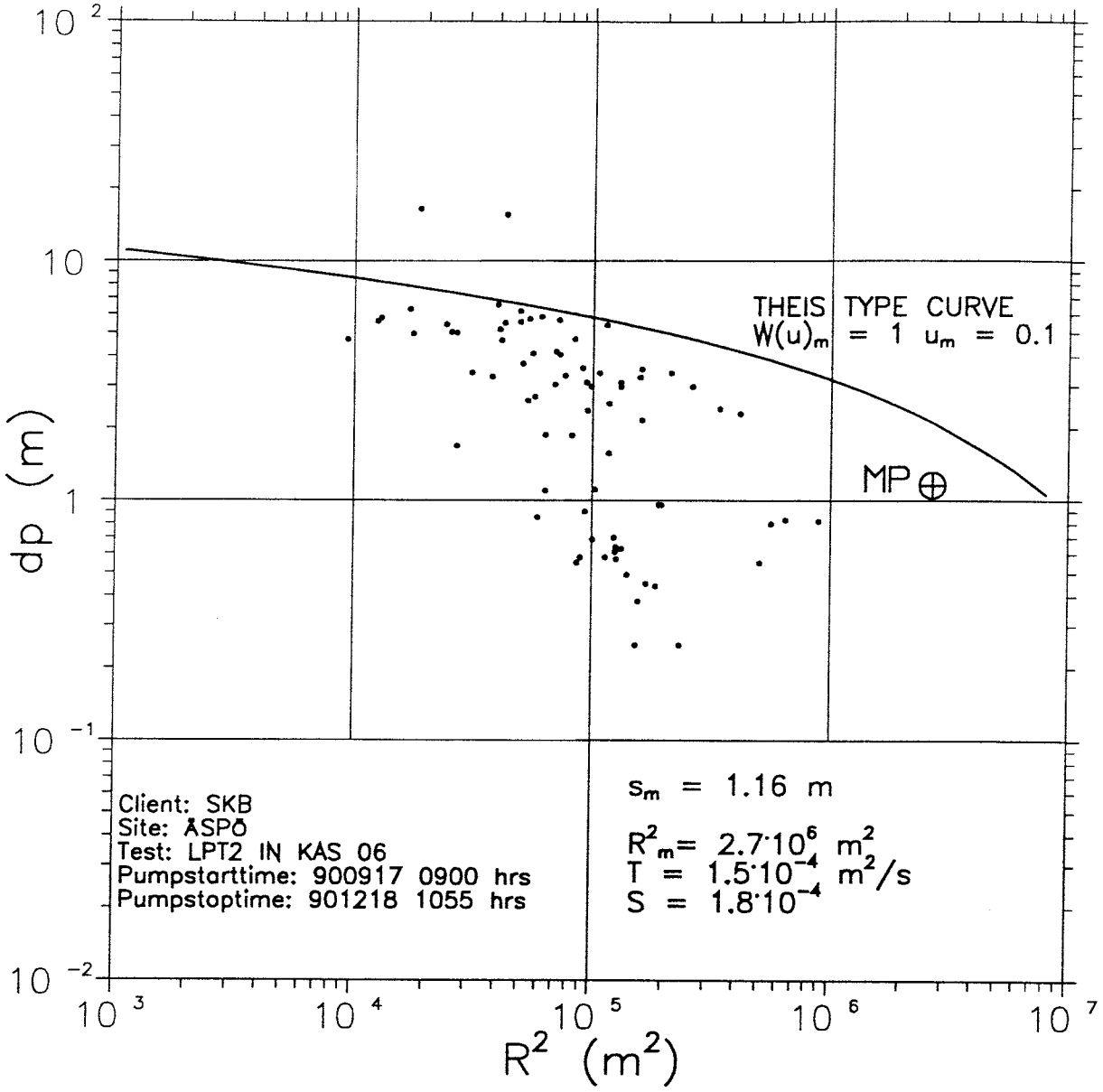

Fig 3.1 *Distance-drawdown graph at stop of pumping during LPT-2. Table 4.1 and figure 4.1 in appendix B give detailed information of drawdown for each observation section.*

3.4 Conclusions

The qualitative and quantitative evaluation of the pumping test LPT-2 is consistent with the overall conceptual model presented in *Wikberg et al /1991/*. The hydraulic importance of Zone EW-5w and the NNW-fracture system and indirectly also NE-1w is clearly demonstrated. However, the test indicated that some modifications of this model are necessary to satisfactorily explain all drawdown responses observed.

The most important points to consider for further investigations are:

- the extension of Zone EW-5w towards northwest beyond Zone EW-1w;
- the extension of Zone EW-5w towards northeast and location of the zone in boreholes KAS04 and KAS12 (and possibly KAS08);
- the extension and hydraulic properties of Zone EW-3w;
- the extension and hydraulic properties of Zones NNW-3w and -4w.

4 THE TRACER EXPERIMENT

4.1 Introduction

A large scale three-dimensional tracer test was performed during LPT2. The aim of this test was to give information on how the fracture zones are interconnected and to determine transport parameters such as residence time, dispersivity, flow porosity and hydraulic fracture conductivity. The experimental results do also provide the data for the validation of the numerical simulation model and constitute a valuable test case for further simulation studies. The details about the experimental design and the test can be found in *appendix C*.

4.2 Method

Before the tracer injections started, dilution measurements were performed to find borehole sections suitable for tracer injections. Altogether ten sections were used for dilution measurements (*see chapter 5*). Out of these, six borehole sections were selected for tracer injections. Dilution measurements are performed with the purpose to determine the flow rate through a borehole section. A tracer is injected in the circulation section (continuously mixed by circulating the water in the section) and the decrease of the tracer concentration is proportional to the flow through the section. A schematic illustration of the borehole equipment is shown in *figure 4.1*.

The first tracers were injected about two weeks after the pumping started, so that the tracers would be injected in a steady state groundwater flow field. Measurements of hydraulic head confirmed that a steady state prevailed during the tracer test.

Tracers were injected in packed-off sections in boreholes which intersected the fracture zones. Injections of tracers were made in boreholes KAS02, KAS05, KAS07, KAS08 and KAS12. The arrival of the tracers were detected in KAS06. The distribution of the water inflow and the tracers along KAS06 was estimated from the measured results.

Three radioactive isotopes (In-114, I-131, Re-186 with half-lifes 49.51 days, 8.04 days and 3.78 days respectively) and one fluorescent dye tracer (Uranine) were injected in four borehole sections into the fracture system around the pumped hole. One tracer per injection point was used.

Towards the end of the tracer test two additional tracer pulses were injected in a second run in two borehole sections not used in the previous run.

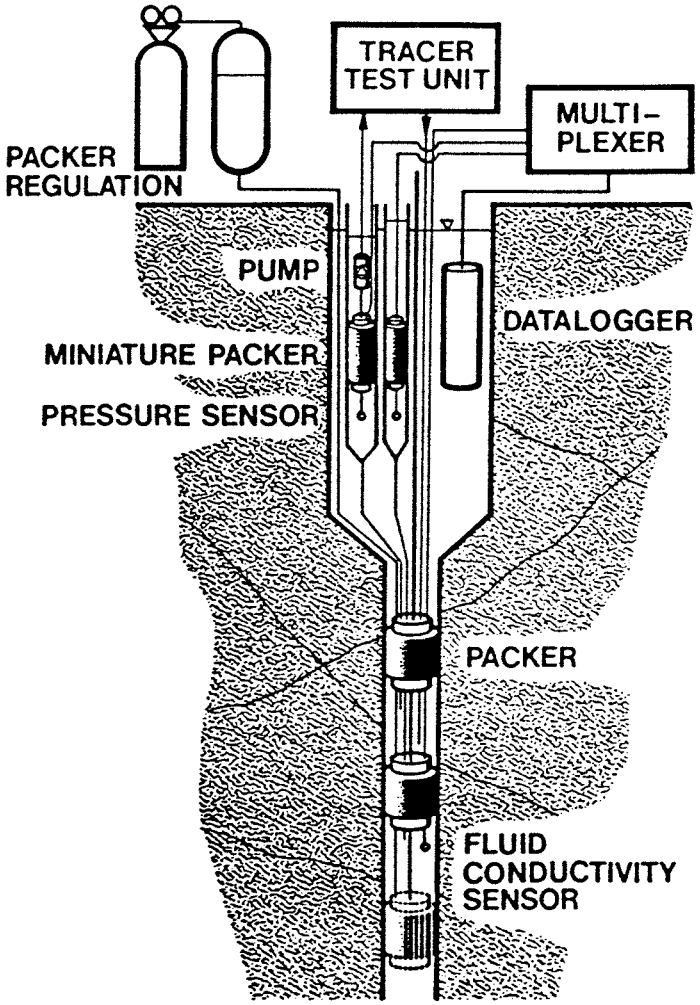

Fig 4.1 *Schematic figure of tracer injection equipment in the borehole. The tracer is injected in the lower part of a section between two packers and the inlet to the circulation pump is close to the upper packer in the section.*

4.3 Results

Tracer injections were made in six borehole sections, see table 4.2. Three of these injections, originating from KAS12 section DB, KAS08 section M1 and KAS05 section E3 could be detected in the withdrawal borehole.

The tracer inflows versus time, i.e. breakthrough, were measured along KAS06 by taking samples intermittently at nine identified inflow levels, *see figure 4.2.*

As an example the breakthrough at sampling level 4 (390 m) of the tracer injected in KAS08 is shown in *figure 4.3.*

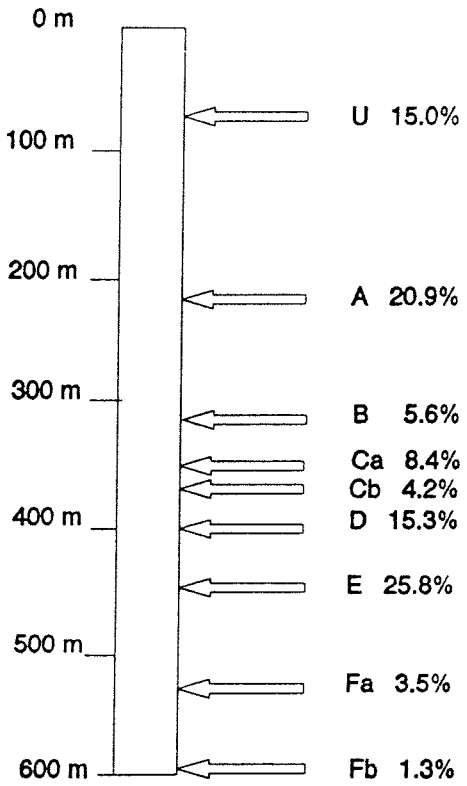

Fig 4.2 *Inflow distribution in KAS06 determined from spinner data and tracer test. Letters A-F refers to the name of the conductor and U to the interval 0-100 m (c f table 4.1).*

Table 4.1 Studied levels and their corresponding major water-conducting fracture zones in KAS06

Level[1] no, depth	Hydraulic label	Conductor[2] depth (m)	Corresponding fracture zone	Borehole[3] identification
	U	60-70	EW-3	G
8 190	A	217	NNW-1,w or EW-5	S, Ch
7 290	B	312	EW-5	S
6 340	C,a	353	EW-5	S
5 360	C,b	364	EW-5	S
4 390	D	399	EW-5	Ch
3 430	E	448	NNW-2,w	S, Ch
2 540	F,a	558	EW-X[4]	
1 570	F,b	596	EW-X[4]	

1 Sampling depth, metres along borehole below casing top.
2 Major hydraulic conductor with its corresponding depth (metres along borehole below casing top).
3 G = geological, S = spinner, Ch = groundwater chemistry */Wikberg et al, 1991/*.
4 Not included in the conceptual model by */Wikberg et al*, 1991/.

Table 4.2 Hydraulically active fractures in the injection sections, according to spinner survey. Underlined numbers are fractures where the main flow occurs

Borehole	Fracture zone	Level of hydraulic active fractures
KAS12, section DB	NE-2 or EW-5	285, 310, 320, 325
KAS08, section M1	NE-1	550-562, 571, 585
KAS08, section M3	NNW-2	141, 184
KAS07, section J4	EW-5	200, 223, 245, 255-276
KAS05, section E3*	EW-5	322, 332, 364, 380
KAS02, section B4	EW-5	318, 342

* = data from hydraulic single hole testing, as no spinner result was obtained

The cumulative apertures of the hydraulically active fractures in the fracture zones were estimated to be 5-10 times greater in EW-5 compared to NNW-1 and NNW-2 ($10 \cdot 10^{-3}$ - $30 \cdot 10^{-3}$ m compared to $2 \cdot 10^{-3}$ - $5 \cdot 10^{-3}$ m). The fracture conductivities are however greater in NNW-1 and NNW-2 compared to EW-5. The conclusion is that EW-5 is built up of many low conductive fractures whereas zones NNW-1 and NNW-2 of a few highly conductive fractures. The calculated flow porosity depends on the estimated width of the zone and if EW-5 is assumed to have a width of 100 m and NNW-1 and NNW-2 5-10 m the flow porosities are in the range of 0.02% for EW-5 and 0.1% for NNW-1 and NNW-2.

The dispersivities were estimated to one tenth to one fifth of the flow path distance and the Peclet number to 4-11, where the lower values are representative for EW-5 and the higher for NNW-1 and NNW-2.

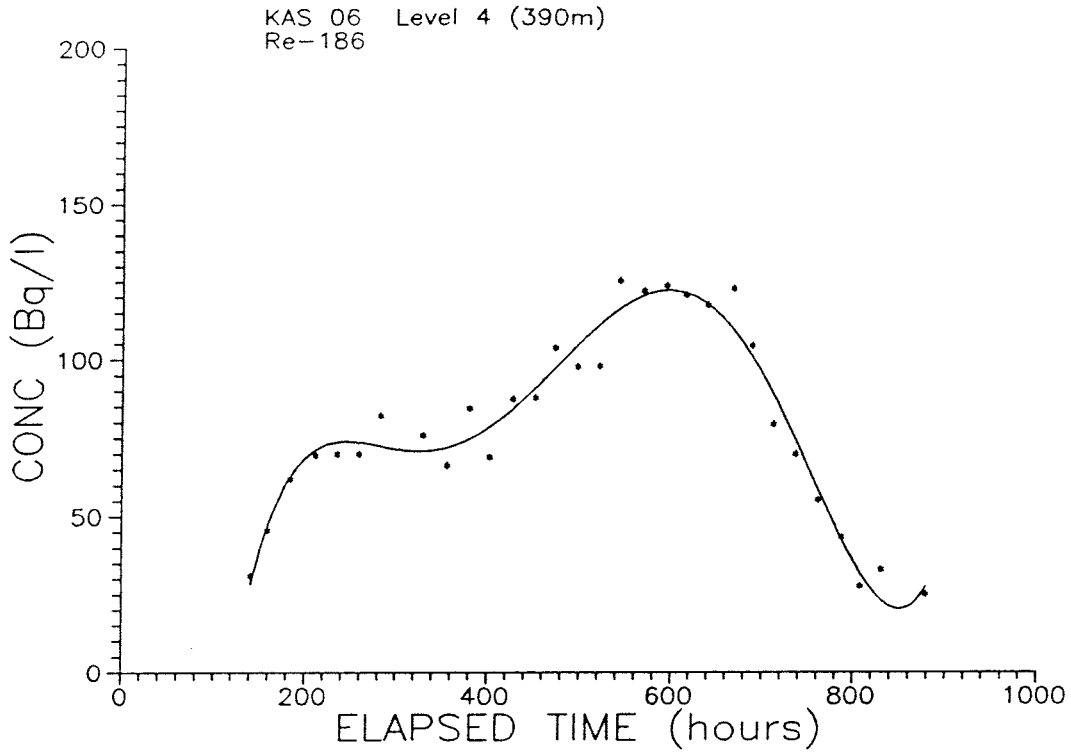

Fig 4.3 *Breakthrough of Re-186 at sampling level 390 m in KAS06. Experimental data points and fitted five-degree polynom (solid line).*

4.4 Conclusions

The report concludes that EW-5 is a good but complex hydraulic conductor with many widely spread but interconnected fracture flow paths. NNW-1 and NNW-2 are very good hydraulic conductors with a few narrowly spaced water conducting fractures. EW-3 should be considered as a more important hydraulic conductor than is assumed in the conceptual model.

The measurements were checked for consistency with the current conceptual model. The general conclusion was that the experimental results support the current conceptual model.

The large scale three-dimensional tracer experiment provides valuable information about the system of fracture zones at Äspö. Both the direct measurements, like the time distribution of tracer inflow at different levels in KAS06, and the derived quantities, like flow porosity and dispersivity, add to the understanding of the groundwater flow.

5 THE TRACER DILUTION MEASUREMENTS

5.1 Introduction

Tracer dilution measurements were performed to determine the groundwater flow in packed-off sections in boreholes, both prior to and during LPT2. The measurements were carried out in altogether 12 boreholes, and 22 different packed-off sections, at depths varying from 40 to 800 meters.

The measurements made prior to LPT2 were carried out under natural gradient conditions and also during a pumptest, called LPT1. During LPT2 ten sections were measured.

The purpose of the tracer dilution measurements was to evaluate the consistency with the conceptual model given by *Wikberg et al /1991/* and to select borehole sections for tracer injections for the LPT2 test. It is within reach to evaluate the consistency with the conceptual model as flow measurements under both natural gradients and pumped conditions, give information for the evaluation of the fracture zones and the way they are connected. The dilution measurements are presented in detail in *appendix D*.

5.2 Method

The measurement of groundwater flow in a borehole section is based on dilution of an added chemical substance that is mixed in the groundwater in the borehole section and thereafter the concentration in the water is determined at regular intervals. The decrease of tracer concentration as a function of time is proportional to the groundwater flow through the section. This way of measuring groundwater flow is termed dilution technique. The borehole section lengths are chosen from considerations of the water conducting fracture zones intersecting the borehole and varies from 7 to 145 m. The major part of the flow measurements were performed within the equipped boreholes in the southern part of Äspö.

The technical design of the experimental set-up is similar to the one used in the tracer experiment discussed earlier; the set-up is illustrated in *figure 4.1*. The injection of the tracer needs to follow a special procedure. *See appendix D* for further details.

5.3 Results

In total 68 dilution measurements have been performed. An example of a dilution curve is shown in *figure 5.1*. In *appendix D* measurements from LPT2 are compiled together with measurements from an earlier pumptest, LPT1, and measurements under natural gradients (NG1 and NG2).

By applying the equation of continuity for the tracer, and using the dilution curve, it is possible to estimate the groundwater flow through the borehole section. In this process the data were also analyzed individually, looking for consistency and possible measurement errors (like leakage in tube fittings). The final result of the analysis is presented in *table 5.1*.

The measured flow rates, both during natural conditions and during LPT2, can be used for an analysis of the consistency of the current conceptual model presented by *Wikberg et al /1991/*. A large difference between the natural and forced groundwater flow indicates that the analyzed section, and hence the fracture zone, is in good hydraulic contact with the pumped borehole. Such an analysis has been carried out, *see appendix D and figure 5.3*. It can, from this analysis, be concluded that the current conceptual model describes the system of fracture zones on Äspö in a realistic way. Improvements are however still possible, as some sections did not respond to the pumping as could be expected (for example KAS02-B4).

The flow during natural gradient is generally between 0 and 35 ml/min and the variation seems, according to the scarce data, to decrease with depth, as can be expected, (*see figure 5.2*).

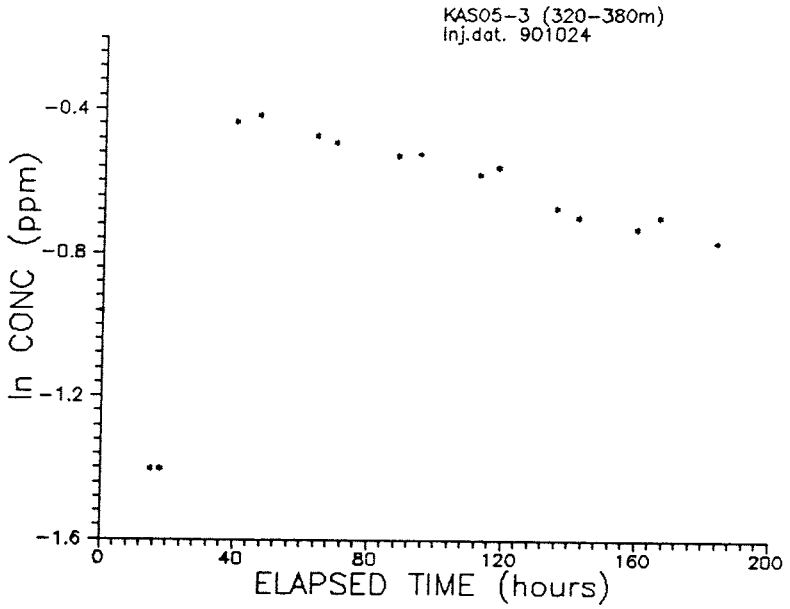

Fig 5.1 Example of a dilution curve.

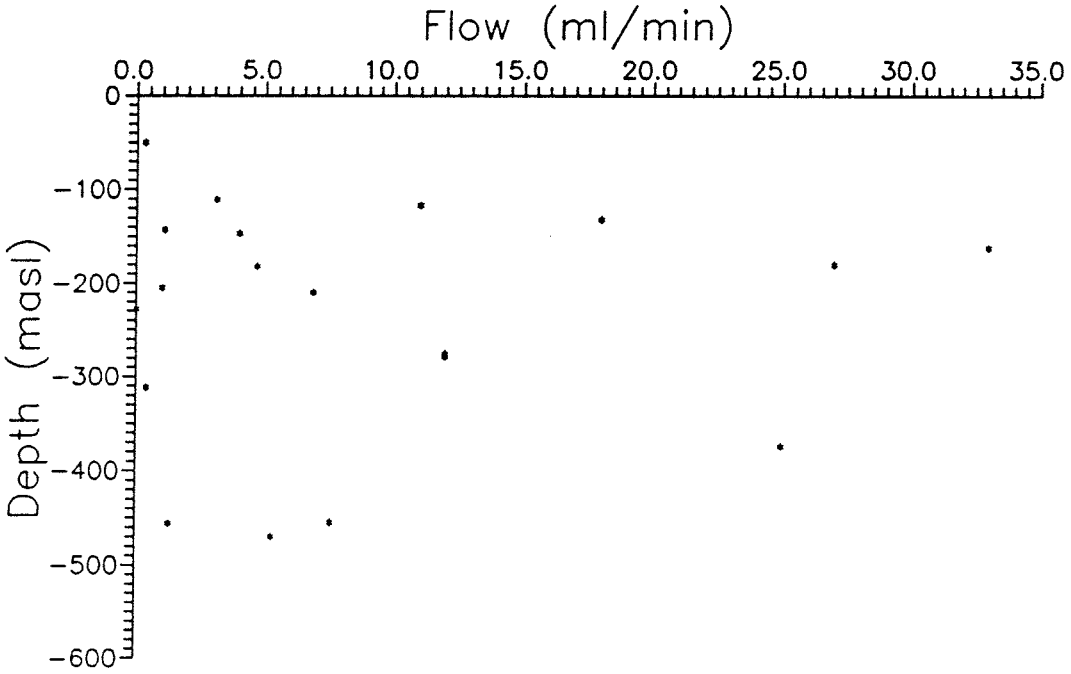

Fig 5.2 Measured flow (through borehole sections) versus depth below ground-surface during natural gradient (NG2), (dilution measurements).

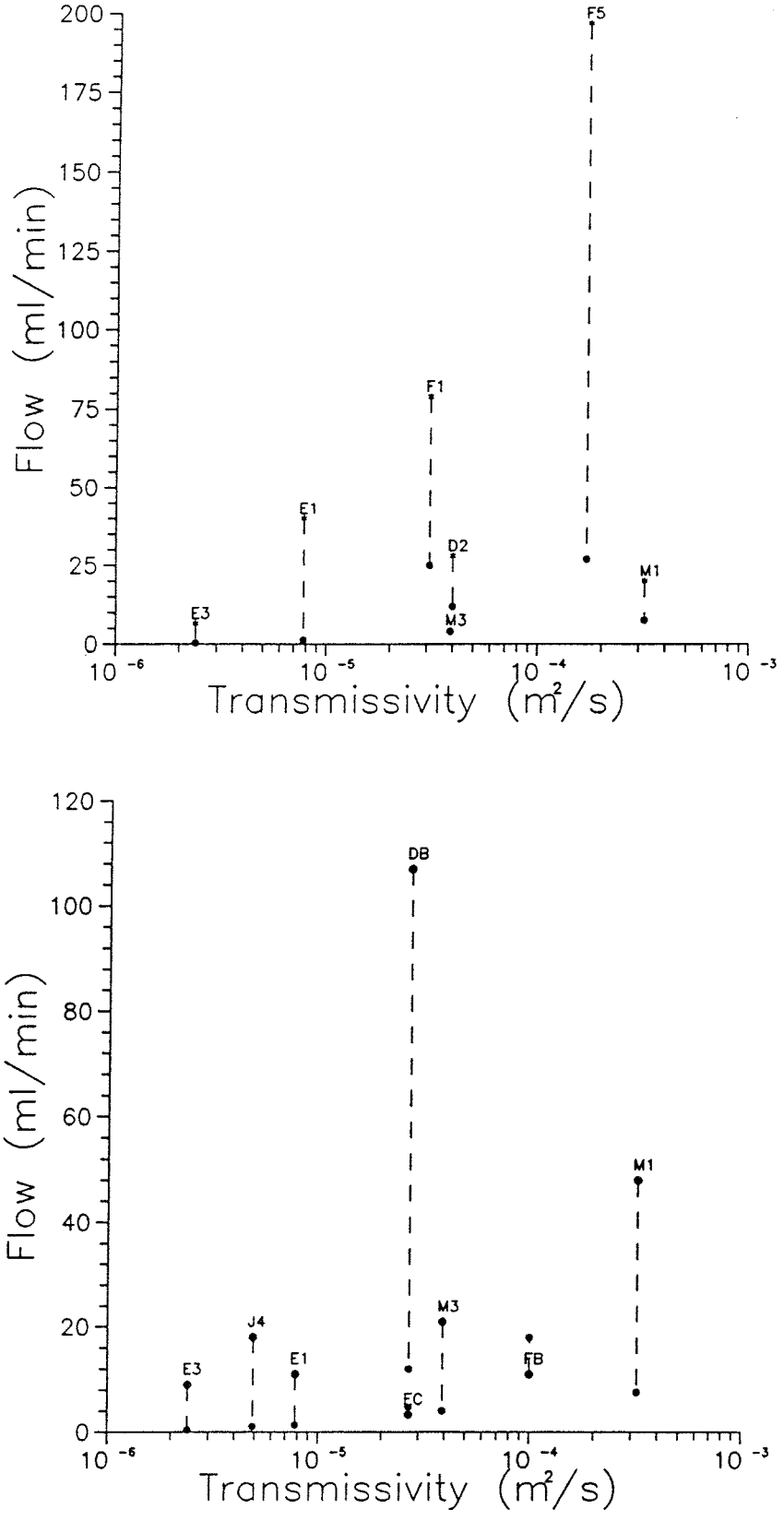

Fig 5.3 *Flow (through borehole sections) versus transmissivity (of the zone(-s) intersecting the section) during LPT1 (top) and LPT2 (bottom) compared to natural gradient conditions (lower-values). The labels on the plot are borehole section codes and these codes can be found in table 5.1.*

Table 5.1 Concluded results of dilution measurements. LPT1 and LPT2 are the Longtime Pumping Test 1 and 2. NG1 and NG2 are the dilution measurements during Natural Gradient - undisturbed conditions.

Borehole	Code	Section (m)	Flow measurements LPT-1 (ml/min)	NG1 (ml/min)	NG2 (ml/min)	LPT-2 (ml/min)
KAS02-4	B4	309-345	1.1	-	(*)	2
KAS02-2	B2	800-854	(*)	-	(*)	4
KAS03-5	C5	107-252	-	-	6.9	-
KAS03-2	C2	533-626	-	-	(120)	-
KAS04-2	D2	332-392	28	-	12	-
KAS05-3	E3	320-380	6.5	-	0.4	9
KAS05-1	E1	440-549	40	1.8	1.3	11
KAS06-5	F5	191-249	197	25	27	ph
KAS06-1	F1	431-500	79	52	25	ph
KAS07-4	J4	191-290	ph	-	1.0	18
KAS07-1	J1	501-604	ph	-	5.3	-
KAS08-3	M3	140-200	4.3	-	4.0	21
KAS08-1	M1	503-601	20	5.5	7.6	48
KAS09-4	AD	116-150			11	-
KAS11-5	CE	47- 64			0.3	-
KAS11-2	CB	153-183			33	-
KAS12-3	DC	235-278			0	-
KAS12-2	DB	279-330			12	107
KAS13-4	ED	151-190			1.1	-
KAS13-3	EC	191-220			4.7	3.3
KAS14-4	FD	131-138			3.1	-
KAS14.2	FB	147-175			18	11

- = No measurement, ph = pumphole
* = Failed measurement (see text)

5.4 Conclusions

The tracer dilution technique provides a fairly direct method of estimating the response on the groundwater flow of a pumptest. The actual flow rate may be affected by local conditions, and disturbances from the borehole, but the change in flow from natural conditions to pump conditions ought to give a good indication of the properties of the network of fracture zones.

The present tracer dilution experiment confirms this and it is also in accordance with the conceptual model of Äspö presented by *Wikberg et al /1991/*.

Some comments about details can however be made:

- The hydraulic connections in EW-5 are possibly better in the E-W direction compared to N-S, which is in accordance with the geological interpretation of the zone. EW-5 seems to be a relatively good hydraulic conductor. Possibly there are conductive structures parallel to EW-5 at deeper levels that connect the lower parts of KAS06 and KAS05.

- Section EC borehole KAS13, which possibly intersects a NNW structure, does not seem to be in good contact with NNW-1, NNW-2, NE-2 or NE-1, because the flow does not increase in this section during pumping in KAS06 (LPT2).

- NE-2 is in good contact with NNW-1 and NNW-2 and possibly the transmissivity is larger than 2.7×10^{-5} m^2/s.

6 VALIDATION OF THE NUMERICAL MODEL

6.1 Introduction

The field measurements presented constitute a most valuable data-base, to be used in future developments of the conceptual and numerical models. Some scoping calculations from a numerical model have also been presented in this report (*chapter 2 and appendix A)*, and an evaluation of these can now be undertaken. It should be noted that the predictions of the travel times were made and presented prior to the experiments, which of course is the correct order. (The drawdown for each borehole section was calculated after the experiments, but with the same boundary conditions and conductivity field). The drawbacks are that the experimental conditions may not be altogether known when the predictions are done. As an example one may note that the predictions were done assuming a pumprate of 2.5 l/s, while the experiment turned out to be done with 2.25 l/s. Also, fracture zone EW3 was considered low conductive in the conceptual model of the summer of 1990, while in fact 15% of the inflow to KAS06 was found to originate from EW3. Finally, when the predictions were made it was expected that injection in KAS12 should be in section DD; it turned out to be in section DB. The injection in the numerical model was therefore done about 70 meters above the correct point.

6.2 Travel times

Results from the tracer experiment can be compared with the numerical predictions for injections in KAS12, DB and KAS08, M1. These comparisons are summarized in *table 6.1*. The predictions presented in *appendix A* assumes a porosity of $n = 10^{-3}$ a value which is not well established for the domain. In Table 6.1 travel times (defined as mean travel time, t_{50}) for a porosity of 5×10^{-4} are also shown. Obviously, good agreement with measured travel times can be obtained with a porosity in the expected range. In fact, both the porosities used in *table 6.1* are in good agreement with the ones estimated from the tracer experiment, see *appendix C*.

In *table 6.1* three measured times are given for KAS12, DB. The reason for this is that the tracer was found in three fracture zones intersecting KAS06. The numerical model does not presently consider any dispersion effect and will hence only predict one flow path and one travel time.

Table 6.1 Measured and predicted mean travel times

Injection point	Travel times Measured (days)	Predicted $n=10^{-3}$ (days)	Predicted $n=5x10^{-4}$ (days)
KAS12, DB	31, 25, 31	61	30
KAS08, M1	10	19	10

6.3 Drawdowns

As can be seen in *appendix B*, extensive measurements of drawdowns were carried out as part of the LPT2 experiment. Drawdowns were not presented in the report for the numerical simulations prior to the experiment (*see appendix A*) and the comparison to be discussed below is thus not, strictly speaking, a validation study. It does anyway illustrate the kind of predictions that can be achieved with a numerical model.

The predictions were subsequently updated with the pumprate in the experiment, i e 2.25 l/s. The conceptual model used in the predictions, presented in *appendix A* was however kept. The distribution of the inflow was in the first run 30% in NNW1 and 70% in NNW2/EW5. This resulted in an average error of -0.7 m in the drawdowns. An analysis showed that the error was concentrated around NNW1. In the experiment 20% of the flow was withdrawn in NNW1 and 15% in EW3. The second run was therefore made with 20% of the flow in NNW1, 65% in NNW2/EW5. It was not possible to pump 15% in EW3 as EW3 had to low transmissivity in the conceptual model used. The withdrawal in EW3 was thus neglected in the second, and final, run. The mean error for this run was -0.07 m and a general agreement with measured drawdowns was obtained, *see appendix E and figure 6.1.* Some large deviations are present, like KAS07-J6 and HAS14. This is however to be expected as all connections between borehole section are not, and can not be, considered in the conceptual model. It should also be noted, see Svensson, (1991) for details, that a stochastic method is used when generating the hydraulic conductivities. Random variations can thus be expected in the calculated error, *see appendix E.*

6.4 Conclusions

A general agreement between measured and predicted travel times and drawdowns has been found . The travel times can be brought to agreement with a reasonable flow porosity. Drawdown predictions were not carried out prior to the experiment and the comparison is thus not to be considered as a validation. The comparison does anyway indicate that a fairly close agreement can be obtained, which is once again a confirmation that the conceptual model is sound.

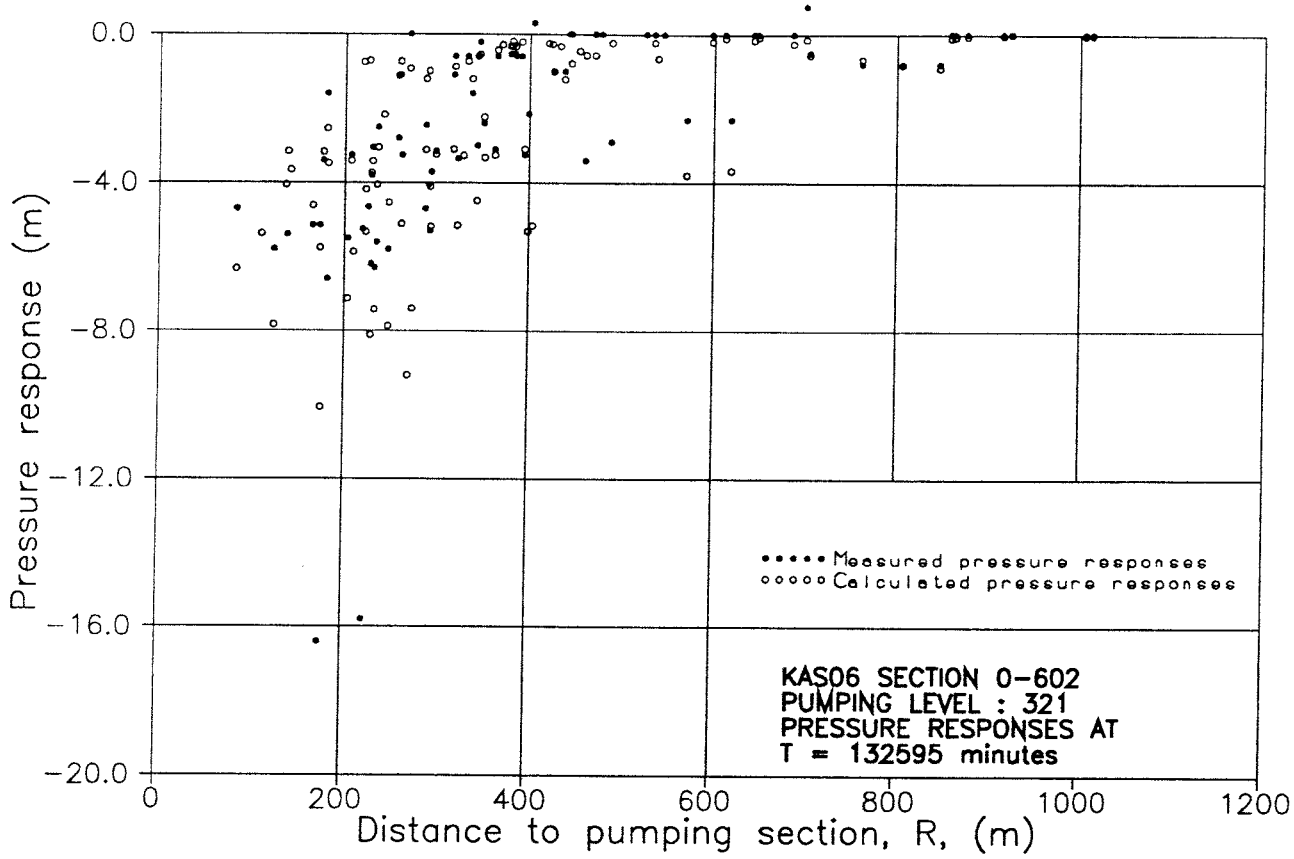

Fig 6.1 Measured (point) and calculated (circles) drawdowns during LPT2.

7 DISCUSSION OF THE CONCEPTUAL MODEL

The general impression of the results from the LPT2 experiment is that the results support the current conceptual model. However, some of the results indicate that the conceptual model possibly can be improved if some changes are made. These changes are put forward in this chapter and they should be discussed considering also geology, geohydrology and groundwater chemistry when an updated conceptual model is made. These changes can also be tested by using the numerical flowmodel over the Äspö area (*see chapter 2*) and the available calibration cases */Rhén I,1991/* and LPT2.

EW-5

The drawdown in the lower part of KAS03 (interval 253-1002 m) indicates that there is a hydraulic contact between southern and northern Äspö and that the response may have been transmitted via EW-5 to EW-1 or via EW-5 alone, if it is extended to the north beyond EW-1. The latter alternative may be the better one as the geologically interpreted EW-1 has a steeper dip than EW-1w. The uppermost section in KAS04 (D6), does however not show any response, which was expected. It must be tested what effect an extension to the north of EW-5 has on the responses in KAS03 and KAS04, D6.

In the report in *appendix B* it is also suggested that EW-5 may extend further to the east. However, geologically, and in hydraulic tests, it has not been seen in KAS08. The possible existence of zone EW-5 in boreholes KAS04 and KAS 12 should be further investigated.

Geologically EW-5 comprises a series of more or less parallel fractures with a dip of 20-30° to NNW and the conductive structure EW-5w was put forward as a single structure with a dip of 37° */Wikberg et al 1991/*. Probably EW-5w has to be divided into several conductive structures and possibly with a dip less than 37°. Possibly there are subzones parallel to EW-5, which were indicated as EW-x in *Wikberg et al /1991/*. According to the dilution measurements the flow increases in section KAS05, E1 (borehole section 440-549 m) which may be an indication of a structure parallel to EW-5 but deeper.

EW-3

It was shown from the tracer test that there was an inflow of water in the upper part of KAS06 during the test, which should correspond to EW-3. This was also indicated by the drawdown response in KAS06 during LPT2. According to *Wikberg et al /1991/* the fracture zone is developed in heterogeneous bedrock , is hydrothermally altered and conductive

sections are probably rare. According to hydraulic tests in KAS07 the transmissivity should be low in EW-3 at deeper levels. One suggestion is that the upper part of EW-3 has a higher transmissivity than the lower part. The properties of EW-3 should be further analyzed.

NNW1 and NNW-2

These structures are important and they probably consist of relatively few interconnected fractures.

NNW-3

This structure is questioned in *appendix B* but it can be seen in several tests that HAS13 is well connected to the boreholes intersecting NE-1 and there is also some geophysical evidences of NNW-3. The properties are however uncertain and possibly the response in HAS13 can be explained with structures parallel to EW-5.

NNW-4

It is suggested in *appendix B* that NNW-4 is possibly not needed in the conceptual model based on the results from LPT2. The responses seen in HAS18 during several tests can possibly be explained by other structures, but as seen in for example *figure 4.1, appendix B* the responses in HAS18 (PA,PB) are quite good compared to for example KAS12 (DA, DF). In any case, NNW-4 should be discussed when the next conceptual model is made.

8 REFERENCES

Rhén I, 1991, Information for numerical modelling 1990. Calibration cases. SKB, Progress report 25-90-17b.

Svensson U, 1991, Groundwater flow at Äspö and changes due to theexcavation of the laboratory. SKB, Progress report 25-91-03.

Wikberg P, Gustafson G, Rhén I, Stanfors R, 1991, Äspö Hard Rock Laboratory. Evaluation and conceptual modelling based on the preinvestigations 1986-1990. SKB, Technical Report 91-22.

SKB, 1986, R&D programme 86, Handling and final disposal of nuclear waste. Programme for research, development and other measures, SKB, Stockholm.

SKB, 1989, R&D programme 89, Handling and final disposal of nuclear waste. Programme for research, development and other measures, SKB, Stockholm.

APPENDIX A Prediction of flow trajectories for the LPT2 test

ÄSPÖ HARD ROCK LABORATORY
- PREDICTIONS OF FLOW TRAJECTORIES FOR THE LPT2 PUMP TEST.

BY
URBAN SVENSSON
COMPUTER-AIDED FLUID ENGINEERING

DATUM 1991-08-28

TABLE OF CONTENTS.

	Page
ABSTRACT/SUMMARY.	1
1. INTRODUCTION	2
2. METHOD	4
3. RESULTS	5
4. CONCLUDING REMARKS	8
5. REFERENCES	9
APPENDIX A	20
Table of trajectory for injection in KAS02, section B4.	
APPENDIX B	25
Table of trajectory for injection in KAS02, section B2.	
APPENDIX C	37
Table of trajectory for injection in KAS04, section D2.	
APPENDIX D	42
Table of trajectory for injection in KAS05, section E3.	
APPENDIX E	47
Table of trajectory for injection in KAS07, section J4.	
APPENDIX F	51
Table of trajectory for injection in KAS08, section M3.	
APPENDIX G	56
Table of trajectory for injection in KAS08, section M1.	
APPENDIX H	60
Table of trajectory for injection in KAS11, section CE.	
APPENDIX I	68
Table of trajectory for injection in KAS12, section DD.	

ABSTRACT/SUMMARY.

Predictions of trajectories during a pumptest are presented and discussed. The pumping is in borehole KAS06 and trajectories are predicted for injections in altogether nine boreholes.

The basic groundwater circulation model has been developed by the author and is fully described elsewhere. This model utilizes the most recent information about conductivity-fields, fracture zone transmissivities, etc. The trajectories are calculated in a Lagrangian manner, i.e. a massless marked fluid element is followed from the injection position to the pump hole.

The predicted trajectories look plausible and are expected to give an indication of the correct trajectories. The typical Darcian flow time for the cases considered is predicted to 10^{10}s. The real flow time can be estimated as a function of the effective porosity.

1. INTRODUCTION

The work presented in this report should be regarded as a complement to the report "Groundwater flow at Äspö and changes due to the excavation of the laboratory" by Svensson /1-1/. In that report the mathematical/numerical model is presented, calibrated and applied. The present report will therefore be brief and concentrate on the presentation of the predictions.

The main objective of the report is to present predictions of tracer trajectories during a pumptest, carried out in September-December 1990. In Figure /1-1/ the Island of Äspö is introduced, with its major fracture zones and some of the boreholes marked. The pumptest, called LPT2, is a long term pumping in KAS06. Tracers will be injected in other boreholes and the path and the travel time to KAS06 noted.

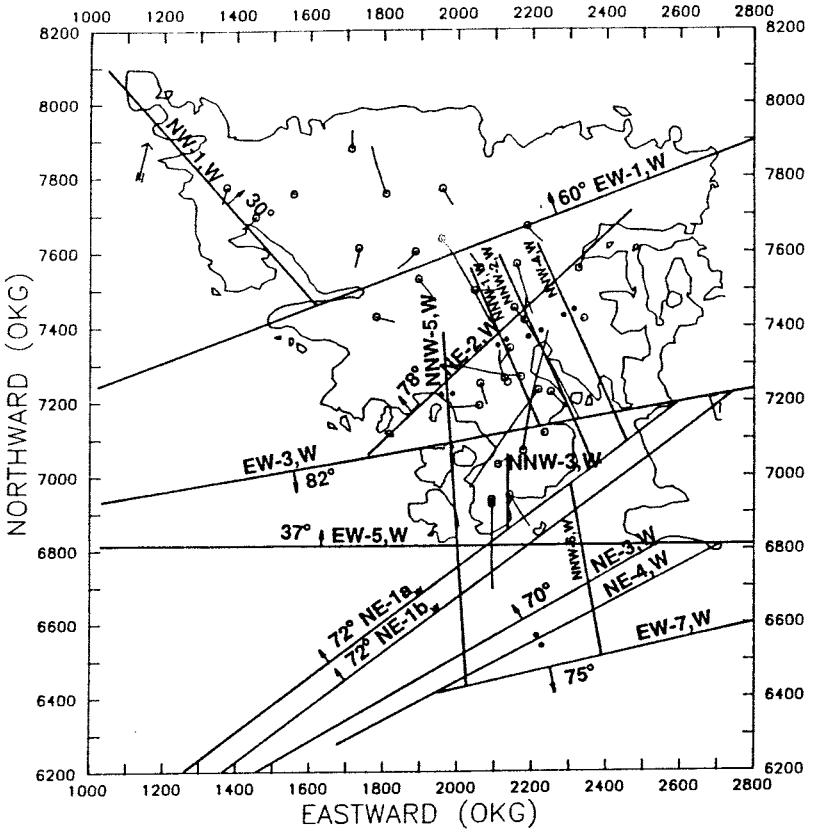

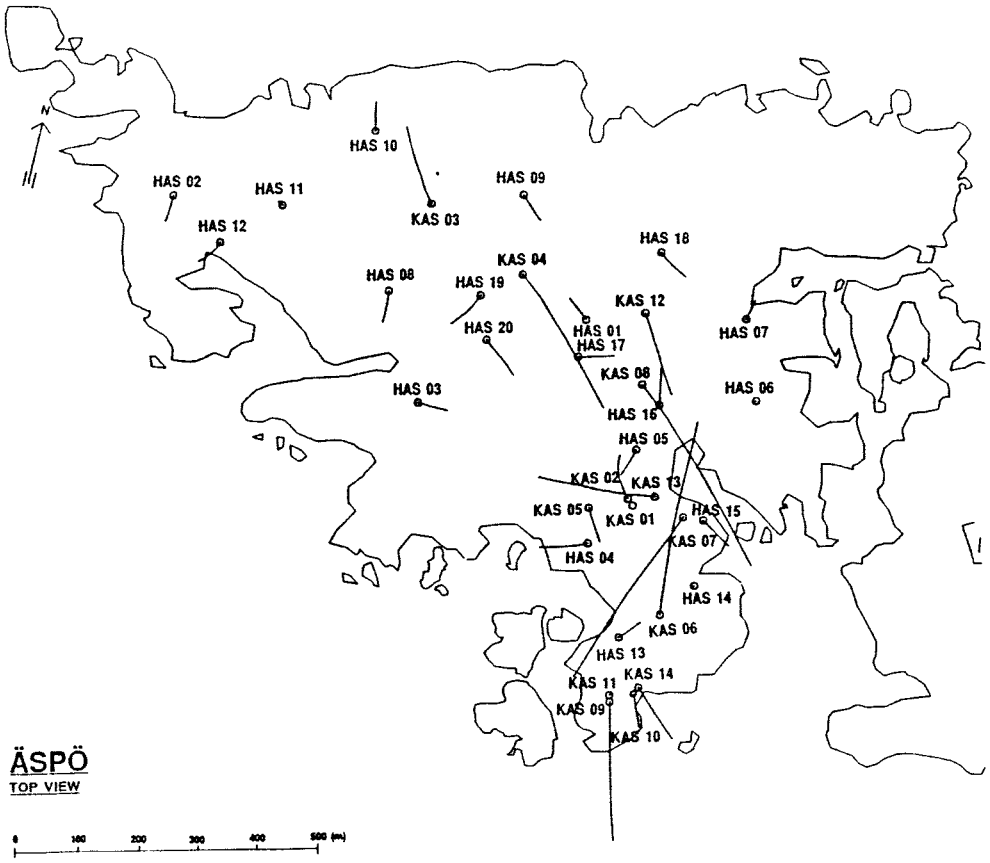

Figure /1-1/ The Island of Äspö. Major fracture zones and boreholes.

2 METHOD

The steady state flow pattern generated when pumping in KAS06 is first predicted using the model described in Svensson /1-1/. This model is based on the most recent conceptual model of Äspö. For the present predictions, the velocity field from this model is used when trajectories are calculated. According to Rhen /1-2/, the pumping rate is around 150 liters/minute distributed along KAS06 as follows:

Zone	Section in borehole (m)	Percent of Flow	Fracture zone
A	217	0,25	NNW1
B	312	0,06	EW5
C	358	0,16	EW5
D	399	0,17	-
E	448	0,28	NNW2
F	577	0,08	-
		≈1.0	

An analysis of the fracture zones, as shown in Figure /1-1/ and represented in the numerical model, shows that the following distribution is in better agreement with the current conceptual and numerical model:

Zone	Section	Percent of Flow	Fracture
A	230	0,30	NNW1,
B	480	0,70	NNW2, EW5

The reason for this idealization is that a fracture zone is required where pumping is to take place. The positions for injection of tracers will be presented when results are discussed.

The tracking of a marked fluid element is done in a Lagrangian manner, i.e.

$$\vec{ds} = \vec{u}\, dt$$

where $\vec{ds}$ denotes increment in space, $\vec{u}$ the local velocity vector and dt the timestep. Instead of having a fixed dt it is of course also possible to put a limit on the step in space. Further details about the algorithm can be found in Svensson /1-1/.
The limited space step was used, with ds_i = 5m, in the predictions to be presented.

3. RESULTS

Results will be presented by considering one injection point at the time. Trajectories will be shown graphically and listed in tables. In the tables cell indexes are used in the description of particle positions. Figure /3-1/ is provided as a reference for these indexes. For each trajectory the Darcian flow time will be estimated. The real travel time can then be estimated with the kinematic porosity, n, assuming the pore velocity $\vec{u}_p = \vec{u}/n$.

3.1 Injection in KAS02, section B4

Starting with the graphical presentation, Figure /3-2/, it is seen that the tracer is injected at a section located about one third of the total length of KAS02. From the horizontal plane (z-y) one can also see that the tracer ends up in zone A in KAS06 (see section 2). The two vertical sections show that the path is quite straight. From the table, see Appendix A, it is seen that the tracer starts in cell IX=27, IY=27, IZ=23 (noted as i = 27, j=27, k=23) and that fracture zone EW5 is crossing this cell. Only cell walls with a fracture zone are listed. The coordinates x, y and z are given in the local coordinate system used in the numerical grid. When a new cell is entered the fracture zones in the cell walls (x+, x-, y+, y-, z+ and z-) are given. Also the pressure in the cell and the neighbouring cells (p, px+, px-, etc) are given when a new cell is entered. This information will not be used in the present report. The final position of the tracer is cell IX=37, IY=33, IZ=23 and the tracer is then in fracture zone NNW1.

3.2 Injection in KAS02, section B2

In the next case to be discussed the tracer is injected at a depth of about 800 meters, still in KAS02. The results of predictions are shown in Figure /3-3/ and Appendix B. A study of the figure and the table shows that the tracer will move vertically in NNW1 then horizontally, more or less, in EW5 and end up in NNW1 at the upper pumplevel in KAS06.

3.3 Injection in KAS04, section D2.

The injection in KAS04 is aiming at an injection in fracture zone NE2. From the table, Appendix C, and Figure /3-4/ one can see that the tracer starts in NE2 then finds its way through NNW2 to the bottom pumplevel in KAS06.

In Figure /3-4/ and the figures to be presented it is sometimes seen that the start or end point of the tracer is not in contact with the borehole. There are two reasons for this. Firstly, the tracer is always injected in a fracture zone which in the numerical model can be a small distance away from the borehole. Secondly, the pumping in KAS06 is done in cells which are in direct contact with the fracture zones. In Figure /3-4/ we can see that the injection cell is slightly displaced from KAS04 for this reason.

3.4 Injection in KAS05, section E3.

A tracer injected at a depth of about 300 meters in KAS05 will find its way to the upper pumplevel in KAS06 through the fracture zones EW5 and NNW1, see Figure /3-5/ and Appendix D.

3.5 Injection in KAS07, Section J4.

In this experiment, see Figure /3-6/ and Appendix E, the tracer is also injected in EW5 but now in KAS07. The path is straight to NNW1 and the upper pumplevel in KAS06.

3.6 Injection in KAS08, section M3.

In this experiment the tracer is located in fracture zone NNW2 all the time mainly experiencing a downward displacement, see Figure /3-7/ and Appendix F. The final position is the lower pumplevel in KAS06.

3.7 Injection in KAS08, section M1.

Next we consider an injection in the bottom of KAS08. It is NE1, and NNW2 which are the main fracture zones at this position. The tracer is found to be in contact with NE1 for a while moving south more or less horizontally, see Figure /3-8/ and Appendix G. However, when the tracer has reached NNW2 it is transported to the bottom pumplevel in KAS06.

3.8 Injection in KAS11, section CE.

A quite complex trajectory is predicted for a tracer released at a depth of 50 meters in KAS11, see Figure /3-9/ and Appendix H. The tracer starts in EW5 moves to EW3 (step 40 in the table) back to EW5, and ends up in NNW1 at the top pumplevel in KAS06.

3.9 Injection in KAS12, section DD.

Looking at the horizontal view in Figure /3-10/ one gets the impression that the tracer moves through NNW2 to the bottom pumplevel in KAS06 in a rather straight forward manner. The table, see Appendix I, shows however that the path is somewhat more complex. The injection is in NE2 and the tracer moves in this fracture zone towards NNW2. However, before the tracer can reach the bottom pump position it must be moved downwards about 200 meters.

4. CONCLUDING REMARKS.

One of the objectives of the study is to estimate the Darcian flow time for the tracer. This can be found in Table /4-1/, where also the flow time in days for a porosity of 10^{-3} is given for convenience.

Injection hole	Darcian time($*10^{10}$)s	Time ($n=10^{-3}$)days
KAS02, section B4	0.68	79
KAS02, section B2	204	23700
KAS04, section D2	11.5	1330
KAS05, section E3	1.1	128
KAS07, section J4	0.41	48
KAS08, section M3	0.20	23
KAS08, section M1	0.16	19
KAS11, section CE	3.5	406
KAS12, section DD	0.53	61

Table /4-1/ Darcian flow times.

The estimate in days is of course directly proportional to the assumed porosity and is included for illustration only. A comment is perhaps needed on the flow time for KAS02, section B2. The explanation is, see Appendix B, that no fracture zone is present at the injection position.

It is hard to estimate the realism of the predictions presented as it all depends on the accuracy of the hydrodynamical model which, in turn, is based on a conceptual model of Äspö. The trajectories do however look plausible and some verification of the hydrodynamical model has been presented in Svensson /1-1/. The tentative conclusion from the work presented is therefore that the predicted trajectories do give an indication of the correct trajectories and that the typical Darcian flow time for the cases considered is 10^{10}s.

5. REFERENCES.

1-1 Svensson U. Groundwater flow at Äspö and changes due to the excavation of the laboratory.
SKB-report. 1991-03-11.
1-2 Rhen I. Personal Communication.

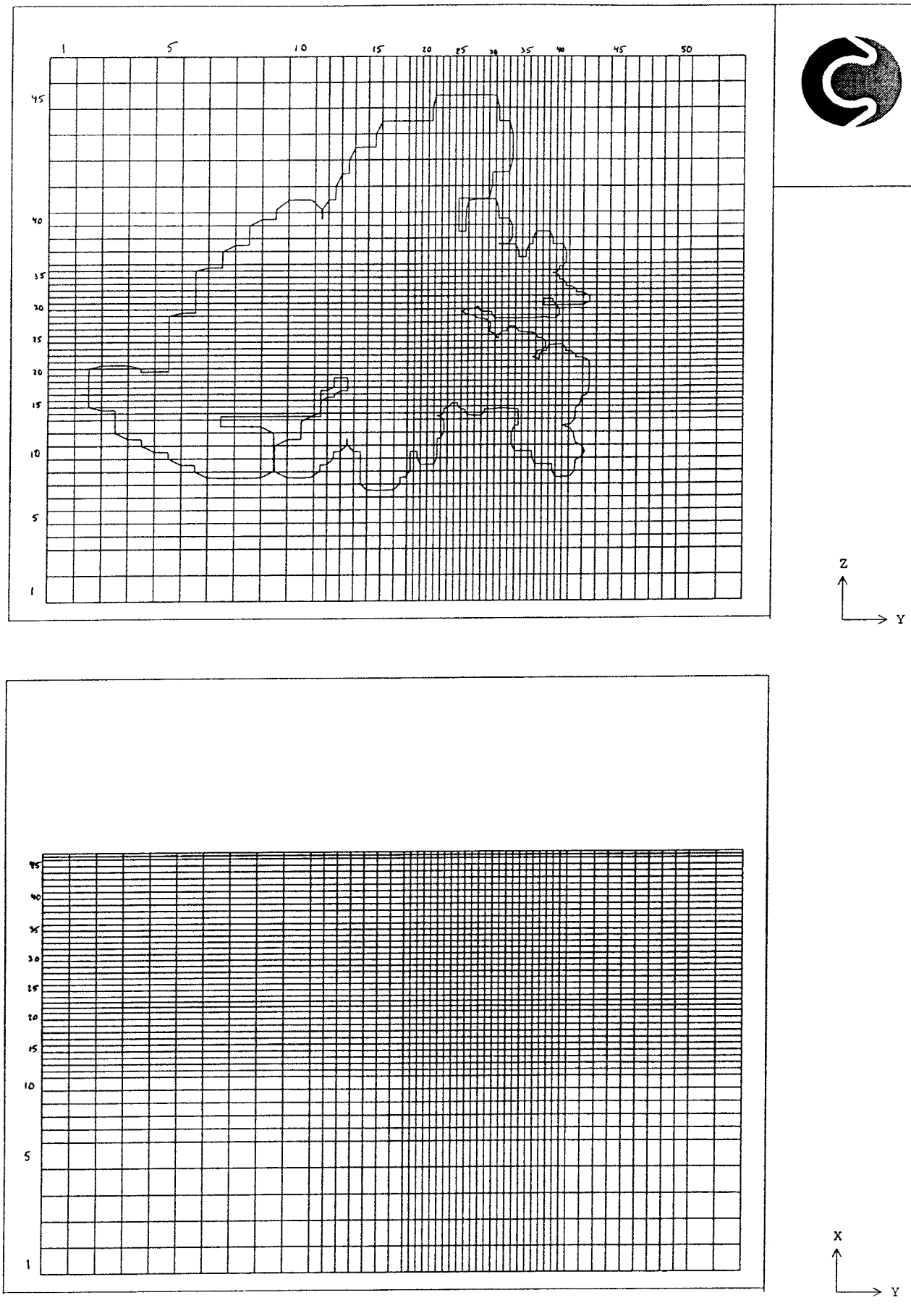

Figure /3-1/. The computational grid.

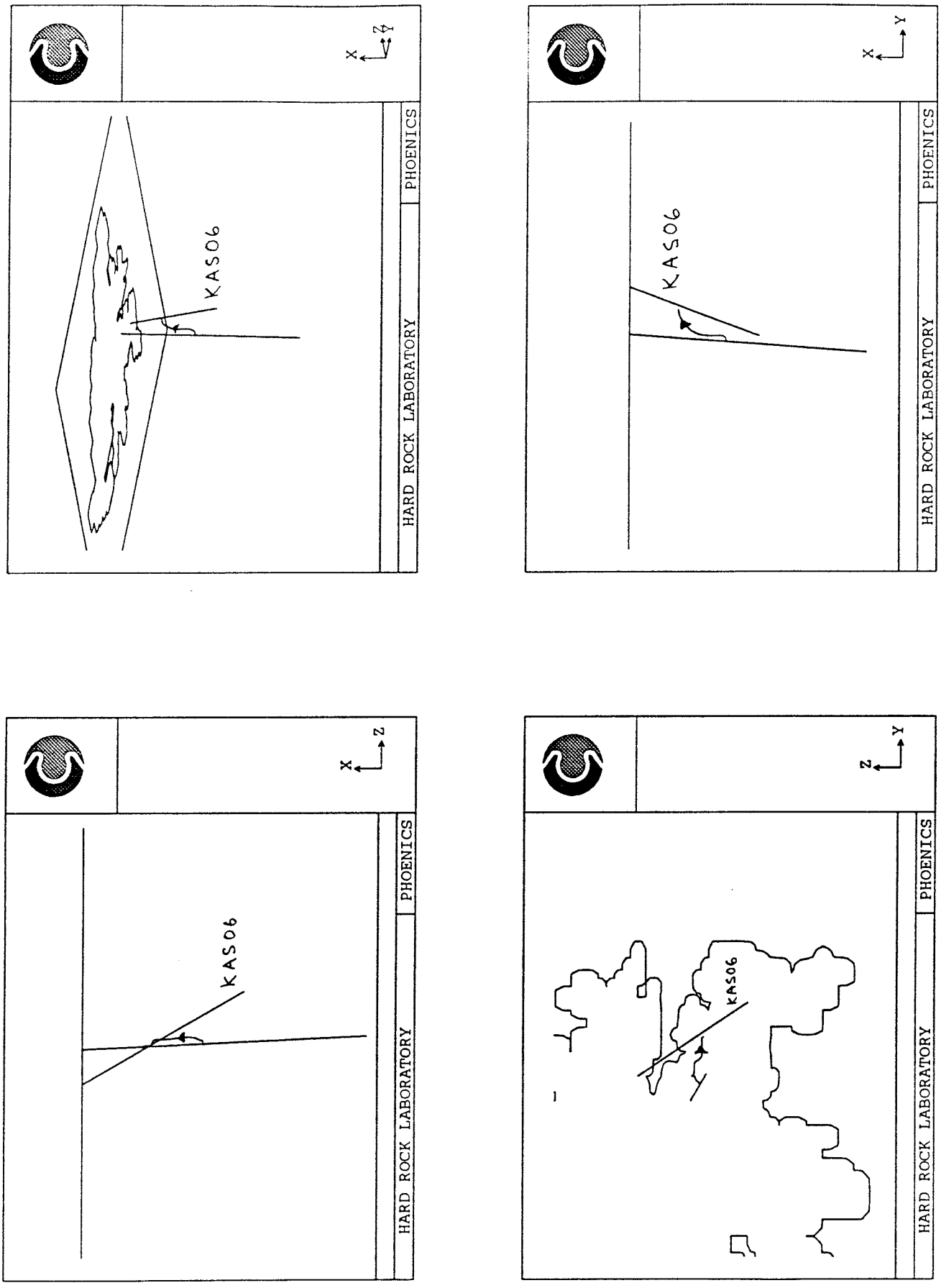

Figure /3-2/. Trajectory when injecting in KAS02, section B4.

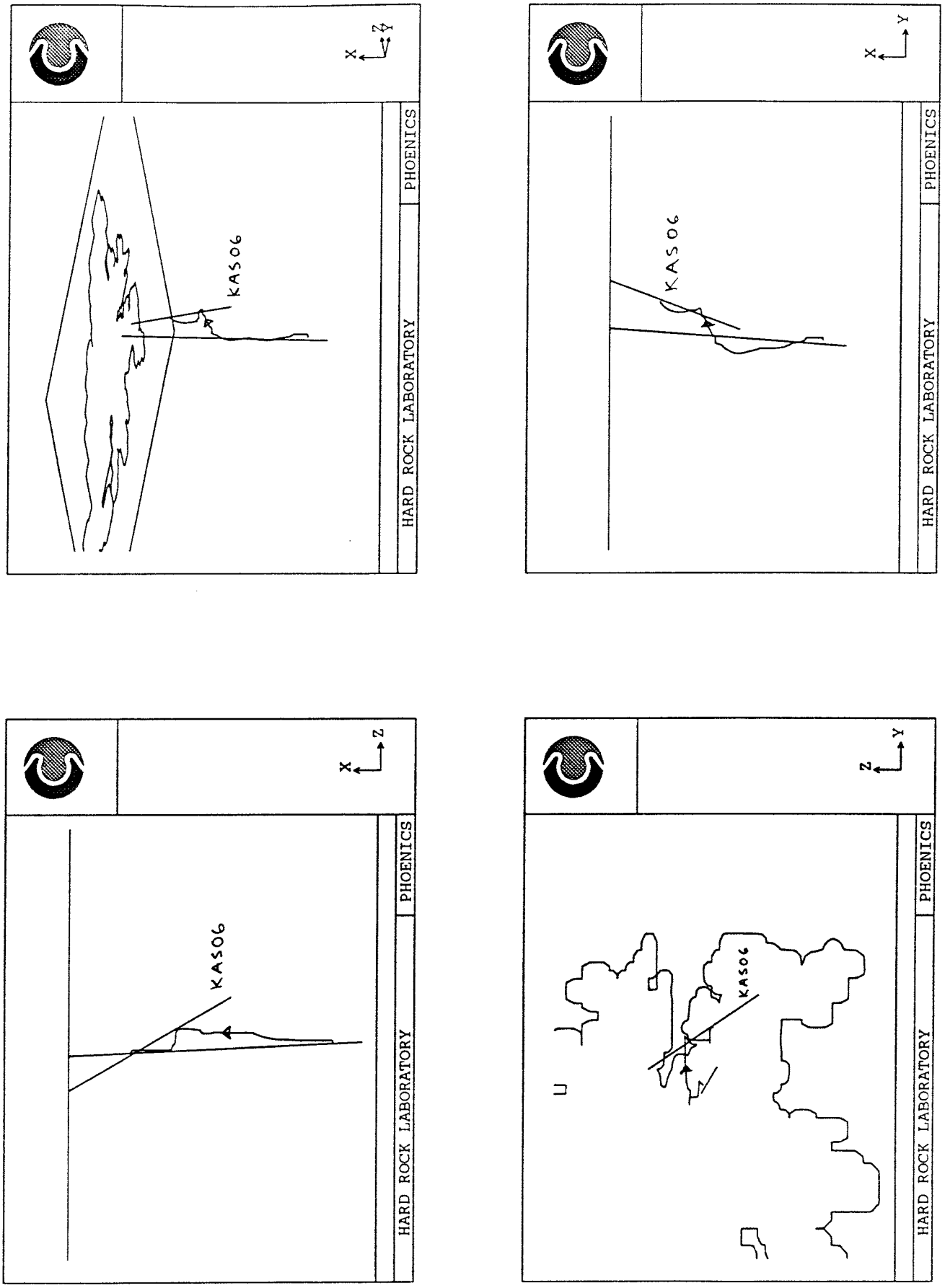

Figure /3-3/. Trajectory when injecting in KAS02, section B2.

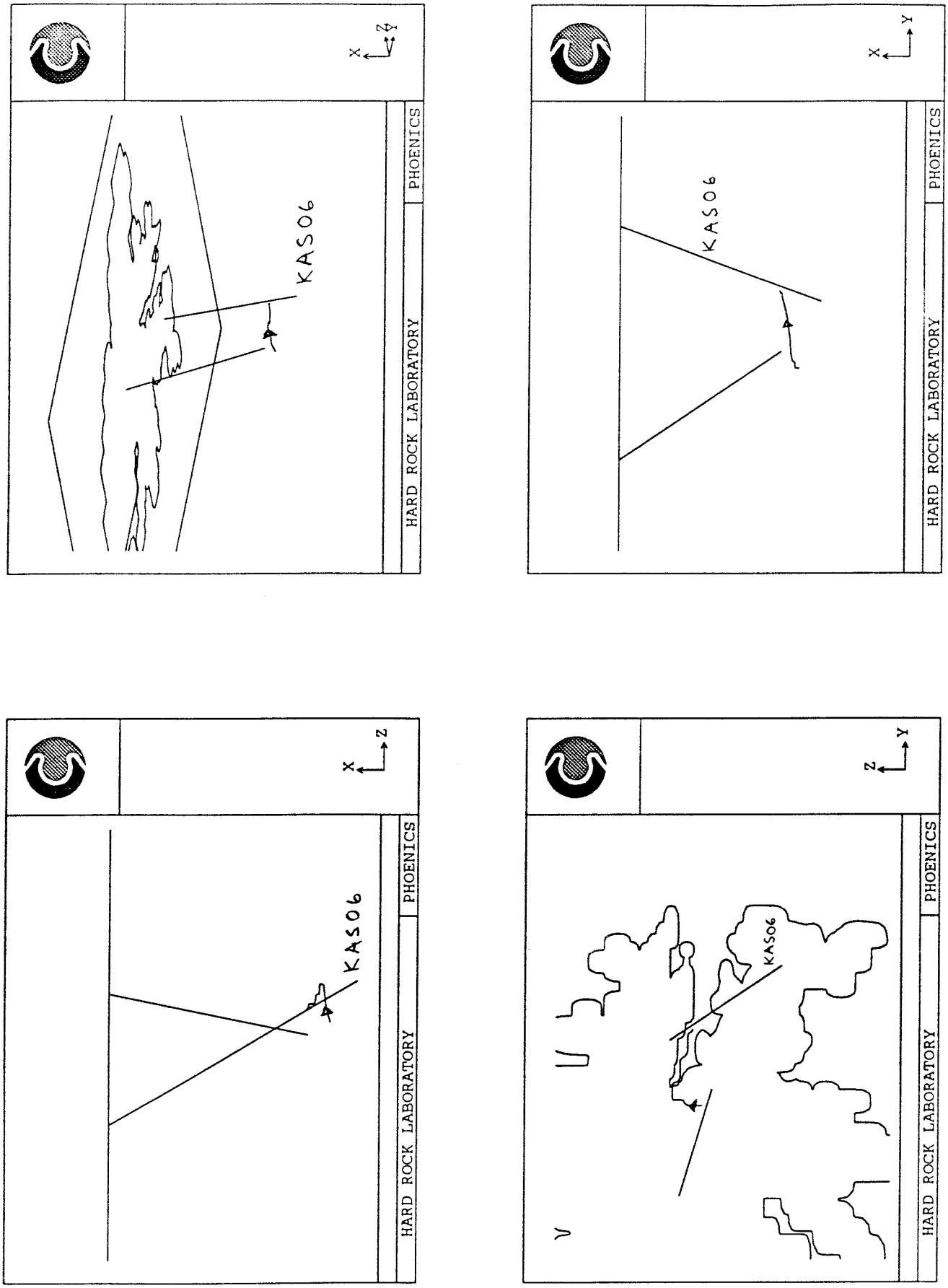

Figure /3-4/. Trajectory when injecting in KAS04, section D2.

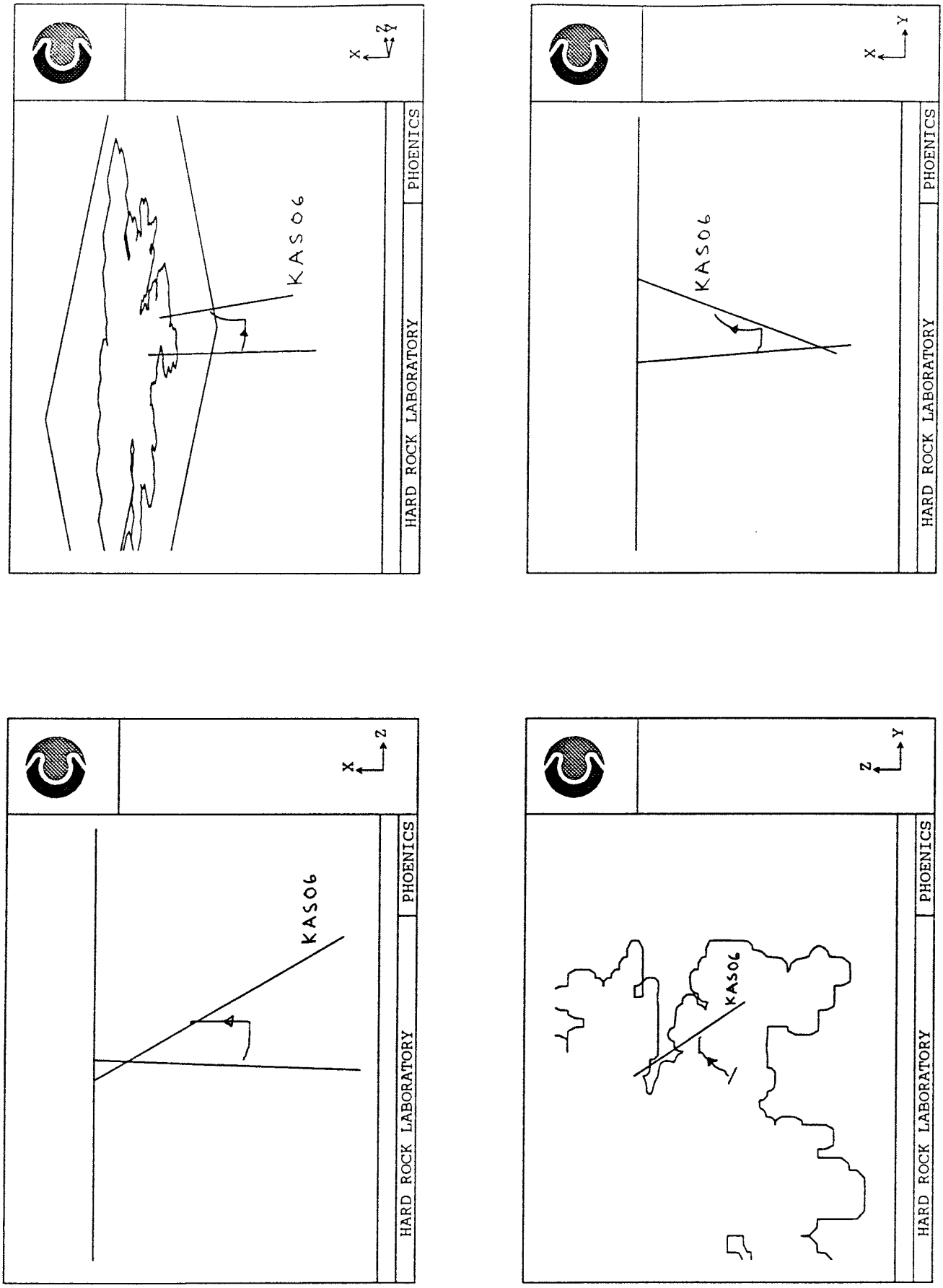

Figure /3-5/. Trajectory when injecting in KAS05, section E3.

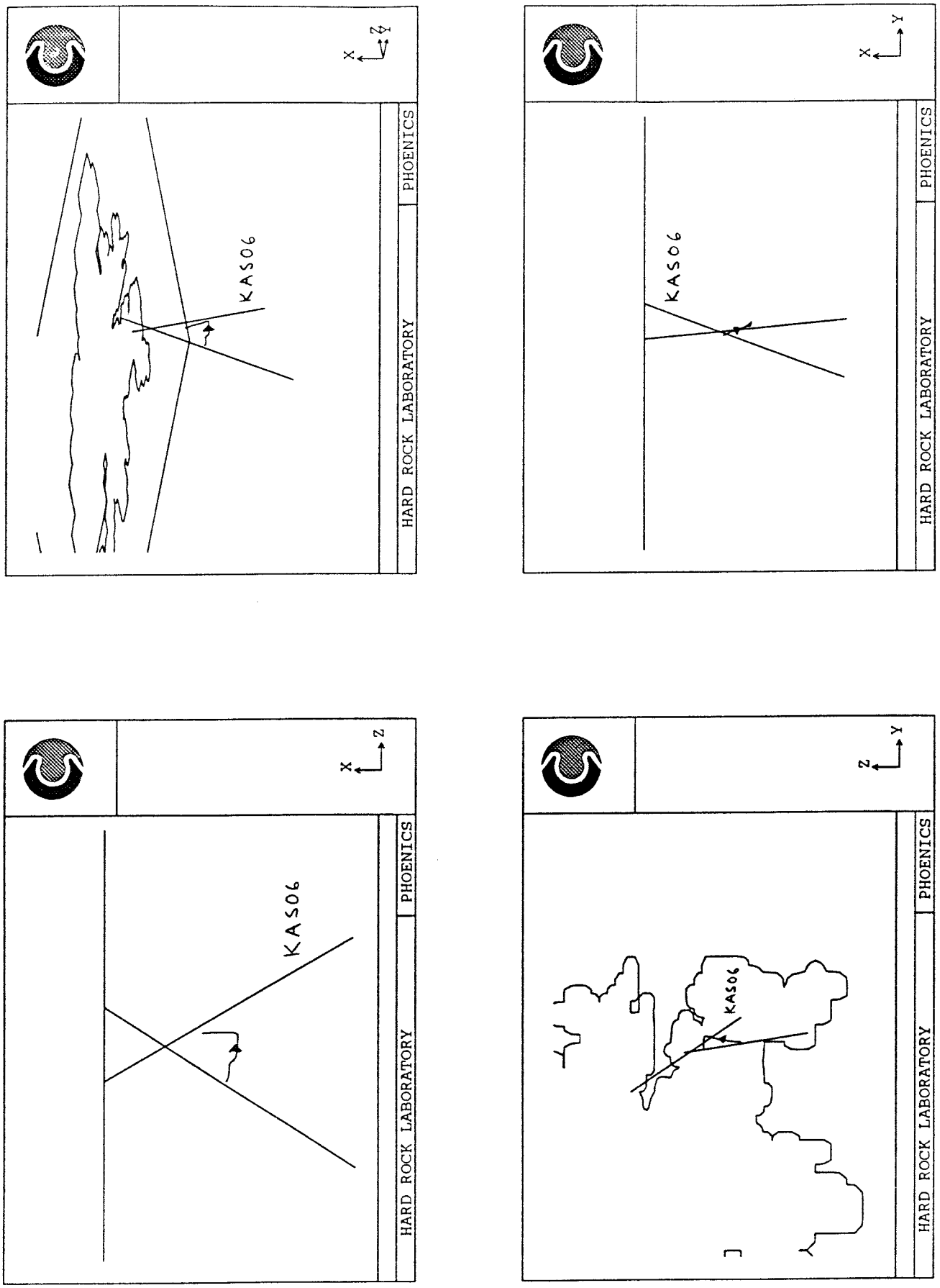

Figure /3-6/. Trajectory when injecting in KAS07, section J4.

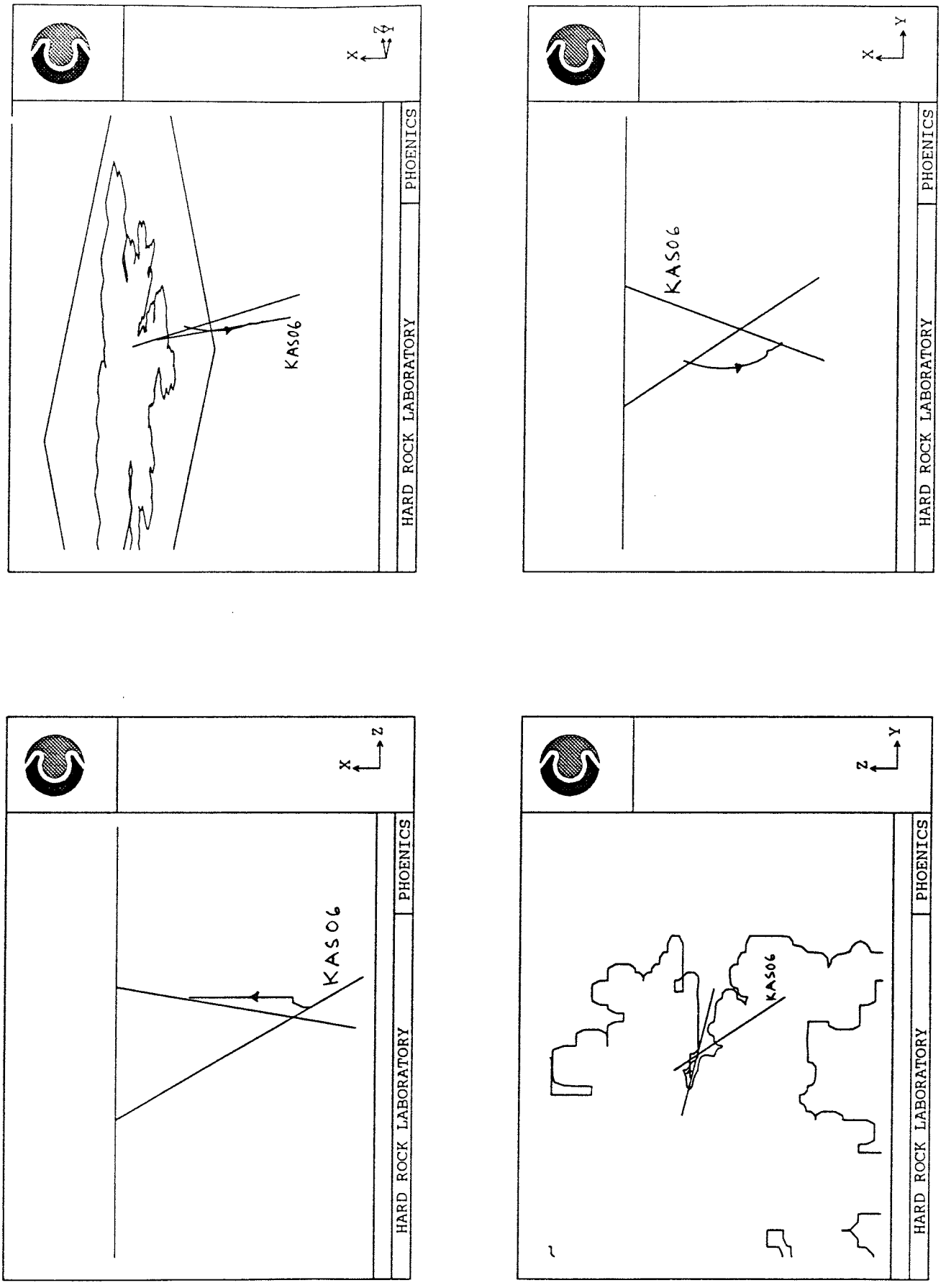

Figure /3-7/. Trajectory when injecting in KAS08, section M3.

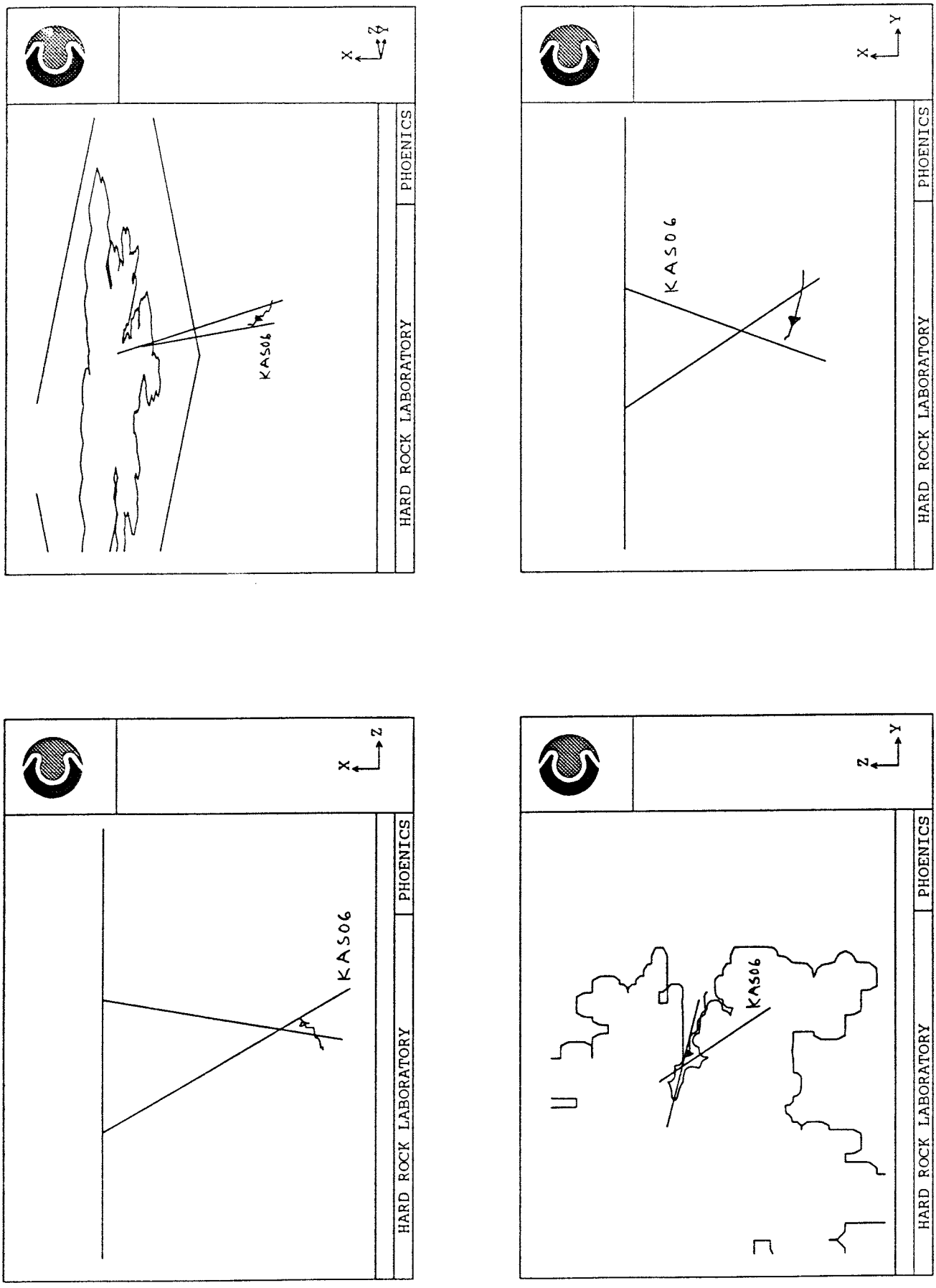

Figure /3-8/. Trajectory when injecting in KAS08, section M1.

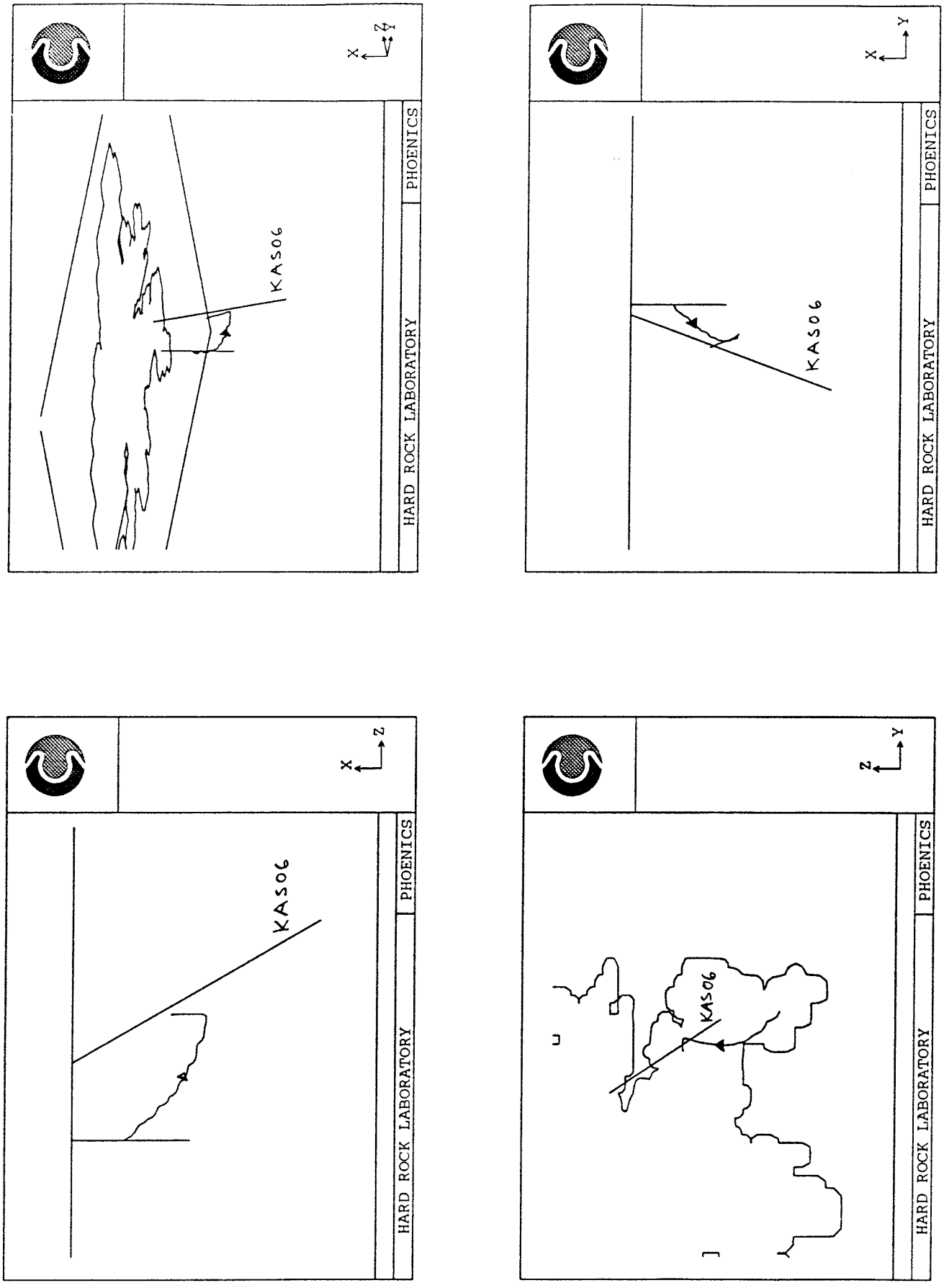

Figure /3-9/. Trajectory when injecting in KAS11, section CE.

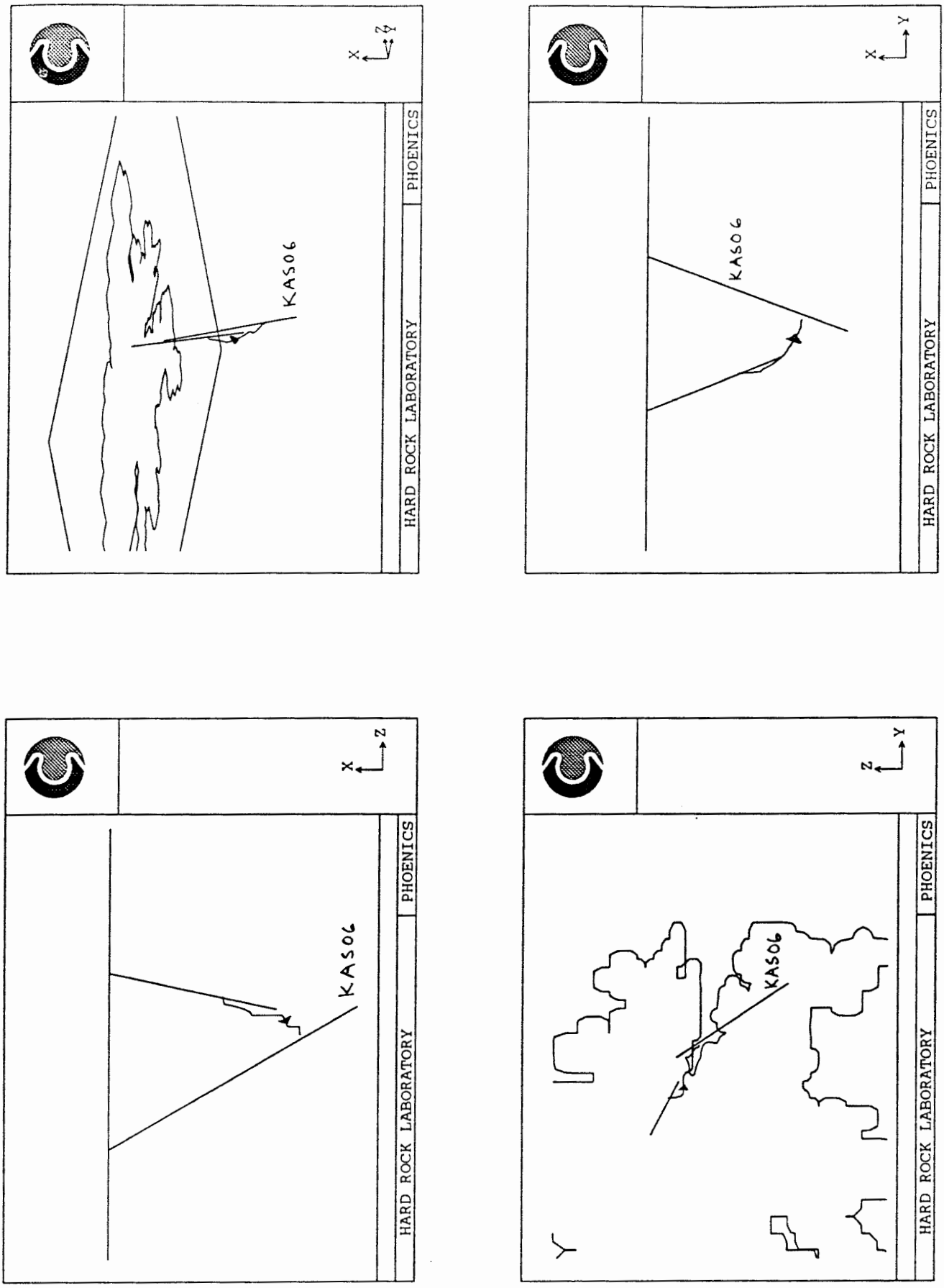

Figure /3-10/. Trajectory when injecting in KAS12, section DD.

APPENDIX A

Table of trajectory for injection in KAS02, B4.

```
Press.       p         px-       px+       py-       py+       pz-       pz+

 i =  27   j =  27   k =  23
Press.  -0.359E+05-0.328E+05-0.373E+05-0.333E+05-0.386E+05-0.335E+05-0.380E+05
 Surface x+   Fracture EW5
 Surface y-   Fracture EW5
 Surface y+   Fracture EW5
 Surface z-   Fracture EW5
 Surface z+   Fracture EW5
 Step    0   x =   913.       y =  0.127E+04   z =   770.
Darcy-time for particle=    3.28451E-02
 Step    1   x =   913.       y =  0.127E+04   z =   773.
Darcy-time for particle=    6.65663E-02
 Step    2   x =   913.       y =  0.128E+04   z =   777.
Darcy-time for particle=    1.00156E-01

 i =  27   j =  28   k =  24
Press.  -0.406E+05-0.375E+05-0.443E+05-0.380E+05-0.414E+05-0.386E+05-0.407E+05
 Surface x-   Fracture NNW1
 Surface x+   Fracture EW5
 Surface x+   Fracture NNW1
 Surface y-   Fracture EW5
 Surface y+   Fracture EW5
 Surface y+   Fracture NNW1
 Surface z-   Fracture EW5
 Surface z+   Fracture EW5
 Surface z+   Fracture NNW1
 Step    3   x =   914.       y =  0.128E+04   z =   781.
Darcy-time for particle=    0.122448
 Step    4   x =   917.       y =  0.128E+04   z =   782.
Darcy-time for particle=    0.144360
 Step    5   x =   921.       y =  0.129E+04   z =   783.
Darcy-time for particle=    0.165063

 i =  28   j =  28   k =  24
Press.  -0.443E+05-0.406E+05-0.520E+05-0.423E+05-0.448E+05-0.403E+05-0.453E+05
 Surface x-   Fracture EW5
 Surface x-   Fracture NNW1
 Surface x+   Fracture NNW1
 Surface y+   Fracture EW5
 Surface y+   Fracture NNW1
 Surface z-   Fracture EW5
 Surface z+   Fracture NNW1
 Step    6   x =   925.       y =  0.129E+04   z =   784.
Darcy-time for particle=    0.184922
 Step    7   x =   929.       y =  0.129E+04   z =   787.
Darcy-time for particle=    0.204122
 Step    8   x =   934.       y =  0.129E+04   z =   789.
Darcy-time for particle=    0.222550
 Step    9   x =   939.       y =  0.129E+04   z =   790.
Darcy-time for particle=    0.240157

 i =  29   j =  28   k =  24
Press.  -0.520E+05-0.443E+05-0.600E+05-0.495E+05-0.516E+05-0.437E+05-0.521E+05
 Surface x-   Fracture NNW1
 Surface x+   Fracture NNW1
 Surface y+   Fracture NNW1
 Surface z+   Fracture NNW1
 Step   10   x =   943.       y =  0.129E+04   z =   792.
Darcy-time for particle=    0.258068
 Step   11   x =   948.       y =  0.129E+04   z =   792.
Darcy-time for particle=    0.275748
 Step   12   x =   953.       y =  0.129E+04   z =   792.
Darcy-time for particle=    0.293203
```

```
 Step   13   x =   958.       y =  0.129E+04   z =   792.
Darcy-time for particle=   0.310438

 i =  30   j =  28   k =  24
Press.  -0.600E+05-0.520E+05-0.686E+05-0.541E+05-0.600E+05-0.466E+05-0.593E+05
 Surface x-   Fracture NNW1
 Surface x+   Fracture NNW1
 Surface y+   Fracture NNW1
 Surface z+   Fracture NNW1
 Step   14   x =   963.       y =  0.129E+04   z =   792.
Darcy-time for particle=   0.327274
 Step   15   x =   968.       y =  0.129E+04   z =   792.
Darcy-time for particle=   0.343723
 Step   16   x =   973.       y =  0.129E+04   z =   791.
Darcy-time for particle=   0.359801

 i =  31   j =  28   k =  24
Press.  -0.686E+05-0.600E+05-0.777E+05-0.606E+05-0.697E+05-0.611E+05-0.669E+05
 Surface x-   Fracture NNW1
 Surface x+   Fracture NNW1
 Surface y+   Fracture NNW1
 Surface z+   Fracture NNW1
 Step   17   x =   978.       y =  0.129E+04   z =   791.
Darcy-time for particle=   0.375417
 Step   18   x =   983.       y =  0.129E+04   z =   791.
Darcy-time for particle=   0.390761
 Step   19   x =   988.       y =  0.129E+04   z =   790.
Darcy-time for particle=   0.405839
 Step   20   x =   993.       y =  0.129E+04   z =   790.
Darcy-time for particle=   0.420659

 i =  32   j =  28   k =  24
Press.  -0.777E+05-0.686E+05-0.869E+05-0.704E+05-0.802E+05-0.728E+05-0.748E+05
 Surface x-   Fracture NNW1
 Surface x+   Fracture NNW1
 Surface y+   Fracture NNW1
 Surface z+   Fracture NNW1
 Step   21   x =   998.       y =  0.129E+04   z =   789.
Darcy-time for particle=   0.435038
 Step   22   x =  0.100E+04   y =  0.129E+04   z =   788.
Darcy-time for particle=   0.449297
 Step   23   x =  0.101E+04   y =  0.129E+04   z =   788.
Darcy-time for particle=   0.463432
 Step   24   x =  0.101E+04   y =  0.129E+04   z =   787.
Darcy-time for particle=   0.477440

 i =  33   j =  28   k =  24
Press.  -0.869E+05-0.777E+05-0.961E+05-0.832E+05-0.912E+05-0.799E+05-0.829E+05
 Surface x-   Fracture NNW1
 Surface x+   Fracture NNW1
 Surface y-   Fracture NNW1
 Surface y+   Fracture NNW1
 Surface z+   Fracture NNW1
 Step   25   x =  0.102E+04   y =  0.129E+04   z =   787.
Darcy-time for particle=   0.490855
 Step   26   x =  0.102E+04   y =  0.130E+04   z =   786.
Darcy-time for particle=   0.504181
 Step   27   x =  0.103E+04   y =  0.130E+04   z =   785.
Darcy-time for particle=   0.517384

 i =  33   j =  29   k =  24
Press.  -0.912E+05-0.802E+05-0.102E+06-0.869E+05-0.954E+05-0.835E+05-0.797E+05
 Surface x-   Fracture NNW1
 Surface x+   Fracture NNW1
```

```
 Surface y-   Fracture NNW1
 Surface y+   Fracture NNW1
 Step   28   x =  0.103E+04   y =  0.130E+04   z =   785.
Darcy-time for particle=   0.528256

 i =  34   j =  29   k =  24
Press.  -0.102E+06-0.912E+05-0.113E+06-0.961E+05-0.109E+06-0.981E+05-0.872E+05
 Surface x-   Fracture NNW1
 Surface x+   Fracture NNW1
 Surface y-   Fracture NNW1
 Surface y+   Fracture NNW1
 Step   29   x =  0.104E+04   y =  0.130E+04   z =   785.
Darcy-time for particle=   0.538522
 Step   30   x =  0.104E+04   y =  0.130E+04   z =   785.
Darcy-time for particle=   0.548866
 Step   31   x =  0.104E+04   y =  0.131E+04   z =   785.
Darcy-time for particle=   0.559287
 Step   32   x =  0.105E+04   y =  0.131E+04   z =   785.
Darcy-time for particle=   0.569782

 i =  35   j =  29   k =  24
Press.  -0.113E+06-0.102E+06-0.122E+06-0.105E+06-0.123E+06-0.971E+05-0.101E+06
 Surface x-   Fracture NNW1
 Surface x+   Fracture NNW1
 Surface y-   Fracture NNW1
 Surface y+   Fracture NNW1
 Step   33   x =  0.105E+04   y =  0.131E+04   z =   785.
Darcy-time for particle=   0.579272
 Step   34   x =  0.106E+04   y =  0.132E+04   z =   785.
Darcy-time for particle=   0.588796
 Step   35   x =  0.106E+04   y =  0.132E+04   z =   785.
Darcy-time for particle=   0.598336

 i =  35   j =  30   k =  24
Press.  -0.123E+06-0.109E+06-0.135E+06-0.113E+06-0.125E+06-0.134E+06-0.870E+05
 Surface x-   Fracture NNW1
 Surface x+   Fracture NNW1
 Surface y-   Fracture NNW1
 Surface z-   Fracture NNW1
 Step   36   x =  0.106E+04   y =  0.132E+04   z =   785.
Darcy-time for particle=   0.607095
 Step   37   x =  0.107E+04   y =  0.133E+04   z =   782.
Darcy-time for particle=   0.615795

 i =  36   j =  30   k =  23
Press.  -0.150E+06-0.134E+06-0.162E+06-0.109E+06-0.167E+06-0.123E+06-0.135E+06
 Surface x-   Fracture NNW1
 Surface x+   Fracture NNW1
 Surface y+   Fracture NNW1
 Surface z+   Fracture NNW1
 Step   38   x =  0.107E+04   y =  0.133E+04   z =   779.
Darcy-time for particle=   0.623714
 Step   39   x =  0.107E+04   y =  0.133E+04   z =   774.
Darcy-time for particle=   0.632723
 Step   40   x =  0.107E+04   y =  0.133E+04   z =   771.
Darcy-time for particle=   0.642042
 Step   41   x =  0.108E+04   y =  0.134E+04   z =   768.
Darcy-time for particle=   0.650489

 i =  36   j =  31   k =  23
Press.  -0.167E+06-0.146E+06-0.183E+06-0.150E+06-0.192E+06-0.160E+06-0.149E+06
 Surface x-   Fracture NNW1
 Surface x+   Fracture NNW1
 Surface y-   Fracture NNW1
```

```
 Surface y+   Fracture NNW1
 Step   42   x =  0.108E+04   y =  0.134E+04   z =   766.
Darcy-time for particle=   0.655449
 Step   43   x =  0.108E+04   y =  0.134E+04   z =   766.
Darcy-time for particle=   0.660453
 Step   44   x =  0.108E+04   y =  0.135E+04   z =   766.
Darcy-time for particle=   0.665452
 Step   45   x =  0.109E+04   y =  0.135E+04   z =   766.
Darcy-time for particle=   0.670396

 i =  37   j =  31   k =  23
Press.  -0.183E+06-0.167E+06-0.184E+06-0.162E+06-0.219E+06-0.180E+06-0.149E+06
 Surface x-   Fracture NNW1
 Surface x+   Fracture NNW1
 Surface y-   Fracture NNW1
 Surface y+   Fracture NNW1
 Step   46   x =  0.109E+04   y =  0.135E+04   z =   766.
Darcy-time for particle=   0.674079
 Step   47   x =  0.109E+04   y =  0.136E+04   z =   766.
Darcy-time for particle=   0.677507

 i =  37   j =  32   k =  23
Press.  -0.219E+06-0.192E+06-0.211E+06-0.183E+06-0.295E+06-0.274E+06-0.161E+06
 Surface x-   Fracture NNW1
 Surface x+   Fracture NNW1
 Surface y-   Fracture NNW1
 Surface y+   Fracture NNW1
 Step   48   x =  0.109E+04   y =  0.136E+04   z =   766.
Darcy-time for particle=   0.680212
 Step   49   x =  0.110E+04   y =  0.137E+04   z =   766.
Darcy-time for particle=   0.682580
 Step   50   x =  0.110E+04   y =  0.137E+04   z =   766.
Darcy-time for particle=   0.684638
 Step   51   x =  0.110E+04   y =  0.138E+04   z =   766.
Darcy-time for particle=   0.686443

 i =  37   j =  33   k =  23
Press.  -0.295E+06-0.223E+06-0.245E+06-0.219E+06-0.164E+06-0.422E+06-0.141E+06
 Surface x-   Fracture NNW1
 Surface x+   Fracture NNW1
 Surface y-   Fracture NNW1
 Surface z-   Fracture NNW1
 Step   52   x =  0.110E+04   y =  0.138E+04   z =   766.
Darcy-time for particle=   0.687635
 Step   53   x =  0.110E+04   y =  0.139E+04   z =   762.
```

APPENDIX B.

Table of trajectory for injection in KAS02, section B2.

```
 Press.        p         px-        px+        py-        py+        pz-        pz+

  i =   7   j =  26   k =  24
 Press.   0.295E+05 0.353E+05 0.235E+05 0.313E+05 0.287E+05 0.310E+05 0.282E+05
  Step    0   x =   460.       y =  0.125E+04   z =   790.
 Darcy-time for particle=    45.6859
  Step    1   x =   461.       y =  0.125E+04   z =   793.
 Darcy-time for particle=    93.1337
  Step    2   x =   462.       y =  0.126E+04   z =   797.
 Darcy-time for particle=    141.269

  i =   7   j =  27   k =  25
 Press.   0.276E+05 0.338E+05 0.219E+05 0.282E+05 0.277E+05 0.287E+05 0.267E+05
  Surface x+   Fracture NNW1
  Surface y+   Fracture NNW1
  Step    3   x =   463.       y =  0.126E+04   z =   800.
 Darcy-time for particle=    142.956
  Step    4   x =   468.       y =  0.126E+04   z =   800.
 Darcy-time for particle=    144.341
  Step    5   x =   473.       y =  0.126E+04   z =   800.
 Darcy-time for particle=    145.516
  Step    6   x =   478.       y =  0.126E+04   z =   801.
 Darcy-time for particle=    146.536

  i =   8   j =  27   k =  25
 Press.   0.219E+05 0.276E+05 0.162E+05 0.220E+05 0.220E+05 0.228E+05 0.202E+05
  Surface x-   Fracture NNW1
  Surface x+   Fracture NNW1
  Surface y-   Fracture NNW1
  Surface y+   Fracture NNW1
  Step    7   x =   483.       y =  0.126E+04   z =   801.
 Darcy-time for particle=    147.416
  Step    8   x =   488.       y =  0.126E+04   z =   801.
 Darcy-time for particle=    148.178
  Step    9   x =   493.       y =  0.126E+04   z =   801.
 Darcy-time for particle=    148.850
  Step   10   x =   498.       y =  0.126E+04   z =   801.
 Darcy-time for particle=    149.451
  Step   11   x =   503.       y =  0.126E+04   z =   801.
 Darcy-time for particle=    149.994
  Step   12   x =   508.       y =  0.126E+04   z =   801.
 Darcy-time for particle=    150.490
  Step   13   x =   513.       y =  0.126E+04   z =   801.
 Darcy-time for particle=    150.946
  Step   14   x =   518.       y =  0.126E+04   z =   801.
 Darcy-time for particle=    151.368

  i =   9   j =  27   k =  25
 Press.   0.162E+05 0.219E+05 0.106E+05 0.161E+05 0.164E+05 0.174E+05 0.135E+05
  Surface x-   Fracture NNW1
  Surface x+   Fracture NNW1
  Surface y-   Fracture NNW1
  Surface y+   Fracture NNW1
  Step   15   x =   523.       y =  0.126E+04   z =   801.
 Darcy-time for particle=    151.756

  i =   9   j =  26   k =  25
 Press.   0.161E+05 0.220E+05 0.104E+05 0.175E+05 0.162E+05 0.175E+05 0.140E+05
  Surface x-   Fracture NNW1
  Surface x+   Fracture NNW1
  Surface y+   Fracture NNW1
  Step   16   x =   527.       y =  0.126E+04   z =   801.
 Darcy-time for particle=    152.987
  Step   17   x =   530.       y =  0.125E+04   z =   801.
```

```
Darcy-time for particle=    154.361
 Step   18   x =   533.       y =  0.125E+04   z =   801.
Darcy-time for particle=    155.732
 Step   19   x =   537.       y =  0.125E+04   z =   801.
Darcy-time for particle=    156.946
 Step   20   x =   542.       y =  0.125E+04   z =   801.
Darcy-time for particle=    157.975
 Step   21   x =   547.       y =  0.124E+04   z =   801.
Darcy-time for particle=    158.847
 Step   22   x =   552.       y =  0.124E+04   z =   801.
Darcy-time for particle=    159.601
 Step   23   x =   557.       y =  0.124E+04   z =   801.
Darcy-time for particle=    160.261

 i =  10   j =  26   k =  25
Press.   0.104E+05 0.161E+05 0.616E+04 0.103E+05 0.106E+05 0.111E+05 0.985E+04
 Surface x-   Fracture NNW1
 Surface x+   Fracture NNW1
 Surface y-   Fracture NNW1
 Surface y+   Fracture NNW1
 Step   24   x =   562.       y =  0.124E+04   z =   801.
Darcy-time for particle=    160.841
 Step   25   x =   567.       y =  0.124E+04   z =   801.
Darcy-time for particle=    161.375
 Step   26   x =   572.       y =  0.124E+04   z =   801.
Darcy-time for particle=    161.868
 Step   27   x =   577.       y =  0.124E+04   z =   801.
Darcy-time for particle=    162.325

 i =  10   j =  25   k =  25
Press.   0.103E+05 0.175E+05 0.603E+04 0.111E+05 0.104E+05 0.122E+05 0.943E+04
 Surface x+   Fracture NNW1
 Surface y+   Fracture NNW1
 Step   28   x =   582.       y =  0.124E+04   z =   801.
Darcy-time for particle=    164.879
 Step   29   x =   585.       y =  0.124E+04   z =   802.
Darcy-time for particle=    167.303
 Step   30   x =   590.       y =  0.123E+04   z =   802.
Darcy-time for particle=    169.520
 Step   31   x =   594.       y =  0.123E+04   z =   802.
Darcy-time for particle=    171.512
 Step   32   x =   599.       y =  0.123E+04   z =   803.
Darcy-time for particle=    173.300

 i =  11   j =  25   k =  25
Press.   0.603E+04 0.103E+05 0.315E+04 0.792E+04 0.616E+04 0.857E+04 0.518E+04
 Surface x-   Fracture NNW1
 Surface x+   Fracture NNW1
 Surface y+   Fracture NNW1
 Step   33   x =   604.       y =  0.123E+04   z =   803.
Darcy-time for particle=    174.464
 Step   34   x =   608.       y =  0.123E+04   z =   803.
Darcy-time for particle=    175.475
 Step   35   x =   613.       y =  0.123E+04   z =   803.
Darcy-time for particle=    176.324
 Step   36   x =   618.       y =  0.122E+04   z =   803.
Darcy-time for particle=    177.043

 i =  12   j =  25   k =  25
Press.   0.315E+04 0.603E+04  269.     0.453E+04 0.329E+04 0.608E+04 0.301E+04
 Surface x-   Fracture NNW1
 Surface x+   Fracture NNW1
 Surface y+   Fracture NNW1
 Surface z+   Fracture NNW1
```

```
 Step   37   x =   623.       y =  0.122E+04   z =   803.
Darcy-time for particle=    177.684
 Step   38   x =   628.       y =  0.122E+04   z =   803.
Darcy-time for particle=    178.280
 Step   39   x =   633.       y =  0.122E+04   z =   803.
Darcy-time for particle=    178.837
 Step   40   x =   638.       y =  0.122E+04   z =   804.
Darcy-time for particle=    179.358

 i =  13   j =  25   k =  25
Press.    269.     0.315E+04-0.261E+04 0.214E+04  418.     0.365E+04  126.
 Surface x-   Fracture NNW1
 Surface x+   Fracture NNW1
 Surface y+   Fracture NNW1
 Surface z+   Fracture NNW1
 Step   41   x =   643.       y =  0.122E+04   z =   804.
Darcy-time for particle=    179.861
 Step   42   x =   648.       y =  0.122E+04   z =   805.
Darcy-time for particle=    180.359
 Step   43   x =   653.       y =  0.122E+04   z =   805.
Darcy-time for particle=    180.854
 Step   44   x =   658.       y =  0.122E+04   z =   806.
Darcy-time for particle=    181.343

 i =  14   j =  25   k =  25
Press.  -0.261E+04  269.    -0.549E+04 -354.    -0.245E+04 0.114E+04-0.275E+04
 Surface x-   Fracture NNW1
 Surface x+   Fracture NNW1
 Surface y+   Fracture NNW1
 Surface z+   Fracture NNW1
 Step   45   x =   662.       y =  0.122E+04   z =   807.
Darcy-time for particle=    181.827
 Step   46   x =   667.       y =  0.122E+04   z =   808.
Darcy-time for particle=    182.302
 Step   47   x =   672.       y =  0.122E+04   z =   809.
Darcy-time for particle=    182.768
 Step   48   x =   677.       y =  0.122E+04   z =   810.
Darcy-time for particle=    183.226

 i =  15   j =  25   k =  25
Press.  -0.549E+04-0.261E+04-0.838E+04-0.259E+04-0.533E+04-0.193E+04-0.564E+04
 Surface x-   Fracture NNW1
 Surface x+   Fracture NNW1
 Surface y+   Fracture NNW1
 Surface z+   Fracture NNW1
 Step   49   x =   682.       y =  0.122E+04   z =   811.
Darcy-time for particle=    183.673
 Step   50   x =   687.       y =  0.122E+04   z =   813.
Darcy-time for particle=    184.110
 Step   51   x =   692.       y =  0.122E+04   z =   814.
Darcy-time for particle=    184.537
 Step   52   x =   696.       y =  0.122E+04   z =   816.
Darcy-time for particle=    184.953

 i =  16   j =  25   k =  25
Press.  -0.838E+04-0.549E+04-0.113E+05-0.700E+04-0.822E+04-0.517E+04-0.852E+04
 Surface x-   Fracture NNW1
 Surface x+   Fracture NNW1
 Surface y+   Fracture NNW1
 Surface z+   Fracture NNW1
 Step   53   x =   701.       y =  0.122E+04   z =   817.
Darcy-time for particle=    185.360
 Step   54   x =   706.       y =  0.122E+04   z =   819.
Darcy-time for particle=    185.756
```

```
 i =  16   j =  25   k =  26
Press.  -0.852E+04-0.564E+04-0.114E+05-0.865E+04-0.131E+05-0.838E+04-0.144E+05
 Surface x-   Fracture NNW1
 Surface x+   Fracture NNW1
 Surface y-   Fracture NNW1
 Surface z-   Fracture NNW1
 Step   55   x =   710.       y =  0.122E+04   z =   821.
Darcy-time for particle=    186.273

 i =  16   j =  24   k =  26
Press.  -0.865E+04-0.577E+04-0.115E+05-0.854E+04-0.852E+04-0.700E+04-0.139E+05
 Surface x-   Fracture NNW1
 Surface x+   Fracture NNW1
 Surface y+   Fracture NNW1
 Step   56   x =   714.       y =  0.122E+04   z =   824.
Darcy-time for particle=    186.622
 Step   57   x =   718.       y =  0.122E+04   z =   824.
Darcy-time for particle=    186.950

 i =  17   j =  24   k =  26
Press.  -0.115E+05-0.865E+04-0.144E+05-0.116E+05-0.114E+05-0.987E+04-0.169E+05
 Surface x-   Fracture NNW1
 Surface x+   Fracture NNW1
 Surface y-   Fracture NNW1
 Surface y+   Fracture NNW1
 Step   58   x =   723.       y =  0.121E+04   z =   824.
Darcy-time for particle=    187.266
 Step   59   x =   728.       y =  0.121E+04   z =   824.
Darcy-time for particle=    187.576
 Step   60   x =   733.       y =  0.121E+04   z =   824.
Darcy-time for particle=    187.881
 Step   61   x =   738.       y =  0.121E+04   z =   824.
Darcy-time for particle=    188.180

 i =  18   j =  24   k =  26
Press.  -0.144E+05-0.115E+05-0.172E+05-0.145E+05-0.143E+05-0.127E+05-0.191E+05
 Surface x-   Fracture NNW1
 Surface x+   Fracture NNW1
 Surface y-   Fracture NNW1
 Surface y+   Fracture NNW1
 Step   62   x =   743.       y =  0.121E+04   z =   824.
Darcy-time for particle=    188.476
 Step   63   x =   747.       y =  0.121E+04   z =   824.
Darcy-time for particle=    188.776
 Step   64   x =   752.       y =  0.121E+04   z =   824.
Darcy-time for particle=    189.080
 Step   65   x =   757.       y =  0.121E+04   z =   824.
Darcy-time for particle=    189.387

 i =  19   j =  24   k =  26
Press.  -0.172E+05-0.144E+05-0.200E+05-0.173E+05-0.171E+05-0.152E+05-0.232E+05
 Surface x-   Fracture NNW1
 Surface x+   Fracture NNW1
 Surface y-   Fracture NNW1
 Surface y+   Fracture NNW1
 Step   66   x =   762.       y =  0.121E+04   z =   824.
Darcy-time for particle=    189.706
 Step   67   x =   767.       y =  0.120E+04   z =   824.
Darcy-time for particle=    190.030
 Step   68   x =   772.       y =  0.120E+04   z =   824.
Darcy-time for particle=    190.359
 Step   69   x =   777.       y =  0.120E+04   z =   824.
Darcy-time for particle=    190.694
```

```
 i =  20   j =  24   k =  26
Press.  -0.200E+05-0.172E+05-0.225E+05-0.200E+05-0.200E+05-0.179E+05-0.280E+05
 Surface x-   Fracture NNW1
 Surface x+   Fracture NNW1
 Surface y-   Fracture NNW1
 Surface y+   Fracture NNW1
 Step   70   x =   782.       y =  0.120E+04   z =   824.
Darcy-time for particle=    191.038
 Step   71   x =   787.       y =  0.120E+04   z =   824.
Darcy-time for particle=    191.384
 Step   72   x =   792.       y =  0.120E+04   z =   824.
Darcy-time for particle=    191.731
 Step   73   x =   797.       y =  0.120E+04   z =   824.
Darcy-time for particle=    192.079

 i =  21   j =  24   k =  26
Press.  -0.225E+05-0.200E+05-0.247E+05-0.223E+05-0.226E+05-0.214E+05-0.307E+05
 Surface x-   Fracture NNW1
 Surface x+   Fracture NNW1
 Surface y-   Fracture NNW1
 Surface y+   Fracture NNW1
 Step   74   x =   802.       y =  0.120E+04   z =   824.
Darcy-time for particle=    192.399
 Step   75   x =   806.       y =  0.120E+04   z =   825.
Darcy-time for particle=    192.707
 Step   76   x =   811.       y =  0.121E+04   z =   825.
Darcy-time for particle=    193.005
 Step   77   x =   816.       y =  0.121E+04   z =   825.
Darcy-time for particle=    193.293

 i =  22   j =  24   k =  26
Press.  -0.247E+05-0.225E+05-0.269E+05-0.243E+05-0.249E+05-0.227E+05-0.318E+05
 Surface x-   Fracture NNW1
 Surface x+   Fracture NNW1
 Surface y-   Fracture NNW1
 Surface y+   Fracture NNW1
 Step   78   x =   820.       y =  0.121E+04   z =   825.
Darcy-time for particle=    193.516
 Step   79   x =   825.       y =  0.121E+04   z =   825.
Darcy-time for particle=    193.731
 Step   80   x =   829.       y =  0.121E+04   z =   825.
Darcy-time for particle=    193.935

 i =  23   j =  24   k =  26
Press.  -0.269E+05-0.247E+05-0.294E+05-0.262E+05-0.273E+05-0.258E+05-0.360E+05
 Surface x-   Fracture NNW1
 Surface x+   Fracture NNW1
 Surface y-   Fracture NNW1
 Surface y+   Fracture NNW1
 Step   81   x =   834.       y =  0.122E+04   z =   825.
Darcy-time for particle=    194.104
 Step   82   x =   838.       y =  0.122E+04   z =   825.
Darcy-time for particle=    194.263

 i =  23   j =  25   k =  26
Press.  -0.273E+05-0.249E+05-0.299E+05-0.269E+05-0.341E+05-0.274E+05-0.365E+05
 Surface x-   Fracture NNW1
 Surface x+   Fracture NNW1
 Surface y-   Fracture NNW1
 Surface z-   Fracture NNW1
 Step   83   x =   842.       y =  0.122E+04   z =   825.
Darcy-time for particle=    194.540
 Step   84   x =   846.       y =  0.122E+04   z =   824.
```

```
Darcy-time for particle=    194.826

 i =  24   j =  25   k =  26
Press.  -0.299E+05-0.273E+05-0.327E+05-0.294E+05-0.363E+05-0.299E+05-0.416E+05
 Surface x-   Fracture NNW1
 Surface x+   Fracture EW5
 Surface x+   Fracture NNW1
 Surface y-   Fracture EW5
 Surface y-   Fracture NNW1
 Surface z-   Fracture EW5
 Surface z-   Fracture NNW1
 Step   85   x =   849.       y =  0.123E+04   z =   822.
Darcy-time for particle=    195.014
 Step   86   x =   852.       y =  0.123E+04   z =   822.
Darcy-time for particle=    195.209
 Step   87   x =   857.       y =  0.123E+04   z =   822.
Darcy-time for particle=    195.380
 Step   88   x =   861.       y =  0.124E+04   z =   822.
Darcy-time for particle=    195.519
 Step   89   x =   866.       y =  0.124E+04   z =   822.
Darcy-time for particle=    195.635

 i =  25   j =  25   k =  26
Press.  -0.327E+05-0.299E+05-0.369E+05-0.332E+05-0.336E+05-0.322E+05-0.408E+05
 Surface x-   Fracture EW5
 Surface x-   Fracture NNW1
 Surface x+   Fracture NNW1
 Surface y-   Fracture NNW1
 Surface y+   Fracture EW5
 Surface z-   Fracture EW5
 Surface z-   Fracture NNW1
 Step   90   x =   871.       y =  0.124E+04   z =   822.
Darcy-time for particle=    195.722
 Step   91   x =   875.       y =  0.124E+04   z =   825.
Darcy-time for particle=    195.815

 i =  25   j =  26   k =  26
Press.  -0.336E+05-0.363E+05-0.361E+05-0.327E+05-0.349E+05-0.335E+05-0.511E+05
 Surface x+   Fracture EW5
 Surface y-   Fracture EW5
 Surface y+   Fracture EW5
 Surface z-   Fracture EW5
 Step   92   x =   879.       y =  0.124E+04   z =   828.
Darcy-time for particle=    196.026
 Step   93   x =   879.       y =  0.125E+04   z =   829.
Darcy-time for particle=    196.223
 Step   94   x =   879.       y =  0.125E+04   z =   831.
Darcy-time for particle=    196.407
 Step   95   x =   879.       y =  0.126E+04   z =   832.
Darcy-time for particle=    196.580

 i =  25   j =  27   k =  26
Press.  -0.349E+05-0.381E+05-0.372E+05-0.336E+05-0.428E+05-0.338E+05-0.570E+05
 Surface x+   Fracture EW5
 Surface y-   Fracture EW5
 Step   96   x =   880.       y =  0.126E+04   z =   833.
Darcy-time for particle=    196.722
 Step   97   x =   882.       y =  0.126E+04   z =   833.
Darcy-time for particle=    196.879

 i =  26   j =  27   k =  26
Press.  -0.372E+05-0.349E+05-0.423E+05-0.361E+05-0.382E+05-0.371E+05-0.614E+05
 Surface x-   Fracture EW5
 Surface y-   Fracture EW5
```

```
 Surface y+   Fracture EW5
 Surface z-   Fracture EW5
 Step   98   x =   885.       y =  0.127E+04   z =   833.
Darcy-time for particle=    197.058
 Step   99   x =   890.       y =  0.127E+04   z =   833.
Darcy-time for particle=    197.254
 Step  100   x =   893.       y =  0.127E+04   z =   834.
Darcy-time for particle=    197.443
 Step  101   x =   896.       y =  0.128E+04   z =   834.
Darcy-time for particle=    197.606

 i =  26   j =  28   k =  26
Press.  -0.382E+05-0.428E+05-0.407E+05-0.372E+05-0.395E+05-0.379E+05-0.787E+05
 Surface x+   Fracture EW5
 Surface y-   Fracture EW5
 Surface y+   Fracture EW5
 Surface z-   Fracture EW5
 Step  102   x =   898.       y =  0.128E+04   z =   834.
Darcy-time for particle=    197.757
 Step  103   x =   900.       y =  0.129E+04   z =   835.
Darcy-time for particle=    197.913
 Step  104   x =   902.       y =  0.129E+04   z =   835.
Darcy-time for particle=    198.071

 i =  27   j =  28   k =  26
Press.  -0.407E+05-0.382E+05-0.491E+05-0.423E+05-0.419E+05-0.407E+05-0.675E+05
 Surface x-   Fracture EW5
 Surface y+   Fracture EW5
 Surface z-   Fracture EW5
 Step  105   x =   905.       y =  0.130E+04   z =   836.
Darcy-time for particle=    198.270
 Step  106   x =   909.       y =  0.130E+04   z =   836.
Darcy-time for particle=    198.469

 i =  27   j =  29   k =  26
Press.  -0.419E+05-0.395E+05-0.494E+05-0.407E+05-0.430E+05-0.418E+05-0.848E+05
 Surface x-   Fracture EW5
 Surface y-   Fracture EW5
 Surface y+   Fracture EW5
 Surface z-   Fracture EW5
 Step  107   x =   912.       y =  0.130E+04   z =   836.
Darcy-time for particle=    198.653
 Step  108   x =   914.       y =  0.131E+04   z =   836.
Darcy-time for particle=    198.811
 Step  109   x =   915.       y =  0.131E+04   z =   836.
Darcy-time for particle=    198.948
 Step  110   x =   916.       y =  0.132E+04   z =   836.
Darcy-time for particle=    199.067

 i =  27   j =  30   k =  26
Press.  -0.430E+05-0.737E+05-0.451E+05-0.419E+05-0.443E+05-0.430E+05-0.105E+06
 Surface x+   Fracture EW5
 Surface y-   Fracture EW5
 Surface y+   Fracture EW5
 Surface z-   Fracture EW5
 Step  111   x =   917.       y =  0.132E+04   z =   836.
Darcy-time for particle=    199.180
 Step  112   x =   919.       y =  0.133E+04   z =   836.
Darcy-time for particle=    199.304
 Step  113   x =   922.       y =  0.133E+04   z =   837.
Darcy-time for particle=    199.435

 i =  28   j =  30   k =  26
Press.  -0.451E+05-0.430E+05-0.509E+05-0.494E+05-0.458E+05-0.453E+05-0.762E+05
```

```
 Surface x-   Fracture EW5
 Surface y+   Fracture EW5
 Surface z-   Fracture EW5
 Step  114   x =   926.       y =  0.133E+04   z =   837.
Darcy-time for particle=    199.607
 Step  115   x =   930.       y =  0.134E+04   z =   837.
Darcy-time for particle=    199.792

 i =  28   j =  31   k =  26
Press.  -0.458E+05-0.443E+05-0.516E+05-0.451E+05-0.462E+05-0.460E+05-0.856E+05
 Surface x-   Fracture EW5
 Surface y-   Fracture EW5
 Surface y+   Fracture EW5
 Surface z-   Fracture EW5
 Step  116   x =   933.       y =  0.134E+04   z =   837.
Darcy-time for particle=    200.008
 Step  117   x =   933.       y =  0.135E+04   z =   837.
Darcy-time for particle=    200.243
 Step  118   x =   934.       y =  0.135E+04   z =   837.
Darcy-time for particle=    200.500
 Step  119   x =   934.       y =  0.136E+04   z =   837.
Darcy-time for particle=    200.785

 i =  28   j =  32   k =  26
Press.  -0.462E+05-0.573E+05-0.474E+05-0.458E+05-0.540E+05-0.463E+05-0.747E+05
 Surface x+   Fracture EW5
 Surface y-   Fracture EW5
 Surface z-   Fracture EW5
 Step  120   x =   935.       y =  0.136E+04   z =   837.
Darcy-time for particle=    201.071
 Step  121   x =   937.       y =  0.137E+04   z =   837.
Darcy-time for particle=    201.392

 i =  29   j =  32   k =  26
Press.  -0.474E+05-0.462E+05-0.547E+05-0.516E+05-0.471E+05-0.479E+05-0.688E+05
 Surface x-   Fracture EW5
 Surface y+   Fracture EW5
 Surface z-   Fracture EW5
 Step  122   x =   941.       y =  0.137E+04   z =   837.
Darcy-time for particle=    201.735
 Step  123   x =   945.       y =  0.137E+04   z =   836.
Darcy-time for particle=    202.155
 Step  124   x =   949.       y =  0.136E+04   z =   834.
Darcy-time for particle=    202.612
 Step  125   x =   952.       y =  0.136E+04   z =   830.
Darcy-time for particle=    202.974
 Step  126   x =   954.       y =  0.136E+04   z =   826.
Darcy-time for particle=    203.229
 Step  127   x =   955.       y =  0.136E+04   z =   821.
Darcy-time for particle=    203.419

 i =  29   j =  32   k =  25
Press.  -0.479E+05-0.463E+05-0.493E+05-0.480E+05-0.472E+05-0.491E+05-0.474E+05
 Surface x-   Fracture EW5
 Surface x+   Fracture EW5
 Surface y-   Fracture EW5
 Surface y+   Fracture EW5
 Surface z-   Fracture EW5
 Surface z+   Fracture EW5
 Step  128   x =   955.       y =  0.136E+04   z =   816.
Darcy-time for particle=    203.557
 Step  129   x =   956.       y =  0.136E+04   z =   811.
Darcy-time for particle=    203.665
 Step  130   x =   956.       y =  0.136E+04   z =   806.
```

```
 Darcy-time for particle=    203.755

  i =  29   j =  31   k =  25
 Press.  -0.480E+05-0.460E+05-0.548E+05-0.498E+05-0.479E+05-0.490E+05-0.516E+05
  Surface x-   Fracture EW5
  Surface y+   Fracture EW5
  Surface z-   Fracture EW5
  Step  131   x =   956.       y =  0.136E+04   z =   801.
 Darcy-time for particle=    203.862

  i =  29   j =  31   k =  24
 Press.  -0.490E+05-0.466E+05-0.515E+05-0.492E+05-0.491E+05-0.494E+05-0.480E+05
  Surface x-   Fracture EW5
  Surface x+   Fracture EW5
  Surface y-   Fracture EW5
  Surface y+   Fracture EW5
  Surface z-   Fracture EW5
  Surface z+   Fracture EW5
  Step  132   x =   957.       y =  0.136E+04   z =   796.
 Darcy-time for particle=    203.966

  i =  29   j =  32   k =  24
 Press.  -0.491E+05-0.464E+05-0.512E+05-0.490E+05-0.475E+05-0.483E+05-0.479E+05
  Surface x+   Fracture EW5
  Surface y-   Fracture EW5
  Surface z+   Fracture EW5
  Step  133   x =   959.       y =  0.136E+04   z =   792.
 Darcy-time for particle=    204.026

  i =  30   j =  32   k =  24
 Press.  -0.512E+05-0.491E+05-0.608E+05-0.515E+05-0.499E+05-0.539E+05-0.493E+05
  Surface x-   Fracture EW5
  Surface y-   Fracture EW5
  Surface y+   Fracture EW5
  Surface z-   Fracture EW5
  Surface z+   Fracture EW5
  Step  134   x =   963.       y =  0.136E+04   z =   789.
 Darcy-time for particle=    204.071
  Step  135   x =   966.       y =  0.136E+04   z =   785.
 Darcy-time for particle=    204.108
  Step  136   x =   967.       y =  0.136E+04   z =   780.
 Darcy-time for particle=    204.137

  i =  30   j =  32   k =  23
 Press.  -0.539E+05-0.483E+05-0.623E+05-0.538E+05-0.529E+05-0.520E+05-0.512E+05
  Surface x-   Fracture NNW1
  Surface x+   Fracture EW5
  Surface x+   Fracture NNW1
  Surface y-   Fracture EW5
  Surface y-   Fracture NNW1
  Surface y+   Fracture EW5
  Surface y+   Fracture NNW1
  Surface z-   Fracture EW5
  Surface z+   Fracture EW5
  Step  137   x =   969.       y =  0.136E+04   z =   775.
 Darcy-time for particle=    204.150
  Step  138   x =   973.       y =  0.136E+04   z =   774.
 Darcy-time for particle=    204.161

  i =  31   j =  32   k =  23
 Press.  -0.623E+05-0.539E+05-0.816E+05-0.674E+05-0.572E+05-0.536E+05-0.608E+05
  Surface x-   Fracture EW5
  Surface x-   Fracture NNW1
  Surface x+   Fracture NNW1
```

```
 Surface y-   Fracture NNW1
 Surface y+   Fracture EW5
 Surface y+   Fracture NNW1
 Surface z-   Fracture EW5
 Step  139   x =   978.       y =  0.136E+04   z =   773.
Darcy-time for particle=    204.170

 i =  31   j =  31   k =  23
Press.  -0.674E+05-0.538E+05-0.839E+05-0.688E+05-0.623E+05-0.499E+05-0.604E+05
 Surface x-   Fracture NNW1
 Surface x+   Fracture NNW1
 Surface y-   Fracture NNW1
 Surface y+   Fracture NNW1
 Step  140   x =   983.       y =  0.136E+04   z =   774.
Darcy-time for particle=    204.178
 Step  141   x =   988.       y =  0.136E+04   z =   774.
Darcy-time for particle=    204.186
 Step  142   x =   992.       y =  0.136E+04   z =   774.
Darcy-time for particle=    204.193

 i =  32   j =  31   k =  23
Press.  -0.839E+05-0.674E+05-0.103E+06-0.833E+05-0.816E+05-0.722E+05-0.730E+05
 Surface x-   Fracture NNW1
 Surface x+   Fracture NNW1
 Surface y-   Fracture NNW1
 Surface y+   Fracture NNW1
 Step  143   x =   997.       y =  0.135E+04   z =   774.
Darcy-time for particle=    204.200
 Step  144   x =  0.100E+04   y =  0.135E+04   z =   774.
Darcy-time for particle=    204.207
 Step  145   x =  0.101E+04   y =  0.135E+04   z =   774.
Darcy-time for particle=    204.214
 Step  146   x =  0.101E+04   y =  0.135E+04   z =   774.
Darcy-time for particle=    204.221

 i =  33   j =  31   k =  23
Press.  -0.103E+06-0.839E+05-0.124E+06-0.994E+05-0.104E+06-0.967E+05-0.912E+05
 Surface x-   Fracture NNW1
 Surface x+   Fracture NNW1
 Surface y-   Fracture NNW1
 Surface y+   Fracture NNW1
 Step  147   x =  0.102E+04   y =  0.135E+04   z =   774.
Darcy-time for particle=    204.227
 Step  148   x =  0.102E+04   y =  0.135E+04   z =   774.
Darcy-time for particle=    204.233
 Step  149   x =  0.103E+04   y =  0.135E+04   z =   774.
Darcy-time for particle=    204.239
 Step  150   x =  0.103E+04   y =  0.135E+04   z =   774.
Darcy-time for particle=    204.245

 i =  34   j =  31   k =  23
Press.  -0.124E+06-0.103E+06-0.146E+06-0.116E+06-0.129E+06-0.113E+06-0.102E+06
 Surface x-   Fracture NNW1
 Surface x+   Fracture NNW1
 Surface y-   Fracture NNW1
 Surface y+   Fracture NNW1
 Step  151   x =  0.104E+04   y =  0.136E+04   z =   774.
Darcy-time for particle=    204.250
 Step  152   x =  0.104E+04   y =  0.136E+04   z =   774.
Darcy-time for particle=    204.256
 Step  153   x =  0.105E+04   y =  0.136E+04   z =   774.
Darcy-time for particle=    204.261

 i =  35   j =  31   k =  23
```

```
 Press.  -0.146E+06-0.124E+06-0.167E+06-0.134E+06-0.159E+06-0.144E+06-0.125E+06
  Surface x-   Fracture NNW1
  Surface x+   Fracture NNW1
  Surface y-   Fracture NNW1
  Surface y+   Fracture NNW1
  Step  154   x =  0.105E+04   y =  0.136E+04   z =   774.
 Darcy-time for particle=    204.266

  i =  35   j =  32   k =  23
 Press.  -0.159E+06-0.129E+06-0.192E+06-0.146E+06-0.170E+06-0.184E+06-0.130E+06
  Surface x-   Fracture NNW1
  Surface x+   Fracture NNW1
  Surface y-   Fracture NNW1
  Surface y+   Fracture NNW1
  Step  155   x =  0.106E+04   y =  0.136E+04   z =   774.
 Darcy-time for particle=    204.269
  Step  156   x =  0.106E+04   y =  0.136E+04   z =   774.
 Darcy-time for particle=    204.273
  Step  157   x =  0.107E+04   y =  0.136E+04   z =   774.
 Darcy-time for particle=    204.277

  i =  36   j =  32   k =  23
 Press.  -0.192E+06-0.159E+06-0.219E+06-0.167E+06-0.223E+06-0.217E+06-0.169E+06
  Surface x-   Fracture NNW1
  Surface x+   Fracture NNW1
  Surface y-   Fracture NNW1
  Surface y+   Fracture NNW1
  Step  158   x =  0.107E+04   y =  0.137E+04   z =   774.
 Darcy-time for particle=    204.280
  Step  159   x =  0.107E+04   y =  0.137E+04   z =   774.
 Darcy-time for particle=    204.283
  Step  160   x =  0.108E+04   y =  0.137E+04   z =   773.
 Darcy-time for particle=    204.286
  Step  161   x =  0.108E+04   y =  0.138E+04   z =   773.
 Darcy-time for particle=    204.289
  Step  162   x =  0.109E+04   y =  0.138E+04   z =   773.
 Darcy-time for particle=    204.292

  i =  36   j =  33   k =  23
 Press.  -0.223E+06-0.170E+06-0.295E+06-0.192E+06-0.162E+06-0.249E+06-0.136E+06
  Surface x-   Fracture NNW1
  Surface x+   Fracture NNW1
  Surface y-   Fracture NNW1
  Surface z-   Fracture NNW1
  Step  163   x =  0.109E+04   y =  0.138E+04   z =   773.
 Darcy-time for particle=    204.295

  i =  37   j =  33   k =  23
 Press.  -0.295E+06-0.223E+06-0.245E+06-0.219E+06-0.164E+06-0.422E+06-0.141E+06
  Surface x-   Fracture NNW1
  Surface x+   Fracture NNW1
  Surface y-   Fracture NNW1
  Surface z-   Fracture NNW1
  Step  164   x =  0.109E+04   y =  0.139E+04   z =   772.
 Darcy-time for particle=    204.297
  Step  165   x =  0.109E+04   y =  0.139E+04   z =   769.
 Darcy-time for particle=    204.298
  Step  166   x =  0.110E+04   y =  0.139E+04   z =   765.
```

APPENDIX C.

Table of trajectory for injection in KAS04, section D2.

```
 Press.       p        px-       px+       py-       py+       pz-       pz+

  i =  23   j =  20   k =  27
 Press.  -0.271E+05-0.245E+05-0.299E+05-0.242E+05-0.286E+05-0.227E+05-0.316E+05
  Surface x-   Fracture NE2
  Surface x+   Fracture NE2
  Surface z-   Fracture NE2
  Surface z+   Fracture NE2
  Step    0   x =   840.       y =  0.113E+04   z =   850.
 Darcy-time for particle=    1.03451E-01
  Step    1   x =   841.       y =  0.113E+04   z =   855.
 Darcy-time for particle=   0.206653
  Step    2   x =   843.       y =  0.113E+04   z =   860.
 Darcy-time for particle=   0.309607

  i =  23   j =  20   k =  28
 Press.  -0.316E+05-0.292E+05-0.341E+05-0.281E+05-0.345E+05-0.271E+05-0.362E+05
  Surface x-   Fracture NE2
  Surface x+   Fracture NE2
  Surface z-   Fracture NE2
  Surface z+   Fracture NE2
  Step    3   x =   844.       y =  0.113E+04   z =   864.
 Darcy-time for particle=   0.413644
  Step    4   x =   846.       y =  0.113E+04   z =   869.
 Darcy-time for particle=   0.517509
  Step    5   x =   847.       y =  0.113E+04   z =   874.
 Darcy-time for particle=   0.621201
  Step    6   x =   848.       y =  0.113E+04   z =   879.
 Darcy-time for particle=   0.724722

  i =  24   j =  20   k =  29
 Press.  -0.381E+05-0.362E+05-0.400E+05-0.340E+05-0.416E+05-0.341E+05-0.398E+05
  Surface x-   Fracture NE2
  Surface y+   Fracture NE2
  Surface z-   Fracture NE2
  Step    7   x =   849.       y =  0.113E+04   z =   884.
 Darcy-time for particle=    3.07818
  Step    8   x =   850.       y =  0.113E+04   z =   888.
 Darcy-time for particle=    5.65750
  Step    9   x =   850.       y =  0.114E+04   z =   892.
 Darcy-time for particle=    8.26055
  Step   10   x =   850.       y =  0.114E+04   z =   895.
 Darcy-time for particle=    10.6464

  i =  24   j =  21   k =  29
 Press.  -0.416E+05-0.393E+05-0.437E+05-0.381E+05-0.467E+05-0.372E+05-0.463E+05
  Surface x-   Fracture NE2
  Surface x+   Fracture NE2
  Surface y-   Fracture NE2
  Surface z-   Fracture NE2
  Surface z+   Fracture NE2
  Step   11   x =   851.       y =  0.114E+04   z =   897.
 Darcy-time for particle=    10.7493

  i =  24   j =  21   k =  30
 Press.  -0.463E+05-0.441E+05-0.482E+05-0.398E+05-0.502E+05-0.416E+05-0.513E+05
  Surface x-   Fracture NE2
  Surface x+   Fracture NE2
  Surface z-   Fracture NE2
  Surface z+   Fracture NE2
  Step   12   x =   851.       y =  0.114E+04   z =   902.
 Darcy-time for particle=    10.8508
  Step   13   x =   852.       y =  0.114E+04   z =   907.
 Darcy-time for particle=    10.9504
```

```
 Step   14   x =   852.       y =  0.114E+04   z =   912.
Darcy-time for particle=    11.0483
 Step   15   x =   853.       y =  0.114E+04   z =   917.
Darcy-time for particle=    11.1444

 i =  24   j =  21   k =  31
Press.  -0.513E+05-0.494E+05-0.529E+05-0.462E+05-0.530E+05-0.463E+05-0.502E+05
 Surface x-   Fracture NE2
 Surface x-   Fracture NNW2
 Surface x+   Fracture NE2
 Surface x+   Fracture NNW2
 Surface y+   Fracture NNW2
 Surface z-   Fracture NE2
 Surface z+   Fracture NE2
 Surface z+   Fracture NNW2
 Step   16   x =   853.       y =  0.114E+04   z =   922.
Darcy-time for particle=    11.1944
 Step   17   x =   856.       y =  0.115E+04   z =   923.
Darcy-time for particle=    11.2275
 Step   18   x =   858.       y =  0.115E+04   z =   923.
Darcy-time for particle=    11.2494
 Step   19   x =   859.       y =  0.116E+04   z =   924.
Darcy-time for particle=    11.2655

 i =  24   j =  22   k =  31
Press.  -0.530E+05-0.510E+05-0.546E+05-0.513E+05-0.551E+05-0.502E+05-0.479E+05
 Surface x-   Fracture NNW2
 Surface x+   Fracture NNW2
 Surface y-   Fracture NNW2
 Surface y+   Fracture NNW2
 Step   20   x =   860.       y =  0.116E+04   z =   924.
Darcy-time for particle=    11.2794
 Step   21   x =   860.       y =  0.117E+04   z =   924.
Darcy-time for particle=    11.2926
 Step   22   x =   861.       y =  0.117E+04   z =   924.
Darcy-time for particle=    11.3052
 Step   23   x =   861.       y =  0.118E+04   z =   924.
Darcy-time for particle=    11.3172

 i =  24   j =  23   k =  31
Press.  -0.551E+05-0.530E+05-0.568E+05-0.530E+05-0.530E+05-0.576E+05-0.465E+05
 Surface x-   Fracture NNW2
 Surface x+   Fracture NNW2
 Surface y-   Fracture NNW2
 Surface z-   Fracture NNW2
 Step   24   x =   862.       y =  0.118E+04   z =   924.
Darcy-time for particle=    11.3263

 i =  24   j =  23   k =  30
Press.  -0.576E+05-0.552E+05-0.594E+05-0.502E+05-0.601E+05-0.464E+05-0.551E+05
 Surface x-   Fracture NNW2
 Surface x+   Fracture NNW2
 Surface y+   Fracture NNW2
 Surface z+   Fracture NNW2
 Step   25   x =   862.       y =  0.119E+04   z =   920.
Darcy-time for particle=    11.3359
 Step   26   x =   862.       y =  0.119E+04   z =   915.
Darcy-time for particle=    11.3477
 Step   27   x =   862.       y =  0.119E+04   z =   911.
Darcy-time for particle=    11.3611
 Step   28   x =   863.       y =  0.119E+04   z =   907.
Darcy-time for particle=    11.3738
 Step   29   x =   863.       y =  0.120E+04   z =   905.
Darcy-time for particle=    11.3841
```

```
 i =  24   j =  24   k =  30
Press.  -0.601E+05-0.575E+05-0.621E+05-0.576E+05-0.634E+05-0.512E+05-0.530E+05
 Surface x-   Fracture NNW2
 Surface x+   Fracture NNW2
 Surface y-   Fracture NNW2
 Surface y+   Fracture NNW2
 Step   30   x =   863.       y =  0.120E+04   z =   904.
Darcy-time for particle=    11.3932
 Step   31   x =   864.       y =  0.121E+04   z =   904.
Darcy-time for particle=    11.4018
 Step   32   x =   865.       y =  0.121E+04   z =   904.
Darcy-time for particle=    11.4100
 Step   33   x =   865.       y =  0.122E+04   z =   904.
Darcy-time for particle=    11.4178

 i =  24   j =  25   k =  30
Press.  -0.634E+05-0.604E+05-0.657E+05-0.601E+05-0.673E+05-0.604E+05-0.559E+05
 Surface x-   Fracture NNW2
 Surface x+   Fracture NNW2
 Surface y-   Fracture NNW2
 Surface y+   Fracture NNW2
 Step   34   x =   866.       y =  0.122E+04   z =   904.
Darcy-time for particle=    11.4252

 i =  25   j =  25   k =  30
Press.  -0.657E+05-0.634E+05-0.667E+05-0.621E+05-0.702E+05-0.634E+05-0.566E+05
 Surface x-   Fracture NNW2
 Surface x+   Fracture NNW2
 Surface y-   Fracture NNW2
 Surface y+   Fracture NNW2
 Step   35   x =   867.       y =  0.123E+04   z =   904.
Darcy-time for particle=    11.4315
 Step   36   x =   868.       y =  0.123E+04   z =   904.
Darcy-time for particle=    11.4374
 Step   37   x =   868.       y =  0.124E+04   z =   904.
Darcy-time for particle=    11.4430

 i =  25   j =  26   k =  30
Press.  -0.702E+05-0.673E+05-0.714E+05-0.657E+05-0.645E+05-0.752E+05-0.576E+05
 Surface x-   Fracture NNW2
 Surface x+   Fracture NNW2
 Surface y-   Fracture NNW2
 Surface z-   Fracture NNW2
 Step   38   x =   869.       y =  0.124E+04   z =   904.
Darcy-time for particle=    11.4473
 Step   39   x =   869.       y =  0.125E+04   z =   900.
Darcy-time for particle=    11.4514

 i =  25   j =  26   k =  29
Press.  -0.752E+05-0.717E+05-0.768E+05-0.634E+05-0.813E+05-0.683E+05-0.702E+05
 Surface x-   Fracture NNW2
 Surface x+   Fracture NNW2
 Surface y+   Fracture NNW2
 Surface z+   Fracture NNW2
 Step   40   x =   869.       y =  0.125E+04   z =   896.
Darcy-time for particle=    11.4565
 Step   41   x =   870.       y =  0.125E+04   z =   892.
Darcy-time for particle=    11.4619
 Step   42   x =   871.       y =  0.125E+04   z =   889.
Darcy-time for particle=    11.4668
 Step   43   x =   872.       y =  0.126E+04   z =   886.
Darcy-time for particle=    11.4708
```

```
 i =  25   j =  27   k =  29
Press.  -0.813E+05-0.766E+05-0.835E+05-0.752E+05-0.899E+05-0.753E+05-0.645E+05
 Surface x-   Fracture NNW2
 Surface x+   Fracture NNW2
 Surface y-   Fracture NNW2
 Surface y+   Fracture NNW2
 Step   44   x =   873.       y =  0.126E+04   z =   885.
Darcy-time for particle=    11.4743
 Step   45   x =   874.       y =  0.127E+04   z =   885.
Darcy-time for particle=    11.4777
 Step   46   x =   876.       y =  0.127E+04   z =   885.
Darcy-time for particle=    11.4808
 Step   47   x =   877.       y =  0.128E+04   z =   885.
Darcy-time for particle=    11.4836

 i =  25   j =  28   k =  29
Press.  -0.899E+05-0.829E+05-0.937E+05-0.813E+05-0.102E+06-0.833E+05-0.681E+05
 Surface x-   Fracture NNW2
 Surface x+   Fracture NNW2
 Surface y-   Fracture NNW2
 Surface y+   Fracture NNW2
 Step   48   x =   878.       y =  0.128E+04   z =   885.
Darcy-time for particle=    11.4862
 Step   49   x =   880.       y =  0.129E+04   z =   885.
Darcy-time for particle=    11.4885
 Step   50   x =   881.       y =  0.129E+04   z =   885.
Darcy-time for particle=    11.4907
 Step   51   x =   882.       y =  0.130E+04   z =   885.
Darcy-time for particle=    11.4928

 i =  25   j =  29   k =  29
Press.  -0.102E+06-0.901E+05-0.111E+06-0.899E+05-0.819E+05-0.114E+06-0.634E+05
 Surface x-   Fracture NNW2
 Surface x+   Fracture NNW2
 Surface y-   Fracture NNW2
 Surface z-   Fracture NNW2
 Step   52   x =   883.       y =  0.130E+04   z =   885.
Darcy-time for particle=    11.4946
 Step   53   x =   884.       y =  0.131E+04   z =   882.
Darcy-time for particle=    11.4964

 i =  25   j =  29   k =  28
Press.  -0.114E+06-0.973E+05-0.129E+06-0.833E+05-0.128E+06-0.884E+05-0.102E+06
 Surface x-   Fracture NNW2
 Surface x+   Fracture NNW2
 Surface y+   Fracture NNW2
 Surface z+   Fracture NNW2
 Step   54   x =   884.       y =  0.131E+04   z =   878.
Darcy-time for particle=    11.4977

 i =  26   j =  29   k =  28
Press.  -0.129E+06-0.114E+06-0.116E+06-0.993E+05-0.180E+06-0.109E+06-0.111E+06
 Surface x-   Fracture NNW2
 Surface x+   Fracture NNW2
 Surface y+   Fracture NNW2
 Surface z+   Fracture NNW2
 Step   55   x =   887.       y =  0.131E+04   z =   875.
Darcy-time for particle=    11.4984
 Step   56   x =   889.       y =  0.132E+04   z =   873.
```

APPENDIX D.

Table of trajectory for injection in KAS05, section E3.

```
Press.       p         px-       px+       py-       py+       pz-       pz+

 i =  31   j =  28   k =  19
Press.  -0.300E+05-0.298E+05-0.372E+05-0.296E+05-0.323E+05-0.266E+05-0.391E+05
 Surface x-   Fracture EW5
 Surface y+   Fracture EW5
 Surface z-   Fracture EW5
 Step    0   x =   987.       y =  0.129E+04   z =   690.
Darcy-time for particle=   0.111940
 Step    1   x =   986.       y =  0.129E+04   z =   694.
Darcy-time for particle=   0.239189
 Step    2   x =   984.       y =  0.130E+04   z =   697.
Darcy-time for particle=   0.353218

 i =  31   j =  29   k =  19
Press.  -0.323E+05-0.321E+05-0.342E+05-0.300E+05-0.346E+05-0.287E+05-0.359E+05
 Surface x-   Fracture EW5
 Surface y-   Fracture EW5
 Surface y+   Fracture EW5
 Surface z-   Fracture EW5
 Surface z+   Fracture EW5
 Step    3   x =   983.       y =  0.130E+04   z =   698.
Darcy-time for particle=   0.398285

 i =  31   j =  29   k =  20
Press.  -0.359E+05-0.356E+05-0.407E+05-0.391E+05-0.386E+05-0.323E+05-0.450E+05
 Surface x-   Fracture EW5
 Surface y+   Fracture EW5
 Surface z-   Fracture EW5
 Step    4   x =   981.       y =  0.130E+04   z =   702.
Darcy-time for particle=   0.468093
 Step    5   x =   980.       y =  0.130E+04   z =   707.
Darcy-time for particle=   0.559924
 Step    6   x =   979.       y =  0.131E+04   z =   712.
Darcy-time for particle=   0.684272

 i =  30   j =  29   k =  20
Press.  -0.356E+05-0.328E+05-0.359E+05-0.330E+05-0.383E+05-0.321E+05-0.391E+05
 Surface x+   Fracture EW5
 Surface y-   Fracture EW5
 Surface y+   Fracture EW5
 Surface z-   Fracture EW5
 Surface z+   Fracture EW5
 Step    7   x =   976.       y =  0.131E+04   z =   716.
Darcy-time for particle=   0.704537
 Step    8   x =   976.       y =  0.131E+04   z =   720.
Darcy-time for particle=   0.724165

 i =  30   j =  29   k =  21
Press.  -0.391E+05-0.383E+05-0.450E+05-0.365E+05-0.421E+05-0.356E+05-0.425E+05
 Surface x-   Fracture EW5
 Surface y-   Fracture EW5
 Surface y+   Fracture EW5
 Surface z-   Fracture EW5
 Surface z+   Fracture EW5
 Step    9   x =   976.       y =  0.131E+04   z =   724.
Darcy-time for particle=   0.747179
 Step   10   x =   976.       y =  0.132E+04   z =   728.
Darcy-time for particle=   0.771576
 Step   11   x =   976.       y =  0.132E+04   z =   731.
Darcy-time for particle=   0.795033

 i =  30   j =  30   k =  21
Press.  -0.421E+05-0.402E+05-0.426E+05-0.391E+05-0.453E+05-0.383E+05-0.459E+05
```

```
 Surface x+   Fracture EW5
 Surface y-   Fracture EW5
 Surface y+   Fracture EW5
 Surface z-   Fracture EW5
 Surface z+   Fracture EW5
 Step   12   x =   976.       y =  0.132E+04   z =   734.
Darcy-time for particle=   0.813153
 Step   13   x =   975.       y =  0.133E+04   z =   738.
Darcy-time for particle=   0.830926

 i =  30   j =  30   k =  22
Press.  -0.459E+05-0.447E+05-0.625E+05-0.425E+05-0.493E+05-0.421E+05-0.557E+05
 Surface x-   Fracture EW5
 Surface y-   Fracture EW5
 Surface y+   Fracture EW5
 Surface z-   Fracture EW5
 Surface z+   Fracture EW5
 Step   14   x =   975.       y =  0.133E+04   z =   742.
Darcy-time for particle=   0.851099
 Step   15   x =   975.       y =  0.133E+04   z =   746.
Darcy-time for particle=   0.873265
 Step   16   x =   975.       y =  0.134E+04   z =   750.
Darcy-time for particle=   0.896027
 Step   17   x =   975.       y =  0.134E+04   z =   753.
Darcy-time for particle=   0.917447

 i =  30   j =  31   k =  22
Press.  -0.493E+05-0.452E+05-0.499E+05-0.459E+05-0.520E+05-0.453E+05-0.538E+05
 Surface x+   Fracture EW5
 Surface y-   Fracture EW5
 Surface y+   Fracture EW5
 Surface z-   Fracture EW5
 Surface z+   Fracture EW5
 Step   18   x =   975.       y =  0.134E+04   z =   756.
Darcy-time for particle=   0.933224
 Step   19   x =   975.       y =  0.135E+04   z =   760.
Darcy-time for particle=   0.948543

 i =  30   j =  31   k =  23
Press.  -0.538E+05-0.494E+05-0.674E+05-0.557E+05-0.539E+05-0.493E+05-0.515E+05
 Surface x-   Fracture EW5
 Surface x-   Fracture NNW1
 Surface x+   Fracture NNW1
 Surface y-   Fracture EW5
 Surface y-   Fracture NNW1
 Surface y+   Fracture EW5
 Surface y+   Fracture NNW1
 Surface z-   Fracture EW5
 Surface z+   Fracture EW5
 Step   20   x =   975.       y =  0.135E+04   z =   764.
Darcy-time for particle=   0.957290

 i =  31   j =  31   k =  23
Press.  -0.674E+05-0.538E+05-0.839E+05-0.688E+05-0.623E+05-0.499E+05-0.604E+05
 Surface x-   Fracture NNW1
 Surface x+   Fracture NNW1
 Surface y-   Fracture NNW1
 Surface y+   Fracture NNW1
 Step   21   x =   980.       y =  0.135E+04   z =   766.
Darcy-time for particle=   0.965981
 Step   22   x =   984.       y =  0.135E+04   z =   766.
Darcy-time for particle=   0.974216
 Step   23   x =   989.       y =  0.135E+04   z =   766.
Darcy-time for particle=   0.982032
```

```
 Step   24   x =   994.       y =  0.135E+04   z =   766.
Darcy-time for particle=   0.989465

 i =  32   j =  31   k =  23
Press.  -0.839E+05-0.674E+05-0.103E+06-0.833E+05-0.816E+05-0.722E+05-0.730E+05
 Surface x-   Fracture NNW1
 Surface x+   Fracture NNW1
 Surface y-   Fracture NNW1
 Surface y+   Fracture NNW1
 Step   25   x =   999.       y =  0.135E+04   z =   766.
Darcy-time for particle=   0.996654
 Step   26   x =  0.100E+04   y =  0.135E+04   z =   766.
Darcy-time for particle=    1.00356
 Step   27   x =  0.101E+04   y =  0.135E+04   z =   766.
Darcy-time for particle=    1.01021
 Step   28   x =  0.101E+04   y =  0.135E+04   z =   766.
Darcy-time for particle=    1.01662

 i =  33   j =  31   k =  23
Press.  -0.103E+06-0.839E+05-0.124E+06-0.994E+05-0.104E+06-0.967E+05-0.912E+05
 Surface x-   Fracture NNW1
 Surface x+   Fracture NNW1
 Surface y-   Fracture NNW1
 Surface y+   Fracture NNW1
 Step   29   x =  0.102E+04   y =  0.135E+04   z =   766.
Darcy-time for particle=    1.02279
 Step   30   x =  0.102E+04   y =  0.135E+04   z =   766.
Darcy-time for particle=    1.02880
 Step   31   x =  0.103E+04   y =  0.135E+04   z =   766.
Darcy-time for particle=    1.03464

 i =  34   j =  31   k =  23
Press.  -0.124E+06-0.103E+06-0.146E+06-0.116E+06-0.129E+06-0.113E+06-0.102E+06
 Surface x-   Fracture NNW1
 Surface x+   Fracture NNW1
 Surface y-   Fracture NNW1
 Surface y+   Fracture NNW1
 Step   32   x =  0.103E+04   y =  0.135E+04   z =   766.
Darcy-time for particle=    1.04016
 Step   33   x =  0.104E+04   y =  0.135E+04   z =   766.
Darcy-time for particle=    1.04561
 Step   34   x =  0.104E+04   y =  0.135E+04   z =   766.
Darcy-time for particle=    1.05100
 Step   35   x =  0.105E+04   y =  0.135E+04   z =   766.
Darcy-time for particle=    1.05632

 i =  35   j =  31   k =  23
Press.  -0.146E+06-0.124E+06-0.167E+06-0.134E+06-0.159E+06-0.144E+06-0.125E+06
 Surface x-   Fracture NNW1
 Surface x+   Fracture NNW1
 Surface y-   Fracture NNW1
 Surface y+   Fracture NNW1
 Step   36   x =  0.105E+04   y =  0.135E+04   z =   766.
Darcy-time for particle=    1.06116
 Step   37   x =  0.106E+04   y =  0.136E+04   z =   766.
Darcy-time for particle=    1.06604
 Step   38   x =  0.106E+04   y =  0.136E+04   z =   766.
Darcy-time for particle=    1.07096
 Step   39   x =  0.107E+04   y =  0.136E+04   z =   766.
Darcy-time for particle=    1.07592

 i =  36   j =  32   k =  23
Press.  -0.192E+06-0.159E+06-0.219E+06-0.167E+06-0.223E+06-0.217E+06-0.169E+06
 Surface x-   Fracture NNW1
```

```
 Surface x+   Fracture NNW1
 Surface y-   Fracture NNW1
 Surface y+   Fracture NNW1
 Step   40   x =  0.107E+04   y =  0.136E+04   z =   766.
Darcy-time for particle=    1.07897
 Step   41   x =  0.107E+04   y =  0.137E+04   z =   766.
Darcy-time for particle=    1.08205
 Step   42   x =  0.108E+04   y =  0.137E+04   z =   766.
Darcy-time for particle=    1.08516
 Step   43   x =  0.108E+04   y =  0.137E+04   z =   766.
Darcy-time for particle=    1.08829
 Step   44   x =  0.109E+04   y =  0.138E+04   z =   766.
Darcy-time for particle=    1.09142
 Step   45   x =  0.109E+04   y =  0.138E+04   z =   766.
Darcy-time for particle=    1.09454

 i =  37   j =  33   k =  23
Press.  -0.295E+06-0.223E+06-0.245E+06-0.219E+06-0.164E+06-0.422E+06-0.141E+06
 Surface x-   Fracture NNW1
 Surface x+   Fracture NNW1
 Surface y-   Fracture NNW1
 Surface z-   Fracture NNW1
 Step   46   x =  0.109E+04   y =  0.138E+04   z =   766.
Darcy-time for particle=    1.09569
 Step   47   x =  0.109E+04   y =  0.139E+04   z =   762.
```

APPENDIX E.

Table of trajectory for injection in KAS07, section J4.

```
Press.        p         px-        px+        py-        py+        pz-        pz+

 i =  34   j =  34   k =  17
Press.  -0.283E+05-0.241E+05-0.260E+05-0.279E+05-0.286E+05-0.230E+05-0.334E+05
 Surface x-   Fracture EW3
 Surface x+   Fracture EW3
 Surface x+   Fracture EW5
 Surface y-   Fracture EW5
 Surface y+   Fracture EW3
 Surface z-   Fracture EW3
 Surface z+   Fracture EW5
 Step    0   x =  0.104E+04   y =  0.141E+04   z =   650.
Darcy-time for particle=    4.01490E-02
 Step    1   x =  0.104E+04   y =  0.141E+04   z =   654.
Darcy-time for particle=    7.48139E-02
 Step    2   x =  0.104E+04   y =  0.141E+04   z =   659.
Darcy-time for particle=    1.02307E-01

 i =  34   j =  34   k =  18
Press.  -0.334E+05-0.323E+05-0.308E+05-0.326E+05-0.337E+05-0.283E+05-0.389E+05
 Surface x+   Fracture EW5
 Surface y-   Fracture EW5
 Surface y+   Fracture EW5
 Surface z-   Fracture EW5
 Surface z+   Fracture EW5
 Step    3   x =  0.104E+04   y =  0.141E+04   z =   664.
Darcy-time for particle=   0.124947
 Step    4   x =  0.104E+04   y =  0.141E+04   z =   668.
Darcy-time for particle=   0.144332
 Step    5   x =  0.104E+04   y =  0.141E+04   z =   673.
Darcy-time for particle=   0.161254
 Step    6   x =  0.104E+04   y =  0.141E+04   z =   678.
Darcy-time for particle=   0.176258

 i =  34   j =  34   k =  19
Press.  -0.389E+05-0.412E+05-0.584E+05-0.378E+05-0.399E+05-0.334E+05-0.451E+05
 Surface x-   Fracture EW5
 Surface y-   Fracture EW5
 Surface y+   Fracture EW5
 Surface z-   Fracture EW5
 Surface z+   Fracture EW5
 Step    7   x =  0.104E+04   y =  0.141E+04   z =   683.
Darcy-time for particle=   0.190238

 i =  33   j =  34   k =  19
Press.  -0.412E+05-0.379E+05-0.389E+05-0.397E+05-0.377E+05-0.323E+05-0.473E+05
 Surface x+   Fracture EW5
 Surface y-   Fracture EW5
 Surface z+   Fracture EW5
 Step    8   x =  0.103E+04   y =  0.141E+04   z =   688.
Darcy-time for particle=   0.210239
 Step    9   x =  0.103E+04   y =  0.141E+04   z =   690.
Darcy-time for particle=   0.231719
 Step   10   x =  0.102E+04   y =  0.141E+04   z =   694.
Darcy-time for particle=   0.251451
 Step   11   x =  0.102E+04   y =  0.141E+04   z =   698.
Darcy-time for particle=   0.267685

 i =  33   j =  34   k =  20
Press.  -0.473E+05-0.490E+05-0.451E+05-0.453E+05-0.492E+05-0.412E+05-0.536E+05
 Surface x-   Fracture EW5
 Surface x+   Fracture EW5
 Surface y-   Fracture EW5
 Surface y+   Fracture EW5
```

```
 Surface z-   Fracture EW5
 Surface z+   Fracture EW5
 Step   12   x =  0.102E+04   y =  0.142E+04   z =   703.
Darcy-time for particle=   0.282111
 Step   13   x =  0.102E+04   y =  0.142E+04   z =   707.
Darcy-time for particle=   0.296425
 Step   14   x =  0.102E+04   y =  0.142E+04   z =   712.
Darcy-time for particle=   0.310627
 Step   15   x =  0.102E+04   y =  0.142E+04   z =   717.
Darcy-time for particle=   0.324720

 i =  33   j =  35   k =  21
Press.  -0.558E+05-0.559E+05-0.546E+05-0.536E+05-0.546E+05-0.492E+05-0.659E+05
 Surface x-   Fracture EW5
 Surface x+   Fracture EW5
 Surface y-   Fracture EW5
 Surface y+   Fracture EW5
 Surface z-   Fracture EW5
 Surface z+   Fracture EW5
 Step   16   x =  0.102E+04   y =  0.142E+04   z =   722.
Darcy-time for particle=   0.337513
 Step   17   x =  0.102E+04   y =  0.142E+04   z =   727.
Darcy-time for particle=   0.349072
 Step   18   x =  0.102E+04   y =  0.142E+04   z =   731.
Darcy-time for particle=   0.359562
 Step   19   x =  0.102E+04   y =  0.142E+04   z =   736.
Darcy-time for particle=   0.369137

 i =  33   j =  35   k =  22
Press.  -0.659E+05-0.583E+05-0.987E+05-0.859E+05-0.559E+05-0.558E+05-0.781E+05
 Surface x-   Fracture EW5
 Surface x-   Fracture NNW1
 Surface x+   Fracture NNW1
 Surface y-   Fracture NNW1
 Surface y+   Fracture EW5
 Surface y+   Fracture NNW1
 Surface z-   Fracture EW5
 Step   20   x =  0.102E+04   y =  0.143E+04   z =   741.
Darcy-time for particle=   0.373016
 Step   21   x =  0.102E+04   y =  0.142E+04   z =   743.
Darcy-time for particle=   0.376752

 i =  33   j =  34   k =  22
Press.  -0.859E+05-0.615E+05-0.119E+06-0.950E+05-0.659E+05-0.536E+05-0.957E+05
 Surface x-   Fracture NNW1
 Surface x+   Fracture NNW1
 Surface y-   Fracture NNW1
 Surface y+   Fracture NNW1
 Step   22   x =  0.103E+04   y =  0.142E+04   z =   745.
Darcy-time for particle=   0.380202
 Step   23   x =  0.103E+04   y =  0.142E+04   z =   745.
Darcy-time for particle=   0.383534

 i =  34   j =  34   k =  22
Press.  -0.119E+06-0.859E+05-0.160E+06-0.129E+06-0.987E+05-0.750E+05-0.114E+06
 Surface x-   Fracture NNW1
 Surface x+   Fracture NNW1
 Surface y-   Fracture NNW1
 Surface y+   Fracture NNW1
 Step   24   x =  0.103E+04   y =  0.141E+04   z =   745.
Darcy-time for particle=   0.386722
 Step   25   x =  0.104E+04   y =  0.141E+04   z =   745.
Darcy-time for particle=   0.389781
 Step   26   x =  0.104E+04   y =  0.141E+04   z =   745.
```

```
Darcy-time for particle=   0.392711
 Step   27   x =  0.105E+04   y =  0.141E+04   z =   745.
Darcy-time for particle=   0.395514

 i =  35   j =  34   k =  22
Press.  -0.160E+06-0.119E+06-0.212E+06-0.175E+06-0.136E+06-0.920E+05-0.132E+06
 Surface x-   Fracture NNW1
 Surface x+   Fracture NNW1
 Surface y-   Fracture NNW1
 Surface y+   Fracture NNW1
 Step   28   x =  0.105E+04   y =  0.141E+04   z =   745.
Darcy-time for particle=   0.398120
 Step   29   x =  0.106E+04   y =  0.141E+04   z =   745.
Darcy-time for particle=   0.400627
 Step   30   x =  0.106E+04   y =  0.140E+04   z =   745.
Darcy-time for particle=   0.403040
 Step   31   x =  0.107E+04   y =  0.140E+04   z =   745.
Darcy-time for particle=   0.405360

 i =  36   j =  34   k =  22
Press.  -0.212E+06-0.160E+06-0.268E+06-0.249E+06-0.174E+06-0.111E+06-0.162E+06
 Surface x-   Fracture NNW1
 Surface x+   Fracture NNW1
 Surface y-   Fracture NNW1
 Surface y+   Fracture NNW1
 Step   32   x =  0.107E+04   y =  0.140E+04   z =   745.
Darcy-time for particle=   0.407317

 i =  36   j =  33   k =  22
Press.  -0.249E+06-0.175E+06-0.422E+06-0.217E+06-0.212E+06-0.159E+06-0.223E+06
 Surface x-   Fracture NNW1
 Surface x+   Fracture NNW1
 Surface y+   Fracture NNW1
 Surface z+   Fracture NNW1
 Step   33   x =  0.108E+04   y =  0.140E+04   z =   745.
Darcy-time for particle=   0.409085
 Step   34   x =  0.108E+04   y =  0.140E+04   z =   745.
Darcy-time for particle=   0.410625
 Step   35   x =  0.108E+04   y =  0.139E+04   z =   744.
Darcy-time for particle=   0.411962
 Step   36   x =  0.109E+04   y =  0.139E+04   z =   744.
```

APPENDIX F.

Table of trajectory for injection in KAS08, section M3.

```
Press.        p         px-        px+        py-        py+        pz-        pz+

 i =  39   j =  28   k =  29
Press.  -0.356E+05-0.388E+05-0.325E+05-0.371E+05-0.340E+05-0.474E+05-0.321E+05
 Surface x-   Fracture NNW2
 Surface x+   Fracture NNW2
 Surface y-   Fracture NNW2
 Surface y+   Fracture NNW2
 Step    0   x =  0.114E+04   y =  0.129E+04   z =   890.
Darcy-time for particle=    5.14183E-03
 Step    1   x =  0.114E+04   y =  0.129E+04   z =   890.
Darcy-time for particle=    1.02614E-02
 Step    2   x =  0.113E+04   y =  0.129E+04   z =   890.
Darcy-time for particle=    1.53588E-02

 i =  38   j =  28   k =  29
Press.  -0.388E+05-0.421E+05-0.356E+05-0.401E+05-0.373E+05-0.420E+05-0.331E+05
 Surface x-   Fracture NNW2
 Surface x+   Fracture NNW2
 Surface y-   Fracture NNW2
 Surface y+   Fracture NNW2
 Step    3   x =  0.113E+04   y =  0.129E+04   z =   890.
Darcy-time for particle=    2.04980E-02
 Step    4   x =  0.112E+04   y =  0.128E+04   z =   890.
Darcy-time for particle=    2.55995E-02
 Step    5   x =  0.112E+04   y =  0.128E+04   z =   890.
Darcy-time for particle=    3.06635E-02
 Step    6   x =  0.111E+04   y =  0.128E+04   z =   890.
Darcy-time for particle=    3.56905E-02

 i =  37   j =  27   k =  29
Press.  -0.431E+05-0.464E+05-0.401E+05-0.439E+05-0.421E+05-0.545E+05-0.388E+05
 Surface x-   Fracture NNW2
 Surface x+   Fracture NNW2
 Surface y-   Fracture NNW2
 Surface y+   Fracture NNW2
 Step    7   x =  0.111E+04   y =  0.128E+04   z =   890.
Darcy-time for particle=    4.10301E-02
 Step    8   x =  0.110E+04   y =  0.128E+04   z =   890.
Darcy-time for particle=    4.63138E-02
 Step    9   x =  0.110E+04   y =  0.128E+04   z =   890.
Darcy-time for particle=    5.15425E-02
 Step   10   x =  0.109E+04   y =  0.128E+04   z =   890.
Darcy-time for particle=    5.67172E-02

 i =  36   j =  27   k =  29
Press.  -0.464E+05-0.498E+05-0.431E+05-0.469E+05-0.456E+05-0.544E+05-0.429E+05
 Surface x-   Fracture NNW2
 Surface x+   Fracture NNW2
 Surface y-   Fracture NNW2
 Surface y+   Fracture NNW2
 Step   11   x =  0.109E+04   y =  0.128E+04   z =   890.
Darcy-time for particle=    6.18831E-02
 Step   12   x =  0.108E+04   y =  0.127E+04   z =   890.
Darcy-time for particle=    6.69820E-02
 Step   13   x =  0.108E+04   y =  0.127E+04   z =   890.
Darcy-time for particle=    7.20154E-02
 Step   14   x =  0.107E+04   y =  0.127E+04   z =   890.
Darcy-time for particle=    7.69849E-02

 i =  35   j =  27   k =  29
Press.  -0.498E+05-0.533E+05-0.464E+05-0.500E+05-0.493E+05-0.589E+05-0.466E+05
 Surface x-   Fracture NNW2
 Surface x+   Fracture NNW2
```

```
 Surface y-   Fracture NNW2
 Surface y+   Fracture NNW2
 Step   15   x =  0.107E+04   y =  0.127E+04   z =   890.
Darcy-time for particle=    8.19169E-02
 Step   16   x =  0.106E+04   y =  0.127E+04   z =   890.
Darcy-time for particle=    8.67749E-02
 Step   17   x =  0.106E+04   y =  0.127E+04   z =   890.
Darcy-time for particle=    9.15609E-02
 Step   18   x =  0.105E+04   y =  0.127E+04   z =   890.
Darcy-time for particle=    9.62770E-02

 i =  34   j =  27   k =  29
Press.  -0.533E+05-0.571E+05-0.498E+05-0.531E+05-0.532E+05-0.609E+05-0.497E+05
 Surface x-   Fracture NNW2
 Surface x+   Fracture NNW2
 Surface y-   Fracture NNW2
 Surface y+   Fracture NNW2
 Step   19   x =  0.105E+04   y =  0.127E+04   z =   890.
Darcy-time for particle=    1.00927E-01
 Step   20   x =  0.104E+04   y =  0.127E+04   z =   890.
Darcy-time for particle=   0.105502
 Step   21   x =  0.104E+04   y =  0.127E+04   z =   890.
Darcy-time for particle=   0.110005

 i =  33   j =  27   k =  29
Press.  -0.571E+05-0.612E+05-0.533E+05-0.564E+05-0.574E+05-0.599E+05-0.553E+05
 Surface x-   Fracture NNW2
 Surface x+   Fracture NNW2
 Surface y-   Fracture NNW2
 Surface y+   Fracture NNW2
 Step   22   x =  0.103E+04   y =  0.127E+04   z =   890.
Darcy-time for particle=   0.114421
 Step   23   x =  0.103E+04   y =  0.127E+04   z =   890.
Darcy-time for particle=   0.118765
 Step   24   x =  0.102E+04   y =  0.127E+04   z =   890.
Darcy-time for particle=   0.123039
 Step   25   x =  0.102E+04   y =  0.127E+04   z =   890.
Darcy-time for particle=   0.127247

 i =  32   j =  27   k =  29
Press.  -0.612E+05-0.655E+05-0.571E+05-0.599E+05-0.620E+05-0.614E+05-0.591E+05
 Surface x-   Fracture NNW2
 Surface x+   Fracture NNW2
 Surface y-   Fracture NNW2
 Surface y+   Fracture NNW2
 Step   26   x =  0.101E+04   y =  0.127E+04   z =   890.
Darcy-time for particle=   0.131340
 Step   27   x =  0.101E+04   y =  0.127E+04   z =   890.
Darcy-time for particle=   0.135375
 Step   28   x =  0.100E+04   y =  0.127E+04   z =   890.
Darcy-time for particle=   0.139353
 Step   29   x =   998.       y =  0.128E+04   z =   890.
Darcy-time for particle=   0.143276

 i =  31   j =  27   k =  29
Press.  -0.655E+05-0.701E+05-0.612E+05-0.635E+05-0.672E+05-0.640E+05-0.615E+05
 Surface x-   Fracture NNW2
 Surface x+   Fracture NNW2
 Surface y-   Fracture NNW2
 Surface y+   Fracture NNW2
 Step   30   x =   993.       y =  0.128E+04   z =   890.
Darcy-time for particle=   0.147056
 Step   31   x =   988.       y =  0.128E+04   z =   890.
Darcy-time for particle=   0.150802
```

```
 Step   32   x =   983.       y =  0.128E+04   z =   890.
Darcy-time for particle=   0.154514

 i =  31   j =  28   k =  29
Press.  -0.672E+05-0.729E+05-0.620E+05-0.655E+05-0.682E+05-0.665E+05-0.626E+05
 Surface x-   Fracture NNW2
 Surface x+   Fracture NNW2
 Surface y-   Fracture NNW2
 Surface y+   Fracture NNW2
 Step   33   x =   978.       y =  0.128E+04   z =   890.
Darcy-time for particle=   0.157612

 i =  30   j =  28   k =  29
Press.  -0.729E+05-0.791E+05-0.672E+05-0.701E+05-0.751E+05-0.693E+05-0.645E+05
 Surface x-   Fracture NNW2
 Surface x+   Fracture NNW2
 Surface y-   Fracture NNW2
 Surface y+   Fracture NNW2
 Step   34   x =   973.       y =  0.128E+04   z =   890.
Darcy-time for particle=   0.160549
 Step   35   x =   969.       y =  0.128E+04   z =   890.
Darcy-time for particle=   0.163448
 Step   36   x =   964.       y =  0.128E+04   z =   890.
Darcy-time for particle=   0.166307
 Step   37   x =   959.       y =  0.129E+04   z =   890.
Darcy-time for particle=   0.169129

 i =  29   j =  28   k =  29
Press.  -0.791E+05-0.855E+05-0.729E+05-0.747E+05-0.833E+05-0.770E+05-0.686E+05
 Surface x-   Fracture NNW2
 Surface x+   Fracture NNW2
 Surface y-   Fracture NNW2
 Surface y+   Fracture NNW2
 Step   38   x =   954.       y =  0.129E+04   z =   890.
Darcy-time for particle=   0.171748
 Step   39   x =   950.       y =  0.129E+04   z =   890.
Darcy-time for particle=   0.174360
 Step   40   x =   945.       y =  0.129E+04   z =   890.
Darcy-time for particle=   0.176965
 Step   41   x =   941.       y =  0.129E+04   z =   890.
Darcy-time for particle=   0.179561

 i =  28   j =  28   k =  29
Press.  -0.855E+05-0.911E+05-0.791E+05-0.791E+05-0.928E+05-0.849E+05-0.714E+05
 Surface x-   Fracture NNW2
 Surface x+   Fracture NNW2
 Surface y-   Fracture NNW2
 Surface y+   Fracture NNW2
 Step   42   x =   936.       y =  0.130E+04   z =   890.
Darcy-time for particle=   0.181804
 Step   43   x =   933.       y =  0.130E+04   z =   890.
Darcy-time for particle=   0.184054

 i =  28   j =  29   k =  29
Press.  -0.928E+05-0.103E+06-0.833E+05-0.855E+05-0.764E+05-0.100E+06-0.680E+05
 Surface x-   Fracture NNW2
 Surface x+   Fracture NNW2
 Surface y-   Fracture NNW2
 Surface z-   Fracture NNW2
 Step   44   x =   929.       y =  0.130E+04   z =   890.
Darcy-time for particle=   0.187469
 Step   45   x =   929.       y =  0.131E+04   z =   887.
Darcy-time for particle=   0.191238
 Step   46   x =   929.       y =  0.131E+04   z =   884.
```

```
Darcy-time for particle=   0.194869

 i =  28   j =  29   k =  28
Press.  -0.100E+06-0.116E+06-0.874E+05-0.849E+05-0.104E+06-0.631E+05-0.928E+05
 Surface x-   Fracture NNW2
 Surface x+   Fracture NNW2
 Surface y+   Fracture NNW2
 Surface z+   Fracture NNW2
 Step   47   x =   928.       y =  0.131E+04   z =   880.
Darcy-time for particle=   0.196159
 Step   48   x =   924.       y =  0.131E+04   z =   878.
Darcy-time for particle=   0.197419

 i =  27   j =  29   k =  28
Press.  -0.116E+06-0.129E+06-0.100E+06-0.100E+06-0.130E+06-0.848E+05-0.103E+06
 Surface x-   Fracture NNW2
 Surface x+   Fracture NNW2
 Surface y+   Fracture NNW2
 Surface z+   Fracture NNW2
 Step   49   x =   919.       y =  0.131E+04   z =   876.
Darcy-time for particle=   0.198479
 Step   50   x =   915.       y =  0.132E+04   z =   874.
Darcy-time for particle=   0.199539
 Step   51   x =   911.       y =  0.132E+04   z =   872.
Darcy-time for particle=   0.200583

 i =  27   j =  30   k =  28
Press.  -0.130E+06-0.180E+06-0.104E+06-0.116E+06-0.112E+06-0.105E+06-0.918E+05
 Surface x-   Fracture NNW2
 Surface x+   Fracture NNW2
 Surface y-   Fracture NNW2
 Surface y+   Fracture NNW2
 Step   52   x =   908.       y =  0.132E+04   z =   870.
Darcy-time for particle=   0.201037

 i =  26   j =  30   k =  28
Press.  -0.180E+06-0.128E+06-0.130E+06-0.129E+06-0.128E+06-0.112E+06-0.995E+05
 Surface x-   Fracture NNW2
 Surface x+   Fracture NNW2
 Surface y-   Fracture NNW2
 Surface y+   Fracture NNW2
 Step   53   x =   903.       y =  0.132E+04   z =   870.
Darcy-time for particle=   0.201423
 Step   54   x =   898.       y =  0.133E+04   z =   870.
Darcy-time for particle=   0.202159
 Step   55   x =   894.       y =  0.133E+04   z =   870.
Darcy-time for particle=   0.207627
 Step   56   x =   893.       y =  0.133E+04   z =   871.
Darcy-time for particle=   0.208747
 Step   57   x =   895.       y =  0.133E+04   z =   871.
Darcy-time for particle=   0.213559
 Step   58   x =   891.       y =  0.133E+04   z =   871.
Darcy-time for particle=   0.214591
 Step   59   x =   895.       y =  0.133E+04   z =   871.
Darcy-time for particle=   0.218458
 Step   60   x =   890.       y =  0.133E+04   z =   871.
```

APPENDIX G.

Table of trajectory for injection in KAS08, section M1.

```
Press.       p         px-       px+       py-       py+       pz-       pz+

 i =  23   j =  39   k =  25
Press.  -0.129E+05-0.118E+05-0.136E+05-0.155E+05-0.763E+04-0.106E+05-0.110E+05
 Surface x-   Fracture NNW2
 Surface x+   Fracture NNW2
 Surface y-   Fracture NNW2
 Surface z-   Fracture NNW2
 Step    0   x =   840.       y =  0.151E+04   z =   810.
Darcy-time for particle=    1.42172E-02
 Step    1   x =   840.       y =  0.151E+04   z =   813.
Darcy-time for particle=    2.67757E-02
 Step    2   x =   840.       y =  0.150E+04   z =   815.
Darcy-time for particle=    3.67436E-02

 i =  23   j =  38   k =  25
Press.  -0.155E+05-0.143E+05-0.162E+05-0.182E+05-0.129E+05-0.136E+05-0.137E+05
 Surface x-   Fracture NNW2
 Surface x+   Fracture NE1
 Surface x+   Fracture NNW2
 Surface y-   Fracture NE1
 Surface y-   Fracture NNW2
 Surface y+   Fracture NNW2
 Surface z+   Fracture NE1
 Step    3   x =   840.       y =  0.150E+04   z =   816.
Darcy-time for particle=    4.53554E-02
 Step    4   x =   840.       y =  0.149E+04   z =   816.
Darcy-time for particle=    5.30369E-02
 Step    5   x =   840.       y =  0.149E+04   z =   816.
Darcy-time for particle=    5.99682E-02
 Step    6   x =   840.       y =  0.148E+04   z =   815.
Darcy-time for particle=    6.62819E-02

 i =  23   j =  37   k =  25
Press.  -0.182E+05-0.170E+05-0.203E+05-0.240E+05-0.155E+05-0.151E+05-0.152E+05
 Surface x-   Fracture NE1
 Surface x-   Fracture NNW2
 Surface x+   Fracture NE1
 Surface x+   Fracture NNW2
 Surface y-   Fracture NNW2
 Surface y+   Fracture NE1
 Surface y+   Fracture NNW2
 Surface z-   Fracture NE1
 Surface z+   Fracture NE1
 Step    7   x =   840.       y =  0.148E+04   z =   815.
Darcy-time for particle=    7.18089E-02
 Step    8   x =   841.       y =  0.147E+04   z =   814.
Darcy-time for particle=    7.68698E-02
 Step    9   x =   842.       y =  0.147E+04   z =   814.
Darcy-time for particle=    8.15339E-02
 Step   10   x =   844.       y =  0.146E+04   z =   814.
Darcy-time for particle=    8.58572E-02

 i =  23   j =  36   k =  25
Press.  -0.240E+05-0.221E+05-0.261E+05-0.292E+05-0.182E+05-0.195E+05-0.297E+05
 Surface x-   Fracture NNW2
 Surface x+   Fracture NNW2
 Surface y+   Fracture NNW2
 Surface z+   Fracture NNW2
 Step   11   x =   845.       y =  0.146E+04   z =   814.
Darcy-time for particle=    8.97452E-02
 Step   12   x =   845.       y =  0.145E+04   z =   817.
Darcy-time for particle=    9.37538E-02
```

```
 i =  23   j =  36   k =  26
Press.  -0.297E+05-0.273E+05-0.319E+05-0.358E+05-0.152E+05-0.240E+05-0.201E+05
 Surface x-   Fracture NNW2
 Surface x+   Fracture NNW2
 Surface y-   Fracture NNW2
 Surface z-   Fracture NNW2
 Step   13   x =   845.       y =  0.145E+04   z =   821.
Darcy-time for particle=    9.75606E-02
 Step   14   x =   846.       y =  0.145E+04   z =   825.
Darcy-time for particle=    1.01761E-01
 Step   15   x =   847.       y =  0.144E+04   z =   829.
Darcy-time for particle=   0.105968

 i =  24   j =  36   k =  26
Press.  -0.319E+05-0.297E+05-0.338E+05-0.384E+05-0.186E+05-0.261E+05-0.230E+05
 Surface x-   Fracture NNW2
 Surface x+   Fracture NNW2
 Surface y-   Fracture NNW2
 Surface z-   Fracture NNW2
 Step   16   x =   849.       y =  0.144E+04   z =   831.
Darcy-time for particle=   0.109579

 i =  24   j =  35   k =  26
Press.  -0.384E+05-0.358E+05-0.405E+05-0.457E+05-0.319E+05-0.348E+05-0.371E+05
 Surface x-   Fracture NNW2
 Surface x+   Fracture NNW2
 Surface y-   Fracture NNW2
 Surface y+   Fracture NNW2
 Step   17   x =   850.       y =  0.144E+04   z =   833.
Darcy-time for particle=   0.113144
 Step   18   x =   851.       y =  0.143E+04   z =   833.
Darcy-time for particle=   0.116620
 Step   19   x =   852.       y =  0.143E+04   z =   833.
Darcy-time for particle=   0.120011
 Step   20   x =   854.       y =  0.142E+04   z =   833.
Darcy-time for particle=   0.123317

 i =  24   j =  34   k =  26
Press.  -0.457E+05-0.426E+05-0.483E+05-0.601E+05-0.384E+05-0.373E+05-0.538E+05
 Surface x-   Fracture NNW2
 Surface x+   Fracture NNW2
 Surface y+   Fracture NNW2
 Surface z+   Fracture NNW2
 Step   21   x =   855.       y =  0.142E+04   z =   833.
Darcy-time for particle=   0.126254
 Step   22   x =   856.       y =  0.141E+04   z =   836.
Darcy-time for particle=   0.129196

 i =  24   j =  34   k =  27
Press.  -0.538E+05-0.498E+05-0.571E+05-0.622E+05-0.371E+05-0.457E+05-0.457E+05
 Surface x-   Fracture NNW2
 Surface x+   Fracture NNW2
 Surface y-   Fracture NNW2
 Surface z-   Fracture NNW2
 Step   23   x =   857.       y =  0.141E+04   z =   840.
Darcy-time for particle=   0.131960
 Step   24   x =   857.       y =  0.141E+04   z =   845.
Darcy-time for particle=   0.135070
 Step   25   x =   858.       y =  0.141E+04   z =   849.
Darcy-time for particle=   0.138231
 Step   26   x =   859.       y =  0.140E+04   z =   852.
Darcy-time for particle=   0.141074

 i =  24   j =  33   k =  27
```

```
Press.  -0.622E+05-0.572E+05-0.664E+05-0.720E+05-0.538E+05-0.601E+05-0.559E+05
 Surface x-   Fracture NNW2
 Surface x+   Fracture NNW2
 Surface y-   Fracture NNW2
 Surface y+   Fracture NNW2
 Step   27   x =   859.       y =  0.140E+04   z =   854.
Darcy-time for particle=   0.143647
 Step   28   x =   861.       y =  0.139E+04   z =   854.
Darcy-time for particle=   0.146161
 Step   29   x =   863.       y =  0.139E+04   z =   854.
Darcy-time for particle=   0.148616
 Step   30   x =   865.       y =  0.138E+04   z =   854.
Darcy-time for particle=   0.151011

 i =  25   j =  32   k =  27
Press.  -0.783E+05-0.720E+05-0.817E+05-0.939E+05-0.664E+05-0.576E+05-0.757E+05
 Surface x-   Fracture NNW2
 Surface x+   Fracture NNW2
 Surface y-   Fracture NNW2
 Surface y+   Fracture NNW2
 Step   31   x =   867.       y =  0.138E+04   z =   854.
Darcy-time for particle=   0.152818
 Step   32   x =   869.       y =  0.137E+04   z =   854.
Darcy-time for particle=   0.154550
 Step   33   x =   871.       y =  0.137E+04   z =   854.
Darcy-time for particle=   0.156208
 Step   34   x =   873.       y =  0.136E+04   z =   854.
Darcy-time for particle=   0.157791

 i =  25   j =  31   k =  27
Press.  -0.939E+05-0.829E+05-0.102E+06-0.897E+05-0.783E+05-0.595E+05-0.111E+06
 Surface x-   Fracture NNW2
 Surface x+   Fracture NNW2
 Surface y+   Fracture NNW2
 Surface z+   Fracture NNW2
 Step   35   x =   874.       y =  0.136E+04   z =   854.
Darcy-time for particle=   0.159058
 Step   36   x =   875.       y =  0.136E+04   z =   856.
Darcy-time for particle=   0.160363

 i =  25   j =  31   k =  28
Press.  -0.111E+06-0.935E+05-0.128E+06-0.128E+06-0.757E+05-0.939E+05-0.884E+05
 Surface x-   Fracture NNW2
 Surface x+   Fracture NNW2
 Surface y-   Fracture NNW2
 Surface z-   Fracture NNW2
 Step   37   x =   876.       y =  0.135E+04   z =   860.
Darcy-time for particle=   0.161501
 Step   38   x =   879.       y =  0.135E+04   z =   864.
Darcy-time for particle=   0.162754
 Step   39   x =   882.       y =  0.135E+04   z =   868.
Darcy-time for particle=   0.164082

 i =  26   j =  31   k =  28
Press.  -0.128E+06-0.111E+06-0.112E+06-0.180E+06-0.796E+05-0.102E+06-0.803E+05
 Surface x-   Fracture NNW2
 Surface x+   Fracture NNW2
 Surface y-   Fracture NNW2
 Surface z-   Fracture NNW2
 Step   40   x =   885.       y =  0.135E+04   z =   870.
Darcy-time for particle=   0.164706
 Step   41   x =   887.       y =  0.134E+04   z =   872.
```

APPENDIX H.

Table of trajectory for injection in KAS11, section CE.

```
Press.       p         px-       px+       py-       py+       pz-       pz+

 i =  41   j =  38   k =  11
Press.  -0.101E+04 -922.    -0.117E+04-0.164E+04 -344.      137.    -0.213E+04
 Surface x-   Fracture EW5
 Surface x+   Fracture EW5
 Surface y-   Fracture EW5
 Surface y+   Fracture EW5
 Surface z-   Fracture EW5
 Surface z+   Fracture EW5
 Step    0   x =  0.118E+04   y =  0.149E+04   z =   500.
Darcy-time for particle=   0.139916
 Step    1   x =  0.118E+04   y =  0.149E+04   z =   502.
Darcy-time for particle=   0.281360
 Step    2   x =  0.118E+04   y =  0.148E+04   z =   504.
Darcy-time for particle=   0.423074

 i =  41   j =  37   k =  11
Press.  -0.164E+04-0.159E+04-0.144E+04-0.221E+04-0.101E+04 -334.    -0.272E+04
 Surface x-   Fracture EW5
 Surface y-   Fracture EW5
 Surface y+   Fracture EW5
 Surface z-   Fracture EW5
 Step    3   x =  0.117E+04   y =  0.148E+04   z =   506.
Darcy-time for particle=   0.547128

 i =  40   j =  37   k =  11
Press.  -0.159E+04-0.157E+04-0.164E+04-0.220E+04 -922.     -196.    -0.304E+04
 Surface x+   Fracture EW5
 Surface y-   Fracture EW5
 Surface y+   Fracture EW5
 Surface z+   Fracture EW5
 Step    4   x =  0.117E+04   y =  0.148E+04   z =   508.
Darcy-time for particle=   0.648176
 Step    5   x =  0.117E+04   y =  0.147E+04   z =   510.
Darcy-time for particle=   0.754222
 Step    6   x =  0.116E+04   y =  0.147E+04   z =   514.
Darcy-time for particle=   0.860722
 Step    7   x =  0.116E+04   y =  0.147E+04   z =   518.
Darcy-time for particle=   0.963556

 i =  40   j =  37   k =  12
Press.  -0.304E+04-0.326E+04-0.272E+04-0.389E+04-0.211E+04-0.159E+04-0.450E+04
 Surface x-   Fracture EW5
 Surface y-   Fracture EW5
 Surface y+   Fracture EW5
 Surface z-   Fracture EW5
 Step    8   x =  0.116E+04   y =  0.147E+04   z =   522.
Darcy-time for particle=    1.06149
 Step    9   x =  0.116E+04   y =  0.147E+04   z =   526.
Darcy-time for particle=    1.15868
 Step   10   x =  0.115E+04   y =  0.147E+04   z =   529.
Darcy-time for particle=    1.25048

 i =  39   j =  37   k =  12
Press.  -0.326E+04-0.310E+04-0.304E+04-0.416E+04-0.231E+04-0.157E+04-0.447E+04
 Surface x+   Fracture EW5
 Surface y-   Fracture EW5
 Surface y+   Fracture EW5
 Surface z+   Fracture EW5
 Step   11   x =  0.115E+04   y =  0.146E+04   z =   532.
Darcy-time for particle=    1.33075
 Step   12   x =  0.114E+04   y =  0.146E+04   z =   533.
Darcy-time for particle=    1.41373
```

```
 i =  39   j =  36   k =  12
Press.  -0.416E+04-0.459E+04-0.389E+04-0.499E+04-0.326E+04-0.228E+04-0.565E+04
 Surface x-   Fracture EW5
 Surface x+   Fracture EW5
 Surface y-   Fracture EW5
 Surface y+   Fracture EW5
 Surface z-   Fracture EW5
 Surface z+   Fracture EW5
 Step   13   x =  0.114E+04   y =  0.146E+04   z =   534.
Darcy-time for particle=    1.49710
 Step   14   x =  0.114E+04   y =  0.145E+04   z =   537.
Darcy-time for particle=    1.58364
 Step   15   x =  0.114E+04   y =  0.145E+04   z =   539.
Darcy-time for particle=    1.67071
 Step   16   x =  0.113E+04   y =  0.145E+04   z =   541.
Darcy-time for particle=    1.75490
 Step   17   x =  0.113E+04   y =  0.144E+04   z =   543.
Darcy-time for particle=    1.83326

 i =  38   j =  36   k =  12
Press.  -0.459E+04-0.382E+04-0.416E+04-0.543E+04-0.310E+04-0.211E+04-0.618E+04
 Surface x+   Fracture EW5
 Surface y-   Fracture EW5
 Surface z+   Fracture EW5
 Step   18   x =  0.113E+04   y =  0.144E+04   z =   545.
Darcy-time for particle=    1.91605
 Step   19   x =  0.112E+04   y =  0.144E+04   z =   548.
Darcy-time for particle=    2.00187

 i =  38   j =  35   k =  12
Press.  -0.543E+04-0.607E+04-0.499E+04-0.614E+04-0.459E+04-0.253E+04-0.742E+04
 Surface x-   Fracture EW5
 Surface x+   Fracture EW5
 Surface y-   Fracture EW5
 Surface y+   Fracture EW5
 Surface z+   Fracture EW5
 Step   20   x =  0.112E+04   y =  0.144E+04   z =   551.
Darcy-time for particle=    2.07701
 Step   21   x =  0.112E+04   y =  0.144E+04   z =   556.
Darcy-time for particle=    2.14766
 Step   22   x =  0.112E+04   y =  0.143E+04   z =   560.
Darcy-time for particle=    2.21300

 i =  38   j =  35   k =  13
Press.  -0.742E+04-0.838E+04-0.946E+04-0.120E+05-0.618E+04-0.543E+04-0.123E+05
 Surface x-   Fracture EW5
 Surface y+   Fracture EW5
 Surface z-   Fracture EW5
 Step   23   x =  0.111E+04   y =  0.143E+04   z =   564.
Darcy-time for particle=    2.25340
 Step   24   x =  0.111E+04   y =  0.143E+04   z =   567.
Darcy-time for particle=    2.28812

 i =  37   j =  35   k =  13
Press.  -0.838E+04-0.659E+04-0.742E+04-0.943E+04-0.703E+04-0.607E+04-0.992E+04
 Surface x+   Fracture EW5
 Surface y-   Fracture EW5
 Surface y+   Fracture EW5
 Surface z-   Fracture EW5
 Surface z+   Fracture EW5
 Step   25   x =  0.111E+04   y =  0.143E+04   z =   568.
Darcy-time for particle=    2.33089
 Step   26   x =  0.110E+04   y =  0.143E+04   z =   570.
```

```
Darcy-time for particle=    2.38255
 Step   27   x =  0.110E+04   y =  0.143E+04   z =   572.
Darcy-time for particle=    2.43929
 Step   28   x =  0.109E+04   y =  0.142E+04   z =   576.
Darcy-time for particle=    2.49289
 Step   29   x =  0.109E+04   y =  0.142E+04   z =   580.
Darcy-time for particle=    2.53966

 i =  37   j =  34   k =  14
Press.  -0.114E+05-0.131E+05-0.192E+05-0.134E+05-0.992E+04-0.943E+04-0.196E+05
 Surface x-   Fracture EW5
 Surface y+   Fracture EW5
 Surface z-   Fracture EW5
 Step   30   x =  0.109E+04   y =  0.142E+04   z =   584.
Darcy-time for particle=    2.56931

 i =  36   j =  34   k =  14
Press.  -0.131E+05-0.972E+04-0.114E+05-0.138E+05-0.118E+05-0.107E+05-0.159E+05
 Surface x+   Fracture EW5
 Surface y-   Fracture EW5
 Surface y+   Fracture EW5
 Surface z-   Fracture EW5
 Surface z+   Fracture EW5
 Step   31   x =  0.109E+04   y =  0.142E+04   z =   586.
Darcy-time for particle=    2.60138
 Step   32   x =  0.108E+04   y =  0.142E+04   z =   588.
Darcy-time for particle=    2.63845
 Step   33   x =  0.108E+04   y =  0.142E+04   z =   591.
Darcy-time for particle=    2.67726
 Step   34   x =  0.108E+04   y =  0.141E+04   z =   595.
Darcy-time for particle=    2.71282
 Step   35   x =  0.107E+04   y =  0.141E+04   z =   600.
Darcy-time for particle=    2.74328

 i =  36   j =  34   k =  15
Press.  -0.159E+05-0.180E+05-0.196E+05-0.168E+05-0.142E+05-0.131E+05-0.195E+05
 Surface x-   Fracture EW5
 Surface y-   Fracture EW5
 Surface y+   Fracture EW5
 Surface z-   Fracture EW5
 Surface z+   Fracture EW5
 Step   36   x =  0.107E+04   y =  0.141E+04   z =   605.
Darcy-time for particle=    2.77065
 Step   37   x =  0.107E+04   y =  0.141E+04   z =   609.
Darcy-time for particle=    2.79854

 i =  35   j =  34   k =  15
Press.  -0.180E+05-0.201E+05-0.159E+05-0.184E+05-0.142E+05-0.972E+04-0.218E+05
 Surface x+   Fracture EW5
 Surface y-   Fracture EW5
 Surface z+   Fracture EW5
 Step   38   x =  0.107E+04   y =  0.141E+04   z =   613.
Darcy-time for particle=    2.85010
 Step   39   x =  0.107E+04   y =  0.141E+04   z =   616.
Darcy-time for particle=    2.90600
 Step   40   x =  0.106E+04   y =  0.141E+04   z =   619.
Darcy-time for particle=    2.96083

 i =  35   j =  34   k =  16
Press.  -0.218E+05-0.230E+05-0.195E+05-0.220E+05-0.211E+05-0.180E+05-0.260E+05
 Surface x-   Fracture EW3
 Surface x+   Fracture EW3
 Surface x+   Fracture EW5
 Surface y-   Fracture EW3
```

```
 Surface y-   Fracture EW5
 Surface y+   Fracture EW5
 Surface z-   Fracture EW5
 Surface z+   Fracture EW3
 Surface z+   Fracture EW5
 Step   41   x =  0.106E+04   y =  0.141E+04   z =   623.
Darcy-time for particle=    2.99735
 Step   42   x =  0.106E+04   y =  0.141E+04   z =   628.
Darcy-time for particle=    3.02849
 Step   43   x =  0.106E+04   y =  0.141E+04   z =   632.
Darcy-time for particle=    3.05356
 Step   44   x =  0.105E+04   y =  0.141E+04   z =   637.
Darcy-time for particle=    3.07412

 i =  35   j =  34   k =  17
Press.  -0.260E+05-0.283E+05-0.269E+05-0.260E+05-0.257E+05-0.218E+05-0.308E+05
 Surface x-   Fracture EW3
 Surface x-   Fracture EW5
 Surface x+   Fracture EW3
 Surface y-   Fracture EW5
 Surface y+   Fracture EW3
 Surface y+   Fracture EW5
 Surface z-   Fracture EW3
 Surface z-   Fracture EW5
 Surface z+   Fracture EW5
 Step   45   x =  0.105E+04   y =  0.141E+04   z =   642.
Darcy-time for particle=    3.09163

 i =  34   j =  34   k =  17
Press.  -0.283E+05-0.241E+05-0.260E+05-0.279E+05-0.286E+05-0.230E+05-0.334E+05
 Surface x-   Fracture EW3
 Surface x+   Fracture EW3
 Surface x+   Fracture EW5
 Surface y-   Fracture EW5
 Surface y+   Fracture EW3
 Surface z-   Fracture EW3
 Surface z+   Fracture EW5
 Step   46   x =  0.105E+04   y =  0.141E+04   z =   647.
Darcy-time for particle=    3.12118
 Step   47   x =  0.105E+04   y =  0.141E+04   z =   649.
Darcy-time for particle=    3.15578
 Step   48   x =  0.104E+04   y =  0.141E+04   z =   652.
Darcy-time for particle=    3.19150
 Step   49   x =  0.104E+04   y =  0.141E+04   z =   656.
Darcy-time for particle=    3.22254

 i =  34   j =  34   k =  18
Press.  -0.334E+05-0.323E+05-0.308E+05-0.326E+05-0.337E+05-0.283E+05-0.389E+05
 Surface x+   Fracture EW5
 Surface y-   Fracture EW5
 Surface y+   Fracture EW5
 Surface z-   Fracture EW5
 Surface z+   Fracture EW5
 Step   50   x =  0.104E+04   y =  0.141E+04   z =   660.
Darcy-time for particle=    3.24775
 Step   51   x =  0.104E+04   y =  0.141E+04   z =   665.
Darcy-time for particle=    3.26912
 Step   52   x =  0.104E+04   y =  0.141E+04   z =   670.
Darcy-time for particle=    3.28758
 Step   53   x =  0.104E+04   y =  0.141E+04   z =   675.
Darcy-time for particle=    3.30381
 Step   54   x =  0.104E+04   y =  0.141E+04   z =   680.
Darcy-time for particle=    3.31827
```

```
 i =  34   j =  34   k =  19
Press.  -0.389E+05-0.412E+05-0.584E+05-0.378E+05-0.399E+05-0.334E+05-0.451E+05
 Surface x-   Fracture EW5
 Surface y-   Fracture EW5
 Surface y+   Fracture EW5
 Surface z-   Fracture EW5
 Surface z+   Fracture EW5
 Step   55   x =  0.104E+04   y =  0.141E+04   z =   685.
Darcy-time for particle=    3.33326

 i =  33   j =  34   k =  19
Press.  -0.412E+05-0.379E+05-0.389E+05-0.397E+05-0.377E+05-0.323E+05-0.473E+05
 Surface x+   Fracture EW5
 Surface y-   Fracture EW5
 Surface z+   Fracture EW5
 Step   56   x =  0.103E+04   y =  0.141E+04   z =   689.
Darcy-time for particle=    3.35176
 Step   57   x =  0.103E+04   y =  0.141E+04   z =   692.
Darcy-time for particle=    3.37088
 Step   58   x =  0.103E+04   y =  0.141E+04   z =   695.
Darcy-time for particle=    3.38823
 Step   59   x =  0.102E+04   y =  0.141E+04   z =   700.
Darcy-time for particle=    3.40278

 i =  33   j =  34   k =  20
Press.  -0.473E+05-0.490E+05-0.451E+05-0.453E+05-0.492E+05-0.412E+05-0.536E+05
 Surface x-   Fracture EW5
 Surface x+   Fracture EW5
 Surface y-   Fracture EW5
 Surface y+   Fracture EW5
 Surface z-   Fracture EW5
 Surface z+   Fracture EW5
 Step   60   x =  0.102E+04   y =  0.141E+04   z =   705.
Darcy-time for particle=    3.41715
 Step   61   x =  0.102E+04   y =  0.142E+04   z =   709.
Darcy-time for particle=    3.43140
 Step   62   x =  0.102E+04   y =  0.142E+04   z =   714.
Darcy-time for particle=    3.44555
 Step   63   x =  0.102E+04   y =  0.142E+04   z =   719.
Darcy-time for particle=    3.45958

 i =  33   j =  34   k =  21
Press.  -0.536E+05-0.554E+05-0.750E+05-0.686E+05-0.558E+05-0.473E+05-0.859E+05
 Surface x-   Fracture EW5
 Surface y+   Fracture EW5
 Surface z-   Fracture EW5
 Step   64   x =  0.102E+04   y =  0.142E+04   z =   724.
Darcy-time for particle=    3.47481

 i =  33   j =  35   k =  21
Press.  -0.558E+05-0.559E+05-0.546E+05-0.536E+05-0.546E+05-0.492E+05-0.659E+05
 Surface x-   Fracture EW5
 Surface x+   Fracture EW5
 Surface y-   Fracture EW5
 Surface y+   Fracture EW5
 Surface z-   Fracture EW5
 Surface z+   Fracture EW5
 Step   65   x =  0.102E+04   y =  0.142E+04   z =   728.
Darcy-time for particle=    3.48596
 Step   66   x =  0.102E+04   y =  0.142E+04   z =   733.
Darcy-time fcr particle=    3.49613
 Step   67   x =  0.102E+04   y =  0.142E+04   z =   738.
Darcy-time for particle=    3.50545
```

```
 i =  33   j =  35   k =  22
Press.  -0.659E+05-0.583E+05-0.987E+05-0.859E+05-0.559E+05-0.558E+05-0.781E+05
 Surface x-   Fracture EW5
 Surface x-   Fracture NNW1
 Surface x+   Fracture NNW1
 Surface y-   Fracture NNW1
 Surface y+   Fracture EW5
 Surface y+   Fracture NNW1
 Surface z-   Fracture EW5
 Step   68   x =  0.102E+04   y =  0.142E+04   z =   743.
Darcy-time for particle=    3.50944
 Step   69   x =  0.102E+04   y =  0.142E+04   z =   745.
Darcy-time for particle=    3.51328

 i =  33   j =  34   k =  22
Press.  -0.859E+05-0.615E+05-0.119E+06-0.950E+05-0.659E+05-0.536E+05-0.957E+05
 Surface x-   Fracture NNW1
 Surface x+   Fracture NNW1
 Surface y-   Fracture NNW1
 Surface y+   Fracture NNW1
 Step   70   x =  0.102E+04   y =  0.142E+04   z =   746.
Darcy-time for particle=    3.51679
 Step   71   x =  0.103E+04   y =  0.142E+04   z =   746.
Darcy-time for particle=    3.52017

 i =  34   j =  34   k =  22
Press.  -0.119E+06-0.859E+05-0.160E+06-0.129E+06-0.987E+05-0.750E+05-0.114E+06
 Surface x-   Fracture NNW1
 Surface x+   Fracture NNW1
 Surface y-   Fracture NNW1
 Surface y+   Fracture NNW1
 Step   72   x =  0.103E+04   y =  0.141E+04   z =   746.
Darcy-time for particle=    3.52340
 Step   73   x =  0.104E+04   y =  0.141E+04   z =   746.
Darcy-time for particle=    3.52650
 Step   74   x =  0.104E+04   y =  0.141E+04   z =   746.
Darcy-time for particle=    3.52946
 Step   75   x =  0.105E+04   y =  0.141E+04   z =   746.
Darcy-time for particle=    3.53229

 i =  35   j =  34   k =  22
Press.  -0.160E+06-0.119E+06-0.212E+06-0.175E+06-0.136E+06-0.920E+05-0.132E+06
 Surface x-   Fracture NNW1
 Surface x+   Fracture NNW1
 Surface y-   Fracture NNW1
 Surface y+   Fracture NNW1
 Step   76   x =  0.105E+04   y =  0.141E+04   z =   746.
Darcy-time for particle=    3.53492
 Step   77   x =  0.106E+04   y =  0.140E+04   z =   746.
Darcy-time for particle=    3.53745
 Step   78   x =  0.106E+04   y =  0.140E+04   z =   746.
Darcy-time for particle=    3.53989
 Step   79   x =  0.107E+04   y =  0.140E+04   z =   746.
Darcy-time for particle=    3.54222

 i =  36   j =  34   k =  22
Press.  -0.212E+06-0.160E+06-0.268E+06-0.249E+06-0.174E+06-0.111E+06-0.162E+06
 Surface x-   Fracture NNW1
 Surface x+   Fracture NNW1
 Surface y-   Fracture NNW1
 Surface y+   Fracture NNW1
 Step   80   x =  0.107E+04   y =  0.140E+04   z =   746.
Darcy-time for particle=    3.54418
```

```
 i =  36   j =  33   k =  22
Press.  -0.249E+06-0.175E+06-0.422E+06-0.217E+06-0.212E+06-0.159E+06-0.223E+06
 Surface x-   Fracture NNW1
 Surface x+   Fracture NNW1
 Surface y+   Fracture NNW1
 Surface z+   Fracture NNW1
 Step   81   x =  0.108E+04   y =  0.140E+04   z =   746.
Darcy-time for particle=    3.54600
 Step   82   x =  0.108E+04   y =  0.140E+04   z =   746.
Darcy-time for particle=    3.54758
 Step   83   x =  0.108E+04   y =  0.139E+04   z =   745.
Darcy-time for particle=    3.54895
 Step   84   x =  0.109E+04   y =  0.139E+04   z =   745.
```

APPENDIX I.

Table of trajectory for injection in KAS12, section DD.

```
Press.       p        px-       px+       py-       py+       pz-       pz+

 i =  35   j =  23   k =  32
Press.  -0.427E+05-0.435E+05-0.419E+05-0.471E+05-0.366E+05-0.491E+05-0.365E+05
 Surface x-   Fracture NE2
 Surface x+   Fracture NE2
 Surface z-   Fracture NE2
 Surface z+   Fracture NE2
 Step    0   x =  0.106E+04   y =  0.119E+04   z =   950.
Darcy-time for particle=    7.32155E-02
 Step    1   x =  0.106E+04   y =  0.119E+04   z =   945.
Darcy-time for particle=   0.146241
 Step    2   x =  0.106E+04   y =  0.119E+04   z =   940.
Darcy-time for particle=   0.219078

 i =  35   j =  23   k =  31
Press.  -0.491E+05-0.505E+05-0.477E+05-0.490E+05-0.450E+05-0.495E+05-0.427E+05
 Surface x-   Fracture NE2
 Surface x-   Fracture NNW2
 Surface x+   Fracture NE2
 Surface x+   Fracture NNW2
 Surface y-   Fracture NNW2
 Surface z-   Fracture NE2
 Surface z-   Fracture NNW2
 Surface z+   Fracture NE2
 Step    3   x =  0.106E+04   y =  0.119E+04   z =   936.
Darcy-time for particle=   0.230189

 i =  34   j =  23   k =  31
Press.  -0.505E+05-0.519E+05-0.491E+05-0.502E+05-0.448E+05-0.512E+05-0.435E+05
 Surface x-   Fracture NE2
 Surface x-   Fracture NNW2
 Surface x+   Fracture NE2
 Surface x+   Fracture NNW2
 Surface y-   Fracture NNW2
 Surface z-   Fracture NE2
 Surface z-   Fracture NNW2
 Surface z+   Fracture NE2
 Step    4   x =  0.105E+04   y =  0.119E+04   z =   935.
Darcy-time for particle=   0.241181
 Step    5   x =  0.105E+04   y =  0.119E+04   z =   934.
Darcy-time for particle=   0.252183
 Step    6   x =  0.104E+04   y =  0.119E+04   z =   933.
Darcy-time for particle=   0.263192
 Step    7   x =  0.104E+04   y =  0.119E+04   z =   932.
Darcy-time for particle=   0.274208

 i =  33   j =  23   k =  31
Press.  -0.519E+05-0.533E+05-0.505E+05-0.514E+05-0.436E+05-0.528E+05-0.442E+05
 Surface x-   Fracture NE2
 Surface x-   Fracture NNW2
 Surface x+   Fracture NE2
 Surface x+   Fracture NNW2
 Surface y-   Fracture NNW2
 Surface z-   Fracture NE2
 Surface z-   Fracture NNW2
 Surface z+   Fracture NE2
 Step    8   x =  0.103E+04   y =  0.119E+04   z =   931.
Darcy-time for particle=   0.285024
 Step    9   x =  0.103E+04   y =  0.119E+04   z =   929.
Darcy-time fcr particle=   0.295842
 Step   10   x =  0.102E+04   y =  0.119E+04   z =   928.
Darcy-time for particle=   0.306654
 Step   11   x =  0.102E+04   y =  0.119E+04   z =   926.
```

```
Darcy-time for particle=   0.317449

 i =  32   j =  23   k =  31
Press.  -0.533E+05-0.548E+05-0.519E+05-0.526E+05-0.477E+05-0.545E+05-0.445E+05
 Surface x-   Fracture NE2
 Surface x-   Fracture NNW2
 Surface x+   Fracture NE2
 Surface x+   Fracture NNW2
 Surface y-   Fracture NE2
 Surface y-   Fracture NNW2
 Surface z-   Fracture NE2
 Surface z-   Fracture NNW2
 Surface z+   Fracture NE2
 Step   12   x =  0.101E+04   y =  0.119E+04   z =   924.
Darcy-time for particle=   0.327772
 Step   13   x =  0.101E+04   y =  0.119E+04   z =   922.
Darcy-time for particle=   0.337961

 i =  32   j =  23   k =  30
Press.  -0.545E+05-0.563E+05-0.528E+05-0.543E+05-0.558E+05-0.551E+05-0.533E+05
 Surface x-   Fracture NNW2
 Surface x+   Fracture NE2
 Surface x+   Fracture NNW2
 Surface y-   Fracture NE2
 Surface y+   Fracture NNW2
 Surface z+   Fracture NE2
 Surface z+   Fracture NNW2
 Step   14   x =  0.100E+04   y =  0.119E+04   z =   920.
Darcy-time for particle=   0.352472
 Step   15   x =  0.100E+04   y =  0.120E+04   z =   916.
Darcy-time for particle=   0.367298

 i =  32   j =  24   k =  30
Press.  -0.558E+05-0.578E+05-0.538E+05-0.545E+05-0.571E+05-0.567E+05-0.477E+05
 Surface x-   Fracture NNW2
 Surface x+   Fracture NNW2
 Surface y-   Fracture NNW2
 Surface y+   Fracture NNW2
 Step   16   x =   999.      y =  0.120E+04   z =   913.
Darcy-time for particle=   0.374036

 i =  31   j =  24   k =  30
Press.  -0.578E+05-0.597E+05-0.558E+05-0.563E+05-0.596E+05-0.564E+05-0.503E+05
 Surface x-   Fracture NNW2
 Surface x+   Fracture NNW2
 Surface y-   Fracture NNW2
 Surface y+   Fracture NNW2
 Step   17   x =   995.      y =  0.120E+04   z =   913.
Darcy-time for particle=   0.380615
 Step   18   x =   990.      y =  0.120E+04   z =   913.
Darcy-time for particle=   0.387255
 Step   19   x =   986.      y =  0.121E+04   z =   913.
Darcy-time for particle=   0.393957
 Step   20   x =   981.      y =  0.121E+04   z =   913.
Darcy-time for particle=   0.400719

 i =  30   j =  24   k =  30
Press.  -0.597E+05-0.612E+05-0.578E+05-0.578E+05-0.619E+05-0.592E+05-0.502E+05
 Surface x-   Fracture NNW2
 Surface x+   Fracture NNW2
 Surface y-   Fracture NNW2
 Surface y+   Fracture NNW2
 Step   21   x =   977.      y =  0.121E+04   z =   913.
Darcy-time for particle=   0.407178
```

```
 Step   22   x =   972.       y =  0.121E+04   z =   913.
Darcy-time for particle=   0.413695
 Step   23   x =   968.       y =  0.122E+04   z =   913.
Darcy-time for particle=   0.420267
 Step   24   x =   964.       y =  0.122E+04   z =   913.
Darcy-time for particle=   0.426887

 i =  30   j =  25   k =  30
Press.  -0.619E+05-0.640E+05-0.596E+05-0.597E+05-0.645E+05-0.629E+05-0.493E+05
 Surface x-   Fracture NNW2
 Surface x+   Fracture NNW2
 Surface y-   Fracture NNW2
 Surface y+   Fracture NNW2
 Step   25   x =   960.       y =  0.122E+04   z =   913.
Darcy-time for particle=   0.432794

 i =  29   j =  25   k =  30
Press.  -0.640E+05-0.656E+05-0.619E+05-0.612E+05-0.673E+05-0.641E+05-0.491E+05
 Surface x-   Fracture NNW2
 Surface x+   Fracture NNW2
 Surface y-   Fracture NNW2
 Surface y+   Fracture NNW2
 Step   26   x =   956.       y =  0.123E+04   z =   913.
Darcy-time for particle=   0.438342
 Step   27   x =   952.       y =  0.123E+04   z =   913.
Darcy-time for particle=   0.443917
 Step   28   x =   949.       y =  0.123E+04   z =   913.
Darcy-time for particle=   0.449505
 Step   29   x =   945.       y =  0.124E+04   z =   913.
Darcy-time for particle=   0.455097
 Step   30   x =   942.       y =  0.124E+04   z =   913.
Darcy-time for particle=   0.460679

 i =  28   j =  26   k =  30
Press.  -0.696E+05-0.711E+05-0.673E+05-0.656E+05-0.649E+05-0.740E+05-0.511E+05
 Surface x-   Fracture NNW2
 Surface x+   Fracture NNW2
 Surface y-   Fracture NNW2
 Surface z-   Fracture NNW2
 Step   31   x =   938.       y =  0.124E+04   z =   913.
Darcy-time for particle=   0.466736
 Step   32   x =   936.       y =  0.125E+04   z =   911.
Darcy-time for particle=   0.473690
 Step   33   x =   934.       y =  0.125E+04   z =   909.
Darcy-time for particle=   0.480907
 Step   34   x =   932.       y =  0.125E+04   z =   905.
Darcy-time for particle=   0.487404
 Step   35   x =   931.       y =  0.126E+04   z =   901.
Darcy-time for particle=   0.492829

 i =  28   j =  26   k =  29
Press.  -0.740E+05-0.762E+05-0.708E+05-0.633E+05-0.791E+05-0.607E+05-0.696E+05
 Surface x-   Fracture NNW2
 Surface x+   Fracture NNW2
 Surface y+   Fracture NNW2
 Surface z+   Fracture NNW2
 Step   36   x =   929.       y =  0.126E+04   z =   896.
Darcy-time for particle=   0.496992
 Step   37   x =   927.       y =  0.126E+04   z =   893.
Darcy-time for particle=   0.500956

 i =  28   j =  27   k =  29
Press.  -0.791E+05-0.824E+05-0.747E+05-0.740E+05-0.855E+05-0.693E+05-0.649E+05
 Surface x-   Fracture NNW2
```

```
 Surface x+   Fracture NNW2
 Surface y-   Fracture NNW2
 Surface y+   Fracture NNW2
 Step   38   x =   925.       y =  0.126E+04   z =   891.
Darcy-time for particle=   0.504287

 i =  27   j =  27   k =  29
Press.  -0.824E+05-0.835E+05-0.791E+05-0.762E+05-0.911E+05-0.736E+05-0.667E+05
 Surface x-   Fracture NNW2
 Surface x+   Fracture NNW2
 Surface y-   Fracture NNW2
 Surface y+   Fracture NNW2
 Step   39   x =   922.       y =  0.127E+04   z =   891.
Darcy-time for particle=   0.507144
 Step   40   x =   919.       y =  0.127E+04   z =   891.
Darcy-time for particle=   0.509923
 Step   41   x =   916.       y =  0.128E+04   z =   891.
Darcy-time for particle=   0.512607

 i =  27   j =  28   k =  29
Press.  -0.911E+05-0.937E+05-0.855E+05-0.824E+05-0.103E+06-0.100E+06-0.677E+05
 Surface x-   Fracture NNW2
 Surface x+   Fracture NNW2
 Surface y-   Fracture NNW2
 Surface y+   Fracture NNW2
 Step   42   x =   914.       y =  0.128E+04   z =   891.
Darcy-time for particle=   0.514902
 Step   43   x =   911.       y =  0.128E+04   z =   891.
Darcy-time for particle=   0.517133
 Step   44   x =   909.       y =  0.129E+04   z =   891.
Darcy-time for particle=   0.519282
 Step   45   x =   906.       y =  0.129E+04   z =   891.
Darcy-time for particle=   0.521338
 Step   46   x =   904.       y =  0.130E+04   z =   891.
Darcy-time for particle=   0.523297

 i =  26   j =  29   k =  29
Press.  -0.111E+06-0.102E+06-0.103E+06-0.937E+05-0.995E+05-0.129E+06-0.747E+05
 Surface x-   Fracture NNW2
 Surface x+   Fracture NNW2
 Surface y-   Fracture NNW2
 Surface z-   Fracture NNW2
 Step   47   x =   902.       y =  0.130E+04   z =   891.
Darcy-time for particle=   0.524693
 Step   48   x =   902.       y =  0.131E+04   z =   888.
Darcy-time for particle=   0.526264
 Step   49   x =   902.       y =  0.131E+04   z =   885.
Darcy-time for particle=   0.527823
 Step   50   x =   902.       y =  0.131E+04   z =   881.
Darcy-time for particle=   0.529181

 i =  26   j =  29   k =  28
Press.  -0.129E+06-0.114E+06-0.116E+06-0.993E+05-0.180E+06-0.109E+06-0.111E+06
 Surface x-   Fracture NNW2
 Surface x+   Fracture NNW2
 Surface y+   Fracture NNW2
 Surface z+   Fracture NNW2
 Step   51   x =   902.       y =  0.131E+04   z =   876.
Darcy-time for particle=   0.529758
 Step   52   x =   901.       y =  0.132E+04   z =   874.
```

APPENDIX B Evaluation of pumping test LPT2 in KAS06 at Äspö

GEOSIGMA AB

Client: SKB

REPORT
ID-no: GRAP 91002
Date: 1991-12-13

EVALUATION OF PUMPING TEST LPT-2 IN KAS06 AT ÄSPÖ

Jan-Erik Andersson

GEOSIGMA AB
UPPSALA, SWEDEN

December 1991

FOREWORD

This report was finalized after discussions of the draft report at a work meeting at VBB - VIAK 1991-10-02.

CONTENTS

		Page
	FOREWORD	i
	CONTENTS	ii
	LIST OF TABLES	iii
	LIST OF FIGURES	iv
1.	INTRODUCTION	1
2.	TEST PERFORMANCE	1
3.	RESPONSE IN THE PUMPING BOREHOLE	2
4.	HYDRAULIC CONNECTIONS TO OBSERVATION BOREHOLES	4
4.1	RESPONSE TIMES	4
4.2	DISCUSSION OF OBSERVATION BOREHOLE RESPONSES	7
5.	ESTIMATION OF HYDRAULIC PARAMETERS	14
6.	DISCUSSION OF THE CONCEPTUAL MODEL	17
7.	CONCLUSIONS	18
8.	REFERENCES	19

LIST OF TABLES

Table 2.1 Average flow rates during the different pumping phases and recovery period together with the duration and observed precipitation during LPT–2. From Jönsson and Nyberg (1991).

Table 3.1 Estimated hydraulic parameters from the pumping borehole KAS06 during LPT–2. (d=drawdown, r=recovery).

Table 3.2 Estimated inflow distribution to the pumping borehole KAS06 during LPT–2 together with corresponding fracture zone intervals and main hydraulic conductors and their estimated transmissivities in KAS06. (G=geological, S=spinner and CH=hydrochemical).

Table 4.1 Drawdown at stop of pumping (s), spherical distance (R), estimated response time (t_e) and response time ratio (t_e/R^2), flow rate under natural gradient (NG–2) and during LPT–2 and electric conductivity at the lower level together with judged hydraulic connection between pumping borehole and observation sections (1=good, 2=intermediate, 3=poor and –=none). NG=natural gradient, n.m.=no measurement, n.r.=no automatic registration, StopD= stop of drawdown, StopR=stop of recovery.

Table 4.2 Recorded electric conductivity at the upper level in cored boreholes during LPT–2. (From Jönsson and Nyberg 1991).

Table 4.3 Compilation of the most distinct hydraulic responses in the observation sections in the cored boreholes during LPT–2 together with interpreted fracture zone intervals and type of indications in the conceptual model of the Äspö area. (S=spinner, G=geological, CH=hydrochemical, I=interference test, P=pumping test and RQD=rock quality design).

Table 5.1 Estimated bulk hydraulic parameters together with possible main pathways from KAS06 to the observation sections with the major hydraulic responses in the cored boreholes during LPT–2.(T_b=bulk transmissivity, S=storativity and K'/m'=leakage coefficient).

Table 5.2 Estimated transmissivity (T) and inflow from some of the dominating fracture zones during LPT–2 (T_b=bulk transmissivity from Table 5.1).

Table 5.3 Estimated range of transmissivity of the dominating fracture zones from LPT–2 and assumed in the conceptual model.

LIST OF FIGURES

Fig. 1.1 Location of boreholes on Äspö and their direction.

Fig. 1.2 Conceptual model of conductive structures on Äspö (From Wikberg et al., 1991).

Fig. 2.1 Overview of the groundwater head in KAS06 during LPT–2. (From Jönsson och Nyberg 1991).

Fig. 2.2 Changes of electric conductivity in the discharged groundwater from KAS06. (From Jönsson och Nyberg 1991).

Fig. 2.3 Instrumentation in the cored boreholes on Äspö. (From Jönsson och Nyberg 1991).

Fig. 2.4 Instrumentation in the percussion boreholes on Äspö. (From Jönsson och Nyberg 1991).

Fig. 3.1 Drawdown in KAS06 during LPT–2, logarithmic graph. (From Jönsson och Nyberg 1991.

Fig. 3.2 Drawdown in KAS06 during LPT–2, semilogarithmic graph. (From Jönsson och Nyberg 1991).

Fig. 3.3 Recovery in KAS06 during LPT–2, logarithmic graph. (From Jönsson och Nyberg 1991.

Fig. 3.4 Recovery in KAS06 during LPT–2, semilogarithmic graph. (From Jönsson och Nyberg 1991).

Fig. 4.1 Distance – drawdown graph at stop of pumping during LPT–2. The variable codes refer to the observation sections listed in Table 4.1.

Fig. 4.2 Drawdown response in KAS02. The section intervals are shown in Table 4.1. (From Jönsson och Nyberg 1991).

Fig. 4.3 Recovery response in KAS02. The section intervals are shown in Table 4.1. (From Jönsson och Nyberg 1991).

Fig. 4.4 Drawdown response in KAS04. The section intervals are shown in Table 4.1. (From Jönsson och Nyberg 1991).

Fig. 4.5 Recovery response in KAS04. The section intervals are shown in Table 4.1. (From Jönsson och Nyberg 1991).

Fig. 4.6 Drawdown response in KAS05. The section intervals are shown in Table 4.1. (From Jönsson och Nyberg 1991).

Fig. 4.7 Recovery response in KAS05. The section intervals are shown in Table 4.1. (From Jönsson och Nyberg 1991).

Fig. 4.8 Drawdown response in KAS07. The section intervals are shown in Table 4.1. (From Jönsson och Nyberg 1991).

Fig. 4.9 Recovery response in KAS07. The section intervals are shown in Table 4.1. (From Jönsson och Nyberg 1991).

Fig. 4.10 Results of the analysis of the drawdown and recovery periods of KAS07 in Fig 4.8–9.

Fig. 4.11 Drawdown response in KAS08. The section intervals are shown in Table 4.1. (From Jönsson och Nyberg 1991).

Fig. 4.12 Recovery response in KAS08. The section intervals are shown in Table 4.1. (From Jönsson och Nyberg 1991).

Fig. 4.13 Drawdown response in KAS12. The section intervals are shown in Table 4.1. (From Jönsson och Nyberg 1991).

1. INTRODUCTION

The long-time pumping test (LPT-2) was carried out in borehole KAS06 on Äspö during september 1990 – january 1991. Observations of drawdown were generally performed in multiple sections in all available cored boreholes and also in the percussion boreholes. The main purpose with LPT-2 was to create a sufficient hydraulic gradient towards the pumping borehole to perform tracer and dilution tests. The location of the boreholes is shown in Fig. 1.1. All borehole and test data from LPT-2 are presented by Jönsson and Nyberg (1991).

The purpose of the present work is to perform a qualitative and quantitative evaluation of the test data and to create a data set for comparison with predicted drawdowns. Finally, the consistency of the results from LPT-2 in relation to the conceptual model of the Äspö area is investigated. As a basis for the latter task the geohydrological conceptual model presented in Wikberg et al. (1991) was used, see Fig. 1.2.

2. TEST PERFORMANCE

A summary of the performance of LPT-2 is presented below. The time periods for the drawdown and recovery period are shown in Table 2.1. KAS06 was used as (open) pumping borehole. The flow rate was changed at two occasions to achieve an optimal drawdown in the pumping borehole for the tracer tests, see Table 2.1. The electric conductivity and redox potential of the discharged groundwater were registered during the drawdown period. An overview of the observed groundwater head and electric conductivity in KAS06 during LPT-2 is shown in Fig. 2.1 and 2.2, respectively. Three short pump stops occurred during the drawdown period.

In all observation boreholes (except HAS01, KAS01 and KAS10) between two and six sections were isolated by packers. The instrumentation in the cored boreholes and percussion boreholes during LPT-2 is shown in Fig. 2.3 and 2.4, respectively. Automatic registration of drawdown was made in most sections. In addition, manual readings were also performed at certain times in all boreholes. In section KAS05-E4 no automatic registration was performed due to technical problems but manual readings were carried out. The instrumentation in the boreholes and the technical performance of the test is described by

Table 2.1 Average flow rates during the different pumping phases and recovery period together with the duration and observed precipitation during LPT-2. From Jönsson and Nyberg (1991).

Phase	Flow rate $x10^{-3}$ (m^3/s)	Duration (min)	Period	Precipitation (mm)
Drawdown phase 1	2.01	4320	900917-900920	9.2
Drawdown phase 2	2.52	6119	900920-900924	34.8
Drawdown phase 3	2.25	122155	900924-901218	129.5
Drawdown, total	2.25	132595	900917-901218	173.5
Recovery	-	c.38800	901218-910118	38.2

Jönsson and Nyberg (1991).

In the cored boreholes KAS02–05 and KAS07–14 the electric conductivity was measured at two different levels. At the lower level automatic registrations of the electric conductivity were performed (Table 4.1) whereas at the higher level manual readings were undertaken. The precipitation during the different drawdown phases and recovery period is shown in Table 2.1.

3. RESPONSE IN THE PUMPING BOREHOLE

According to the conceptual model several fracture zones are assumed to intersect the pumping borehole KAS06 (Table 3.2). In this borehole the first phase of the drawdown period with constant flow rate (up to c. 4320 min) and the recovery period is evaluated. The subsequent pumping phases are affected by the changes of the flow rate (Table 2.1). During the first drawdown phase and recovery period low precipitation was observed (Table 2.1).

During early times (to c. 1 min) the drawdown curve in the pumping borehole is dominated by borehole effects storage due to open borehole conditions (Fig. 3.1). Then a rather long transition period follows up to about 120 min. During the transition period threedimensional (pseudospherical) flow may occur. A first radial flow period is interpreted between c. 120–360 min (Fig. 3.2). This period may possibly represent radial flow in the most conductive zone intersecting the pumping borehole (EW–5w), c.f. Tables 3.1 and 3.2. Then another transition period follows (c. 360–2000 min). During this period crossflow between the fracture zones intersecting the borehole may occur.

A second radial flow period is interpreted between 2000–4320 min in Fig. 3.2. During this period all fracture zones in the borehole are assumed to be hydraulically active, thus representing the total transmissivity of all zones. During later times of the drawdown period (after c. 50 000 min) the effects of a small leakage inflow from the upper parts of the bedrock can be seen. The leakage inflow starts much earlier during drawdown but the effects are obscured by the changes of flow rate. During the recovery period effects of leakage appear after c. 1500 min, see Fig. 3.4. Due to interruptions in the data sampling the first radial flow period during the recovery period is not evaluated (Fig. 3.4).

The interpreted flow regimes during the first pumping phase (Fig. 3.1–2) are summarized below. The recovery curves (Fig. 3.3–4) exhibit the same general pattern.

0–1 min	borehole storage	
1–120 min	transition period	
120–360 min	first radial flow period	(Zone EW–5w)
360–2000 min	transition period	
2000–4320 min	second radial flow period	(All fracture zones)
(> c. 50 000 min)	leakage, c.f. recovery period	

The hydraulic parameters in the pumping borehole KAS06 are mainly calculated from the semilogarithmic diagrams of the drawdown and recovery periods (Fig. 3.2 and 3.4). The borehole storage coefficient is determined from the logarithmic diagrams (Fig. 3.1 and 3.3). The estimated hydraulic parameters from KAS06 during LPT-2 are shown in Table 3.1. The storativity value is derived from the responses in the observation sections, see Table 5.1. In Table 3.1, T=transmissivity, S=storativity, SK=skin factor, r_{wf}=effective borehole radius and C=borehole storage coefficient.

Table 3.1 Estimated hydraulic parameters from the pumping borehole KAS06 during LPT-2. (d=drawdown, r=recovery).

Hydraulic unit	$Tx10^{-5}$ (m^2/s)	$Sx10^{-5}$ (-)	SK (-)	r_{wf} (m)	$Cx10^{-2}$ (m^2)	Remarks
Cond. zone	5.4	5.0	-2.8	0.46	-	d
All zones	14	5.0	6.6	$3.8x10^{-5}$	2.1	d
-"-	15	5.0	10	$1.3x10^{-6}$	2.2	r

The dimensionless borehole storage coefficient is estimated at $C_D=10^5$. Similar values on the hydraulic parameters were calculated from the drawdown and recovery periods. The estimated values of total transmissivity and skin factor are in reasonable agreement with the values calculated from a previous short-time pumping test in KAS06 ($T=1.0x10^{-4}$ m^2/s and SK=5.7) presented by Nilsson (1989).

The inflow distribution to KAS06 during pumping has mainly been estimated from spinner measurements (Nilsson 1989). The inflow from Zone EW-3w in the upper part of the borehole, not covered by the spinner survey, is estimated from tracer dilution measurements (Gustafsson et al. 1991), see Table 3.2. In this table also the corresponding fracture zone intervals and main hydraulic conductors, mainly according to the conceptual model (Wikberg et al. 1991), are presented. Zone EW-X is in the conceptual model interpreted as a possible, deeper zone parallel to Zone EW-5 mainly from geological information. The spinner survey in KAS06 indicated a minor hydraulic conductor below 557 m.

Table 3.2 Estimated inflow distribution to the pumping borehole KAS06 during LPT-2 together with corresponding fracture zone intervals and main hydraulic conductors and their estimated transmissivities in KAS06. (G=geological, S=spinner and CH=hydrochemical).

Fracture zone	Interval (m)	Inflow (fraction)	$Tx10^{-5}$ (m^2/s)	Hydraulic conductor	Indication
EW-3	c. 60-70	0.15	2.1	U	G
NNW-1w	208-234	0.21	2.9	A	S
EW-5w	312-406	0.33	4.6	B,Ca,Cb,D	312-365 m : S 389-406 m : CH
NNW-2w	447-450	0.26	3.6	E	S
EW-X	558-596	0.05	0.7	Fa, Fb	G
All zones	0-602	1.0	14	All	

From the total transmissivity, assumed to represent all fracture zones, together with the presumed inflow distribution the transmissivity of each fracture zone can be estimated, provided that the zones are virtually hydraulically independent and that the flow in each fracture zone is directed radially towards the pumping borehole. The total transmissivity of all zones in Table 3.2 is evaluated from the drawdown period, see Table 3.1.

4. HYDRAULIC CONNECTIONS TO THE OBSERVATION BOREHOLES

4.1 RESPONSE TIMES

To assess the hydraulic connection between the different observation sections and the pumping borehole, the response times were estimated for each section in the observation boreholes from the logarithmic drawdown plots (Fig. 4.2–13). The response time chosen corresponds to the approximative time after start of pumping when a drawdown of 0.1 m was observed in the actual borehole section. Due to long data scan intervals in the beginning of the drawdown period, the drawdown curves must in some cases be extrapolated backward to intersect the 0.1 m drawdown line. The extrapolation was generally made from the type curve used for interpretation, see Chapter 5.

A response time ratio was then calculated for each section by dividing the estimated response time by the squared (spherical) distance to the pumping borehole. The distances were calculated from the midpoint of the observation sections to the midpoint of the pumping borehole. For radial flow, this ratio is inversely proportional to the hydraulic diffusivity (T/S) between the observation section and the pumping borehole, i.e. the lower the ratio the higher the hydraulic diffusivity. Low ratios (small response times at large distances) can be expected for borehole sections located in fracture zones while higher ratios can be expected for sections in the rock mass with decreased hydraulic connection.

It should be observed that the response time ratio is no absolute measure of the hydraulic connection due to (conceptual) uncertainties in the calculated distances as well as in the estimated response times, e.g. due to leakage between sections in the boreholes. Also any inaccuracies in the drawdown curves at short times, e.g. due to sparse scanning density, may cause uncertain response times. Thus, the calculated response time ratios should be used in combination with other information, e.g the total drawdown in the borehole sections, results from tracer tests, dilution and electric conductivity measurements, spinner surveys, packer and pumping tests and other available information.

To assist in assessing the hydraulic connection to the observation sections, a distance–drawdown plot was also prepared, see Fig. 4.1. In this plot the total drawdown in each observation section at stop of pumping versus the squared distance to the pumping borehole is shown. It should be observed that the recorded drawdown in some of the sections listed in the data report (Jönsson and Nyberg 1991, Tabell 4.1) has been corrected due to non–representative drawdown values, e.g. due to circulation of tracer in the sections by the end of pumping. These drawdowns are marked with an asterix in Table 4.1 below.

The estimated response times, distances, response time ratios, total drawdowns together with the assessed hydraulic connection for each borehole section are listed in Table 4.1. In addition, the calculated flow through some of the borehole sections during natural and pumping conditions as estimated from the tracer dilution measurements (Ittner et al. 1991) together with the recorded electric conductivity at the lower level are shown in the table. As pointed out by Jönsson and Nyberg (1991) there are certain "jumps" in the latter recordings which must be considered by the interpretation. The electric conductivity recordings at the higher levels are shown in Table 4.2. The recorded values at these levels in KAS04 and KAS12 are uncertain.

The hydraulic connections are classified in 1 (good), 2 (intermediate), 3 (poor) and – (no response). Hydraulic connections classified as "good" are assumed to correspond to response time ratios less (or equal to) than 10^{-3} (min/m^2) and connections classified as "poor" to ratios higher than $5x10^{-3}$ (min/m^2). Observation borehole sections judged to have a "good" hydraulic connection with the pumping borehole in Table 4.1 may correspond to interpreted fracture zone intervals. A compilation of the most distinct hydraulic response sections in the cored boreholes and interpreted major fracture zone intervals in the Äspö area presented in Wikberg et al. (1991, Table 4.1), is shown in Table 4.3.

Table 4.1 Drawdown at stop of pumping (s), spherical distance (R), estimated response time (t_e) and response time ratio (t_e/R^2), flow rate under natural gradient (NG–2) and during LPT–2 and electric conductivity at the lower level together with judged hydraulic connection between pumping borehole and observation sections (1=good, 2=intermediate, 3=poor and –=none). NG=natural gradient, n.m.=no measurement, n.r.=no automatic registration, StopD= stop of drawdown, StopR=stop of recovery.

Borehole section	Variable code	Interval (m)	s (m)	R (m)	t_e (min)	t_e/R^2x10^{-3} (min/m^2)	Flow rate (ml/min) NG–2	LPT–2	El. cond.x10^3 (mS/m) Start	StopD	StopR	Hydr. conn.
KAS01–1	A1	0–101*	6.20	223	150	3.0						2
KAS02–6	B6	0–113	6.30	222	300	6.1						3
–5	B5	114–308	5.79	114	70	5.4						3
–4	B4	309–345	6.30[1]	131	23	1.3	(–)[2]	2				2
–3	B3	346–799	5.40	338	42	0.4			1.76	2.12	2.12	1
–2	B2	800–854	2.41	584	1300	3.8	(–)[2]	4				2
–1	B1	855–924*	2.30	645	600	1.4						2
KAS03–6	C6	0–106	0	710	–	–						–
–5	C5	107–252	0	698	–	–	6.9	n.m.				–
–4	C4	253–376	0.55	711	20000	40						3
–3	C3	377–532	0.80	751	7500	13						3
–2	C2	533–626	0.83	806	7500	12	(120)	n.m.				3
–1	C1	627–1002*	0.82	948	7500	8.3			2.53	2.51	2.51	3
KAS04–6	D6	0–185	0	479	–	–						–
–5	D5	186–214	3.27	397	(200)	(1.3)						2?
–4	D4	215–287	3.11	362	(300)	(2.3)						2?
–3	D3	288–331	3.42	327	(160)	(1.5)						2?
–2	D2	332–392	3.58	301	(240)	(2.6)	12	n.m.				2?
–1	D1	393–481*	3.33	277	(200)	(2.5)			2.10	2.26	2.08	2?
KAS05–5	E5	0–171	5.58	223	100	2.0						2
–4	E4	172–319	4.97[3]	133	n.r.	n.r.						1?
–3	E3	320–380	5.45[1]	156	18	0.7	0.4	9				1
–2	E2	381–439	3.30	195	50	1.3			1.14	1.23	–	2
–1	E1	440–550*	3.06	264	90	1.3	1.5	11				2
KAS06–1	P	0–602*	51.77	0	0.01	–						

cont. Table 4.1

Borehole section	Variable code	Interval (m)	s (m)	R (m)	t_c (min)	$t_c/R^2 \times 10^{-3}$ (min/m^2)	Flow rate (ml/min) NG-2	LPT-2	El. cond.x10^3 (mS/m) Start	StopD	StopR	Hydr. conn.
KAS07-6	J6	0-109	15.64	208	4	0.09						1
-5	J5	110-190	16.53	137	5	0.3						1
-4	J4	191-290	5.61	112	10	0.8	1.0	18				1
-3	J3	291-410	1.69	165	2000	73						3
-2	J2	411-500	1.88?	253	7	0.1			2.7	2.7	2.7	1?
-1	J1	501-604*	2.54	343	100	0.8	5.3	n.m.				1
KAS08-4	M4	0-139	4.73	290	110	1.3						2
-3	M3	140-200	6.58	200	4	0.1	4.0	21				1
-2	M2	201-502	4.70	97	10	1.1			1.98	2.20	2.22	2
-1	M1	503-601*	3.74	226	53	1.0	7.6	48				1
KAS09-5	AE	0-115	0.25	392	300	2.0						2
-4	AD	116-150	0.38[3]	396	550	3.5	11	n.m.				2
-3	AC	151-240	0.45[3]	411	440	2.6						2
-2	AB	241-260	0.44[3]	431	440	2.4			2.26	-	-	2
-1	AA	261-450*	0.25[3]	484	400	1.7						2
KAS10-1	BA	0-100*	0.63	365	c.1000	c.7.5						3
KAS11-6	CF	0-46	0.49	375	(205)	(1.5)						2?
-5	CE	47-64	0.57	356	(180)	(1.4)	0.3	n.m.				2?
-4	CD	65-115	0.58	338	(180)	(1.6)						2?
-3	CC	116-152	0.69	318	(205)	(2.0)						2?
-2	CB	153-183	0.90	306	(240)	(2.6)	33	n.m.				2?
-1	CA	184-249*	0.55	295	(240)	(2.8)			2.3	2.3	2.1	2?
KAS12-5	DE	0-101	3.54[4]	400	120	0.7						1
-4	DD	102-233	3.00[3]	314	90	0.9						1
-3	DC	234-277	4.20[3]	265	32	0.5	0	n.m.				1
-2	DB	278-329	5.87[3]?	247	19	0.3	12	107	0.62	-	-	1
-1	DA	330-380*	4.13[3]	237	130	2.3						2
KAS13-5	EE	0-150	5.53	207	220	5.0						3
-4	ED	151-190	5.03	164	240	8.9	1.1	n.m.				3
-3	EC	191-220	5.06	160	260	10	4.7	3.3				3
-2	EB	221-330	3.43	177	220	7.0						3
-1	EA	331-407*	2.62	232	550	10			0.28	0.34	0.34	3
KAS14-5	FE	0-130	0.64	355	(260)	(2.1)						2?
-4	FD	131-138	0.70	352	(260)	(2.1)	3.1	n.m.				2?
-3	FC	139-146	0.72	352	(250)	(2.0)						2?
-2	FB	147-175	0.61	354	(260)	(2.1)	18	11				2?
-1	FA	176-212*	0.63	359	(260)	(2.0)			1.97	1.94	1.94	2?
HAS01-1	G1	0-100*	0	451	-	-						-
HAS02-2	H2	0-72	0	1020	-	-						-
-1	H1	73-93*	0	1006	-	-						-
HAS03-2	I2	0-50	0	513	-	-						-
-1	I1	51-100*	0	472	-	-						-
HAS04-2	K2	0-100	4.08	270	460	6.3						3
-1	K1	101-201*	2.72	240	230	4.0						2
HAS05-3	L3	0-15	1.87[4]	287	2800	34						3
-2	L2	16-40	5.68	269	190	2.6						2
-1	L1	41-100*	5.75	233	100	1.9						2
HAS06-2	N2	0-40	1.57	343	570	4.3						2
-1	N1	41-100*	2.37	309	85	0.9						1
HAS07-2	O2	0-40	0.96	442	1600	8.0						3
-1	O1	41-100*	0.96	436	900	4.7						2

cont. Table 4.1

Borehole section	Variable code	Interval (m)	s (m)	R (m)	t_c (min)	$t_c/R^2 x10^{-3}$ (min/m^2)	Flow rate (ml/min) NG-2	LPT-2	El. cond.x10^3 (mS/m) Start	StopD	StopR	Hydr. conn.
HAS08-2	P2	0-65	0	649	-	-						-
-1	P1	66-125*	0	620	-	-						-
HAS09-2	Q2	0-10	0	656	-	-						-
-1	Q1	11-125*	0	610	-	-						-
HAS10-2	R2	0-10	0	865	-	-						-
-1	R1	11-125*	0	873	-	-						-
HAS11-2	S2	0-30	0	878	-	-						-
-1	S1	31-125*	0	867	-	-						-
HAS12-2	T2	0-60	0	922	-	-						-
-1	T1	61-125*	0	918	-	-						-
HAS13-2	U2	0-50	0.58	300	140	1.6						2
-1	U1	51-100*	1.10	253	40	0.6						1
HAS14-2	V2	0-50	0	249	-	-						-
-1	V1	51-100*	4.67	204	330	7.9						3
HAS15-2	X2	0-40	0.85[4]	244	820	14						3
-1	X1	41-120*	5.20[4]	202	210	5.1						3
HAS16-2	Y2	0-40	1.11[4]	321	>200	>2.0						2?
-1	Y1	41-120*	3.12	307	200	2.1						2
HAS17-2	Z2	0-40	2.16[4]	401	>260	>1.6						2?
-1	Z1	41-120*	2.99[4]	362	260	2.0						2
HAS18-2	PB	0-35	2.99[4]	512	720	2.8						2
-1	PA	36-150*	3.41[4]	461	720	3.4						2
HAS19-2	QB	0-60	0	550	-	-						-
-1	QA	61-150*	0	526	-	-						-
HAS20-2	RB	0-68	0	484	-	-						-
-1	RA	69-150*	0	420	-	-						-

* Total borehole length
1 circulation of tracer at stop of pumping
2 measurement failure
3 manual reading 901203
4 -"- at stop of pumping 901218
( ) values within brackets are uncertain

4.2 DISCUSSION OF OBSERVATION BOREHOLE RESPONSES

Below, the responses in each of the observation sections of the cored boreholes are discussed qualitatively in the context of interpreted fracture zone intervals in the conceptual model. A compilation of the most distinct hydraulic responses in the cored boreholes during LPT-2 together with the corresponding fracture zone intervals assumed in the conceptual model according to Wikberg et al.(1991) is shown in Table 4.3.

KAS01

In borehole KAS01 the hydraulic response is classified as "Intermediate". This is consistent with the conceptual model in which no fracture zones are interpreted to intersect the borehole. The response was probably transmitted

through the upper part of the bedrock.

Table 4.2 Recorded electric conductivity at the upper level in cored boreholes during LPT-2. (From Jönsson and Nyberg 1991).

Borehole section	Date	El. cond. (mS/m)	Borehole section	Date	El. cond. (mS/m)
KAS02-B5	901203	660	KAS09-AD	901005	1672
	910105	571		901104	1653
				901203	1653
KAS03-C3	901005	1434		910105	1638
	901104	1426			
	901203	1434	KAS11-CC	901005	1854
	910105	1434		901104	1849
				901203	1817
KAS04-D3	901005	138		910105	1918
	901104	95			
	901203	69	KAS12-DD	901104	-168
	910105	-8		901203	-163
				910105	-157
KAS05-E4	901005	407			
	901104	393	KAS13-EB	901104	449
	901203	393		901203	456
	910105	388		910105	449
KAS07-J5	901203	609	KAS14-FC	901005	1666
	910105	605		901104	1677
				901203	1677
KAS08-M4	901203	3948		910105	1688
	910105	4064			

KAS02

The responses in KAS02 during drawdown and recovery are shown in Fig. 4.2 and 4.3, respectively. Section B3 (346–799 m) shows "good" hydraulic connection with the pumping borehole according to Table 4.1 whereas section B4 (309–345 m) shows an intermediate response. Zone EW–5w is interpreted to intersect section B4 in the conceptual model (Table 4.3). According to the spinner measurements the lower hydraulic conductor in Zone EW–5w is located at 342 m (Nilsson 1988). The responses in these two sections may be explained by the fact that the interpreted lower conductor in Zone EW–5w is located close to the border between the two sections. Alternatively, the response in section B3 may be transmitted along Zone EW–X, which is interpreted geologically to intersect this section (Table 4.3). The tracer dilution measurements indicate a rather poor hydraulic connection between the pumping borehole and section B4 (Table 4.1).

The observed rather poor hydraulic connection to section B2 (800–854 m), assumed to be intersected by Zone NE–1w (Table 4.3), is consistent with the dilution measurements which indicate no significant hydraulic connection with the pumping borehole. An intermediate–good hydraulic response was observed in section B1 (855–924 m), also assumed to intersect Zone NE–1w. A rather strong hydraulic conductor was identified at 868–887 m in this section from the spinner survey. Poor responses were obtained in the upper part of KAS02 (section B5 and B6) which is consistent with the conceptual model.

KAS03

In KAS03 appreciable drawdowns were observed in the lower part of the borehole in sections C1–C3 located about 750–950 m from the pumping borehole (Table 4.1). The responses may possibly have been transmitted via Zones EW–5w and EW–1w. The latter zone is assumed to intersect the lower part of KAS03 (Table 4.3). However, Zone EW–5w is believed to terminate at the southern part of EW–1 in the conceptual model. No response was observed in sections C5 and C6 in which no fracture zones are interpreted.

An alternative, and more plausible, interpretation of the responses in the lower part of KAS03 is that Zone EW–5w continues to the north of the outcrop of EW–1 (Fig. 1.2). The latter zone (and possibly also NW–1) may also be steeper than assumed in the conceptual model. Such an interpretation would certainly explain the responses in the lower part of KAS03 as well as the non–responses in KAS04–D6, HAS08 and HAS11 (Table 4.1). However, it is not sure that any responses would be seen (during the time of the pumping test) in the latter three boreholes with the assumed dip of Zone EW–1w in the conceptual model even if Zone EW–5w intersects KAS03 (and Zone EW–1w). The borehole radar measurements in KAS03 (Niva and Gabriel 1987) indicate a low–angle structure at 620, 625 and 790 m in this borehole which may possibly correspond to Zone EW–5w (Carlsten 1991).

Table 4.3 Compilation of the most distinct hydraulic responses in the observation sections in the cored boreholes during LPT–2 together with interpreted fracture zone intervals and type of indications in the conceptual model of the Äspö area. (S=spinner, G=geological, CH=hydrochemical, I=interference test, P=pumping test and RQD=rock quality design).

Borehole–section	Hydraulic connection	Interval (m)	Interpreted fracture zone and interval (m)	Indication
KAS02–B4	2	309–345	EW–5w : 309–343	S
–B3	1	346–799	EW–X : c.400, 490	G
–B1	2	855–924*	NE–1w : 803–920	S
KAS04–D3	2?	288–331	EW–5 : c.330	G
–D2	2?	332–392	EW–1 : 334–343	CH
			NE–2w: 388–436	S
–D1	2?	393–481*	–"– –"–	S
			–"– 440–481	CH
KAS05–E4	1?	172–319	EW–5w: 274–383	I
–E3	1	320–380	–"– –"– , 362–365	I
–E1	2	440–550*	EW–X : c.400, 480	G
KAS07–J6	1	0–109	NNW–1w: 50–80	RQD,P
–J5	1	110–190	–	–
–J4	1	191–290	EW–5w: 222–224, 235–246	S
			–"– : 212–304	CH
–J2	1?	411–500	EW–3w: 383–451	I
			EW–3 : c.420	G
–J1	1	501–604*	NE–1w: 508–604	S
			NE–1 : 462–604	CH
KAS08–M3	1	140–200	NNW–2w: 183–186	S
–M1	1	503–601*	NE–1w: 555–601*	S
KAS12–DC	1	234–277	(NE–2w : 240–325)	S
–DB	1	278–329	NE–2w : 240–325	S
			NE–2 : 303–380	CH

* Total length of borehole

KAS04

The responses in KAS04 during the drawdown and recovery are shown in Fig. 4.4 and 4.5, respectively. Only intermediate hydraulic responses are interpreted. However, the estimation of response times in this borehole is uncertain. The first scan sequence during drawdown indicates a faster response than during recovery. The beginning of the drawdown is probably affected by tidal effects and therefore uncertain due to sparse scanning before start of pumping (uncertain background pressure). Relatively good responses were observed in the lowermost sections D1–D3 (Table 4.1). During both drawdown and recovery section D3 (288–331 m) responded first but the largest total drawdown was observed in section D2 (332–392 m). In the conceptual model Zone NE–2w is interpreted in sections D1 and D2 (and possibly also Zone EW–1 in section D2), see Table 4.3. These zones are not assumed to intersect KAS06. A rather large natural flow rate was measured in section D2 from the tracer dilution measurements, see Table 4.1.

According to the geological interpretation Zone EW–5 intersects the lowermost part of section D3 at about 330 m (Table 4.3). The most conductive part of KAS04 is in the interval 335–345 m in section D2 according to the spinner measurements and packer tests (Nilsson 1988). This interval may possibly belong to EW–5w (instead of EW–1 assumed in the conceptual model). This may explain the rather good response (and total drawdown) observed in section D2 (and possibly also in D1). This would not be expected if the response were (indirectly) transmitted via Zones NE–2w (and EW–1). In section D1 (393–481 m) two minor hydraulic conductors are identified from the spinner measurements.

Section D2 also responded rather good during the pumping test LPT–1 in KAS07 (Rhén 1990). KAS07 is also assumed to intersect Zone EW–5w in the conceptual model (but neither NE–2w nor EW–1). During LPT–1 a relatively high flow rate was measured through section D2 from the dilution tests (Ittner et al. 1991). These facts indicate that Zone EW–5w intersects section D2.

As discussed above (borehole KAS03) the uppermost part of KAS04 (section D6), in which no response was observed, is assumed to intersect Zone EW–1w in the conceptual model (Table 4.3).

KAS05

The responses in KAS05 during drawdown and recovery are shown in Fig. 4.6 and 4.7, respectively. The most distinct response was observed in section E3 (320–380 m) where Zone EW–5w is assumed to intersect the borehole, see Table 4.3. This response is confirmed by the increased flow rate calculated from the tracer dilution measurements. The spinner measurements indicate a strong hydraulic conductor in the interval 319–325 m in section E3 (Nilsson 1989).

Also at the bottom of the borehole (sections E2 and E1) rather good hydraulic responses were observed (Table 4.1). The flow rate through section E1 (440–550 m) was estimated to be in the same order as in section E3. The responses in the lower part of KAS05 may be transmitted along Zone EW–X which is geologically interpreted to intersect KAS05 at c. 400 m and 480 m in the

conceptual model, i.e. sections E1 and E2. The spinner measurements indicate major hydraulic conductors at 442–445 m and 466–469 m.

It should be observed that no automatic head registrations were undertaken in the presumably high-conductive section E4 (172–319 m), also assumed to intersect Zone EW–5w, due to technical problems (Jönsson and Nyberg 1991). However, a few manual readings were performed during the test. The spinner measurements indicate several hydraulic conductors in this section.

KAS07

The responses in KAS07 during drawdown and recovery are shown in Fig. 4.8 and 4.9, respectively. Distinct hydraulic responses occurred in all sections except J3 (Table 4.1). Very fast and large responses occurred in the upper part of the borehole (sections J6 and J5), c.f Fig 4.1. The uppermost section J6 (0–109 m) is assumed to intersect Zone NNW–1w (Table 4.3) which also intersects the pumping borehole KAS06 (Table 3.2), thus implying a direct hydraulic connection through this zone. In section J5 (110–190 m) no fracture zone is interpreted but a minor hydraulic conductor is indicated at 122–128 m by the spinner measurements (Nilsson 1989). Since KAS06 runs close to this section the response may be transmitted through the upper part of the bedrock.

The response in section J4 (191–290 m), classified as "good" in Table 4.1, is probably transmitted through Zone EW–5w as assumed in the conceptual model (Table 4.3). This is supported by the relatively high flow rate calculated from the dilution measurements in this section. Two minor hydraulic conductors are identified at 222–224 m and 235–246 m by the spinner survey. Section J3, in which no fracture zones or hydraulic conductors are interpreted, shows a poor response to the pumping.

Good responses were also obtained in the lower part of KAS07, particularly in section J2 (411–500 m) which is assumed to be intersected by Zone EW–3w (Table 4.3). This zone also intersects KAS06 at c. 60–70 m according to the geological interpretation (Table 3.2). However, the recorded electric conductivity in this section is rather stable during pumping, indicating a low flow rate through this section. A minor hydraulic conductor is indicated at 417–418 m by the spinner survey but the packer tests only show a slight increase of the hydraulic conductivity at c. 430 m (Nilsson 1989). Possibly, the response in section J2 is not representative but could be transmitted via the lowermost section J1 (501–604 m).

In section J1, assumed to intersect Zone NE–1w, the response is classified as "good". No spinner survey is performed in this part of the borehole but the packer tests show high hydraulic conductivities in several intervals. The dilution measurements show a rather high natural flow rate through section J1 (Table 4.1). The response may have been transmitted from the pumping borehole either via NNW–1w or NNW–2w (or both) or possibly via EW–X to Zone NE–1w.

KAS08

The responses in KAS08 during drawdown and recovery are shown in Fig. 4.11 and 4.12, respectively. Relatively good responses were observed in all sections

with the most distinct response in section M3 (140–200 m), assumed to intersect Zone NNW–2w, also intersecting KAS06 at c. 450 m according to the conceptual model (Table 3.2). Thus, the response may have been transmitted upward from KAS06 through this zone to section M3. The spinner measurements show a major hydraulic conductor at 183–186 m in section M3 (Nilsson 1989). The calculated dilution flow rate through this section is relatively high, see Table 4.1.

Also the lowermost section M1 (503–601 m), assumed to be intersected by Zone NE–1w, shows good response to the pumping. The spinner survey indicate major hydraulic conductors at 555–571 m and 577–585 m in section M1. In this section, a high flow rate was calculated from the dilution measurements (Table 4.1). Furthermore, the injected tracer in this section was recovered in the pumping borehole KAS06 during LPT–2 (Gustafsson et al 1991). The response may have transmitted via Zones NNW–2w (and NE–1w) to section M1 (Table 5.1). Also sections M2 and M4 were responding relatively good to the pumping but no hydraulic conductors are interpreted in these sections.

KAS09

In KAS09 only intermediate–relatively poor responses were observed. In the conceptual model Zones EW–5w and NE–1w are assumed to intersect the upper part of the borehole in sections AE (0–115 m) and AD (116–150 m), respectively. However, poor responses were observed in these sections, c.f. Table 4.1 and the distance–drawdown plot in Fig. 4.1. This is surprising since a distinct response was observed in KAS06 in all sections below 250 m during the pumping test in KAS09 (Rhén et al. 1991). Major hydraulic conductors are identified at 100–119 m, 131–132 m and 146–148 m in sections AE and AD by the spinner survey (Rhén et al. 1991). Possibly, Zone NE–1w acts as a major recharge source to borehole KAS09 during pumping, extinguishing the drawdown towards south.

KAS10

In KAS10 a poor response was obtained (Table 4.1). No fracture zones are interpreted in this borehole.

KAS11

In KAS11 relatively poor responses were observed in all sections (Table 4.1). The estimated response times from the drawdown period are however uncertain due to sparse scanning in the beginning of the test and presumed tidal effects, c.f. KAS04. The only hydraulic zone interpreted in this borehole is EW–5w, assumed to intersect the upper part of the borehole in sections CE (47–64 m) and CD (65–115 m) in the conceptual model (Table 4.3). The spinner survey indicate a hydraulic conductor at 52–104 m in these sections (Rhén et al. 1991). However, the response in these sections was rather poor, c.f. Fig. 4.1. As in KAS09 Zone NE–1w possibly extinguishes the drawdown in this region. Dilution measurements in section CE under natural gradient before LPT–2 indicated a low natural flow rate through this section.

In section CB (153–183 m) there are geological evidence of Zone NE–1 and

possibly Zone EW–X (Wikberg et al 1991). A strong hydraulic conductor is identified at 157–174 m by the spinner measurements. The high natural flow rate measured in section CB (Table 4.1) may possibly be explained by natural flow in Zone NE–1w, but since this zone is not assumed to intersect KAS06, the hydraulic response in the section will yet be poor.

KAS12

The drawdown response in KAS12 is shown in Fig. 4.13. The most distinct response was observed in section DB (278–329 m). Also in section DC (234–277 m) a good response was registered, see Table 4.1. Both sections are assumed to be intersected by Zone NE–2w in the conceptual model (Table 4.3). This zone is not assumed to be intersected by KAS06. The strongest hydraulic conductors are located at 281–285 m and 308–324.5 m in section DB according to the spinner measurements (Rhén et al. 1991). A very high flow rate was monitored through section DB during LPT–2 by the dilution tests (Table 4.1), indicating an excellent hydraulic connection between this section and KAS06. No dilution measurements were carried out in section DC during pumping but measurements under a natural gradient indicated zero natural flow rate through this section (Table 4.1). The hydraulic responses in section DB (and DC) may possibly have been transmitted via Zones NNW–1w and –2w and Zone NE–2w.

An alternative interpretation is that Zone EW–5w intersects section DB somewhere in the most conductive interval 278–329 m. During the pumping test in KAS12 rather distinct responses were observed in borehole sections KAS02–B4, KAS05–E3 and E4, KAS06–F3 and F4 and KAS07–J4 (Rhén et al. 1991), i.e. in the intervals where Zone EW–5w is interpreted in the conceptual model. This fact indicates that Zone EW–5w intersects KAS12.

According to the conceptual model, KAS06 is assumed to intersect Zone EW–5w in the interval 312–365 m from spinner measurements and 389–406 m from the hydrochemical interpretation (Table 3.2). The tracer breakthrough measurements during LPT–2 showed that the inflow of Uranine to KAS06 from KAS12–DB mainly occurred at the 390 m–level in EW–5w and to a minor extent at the 430 m–level in NNW–2w (Gustafsson et al 1991). This indicates that the main part of the tracer travelled directly along Zone EW–5w to KAS06.

In section DA (330–380 m) an intermediate reponse time ratio was observed whereas in the uppermost sections DD (102–233 m) and DE (0–101 m) apparently good hydraulic responses are indicated, see Table 4.1. However, the latter responses are probably non–representative and may have been transmitted by hydraulic connections along the borehole or through the upper part of the bedrock. No hydraulic conductors are interpreted in these sections (Rhén et al. 1991).

KAS13

In KAS13 poor responses were observed in all sections, see Table 4.1. According to the map of conceptual hydraulic model (Fig. 1.2), the uppermost part of KAS13 is indicated to intersect Zone NNW–1w. Hydraulic conductors are identified at 160–170 m and 195–215 m, i.e. in sections ED (151–190 m) and EC (191–220 m) by the spinner survey (Rhén et al. 1991). The responses

in these sections are poor and do not support this interpretation unless KAS13 also intersects other zones. According to the geological interpretation KAS13 intersects Zone NE-2 at c.370-410 m (Wikberg et al. 1991). However, no hydraulic conductor is identified in this interval. If KAS13 intersected Zone NNW-1w a better hydraulic connection with KAS06 would be expected, since the latter borehole is also assumed to intersect this zone (Table 3.2). Dilution measurements in section EC during LPT-2 also indicate no hydraulic connection with KAS06, see Table 4.1.

KAS14

In KAS14 intermediate responses were observed in all sections, see Table 4.1. The estimated response times during drawdown are uncertain due to tidal effects and sparse scanning. The distance-drawdown plot also indicates relatively poor responses (Fig. 4.1). According to the conceptual model, Zone EW-5w is assumed to intersect the uppermost section FE (0-130 m) and Zone NE-1w the next three lower sections (FB, FC and FD). The latter zone is not assumed to intersect KAS06 which may explain the rather poor responses in these sections. Dilution measurements in section FB (147-175 m) during LPT-2 indicate no significant hydraulic connection with KAS06 although a certain flow through the section was measured during the pumping test, see Table 4.1. This flow is assumed to be natural flow along Zone NE-1w, c.f. section KAS11-CB.

In section FE a strong hydraulic conductor is identified at 110-122 m by the spinner survey (Rhén et al. 1991). The response in these section is rather poor which possibly may be explained by the extinguishing effect of Zone NE-1w, c.f. boreholes KAS09 and KAS11. During the pumping in KAS14 distinct responses were obtained in KAS06 in all sections below 250 m (Rhén et al. 1991).

5. ESTIMATION OF HYDRAULIC PARAMETERS

The hydraulic parameters of some of the fracture zones have been estimated by transient analysis of the most distinct responses in the observation boreholes (Table 4.3), assuming a leaky confined aquifer system according to Walton (see e.g. Carlsson and Gustafson 1984). This model, which assumes radial flow towards the pumping borehole supported by a certain leakage flow, generally from above, is considered to be a reasonable approximation in this case. This is supported by the declining electric conductivity of the discharged groundwater from the pumping borehole during LPT-2 (Fig.2.2), indicating a small inflow of shallow, non-saline water from above. During the drawdown period the electric conductivity in KAS06 decreased from about 1400 to c. 1320 mS/m (Jönsson and Nyberg 1991).

In Table 5.1, bulk values on the hydraulic parameters (based on the total flow rate) are estimated assuming flow in a porous, isotropic leaky aquifer, i.e in an equivalent porous media together with possible pathways of the major hydraulic responses in the cored boreholes. The evaluation has mainly been performed of the first drawdown phase and the recovery period from the logarithmic diagrams. No corrections of the raw-data (e.g. due to tidal effects) have been made before the evaluation. Consistent results were obtained from both drawdown and recovery.

In the distance-drawdown diagram in Fig. 4.1 the theoretical Theis' curve is shown. By the matching, emphasis is put on responses in borehole sections assumed to be located in Zone EW-5w according to Table 5.1. These sections are marked with a circle in Fig. 4.1. The curve thus roughly represents the bulk hydraulic properties of Zone EW-5w. Responses located above the curve generally represent borehole sections in other fracture zones (e.g. NNW-1w and -2w) and preferential flow paths (e.g. sections J5 and J6) whereas responses below the curve generally represent sections in the rock mass with intermediate and poor hydraulic connections to the pumping borehole.

An approximative distance-drawdown analysis was also made in Fig. 4.1 by the end of the drawdown period according to Theis (see e.g. Carlsson and Gustafson 1984). The (total) transmissivity was estimated at $T=1.5\times10^{-4}$ m^2/s (corresponding to a transmissivity of about 5×10^{-5} m^2/s for Zone EW-5w) which is in good agreement with the results of the time-drawdown/recovery analyses (Table 5.1). The calculated storativity value ($S=1.8\times10^{-4}$) is likely to be somewhat overestimated due to the leakage inflow occuring by the end of the test.

Table 5.1 Estimated bulk hydraulic parameters together with possible main pathways from KAS06 to the observation sections with the major hydraulic responses in the cored boreholes during LPT-2.(T_b=bulk transmissivity, S=storativity and K'/m'=leakage coefficient).

Borehole-section	$T_b\times10^{-5}$ (m^2/s)	$S\times10^{-5}$ (-)	$K'/m'\times10^{-10}$ (s^{-1})	Possible pathway	Test phase
KAS02-B4	12	6.3	2.8	EW-5w	drawdown
-B4	14	4.5	0.8	-"-	recovery
-B3	11	1.8	1.6	EW-5w/EW-X	drawdown
-B3	15	1.6	0.5	-"-	recovery
KAS04-D2	14	12	1.4	EW-5w? (NNW-1w-NE-2w)	drawdown -"-
-D2	11	12	1.1	-"-	recovery
KAS05-E3	14	4.0	2.4	EW-5w	drawdown
-E3	14	5.2	2.3	-"-	recovery
KAS07-J6	4.1	0.27	0.095	NNW-1w	drawdown
-J6	4.7	0.63	0.11	-"-	recovery
-J5	4.9	0.82	0.26	NNW-1w ?	drawdown
-J5	4.7	1.4	0.25	-"-	recovery
-J4	17	4.9	1.3	EW-5w	drawdown
-J4	16	4.2	1.2	-"-	recovery
-J2	6.1	0.37	0.096	EW-3w?	drawdown
-J1	19	5.5	2.5	NNW-1w-NE-1w (EW-X-NE-1w)	drawdown -"-
-J1	17	5.7	2.3	-"-	recovery
KAS08-M3	14	0.56	0.35	NNW-2w	drawdown
-M3	15	0.98	0.37	-"-	recovery
-M1	10	4.6	5.0	NNW-2w-NE-1w	drawdown
-M1	8.9	5.0	4.4	-"-	recovery
KAS12-DC	15	2.5	0.88	EW-5w? (NNW-1&2w-NE-2w)	drawdown
-DB	13	1.6	0.87	D:o	-"-

According to the conceptual model the pumping borehole KAS06 is assumed to intersect several fracture zones (Table 3.2). Since the pumping test was performed in the open borehole, all these fracture zones are thus pumped

simultaneously with various inflows to the pumping borehole. The estimated inflow distribution in the pumping borehole for each fracture zone is shown in Table 3.2.

By considering each fracture zone as an individual hydraulic conductor, pumped by the flow rate fraction of the total flow rate in Table 3.2, the transmissivity of some of the dominating fracture zones during LPT–2 is estimated in Table 5.2. The transmissivity values were calculated by multiplying the bulk transmissivity values in Table 5.1 by the corresponding estimated inflow portion shown in Table 3.2. Thus, the calculated transmissivity values are dependent on the conceptual model and the interpretation of fracture zones. In Table 5.3 the estimated range of transmissivity for the actual fracture zones calculated from LPT–2 and assumed in the conceptual model is shown.

The estimated ranges of transmissivity of the dominating fracture zones from LPT–2 are in reasonable agreement with the ranges assumed in the conceptual model. Also, the estimated transmissivities from these fracture zones in KAS06 (Table 3.2) generally are within this range.

Table 5.2 Estimated transmissivity (T) and inflow from some of the dominating fracture zones during LPT–2 (T_b=bulk transmissivity from Table 5.1).

Borehole–section	Dominating fracture zone	Inflow (%)	$T_b x10^{-5}$ (m^2/s)	$Tx10^{-5}$ (m^2/s)
KAS02–B4	EW–5w	33	12	4.0
–B3	EW–5w	33	11	3.3
KAS04–D2	EW–5w?	33	14	4.6
KAS05–E3	EW–5w	33	14	4.6
KAS07–J6	NNW–1w	21	4.1	0.84
–J5	NNW–1w?	21	4.9	1.0
–J4	EW–5w	33	17	5.6
–J2	EW–3w?	15	6.1	0.91
–J1	NNW–1w?	21	19	4.0
	EW–X?	5	19	0.95
KAS08–M3	NNW–2w	26	14	3.6
–M1	NNW–2w	26	10	2.6
KAS12–DC	EW–5w?	33	15	4.9
–DB	EW–5w	33	13	4.3

In total, ten percussion boreholes responded to the pumping in KAS06. In the other boreholes no significant drawdown was observed. The most distinct responses (relative to the distance from the pumping borehole) were observed in HAS06–N1 and HAS13–U1, see Table 4.1. A rather low specific capacity (Q/s_w=2.8x10^{-7} m^2/s) was calculated in HAS06 from the air–lift tests (Wikberg et al. 1991, p.81). No fracture zone is interpreted to intersect the borehole.

In HAS13 a high transmissivity (T=2.5x10^{-4} m^2/s) was calculated from the air–lift tests (Nilsson 1989). According to the conceptual model Zone EW–3w is assumed to intersect HAS13 (Wikberg et al. 1991, p.181). From LPT–2 an apparent high transmissivity of T=5.0x10^{-4} m^2/s (based on the total flow rate), a storativity of S=6.0x10^{-5} and a leakage coefficient of K'/m'=7.0x10^{-10} s^{-1} were

calculated. It is uncertain whether the response in HAS13–U1 was propagated along fracture zones or in the upper part of the bedrock and accordingly, if the calculated hydraulic parameters in this section are representative. The response may possibly have been transmitted via Zones EW–3w and NNW–3w.

In general, no quantitative evaluation of the responses in the percussion boreholes has been performed since most responses are interpreted as intermediate–poor (Table 4.1) and probably have been indirectly transmitted along the upper part of the bedrock in most cases.

Table 5.3 Estimated range of transmissivity of the dominating fracture zones from LPT–2 and assumed in the conceptual model.

Fracture zone	LPT–2 $Tx10^{-5}$ (m^2/s)	Conceptual model $Tx10^{-5}$ (m^2/s)
EW–5w	3.3 – 5.6	1 – 4
NNW–1w	0.84– 4.0	0.5–2
NNW–2w	2.6 – 3.6	2 – 6
EW–3w	0.91 ?	0.01–0.1
EW–X	0.95	–

6. DISCUSSION OF THE CONCEPTUAL MODEL

According to Table 4.3 and the conceptual model, fracture zones are assumed to intersect most of the observation sections with the most distinct hydraulic responses during LPT–2. In several of these sections the hydraulic connections with the pumping borehole are confirmed by tracer dilution measurements. These observations thus support the overall conceptual model. However, some modifications of the latter model are necessary to satisfactory explain all observation borehole responses.

Conversely, fracture zones are interpreted in a few sections with rather poor (delayed) responses. These are KAS09–AE and AD which are assumed to be intersected by Zone EW–5w (50–100 m) and Zone NE–1w (110–148 m), respectively in the geohydrological conceptual model. Also in sections KAS11–CE and CD (Zone EW–5w), KAS13–ED and EC (Zone NNW) and KAS14–FE (Zone EW–5w) rather poor or delayed hydraulic responses were observed, see Table 4.1. Several of these sections are located in the upper part of the bedrock and in boreholes close to Zone NE–1w. As discussed above, this zone may possibly have an extinguishing effect on the responses in observation boreholes close to the zone.

Some of the fracture zones interpreted in the observation sections are assumed to also intersect the pumping borehole KAS06, i.e. Zones EW–3w, NNW–1w and 2w, EW–5w (and possibly also EW–X). Of these zones, EW–5w (and possibly EW–X) and NNW–1w and 2w seem to play an important role as major hydraulic conductors during LPT–2. The responses in observation sections intersected by the other interpreted fracture zones in the southern part of the Äspö area, i.e. NE–1w, EW–1w and NE–2w seem to have been indirectly

transmitted via the above mentioned fracture zones from the pumping borehole.

The distinct response in the lower part of KAS03 indicates that Zone EW–5w probably also extends to the north of Zone EW–1w. This is considered to be an important result of LPT–2.

LPT–2 also indicates that Zone EW–5w may intersect section D2 (332–392 m) in KAS04. In the hydraulic conceptual model Zone NE–2w (and possibly also EW–1) is assumed to intersect this section. However, the geological interpretation indicates the presence of Zone EW–5 .

Zone EW–5w may also intersect section DB (278–329 m) in KAS12. In the conceptual model this section is assumed to be intersected by Zone NE–2w.

Zone EW–X may possibly be of hydraulic importance in the deeper parts of the bedrock.

Considering the uncertainties in the quantitative evaluation of LPT–2 the estimated transmissivities of the dominating fracture zones on Äspö are generally within (or close to) the range of transmissivities of these zones assumed in the conceptual model. The only exception is Zone EW–3w for which the estimated transmissivity from LPT–2 is 10–100 times higher than assumed in the conceptual model. The estimated value from LPT–2 is considered as very uncertain since it is only based on the hydraulic response in borehole section KAS07–J2 (which is uncertain).

However, Zone EW–3w is probably hydraulically significant in the pumping borehole KAS06. Except the results from the tracer dilution tests in KAS06 during LPT–2, this zone probably affects the drawdown behavior in KAS06. This is indicated by the rapid increase of drawdown in KAS06 when the flow rate was increased 900920 (Table 2.1). The drawdown increased more than was expected, indicating changed hydraulic conditions in the borehole (increased skin factor). This may be explained by the groundwater table in the borehole falling below a major hydraulic conductor of Zone EW–3w, located at a vertical depth of about 50–60 m. This figure approximately coincides with the measured groundwater head at this time (Fig. 2.1) and the interpreted location of Zone EW–3w from the tracer dilution measurements (Table 3.2).

The interpretation of Zones NNW–3w and –4w in the conceptual model must be regarded as uncertain. The observed rather large drawdown across Zone NNW–4w in the upper part of the bedrock in boreholes HAS06 and 07, see Table 4.1, may speak against the present interpretation of this zone.

7. CONCLUSIONS

The qualitative and quantitative evaluation of the pumping test LPT–2 is consistent with the overall conceptual model presented in Wikberg et al. (1991). The hydraulic importance of Zone EW–5w and the NNW–fracture system, and indirectly also NE–1w, is clearly demonstrated. However, the test indicated that some modifications of this model are necessary to satisfactory explain all drawdown responses observed.

The most important points to further investigate are considered to be:

-the extension of Zone EW-5w towards northwest beyond Zone EW-1w (KAS03).

-the extension of Zone EW-5w towards northeast and location of the zone in boreholes KAS04 and KAS12 (and possibly in KAS08).

-the extension and hydraulic properties of Zone EW-3w.

-the extension and hydraulic properties of Zones NNW-3w and -4w.

8. REFERENCES

Carlsson L och Gustafson G (1984): Provpumpning som geohydrologisk undersökningsmetodik. R41 : 1984, Byggforskningsrådet.

Carlsten S (1991): Pers. comm.

Gustafsson E, Andersson P, Ittner T and Nordqvist R (1991): Large scale three dimensional tracer test at Äspö. GRAP 91001, Geosigma AB, Uppsala.

Ittner T, Gustafsson E, Andersson P and Eriksson C-O (1991): Groundwater flow measurements at Äspö with the dilution method. PR 25-91-18.

Jönsson S och Nyberg G (1991): Data från långtidspumptest i borrhål KAS06. SGAB IRAP 91223, Uppsala.

Nilsson L (1988): Hydraulic tests at Äspö and Laxemar. Evaluation. PR 25-88-14, Stockholm.

Nilsson L (1989): Hydraulic tests at Äspö. KAS05-KAS08, HAS13-HAS17. Evaluation. PR 25-89-20, Stockholm.

Rhén I (1990): Transient interference tests on Äspö in KAS06, HAS13 and KAS07. Evaluation. PR 25-90-09, Stockholm.

Rhén I, Forsmark T and Nilsson L (1991): Hydraulic tests on Äspö, Bockholmen and Laxemar 1990 in KAS09, KAS11-14, HAS18-20, KBH01-02 and KLX01. Evaluation. PR 25-91-01, Stockholm.

Wikberg P (ed), Stanfors R, Rhén I and Gustafson G (1991): Evaluation and conceptual modelling based on the pre-investigations for the Äspö Hard Rock Laboratory. SKB Technical Report 91-22.

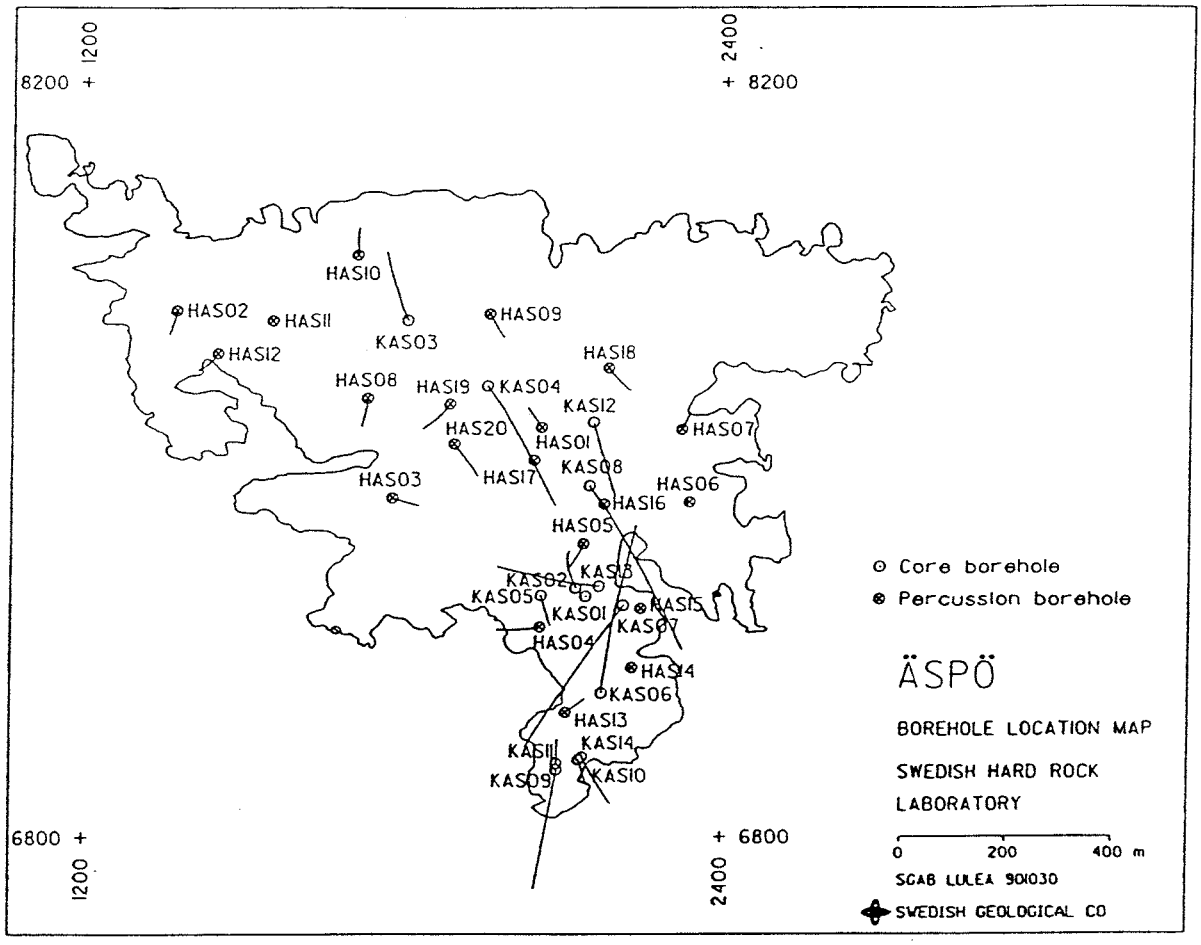

Fig. 1.1 Location of boreholes on Äspö and their direction.

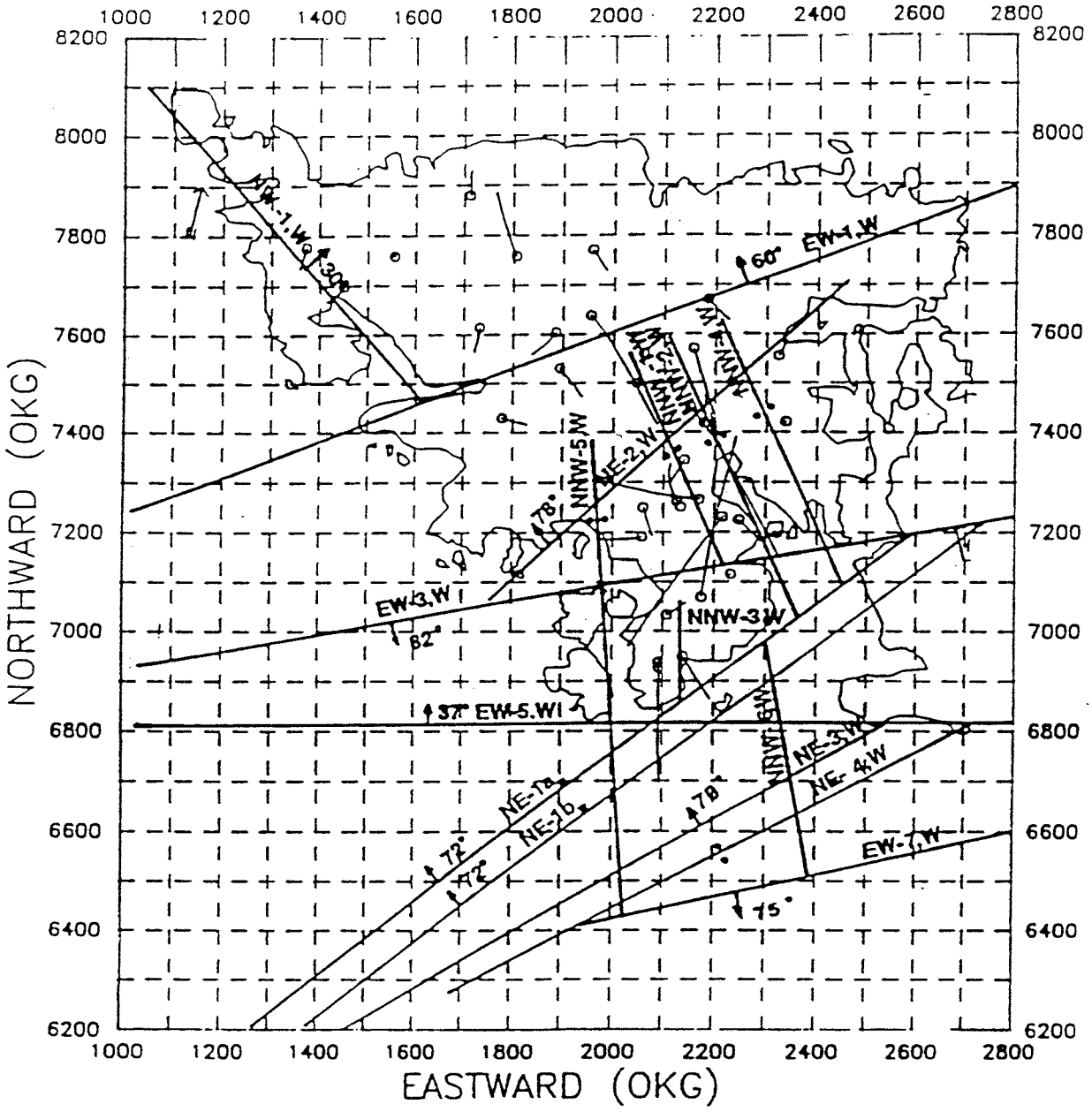

Fig. 1.2 Conceptual model of conductive structures on Äspö (From Wikberg et al., 1991).

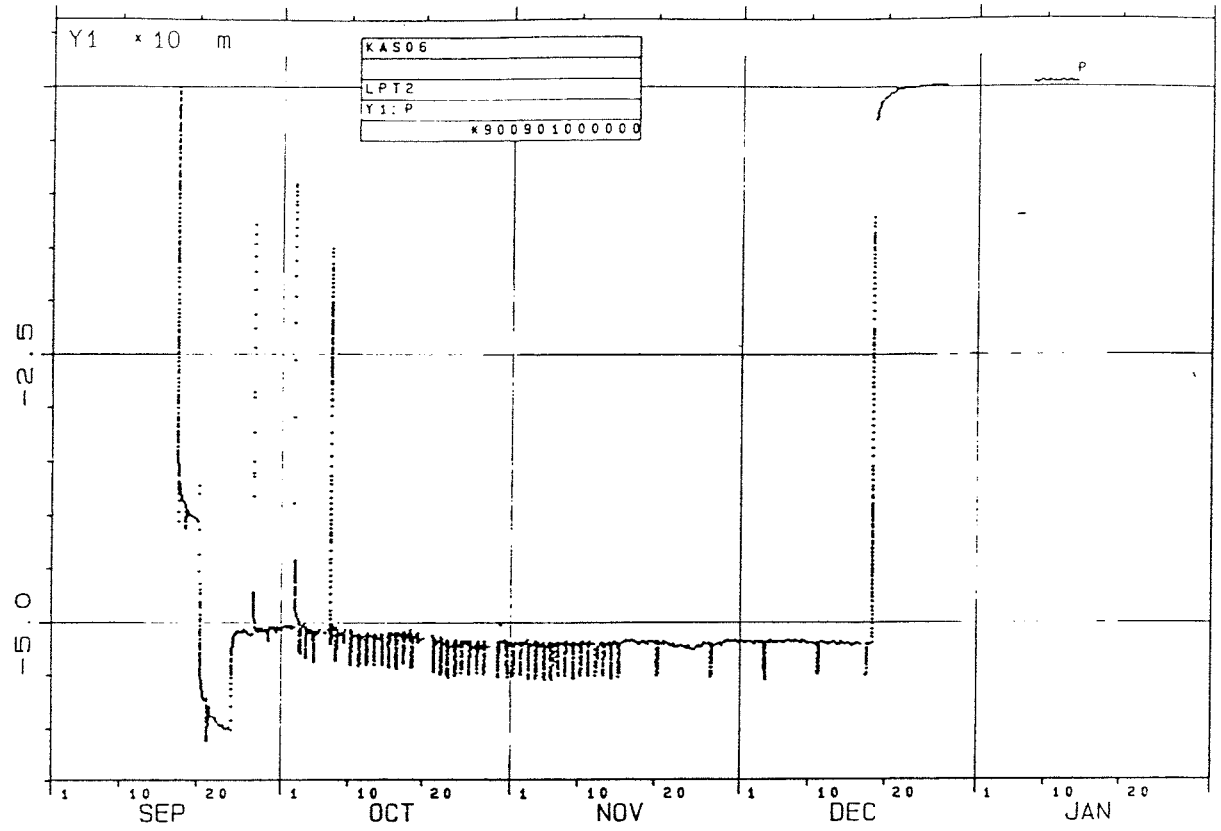

Fig. 2.1 Overview of the groundwater head in KAS06 during LPT–2. (From Jönsson och Nyberg 1991).

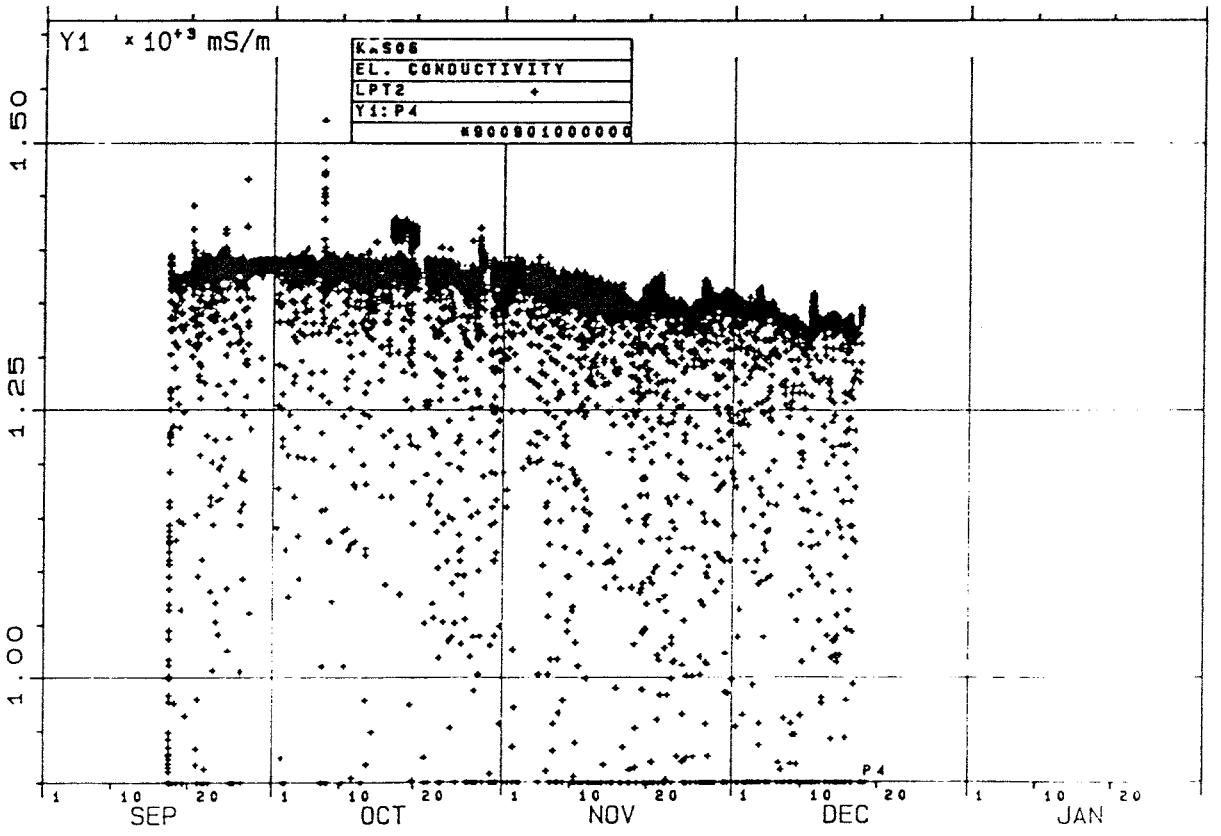

Fig. 2.2 Changes of electric conductivity in the discharged groundwater from KAS06. (From Jönsson och Nyberg 1991).

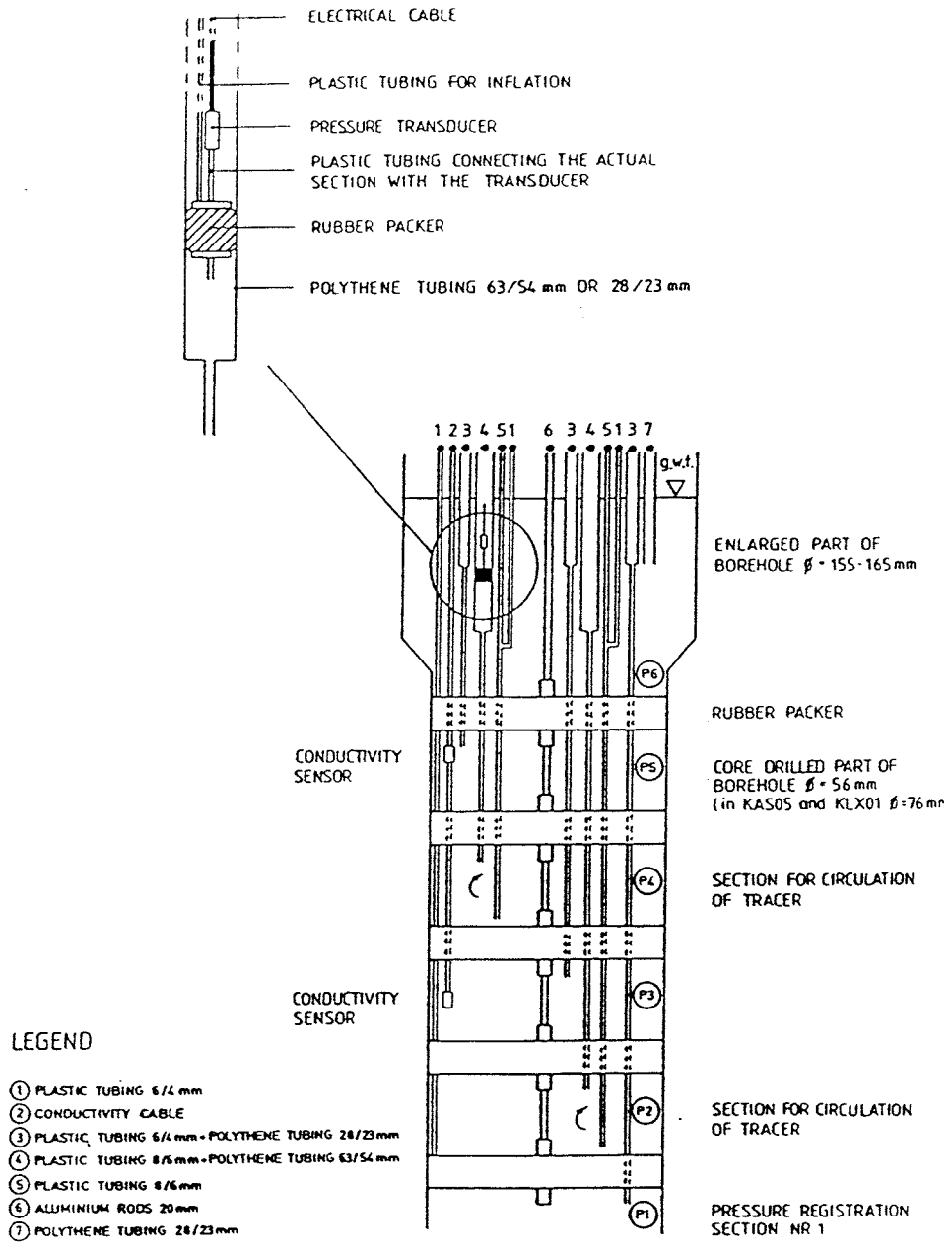

Fig. 2.3 Instrumentation in the cored boreholes on Äspö. (From Jönsson och Nyberg 1991).

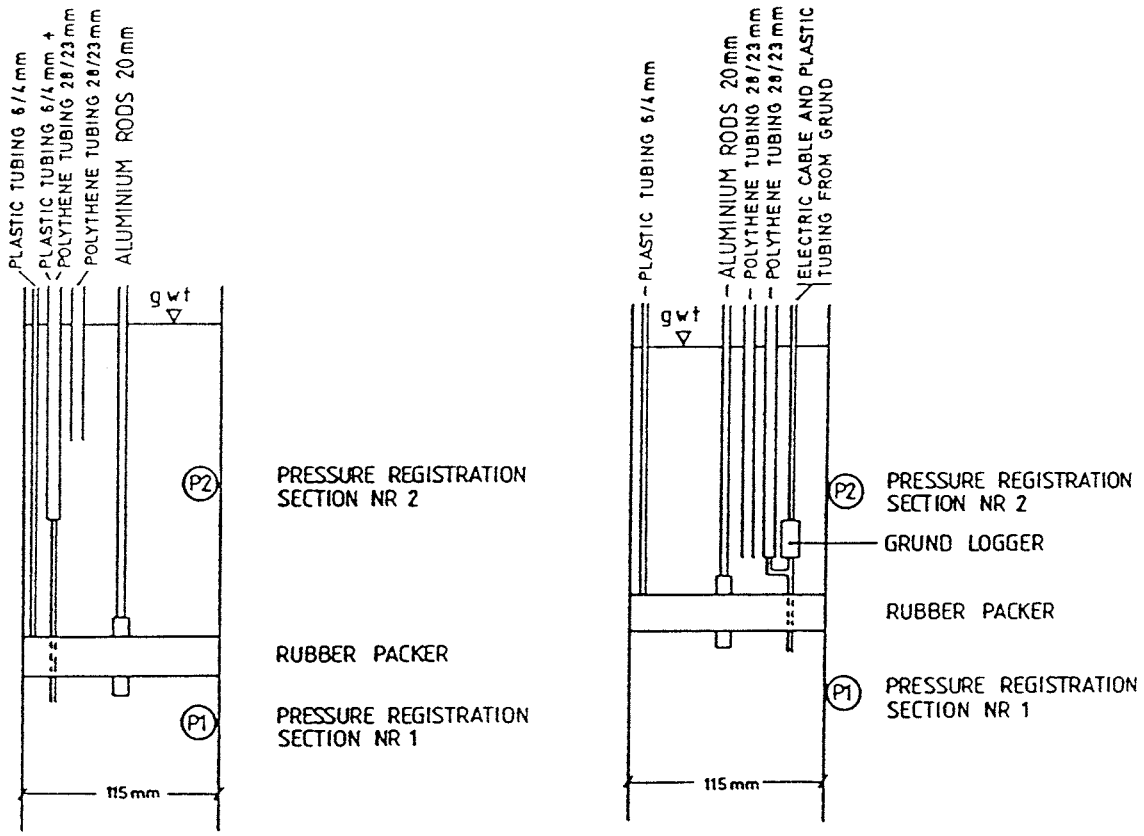

Fig. 2.4 Instrumentation in the percussion boreholes on Äspö. (From Jönsson och Nyberg 1991).

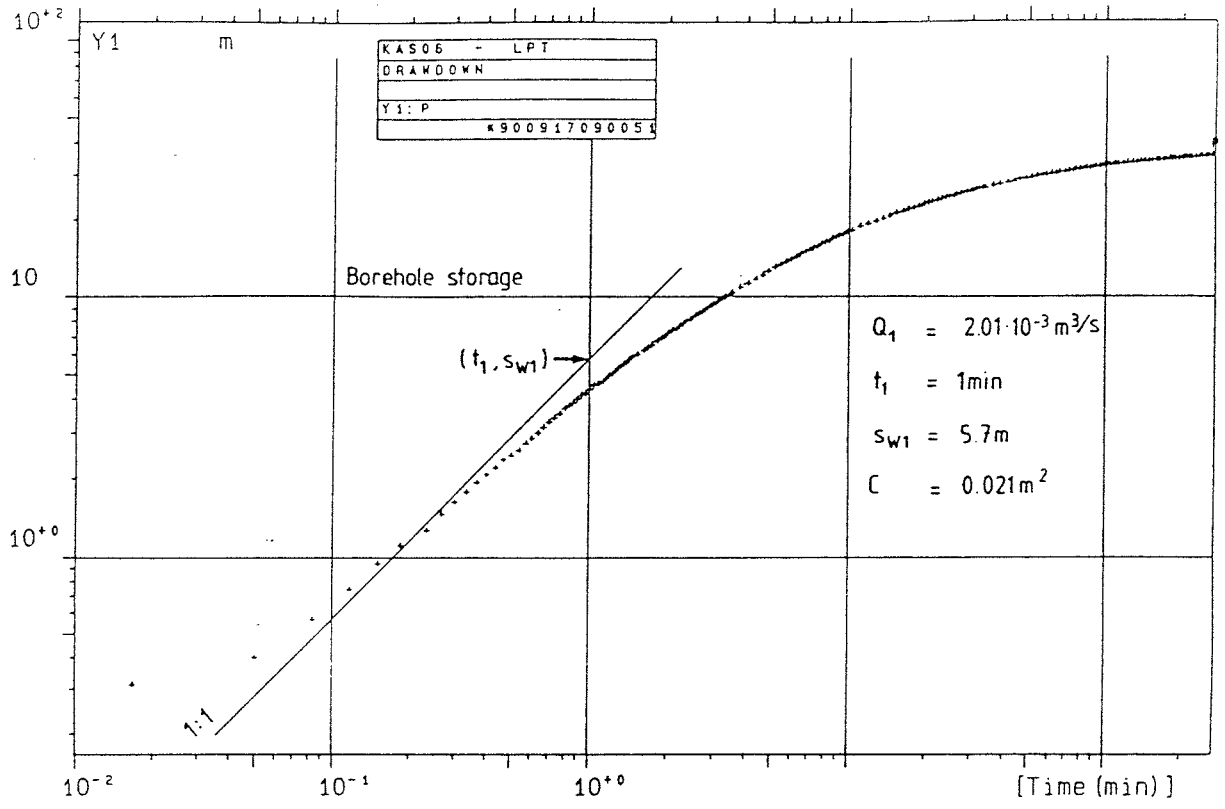

Fig. 3.1 Drawdown in KAS06 during LPT–2, logarithmic graph. (From Jönsson och Nyberg 1991.

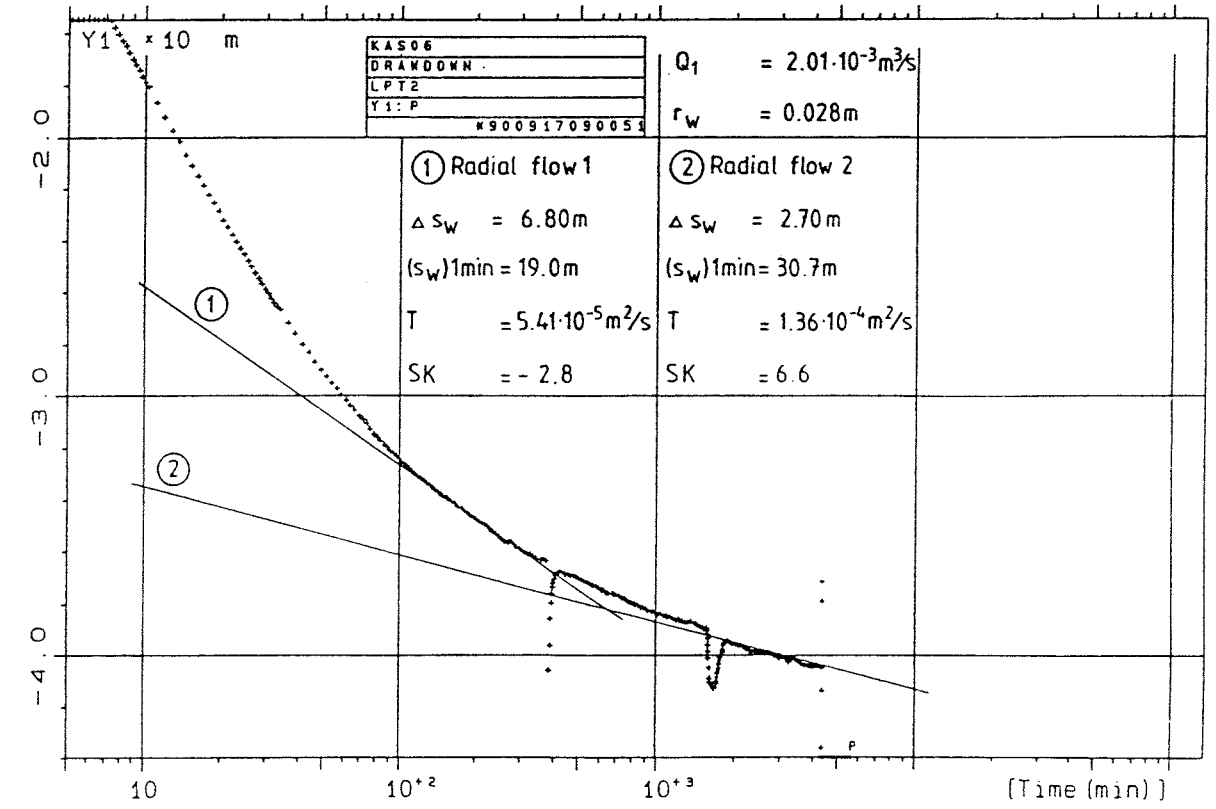

Fig. 3.2 Drawdown in KAS06 during LPT–2, semilogarithmic graph. (From Jönsson och Nyberg 1991).

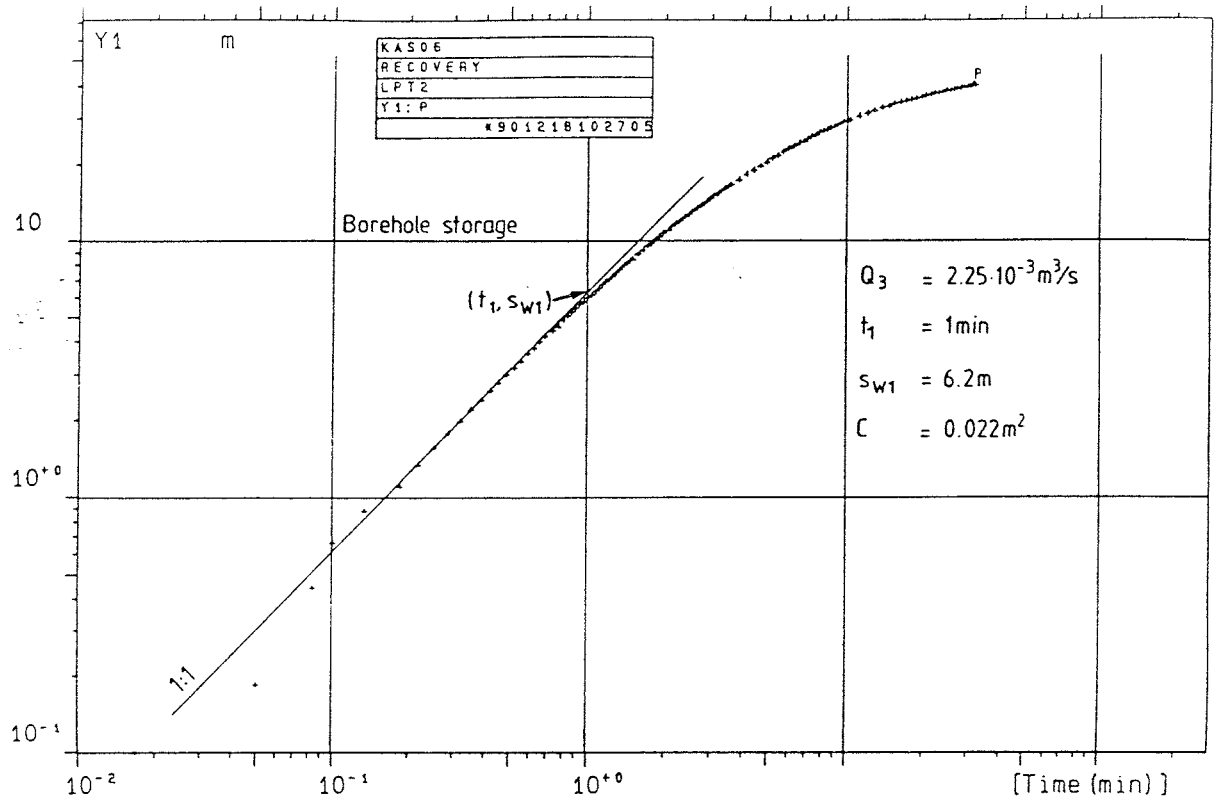

Fig. 3.3 Recovery in KAS06 during LPT–2, logarithmic graph. (From Jönsson och Nyberg 1991.

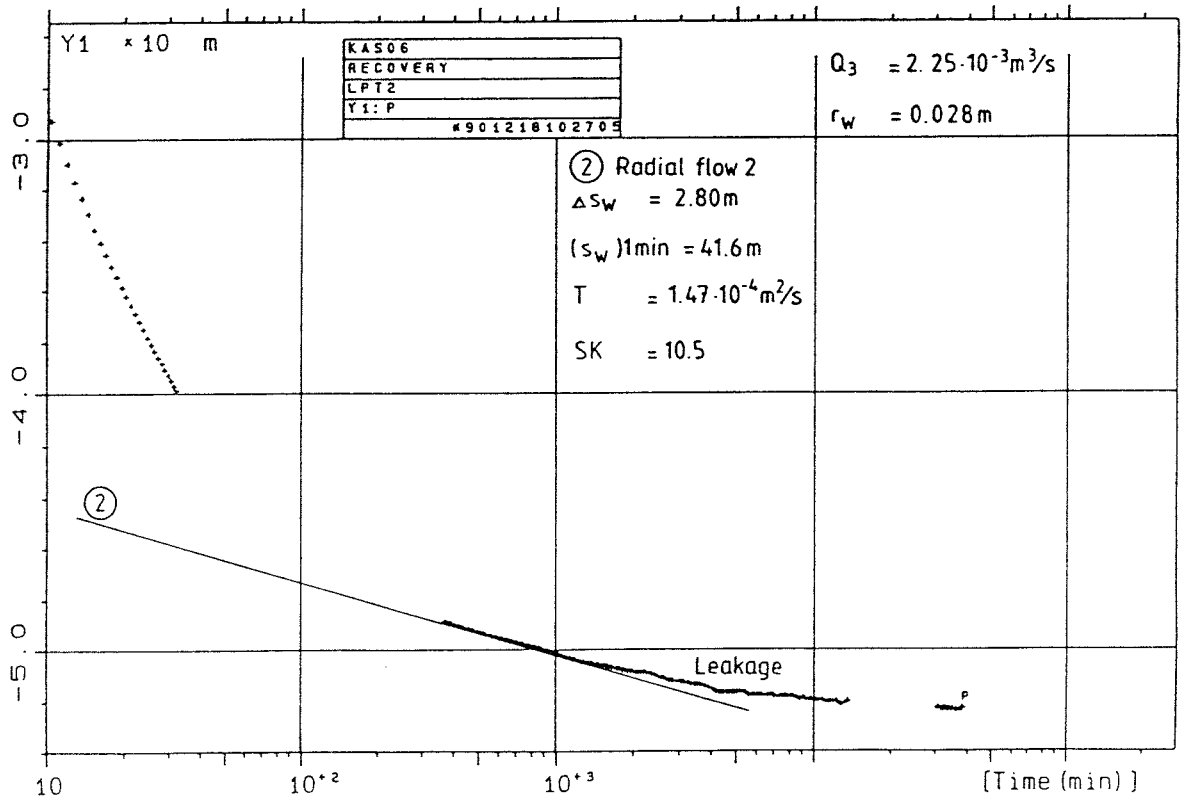

Fig. 3.4 Recovery in KAS06 during LPT–2, semilogarithmic graph. (From Jönsson och Nyberg 1991).

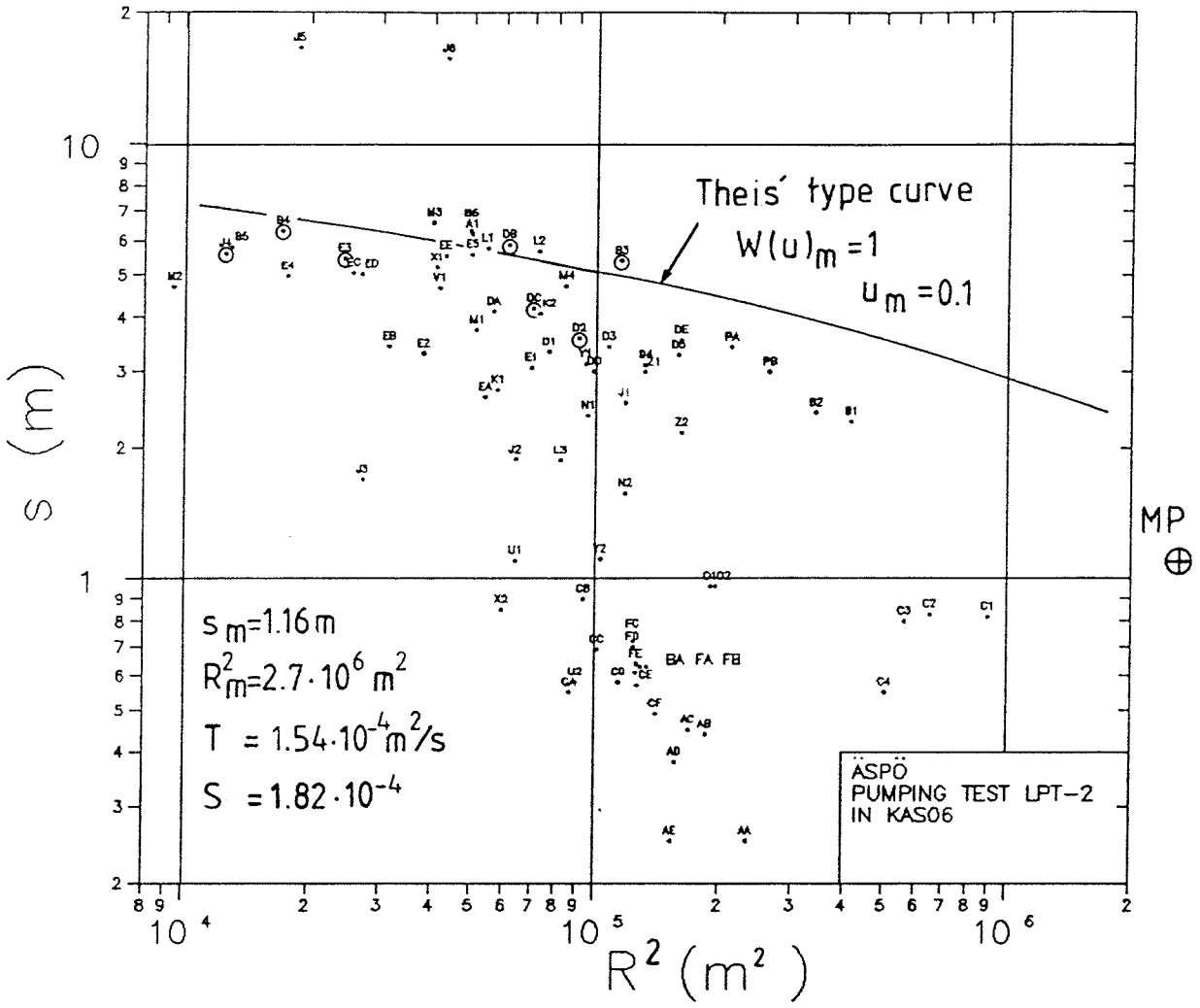

Fig. 4.1 Distance – drawdown graph at stop of pumping (t=132 595 min) during LPT–2 together with theoretical Theis' curve. The variable codes refer to the observation sections listed in Table 4.1. Sections assumed to be located in Zone EW–5w are marked with a circle.

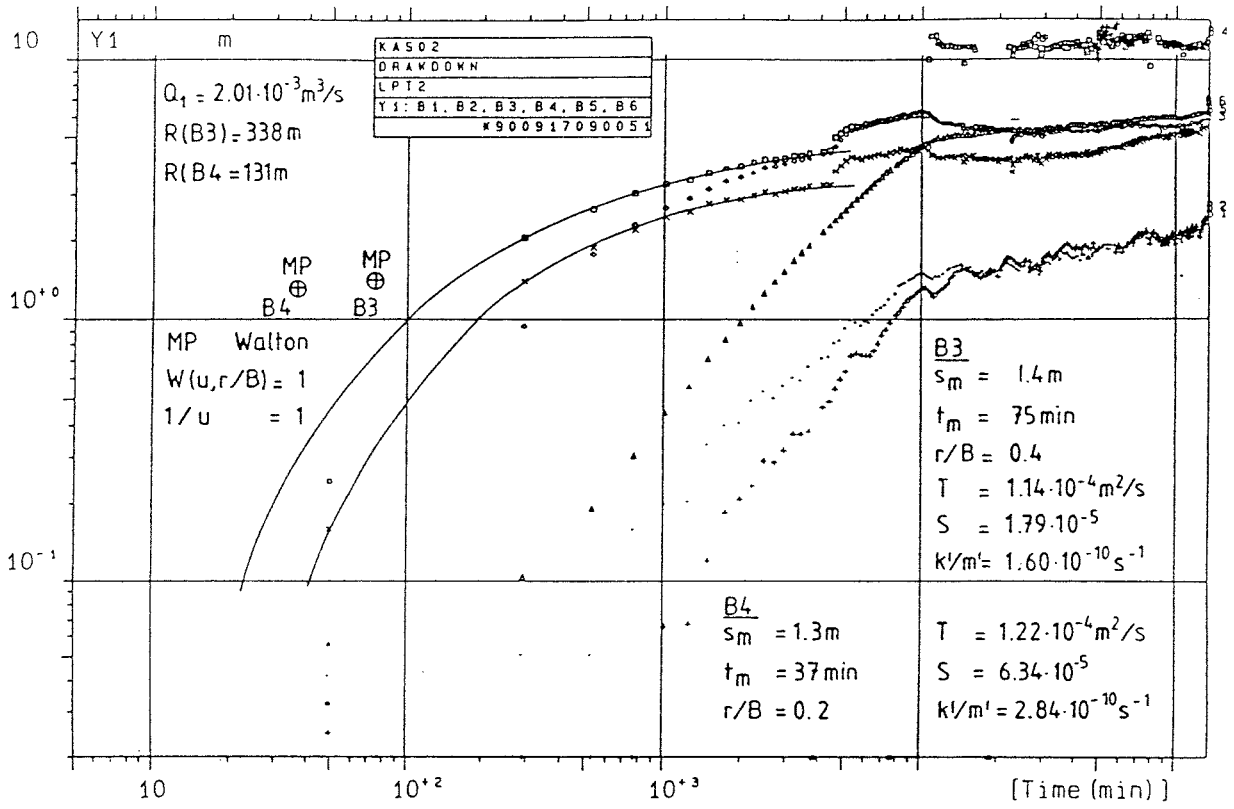

Fig. 4.2 Drawdown response in KAS02. The section intervals are shown in Table 4.1. (From Jönsson och Nyberg 1991).

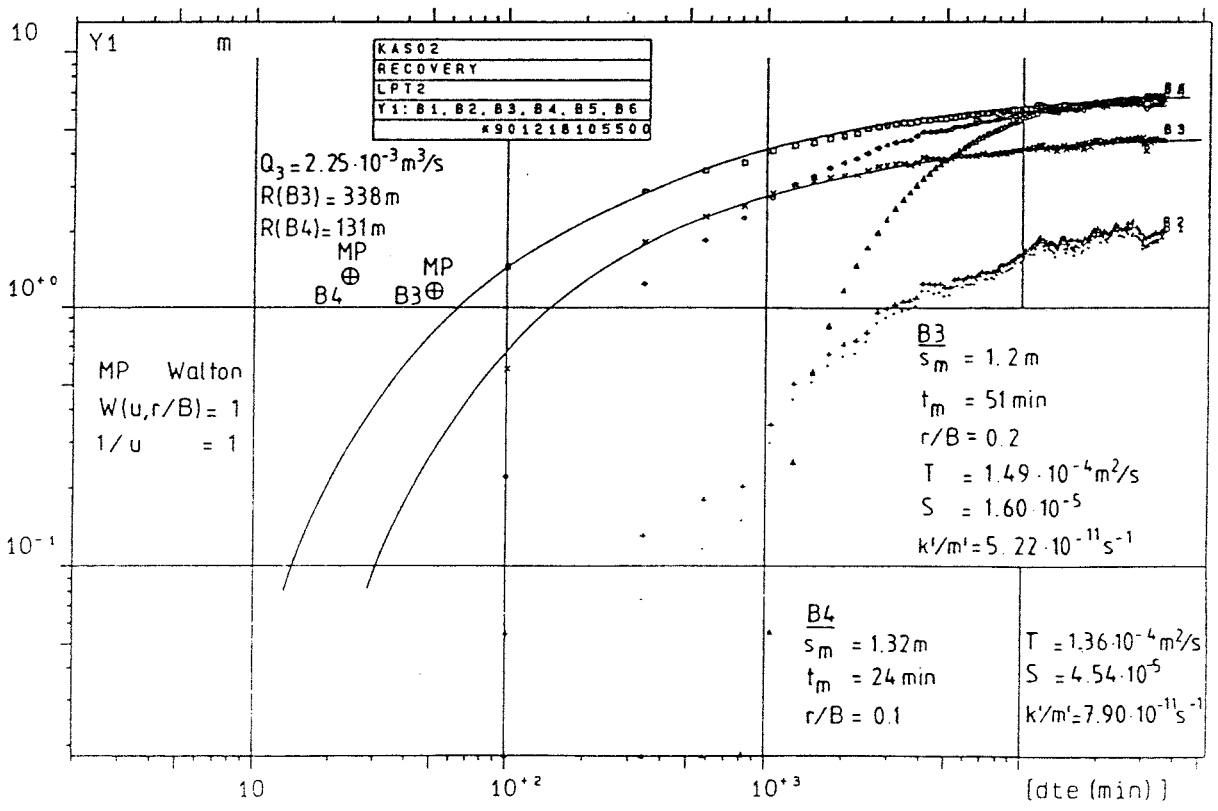

Fig. 4.3 Recovery response in KAS02. The section intervals are shown in Table 4.1. (From Jönsson och Nyberg 1991).

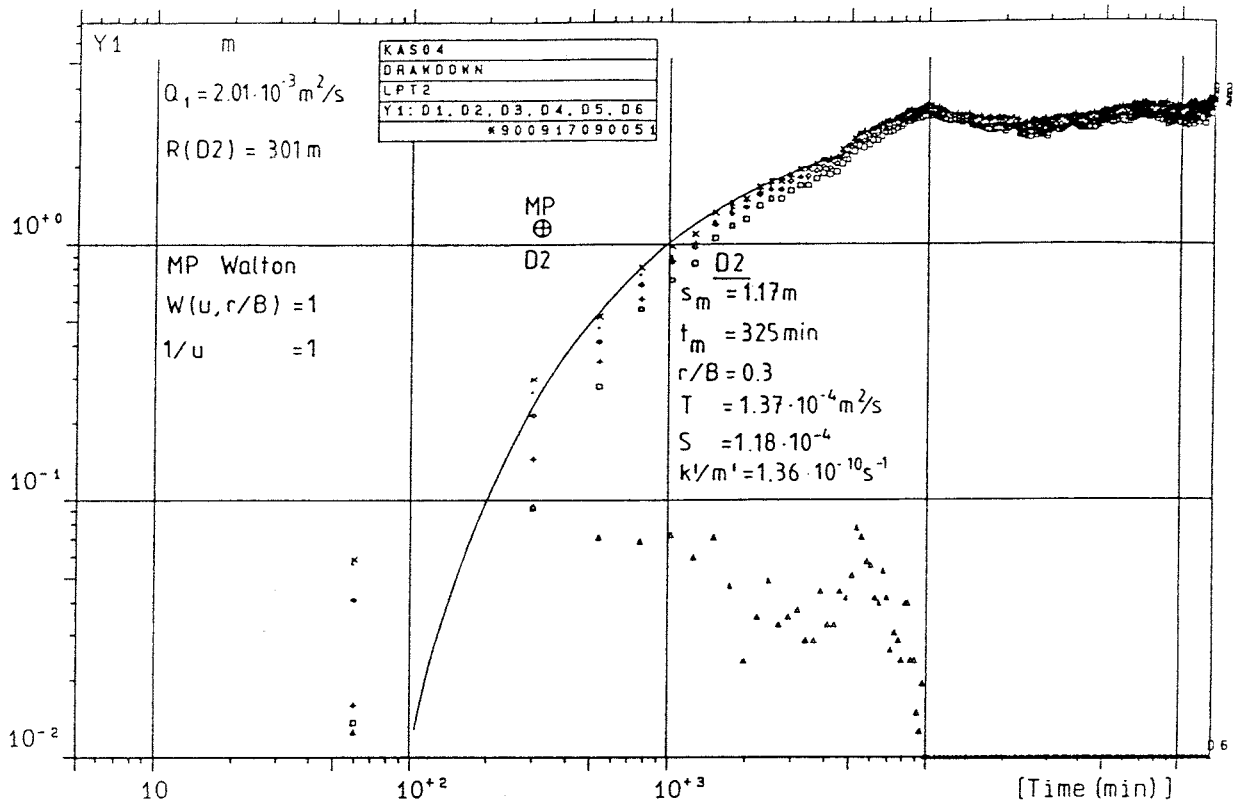

Fig. 4.4 Drawdown response in KAS04. The section intervals are shown in Table 4.1. (From Jönsson och Nyberg 1991).

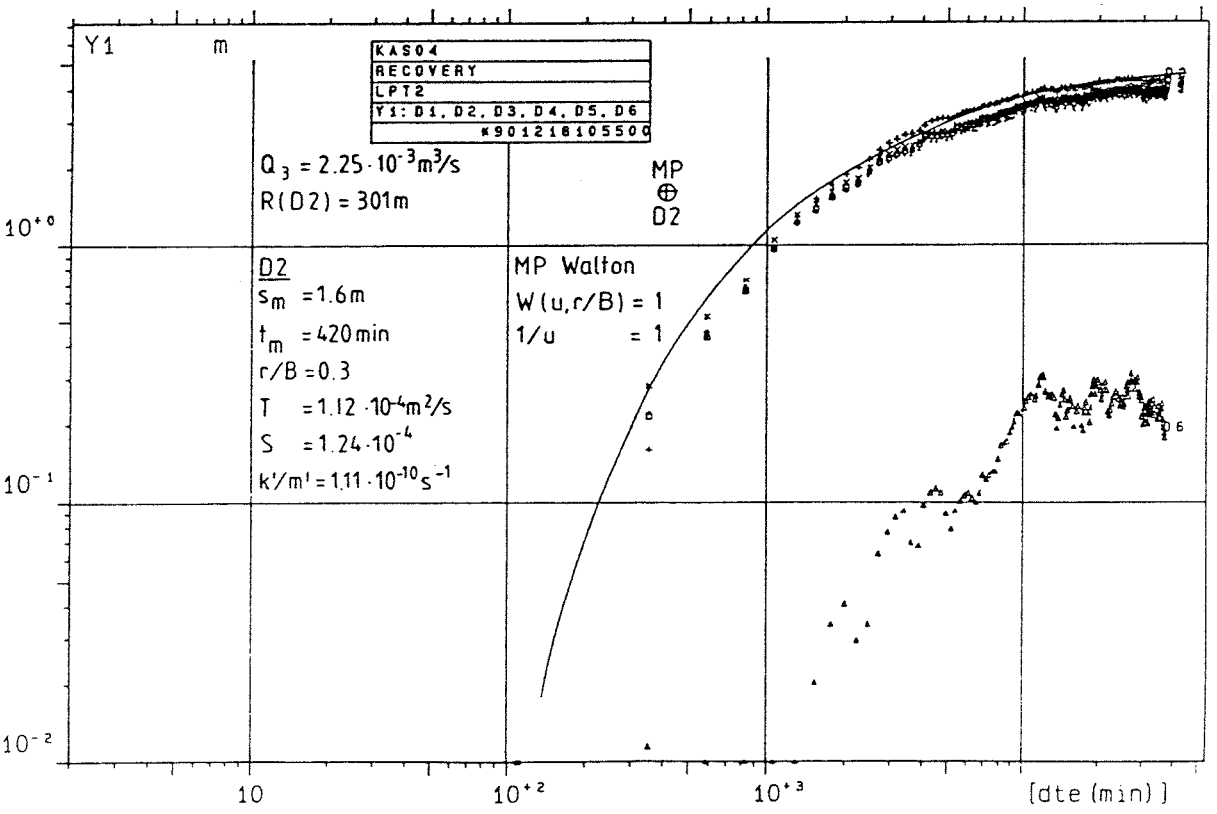

Fig. 4.5 Recovery response in KAS04. The section intervals are shown in Table 4.1. (From Jönsson och Nyberg 1991).

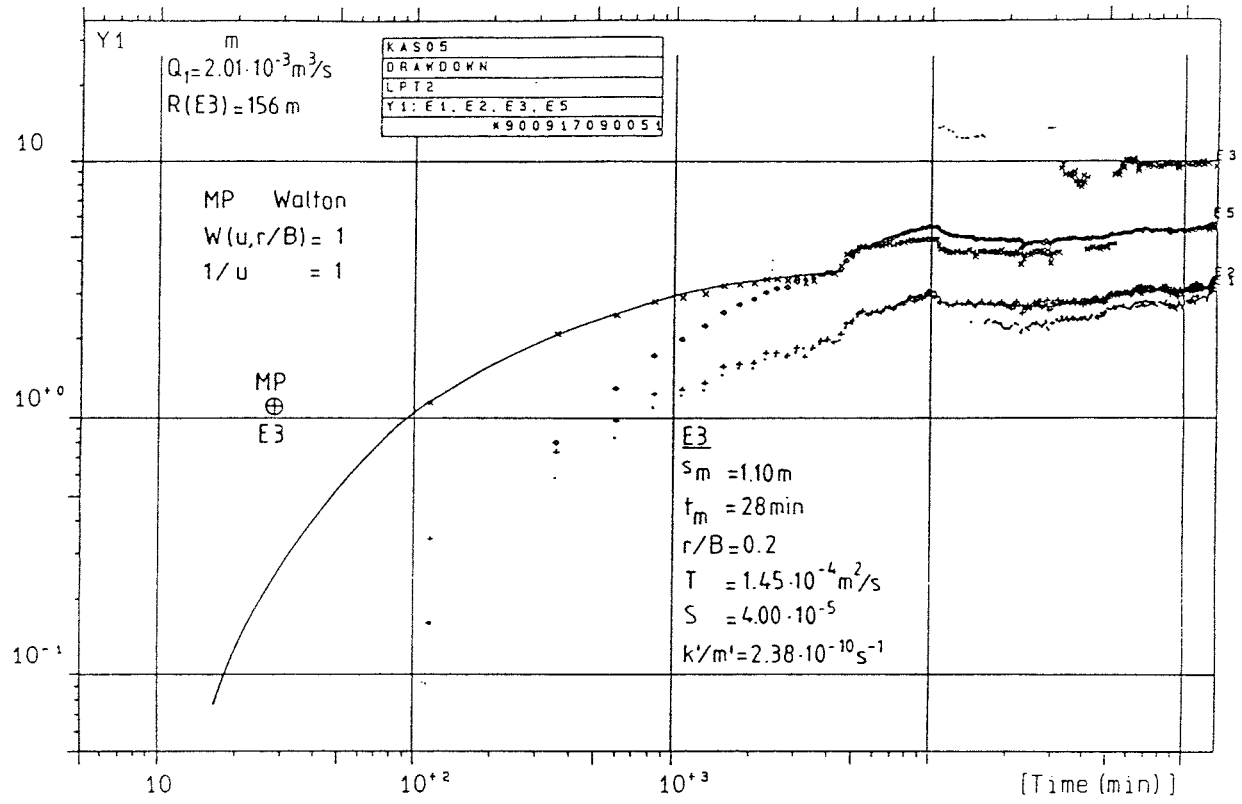

Fig. 4.6 Drawdown response in KAS05. The section intervals are shown in Table 4.1. (From Jönsson och Nyberg 1991).

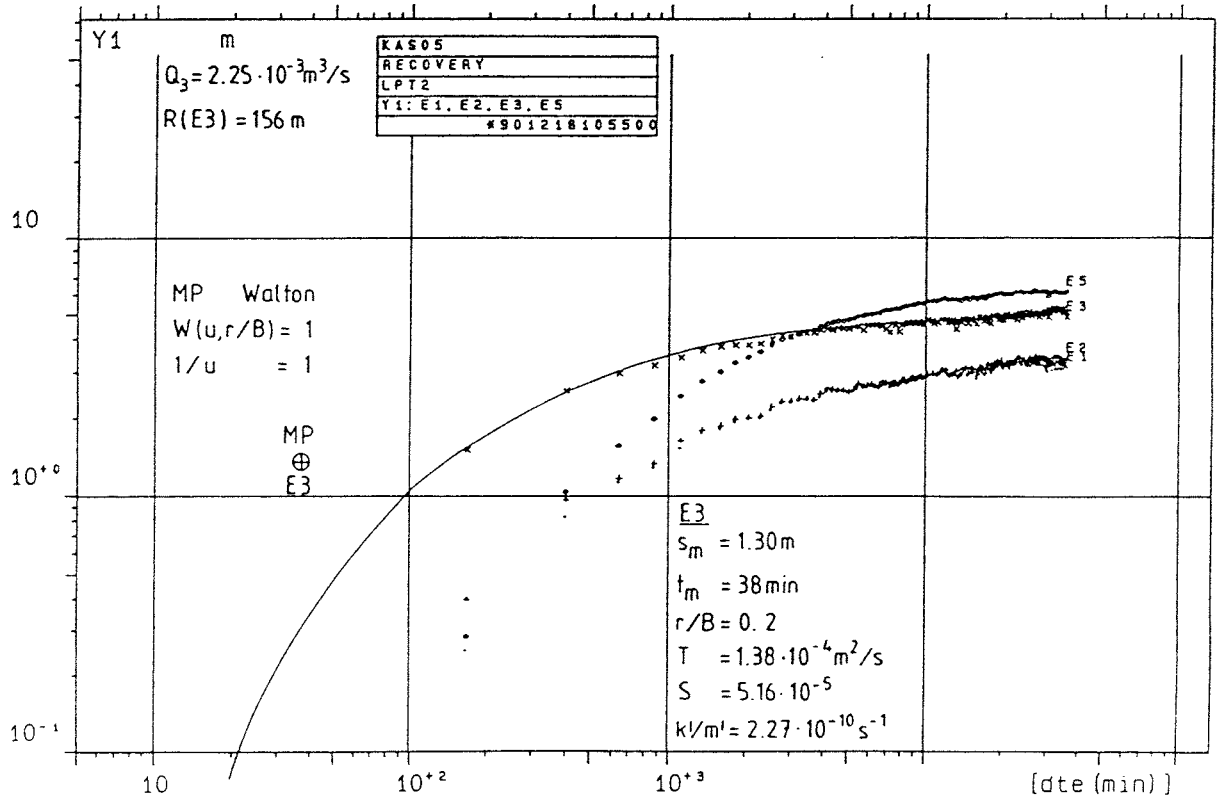

Fig. 4.7 Recovery response in KAS05. The section intervals are shown in Table 4.1. (From Jönsson och Nyberg 1991).

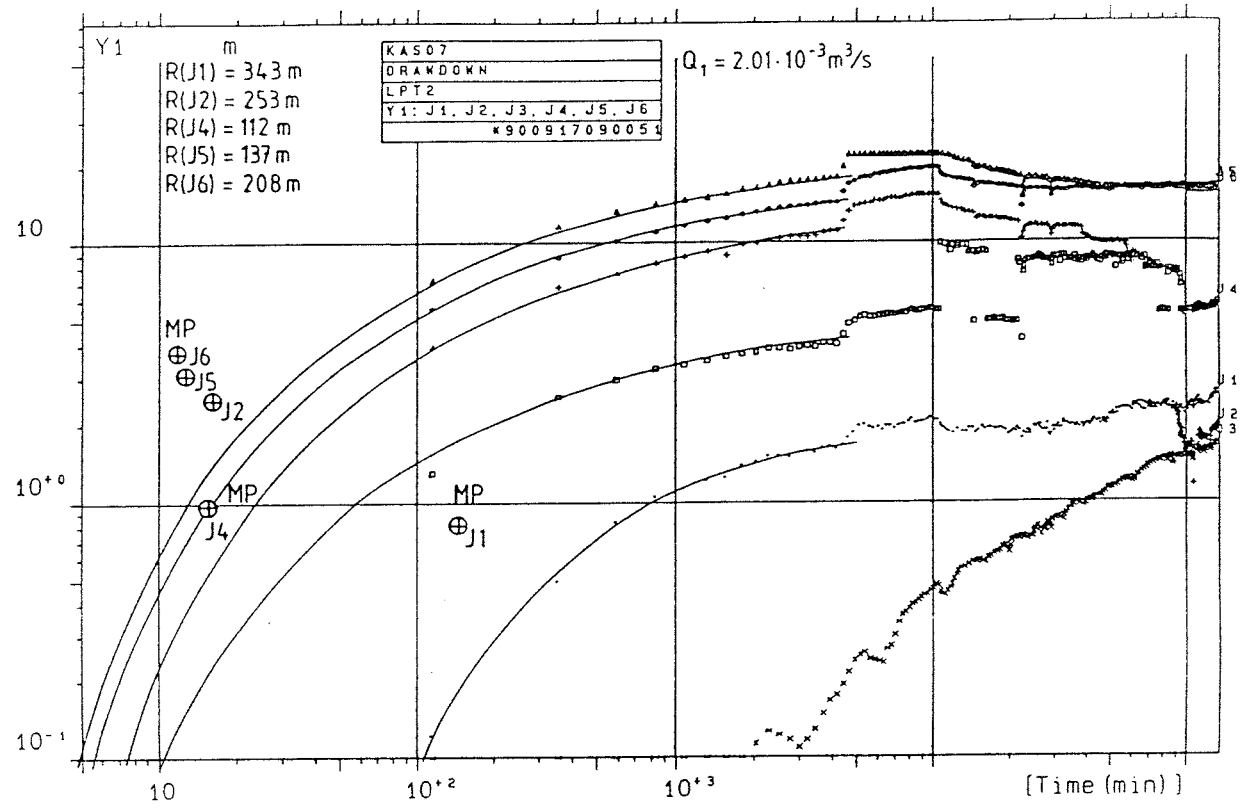

Fig. 4.8 Drawdown response in KAS07. The section intervals are shown in Table 4.1. (From Jönsson och Nyberg 1991).

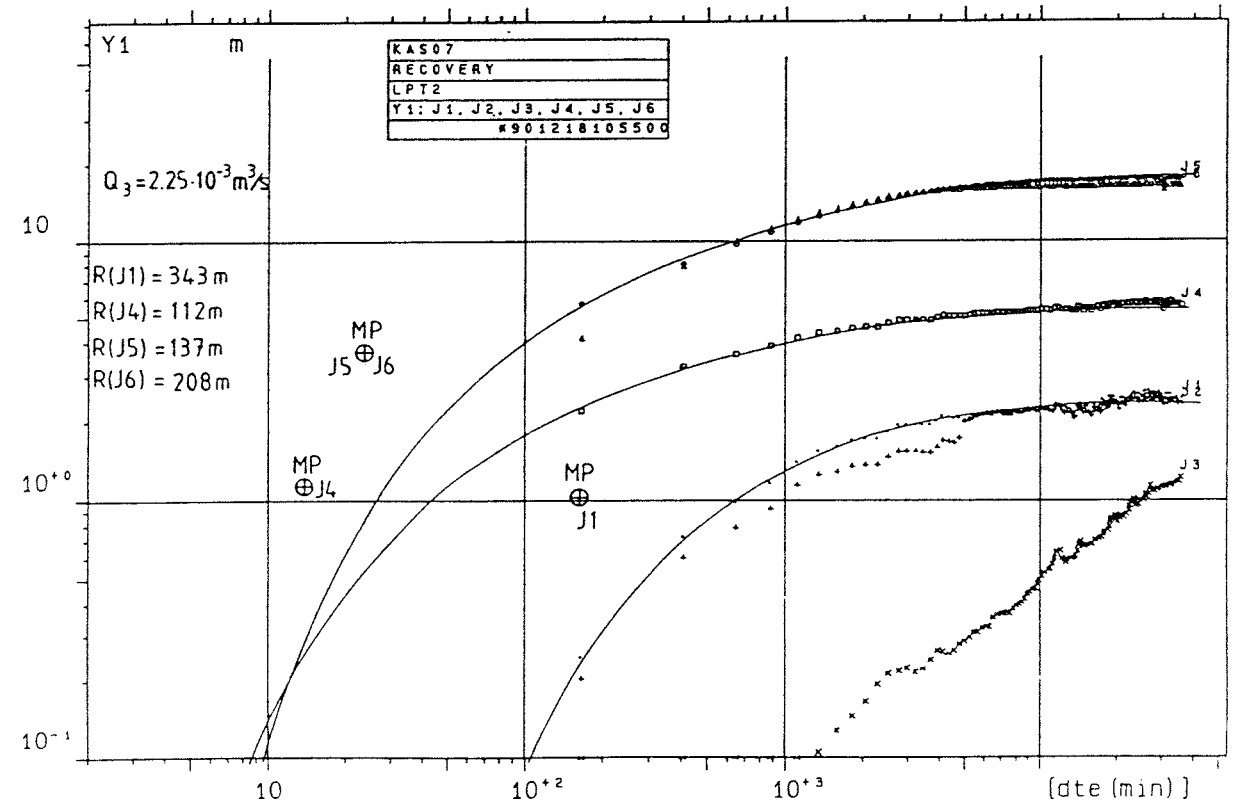

Fig. 4.9 Recovery response in KAS07. The section intervals are shown in Table 4.1. (From Jönsson och Nyberg 1991).

KAS07
LPT-2
DRAW-DOWN

MP Walton
W(u,r/B) = 1
1/u = 1

J1
s_m = 0.85m
t_m = 145min
r/B = 0.4
T = $1.87 \cdot 10^{-4} m^2/s$
S = $5.54 \cdot 10^{-5}$
$k'/m' = 2.54 \cdot 10^{-10} s^{-1}$

J2
s_m = 2.60m
t_m = 16min
r/B = 0.1
T = $6.12 \cdot 10^{-5} m^2/s$
S = $3.67 \cdot 10^{-6}$
$k'/m' = 9.56 \cdot 10^{-12} s^{-1}$

J4
s_m = 0.96m
t_m = 15.5min
r/B = 0.1
T = $1.66 \cdot 10^{-4} m^2/s$
S = $4.94 \cdot 10^{-5}$
$k'/m' = 1.32 \cdot 10^{-10} s^{-1}$

J5
s_m = 3.22m
t_m = 13min
r/B = 0.1
T = $4.94 \cdot 10^{-5} m^2/s$
S = $8.22 \cdot 10^{-6}$
$k'/m' = 2.63 \cdot 10^{-11} s^{-1}$

J6
s_m = 3.9m
t_m = 12min
r/B = 0.1
T = $4.10 \cdot 10^{-5} m^2/s$
S = $2.73 \cdot 10^{-6}$
$k'/m' = 9.48 \cdot 10^{-12} s^{-1}$

RECOVERY

J1
s_m = 1.05m
t_m = 165min
r/B = 0.4
T = $1.70 \cdot 10^{-4} m^2/s$
S = $5.73 \cdot 10^{-5}$
$k'/m' = 2.31 \cdot 10^{-10} s^{-1}$

J4
s_m = 1.15m
t_m = 14min
r/B = 0.1
T = $1.56 \cdot 10^{-4} m^2/s$
S = $4.17 \cdot 10^{-5}$
$k'/m' = 1.24 \cdot 10^{-10} s^{-1}$

J5
s_m = 3.8m
t_m = 24min
r/B = 0.1
T = $4.71 \cdot 10^{-5} m^2/s$
S = $1.44 \cdot 10^{-5}$
$k'/m' = 2.51 \cdot 10^{-11} s^{-1}$

J6
s_m = 3.8m
t_m = 24min
r/B = 0.1
T = $4.71 \cdot 10^{-5} m^2/s$
S = $6.27 \cdot 10^{-6}$
$k'/m' = 1.09 \cdot 10^{-11} s^{-1}$

Fig. 4.10 Results of the analysis of the drawdown and recovery periods of KAS07 in Fig 4.8–9.

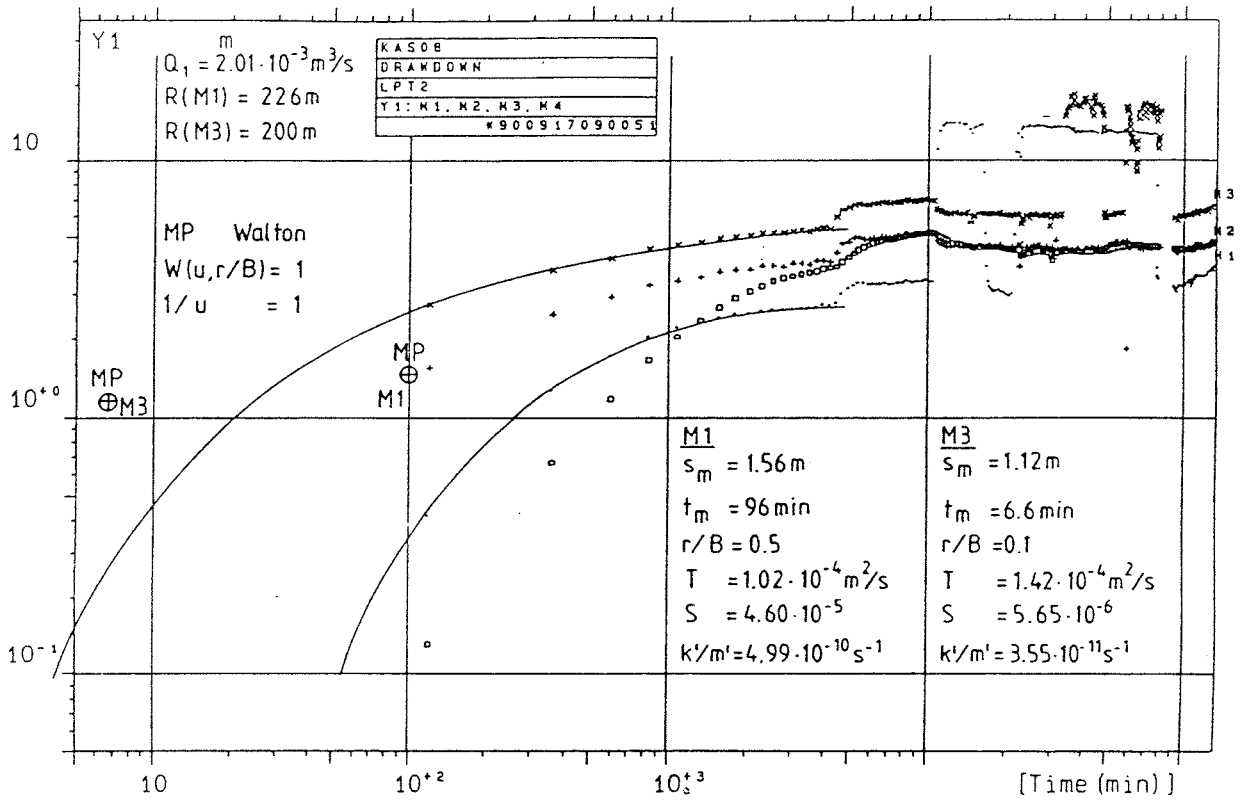

Fig. 4.11 Drawdown response in KAS08. The section intervals are shown in Table 4.1. (From Jönsson och Nyberg 1991).

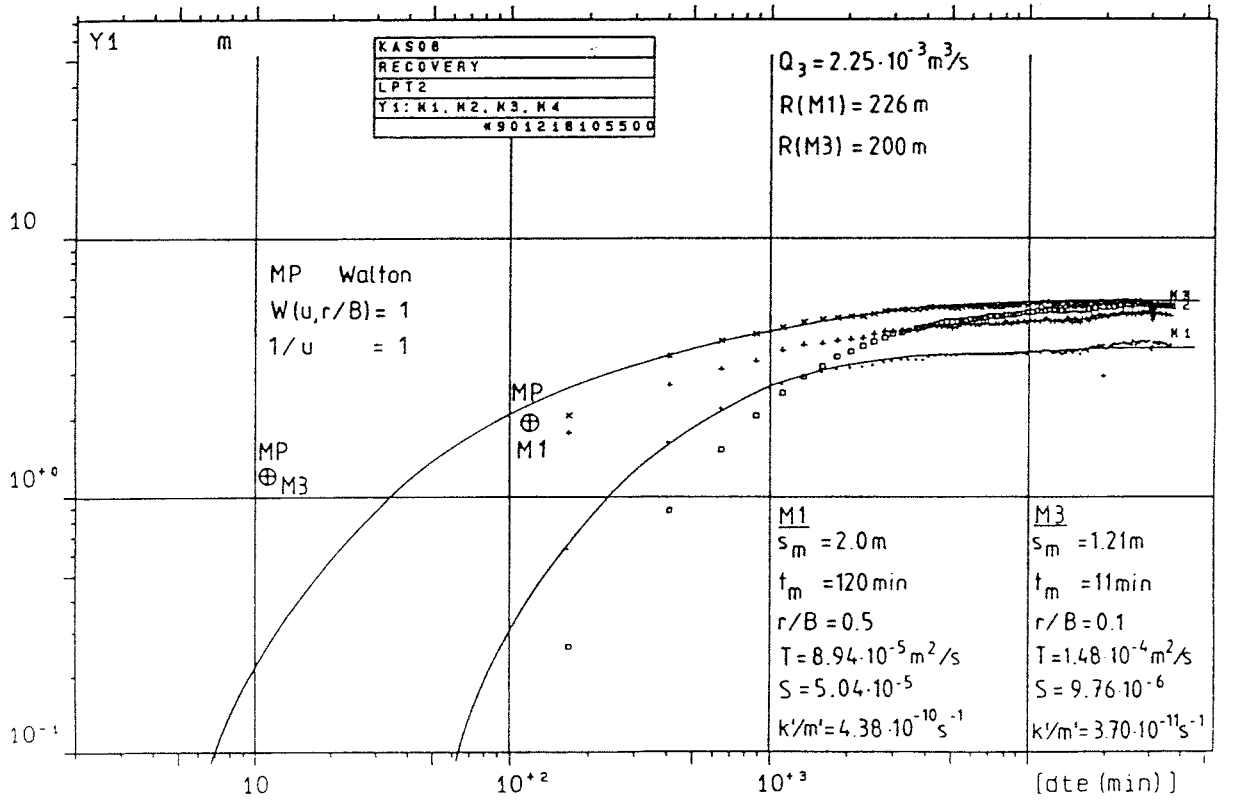

Fig. 4.12 Recovery response in KAS08. The section intervals are shown in Table 4.1. (From Jönsson och Nyberg 1991).

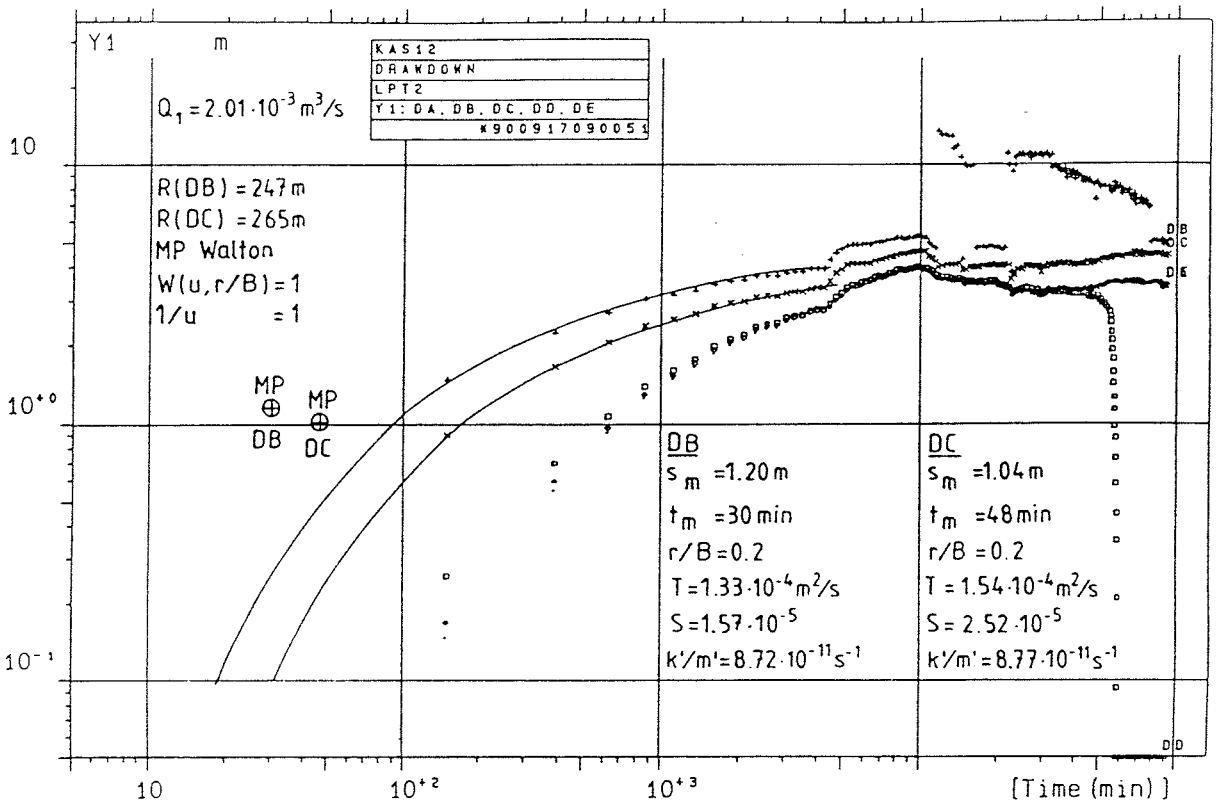

Fig. 4.13 Drawdown response in KAS12. The section intervals are shown in Table 4.1. (From Jönsson och Nyberg 1991).

APPENDIX C Large scale three-dimensional tracer test at Äspö

GEOSIGMA AB

Client: SKB

REPORT
ID-no: GRAP 91001
Date: 1991-12-12

LARGE SCALE THREE-DIMENSIONAL TRACER TEST AT ÄSPÖ

Erik Gustafsson
Peter Andersson
Thomas Ittner
Rune Nordqvist

GEOSIGMA AB
UPPSALA, SWEDEN

December 1991

ABSTRACT

A large scale three-dimensional tracer test was performed in fractured crystalline rock autumn 1990 in the target area at Äspö, Sweden where the hard rock laboratory is to be constructed. The objective of this tracer test was to determine how the major fracture zones are interconnected and by comparison with the experimentally obtained results verify or refute the framework of fracture zones presented in the conceptual model of Äspö. The aim was also to determine transport parameters such as residence time, dispersivity, flow porosity and hydraulic conductivity of the fracture flow paths. Predictions of tracer flow paths and residence times have previously been made by numerical modeling and the experimemtal results are compared with the predicitons.

The large scale three-dimensional tracer test included tracer withdrawal by pumping in an 600 metres deep open borehole, creating a converging flow field in the hydraulic conductive fracture zones surrounding the borehole. One dye tracer and three radionuclide tracers were injected in packed-off sections in nearby boreholes, where these intersects the hydraulic conductors. Two of the tracers were subjected to repeated injection, resulting in tracer injections from totally six locations in the fracture system. The geometric (straight line) distances from point of injection to point of detection in the withdrawal borehole ranged from 100 to 300 metres. The longest tracer flow path (trajectory) distance along interconnected fracture zones is calculated to approximately 380 metres. The depths ranged from 140 to 600 metres.

The experimental design and performance included the intermittent decaying pulse injection technique to minimize disturbance of the groundwater flow field and handling of radioactive tracers whilst also optimum conditions for tracer detection in the withdrawal borehole are given. Groundwater flow measurements by the dilution method were utilized to determine which borehole sections to be subjected to tracer injection, and a multilevel sampler were used to make it possible to detect tracer inflow levels in the withdrawal borehole.

The results of the tracer test are consistent with the framework of fracture zones presented in the existing conceptual model of the Äspö area. The dispersivities in the fracture zones at Äspö obtained by model fit to the breakthrough curves are compareable to a large fracture zone (Zone 2) investigated at the Finnsjön site, central Sweden. In general, the dispersivities was in the order of one tenth to one fifth of the flow path distance. From the results it is judged that macro dispersion is an important process during the prevailed pumped conditions. The hydraulic conductivity of fracture flow paths and flow porosities were calculated for three fracture zones, and a clear distinction between these could be done. The fracture conductivities ranged from $1.3 \cdot 10^{-4}$ to $8.6 \cdot 10^{-3}$ m/s and the flow porosities $2.0 \cdot 10^{-4}$ to $5.0 \cdot 10^{-2}$.

SUMMARY AND CONCLUSIONS

The objective of this tracer test was to determine how the major fracture zones are interconnected and by comparison with the experimentally obtained results verify or refute the framework of fracture zones presented in the conceptual model of Äspö. The aim was also to determine transport parameters such as residence time, dispersivity, flow porosity and hydraulic conductivity of the fracture flow paths. Predictions of tracer flow paths and residence times have previously been made by numerical modeling and the experimemtal results are compared with the predicitons.

The large scale three-dimensional tracer test included tracer withdrawal by pumping in an 600 metres deep open borehole, creating a converging flow field in the hydraulic conductive fracture zones surrounding the borehole. One dye tracer and three radionuclide tracers were injected in packed-off sections in nearby boreholes, where these intersects the hydraulic conductors. Two of the tracers were subjected to repeated injection, resulting in tracer injections from totally six locations in the fracture system. The geometric (straight line) distances from point of injection to point of detection in the withdrawal borehole ranged from 100 to 300 metres. The longest tracer flow path (trajectory) distance along interconnected fracture zones is calculated to approximately 380 metres. The depths ranged from 140 to 600 metres.

The experimental design and performance included the intermittent decaying pulse injection technique to minimize disturbance of the groundwater flow field and handling of radioactive tracers whilst also optimum conditions for tracer detection in the withdrawal borehole are given. Groundwater flow measurements by the dilution method were utilized to determine which borehole sections to be subjected to tracer injection, and a multilevel sampler were used to make it possible to detect tracer inflow levels in the withdrawal borehole.

Five fracture zones contributed to tracer transport from points of injection to detection in the withdrawal borehole; NE-1, NE-2, NNW-1, NNW-2 and EW-5.

Within the time limits given for this tracer test, 76 days, and considering the half-life of the radionuclide tracers used, tracers reached the withdrawal borehole from three out of six injection points. However, the interpretation is that tracer possibly also reached KAS06 from a fourth injection point.

The results of the tracer test are consistent with the framework of fracture zones presented in the conceptual model of Äspö by Wikberg et al.(1991), i.e. geometry and intersections between fracture zones agree with the obtained tracer flow paths. However, the flow paths predicted by numerical modeling (Svensson, 1991) did not agree completely with the experimental data. To some degree this is due to the fact that the computer code used for the predictions by definition only can develop one flow path from a point of injection.

Out of six injection points the predicted residence time was a bit overestimated (a factor of 2–3) from four points and underestimated from one injection point. From the sixth injection point no fair comparison can be made between experimental and predicted residence time since the pumping for tracer withdrawal stopped three days before the predicted time of tracer arrival. The predicted residence time was anyway then not overestimated from that injection point. The discrepancy shows how sensitive the residence times are to flow porosity. In the predictive modeling a flow porosity of 1.0 10^{-3} was applied to all zones, but from the tracer test the flow porosity was determined to vary between $2.0 \cdot 10^{-4}$ and $5.0 \cdot 10^{-2}$.

Zone EW–3 carried no tracer but from the tracer test results it was possible to calculate its contribution to the inflow in the withdrawal borehole KAS06. The inflow from zone EW–3 amounted to 15 % of the total inflow, i.e. it is indicated that EW–3 must be considered being a more important hydraulic conductor than is assumed in the conceptual model.

Within the distances involved in the performed tracer test zone EW–5 is judged to be a good but complex hydraulic conductor, with many widely spread but interconnected fracture flow paths.

Zones NNW–1 and NNW–2 are very good hydraulic conductors with a few narrow spaced water–conducting fractures.

The transport parameters for fracture zones NE–1 and NE–2 can not be quantitatively determined, but based on the tracer test results it is assumed that NE–1, having higher conductivities in the fracture flow paths and lower dispersivities is a more distinct hydraulic conductor than NE–2.

The dispersivities obtained by model fit to the breakthrough curves for NNW–1, NNW–2 and EW–5 are compareable to a large fracture zone investigated at the Finnsjön site, central Sweden. In general, the dispersivities was in the order of one tenth to one fifth of the flow path distance. Expressed as Peclet numbers, 4.2 – 11.3 where the lower values are representative for EW–5 and the higher for NNW–1 and NNW–2, i.e. largest dispersion in EW–5, which is not suprisingly the most geometrically complex zone according to the conceptual model.

From the results it is judged that macro dispersion is an important process during the prevailed pumped conditions.

The hydraulic conductivity of the fracture flow paths were calculated. The fracture conductivities are obviously smaller in EW–5 than in NNW–1 and NNW–2, out of which NNW–1 has somewhat higher conductivities. The mean value is $6.3 \cdot 10^{-4}$ m/s in EW–5 and $3.6 \cdot 10^{-3}$ and $1.5 \cdot 10^{-3}$ m/s in NNW–1 and NNW–2 respectively. The cumultative width of the hydraulically active fractures in the zones is about five to ten times higher for EW–5 than NNW–1 and NNW–2. The conclusion is that zone EW–5 consists of many low conductive fractures, whereas zones NNW–1 and NNW–2 consists of a few highly conductive fractures.

The flow porosity was calculated over the entire width of the fracture zones. Based on the results of the calculations the flow porosity in EW–5 is estimated to vary between $2.0 \cdot 10^{-4}$ and $2.0 \cdot 10^{-3}$, in NNW–1 between $6.0 \cdot 10^{-4}$ and $3.0 \cdot 10^{-2}$, and in NNW–2 between $5.0 \cdot 10^{-3}$ and $5.0 \cdot 10^{-2}$. However, due to the much greater width of EW–5, 100 metres compared to 1 to 3 metres for NNW–1 and NNW–2 the total effective pore volume in EW–5 is in the same order or even larger than in the other two zones.

CONTENTS

		Page
	ABSTRACT	i
	SUMMARY AND CONCLUSIONS	ii
	CONTENTS	v
	LIST OF FIGURES	vii
	LIST OF TABLES	ix
1.	INTRODUCTION	1
2.	EXPERIMENTAL DESIGN	2
2.1	GENERAL OUTLINE	2
2.2	PUMPING FOR TRACER WITHDRAWAL	5
2.3	TRACER INJECTIONS	6
2.3.1	Tracers used	6
2.3.2	Dilution measurements	7
2.3.3	Injection procedures	11
2.4	TRACER SAMPLING AND ANALYSIS IN WITHDRAWAL BOREHOLE	14
2.5	SUPPORTING MEASUREMENTS	19
2.5.1	Hydraulic head	19
2.5.2	Electrical conductivity and Redox potential	19
2.5.3	Temperature and Water chemistry	19
3.	EXPERIMENTAL RESULTS	21
3.1	LOG OF EVENTS	21
3.2	TRACER INJECTIONS	21
3.2.1	Dilution measurements	21
3.2.2	Injection schedules	22
3.3	TRACER BREAKTHROUGH IN WITHDRAWAL BOREHOLE	26
3.3.1	Breakthrough in total discharge	26
3.3.2	Breakthrough at the different sampling levels	26
3.4	SUPPORTING MEASUREMENTS	27
3.4.1	Hydraulic head	27
3.4.2	Electrical conductivity and Redox potential	27
3.4.3	Temperature and Water chemistry	28

4.	INTERPRETATION OF TRACER BREAKTHROUGH DATA	29
4.1	CALCULATED BREAKTHROUGH IN MAJOR CONDUCTORS	29
4.1.1	Processing of measured breakthrough data	29
4.1.2	Tracer breakthrough in major conductors	32
4.2	CONCEPTUAL MODEL OF FLOW PATHS	37
4.2.1	Description of fracture zones	37
4.2.2	Interpreted flow paths	38
4.3	MODELING OF TRACER BREAKTHROUGH DATA	43
4.3.1	Model used	43
4.3.2	Parameter estimation method	45
4.3.3	Modeling preformed	45
4.4	MODELING RESULTS	47
4.5	COMPARISON WITH PREDICTIONS AND AND THE ÄSPÖ CONCEPTUAL MODEL	50
4.6	PARAMETER DETERMINATIONS USING ANALYTICAL EXPRESSIONS	52
4.6.1	Hydraulic fracture conductivity and width	52
4.6.2	Flow porosity	54
4.6.3	Recovery calculations	56
5.	DISCUSSION AND CONCLUSIONS	57
5.1	EXPERIMENTAL	57
5.2	CONCEPTUAL MODEL	57
5.3	FRACTURE ZONES	58
5.4	TRANSPORT PARAMETERS	58
6.	REFERENCES	60

APPENDICES

APPENDIX A: Dilution measurements
APPENDIX B: Tracer injections
APPENDIX C: Tracer breakthrough at the sampling levels
APPENDIX D: Electric conductivity and redox potential
APPENDIX E: Calculated breakthrough in major conductors
APPENDIX F: 1-D modelling
APPENDIX G: Statistics of the 1-D modeling

LIST OF FIGURES

		page
Figure 1.1	Key map for the Äspö hard rock laboratory.	1
Figure 2.1	Borehole locations at southern Äspö. Borehole projections at ground surface are indicated.	3
Figure 2.2	Conceptual model of conductive structures on Äspö (From Wikberg et al., 1991).	4
Figure 2.3	Sketch showing the outline of a three–dimensional tracer test in fractured crystalline rock.	5
Figure 2.4	Schematic of injection borehole equipment. Trace element unit and circulation pump system is shown in Figure 2.5.	9
Figure 2.5	Description of detailsfrom Figure 2.4. Left: circulation pump system in PEM tube. Right: trace element unit.	10
Figure 2.6	Intermittent decying pulse injection. Example of a theoretical breakthrough curve resulting from an intermittent decying pulse injection in a stream tube 70 m long and 1m^2 cross sectional area (Gustafsson 1990b).	13
Figure 2.7	Sketch of equipment at withdrawal borehole for regulation of flow, sampling and analysis of water.	15
Figure 2.8	Measurement performed with gamma spectrometer probe. Framed part shown in detail in Figure 2.7.	16
Figure 2.9	Sampling performed with multi level sampler. Framed part shown in detail in Figure 2.7.	17
Figure 2.10	Hydraulic conductivity and inflow levels in KAS06, withdrawal borehole (Ekman and Gentzschein, 1989).	18
Figure 2.11	Principal outline of instrumentation in core boreholes (with prefix KAS). Encircled detail is shown in Figures 2.5 and 2.6.	20
Figure 2.12	Principal outline of instrumentation in percussion boreholes (Nyberg et al., 1991).	20
Figure 3.1	Gamma spectrometer probe measurements in KAS06 (c.f. Table 2.5).	27
Figure 4.1	Schematic view of the relation between sampling levels and inflow sections in KAS06 during pumping for tracer withdrawal.	29

Figure 4.2 Inflow distribution in KAS06 determined from spinner data. Letters A–F refers to name of conductor and U to the interval 0–100 m (c.f. Table 4.1). 31

Figure 4.3 Breakthrough of Re–186 at sampling level 390 m in KAS06. Experimental data points and fitted five–degree polynom (solid line). 32

Figure 4.4 Corrected breakthrough curve for Uranine at sampling level 4 (Conductor D) in KAS06. 33

Figure 4.5 Breakthrough of Uranine in KAS06. Sum of all levels, 0–600 m. 34

Figure 4.6 Corrected breakthrough of Rhenium at sampling level 3 (Conductor E) in KAS06. Comparison between corrected curve based on polynomial fit (solid line) and based on actual measured values (points). 35

Figure 4.7 Corrected breakthrough of Rhenium at sampling level 4 (Conductor D) in KAS06. Comparison between corrected curve based on the polynomial fit (solid line) and based on measured values (points). 36

Figure 4.8 Breakthrough of Rhenium (Re–186) for the sum of all levels, 0–600 m, in KAS06. 37

Figure 4.9 Injection schedule in KAS12, used in the 1–D modeling. 46

Figure 4.10 Injection schedule in KAS08, used in the 1–D modeling. 47

LIST OF TABLES

		page
Table 2.1	Configuration of boreholes and sections used in the tracer test.	3
Table 2.2	Tracers used.	6
Table 2.3	Tracer injection data.	12
Table 2.4	Tracer runs.	13
Table 2.5	Sampled levels and their corresponding waterconducting fracture zones in KAS06 (Interpretations made in connection with prediction and planning of this tracer test).	14
Table 3.1	Log of events during the large scale three–dimensional tracer test.	21
Table 3.2	Result of flow measurements in borehole sections (c.f. Appendix A).	22
Table 3.3	Flow measurements in connection with tracer injections.	23
Table 3.4	Radiotracer injections. Measured and calculated concentrations at injection start.	24
Table 3.5	Dye tracer (Uranine) injections. Measured and calculated concentrations at injection start.	24
Table 3.6	Radiotracer injections. Measured concentrations of samples taken from studied borehole section and mass release.	25
Table 3.7	Dye tracer (Uranine) injections. Measured concentrations of samples taken from studied borehole sections and mass release.	25
Table 3.8	Calculated head difference, Δh, between point of tracer injection and detection.	28
Table 4.1	Studied levels and their corresponding major water–conducting fracture zones in KAS06.	39
Table 4.2	Hydraulically active fractures in the injection sections, according to spinner survey. Underlined numbers are fractures where the main flow occurs.	39
Table 4.3	Assumed fracture flow paths for Uranine tracer from KAS12, section DB (279 – 330 m) to KAS06.	40
Table 4.4	Assumed fracture flow path for Rhenium tracer from KAS08, section M3 (140 – 200 m) to KAS06.	40

Table 4.5	Assumed fracture flow paths for Rhenium tracer from KAS08, section M1 (503 – 601 m) to KAS06.	41
Table 4.6	Assumed fracture flow paths for Iodine tracer from KAS07, section J4 (191 – 290 m) to KAS06.	41
Table 4.7	Assumed fracture flow paths for Uranine tracer from KAS05, section E3 (320 – 380 m) to KAS06.	42
Table 4.8	Assumed fracture flow paths for Indium tracer from KAS02, section B4 (309 – 345 m) to KAS06.	42
Table 4.9	Results of 1–D modeling of Uranine breakthrough in borehole KAS06. The tracer originates from injection in borehole KAS12, section DB.	48
Table 4.10	Results of 1–D modeling of Rhenium breakthrough in borehole KAS06. The tracer originates from injection in borehole KAS08, section M1.	49
Table 4.11	Results of 1–D modeling of uranine breakthrough in borehole KAS06, assuming tracer originating from two different boreholes. Borehole KAS05, section E3 and KAS12, section DB.	49
Table 4.12	Hydraulic parameters for fracture zones EW–5, NNW–1 and NNW–2. Determined from tracer breakthrough in borehole KAS06.	53
Table 4.13	Average hydraulic conductivity of fracture zones.	55
Table 4.14	Flow porosities in fracture zones EW–5, NNW–1 and NNW–2. Determined from tracer breakthrough in borehole KAS06.	56

1. INTRODUCTION

Groundwater and its capability to dissolve and transport spent reactor fuel from a repository to the biosphere is one of the critical questions when dealing with deep underground disposal of the radioactive material from nuclear power plants. The potential repository for spent reactor fuel will be placed in crystalline rock at a depth of 500 m below ground surface. Since the active transport in non-fractured rock is negligible, the transport with groundwater in fractured rock will be the most important mechanism to dislocate the radioactive elements and transport them to the biosphere.

The fracture zones on the island of Äspö have been observed both from the ground surface and in boreholes. In borehole sections isolated by packers, fracture zones have been noticed as hydraulic conductors. In order to quantify transport parameters of these fracture zones, a large scale three-dimensional tracer test was performed in the autumn of 1990. The aim of this tracer test was to give information on how these fracture zones are interconnected, and to determine transport parameters such as residence time, dispersivity, flow porosity and hydraulic fracture conductivity. For further information about geology, geohydrology and hydrochemistry of Äspö island see Gustafson et al 1989.

The field experiments were performed at the Äspö site (Fig 1.1) during October and November 1990 and sparse sampling was continued until pump stop in December 1990. The field work was coordinated with the Department of Nuclear Chemistry, Chalmers University of Technology who handled and analyzed the radioactive tracers.

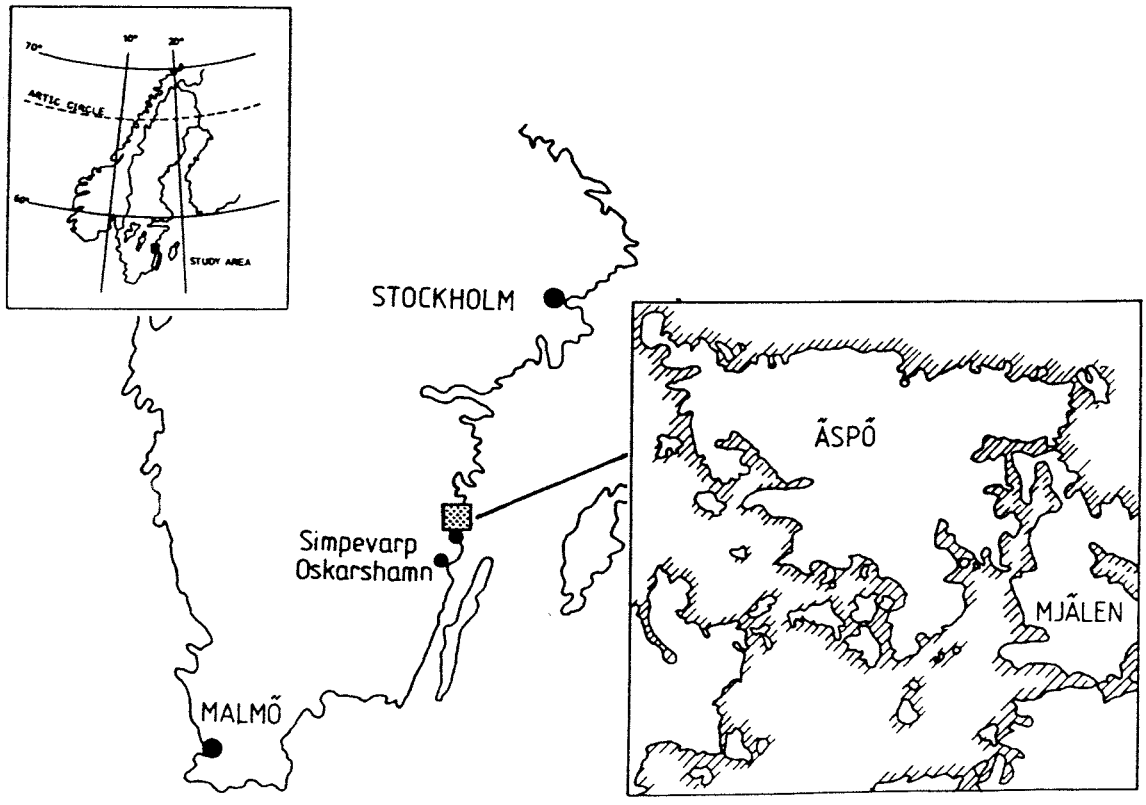

Figure 1.1 Key map for the Äspö hard rock laboratory.

2. EXPERIMENTAL DESIGN

2.1 GENERAL OUTLINE

The large scale three dimensional tracer test described in this report was performed on the southern part of Äspö (Figure 2.1) in the area where the hard rock laboratory will be constructed. Groundwater was discharged from the 600 m deep borehole KAS06 creating a converging flow field through hydraulic conductors, i.e. fracture zones, surrounding the borehole. Tracers were injected in packed-off sections in nearby boreholes, where these intersects the hydraulic conductors (Figure 2.3). The interpretation of the fracture system in and around southern Äspö has been dealt with by several authors (e.g. Carlsten, 1989) and summarized by Wikberg et al.(1991) in a conceptual model (Figure 2.2). The configuration of the fracture system is the key to the understanding of possible hydraulic contact between boreholes. The extension and magnitude of the hydraulic conductivity of the fracture zones, including intersecting zones, has to be determined. Since the withdrawal pump is situated in an open 600m long borehole, and the fracture configuration in the crystalline rock has a complex structure, there is a difference from the "classical" radial converging flow geometry. The transport parameters of the hydraulic conductors are determined from the breakthrough curves of the tracers.

The pumping was performed during three months and the pumped groundwater was discharged into the sea. The first tracers were injected about two weeks after pumping started so that the tracers would be injected in a steady state groundwater flow field. Measurements of hydraulic head confirmed a groundwater situation very near a steady state during the tracer test.

Three radioactive isotopes and one fluorescent dye tracer were injected in four borehole sections into the fracture system around the pumped hole. One tracer per injection point was used. Towards the end of the tracer test two additional tracer pulses were injected in a second run in two borehole sections not used in the previous run. Boreholes and sections considered for tracer injections are presented in Table 2.1.

All boreholes at Äspö are equipped with packers in order to isolate the different hydraulic units. In most of these sections the groundwater pressure was registered with pressure transducers and data logger, in the same way as the previous long term pump test on Äspö in KAS07 performed in August 1989 (Gentzschein and Nyberg, 1989). The principle design of the instrumentation in the boreholes is shown in Figures 2.11 and 2.12.

Table 2.1 Configuration of boreholes and sections used in the tracer test.

Borehole –section	Code	Depth[1] (m)	Section length (m)	Borehole diameter (m)	length (m)	inc[2]
KAS02–4*	B4	309 - 345	36	0.056	924	84
KAS02–2*	B2	800 - 854	54	0.056		
KAS05–3*	E3	320 - 380	60	0.076	549	85
KAS05–1*	E1	440 - 549	109	0.076		
KAS07–4*	J4	191 - 290	99	0.056	604	59
KAS08–3*	M3	140 - 200	60	0.056	601	59
KAS08–1*	M1	503 - 601	98	0.056		
KAS12–2*	DB	279 - 330	51	0.056	380	60
KAS13–3	EC	191 - 220	29	0.056	407	60
KAS14–2	FB	147 - 175	28	0.056	212	60

[1] Distance from casing top, isolated by packers.
[2] Inclination in degrees to the horizontal plane. Borehole orientation is shown in Figure 2–1.
* Chemical analysis of section water available, sampled in May and June 1990. (Nilsson 1991)

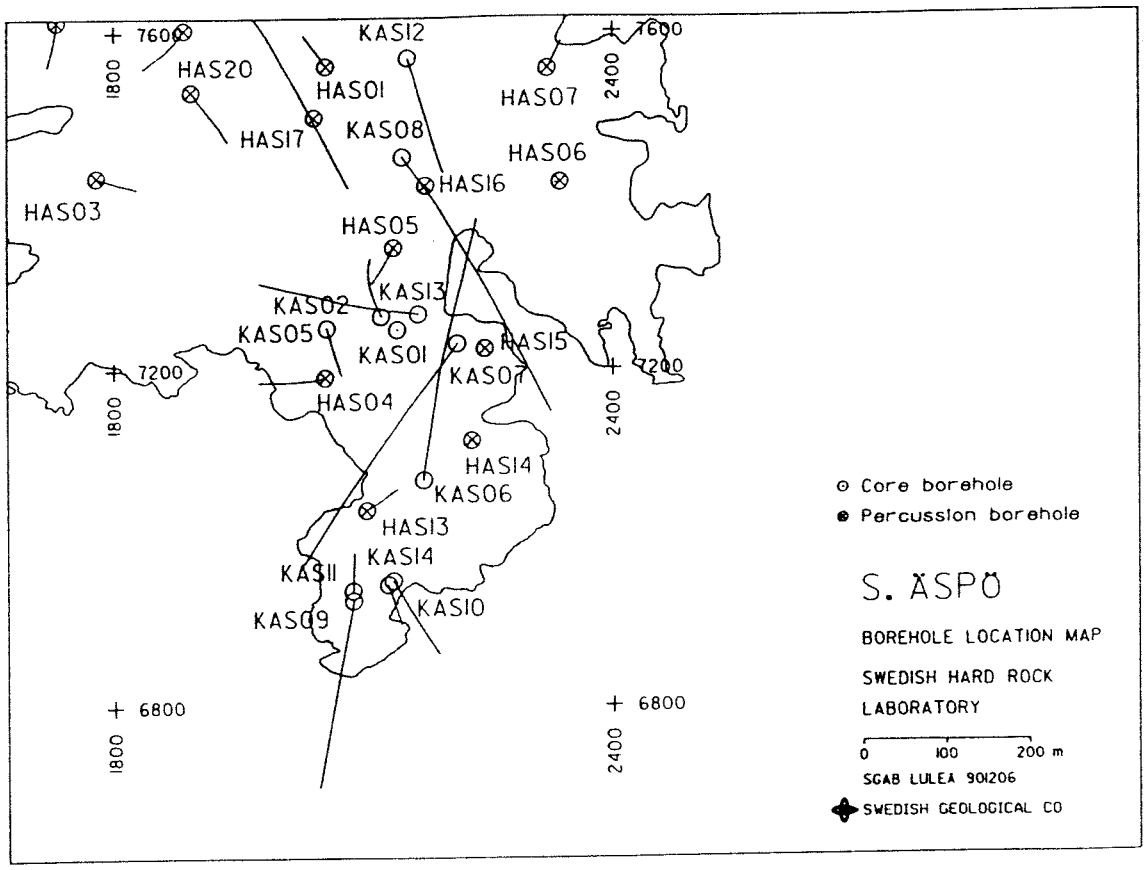

Figure 2.1 Borehole locations at southern Äspö. Borehole projections at ground surface are indicated.

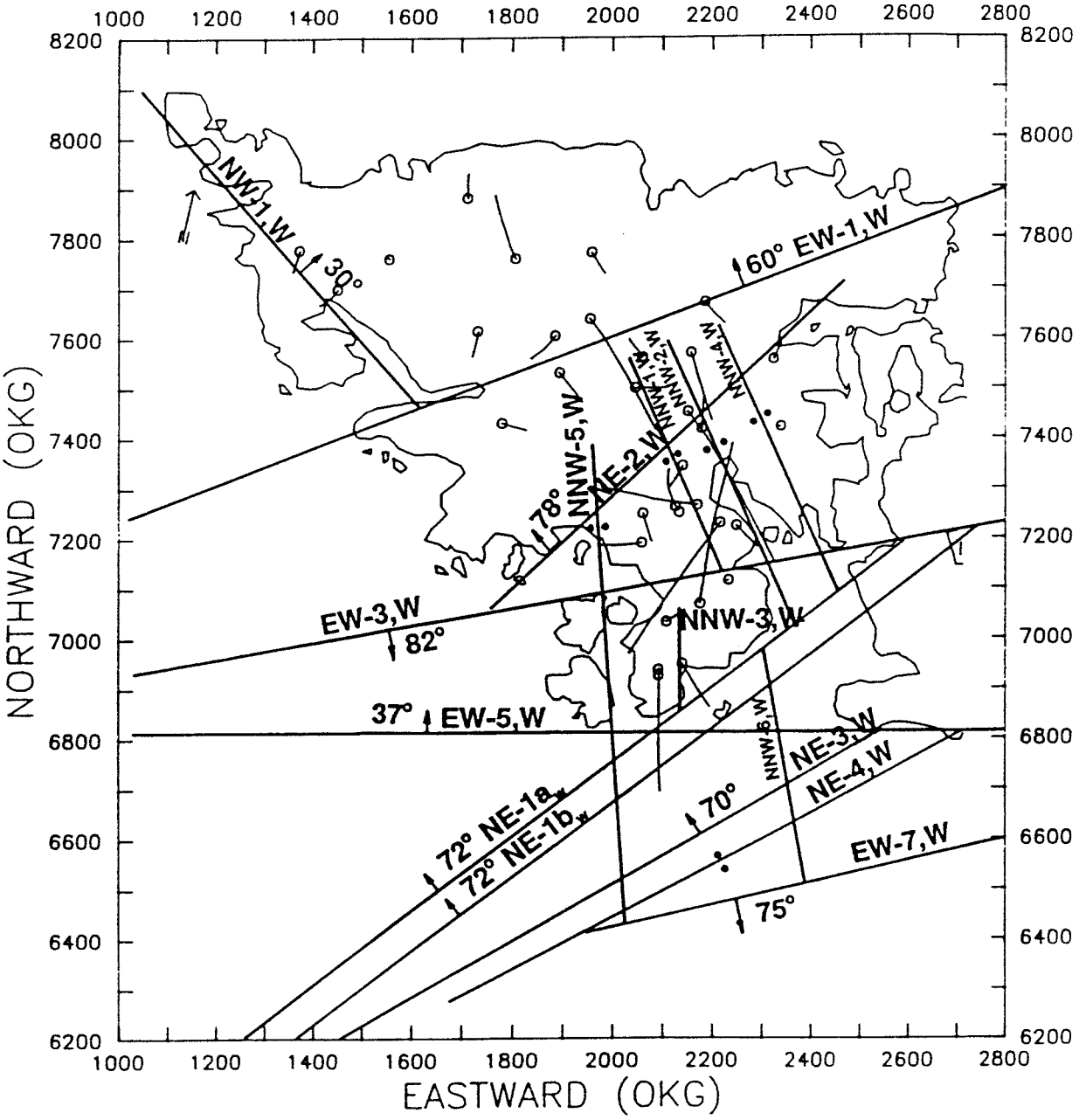

Figure 2.2 Conceptual model of conductive structures on Äspö (From Wikberg et al.,1991).

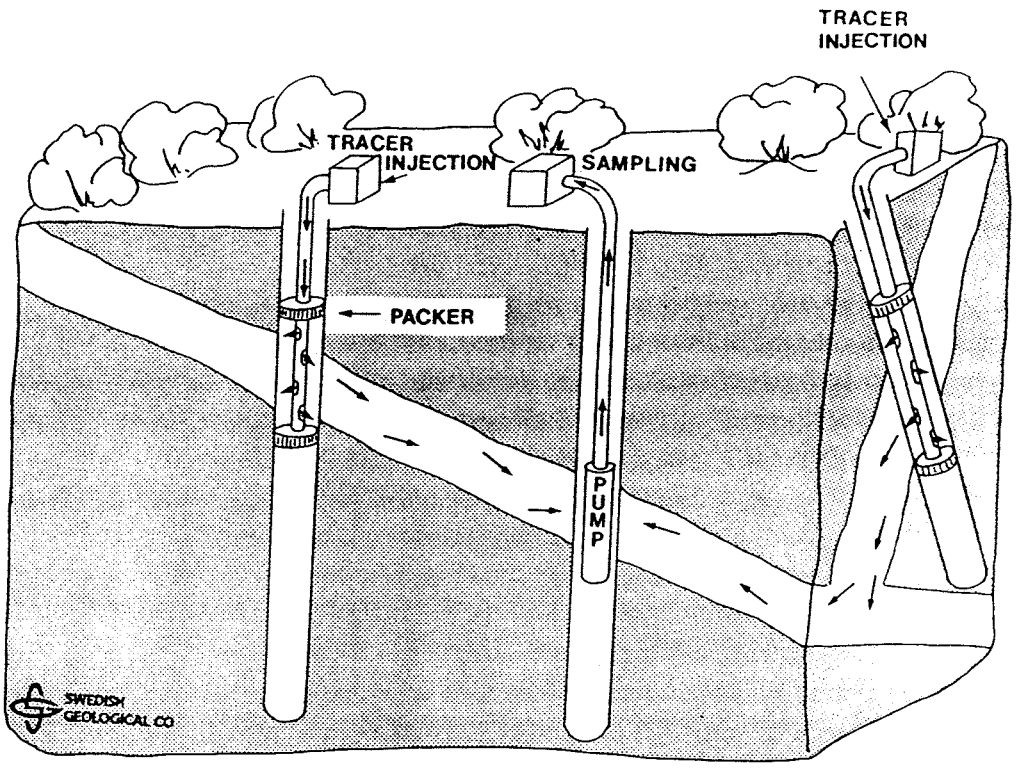

Figure 2.3 Sketch showing the outline of a three-dimensional tracer test in fractured crystalline rock.

2.2 PUMPING FOR TRACER WITHDRAWAL

The tracer test was carried out in a converging flow geometry established by pumping in borehole KAS06. The borehole is 602m deep and has an inclination to the horizontal plane of 60° towards north. Borehole KAS06 is of telescope type and has a diameter of 164mm in the uppermost 100m and 56mm below. The pumping was made in an open borehole configuration with a submersible pump placed 85 m below top of casing. The withdrawn water was discharged into a container at the ground surface, through PVC pipes with an inner diameter of 40.8 mm. A big bilgepump in the container pumped the water further into the sea through a large diameter tube.

The withdrawal rate was continuously measured and regulated to a constant flow. The groundwater level in the borehole was also continuously monitored. The pump flow rate was changed at two occations in the beginning of the test to obtain the largest pump capacity possible without any risk that the pump would run dry. The objective was to create a large hydraulic gradient, giving an optimum chance for injected tracers to reach the pumped borehole within the time limits stated for this tracer test. At a constant pump flow rate of 135 l/min the mean drawdown established by the pumping was about 65m in the pumping borehole.

The pump was equipped with a check valve and in the top of the borehole a branch pipe for the possibility either to lead the water into the flow meter and further on into the sea or to lead the water back into the borehole. This is useful when starting up again after a pump stop. For measurement and detection of the tracers a shunt has been used to detach the analysis and sampling equipment to the main flow pipe (c.f. section 2.4, Figure 2.7).

The pumping started on September 17th 1990 and the transient (initial) stage, regarding the head distribution in the tracer test area was estimated to last for about two weeks, based on data from the previous pump test LPT-1. The 18th of December 1990 the pump was shut off and the recovery period started. No major pump stops that could interfere with the tracer test have been reported during this period. All events during the test including the the tracer injections are summarized in Table 3.1, below. Measurements of hydraulic head confirmed a groundwater situation very near a steady state during the tracer test.

2.3 TRACER INJECTIONS

2.3.1 Tracers used

Four different non-sorbing tracers were used during this tracer test, three short-lived radioactive isotopes and one fluorescent dye, Uranine. The chemical form and half-lives of the radiotracers are given in Table 2.2. Uranine is also used as marker of the flushing water during borehole drilling at Äspö.

Table 2.2 Tracers used.

Tracer	Half-life	Chemical form	Remarks
In-114	49.51 d	In(III)-EDTA	metal complex
I-131	8.04 d	$I(I)^-$	negative ion
Re-186	3.78 d	$Re(VII)O_4^-$	negative ion
Uranine	-	Fluorescent dye	

note: Gamma ray energies and detection limits are presented in Byegård et al.(1991).

The advantages of using short-lived radioactive isotopes as tracers are that they can be detected in very low concentrations, equipment for detecting them in situ in boreholes are available and that they never will interfere with experiments in the future. The main drawback is that one needs a very precise description of the prevailing hydraulic conditions at the study site. The prediction has to be so precise that the breakthrough is made before the detection limit is reached due to decay. Another disadvantage is that the radiotracers in general has a relatively narrow dynamic concentration range due to safety regulations that limit the amount that can be injected.

The radiotracers are possible to detect with a gamma spectrometer probe in the pumped borehole. The radiotracers have been chosen so that their detectable gamma energy levels will not interfere with each other.

Continuously during the tracer test all tracers were analyzed in the field laboratories. One field laboratory was prepared and used as a radiochemical laboratory. Here the injection solutions were prepared from transport stock solutions as well as calibration solutions for concentration determinations. In another laboratory, physically separated from the radiochemical laboratory, samples were measured and gamma spectras were analyzed. The gamma spectrometer probe used for detection of inflow levels in the pumped borehole was connected to a multi channel analyzer in the detector laboratory. For further information about the radio analyses see Byegård et al. (1991). The dye tracer Uranine was analyzed with the fluorescence technique. A fluorescence spectrophotometer was installed in a third field laboratory and samples were measured every day for Uranine content.

Prior to the large scale three-dimensional tracer test, a small field test in a borehole was performed to determine the necessary conditions for using the gamma spectrometer probe to detect tracer inflow levels in a pumped borehole (Gustafsson 1990a).

2.3.2 Dilution measurements

Before the tracer injections started, dilution measurements were performed in six candidate borehole sections to find the four best for the tracer injections. Then, during the first part of the tracer test additional dilution measurements were made in four new borehole sections to find sections suitable for the large tracer pulse injections at the end of the test. The sections measured are presented in Table 2.1.

Dilution measurements are performed for determination of groundwater flow through boreholes or packed-off sections (hydraulic units) of boreholes. The groundwater flow is usually calculated as a mean value over a period of a few days in a borehole section limited by borehole packers. The borehole section lengths at Äspö varies from about 30 to 100 m. The dilution (circulation) section in the borehole is connected to the ground surface with two plastic tubes, as shown in Figure 2.4 (with an inner diameter of 6 mm). The downward tube outlet is situated at the bottom of the section and the inlet at the top. The circulation pumps placed in the near surface PEM tube establishes a circulating system where the groundwater in the borehole section will be mixed.

A small amount of tracer is constantly added during one circulation cycle to the circulating water system. This tracer must posses the quality that it can be added to the studied water in either low or high concentrations and then still be possible to detect in very low concentrations i.e. a wide concentration range.

The tracer concentration in the borehole section will then decrease as the through flowing groundwater dilutes the tracer labelled section water. The dilution of the tracer in the water is proportional to the groundwater flow through the section.

As the amount of the injected tracer solution usually is limited to four or five liters and injected over at least five hours, the tracers will not be forced out into the fracture system with excess pressure. If the fracture is judged to have a low hydraulic conductivity it is possible to withdraw the same amount of water from the circulating system as injected.

The groundwater flow through the borehole sections is generally detemined with an error less than a few percent. If the flow rate through the borehole section is to be converted to groundwater flow in the straddeled fracture zone some factors that may cause errors in the calculated value have to be considered. The disturbance in the flow field due to the presence of the borehole and the presence of several water conducting fractures within the measured section may provide short circuits between the fractures (with different hydraulic head) resulting in enhanced flow rates. The flow in the fractures has spatial differences due to uneven distribution of fracture apertures and other heterogeneities. Consequently, if a borehole penetrates a highly conductive fracture in a location were the fracture surfaces are in contact with each other it will show lower values of groundwater flow than if the borehole had penetrated a "flow channel" in the fracture. Also the angle between the borehole and the fracture zone as well as the direction of the groundwater flow has to be considered in that case (Gustafsson, 1986).

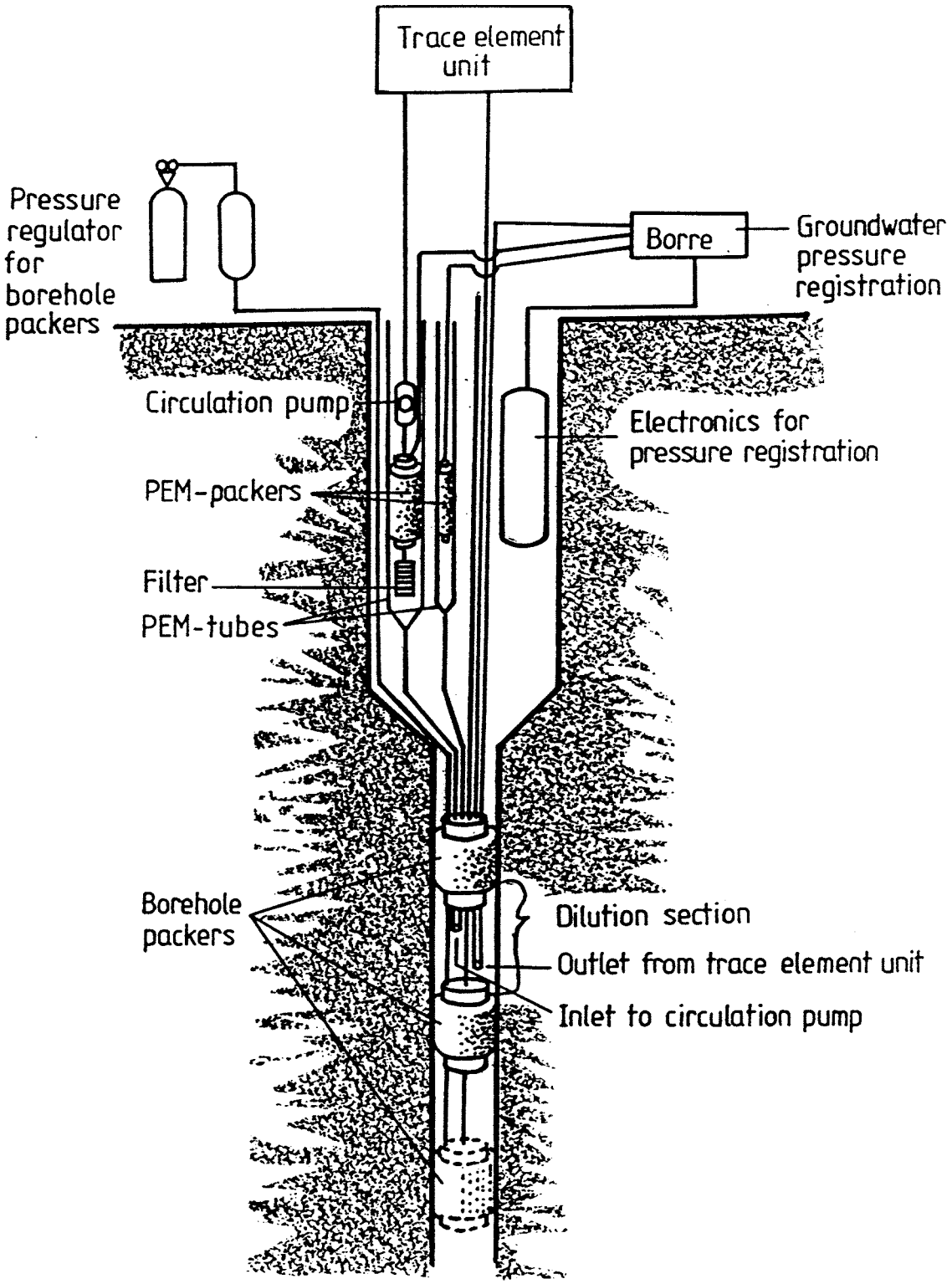

Figure 2.4 Schematic of injection borehole equipment.
Trace element unit and circulation pump system is shown in Figure 2.5.

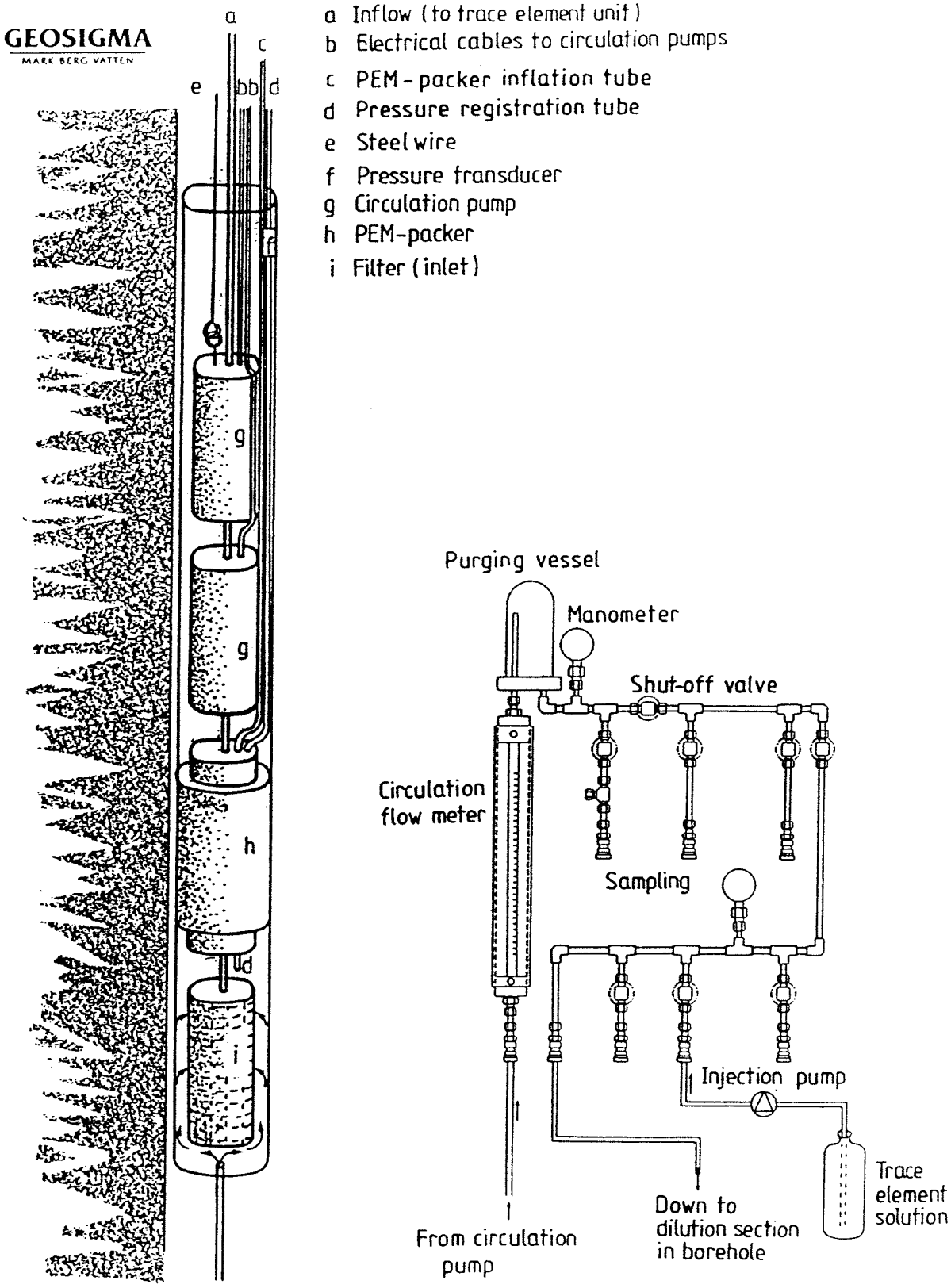

Figure 2.5 Description of details from Figure 2.4.
Left: circulation pump system in PEM tube.
Right: trace element unit.

2.3.3 Injection procedures

In the core boreholes, with prefix KAS, usually two sections are available to circulate the groundwater from the isolated section up the ground surface and back again. This circulation makes it possible to use tracers in one section without contaminating adjacent sections. The circulation system is shown in Figure 2.4. The circulation pump is located in the upper enlarged part of the borehole in a plastic (PEM) tube. The pump system in the borehole and the trace element unit on the ground surface are shown in Figure 2.5. The circulation capacity of the section water is measured by a float type flow meter. Pressure gauges are used for monitoring the pressure situation. Injection of the tracers into the circulating section is made with an injection pump which is temporary connected to the trace element unit. The injection of the tracer solution is made during one circulation/mixing cycle in order to achieve the best possible initial mixing. Manual sampling of section water for analysis of tracer concentration is also made in the trace element unit.

The tracers were injected with **the intermittent decaying pulse injection technique** that meets the following requirements:

- Possibilities to in situ measurements of the tracer inflow levels with gamma spectrometric probe and multi level sampler when the tracers reach the pumping borehole.

- Well defined in time and space, eg. no dispersion of the tracers in the injection borehole section. No disturbance of the ground water flow field and no tracers forced out to a unknown distance in the adjacent fracture system.

- Minimize the handling and storing of radioactive tracers at the injection borehole.

Intermittent decaying pulse injection means that pulses of tracers are injected in an clearly defined borehole section with constant time interval and without excess pressure, eg. one pulse every third or sixth day. The equipment needed is the same as for measuring groundwater flow with the dilution technique. The injected tracer is diluted by the groundwater flowing through the borehole section and when the concentration has reached a lower limit, after a couple of days, a new pulse is injected containing the same mass of tracer that has been released from the borehole section during the dilution process. Figure 2.6 shows an example of tracer concentration versus time in both the injection section and in the withdrawal water.

The tracers were injected with the following schedule:

(1) 4000 ml of concentrated of tracer solution (C_{oo}) was injected with constant flow into the circulation system during one mixing cycle (c.f. Table 2.3).

(2) The magnitude of the groundwater flow in the studied section was determined by sampling and analysis of the tracer concentration (C_o). The dilution of the tracer with time is proportional to the groundwater flow.

(3) From the groundwater flow and mass balance calculations, the amount of tracer that has to be added to reach the initial C_o concentration in the borehole section during the next injection pulse is determined. (c.f. Table 3.4)

(4) Repeated injection of 4000 ml concentrated tracer solution every third (sixth) day according to the procedure (1) – (3) above.

(5) Continuous monitoring of the groundwater flow by sampling and analysis of the tracer concentration in field every day.

Table 2.3 Tracer injection data.

Borehole section	Injection time (h min)	Injection flow (ml/min)	Injection volume (ml)	Inj. no (a)	Inj. int (b)
KAS02–4	5 21	12.5	4000	1	–
KAS05–3	14 56	27.9	25000	1	–
KAS07–4	13 31	4.9	4000	5	6
KAS08–1	7 2	9.5	4000	7	3
KAS08–3	6 53	9.7	4000	1	–
KAS12–2	6 42	12.0	5000	7	3

Injection time = one mixing cycle
a) number of injections during the test
b) number of days between each injection

During the field test a continuous follow up of the tracer concentration in the actual injection sections were made. Samples were taken and analyzed morning and evening. In the morning of injection day the last sample were taken and analyzed before injection. Together with analyses from previous days a predictive dilution calculation was made for the injection later that day. This was made in order to optimize the injected concentration so that every intermittent pulse injection would contribute to the same initial tracer concentration in the groundwater.

Table 2.4 Tracer runs.

Borehole section	Tracer	Run no[1]	Inj[2] type
KAS02–4	Indium (In–114)	1	dp
KAS05–3	Uranine	2	dp
KAS07–4	Iodine (I–131)	1	idp
KAS08–1	Rhenium (Re–186)	1	idp
KAS08–3	Rhenium (Re–186)	2	dp
KAS12–2	Uranine	1	idp

[1] 1 = initial choice, 2 = additional pulse injection
[2] idp = intermittent decaying pulse injection, dp = decaying pulse injection

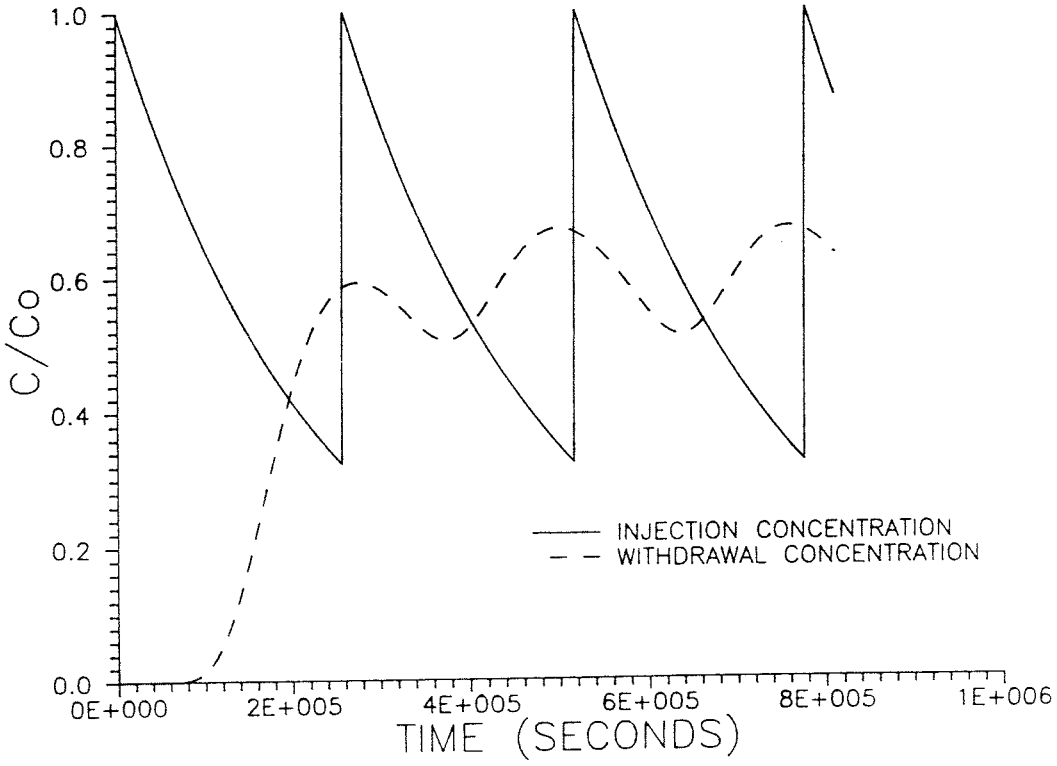

Figure 2.6 Intermittent decying pulse injection. Example of a theoretical breakthrough curve resulting from an intermittent decaying pulse injection in a stream tube 70 m long and 1 m^2 cross sectional area (Gustafsson, 1990b).

2.4 TRACER SAMPLING AND ANALYSIS IN WITHDRAWAL BOREHOLE

Besides sampling of tracers also Eh, temperature and electrical conductivity were continuously monitored in the pumping borehole KAS06 (Figure 2.7). The tracers were detected in the withdrawn water as well as in the borehole with the gamma spectrometer probe to distinguish between the different inflow paths to the pumping hole (Figure 2.8). Another device, called the multi level sampler, was constructed and used for the same purpose but also for the possibility of probe failure and if the radioactivity of the water in KAS06 should be below detection limit. The dye tracer can not be measured with the probe and the multilevel sampler is necessary if tracer breakthrough at different inflow levels is to be determined. The multi level sampler is a bundle of eight tubes of different lengths fitted with check valves at the inlets. This multi level sampler is lowered into the borehole, with an excess pressure applied to the check valves thereby closing the tubes, passing–by the main withdrawal pump, to each level studied. The tube outlets, on the ground surface, are then opened and the tubes are filled at each sampling level. The multi level sampler tube was then brought up to the ground surface and each tube was emptied on water from the studied levels (Figure 2.9)

The studied levels in the withdrawal hole have been chosen on basis of the spinner measurements performed (Ekman and Gentzschein, 1989). These flow measurements are shown in Figure 2.10. The various inflow levels increases the water velocity and shows a step formed velocity distribution in the borehole. The inflow levels correspond to sections of increased hydraulic conductivity (Nilsson, 1990).

Table 2.5 Sampled levels and their corresponding waterconducting fracture zones in KAS06 (Interpretations made in connection with prediction and planning of this tracer test).

Level[1] no – m	Hydraulic conductor[2] label	level(m)	Corresponding[3] fracture zone
8 – 190	A	217	NNW–1
7 – 290	B	312	EW–5
6 – 340	C,a	353	EW–5
5 – 360	C,b	364	EW–5
4 – 390	D	399	?
3 – 430	E	448	NNW–2
2 – 540	F,a	558	?
1 – 570	F,b	596	?

[1] Instrumental level, m below casing top.
[2] Major hydraulic conductor with its corresponding level
[3] Fracture zone interpretation made before this tracer test.

From the results in Figure 2.10 the eight levels presented in Table 2.5 were chosen. Since the flow direction in the pumped borehole is upwards the sampling levels were chosen just above the level where the hydraulic conductor intersects the borehole. Note that each sampled level is a sum of all underlying levels and the net inflow to each level is obtained by calculations based on the water inflow distribution in the borehole.

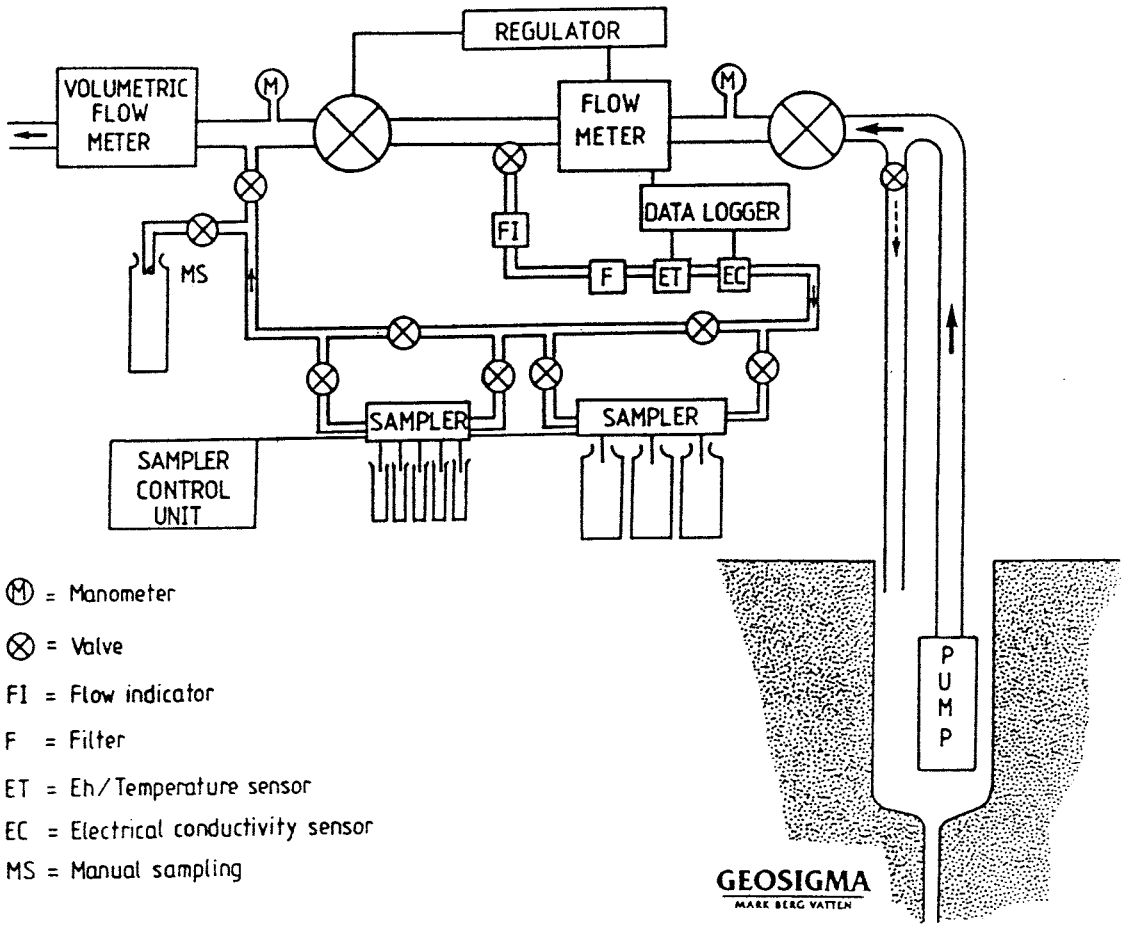

Figure 2.7 Sketch of equipment at withdrawal borehole for regulation of flow, sampling and analysis of water.

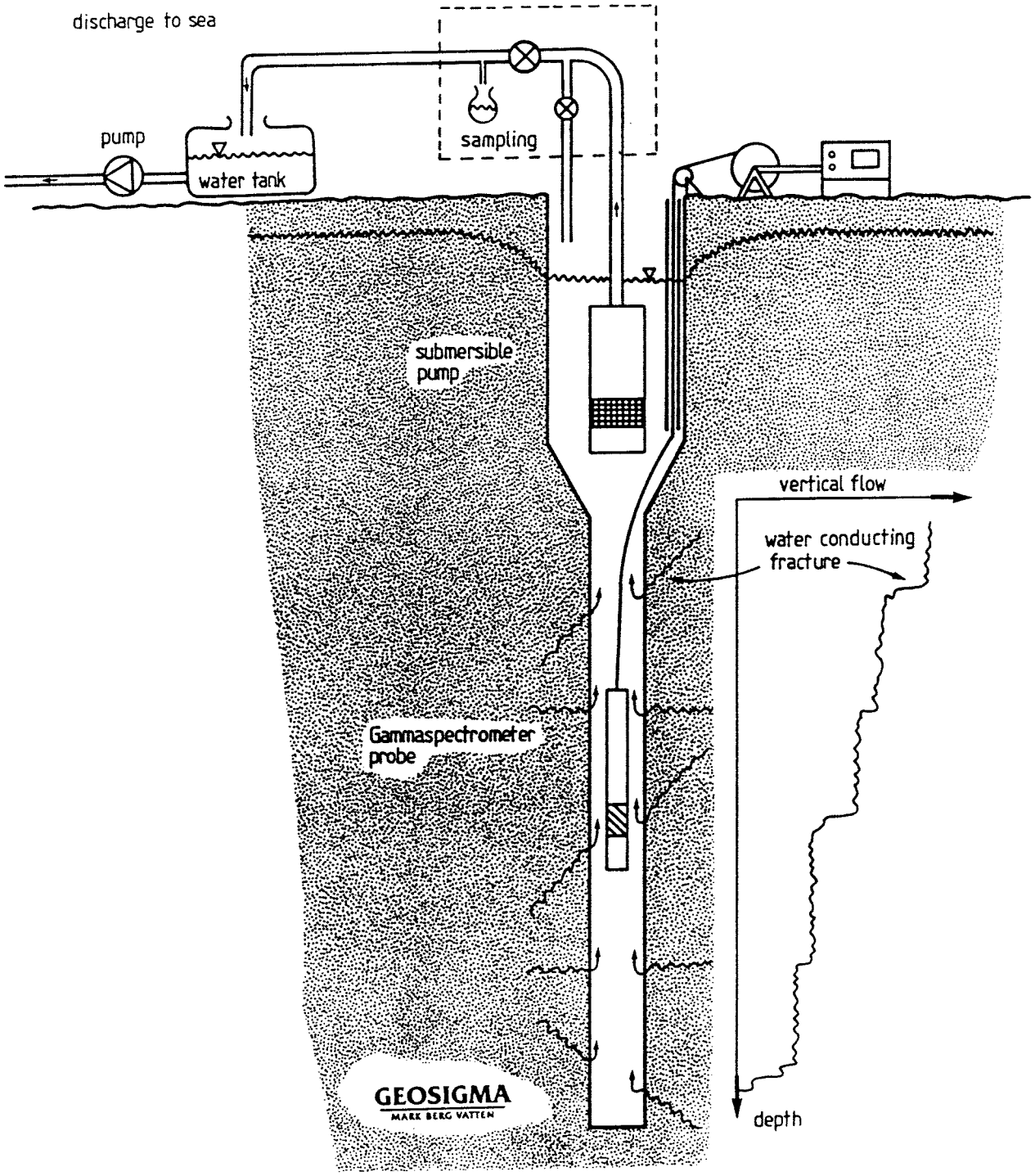

Figure 2.8 Measurement performed with gamma spectrometer probe. Framed part shown in detail in Figure 2.7.

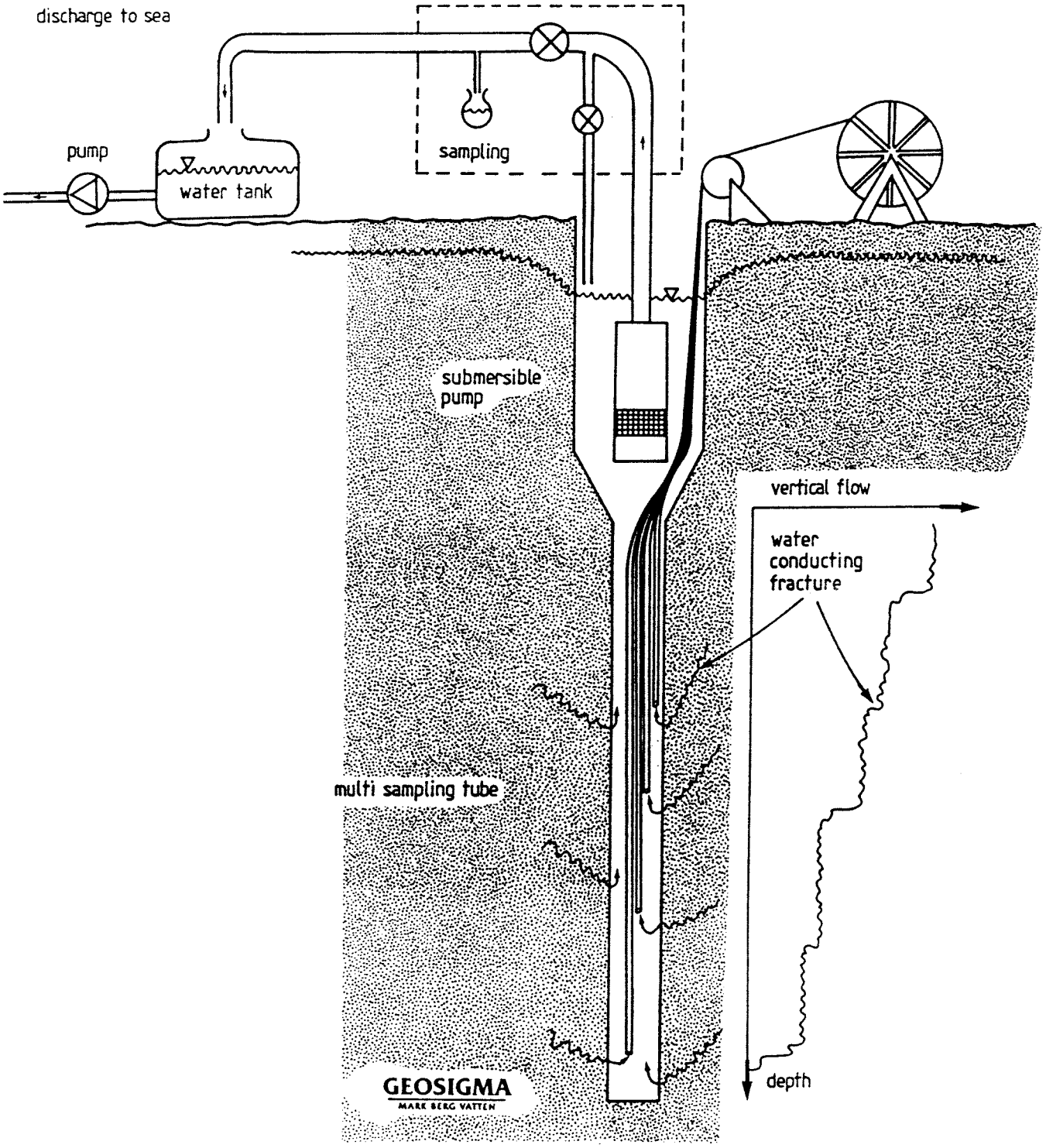

Figure 2.9 Sampling performed with multi level sampler. Framed part shown in detail in Figure 2.7.

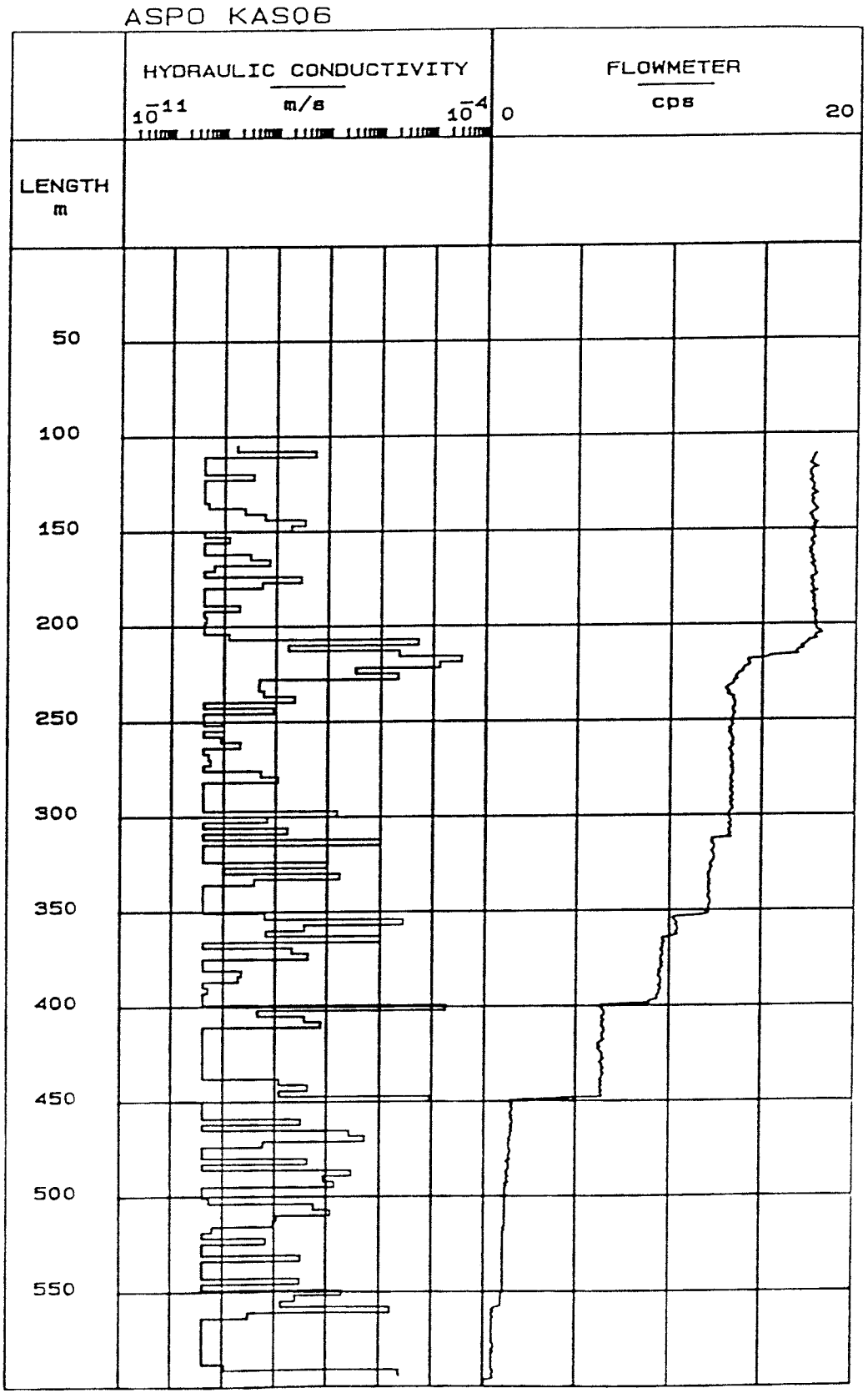

Figure 2.10 Hydraulic conductivity and inflow levels in KAS06, withdrawal hole (Ekman and Gentzschein, 1989)

2.5 SUPPORTING MEASUREMENTS

2.5.1 Hydraulic head

The hydraulic head was monitored in all boreholes on Äspö (Jönsson and Nyberg, 1991). At the Äspö site most of the boreholes are equipped with data loggers which continuously collects values of automatically measured hydraulic heads in the boreholes. The logged data are dumped with a portable computer at the boreholes every two months. In the boreholes KAS02 – KAS14 the hydraulic head was monitored in 4 – 6 packed–off sections. In KAS01 and KAS10 the groundwater level was measured in open boreholes. In the percussion boreholes HAS02 – HAS20 the hydraulic heads were registered in two or three packed–off sections. In HAS01 the groundwater level was registered in the open borehole. The principal outline of the instrumentation for hydraulic head measurements is shown in Figures 2.11 and 2.12. In the pumped borehole, KAS06 the hydraulic head was measured by a pressure transducer placed downhole and connected to a data logger at the ground surface. A check plot was made every day to control the hydraulic head status.

In the borehole sections that are used for tracer injection it is not possible to measure the correct hydraulic head during circulation and mixing. Measurements of hydraulic head during circulation of the section water will only register an underpressure due to the technical solution that is chosen, i.e. pressure gauge connected to the inlet tube of the circulation pumps, cf Figure 2.4. A real pressure drop in the section due to circulation does not exist. At the end of the pumping period the circulation pumps in the injection borehole were stopped for a period of about four to five days in order to monitor the correct hydraulic heads in the injection sections.

2.5.2 Electrical conductivity and Redox potential

During the pumping in KAS06 the redox potential,Eh, and electrical conductivity was continuously registered in the withdrawal water, as outlined in Figure 2.7.

2.5.3 Temperature and Water Chemistry

The temperature in the water withdrawn from KAS06 was noted once a day from readings on the temperature sensor display (Fig. 2.7).

Groundwater was sampled in May and June 1990 in injection sections and in level 3 and 8 in KAS06 for chemical analysis of main constituents. In KAS02–2, KAS07–4 and KAS12–2 analyses were made for elements in trace concentrations. For further information see Nilsson (1991).

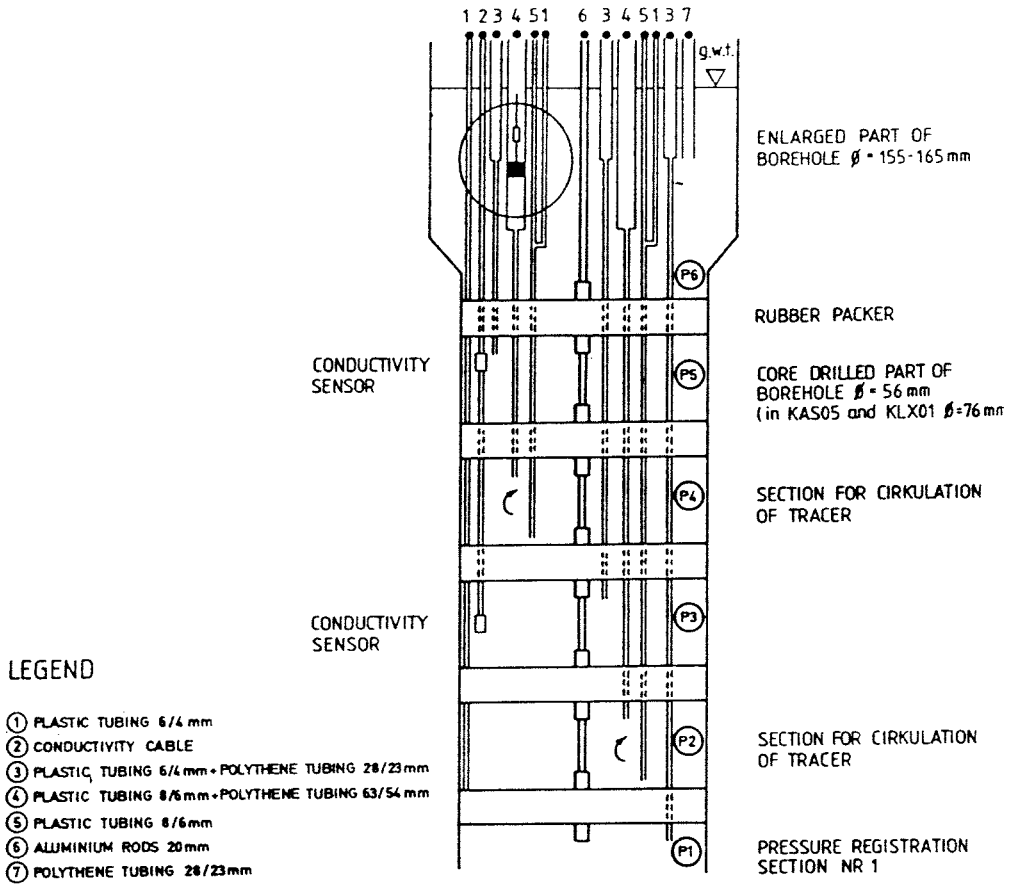

Figure 2.11 Principal outline of instrumentation in core boreholes (with prefix KAS). Encircled detail is shown in Figure 2.5.

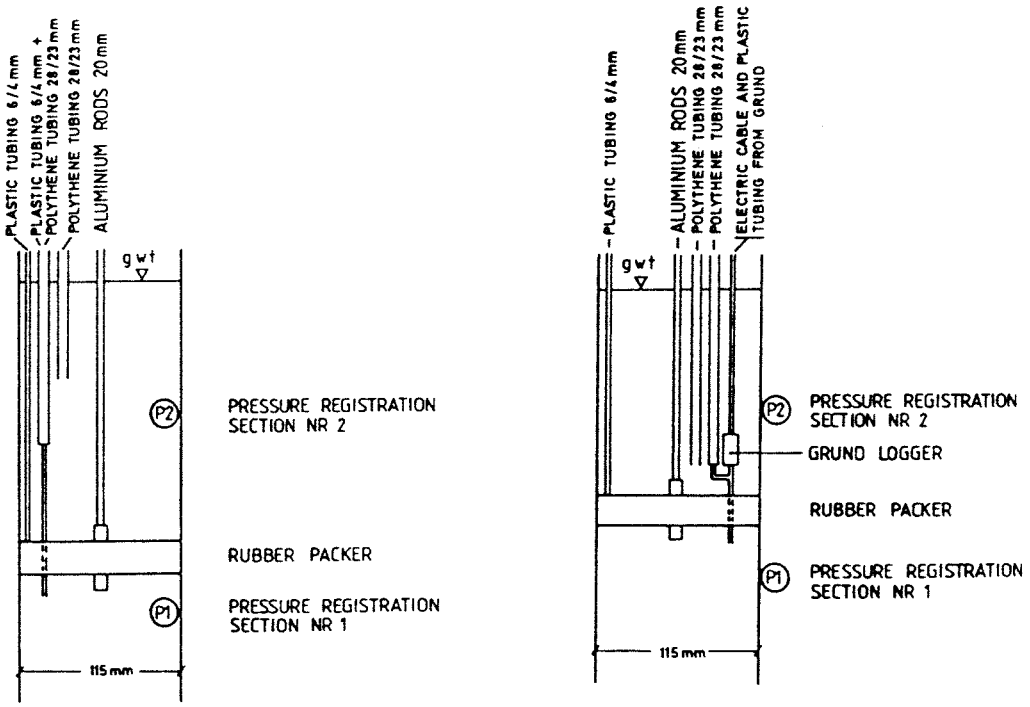

Figure 2.12 Principal outline of instrumentation in percussion boreholes (Nyberg et al.,1991)

3. EXPERIMENTAL RESULTS

3.1 LOG OF EVENTS

In order to be able to compare different events during the LPT–2, it is practical to use a common time basis. In this test, the different events have been compared to the start of the Uranine and Rhenium injections which started simultaneously. The log of events, presented in Table 3.1 also lists each major event during the entire pumping period for the tracer test.

Table 3.1 Log of events during the large scale three–dimensional tracer test.

Date	Time	El.time (hours)	Event
900917	09.00	–396	Pump start in KAS06. Q= 120 l/min.
900920	09.00	–324	Q changed to 150 l/min
900924	15.00	–227	Q changed to 135 l/min
901002	21.00	– 14	Pump stop 1 hour, power failure
901003	10.55	0	Start tracer inj. in KAS12–2 (DB)
901003	11.01	0	Start tracer inj. in KAS08–1 (M1)
901003	14.59	4	Start tracer inj. in KAS02–4 (B4)
901003	17.22	6	Start tracer inj. in KAS07–4 (J4)
901031	15.52	677	Start tracer inj. in KAS08–3 (M3)
901031	16.30	678	Start tracer inj. in KAS05–3 (E3)
901218	10.55	1824	Pumping in KAS06 finished

3.2 TRACER INJECTIONS

3.2.1 Dilution measurements

Dilution measurements were performed in ten candidate injection sections in order to decide the borehole sections best suited for tracer injections. The decision was based on the groundwater flow through the sections. To measure the groundwater flow in the candidate borehole sections by means of the dilution technique a small amount (20–40 mg) of the fluorescent dye Uranine was injected. In the first run six borehole sections were measured, out of which four were chosen for tracer injection. In the second run additional four sections were measured to decide two extra borehole sections possible to inject, in case of fast breakthrough of any of the earlier injected four tracers. The results from the dilution measurements are presented in Table 3.2.

Table 3.2 Result of flow measurements in borehole sections (c.f. Appendix A).

Borehole section*	Start	Duration[1] (h)	Flow (ml/min)	Remarks
KAS02–4	900927	55	14	First run
KAS05–1	900925	80	11	
KAS07–4	900927	55	33	
KAS08–1	900926	65	54	
KAS12–2	900926	60	111	
KAS13–3	900925	76	3	
KAS02–2	901023	110	4	Second run
KAS05–3	901009	80	12	
	901025	80	10	
KAS08–3	901011	200	16	
	901029	55	5	
KAS14–2	901022	90	11	

* See Table 3.3 for borehole section code
[1] Duration of dilution measurements.

3.2.2 Injection schedules

The tracers were injected with the intermittent decaying pulse injection technique as described in section 2.3. The concentrations of the injected tracer solutions C_{00} were measured before injection into the studied borehole sections (Tables 3.4 and 3.5). The concentration were also measured during the injection progress via the continuous sampling of the circulating water in the injected borehole sections. In Table 3.3 the calculated groundwater flow is shown.

The peak concentration of the intermittent decaying pulse injection C_0 can be determined in two different ways, firstly by using the measured values of the injection solution C_{00} and the water volume of the borehole section and secondly by extrapolating the actually measured concentration to the time of injection start. The maximum concentration $(C_0)_a$ calculated from the measured concentrations of injection solutions C_{00} is shown in Tables 3.4 and 3.5. The maximum concentration in the injected borehole section calculated from the measured concentration in the circulating water, assigned $(C_0)_b$ is presented in Tables 3.6 and 3.7. The discrepancy between these two methods of calculating the maximum concentration can be assigned to losses in the circulation system due to sorption and to initial losses. The mass release calculations in Tables 3.6 and 3.7 are based on measured concentrations of the circulating section water. The tracer concentration in the circulating section water, during injection, is shown in Appendix B.

The radiotracer concentrations presented in Table 3.4 are decay corrected to each injected pulse start time.

Table 3.3 Flow measurements in connection with tracer injections.

Borehole section	Code	Inj no	Start	Flow (ml/min)	Duration (h)
KAS02–4	B4	1	901003	1.4	900
				2.8	2400
KAS05–3	E3	1	901031	9	1400
KAS07–4	J4	1	901003	20	144
		2	901009	17	144
		3	901015	18	143
		4	901021	18	369
KAS08–3	M3	1	901031	21	300
KAS08–1	M1	1	901003	51	72
		2	901006	50	68
		3	901009	48	75
		4	901012	46	68
		5	901015	47	75
		6	901018	45	71
		7	901021	44	189
KAS12–2	DB	1	901003	99	73
		2	901006	94	71
		3	901009	122	78
		4	901012	116	65
		5	901015	115	78
		6	901018	100	66
		7	901021	97	139

Table 3.4 Radiotracer injections.
Measured and calculated concentrations at injection start.

Borehole section	Code	Inj[1] no	C_{∞}[2] (Bq/l)	C_0[3] (Bq/l)	Injected amount (Bq)
KAS02–4	B4	1	3.073E8	1.154E7	1.229E9
KAS07–4	J4	1	3.125E8	5.760E6	1.275E9
		2	2.224E8	4.018E6	8.894E8
		3	2.078E8	3.771E6	8.348E8
		4	2.310E8	4.179E6	9.250E8
		Total			3.924E9
KAS08–3	M3	1	2.279E9	6.288E7	9.114E9
KAS08–1	M1	1	5.410E8	2.159E7	2.164E9
		2	4.952E8	1.975E7	1.980E9
		3	7.310E7	2.917E6	2.924E8
		4	3.990E8	1.592E7	1.596E9
		5	5.385E8	2.149E7	2.154E9
		6	6.910E8	2.757E7	2.764E9
		7	6.255E8	2.496E7	2.502E9
		Total			1.345E10

[1] Injection number (c.f. Table 3.2)
[2] Tracer concentration in injection solution (c.f. Tables 2.3 and 2.4)
[3] Calculated tracer concentration in borehole section. Referring to $(C_0)_a$ in text.

Table 3.5 Dye tracer (Uranine) injections.
Measured and calculated concentrations at injection start.

Borehole section	Code	Inj no	C_{∞}[1] (mg/l)	C_0[2] (mg/l)	Injected amount (g)
KAS05–3	E3	1	23590	2110	590
KAS12–2	DB	1	25000	710	100
		2	10000	355	50
		3	10000	340	48
		4	10000	355	50
		5	10000	324	46
		6	10000	350	49
		7	10000	341	48
		Total			390

[1] Tracer concentration in injection solution (c.f. Tables 2.3 and 2.4)
[2] Referring to $(C_0)_a$ in text.

Table 3.6 Radiotracer injections.
Measured concentrations of samples taken from studied borehole section and mass release.

Borehole section	Code	Inj no	C_0[1] (Bq/l)	Interval (h)	Mass release (Bq/min)	Mass release (Bq)
KAS02–4	B4	1	9.588E6	0 – 900	9.862E3	5.325E8
				0 – 2400	6.821E3	9.823E8
KAS07–4	J4	1	4.789E6	0 – 144	6.790E4	5.846E8
		2	4.917E6	144 – 288	6.331E4	5.470E8
		3	5.009E6	288 – 431	6.774E4	5.833E8
		4	5.441E6	431 – 800	4.540E4	1.005E9
		Total		0 – 800		2.720E9
KAS08–3	M3	1	6.062E7	0 – 350	4.001E5	8.403E9
KAS08–1	M1	1	1.973E7	0 – 72	4.075E5	1.756E9
		2	1.834E7	72 – 140	4.003E5	1.646E9
		3	4.115E6	140 – 216	8.089E4	3.655E8
		4	1.382E7	216 – 284	2.864E5	1.174E9
		5	2.072E7	284 – 359	4.037E5	1.827E9
		6	2.546E7	359 – 431	5.068E5	2.172E9
		7	2.283E7	431 – 620	2.002E5	2.272E9
		Total		0 – 620		1.121E10

[1] Referring to $(C_0)_b$ in text.

Table 3.7 Dye tracer (Uranine) injections.
Measured concentrations of samples taken from studied borehole sections and mass release.

Borehole section	Code	Inj no	C_0[1] (mg/l)	Interval (h)	Mass release (mg/min)	Mass release (g)
KAS05–3	E3	1	905	0 – 1400	2.8	238.00
KAS12–2	DB	1	229	0 – 73	7.0	30.74
		2	214	73 – 144	6.7	28.40
		3	575	144 – 222	17.0	79.55
		4	556	222 – 288	19.2	75.21
		5	222	288 – 366	6.5	30.60
		6	212	366 – 432	7.0	28.05
		7	222	432 – 571	3.7	31.17
		Total		0 – 571		303.72

[1] Referring to $(C_0)_b$ in text.

3.3 TRACER BREAKTHROUGH IN WITHDRAWAL BOREHOLE

The monitoring of the tracer breakthrough in the withdrawal borehole was made with three different methods:
- Sampling of the total discharge at ground surface.
- Sampling of the different inflow levels with the multi level sampler.
- Measurements at the different inflow levels with the gamma spectrometer probe.

3.3.1 Breakthrough in total discharge

The tracer breakthrough in the total discharge is a sum of all water bearing fractures in KAS06. The tracer concentration is very low, about 15 ppb Uranine at the most (Figure 4.5) and 60 Bq/l of Rhenium as shown in Figure 4.8. About six and a half days after the first pulse injection in KAS12, section DB the Uranine content in the withdrawal water slowly starts to increase. The Rhenium concentration starts to increase in the withdrawal water four days after the first injection in KAS08, section M1. Indium injected in KAS02, section B4 and Iodine injected in KAS07, section J4 (191–290m) was not found in the withdrawal water, which was sampled an analyzed for all three tracers until pumpstop at 1824 hours of elapsed time after injection.

3.3.2 Breakthrough at the different sampling levels

The results obtained from **the multi level sampler** showed inflow of Uranine from KAS12, section DB is mainly observed at two levels in KAS06, namely level 4, 390m and level 3, 430m. The inflow of Rhenium from KAS08, section M1 is detected in level 3, 430m. Indium from KAS02, section B4 and Iodine from KAS07, section J4 were not detected in samples taken with the multi level sampler. Breakthrough curves for the various levels are shown in Appendix C. It should be noted that the breakthrough curve for each level presented in Appendix C represents a sum of all underlying levels. Therefore the breakthrough curves were processed as described in section 4.1 to determine the actual breakthrough for each individual level.

The **gamma spectrometer probe** was used in the first part of the tracer test and various levels in the borehole were measured with the gamma spectrometer probe without detecting any tracers. However, in an early stage during the field test, samples taken with the multi level sampler showed that a breakthrough for both Uranine and Rhenium slowly started at the 430m level. Because of that it was then decided to measure only at the 430m level, but no breakthrough was observed in the analysis of the gamma spectras due to low tracer concentration. In Figure 3.1 the measured levels and the duration of the measurements are shown. For further information about detection limits and gamma energies see Byegård et al. (1991) and Gustafsson (1990a).

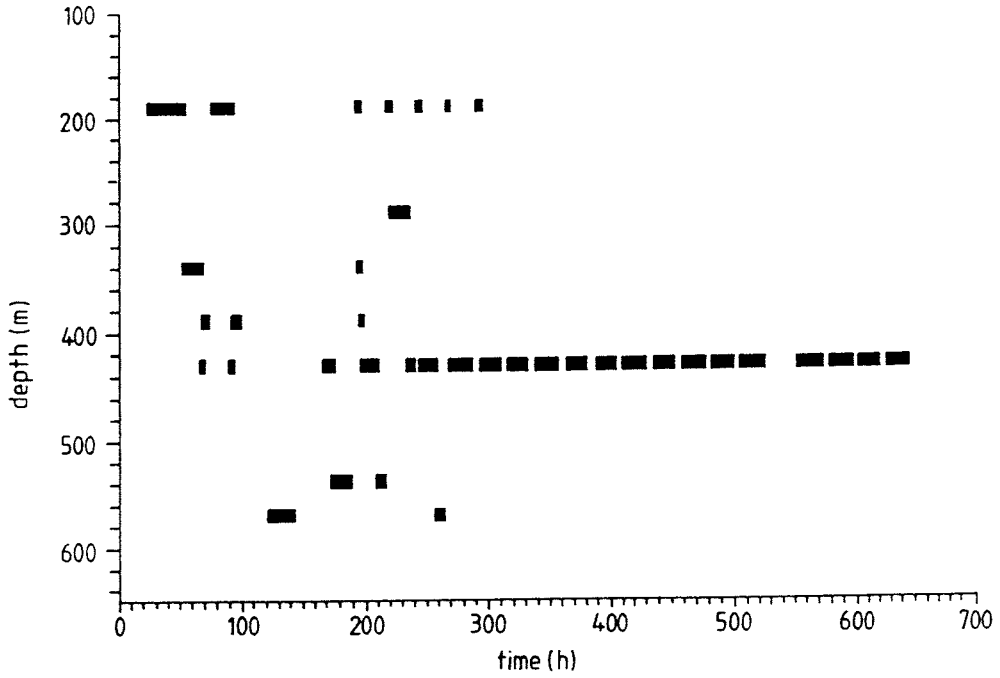

Figure 3.1 Gamma spectrometer probe measurements in KAS06 (c.f. Table 2.5).

3.4 SUPPORTING MEASUREMENTS

3.4.1 Hydraulic head

Hydraulic head was registered in all boreholes on Äspö before, during and after pumping. Detailed data compilation is available in Jönsson and Nyberg (1991).

From the head measurements the head difference, Δh, between the tracer injection borehole sections and the pumped tracer withdrawal borehole was calculated. The results are presented in Table 3.8. The Δh value is one of the input data needed when determining some of the hydraulic transport parameters considered in this study.

3.4.2 Electrical conductivity and Redox potential

The electrical conductivity and redox potential were continuously monitored in the withdrawn water from KAS06. In Appendix D the values of the oxidation-reduction potential and electrical conductivity during the tracer test are shown.

The mean value of the electrical conductivity was about 1350 mS/m. Starting with 1375 mS/m during the first six weeks of pumping, after which it started to decrease. At the end of the 12 weeks of pumping it reached 1325 mS/m.

According to the flow-through cell used for the redox measurements the value was steady throughout the whole tracer test. The Eh value obtained from the cell, -100 mV shall be multiplied by a calibration constant to give a correct redox potential in the withdrawn water of about +150 - +200 mV. However, this positive Eh value is not representative for the water in the fracture flow paths, instead it is due to the hydraulic conditions in the borehole. The pumping created so large drawdown that the groundwater level was lowered below the intersection with zone EW-3. The water from EW-3, making up 15 % of the total discharge, was aireated when it was flowing at the borehole wall down to the water table giving positive Eh values in the discharged water.

3.4.3 Temperature and Water chemistry

The temperature showed no trends, to increase or decrease. It was steady between 11 and 12 °C during the whole pumped period.

The deep waters in the fracture zones on Äspö, involved in the tracer transport during this tracer test can generally be judged as saline with a high content of dissolved inorganic constituents. For further detailes see Wikberg et al.(1991).

Table 3.8 Calculated head difference, Δh, between point of tracer injection and detection.

Borehole / section	H^+ (m.a.s.l.)	Route	Δh (m)
KAS02, B2*	- 5.0	KAS02, B2 - KAS06	46.8
KAS02, B4	- 5.6	KAS02, B4 - KAS06	46.2
KAS05, E1*	- 3.8	KAS05, E1 - KAS06	48.0
KAS05, E3	- 5.0	KAS05, E3 - KAS06	46.8
KAS06	- 51.8		
KAS07, J4*	- 5.1	KAS07, J4 - KAS06	46.7
KAS08, M1*	- 3.8	KAS08, M1 - KAS06	48.0
KAS08, M3	- 5.5	KAS08, M3 - KAS06	46.3
KAS12, DB*	- 4.8	KAS12, DB - KAS06	47.0
KAS13, EC	- 4.3	KAS13, EC - KAS06	47.5
KAS14, FB	- 0.2	KAS14, FB - KAS06	51.6

* = Borehole section in which tracer were injected
+ = Hydraulic head during the tracer test

4. INTERPRETATION OF TRACER BREAKTHROUGH DATA

4.1 CALCULATED BREAKTHROUGH IN MAJOR CONDUCTORS

The sampling for tracers in KAS06 was made at 8 different levels and also in the total discharge as described in Section 2.4. However, each sample represents a sum of the tracer concentration in the water coming from the sampling levels below and the concentration of tracer at the actual sampling level, see Figure 4.1. This means that the measured concentrations, Cm_1,....,Cm_8, have to be corrected in order to determine the true concentration, C_1,....,C_8, of tracer at each sampling level.

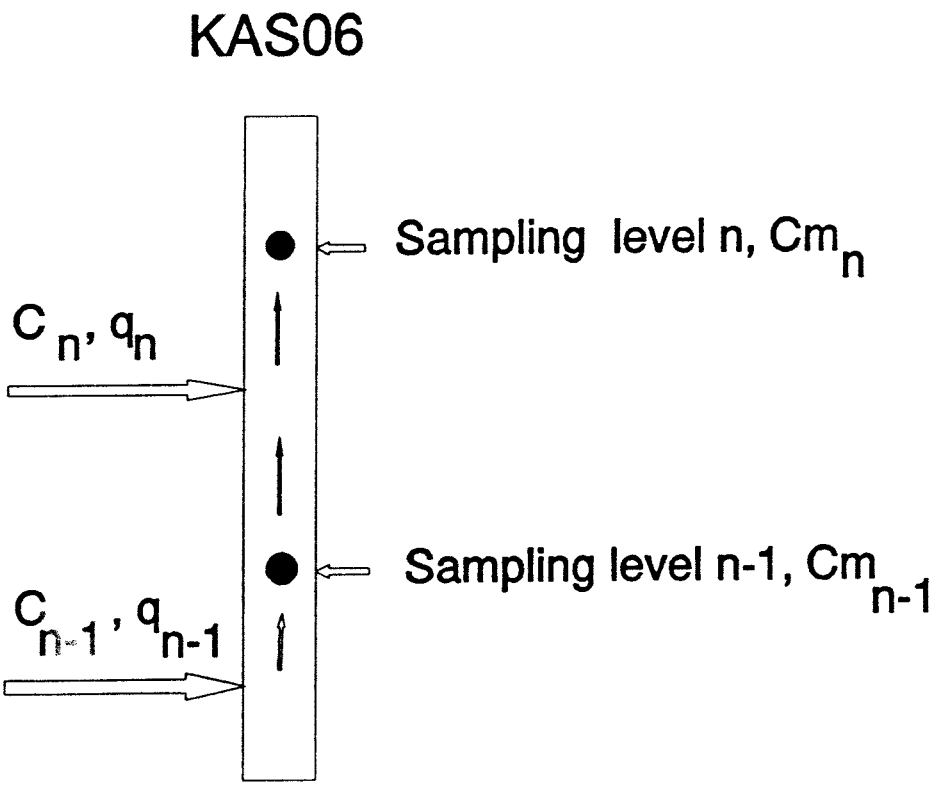

Figure 4.1 Schematic view of the relation between sampling levels and inflow sections in KAS06 during pumping for tracer withdrawal.

4.1.1 Processing of measured breakthrough data

The following expression has been used to determine the true concentration at each level, C_n;

$$C_n = Cm_n + A \cdot (Cm_n - Cm_{n-1}) \qquad (4.1)$$

where A is defined by:

$$A = \frac{\sum_{i=1}^{n-1} q_i}{q_n} \qquad (4.2)$$

Thus, the correction according to Equation (4.1) is entirely dependent on the inflow distribution during the pumping.

There are two ways to determine the inflow distribution; either by using the hydraulic conductivity distribution determined from packer tests in 3 m intervals or by using the spinner survey (Nilsson, 1990). The spinner survey was performed during similar pumping conditions as during the tracer test, therefore this was considered to be the best basis to determine the value of A in Equation (4.2). It should however be noted that the spinner survey was made after a short period of pumping (1–4 hours) and with about half the pumping rate compared to the tracer test. The results may therefore not be entirely representative of the conditions during pumping for tracer withdrawal.

Assuming that the inflow distribution is correctly chosen, the breakthrough curves determined from Equation (4.1) should only be a scatter around zero concentration if no tracer has arrived. A wrongly chosen flow distribution may either give a false breakthrough curve or negative values.

Another way to test whether a breakthrough determined from Equation (4.1) is correct or not is by studying the ratio Cm_n/Cm_{n-1}. If no tracer is added between sampling level n–1 and n, the ratio should be constant and only dependent on the dilution with unlabelled water. This ratio was also used to determine the inflow of water from fracture zone EW–3 between the uppermost sampling level and the pump as no spinner survey was performed in the upper 100 m of KAS06.

The inflow distribution determined from the spinner survey and combined with the calculation of the inflow from the upper 100 m of the borehole is presented in Figure 4.2. The uppermost inflow level, U, representing fracture zone EW–3 contributet with a suprisingly large portion to the total inflow, 15 % or $3.38 \cdot 10^{-4}$ m^3/s.

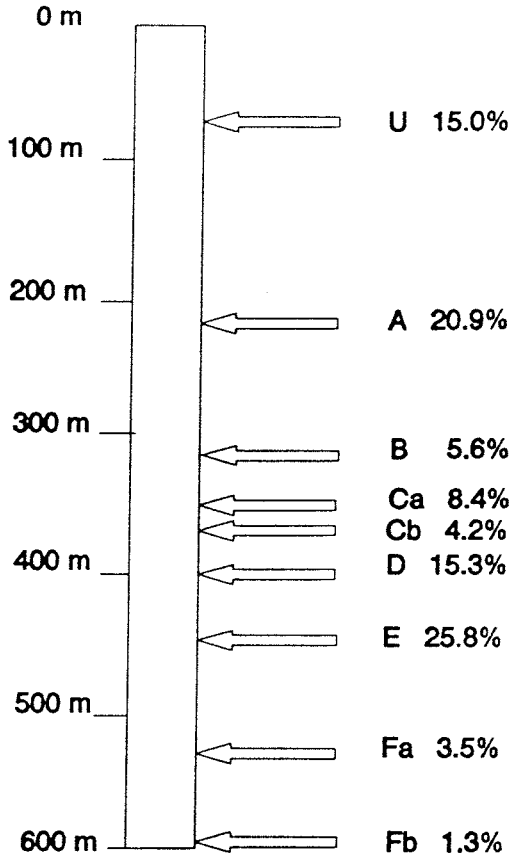

Figure 4.2 Inflow distribution in KAS06 determined from spinner data. Letters A–F refers to name of conductor and U to the interval 0–100 m (c.f. Table 4.1).

This way of interpreting the breakthrough at individual levels in the sampling hole demands that the analysis errors are small. Otherwise, the breakthrough curve resulting from Equation (4.1) will be very noisy. For the analysis of the Rhenium breakthrough, which compared to Uranine displays much larger uncertainties in the analyses, another technique had to be used to determine the corrected breakthrough curves. Instead of using the original data, a least square fit to a five degree polynom was made for each sampling level. This curve was then used to determine the corrected curves according to Equation (4.1). An example of the fitted curve to the breakthrough at sampling level 4 is shown in Figure 4.3.

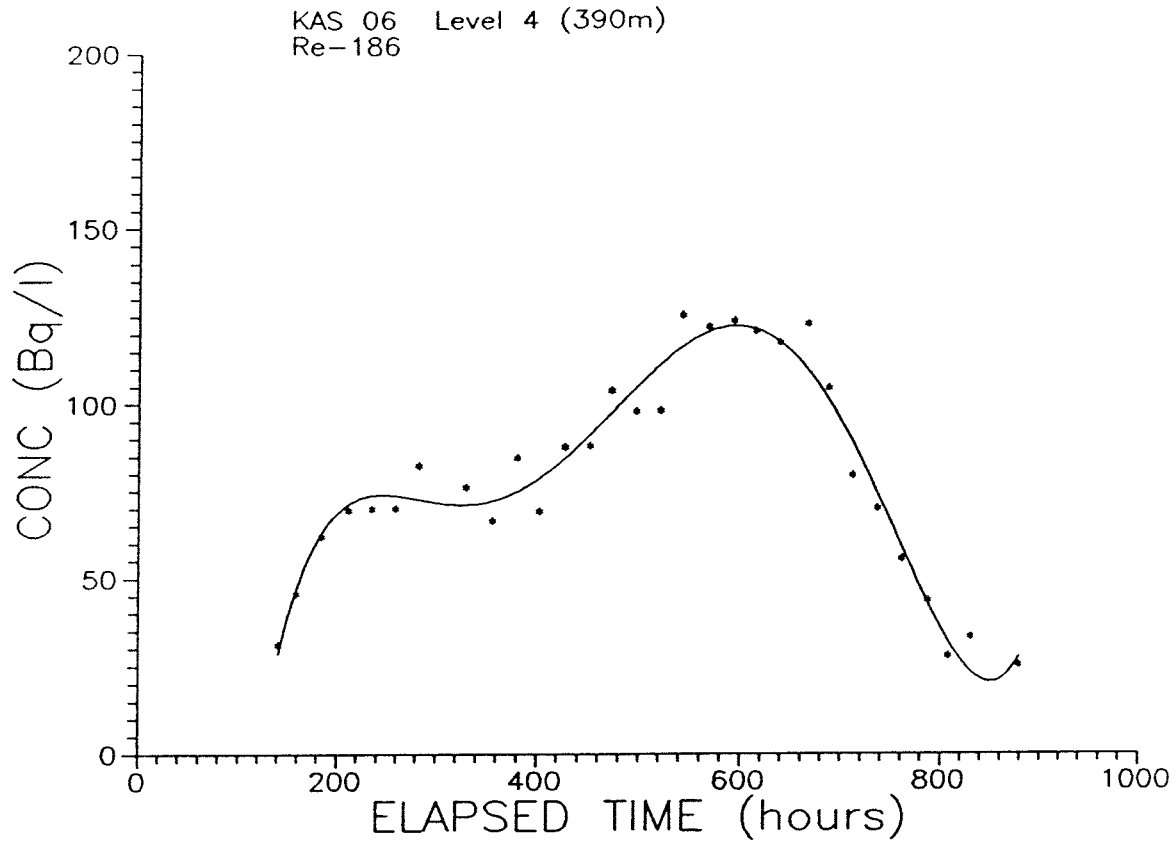

Figure 4.3 Breakthrough of Re-186 at sampling level 390 m in KAS06. Experimental data points and fitted five-degree polynom (solid line).

4.1.2 Tracer breakthrough in major conductors

Breakthrough of Uranine from KAS12, section DB

The corrected breakthrough curves indicate that tracer breakthrough occurs in sampling levels 3 to 8, see Appendix C. However, a closer analysis involving analysis of the ratio between concentrations at different levels as described in Section 4.1.1 shows that the tracer breakthrough curves for sampling level 7 most probably are resulting from a slightly wrongly chosen inflow distribution. Hence, breakthrough is measured in sampling levels 3-6 and 8, corresponding to flow conductors E,D,C_b, C_a and A.

Breakthrough of Uranine was first registered at sampling levels 3 and 4, corresponding to conductors E and D, after about 140 hours of elapsed time. Breakthrough in sampling levels 5 and 8, corresponding to conductors Cb and A, are slightly delayed with a first arrival of about 160 hours.

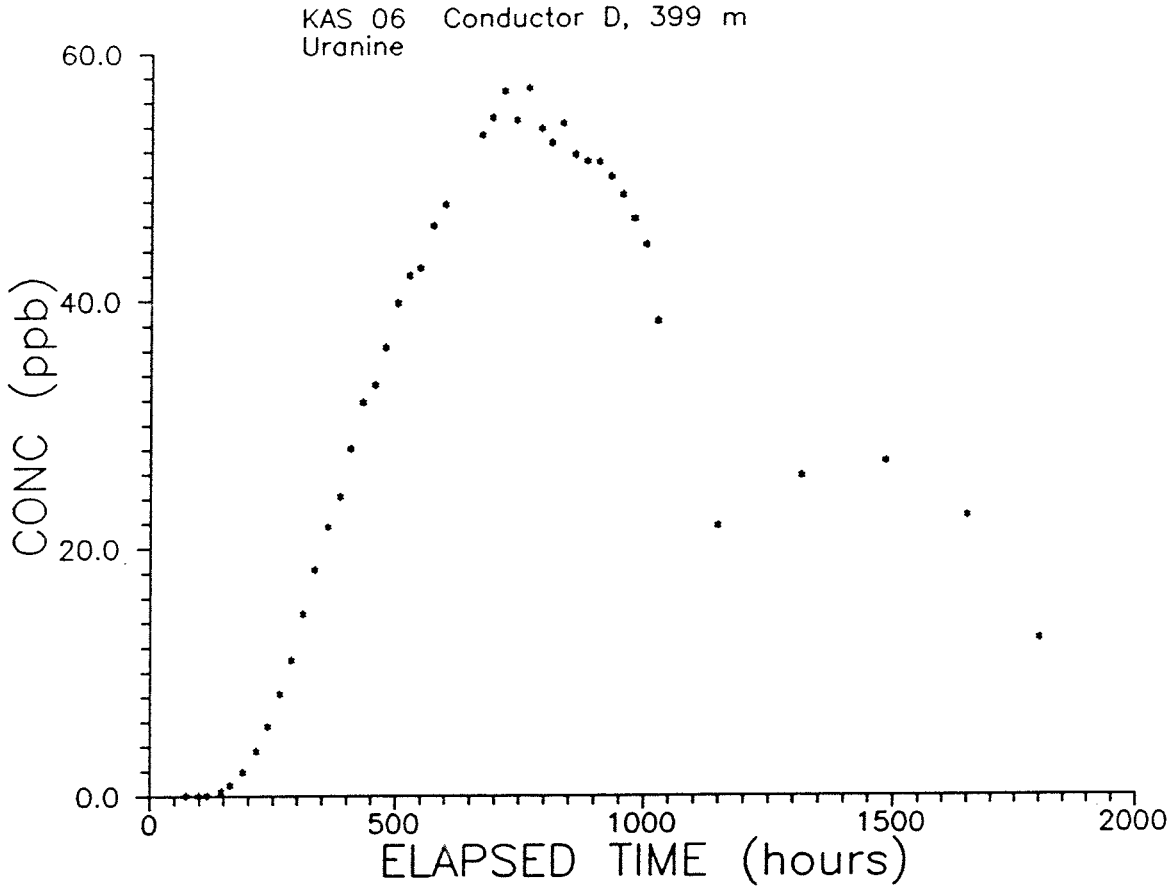

Figure 4.4 Corrected breakthrough curve for Uranine at sampling level 4 (Conductor D) in KAS06.

None of the curves reaches steady state concentration before injection stop at 677 hours of elapsed time. The highest concentration is reached in conductor D, about 60 ppb or given as C/C_0, $2.0 \cdot 10^{-4}$, see Figure 4.4.

The breakthrough curve for the total breakthrough (Figure 4.5), determined from the sampling of the discharge water from KAS06, is dominated by the contribution from Conductor D, c.f. Section 4.5.1. The curve displays a relatively large spread of data points at the descending part of the curve. This is due to iron precipitations present in the samples from the total discharge and possible sorption of the tracer on the precipitations. The iron precipitations occur as a result of the depressurisation of the pumped water and was not a problem as long as the sampling was intense. However, longer time intervals between samples towards the end of the test resulted in accumulation of iron precipitations in the tubing to the sampler. When the sampler valve opened the precipitations followed with the water sampled into the test-tube. Therefore, samples with higher concentrations are probably more unaffected and thus also more representative. This interpretation is also supported by comparison with the samples taken in-situ at the upper sampling level with the multi level sampler (sampling level 8) where no precipitations occured.

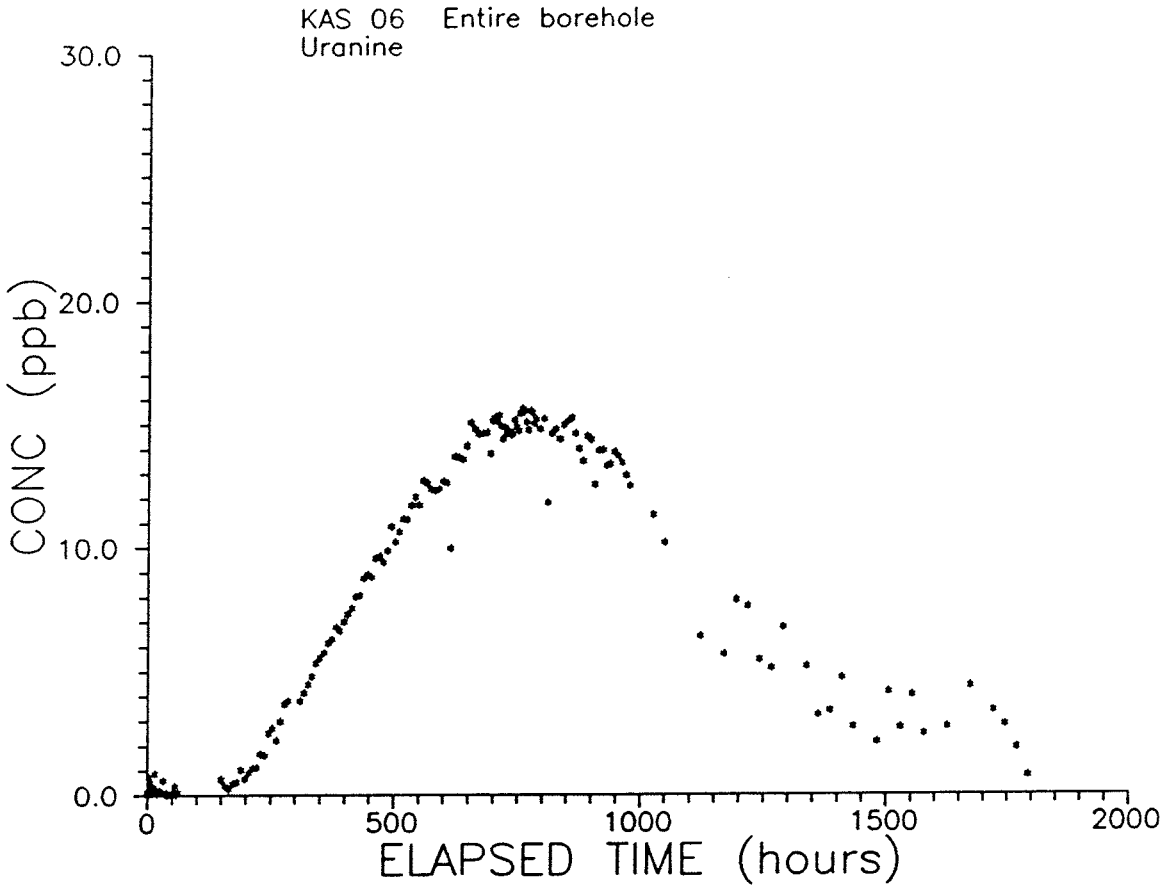

Figure 4.5 Breakthrough of Uranine in KAS06. Sum of all levels, 0–600 m.

Breakthrough of Re–186 from KAS08, section M1

Rhenium breakthrough is interpreted to occur at sampling levels 3, 4, 6 and 8 corresponding to conductors E, D, C and A, respectively. The dominant breakthrough regarding mass was registered in sampling level 3, corresponding to Conductor E, see Figure 4.6. The figure shows the corrected breakthrough curve using the polynomial fit as earlier described and also the corrected curve without polynomial fit. At this level they coincide quite well. In Figure 4.7 the same picture is shown for sampling level 4 (Conductor D) and here it is obvious that the breakthrough data without making the polynomial fit is quite difficult to interpret. First arrival is registered at about 130 hours for the two dominant sampling levels, 3 and 4, whereas the first arrival to sampling levels 6 and 8 is registered after about 190 hours. None of the breakthrough curves seem to have reached steady state concentration before injection stop at 678 hours of elapsed time. The breakthrough for the entire borehole, presented in Figure 4.8, also displays somewhat scattered data. This has to do with the low concentration levels in combination with relatively short measurement times (Byegård et al, 1991) which gives higher uncertainties in the analyses.

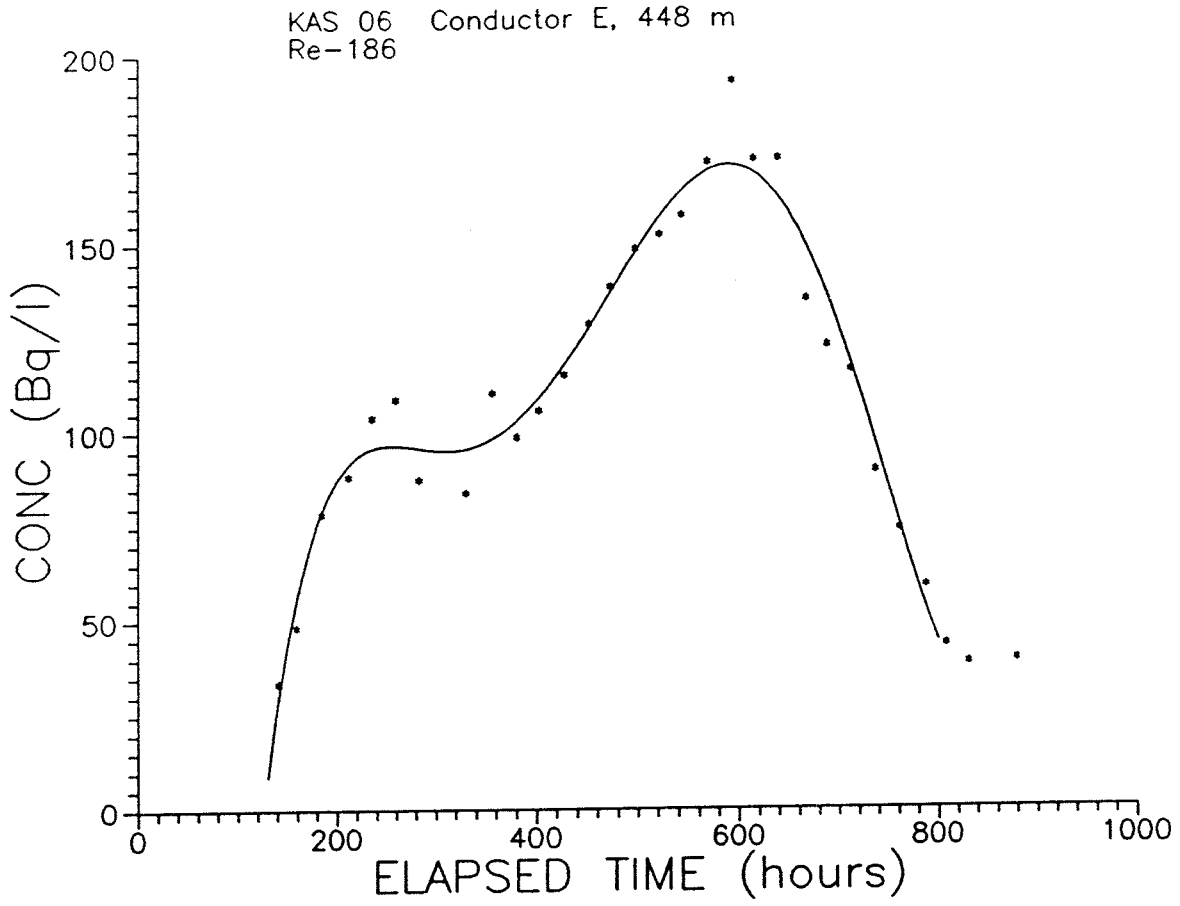

Figure 4.6 Corrected breakthrough of Rhenium at sampling level 3 (Conductor E) in KAS06. Comparison between corrected curve based on polynomial fit (solid line) and based on actual measured values (points).

Breakthrough of Re-186 from KAS08, section M3

A large pulse of Rhenium was injected in KAS08, section M3 at 677 hours after the injection start of Rhenium in section M1. The corrected breakthrough curves of Rehnium in the withdrawal borehole KAS06 (Appendix E) show no maximum that certainly can be judged to originate from the injection in section M3. However, at the lowest Rhenium tracer inflow level at 448 m (sampling level 430 m) it is possible that the little bulb on the descending part of the breakthrough curve is the result of Rheniun injection in KAS08 section M3 (Appendix C page C:6). Note that at the lowest inflow level the corrected and uncorrected breakthrough curves are compareable, since water inflow quotient don't has to be considered according to Equation 4.1 and the corrected curve is only a polynomial fit to the experimental data.

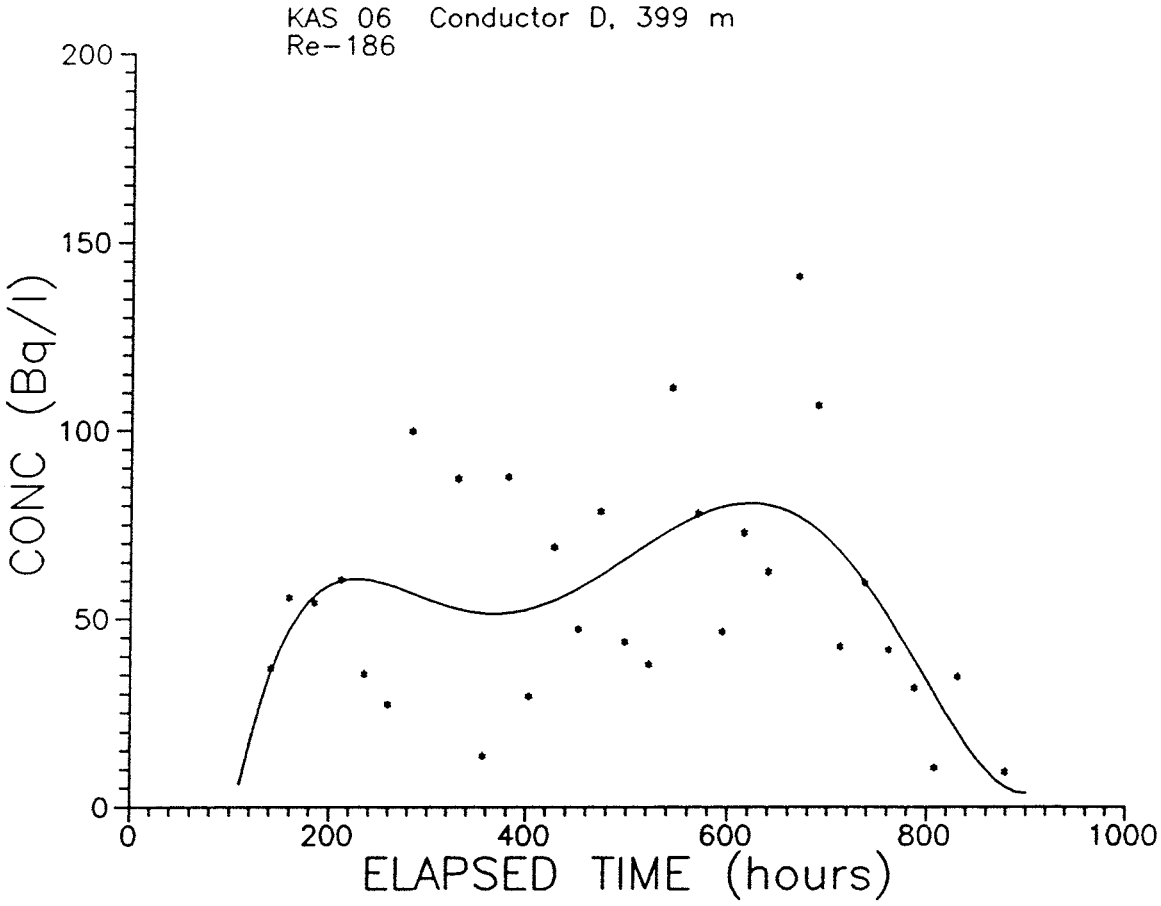

Figure 4.7 Corrected breakthrough of Rhenium at sampling level 4 (Conductor D) in KAS06. Comparison between corrected curve based on the polynomial fit (solid line) and based on measured values (points).

Breakthrough of Uranine from KAS05, section E3

A pulse of Uranine was injected in KAS05, section E3 at 678 hours after injection start of Uranine in KAS12, section DB. The breakthrough curves at inflow levels 353 m (conductor C,a) and 399 m (conductor D) both have a second peak with the maximum concentration at about 1500 hours of elapsed time since start of injection in KAS12 (Appendix E). It is most possible that this second peak originate from Uranine injection in KAS05, section E3.

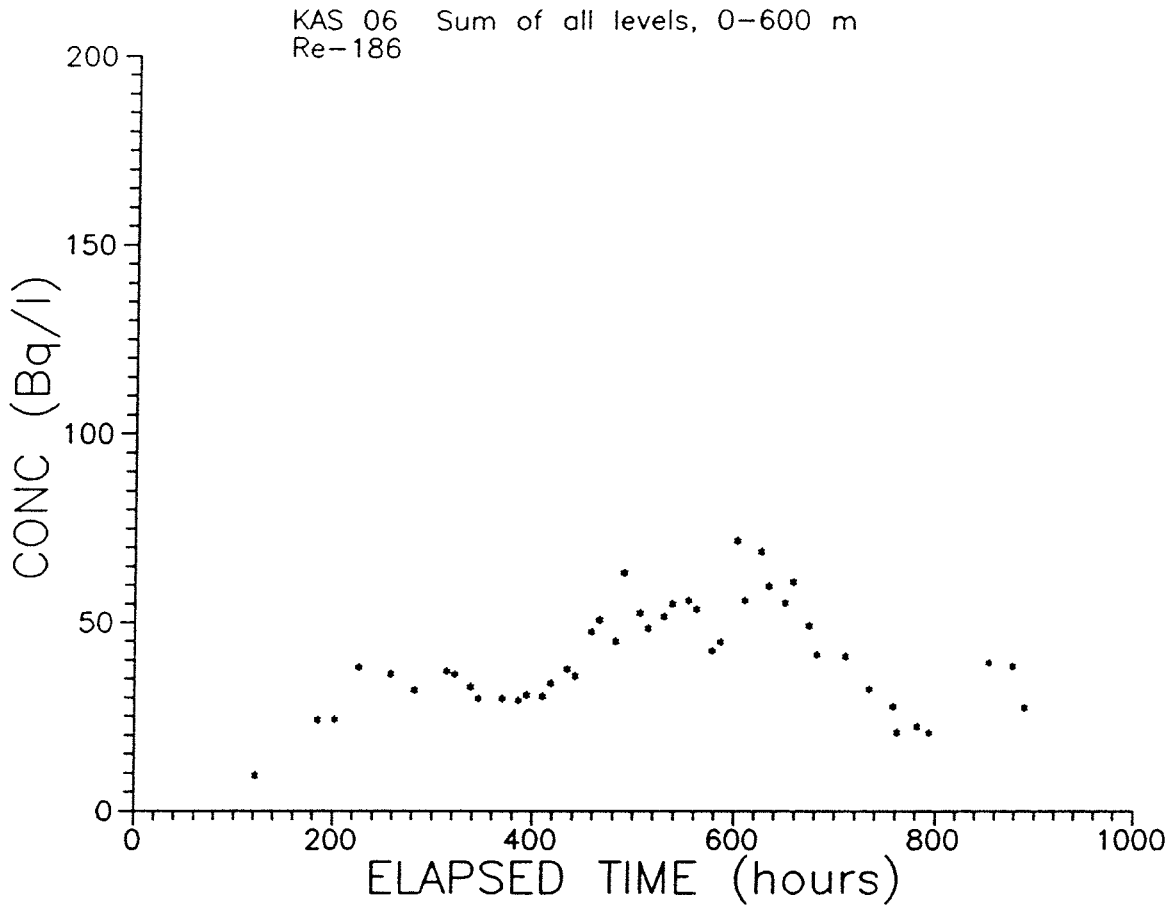

Figure 4.8 Breakthrough of Rhenium (Re-186) for the sum of all levels, 0-600 m, in KAS 06.

4.2 CONCEPTUAL MODEL OF FLOW PATHS

The assumed tracer flow paths from the point of injection in a packed-off borehole section to one or several inflow levels in KAS06 are based on the obtained tracer breakthroughs and the conceptual model of Äspö (Wikberg et al., 1991) considering the presented framework of major fracture zones. Below is also a geologic and hydraulic description of fracture zones relevant to the tracer test carried out.

4.2.1 Description of fracture zones

According to Wikberg et al.(1991) Zone NE-1 is estimated to be complex, with both more steeply dipping and gently dipping elements. NE-1 consists of sub-zones, several meters wide, highly fractured and mineralogically altered. They are considered to be important hydraulic conductors. Some of the sub-zones are probably connected with EW-5.

Zone NE–2 may, according to the geological information, not be very conductive.

Zones NNW–1 and NNW–2 are from geological and geophysical information judged to consist of single fractures, which are open due to the actual stress field in the area. The axes of common intersection of fractures in the almost vertical NNW–1 and NNW–2 with fractures in the low–dipping zone EW–5 are probably of great importance as hydraulic conductors.

Zone EW–5 comprises according to the conceptual model of a series of more or less parallel fractures, partly open with stepwise offsets in the dip direction. This means that the most significant hydraulic pathways will run parallel to the strike of the zone. The different steps of EW–5 are assumed to be badly hydraulically connected for the most part, according to Wikberg et al. (1991). They are probably intersected by the narrow NNW–NNE trending fracture zones, which are judged to be highly permeable. The possibility of several parallel fracture zones with a centerline vertical spacing of about 90–130 m is also discussed. The zone is probably very complex.

According to Wikberg et al. (1991) conductive sections are probably rare in zone EW–3 and mostly coincide with open fractures along the contacts to the surrounding fresh rock. On a geological basis the structure is expected to have low transmissivity.

4.2.2 Interpreted flow paths

The geometric (straight line) distances from point of injection to inflow level in the withdrawal borehole ranged from 100 to 300 metres, see Tables 4.3 – 4.8. The longest trajectory (tracer flow path) distance along interconnected fracture zones is calculated to approx. 380 metres.

Five fracture zones contributed to tracer transport from points of injection to detection in withdrawal borehole; NE–1, NE–2, NNW–1, NNW–2 and EW–5. Zone EW–3 carried no tracer but contributed with about 15 % to the total inflow in the withdrawal borehole.

From the number of hydraulically active fractures (inflow levels) and the estimated width of the zones (Table 4.13) the fracture zones NNW–1 and NNW–2 seem to differ from the other zones involved (Table 4.1 and 4.2). A few narrow spaced water–conducting fractures.

Within the time limits given for the pumping in this test, 76 days, and considering the half–life of the radionuclide tracers used, tracers reached the withdrawal borehole from three out of six injection points (Tables 4.3 – 4.8). However, there is a possibility that tracer also reached KAS06 from a fourth injection point, c.f. Sections 4.1.2 and 4.5.

Table 4.1 Studied levels and their corresponding major water-conducting fracture zones in KAS06.

Level[1] no, depth	Hydraulic conductor[2] label	depth(m)	Corresponding fracture zone	Borehole[3] identification
	U	60-70	EW-3	G
8 190	A	217	NNW-1,w or EW-5	S,Ch
7 290	B	312	EW-5	S
6 340	C,a	353	EW-5	S
5 360	C,b	364	EW-5	S
4 390	D	399	EW-5	Ch
3 430	E	448	NNW-2,w	S,Ch
2 540	F,a	558	EW-X[4]	
1 570	F,b	596	EW-X[4]	

[1] Sampling depth, metres below casing top.
[2] Major hydraulic conductor with its corresponding level
[3] G = geological, S = spinner, Ch = groundwater chemistry (Wikberg et al 1991)
[4] Not included in the conceptual model by Wikberg et al. (1991).

Table 4.2 Hydraulically active fractures in the injection sections, according to spinner survey. Underlined numbers are fractures where the main flow occurs.

Borehole	Fracture zone	Levels of hydraulic active fractures
KAS12, section DB	NE-2 or EW-5	285, <u>310</u>, 320, <u>325</u>
KAS08, section M1	NE-1	<u>550-562</u>, <u>571</u>, <u>585</u>
KAS08, section M3	NNW-2	141, <u>184</u>
KAS07, section J4	EW-5	200, <u>223</u>, <u>245</u>, 245-276
KAS05, section E3*	EW-5	<u>322</u>, 332, 364, 380
KAS02, section B4	EW-5	<u>318</u>, 342

* = data from hydraulic single hole testing, as no spinner result was obtained.

Table 4.3 Assumed fracture flow paths for Uranine tracer from KAS12, section DB (279 - 330 m) to KAS06.

KAS12 to KAS06	Level in KAS06*	TR(%)	GD(m)	TD(m)
NE-2 → NNW-1,w (EW-5)	217 (190)	3.2	292	331
	312 (290)	0		
	353 (340)	0		
EW-5	364 (360)	2.8	213	-
NE-2 → NNW-2 →EW-5 (EW-5)	399 (390)	16.6	200	234
NE-2 → NNW-2,w +	448 (430)	5.4	190	220,312++
	558 (590)	0		
	596 (570)	0		

+ = fracture flow path according to the predictive modeling (Svensson, 1991)
++ = trajectory distance according to the predictive modeling
* = Sampling levels are given in brackets
TR = Tracer recovery, GD = Geometric distance, TD = Trajectory distance

Table 4.4 Assumed fracture flow path for Rhenium tracer from KAS08, section M3 (140 - 200 m) to KAS06.

KAS08 to KAS06	Level in KAS06*	TR(%)	GD(m)	TD(m)
NNW-2,w +	448 (430)	0	235	323++

* = Sampling level is given in brackets
TR = Tracer recovery, GD = Geometric distance, TD = Trajectory distance

Table 4.5 Assumed fracture flow paths for Rhenium tracer from KAS08, section M1 (503 - 601 m) to KAS06.

KAS08 to KAS06	Level in KAS06*	TR(%)	GD(m)	TD(m)
NE-1 → NNW-1,w (EW-X → NNW-1,w)	217 (190)	4.9	301	381
	312 (290)	0		
NE-1 → NNW-2,w → EW-5 (EW-X → NNW-2,w → EW-5)	353 (340)	2.1	212	277
	364 (360)	0		
NE-1 → NNW-2,w → EW-5 (EW-X → NNW-2,w → EW-5)	399 (390)	5.7	190	238
NE-1 → NNW-2,w + (EW-X → NNW-2,w)	448 (430)	17.7	181	234++
	558 (540)	0		
	596 (570)	0		

\+ = fracture flow path according to the predictive modeling (Svensson, 1991)
++ = trajectory distance according to the predictive modeling
* = Sampling levels are given in brackets
TR = Tracer recovery, GD = Geometric distance, TD = Trajectory distance

Table 4.6 Assumed fracture flow paths for Iodine tracer from KAS07, section J4 (191 - 290 m) to KAS06.

KAS07 to KAS06	Level in KAS06*	TR(%)	GD(m)	TD(m)
EW-5 → NNW-1,w +	217 (190)	0	-	227++
EW-5	353 (340)	0	174	-

* = Sampling levels are given in brackets
TR = Tracer recovery, GD = Geometric distance, TD = Trajectory distance

Table 4.7 Assumed fracture flow paths for Uranine tracer from KAS05, section E3 (320 – 380 m) to KAS06.

KAS05 to KAS06	Level in KAS06*	TR(%)	GD(m)	TD(m)
EW-5 → NNW1 +	217 (190)	0	181	245,262++
EW-5	353 (340)	X	141	–
	364 (360)	0		
	399 (390)	X		

\+ = fracture flow path according to the predictive modeling (Svensson, 1991)
++ = trajectory distance according to the predictive modeling
* = Sampling levels are given in brackets
X = Breakthrough is most likely to have occured, but no recovery is calculated
TR = Tracer recovery, GD = Geometric distance, TD = Trajectory distance

Table 4.8 Assumed fracture flow paths for Indium tracer from KAS02, section B4 (309 – 345 m) to KAS06.

KAS02 to KAS06	Level in KAS06*	TR(%)	GD(m)	TD(m)
EW-5 → NNW1 +	217 (190)	0	184	306++
EW-5	353 (340)	0	104	–

* = Sampling levels are given in brackets
TR = Tracer recovery, GD = Geometric distance, TD = Trajectory distance

4.3 MODELING OF TRACER BREAKTHROUGH DATA

The general modeling purpose was to evaluate and interpret the experimental data with respect to injection schedules, occurrence of multiple flow paths, etc. In addition, model simulations were performed in order to illustrate and increase the understanding of the possible flow geometries during the tracer test.

4.3.1 Model used

The evaluation and interpretation of the tracer breakthrough curves was made with a one-dimensional porous media model. The dispersion and fluid velocity are determined by fitting the tracer breakthrough curve to the theoretical solutions. They can be determined for each identified flow path as well as the total breakthrough curve (macro dispersion).

The dispersion is defined as the spreading in time and space of a solute transported with the groundwater. The dispersion originates from (Bear, 1979):

- local variations of the velocity in the flow field
- molecular diffusion in the groundwater

The first process is called mechanical dispersion. The second one, molecular diffusion, takes place also in the absence of advection but is a time depending process. Its effect on the overall dispersion will thus be more significant at low flow velocities. Hence, these two processes can not be separated.

In the model fluid velocity is assumed to be a constant, and transverse dispersion is ignored. The governing equation is (Van Genuchten and Alves, 1982):

$$D \frac{\partial^2 C}{\partial x^2} - v \frac{\partial C}{\partial x} = R \frac{\partial C}{\partial t} \qquad (4.3)$$

where
D = dispersion coefficient
v = fluid velocity (m/s)
C = concentration of solute (kg/m^3)
x = distance from injection point (m)
R = retardation factor
t = time (s)

This model was applied in the evaluation of the experiment. Although a linear flow model (constant velocity) is used for a convergent flow field, it can be demonstrated that breakthrough curves and parameter estimates are similar for Peclet numbers of about 10 and higher. For Peclet numbers on the order of 1 the linear flow model will underestimate the mean travel time and dispersivity with 35 – 40 % compared to a radial flow model (Nordqvist, 1991) The Peclet number (Pe) is defined by:

$$Pe = x \cdot v / D \tag{4.4}$$

Mixing in the sampled borehole of tracers travelling through several different major flowpaths is considered. The concentration in the sampled section is assumed to be a volume–averaged concentration:

$$C = \sum_i f_i C_i \tag{4.5}$$

where C = tracer concentration in borehole
f_i = fractional volume parameter
C_i = tracer concentration from flowpath i

The one–dimensional models were solved using analytical solutions as given by Van Genuchten and Alves (1982). The variable injection schemes (Fig 4.9 and 4.10) were simulated by superposition of these solutions.

The boundary condition used for the injection well is a so called third type boundary condition for a step input, defined as:

$$-D \frac{\partial C}{\partial x} + vC = vC_0 \tag{4.6}$$

This boundary condition represent a convected input of solute at the upstre–am boundary, where C_0 is the injection concentration which is constant during the step input.

The fitting was generally made for three parameters, dispersion coefficient, D, mean velocity, v, and proportionality factor, f, which is a factor describing the dilution in the sampling borehole and, in the case of several flow paths, the volumetric fraction for each flow path. The fitted parameters were transformed into the form of more conventional transport parameters; mean travel time, t_0 (hours), dispersivity, D/v (m), and Peclet number.

4.3.2 Parameter estimation method

For the one–dimensional analysis, non–linear least squares regression was used. The technique that was used for regression is sometimes referred to as the Marquardt method (Marquardt, 1963) and is in this report formulated as, in an iterative form (see also Cooley, 1985):

$$\mathbf{B}_{r+1} = \mathbf{B}_r + p_{r+1}(\mathbf{X}_r^T\mathbf{W}\mathbf{X}_r + u_{r+1})^{-1}\mathbf{X}_r^T\mathbf{W}(\mathbf{C}_r^o - \mathbf{C}_r^m) \qquad (4.7)$$

where
$\mathbf{B}_r$ = vector of parameter estimates
$\mathbf{X}$ = vector of parameter sensitivities
$\mathbf{W}$ = reliability weight matrix
$\mathbf{C}_r^o$ = vector of observed concentrations
$\mathbf{C}_r^m$ = vector of model concentrations
p = damping parameter (≤ 1)
u = Marquardt parameter

Equation (4.7) gives the updated parameter estimate at the (r+1)th iteration. The parameter sensitivity vector is obtained by taking partial derivatives of the dependent variable with respect to each parameter. Thus, for an element in the $\mathbf{X}$ matrix:

$$X_{ij} = \partial C_j^m / \partial B_i \qquad (4.8)$$

The parameter sensitivities are obtained by taking analytical derivatives.

The reliability weight matrix, $\mathbf{W}$, usually reflects the error structure of the observed data. However, it may also be used by the modeller to empha–size/de–emphasize certain components of the data. If the observations are assumed to be random (no correlation between observations) and have a common variance $\mathbf{W}$ reduces to an identity matrix, and that is what is assumed in this work.

Standard errors of the parameters and linear correlation between parameters were obtained from the variance–covariance matrix, $s^2(\mathbf{X}^T\mathbf{W}\mathbf{X})^{-1}$, where s^2 is the error variance. Details of the statistical analysis procedures of regression results are also given by Cooley (1979).

4.3.3 Modeling performed

As a first step, the delay and dispersivity in the withdrawal borehole KAS06 and in the tubing system up to the sampling equipment at ground surface was examined. The flow was turbulent from the inflow at the 558 m level and upwards in the borehole. From the inflow level at 448 m and up to the sampling equipment at the ground surface the transport time was calculated to 15 minutes, i.e. for the tracers studied there was no delay in the borehole compared to the residense time in the fracture zones.

The transport time was calculated to be a bit longer from the lowest two inflow levels, but they were not used for modeling because of no tracer inflow (24 minutes between sampling levels 570 and 540 metres and 36 minutes between 540 and 430 metres). The short transport time and the turbulent flow together indicates negligible dispersion in the borehole and tubing.

The 1-D modeling was performed for all breakthrough curves obtained in the major conductors. Special emphasis was placed on classifying the uniqueness of the parameter determination. This was made by studying the regression estimates of each model run, in particular the correlation coefficients, standard errors of the parameters and the correlation between the parameters. If the correlation coefficient is high, the standard errors are low and the correlation between parameters are low, the model is good. If there is a high degree of correlation between parameters, there are too many parameters and the model should be rejected. The classification was made on a scale from 1 to 3 where 1 represents a poor model, 2 represents an acceptable model and 3 a good model. The regression statistics are presented in Appendix G.

Another important factor which was considered was the varying injection schedule. In practice, this was done by taking mean values of tracer mass release per time unit between the injection events (Figs. 4.9 and 4.10).

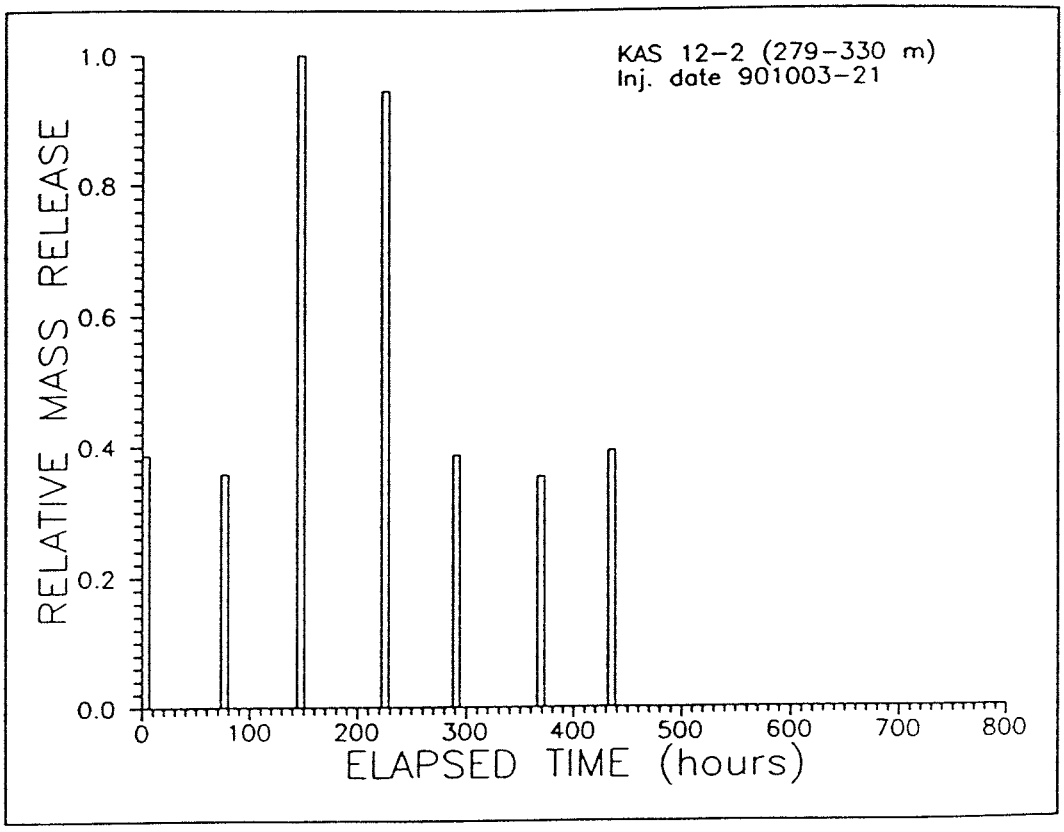

Figure 4.9 Injection schedule in KAS12, used in the 1-D modeling.

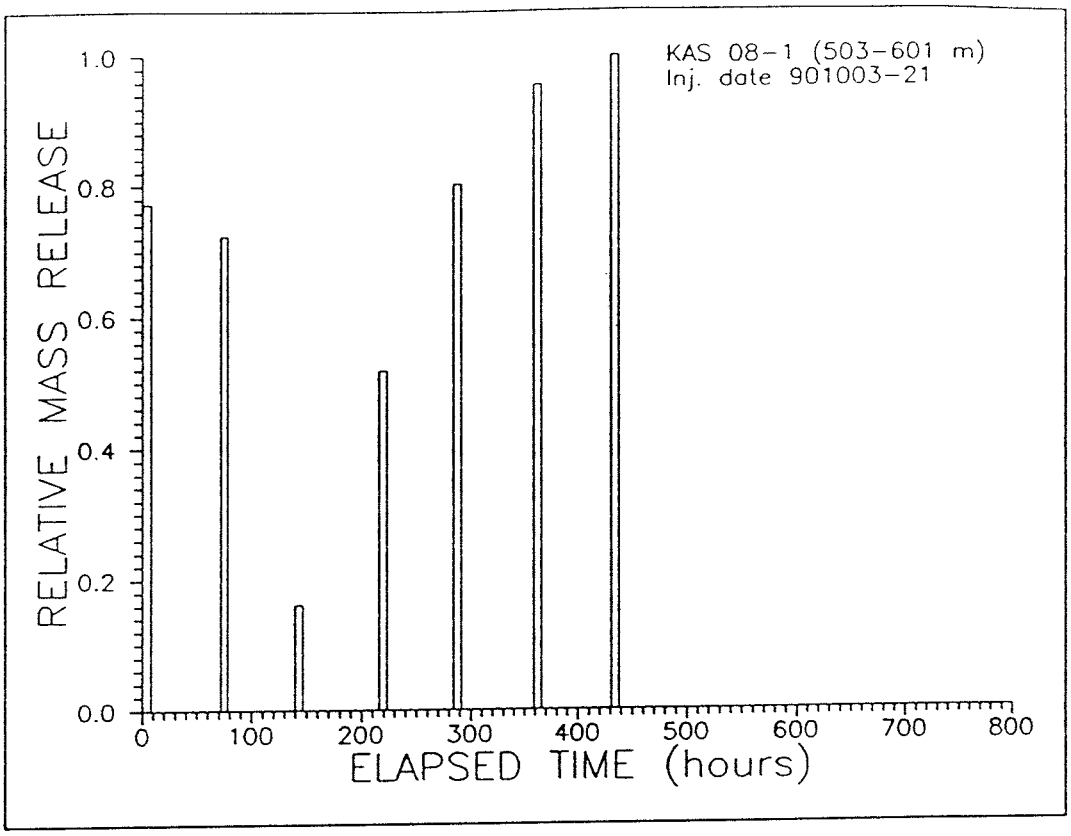

Figure 4.10 Injection schedule in KAS08, used in the 1-D modeling.

4.4 MODELING RESULTS

Modeling was performed using the 1-D models earlier described. The results of the modeling are summarized in Tables 4.9 to 4.11. The model fits to the breakthrough curves are visualised in Appendix F and statistics of model fits are presented in Appendix G.

In general the best fit (Class 2) is with only one main flow path to the inflow level in KAS06. Note that here it is assumed that each main flow path constitutes of so many minor flow paths with different velocities that it has the same transport properties as a porous media. The fracture zones are in spite of that different since the fracture zones NNW-1 and NNW-2 only have one distinct main flow path, whereas EW-5 has three main flow paths (353, 364 and 399 m) that carried tracer. The modeling of Uranine inflow to level 399 m could not fit the second peak on the breakthrough curve otherwise than injection from both KAS12 and KAS05 were included.

The obtained mean travel times, t_0, are the result from both distance, hydraulic gradient and the conductivity of the fracture flow paths. Thus, they are not suited to directly compare to other tests performed during different conditions. In this test the obtained travel times can be compared to the predictive modeling (Svensson, 1991).

The tracers that reached the withdrawal borehole all showed shorter travel times than predicted by the model.In the low-angle and complex fracture zone EW-5 the dispersivities, D/v, fitted by the 1-D model ranged from 18 to 47 metres over the flow path distances 190 to 238 m. In the flow paths from KAS05 to KAS06 with a travel distance of 141 m the dispersivity was between 1.3 and 1.7 m. These numbers can be compared to a major low-angle fracture zone at the Finnsjön site, Sweden (Gustafsson et al.,1990 and Gustafsson & Andersson 1991). Over distances 155 - 190 m the dispersivities obtained were 5 - 28 metres during low gradient conditions and 1.3 - 3.9 m in the upper highly conductive sub-zone during high gradient conditions.

The analysis of the dispersivities obtained by model fit of the inflow from NNW-1 and NNW-2 to KAS06 are difficult, since the fracture flow paths from KAS08 starts in zone NE-1 and the fracture flow paths from KAS12 starts in NE-2. The magnitude of the dispersivities are the same in NNW-1 and NNW-2, but in flow paths starting from NE-2 dispersivities are larger. If it is assumed that NNW-1 and NNW-2 displays the same dispersivity in all directions, then the dispersivity is higher in NE-2 than in NE-1 and the dispersivity in NNW-1 is between 28 and 36 m over the travel distances 301 to 381 metres. The dispersivity in NNW-2 then consequently ranged from 16 to 21 m over the distance 181 to 234 metres.

Table 4.9 Results of 1-D modeling of Uranine breakthrough in borehole KAS06. The tracer originates from injection in borehole KAS12, section DB.

Level in KAS06	Number of flow paths	Distance (m)	t_0 (h)	D/v (m)	Pe	f	Classification
217 (190)	1	GD 292	752	110	2.6	-	2
	2	GD 292	558 / 907	70 / 137	4.2 / 2.1	0.34 / 0.66	1
	1	TD 331	741	121	2.7	-	2
	2	TD 331	474 / 1105	68 / 169	4.9 / 2.0	0.19 / 0.81	1
364 (360)	1	GD 213	1053	47	4.5	-	1
	2	GD 213	421 / 995	11 / 7.0	19.4/30.4	0.22 / 0.78	1
399 (390)	1	GD 200	735	60	3.3	-	2
	2	GD 200	595 / 1135	8.4 / 221	23.8/ 0.9	0.15 / 0.85	1
	1	TD 234	735	70	3.3	-	2
	2	TD 234	538 / 1052	22 / 135	10.6/ 1.7	0.17 / 0.83	1
448 (430)	1	GD 190	605	41	4.6	-	2
	2	GD 190	275 / 666	16 / 15	11.9/12.7	0.24 / 0.76	1
	1	TD 220	605	47	4.7	-	2
	2	TD 220	271 / 642	12 / 11	18.3/20.0	0.27 / 0.0.73	1
	1	TD 312	605	66	4.7	-	2
	2	TD 312	346 / 690	44 / 16	7.1 /19.5	0.42 / 0.58	1
TOT 0 - 600	1	200	643	40	5.0	-	2
	2	200	446 / 773	32 / 11	6.2 /18.2	0.55 / 0.45	1

Table 4.10 Results of 1-D modeling of Rhenium breakthrough in borehole KAS06. The tracer originates from injection in borehole KAS08, section M1.

Level in KAS06	Number of flow paths	Distance (m)	t_0 (h)	D/v (m)	Pe	f	Classification
217 (190)	1	GD 301	284	28	10.8	-	2
	2	GD 301	226 / 559	6.3 / 1.6	47.8/188.1	0.42 / 0.48	2
	1	TD 381	284	36	10.6	-	2
	2	TD 381	227 / 558	7.5 / 2.1	50.8/181.4	0.42 / 0.58	2
399 (390)	1	GD 190	252	18	10.6	-	2
	2	GD 190	193 / 335	7.8 / 3.5	24.4/ 54.3	0.56 / 0.44	1
	1	TD 238	252	23	10.4	-	2
	2	TD 238	193 / 335	9.8 / 4.4	24.3/ 54.1	0.56 / 0.44	1
448 (430)	1	GD 181	251	16	11.3	-	2
	2	GD 181	240 / 262	22 / 11	8.2 / 16.4	0.57 / 0.43	1
	1	TD 234	251	21	11.1	-	2
	2	TD 234	194 / 321	9.6 / 8.8	24.4 /26.6	0.49 / 0.51	1
TOT 0 - 600	1	181	254	13	13.9	-	2
	2	181	235 / 386	32 / 11	43.1/ 1.5	0.40 / 0.60	1.5
	1	234	254	16	14.6	-	2
	2	234	230 / 332	8.2 / 36	28.5/ 6.5	0.55 / 0.45	1.5

Table 4.11 Results of 1-D modeling of Uranine breakthrough in borehole KAS06, assuming tracer originating from two different boreholes. Borehole KAS05, section E3 and KAS12, section DB.

Level in KAS06	Number of* flow paths	Distance (m)	t_0 (h)	D/v (m)	Pe	f	Classification
353 (340)	1	KAS05 141	960	1.3	106.9	0.15	1
	1	KAS12 200	618	33	6.1	0.85	1
399 (390)	1	KAS05 141	900	1.7	84.8	0.11	2
	1	KAS12 200	670	47	4.2	0.89	2

* = The breakthrough curve (inflow level) is fitted with two main flow paths, one from each injection point.

4.5 COMPARISON WITH PREDICTIONS AND THE ÄSPÖ CONCEPTUAL MODEL

The results from the tracer test can be compared with the conceptual model of Äspö, i.e. the framework of fracture zones and their hydraulic properties (Wikberg et al.,1991) and also with the predictive modeling (Svensson, 1991) regarding tracer flow paths and mean residence times. Note that the predictive modeling was made with the computer code PHOENICS using a simplified version of the fracture zone framework. The computer code gives Darcian times and a porosity of 0.001 was applied to all fracture zones to obtain mean travel times.

The results of the tracer test are consistent with the framework of fracture zones presented in the conceptual model of Äspö, i.e. geometry and intersections between fracture zones agree with the obtained tracer flow paths. However, the flow paths predicted by numerical modeling did not agree completely with the experimental data. To some degree this is due to the fact that the computer code used for the predictions by definition only can develop one flow path from a point of injection.

Out of six injection points the predicted residence time was a bit overestimated (a factor of 2–3) from four points and underestimated from one injection point. From the sixth injection point no fair comparison can be made between experimental and predicted residence time since the pumping for tracer withdrawal stopped three days before the predicted time of tracer arrival. The predicted residence time was anyway then not overestimated from that injection point. The discrepancy shows how sensitive the residence times are to flow porosity. In the predictive modeling a flow porosity of 1.0 10^{-3} was applied to all zones, but from the tracer test the flow porosity was determined to vary between $2.0 \cdot 10^{-4}$ and $5.0 \cdot 10^{-2}$, see Section 4.6.2.

In **borehole KAS12, section DB** the Uranine tracer was injected in fracture zone NE–2 or EW–5. The pumping for tracer withdrawal in KAS06 had a great impact on the groundwater flow through this borehole section. The flow increased from 12 ml/min during natural gradient conditions (Ittner et al., 1991) to approx. 100 ml/min, and hence there would be a good chance to obtain tracer breakthrough in the withdrawal borehole KAS06. According to the predictive modeling the tracer should reach KAS06 through the fracture zone NNW–2 with a mean travel time of 61 days, but tracers actually reached KAS–06 through both NNW–1, NNW–2 and EW–5 where the main flow was in EW–5. The travel times was 31, 25 and 31 days for NNW–1, NNW–2 and EW–5 respectively.

In **borehole KAS08, section M1** the Rhenium tracer was injected in fracture zone NE–1. Also in this section the groundwater flow increased considerably due to the pumping in KAS06, from 7 ml/min during natural gradient conditions to about 50 ml/min. Here the tracer was spread out to reach KAS06 in three major fracture zones NNW–1, EW–5 and NNW–2. Most of the tracer arrived in NNW–2. This was also the predicted flow path by the model, which, according to the theory only can give one flow path.

The predicted travel time was 19 days in NNW–2. The actual travel time was 10 days. In NNW–1 and EW–5 the travel times was respectively 12 and 11 days.

In **borehole KAS08, section M3** the Rhenium tracer was injected in fracture zone NNW–2 (677 hours after the injection start of Rhenium in KAS08, section M1). The groundwater flow increased from 4 ml/min to about 20 ml/min due to the pumping in KAS06. The tracer was expected to follow zone NNW–2 straight forward to KAS06. However, the Rhenium tracer from this injection was not found, i.e. no second maximum could by sure be identified on the breakthrough curves (Appendix E). It may be a possibility that the little bulb on the descending part of the breakthrough curve at inflow level 448 m representing NNW–2 originates from the injection in section M3 (Appendix C). In that case the residence time is estimated to approximately 200 hours (8 days). Zone NNW–2 is also supposed to consist of single fractures and to be an important hydraulic conductor (Wikberg et al.,1991). The breakthrough curve is plotted only to 1000 hours, but samples were measured to 1500 hours after which it was judged meaningless to continue due to half–lives, detection limits and background scatter. The predicted travel time was 23 days.

In **borehole KAS07, section J4** the Iodine tracer was injected in fracture zone EW–5. The pumping in KAS06 increased the groundwater flow through the borehole section from 1 ml/min during natural gradient conditions to about 18 ml/min during pumping. Thus it seemed reasonable that the tracer should reach the withdrawal borehole, even though zone EW–5 according to the conceptual model is complex. The predicted mean travel time was 48 days, but no tracer was detected in the withdrawal borehole during the 76 days time of the tracer test. The explanation may be large pore volume in combination with low hydraulic conductivity in the fracture flow paths, c.f. below.

In **borehole KAS05, section E3** the Uranine tracer was injected in fracture zone EW–5 (678 hours after injection start of Uranine in KAS12, section DB). In this section the very low natural groundwater flow, 0.4 ml/min increased to 9 ml/min due to pumping for tracer withdrawal in KAS06. The tracer reached KAS06 through zone EW–5 with a mean travel time of about 39 days. The predicted flow path was EW–5 to NNW–1, with a travel time of 128 days. It must be pointed out that the interpretation of tracer breakthrough from KAS05 is a bit uncertain, but if tracer has reached KAS06 it has been through the EW–5 zone.

In **borehole KAS02, section B4** the Indium tracer was injected in fracture zone EW–5. In this section there is no data on groundwater flow during natural gradient conditions. During the pumping in KAS06 the groundwater flow through the section was first measured to 14 ml/min when the injection sections should be chosen out of a number of candidates. However, during the tracer injection the flow was only 2 ml/min. The explanation is probably that the magnitude and/or the direction of the gradient was in a transient stage during the first measurement, made only one week after start of

pumping in KAS06. The predicted travel time was 79 days and the tracer did not reach the withdrawal borehole during the 76 days of pumping.

4.6 PARAMETER DETERMINATIONS USING ANALYTICAL EXPRESSIONS

4.6.1 Hydraulic fracture conductivity and width

The hydraulic properties of a fractured crystalline rock aquifer can be expressed as an average hydraulic conductivity for the whole thickness of the aquifer or parts thereof, e.g. fracture zones. The hydraulic average conductivity is then determined from single hole hydraulic tests or multiple borehole pumping tests (interference tests). If a tracer is injected at some distance from a pumped well the hydraulic conductivity of the actual flow paths can be calculated with the residence time as the basic variable, assuming radial flow field (Gustafsson & Andersson, 1991).

$$K_e^r = [(r^2 - r_w^2) \cdot \ln(r/r_w)] / (2 \cdot t_0 \cdot \Delta h) \qquad (4.9)$$

where: t_0 = residence time
r = distance to point of tracer injection
r_w = well radius
Δh = hydraulic head difference

In a linear flow field the hydraulic fracture conductivity is given by.

$$K_e^l = L^2 / (t_0 \cdot \Delta h) \qquad (4.10)$$

where: L = length

The sum of the widths of all hydraulically active fractures in a fracture zone, or part thereof (sub-zone) can be determined from the mass balance utilizing the residence time of a tracer.

$$e^m = q_n \cdot t_0 / [\pi(r^2 - r_w^2)] \qquad (4.11)$$

where: q_n = discharge from fracture zone

The results of the parameter caculations are presented in Table 4.12. The hydraulic fracture conductivities (K_e^r and K_e^l) are all higher assuming radial than linear flow. About four times higher for radial flow. A distinction between the fracture zones can anyway be made. The fracture conductivities in zone EW–5 are obviously smaller than in NNW–1 and NNW–2, out of which NNW–1 shows somewhat higher values. In EW–5 the hydraulic fracture conductivities ranged from $1.3 \cdot 10^{-4}$ to $1.5 \cdot 10^{-3}$ m/s and in NNW–1 and NNW–2 from $3.5 \cdot 10^{-4}$ to $8.6 \cdot 10^{-3}$ m/s.

The cumulative width of the hydraulically active fractures in the zones is in contrary to the fracture conductivities about five to ten times higher for EW–5 than NNW–1 and NNW–2. The conclusion is that zone EW–5 constitutes of many low conductive fractures, whereas zones NNW–1 and NNW–2 of a few highly conductive fractures.

Table 4.12 Hydraulic parameters for fracture zones EW–5, NNW–1 and NNW–2. Determined from tracer breakthrough in borehole KAS06.

Fracture zone	Level in KAS06	Distance (m)	t_0 (h)	K_e^r (m/s)	K_e^l (m/s)	e^m (m)
EW–5	353 (340)	KAS05 141	960	$5.3 \cdot 10^{-4}$	$1.2 \cdot 10^{-4}$	$1.1 \cdot 10^{-2}$
		KAS12 200	618	$1.7 \cdot 10^{-3}$	$3.9 \cdot 10^{-4}$	$3.4 \cdot 10^{-3}$
	364 (360)	KAS12 213	1053	$1.2 \cdot 10^{-3}$	$2.5 \cdot 10^{-4}$	$2.5 \cdot 10^{-3}$
	399 (390)	KAS05 141	900	$5.6 \cdot 10^{-4}$	$1.3 \cdot 10^{-4}$	$1.8 \cdot 10^{-2}$
		KAS12 200	670	$1.6 \cdot 10^{-3}$	$3.6 \cdot 10^{-4}$	$6.6 \cdot 10^{-3}$
	mean of all levels	KAS05	–	$5.5 \cdot 10^{-4}$	$1.3 \cdot 10^{-4}$	–
		KAS12	–	$1.5 \cdot 10^{-3}$	$3.3 \cdot 10^{-4}$	–
	sum of all levels	KAS05	–	–	–	$2.9 \cdot 10^{-2}$
		KAS12	–	–	–	$1.3 \cdot 10^{-2}$
NNW–1	217 (190)	KAS08 301	284	$8.6 \cdot 10^{-3}$	$1.9 \cdot 10^{-3}$	$1.7 \cdot 10^{-3}$
		KAS12 292	752	$3.1 \cdot 10^{-3}$	$6.8 \cdot 10^{-4}$	$4.8 \cdot 10^{-3}$
NNW–2	448 (430)	KAS08 181	251	$3.3 \cdot 10^{-3}$	$7.6 \cdot 10^{-4}$	$5.1 \cdot 10^{-3}$
		KAS12 190	605	$1.6 \cdot 10^{-3}$	$3.5 \cdot 10^{-4}$	$1.1 \cdot 10^{-2}$

4.6.2 Flow porosity

The flow porosity of a rock is defined as the volume of pore space involved in fluid transportation and is a part of the total porosity of the rock, as given by Norton and Knapp (1977).

$$\theta_T = \theta_k + \theta_d + \theta_r \qquad (4.12)$$

where: θ_T = total porosity
θ_k = flow porosity
θ_d = diffusion porosity
θ_r = residual porosity

Besides the flow porosity the total porosity also includes the diffusion porosity representing discontinuous (dead end) fractures and fractures and parts of fractures of such small aperture that water cannot move under the prevailing hydraulic conditions.

Flow paths participating in the transport are mainly concentrated to interconnected patches of elevated aperture in the single fracture, which in turn is a part of a system of interconnected fractures and zones. The configuration of the participating flow paths, and thus the magnitude of the diffusion- and flow porosity will depend on the flow conditions, i.e. change with the direction of the hydraulic gradient. Consequently, in fractured rock flow porosity is a directional property.

The flow porosity can be determined as the ratio between the average hydraulic conductivity of the fracture zone, K, and the hydraulic fracture conductivity of the flow paths, K_e, providing that Darcy's law applies.

$$\theta_k = K / K_e \qquad (4.13)$$

The flow porosity can also be determined as the ratio between the volume of flowing water in the fracture zone and the total volume of the fracture zone. In a radial flow field the ratio is.

$$\theta_k^m = e^m / W \qquad (4.14)$$

where: W = width of fracture zone

Note that by definition e^m and θ_k^m will be equal if determined for a one metre thick aquifer.

Contrary to the porous media case, values of porosity determined in a heterogeneous rock aquifer from eqn. (4.13) or (4.14) are dependent on the length of the interval where the hydraulic conductivity, K, was determined, or on W being the assumed thickness of the aquifer contributing to the flow. For example, this is the case for one single fracture (or a few closely spaced fractures) in an otherwise low conductive rock mass.

The flow porosities have been calculated over the entire thickness of the fracture zones presented in Table 4.13 and the results are presented in Table 4.14. Based on the results presented in Table 4.14 the flow porosity in fracture zone EW–5 is estimated to vary between $2.0 \cdot 10^{-4}$ and $2.0 \cdot 10^{-3}$. In fracture zone NNW–1 between $6.0 \cdot 10^{-4}$ and $3.0 \cdot 10^{-2}$, and in NNW–2 between $5.0 \cdot 10^{-3}$ and $5.0 \cdot 10^{-2}$.

Note that the total pore volume in EW–5 is of the same order as in NNW–1 and NNW–2 due to the much greater width, 100 metres compared to 1–3 m.

Table 4.13 Average hydraulic conductivity of fracture zones.

Fracture zone	Width* (m)	T* (m^2/s)	T** (m^2/s)	K+ (m/s)
NE–2	5 – 10	$0.2 \cdot 10^{-5}$ – $1.0 \cdot 10^{-5}$	–	$2.0 \cdot 10^{-7}$ – $2.0 \cdot 10^{-6}$
NE–1	50	$4.0 \cdot 10^{-5}$ – $4.0 \cdot 10^{-4}$	–	$8.0 \cdot 10^{-7}$ – $8.0 \cdot 10^{-6}$
EW–5	100	$1.0 \cdot 10^{-5}$ – $4.0 \cdot 10^{-5}$	$3.3 \cdot 10^{-5}$ – $5.6 \cdot 10^{-5}$	$3.3 \cdot 10^{-7}$ – $5.6 \cdot 10^{-7}$
NNW–1	1 – 3	$0.5 \cdot 10^{-5}$ – $2.0 \cdot 10^{-5}$	$0.8 \cdot 10^{-5}$ – $4.0 \cdot 10^{-5}$	$2.7 \cdot 10^{-6}$ – $4.0 \cdot 10^{-5}$
NNW–2	1 – 3	$2.0 \cdot 10^{-5}$ – $6.0 \cdot 10^{-5}$	$2.6 \cdot 10^{-5}$ – $3.6 \cdot 10^{-5}$	$8.7 \cdot 10^{-6}$ – $3.6 \cdot 10^{-5}$
EW–3	10 – 15	$0.1 \cdot 10^{-6}$ – $1.0 \cdot 10^{-6}$	$0.9 \cdot 10^{-5}$	$6.1 \cdot 10^{-7}$ – $9.1 \cdot 10^{-7}$
EW–X	100	_	$9.5 \cdot 10^{-6}$	$9.5 \cdot 10^{-8}$

* = according to conceptual model (Wikberg et al.,1991)
** = according to interpretation of drawdowns due to pumping during the tracer test (Andersson, 1991)
\+ = calculated with T-values from Andersson (1991), if available

Table 4.14 Flow porosities in fracture zones EW–5, NNW–1 and NNW–2. Determined from tracer breakthrough in borehole KAS06.

Fracture zone	Direction	θ_k^r	θ_k^i	θ_k^m
EW–5	KAS05 → KAS06	$6.0 \cdot 10^{-4}$ – $1.0 \cdot 10^{-3}$	$2.5 \cdot 10^{-3}$ – $4.3 \cdot 10^{-3}$	$2.9 \cdot 10^{-4}$
	KAS12 → KAS06	$2.2 \cdot 10^{-4}$ – $3.7 \cdot 10^{-4}$	$1.0 \cdot 10^{-3}$ – $1.7 \cdot 10^{-3}$	$1.3 \cdot 10^{-4}$
NNW–1	KAS08 → KAS06	$3.1 \cdot 10^{-4}$ – $4.7 \cdot 10^{-3}$	$1.4 \cdot 10^{-3}$ – $2.1 \cdot 10^{-2}$	$5.7 \cdot 10^{-4}$ – $1.7 \cdot 10^{-3}$
	KAS12 → KAS06	$8.7 \cdot 10^{-4}$ – $1.3 \cdot 10^{-2}$	$4.0 \cdot 10^{-3}$ – $5.9 \cdot 10^{-2}$	$1.6 \cdot 10^{-3}$ – $4.8 \cdot 10^{-3}$
NNW–2	KAS08 → KAS06	$2.6 \cdot 10^{-3}$ – $1.1 \cdot 10^{-2}$	$1.1 \cdot 10^{-2}$ – $4.7 \cdot 10^{-2}$	$1.7 \cdot 10^{-3}$ – $5.1 \cdot 10^{-3}$
	KAS12 → KAS06	$5.4 \cdot 10^{-3}$ – $2.2 \cdot 10^{-2}$	$2.5 \cdot 10^{-2}$ – $1.0 \cdot 10^{-1}$	$3.7 \cdot 10^{-3}$ – $1.1 \cdot 10^{-2}$

4.6.3 Recovery calculations

Calculations for Uranine in the total discharge shows a recovery of 28 % of the total injected amount in KAS12–2. The recovery is calculated over the breakthrough interval 100 – 1800 h. The recovery in the individual fracture zone flow paths is presented in Table 4.3. The main part of the tracer is recovered in fracture zone EW–5.

Preliminary calculations for Rhenium (Re–186) in the total discharge shows a recovery of 23 % of the total injected amount in KAS08–1. The recovery is calculated over the breakthrough interval 100 – 800 h. The recovery in the individual fracture zone flow paths is presented in Table 4.5. The main part of the tracer is recovered in fracture zone NNW–2.

The other tracers injected, In–114 and I–131, were not recovered in the withdrawal borehole KAS06.

5. DISCUSSION AND CONCLUSIONS

5.1 EXPERIMENTAL

The experimental design and performance was very successful, including the intermittent decaying pulse injection technique, the utilization of groundwater flow measurements by the dilution method and the multilevel sampler to detect tracer inflow levels in the withdrawal borehole.

The geometric (straight line) distances from point of injection to point of inflow in the withdrawal borehole ranged from 100 to 300 metres. The longest tracer flow path (trajectory) distance along interconnected fracture zones is calculated to approximately 380 metres.

Five fracture zones contributed to tracer transport from points of injection to detection in the withdrawal borehole; NE–1, NE–2, NNW–1, NNW–2 and EW–5.

Within the time limits given for this tracer test, 76 days, and considering the half–life of the radionuclide tracers used, tracers reached the withdrawal borehole from three out of six injection points. However, the interpretation is that tracer possibly also reached KAS06 from a fourth injection point.

5.2 CONCEPTUAL MODEL

The results of the tracer test are consistent with the framework of fracture zones presented in the conceptual model of Äspö by Wikberg et al.(1991), i.e. geometry and intersections between fracture zones agree with the obtained tracer flow paths. However, the flow paths predicted by numerical modeling (Svensson, 1991) did not agree completely with the experimental data. To some degree this is due to the fact that the computer code used for the predictions by definition only can develop one flow path from a point of injection.

Out of six injection points the predicted residence time was a bit overestimated (a factor of 2–3) from four points and underestimated from one injection point. From the sixth injection point no fair comparison can be made between experimental and predicted residence time since the pumping for tracer withdrawal stopped three days before the predicted time of tracer arrival. The predicted residence time was anyway then not overestimated from that injection point. The discrepancy shows how sensitive the residence times are to flow porosity. In the predictive modeling a flow porosity of $1.0 \cdot 10^{-3}$ was applied to all zones, but from the tracer test the flow porosity was determined to vary between $2.0 \cdot 10^{-4}$ and $5.0 \cdot 10^{-2}$.

5.3 FRACTURE ZONES

Zone EW–3 carried no tracer but from the tracer test results it was possible to calculate its contribution to the inflow in the withdrawal borehole KAS06. The inflow from zone EW–3 amounted to 15 % of the total inflow, i.e. it is indicated that EW–3 must be considered being a more important hydraulic conductor than is assumed in the conceptual model.

Within the distances involved in the performed tracer test zone EW–5 is judged to be a good but complex hydraulic conductor, with many widely spread but interconnected fracture flow paths.

Zones NNW–1 and NNW–2 are very good hydraulic conductors with a few narrow spaced water–conducting fractures.

The transport parameters for fracture zones NE–1 and NE–2 can not be quantitatively determined, but based on the tracer test results it is assumed that NE–1, having higher conductivities in the fracture flow paths and lower dispersivities is a more distinct hydraulic conductor than NE–2.

5.4 TRANSPORT PARAMETERS

The dispersivities obtained by model fit to the breakthrough curves for NNW–1, NNW–2 and EW–5 are compareable to a large fracture zone investigated at the Finnsjön site, central Sweden. In general, the dispersivities was in the order of one tenth to one fifth of the flow path distance. Expressed as Peclet numbers, 4.2 – 11.3 where the lower values are representative for EW–5 and the higher for NNW–1 and NNW–2, i.e. largest dispersion in EW–5, which is not suprisingly the most geometrically complex zone according to the conceptual model.

The tracer labelled groundwater flowing through the injection borehole sections are widely spread within the the fracture zones and between fracture zones until it eventually emerges in the withdrawal borehole KAS06. As an example the uranine injected in KAS12, section DB has been spread into three fracture zones before it reaches KAS06. Macro dispersion is thus judged to be an important process in the fractured rock during the prevailed high flow rate pumped conditions.

The hydraulic conductivity of the fracture flow paths were calculated. The fracture conductivities are obviously smaller in EW–5 than in NNW–1 and NNW–2, out of which NNW–1 has somewhat higher conductivities. The mean value is $6.3 \cdot 10^{-4}$ m/s in EW–5 and $3.6 \cdot 10^{-3}$ and $1.5 \cdot 10^{-3}$ m/s in NNW–1 and NNW–2 respectively. The cumultative width of the hydraulically active fractures in the zones is about five to ten times higher for EW–5 than NNW–1 and NNW–2. The conclusion is that zone EW–5 consists of many low conductive fractures, whereas zones NNW–1 and NNW–2 consists of a few highly conductive fractures.

The flow porosity was calculated over the entire width of the fracture zones. Based on the results of the calculations the flow porosity in EW–5 is estimated to vary between $2.0 \cdot 10^{-4}$ and $2.0 \cdot 10^{-3}$, in NNW–1 between $6.0 \cdot 10^{-4}$ and $3.0 \cdot 10^{-2}$, and in NNW–2 between $5.0 \cdot 10^{-3}$ and $5.0 \cdot 10^{-2}$. However, due to the much greater width of EW–5, 100 metres compared to 1 to 3 metres for NNW–1 and NNW–2 the total effective pore volume in EW–5 is in the same order or even larger than in the other two zones.

6. REFERENCES

Andersson J-E. 1991. Evaluation of pumping test LPT-2 in KAS06 at Äspö. GEOSIGMA GRAP 91002. GEOSIGMA AB. Uppsala.

Bear J. 1979. Hydraulics of groundwater. Mc Graw-Hill. New York.

Byegård J., Skarnemark G., Skålberg M. 1991. Radioactive tracer experiment performed at the Finnsjön area and at Äspö. SKB Technical Report TR 91-xx. in prep.

Carlsten S. 1989. Results from borehole radar measurements in KAS05, KAS06, KAS07 and KAS08 at Äspö - Interpretation of fracture zones by including radar measurements from KAS02 and KAS04. Äspö Hard Rock Laboratory. SKB PR 25-89-10. Swedish Nuclear Fuel and Waste Management Co. Stockholm.

Cooley R.L. 1979. A method for estimating parameters and assessing reliability for models of steady state groundwater flow. 2, Application of statistical analysis. Water Resourses Research. Vol 15, No 3. Washington D.C.

Cooley R.L. 1985. A comparison of several methods of solving nonlinear regression groundwater flow problems. Water Resourses Research. Vol 21, No 10. Washington D.C.

Ekman L., Gentzschein B. 1989. Projekt berglaboratorium. Sammanställning av preliminära värden på hydraulisk konduktivitet från vatteninjektionstester i 3-m sektioner i kärnborrhålen KAS05 - KAS08 på Äspö. SGAB IRAP 89238. Sveriges Geologiska AB. Uppsala.

Gentzschein B., Nyberg G. 1989. Data från långtidspumptest i borrhål KAS07. SGAB IRAP 89236. Sveriges Geologiska AB. Uppsala.

Gustafson G., Stanfors R., Wikberg P. 1989. Swedish hard rock laboratory. Evaluation of 1988 Year Pre-investigations and Description of the Target Area, the Island of Äspö. SKB Tech. Rep. 89-16. Swedish Nuclear Fuel and Waste Management Co. Stockholm.

Gustafsson E., Andersson P., Eriksson C-O., Nordqvist R. 1990. Radially converging tracer experiment in a low-angle fracture zone at the Finnsjön site, central Sweden: The fracture zone project - phase 3. SKB Progress Report AR 90-27. Swedish Nuclear Fuel and Waste Management Co. Stockholm.

Gustafsson E., Andersson P. 1991. Groundwater flow conditions in a low-angle fracture zone at Finnsjön, Sweden. Journal of Hydrology. 126, pp 79 - 111. Elsvier Science Publishers B.V.. Amsterdam.

Gustafsson E. 1986. Bestämning av grundvattenflödet med utspädningsteknik – Modifierad utrustning och kompletterande fältmätningar. SKB Progress Report AR 86–21. Swedish Nuclear Fuel and Waste Management Co. Stockholm.

Gustafsson E. 1990a. Test av gammaspektrometersond för bestämmning av inflödesnivåer i borrhål. SGAB IRAP 90205. Sveriges Geologiska AB. Uppsala.

Gustafsson E. 1990b. Radiellt konvergerande spårförsök vid LPT–2: Förslag till genomförande. SGAB IRAP 90203. Sveriges Geologiska AB. Uppsala.

Ittner T., Gustafsson E., Andersson P., Eriksson C–O. 1991. Groundwater flow measurements at Äspö with the dilution method. Äspö Hard Rock Laboratory. SKB PR 25–91–18. Swedish Nuclear Fuel and Waste Management Co. Stockholm.

Jönsson S., Nyberg G. 1991. Data från långtidspumptest i borrhål KAS06. SGAB IRAP 91223. Sveriges Geologiska AB. Uppsala.

Marquardht D.W. 1963. An algortihm for least squares estimation of nonlinear parameters. J. Soc. Ind. Appl. Math. 11(2). pp 431–441.

Nilsson A–C. 1991. Groundwater chemistry monitoring at Äspö during 1990. Äspö Hard Rock Laboratory. SKB PR 25–91–04. Swedish Nuclear Fuel and Waste Management Co. Stockholm.

Nilsson L. 1990. Hydraulic tests at Äspö, KAS05–KAS08, HAS13–HAS17, Evaluation. Äspö Hard Rock Laboratory. SKB PR 25–89–20. Swedish Nuclear Fuel and Waste Management Co. Stockholm.

Nordqvist R. 1991. Personal communication. GEOSIGMA AB. Uppsala.

Norton D., Knapp R. 1977. Transport phenomena in hydrothermal systems: The nature of porosity. Amer. Journal of Science. Vol 277. PP 913–936.

Nyberg G., Jönsson S., Ekman L. 1991. Äspö Hard Rock Laboratory: Groundwater level program, report for the period 1987 – 1989. Äspö Hard Rock Laboratory. SKB PR 25–90–18. Swedish Nuclear Fuel and Waste Management Co. Stockholm.

Svensson U. 1991. Predictions of flow trajectories for the LPT–2 test. Äspö Hard Rock Laboratory. SKB PR 25–91–17. Swedish Nuclear Fuel and Waste Management Co. Stockholm.

Van Genuchten M. Th., Alves W.J. 1982. Analytical solutions of the one–dimensional convective–dispersive solute transport equation. U.S. Dep. Agric. Tech. Bull. 1661. pp 151.

Wikberg P. (ed), Gustafson G., Rhén I., Stanfors R. 1991. Äspö Hard Rock Laboratory. Evaluation and conceptual modelling based on the pre-investigations 1986–1990. SKB TR 91–22. Swedish Nuclear Fuel and Waste Management Co. Stockholm.

APPENDIX A

DILUTION MEASUREMENTS

Dilution measurement in borehole sections:

Figure	Page
A- 1: KAS02-2	A:1
A- 2: KAS02-4	
A- 3: KAS05-3	A:2
A- 4: KAS05-3	
A- 5: KAS05-1	A:3
A- 6: KAS07-4	
A- 7: KAS08-3	A:4
A- 8: KAS08-3	
A- 9: KAS08-1	A:5
A-10: KAS12-2	
A-11: KAS13-3	A:6
A-12: KAS14-2	

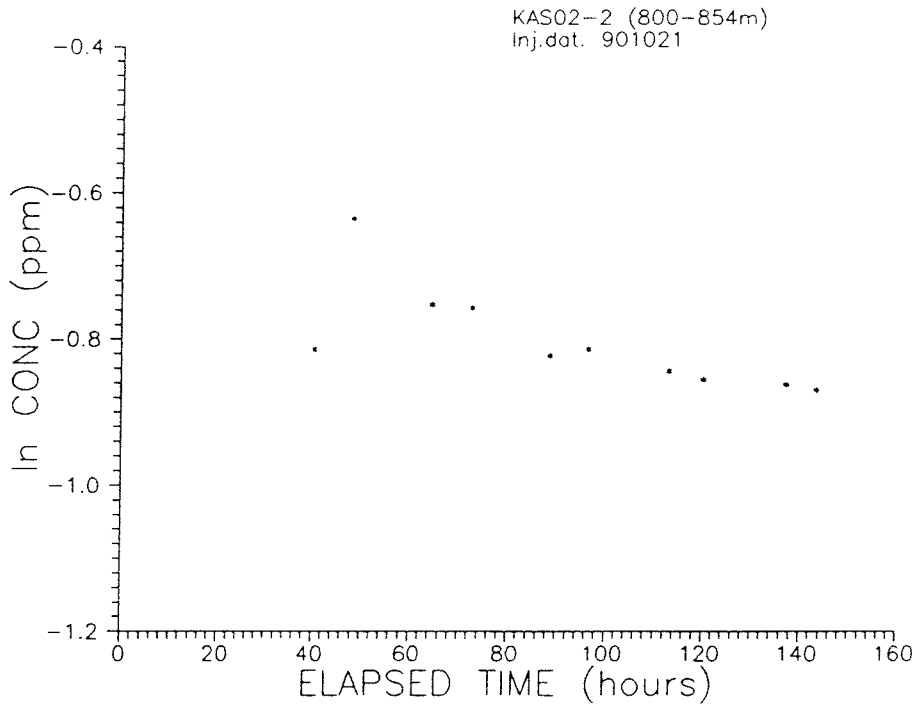

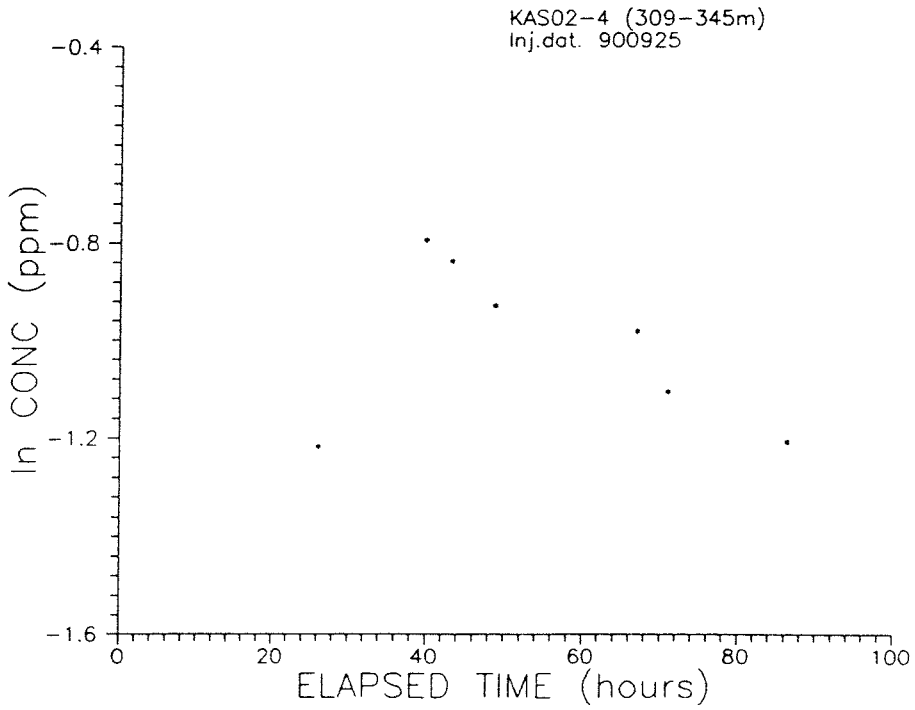

Dilution measurements in KAS02-2 and KAS02-4.

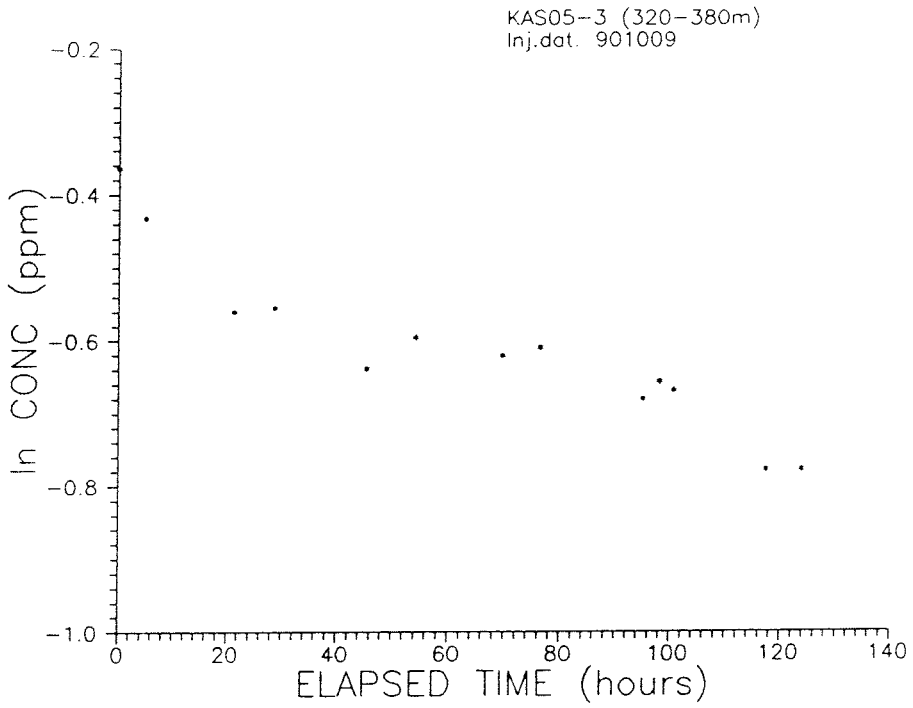

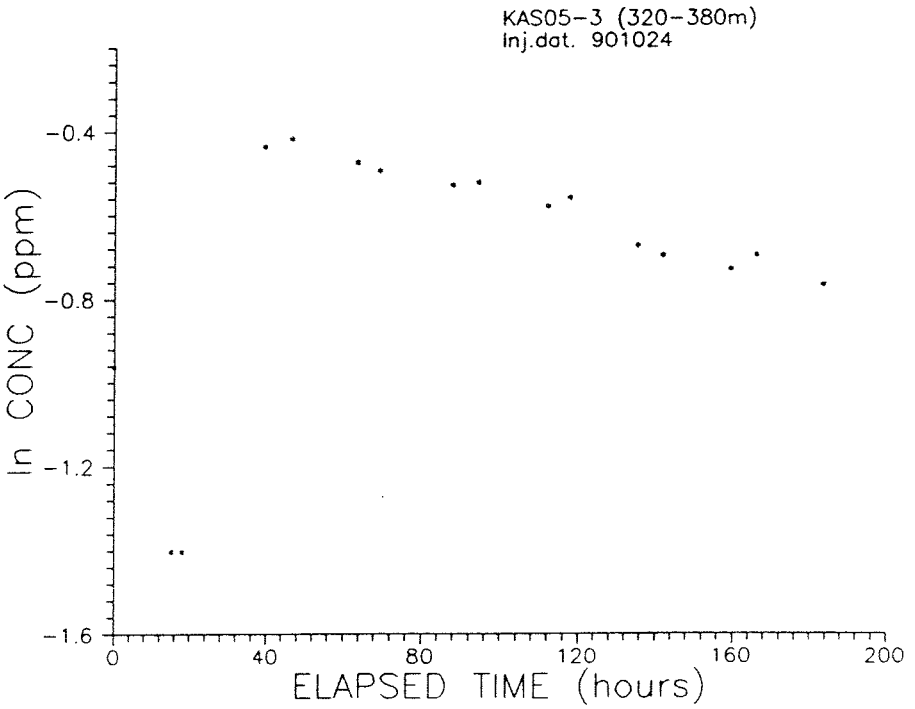

Dilution measurements in KAS05-3.

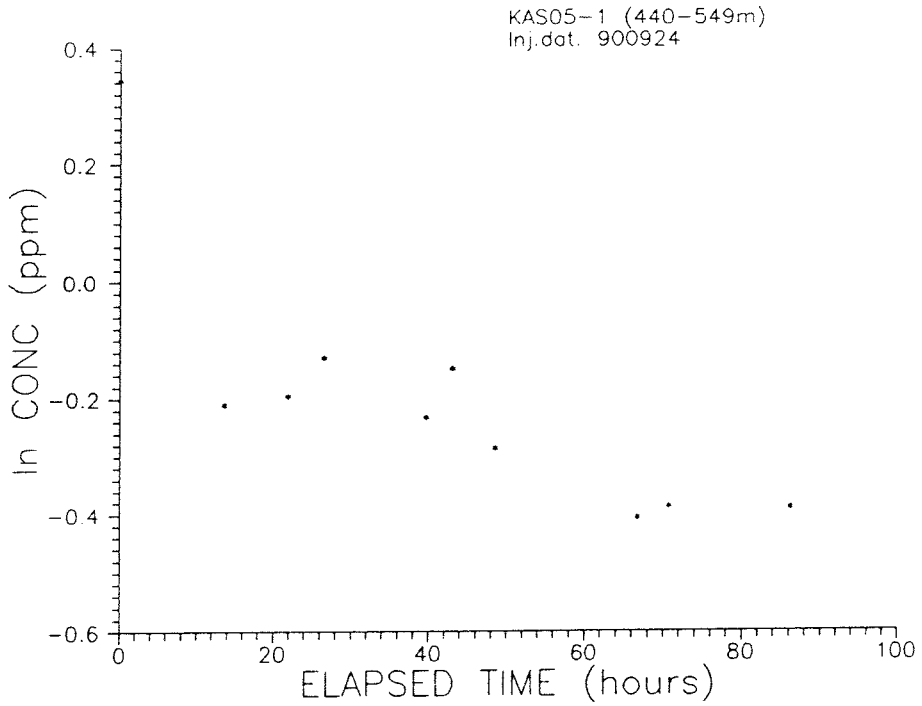

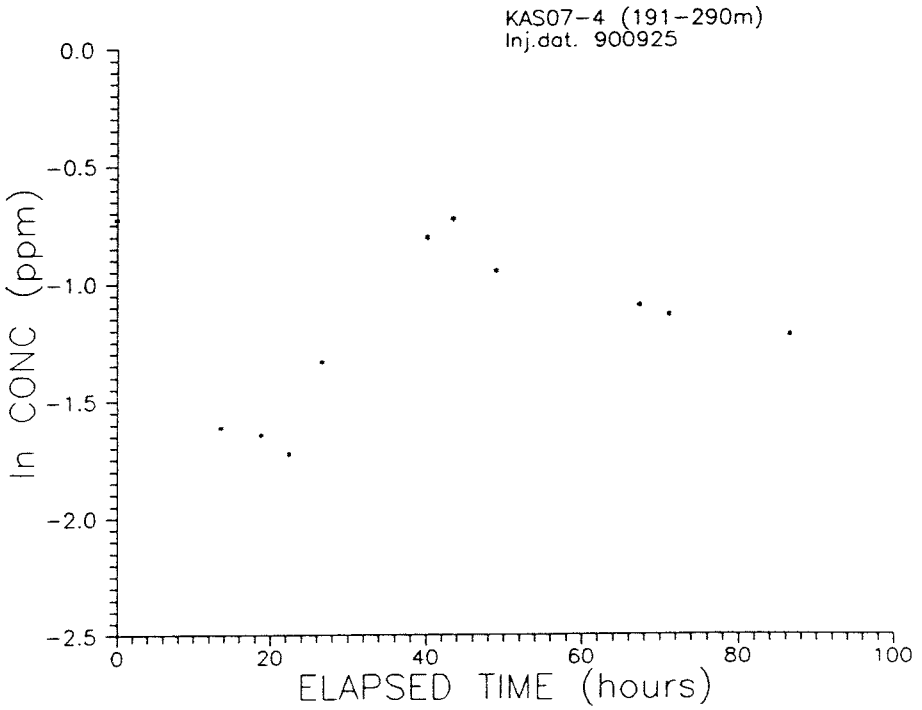

Dilution measurements in KAS05-1 and KAS07-4.

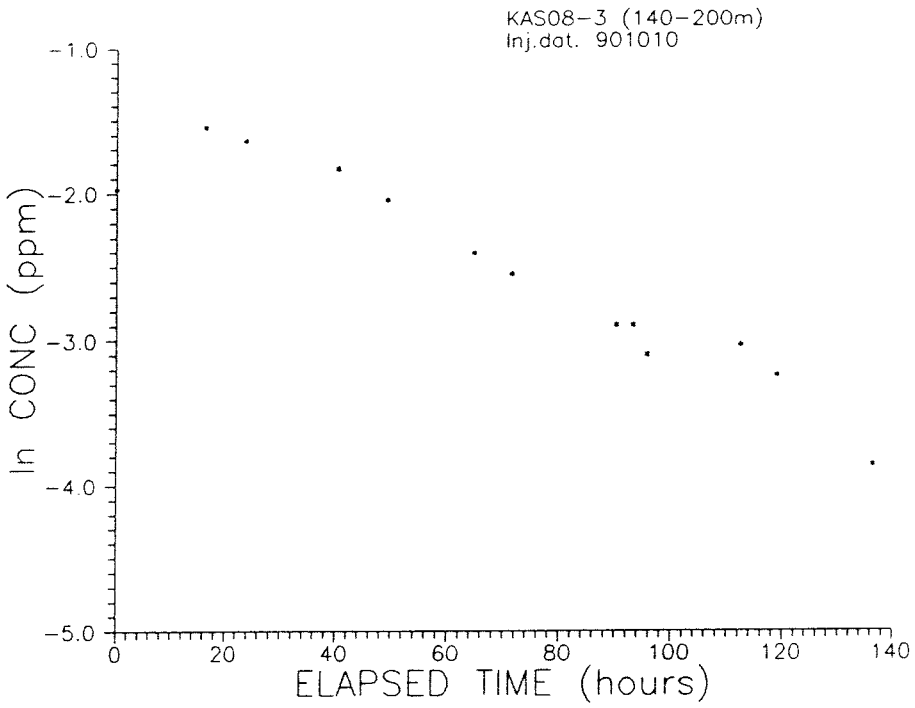

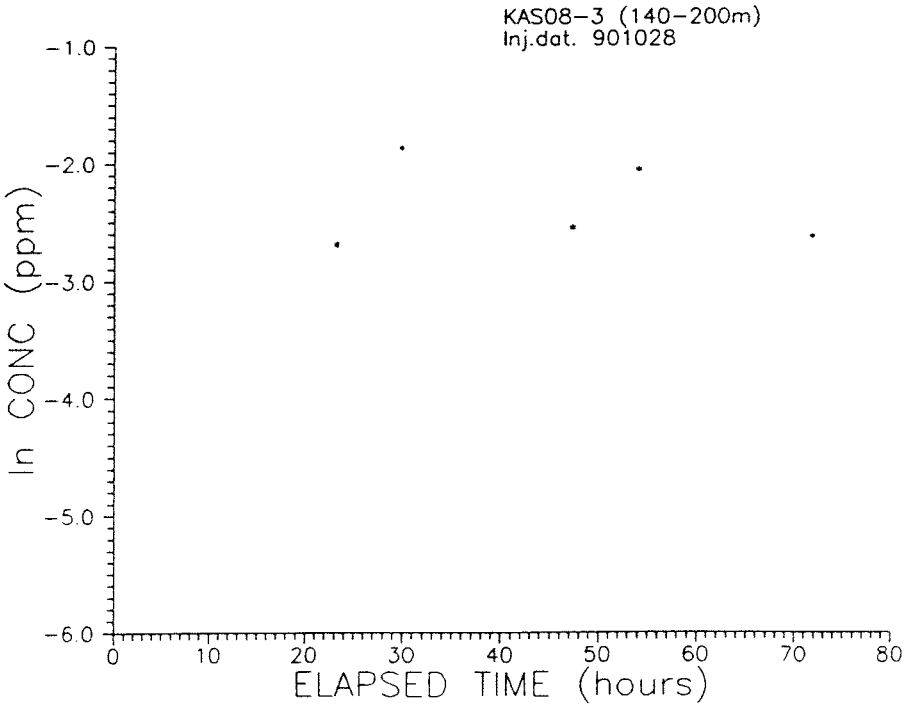

Dilution measurements in KAS08-3.

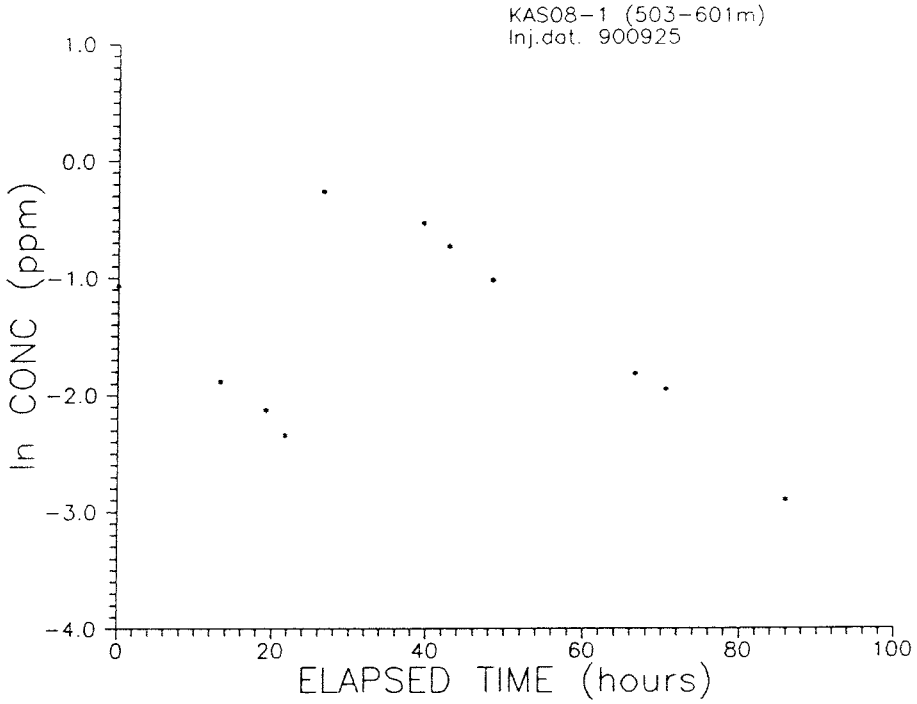

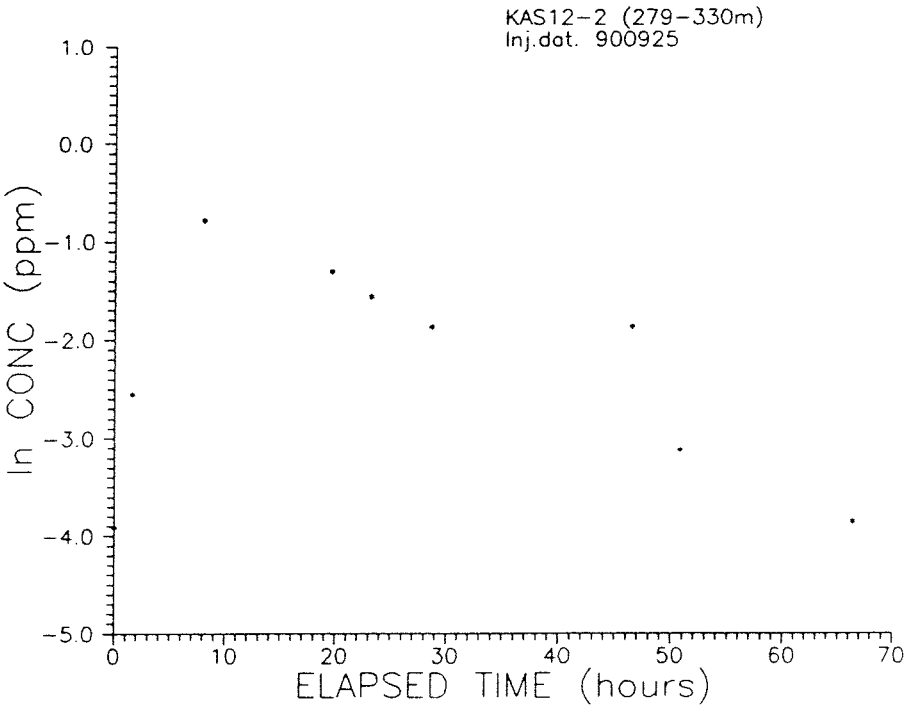

Dilution measurements in KAS08-1 and KAS12-2.

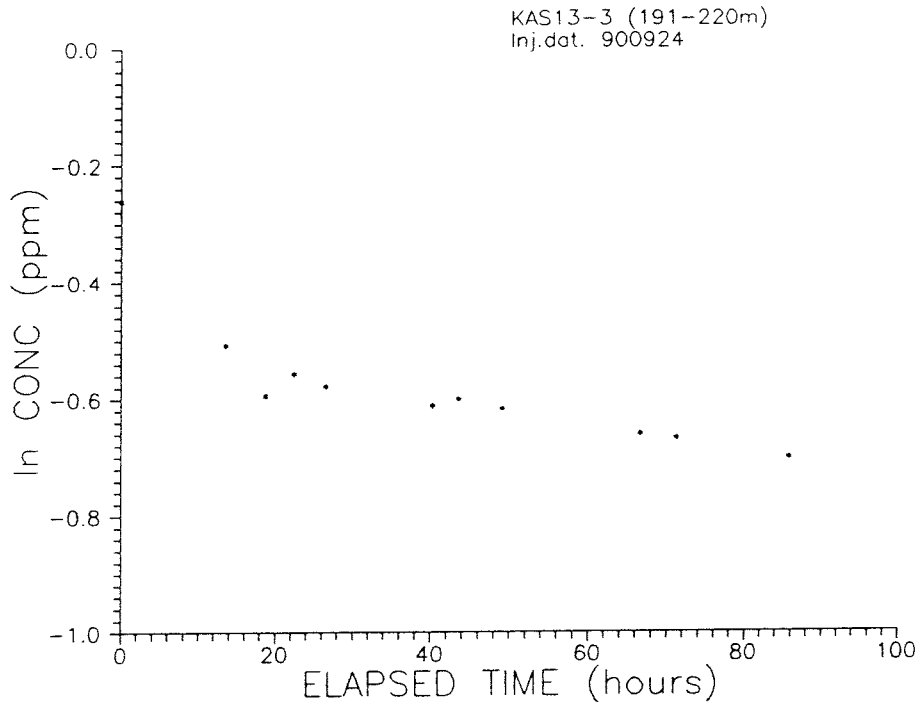

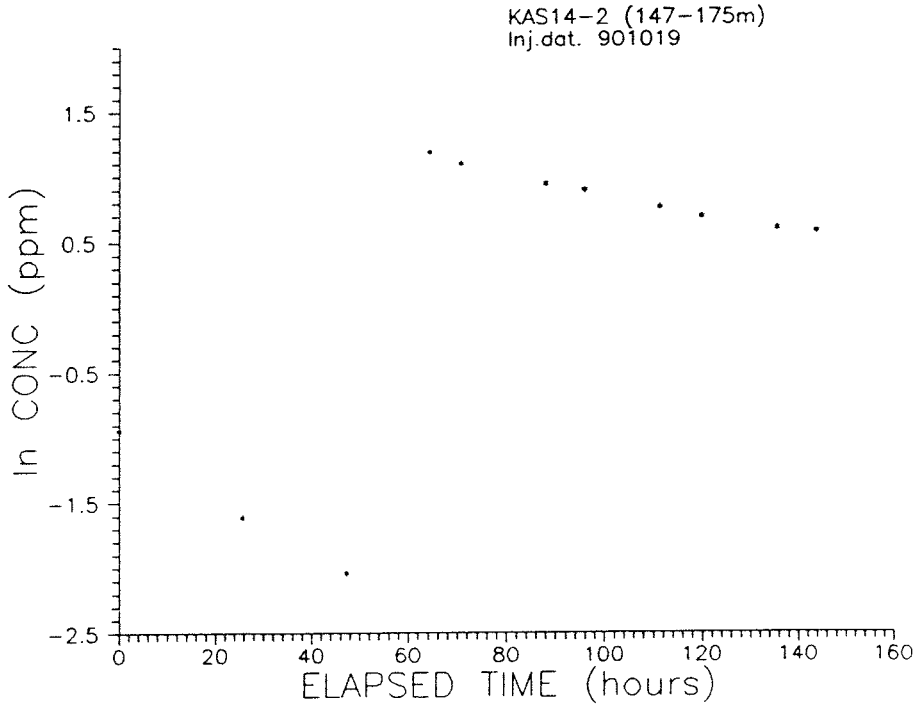

Dilution measurements in KAS13-3 and KAS14-2.

APPENDIX B

TRACER INJECTIONS

Tracer injections in borehole sections:

Figure		Page
B- 1: KAS02-4	Indium-114	B:1
B- 2: KAS05-3	Uranine	
B- 3: KAS07-4	Iodine-131	B:2
B- 4: KAS08-1	Rhenium-186	
B- 5: KAS08-3	Rhenium-186	B:3
B- 6: KAS12-2	Uranine	

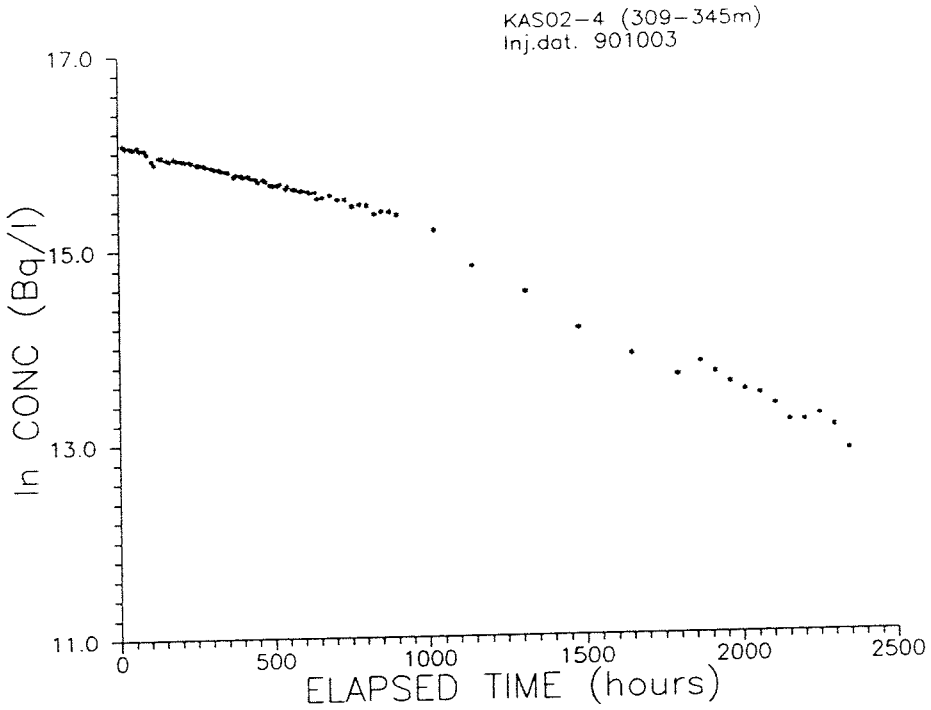

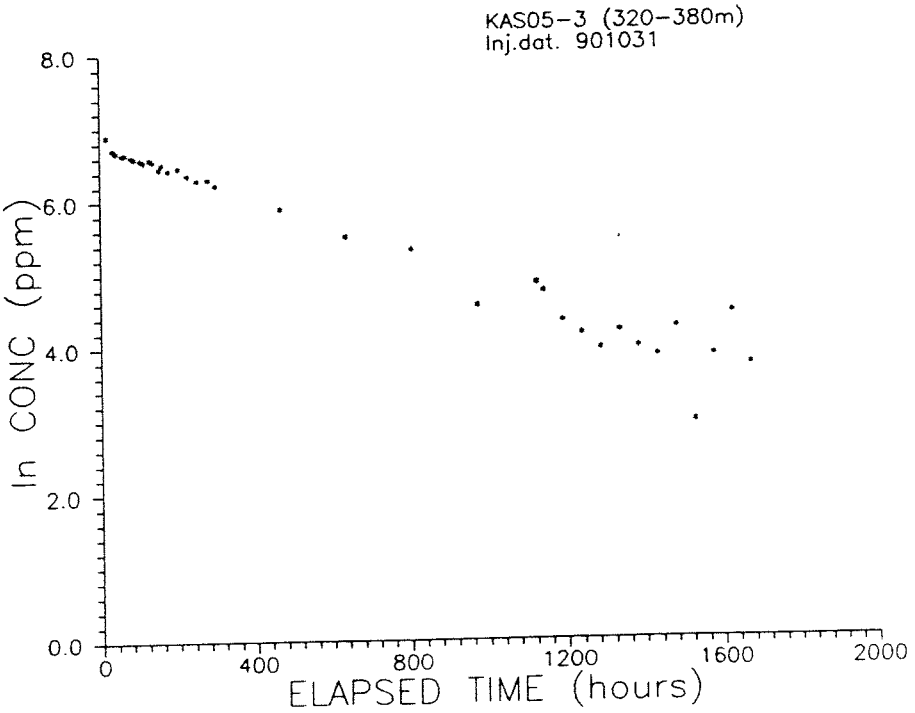

Tracer injection in KAS02-4 (In-114) and KAS05-3 (Uranine).

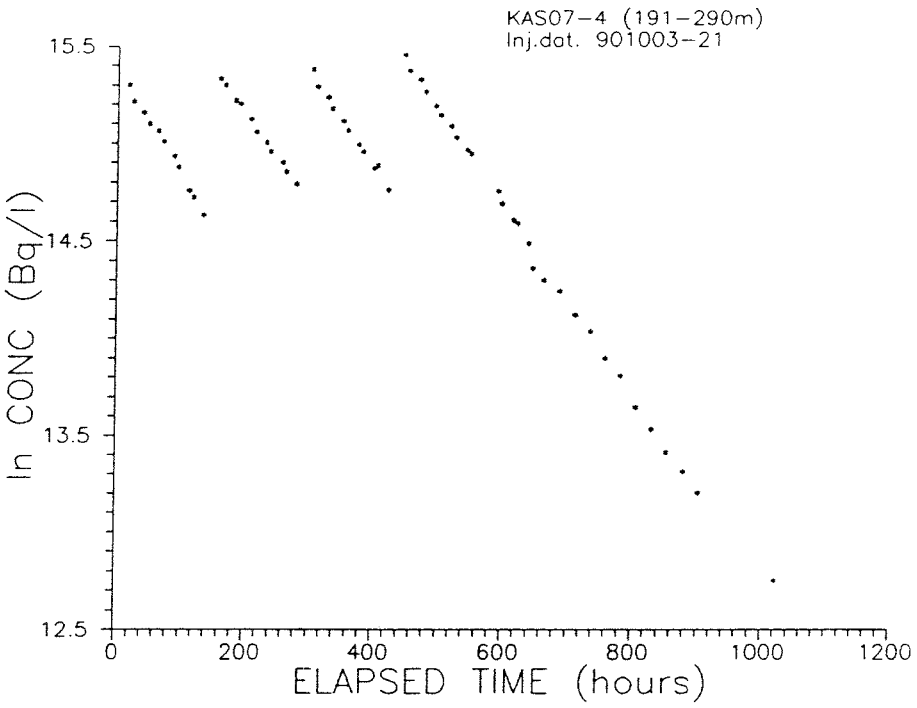

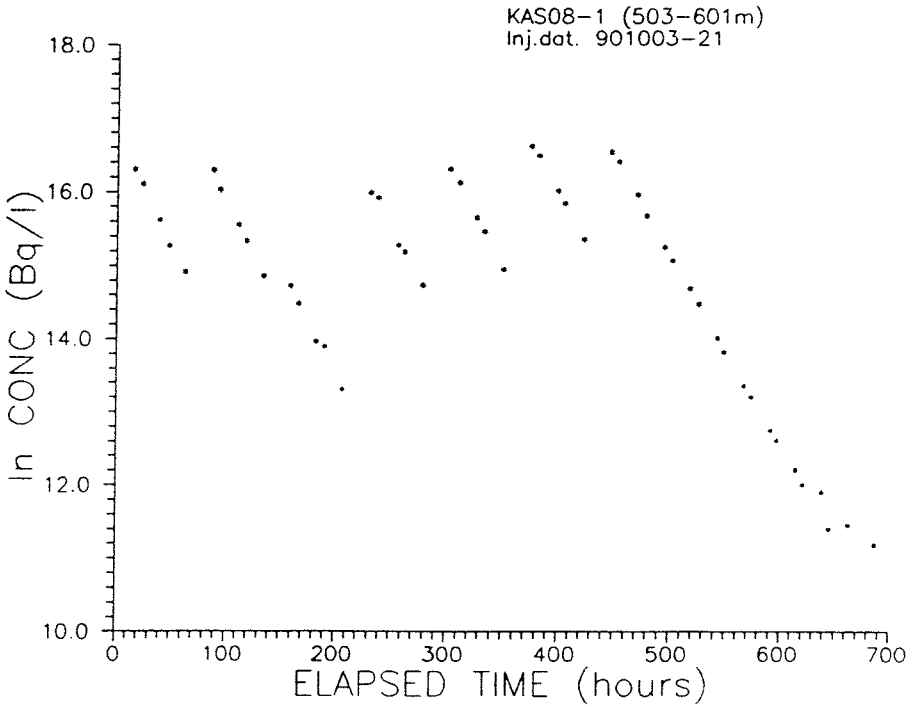

Tracer injection in KAS07-4 (I-131) and KAS08-1 (Re-186).

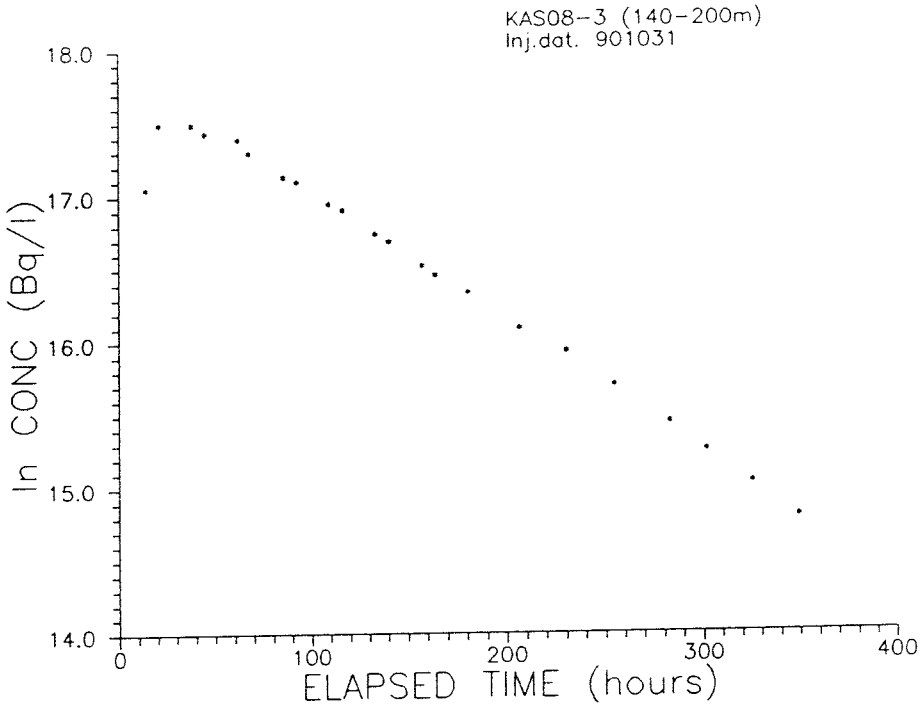

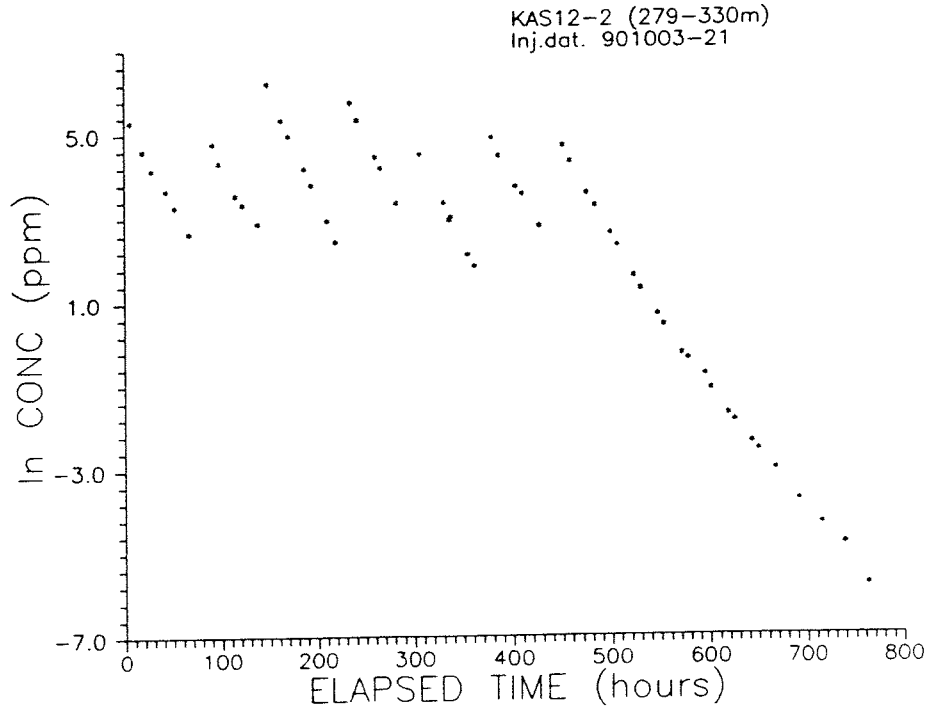

Tracer injection in KAS08-3 (Re-186) and KAS12-2 (Uranine).

APPENDIX C

TRACER BREAKTHROUGH AT THE SAMPLING LEVELS

Tracer breakthrough in withdrawal borehole, KAS06

Figure		Page
C- 1: level 1 570m	Uranine	C:1
C- 2: level 2 540m		
C- 3: level 3 430m		C:2
C- 4: level 4 390m		
C- 5: level 5 360m		C:3
C- 6: level 6 340m		
C- 7: level 7 290m		C:4
C- 8: level 8 190m		
C- 9: total discharge		C:5
C-10: level 3 430m	Rhenium-186	C:6
C-11: level 4 390m		
C-12: level 5 360m		C:7
C-13: level 6 340m		
C-14: level 7 290m		C:8
C-15: level 8 190m		
C-16: total discharge		C:9

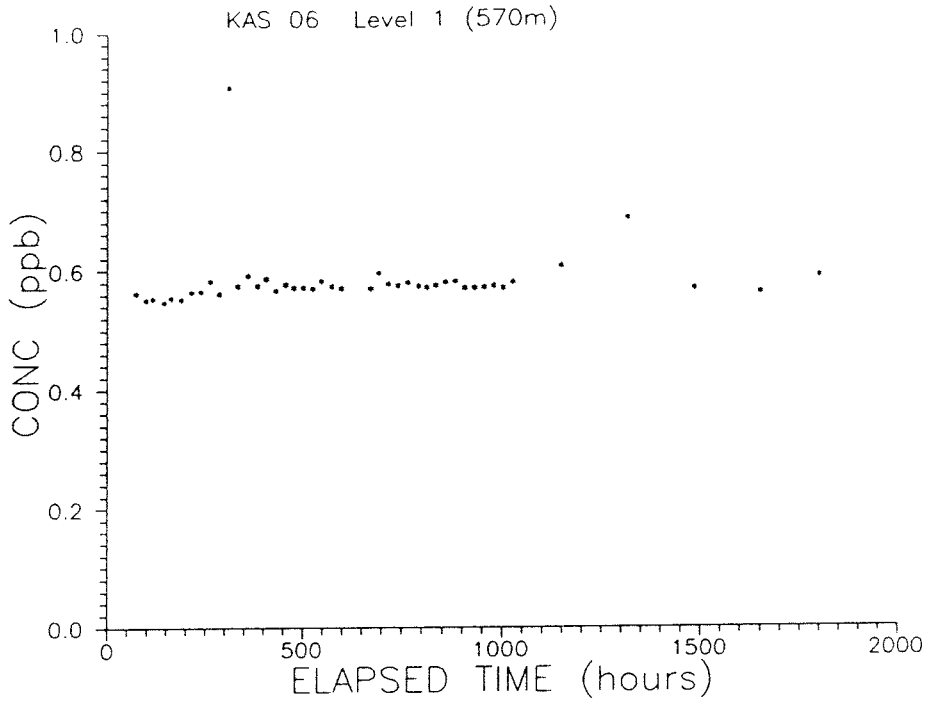

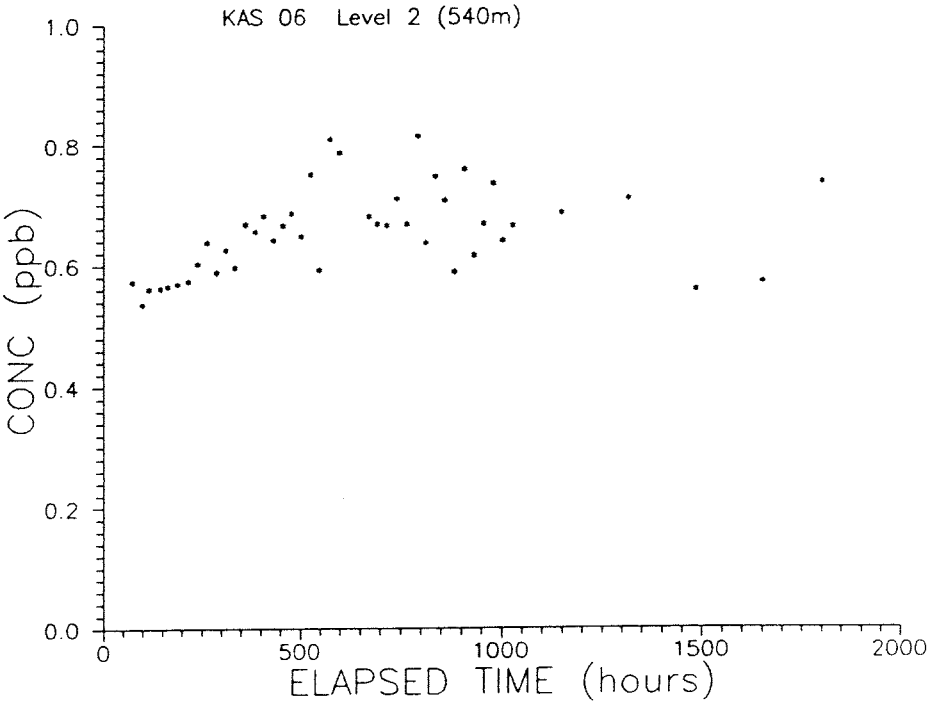

Tracer breakthrough (Uranine) in withdrawal hole, KAS06.

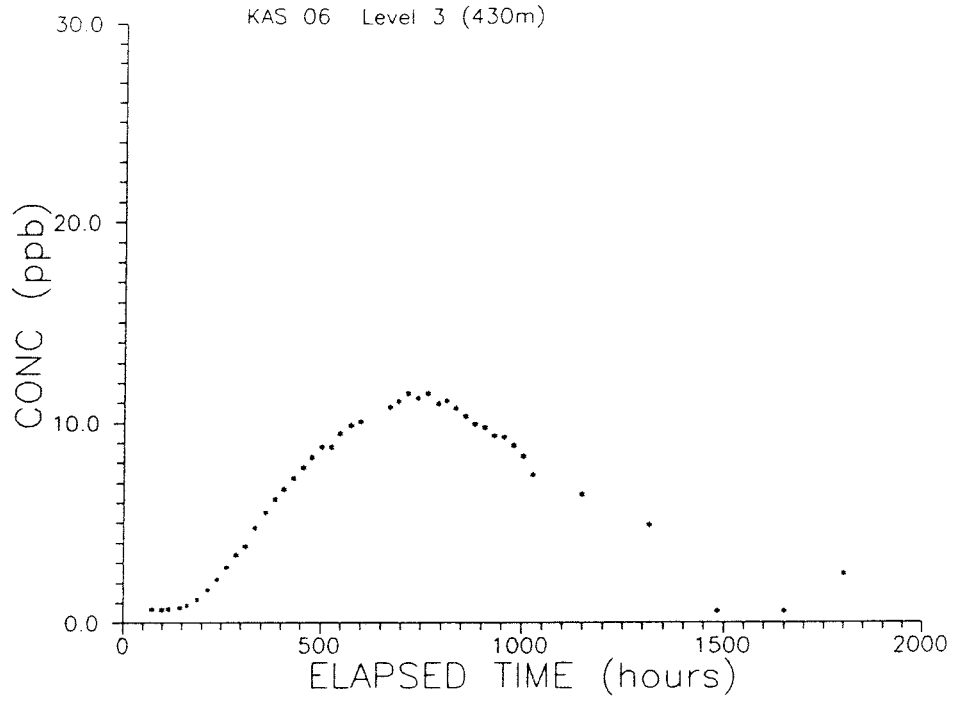

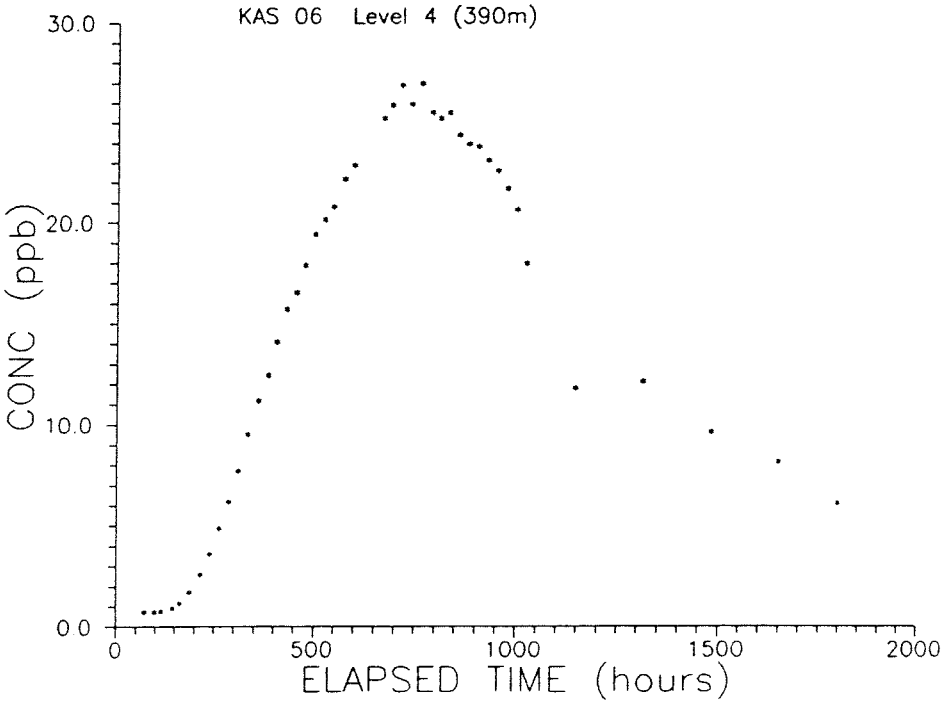

Tracer breakthrough (Uranine) in withdrawal hole, KAS06.

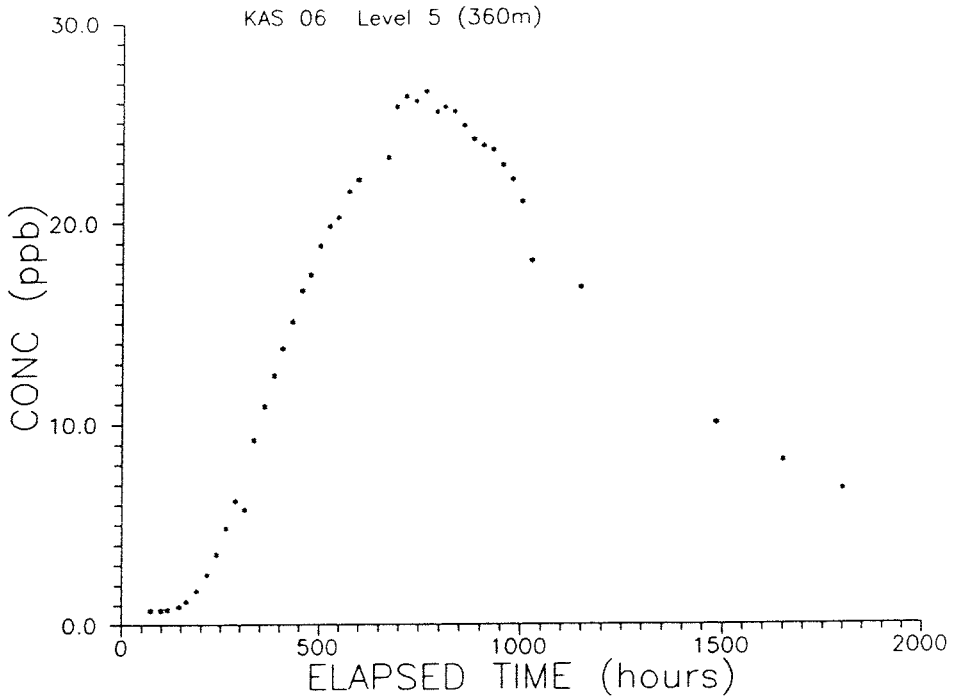

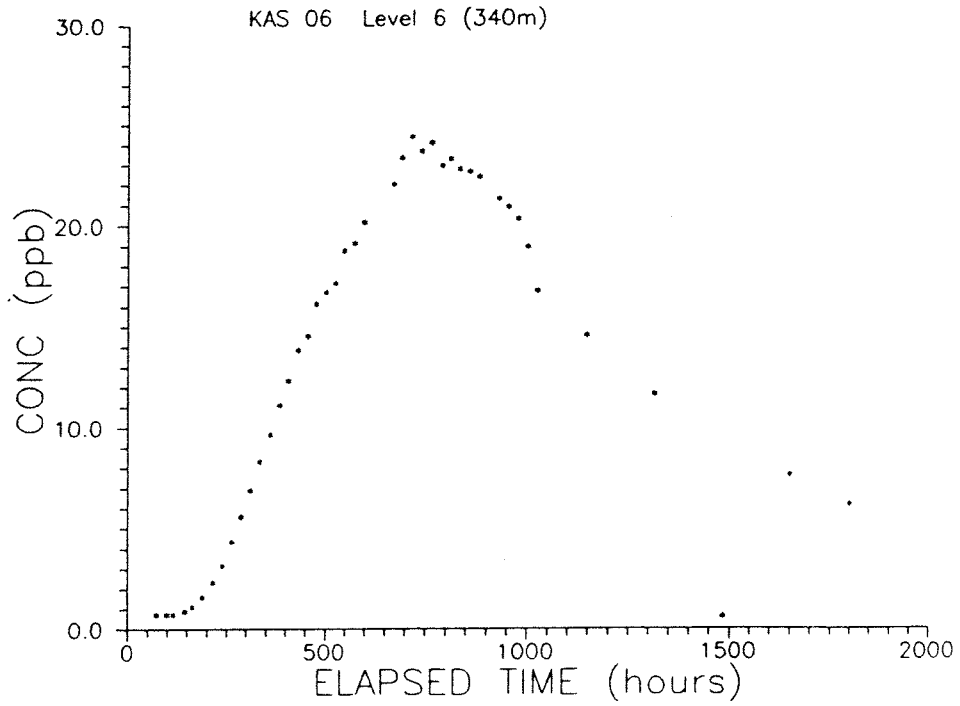

Tracer breakthrough (Uranine) in withdrawal hole, KAS06.

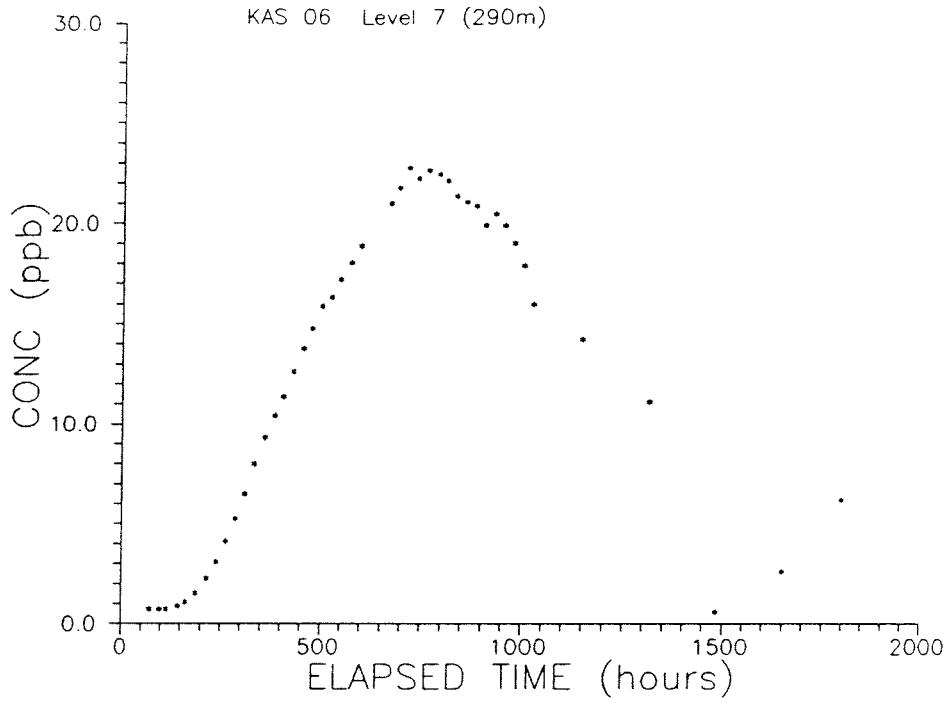

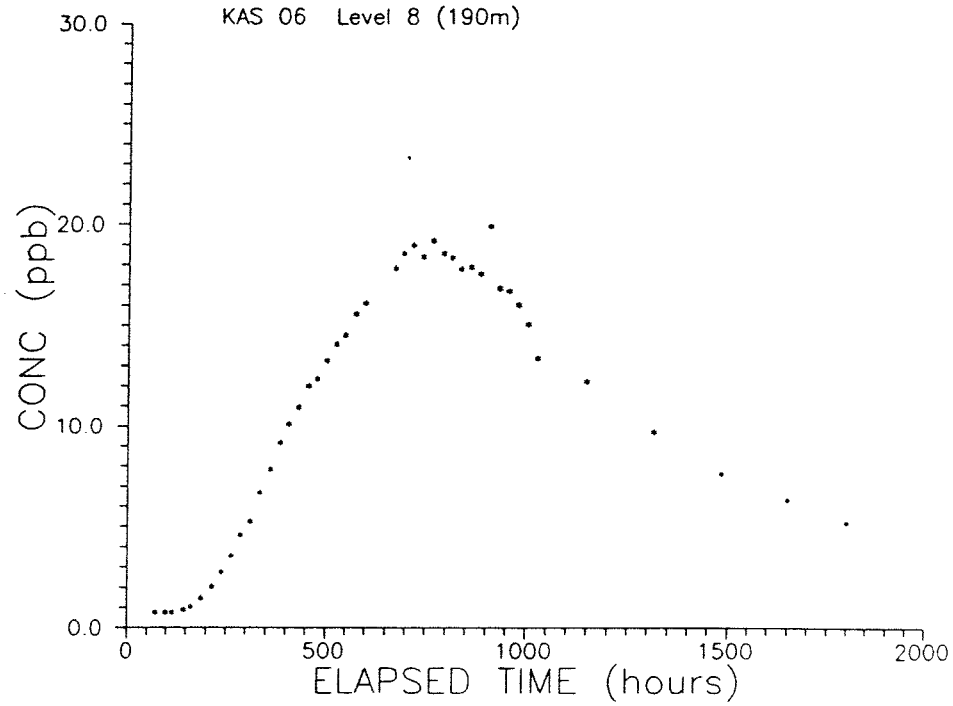

Tracer breakthrough (Uranine) in withdrawal hole, KAS06.

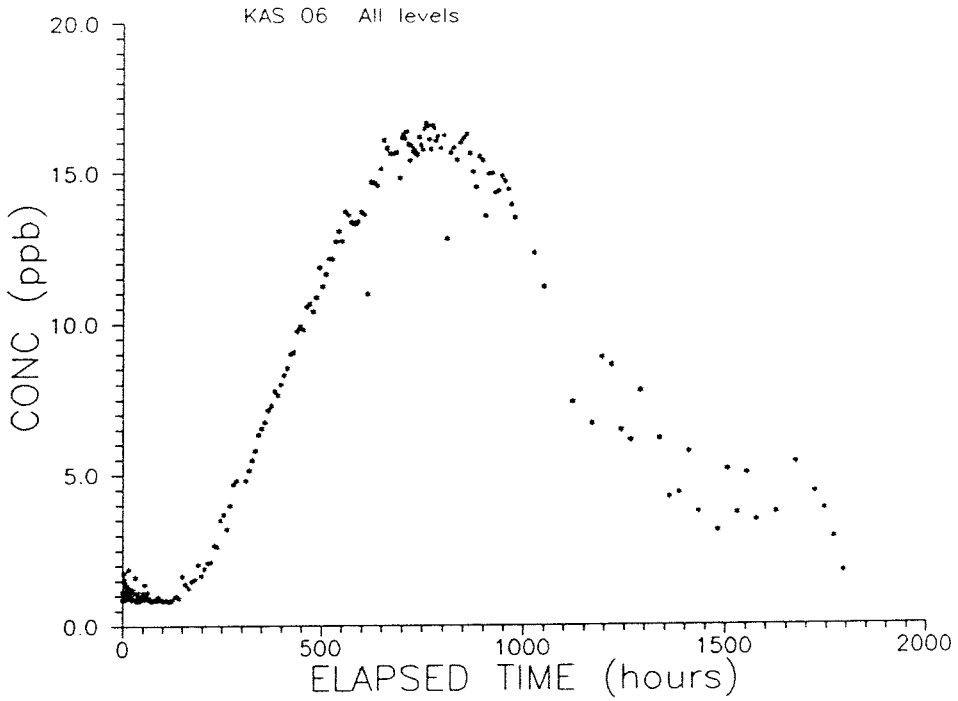

Tracer breakthrough (Uranine) in total discharge, KAS06.

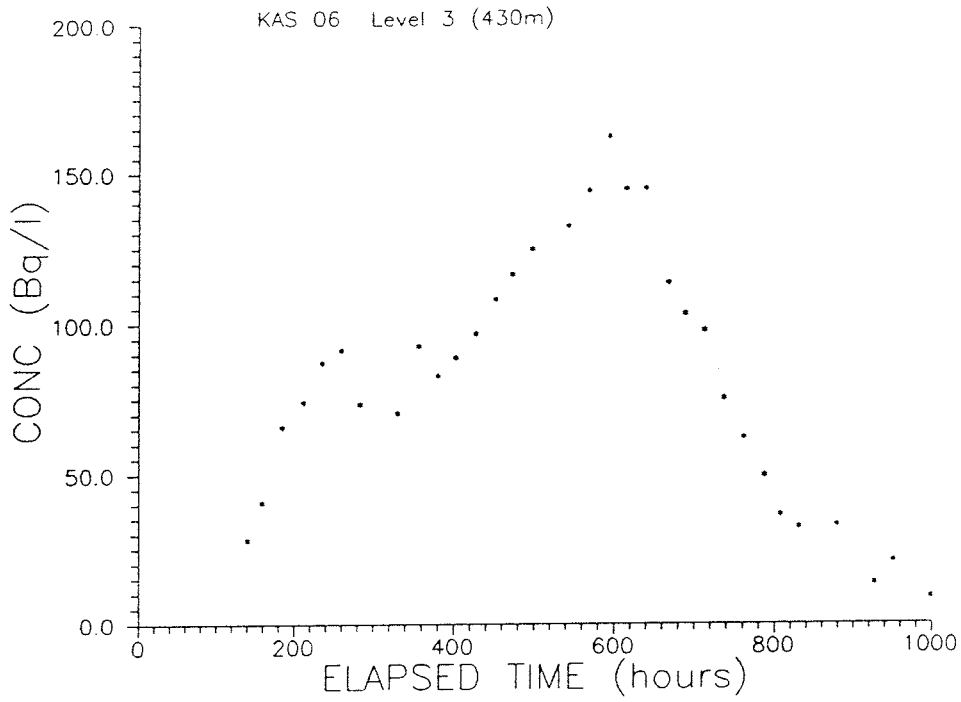

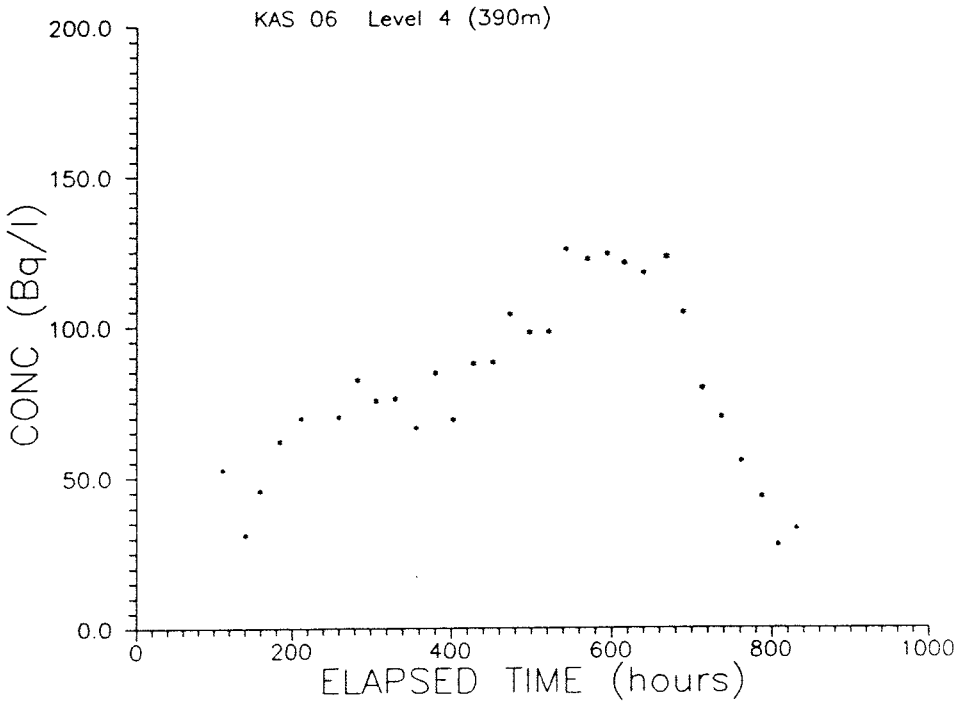

Tracer breakthrough (Rhenium) in withdrawal hole, KAS06.

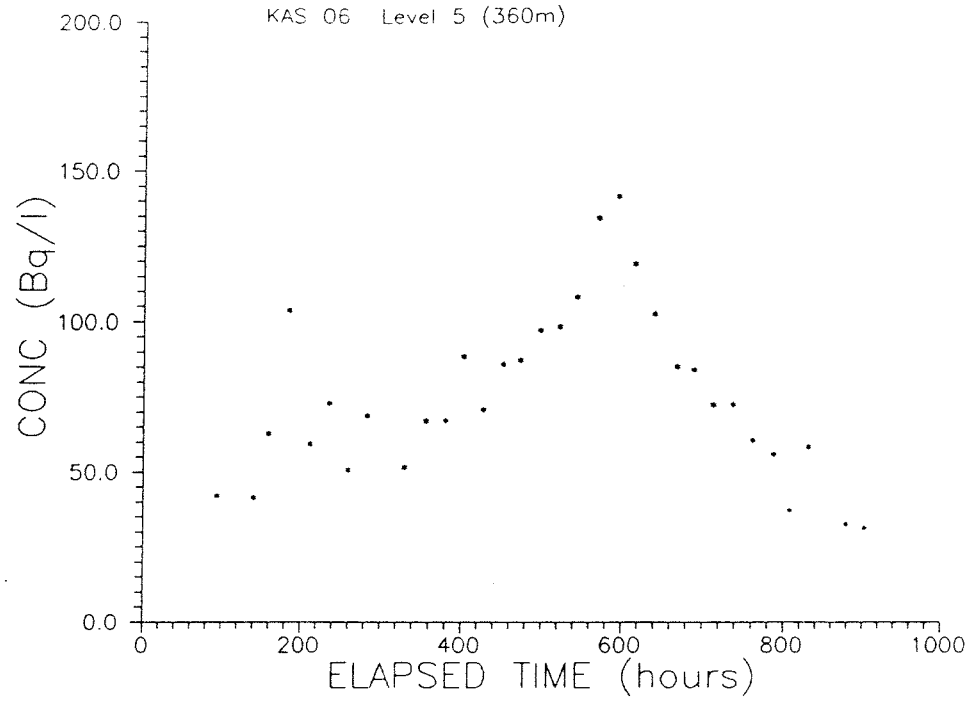

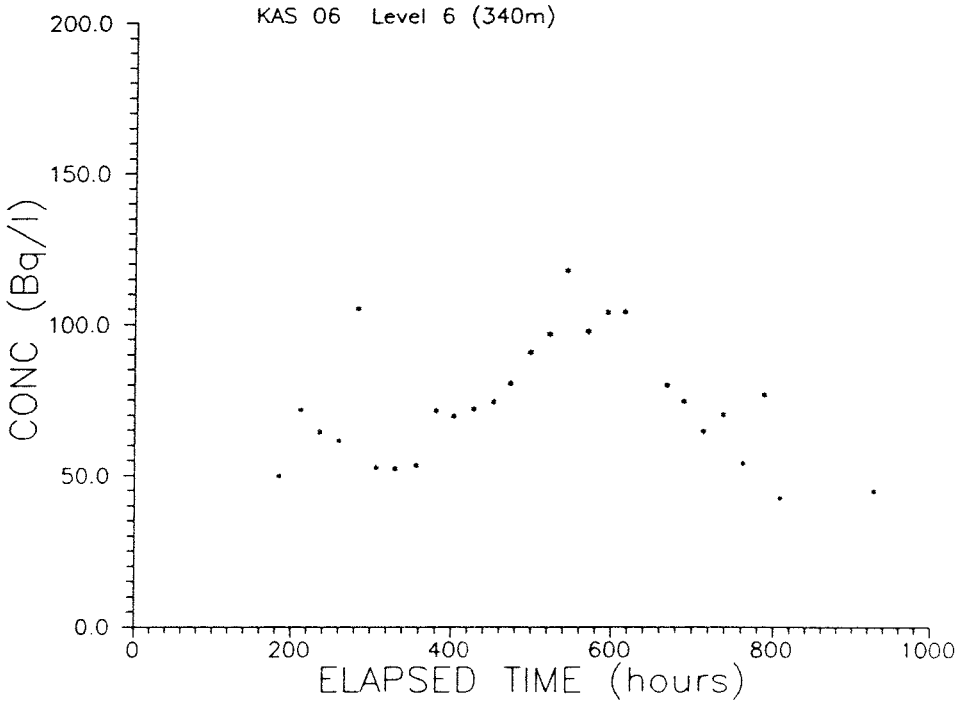

Tracer breakthrough (Rhenium) in withdrawal hole, KAS06.

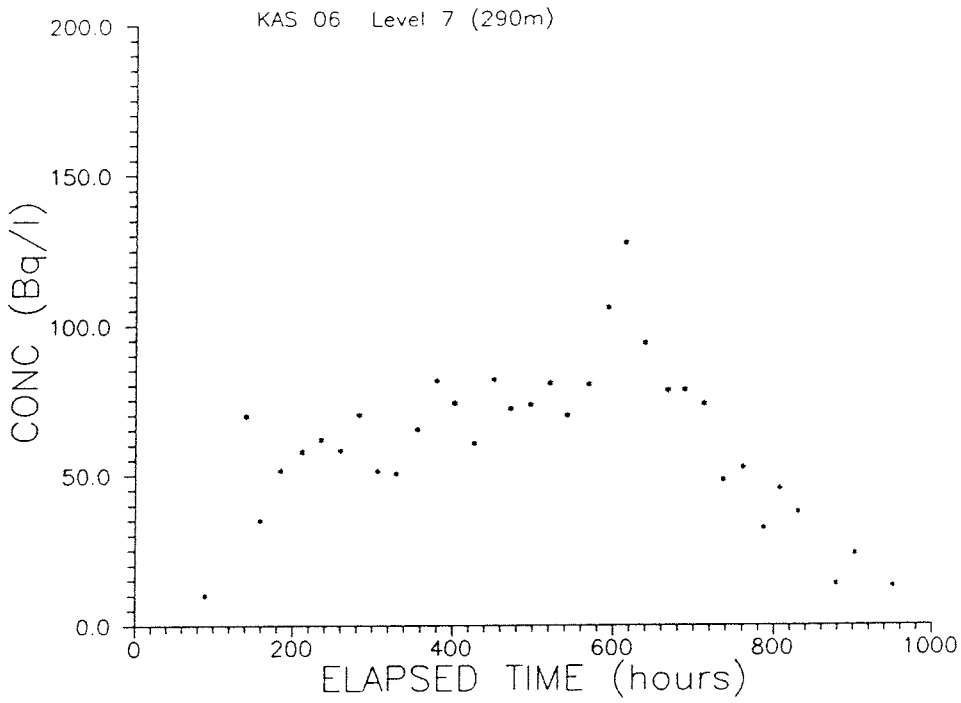

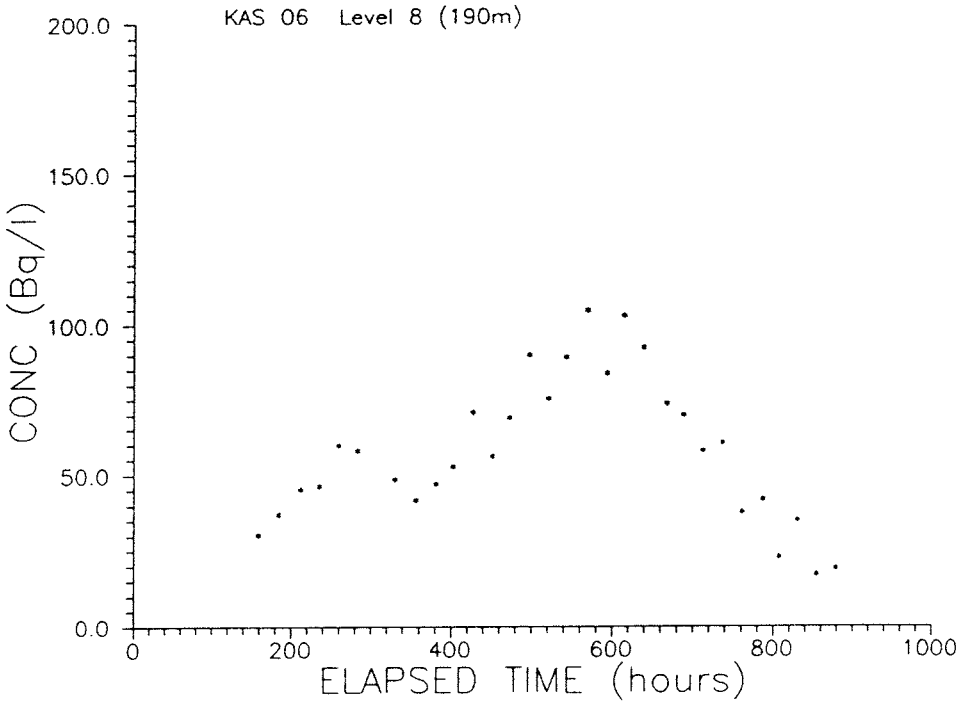

Tracer breakthrough (Rhenium) in withdrawal hole, KAS06.

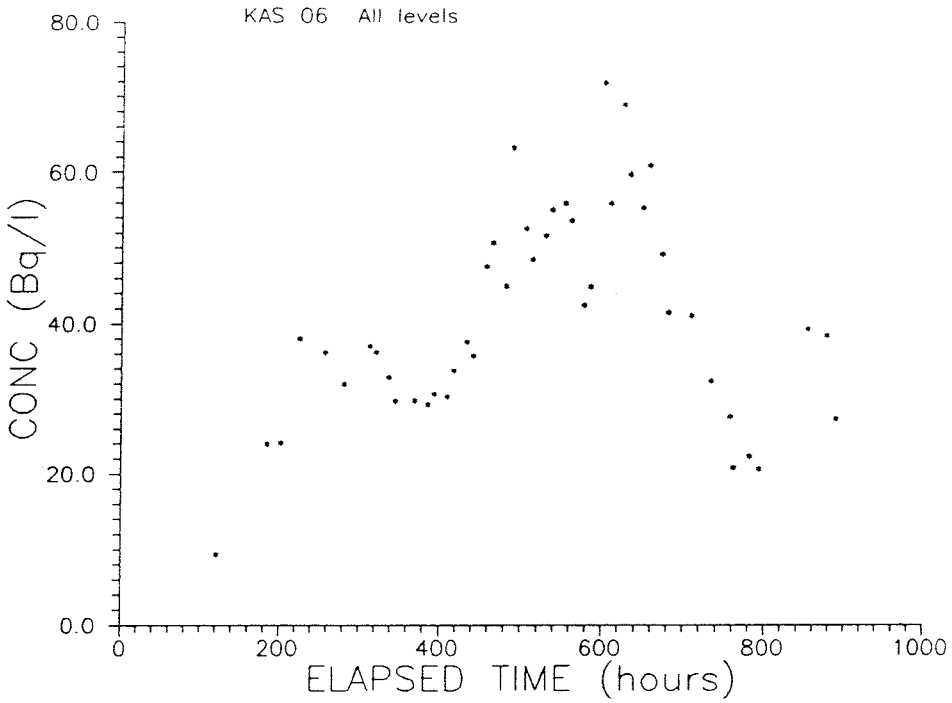

Tracer breakthrough (Rhenium) in total discharge, KAS06.

APPENDIX D

ELECTRIC CONDUCTIVITY AND REDOX POTENTIAL

Supporting measurements during pumptest in discharge water, KAS06

Figure	Page
D– 1: Oxidation–reduction potential	D:1
D– 2: Electrical coductivity	

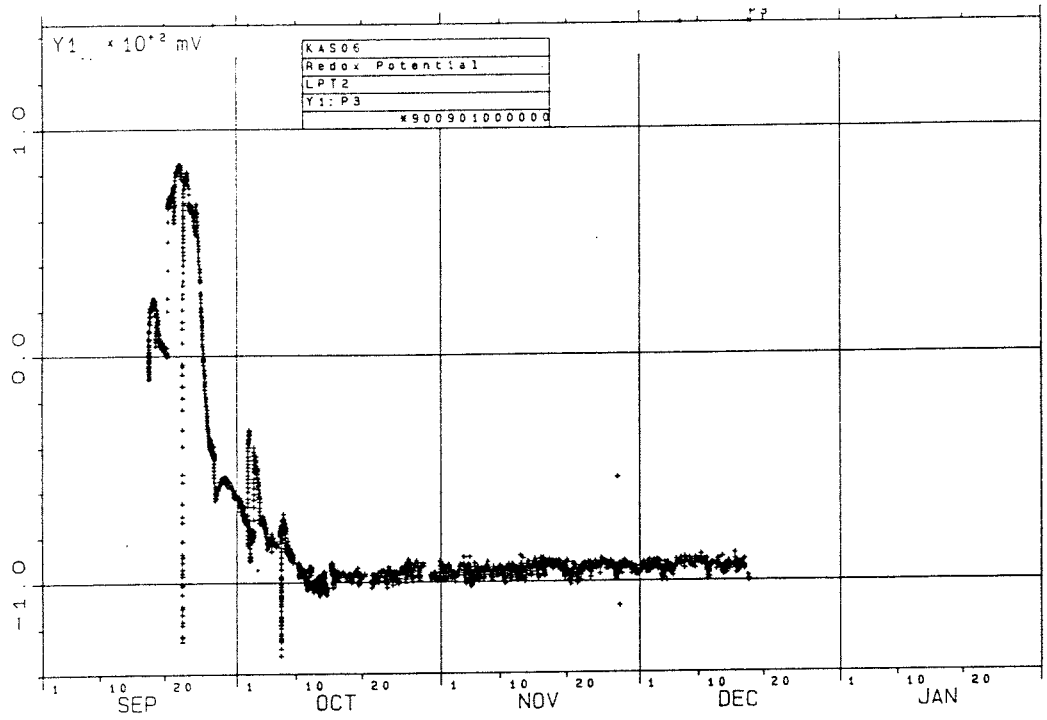

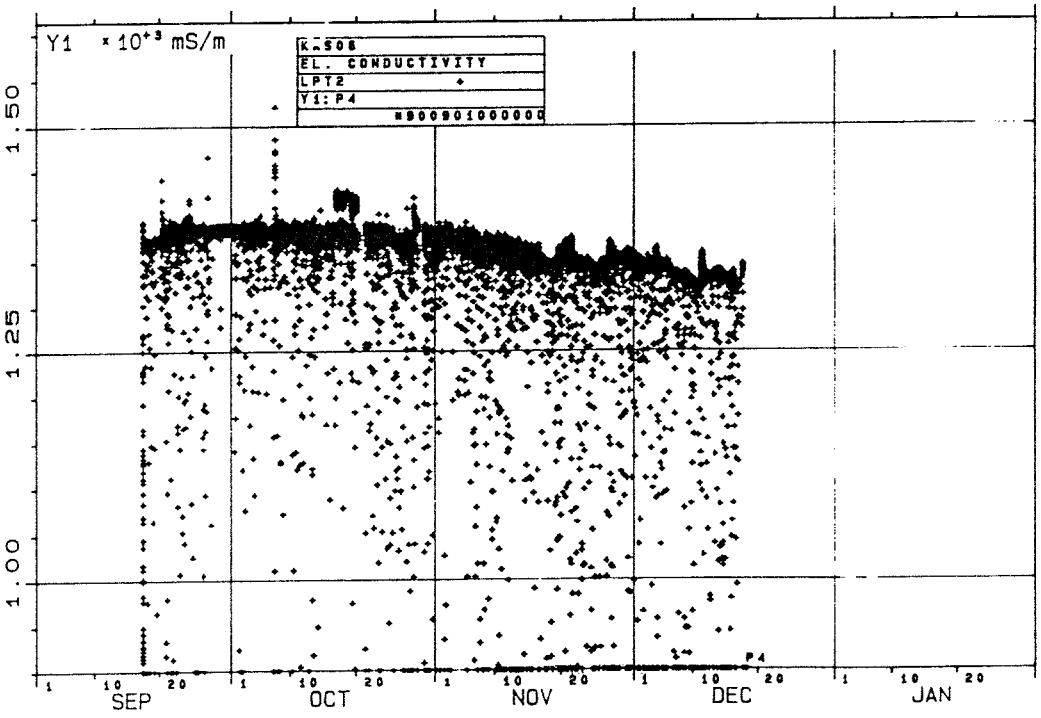

Redox potential and electrical conductivity in discharge water, KAS06.

APPENDIX E

CALCULATED BREAKTHROUGH IN MAJOR CONDUCTORS

Corrected breakthrough curves for Uranine and Rhenium in KAS06

Figure		Page
E- 1: level 3 430m	Rhenium	E:1
E- 2: level 4 390m		
E- 3: level 5 360m		E:2
E- 4: level 6 340m		
E- 5: level 7 290m		E:3
E- 6: level 8 190m		
E- 7: level 3 430m	Uranine	E:4
E- 8: level 4 390m		
E- 9: level 5 360m		E:5
E-10: level 6 340m		
E-11: level 7 290m		E:6
E-12: level 8 190m		
E-13: entire borehole		E:7

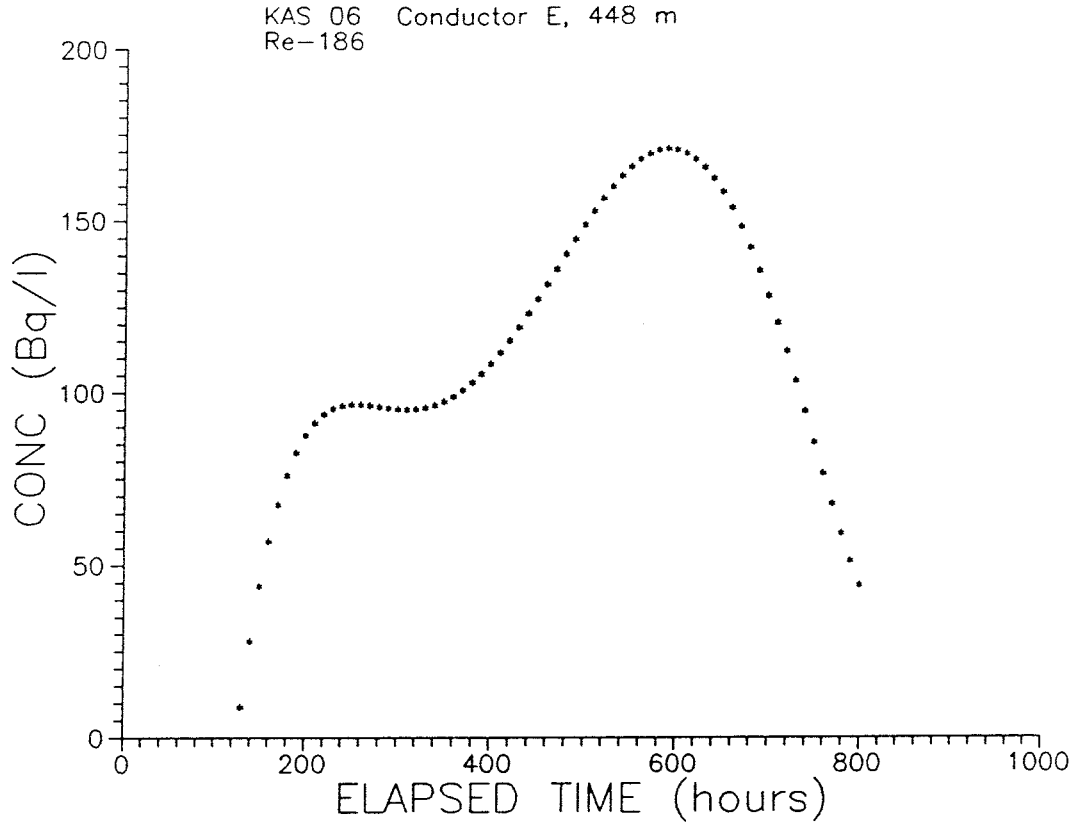
KAS 06 Conductor E, 448 m
Re-186
CONC (Bq/l)
ELAPSED TIME (hours)
0
50
100
150
200
0
200
400
600
800
1000

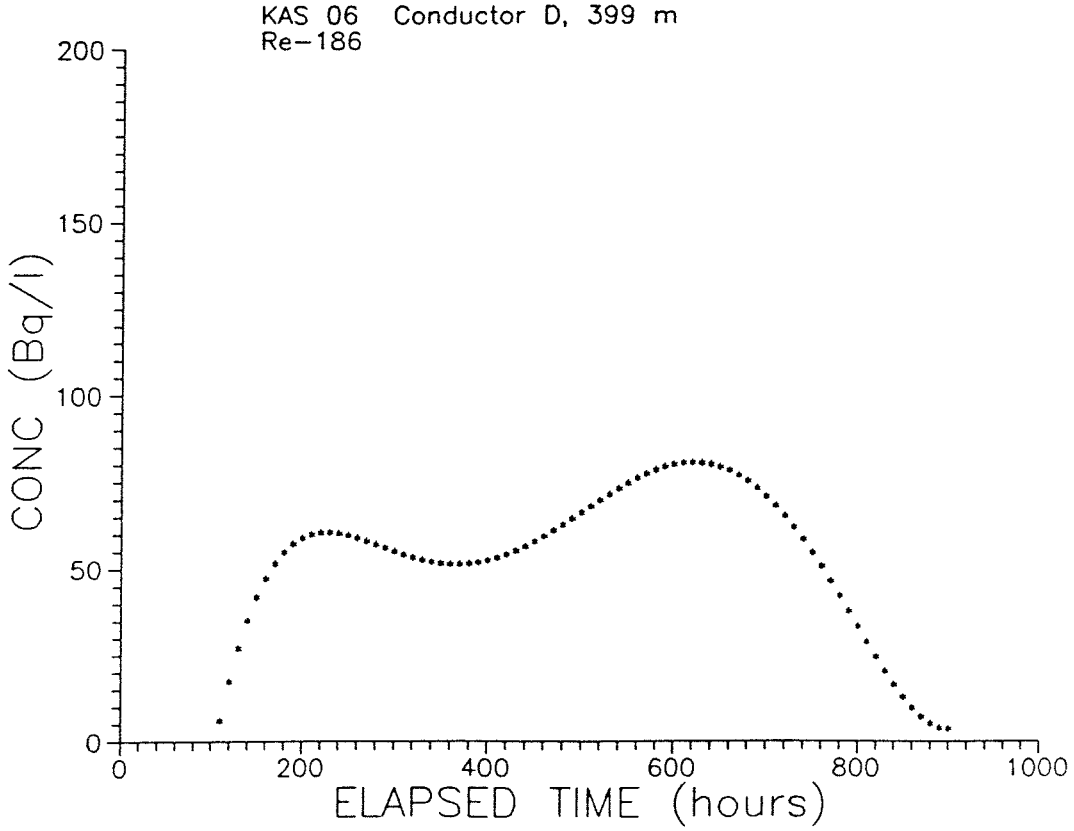
KAS 06 Conductor D, 399 m
Re-186
CONC (Bq/l)
ELAPSED TIME (hours)
0
50
100
150
200
0
200
400
600
800
1000

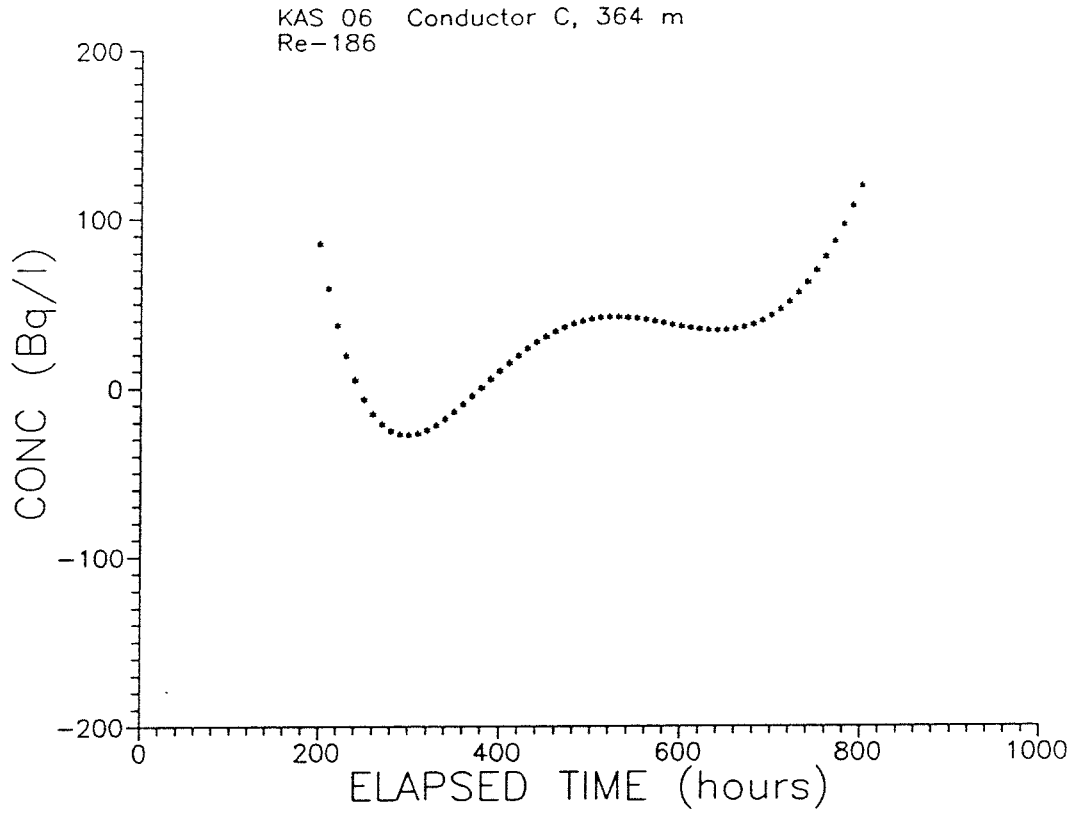
KAS 06 Conductor C, 364 m
Re-186
CONC (Bq/l)
200
100
0
-100
-200
0
200
400
600
800
1000
ELAPSED TIME (hours)

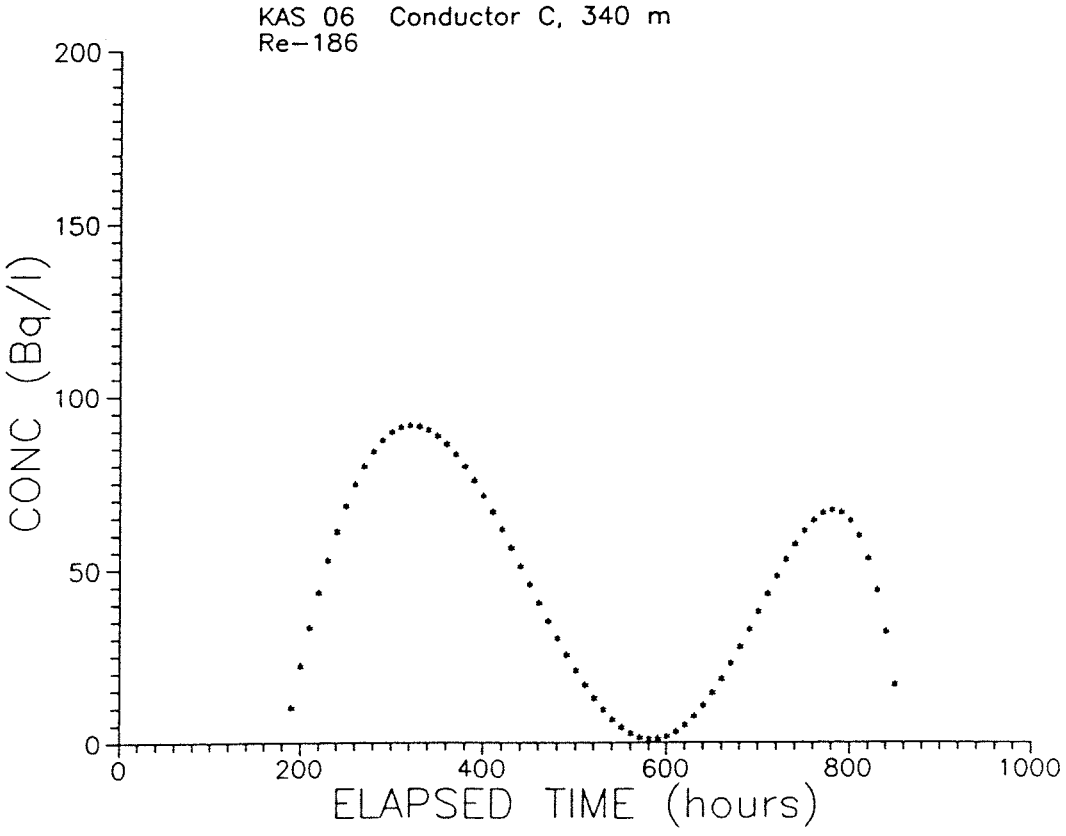
KAS 06 Conductor C, 340 m
Re-186
CONC (Bq/l)
200
150
100
50
0
0
200
400
600
800
1000
ELAPSED TIME (hours)

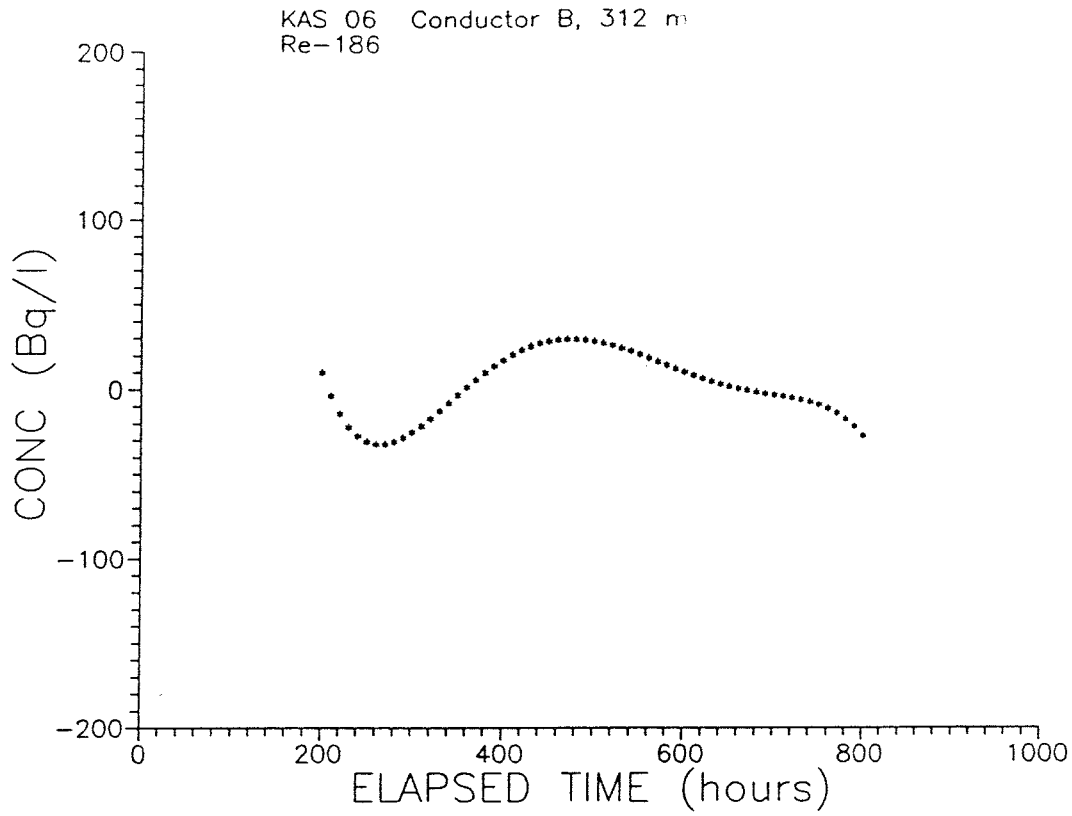
KAS 06 Conductor B, 312 m
Re-186
CONC (Bq/l)
200
100
0
-100
-200
0
200
400
600
800
1000
ELAPSED TIME (hours)

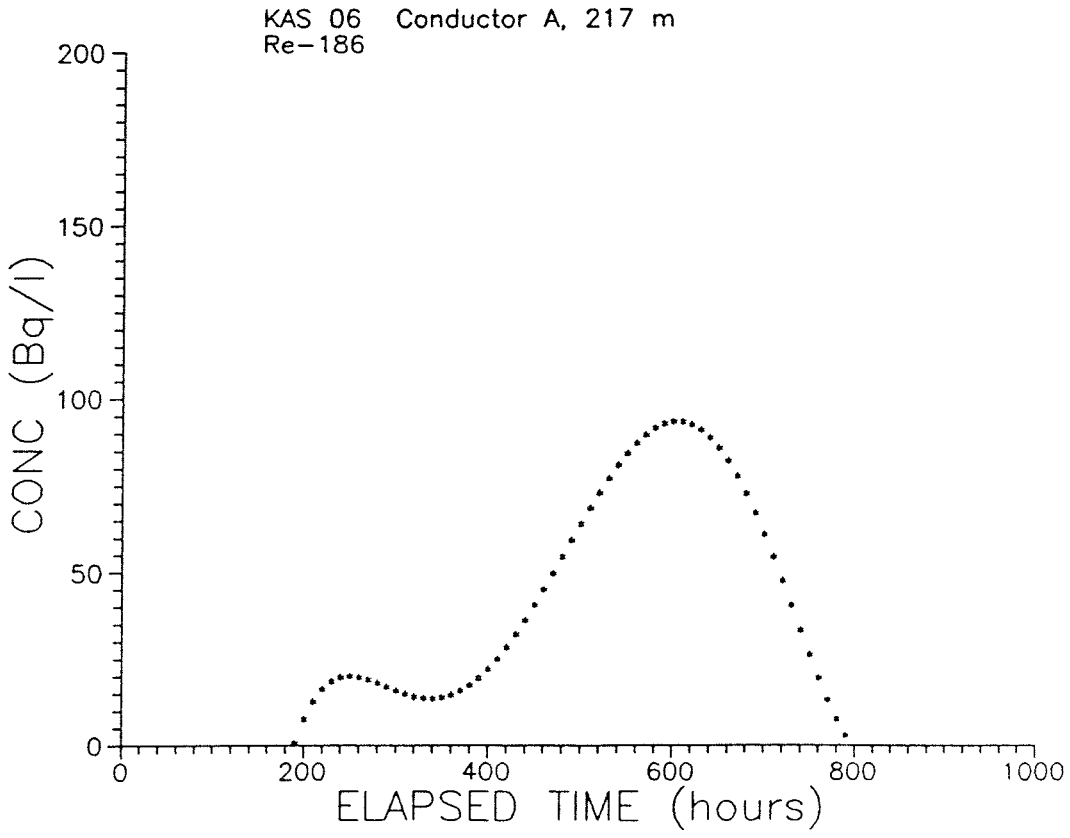
KAS 06 Conductor A, 217 m
Re-186
CONC (Bq/l)
200
150
100
50
0
0
200
400
600
800
1000
ELAPSED TIME (hours)

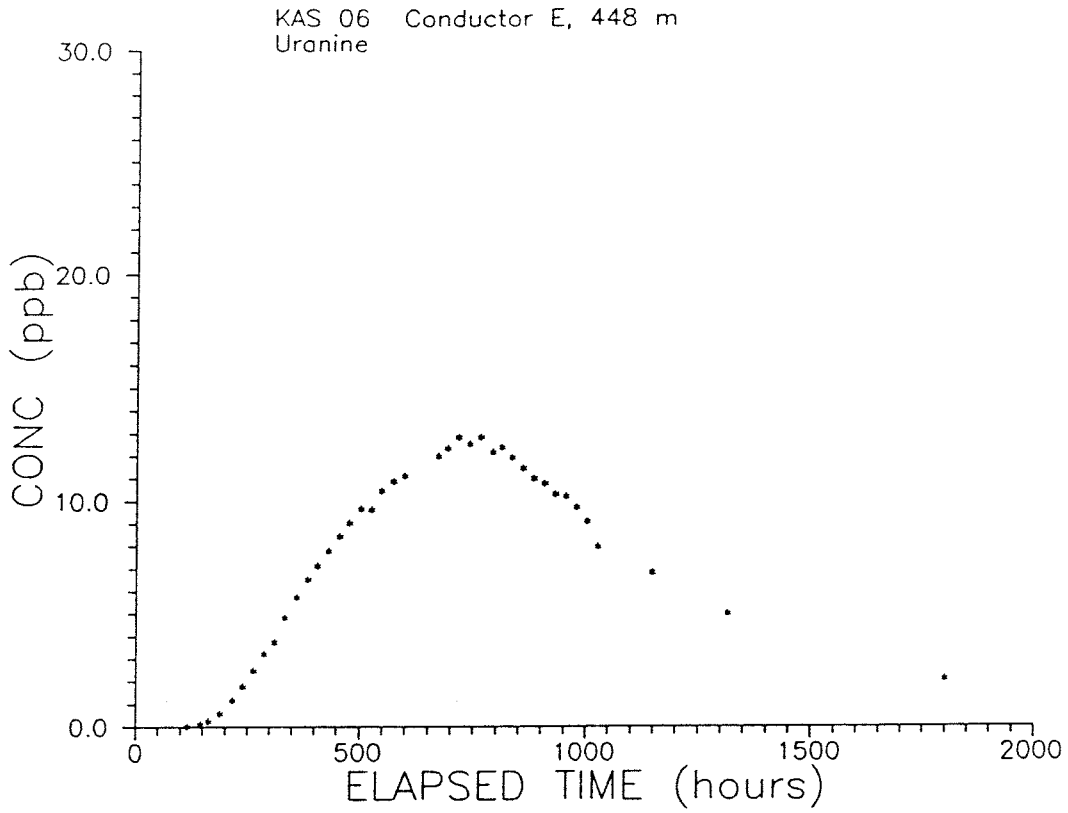
KAS 06 Conductor E, 448 m
Uranine
30.0
20.0
10.0
0.0
CONC (ppb)
0
500
1000
1500
2000
ELAPSED TIME (hours)

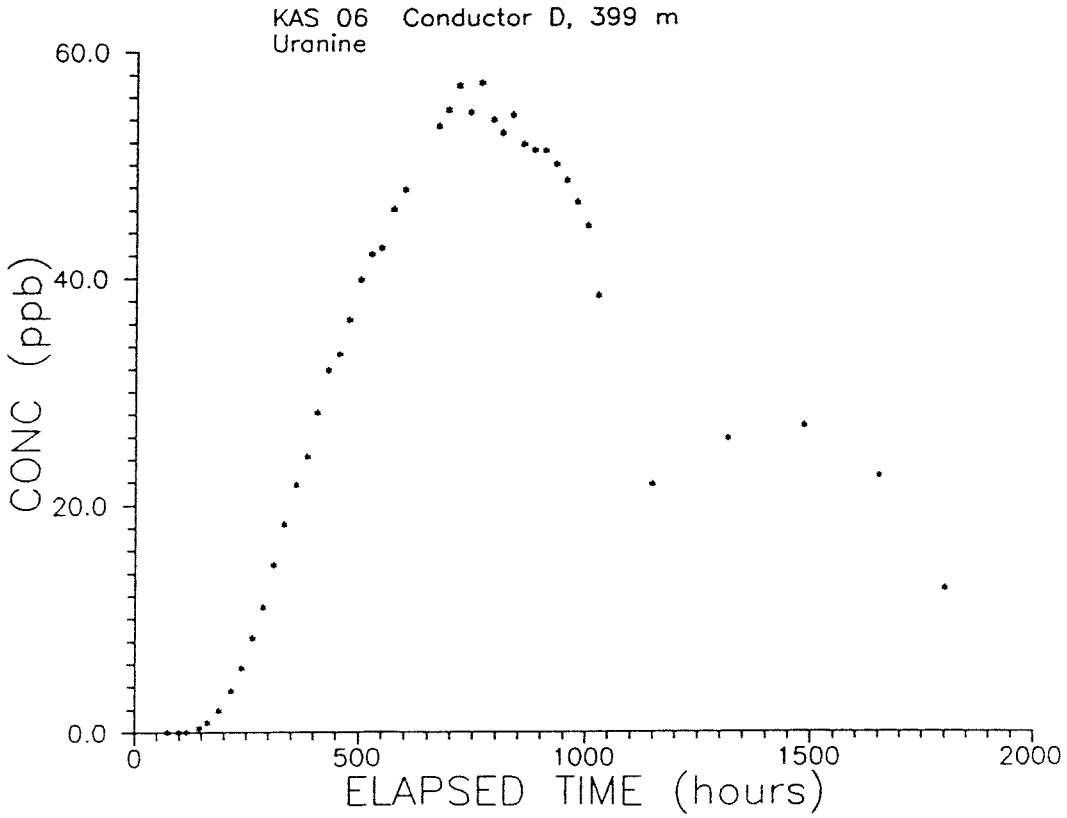
KAS 06 Conductor D, 399 m
Uranine
60.0
40.0
20.0
0.0
CONC (ppb)
0
500
1000
1500
2000
ELAPSED TIME (hours)

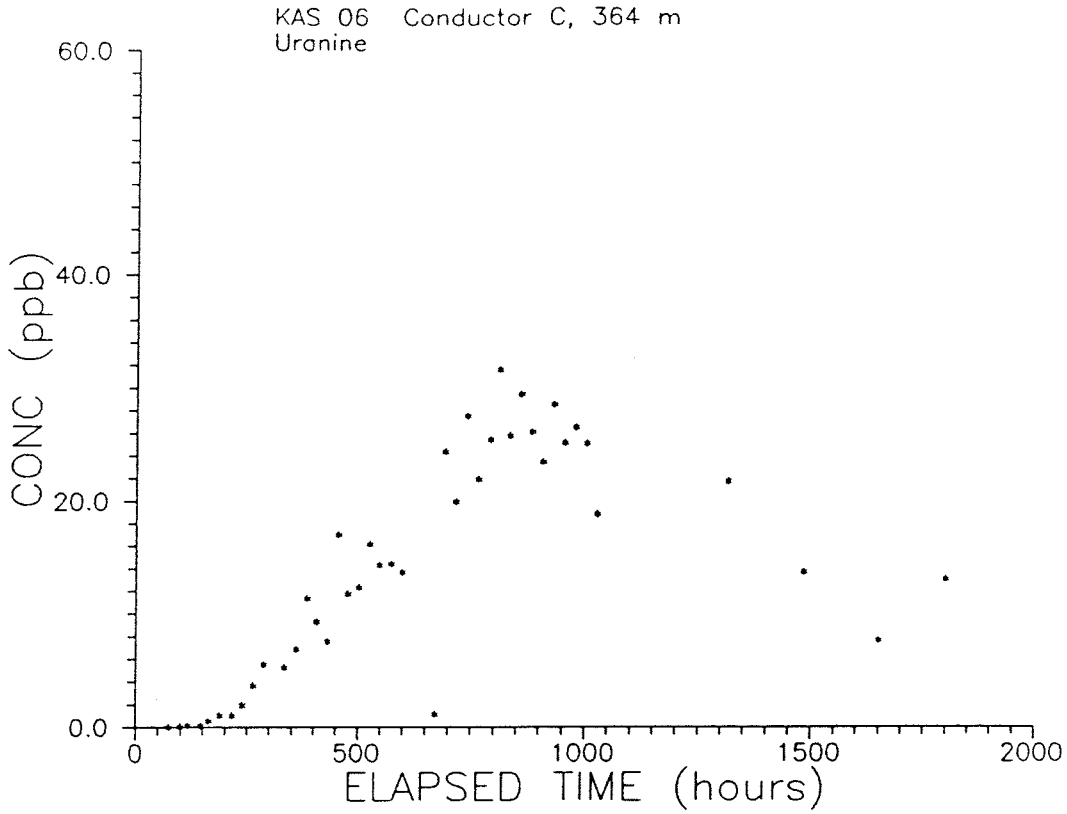
KAS 06 Conductor C, 364 m
Uranine
60.0
40.0
20.0
0.0
CONC (ppb)
0
500
1000
1500
2000
ELAPSED TIME (hours)

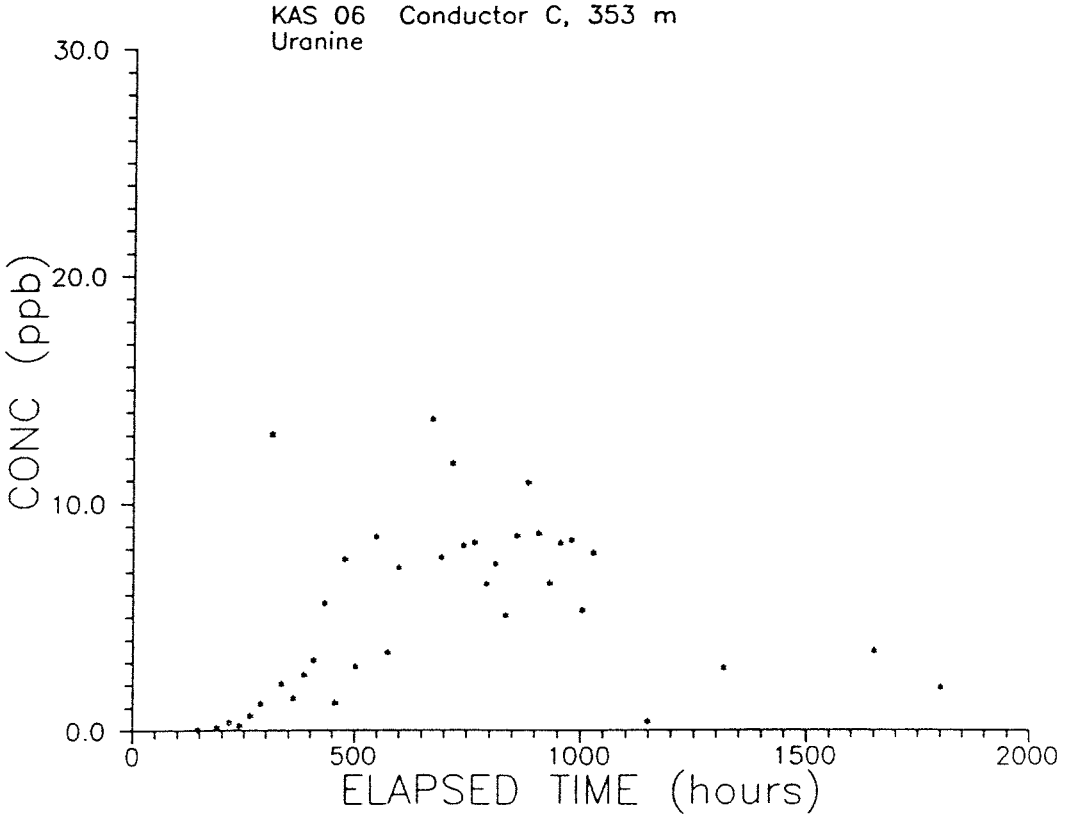
KAS 06 Conductor C, 353 m
Uranine
30.0
20.0
10.0
0.0
CONC (ppb)
0
500
1000
1500
2000
ELAPSED TIME (hours)

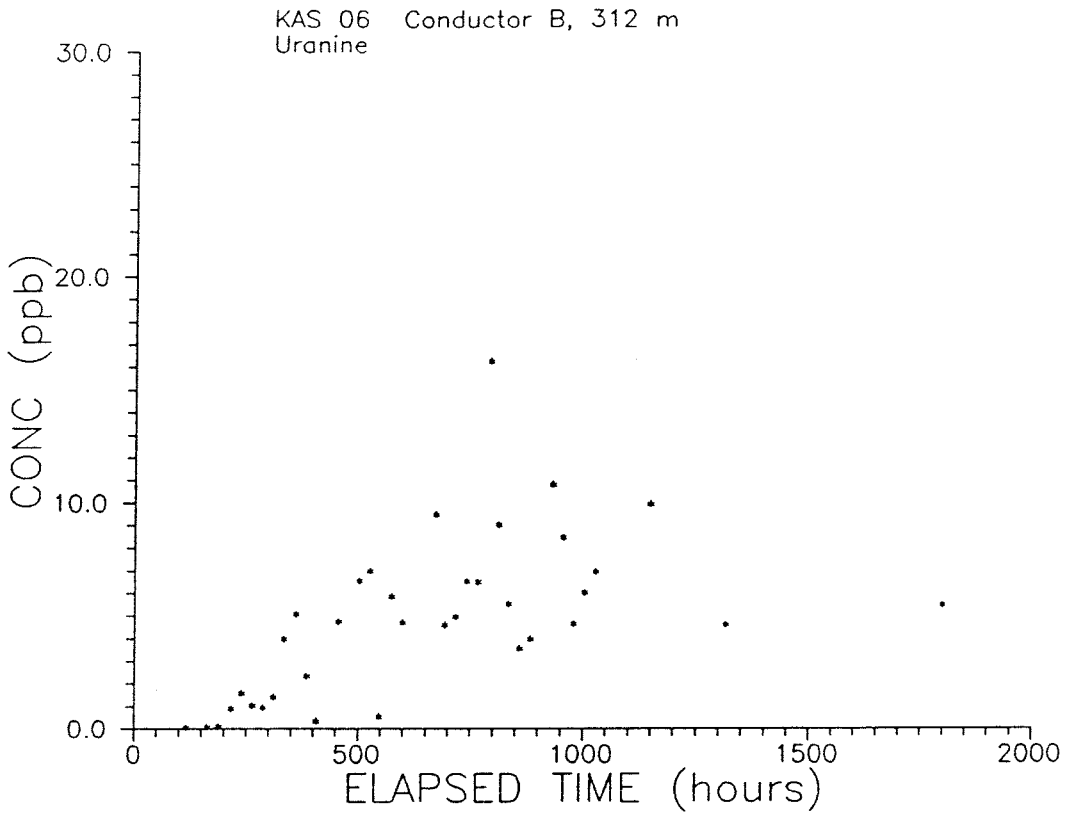
KAS 06 Conductor B, 312 m
Uranine
30.0
20.0
10.0
0.0
CONC (ppb)
0
500
1000
1500
2000
ELAPSED TIME (hours)

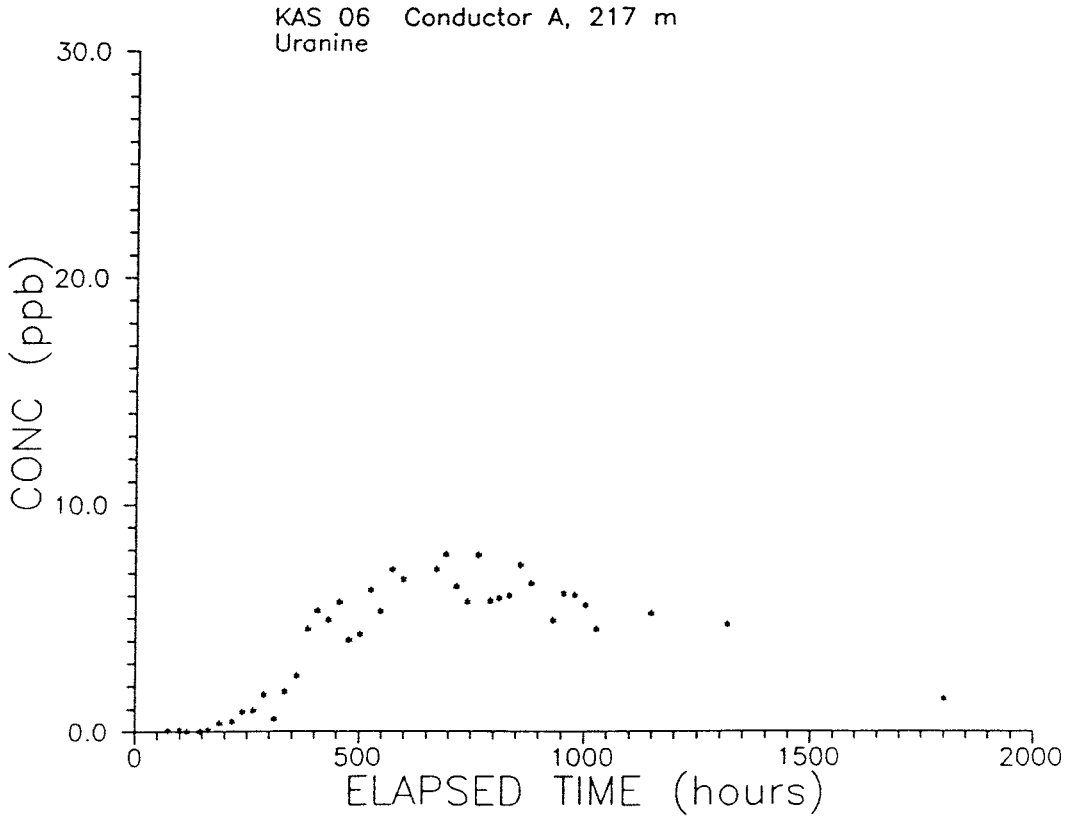
KAS 06 Conductor A, 217 m
Uranine
30.0
20.0
10.0
0.0
CONC (ppb)
0
500
1000
1500
2000
ELAPSED TIME (hours)

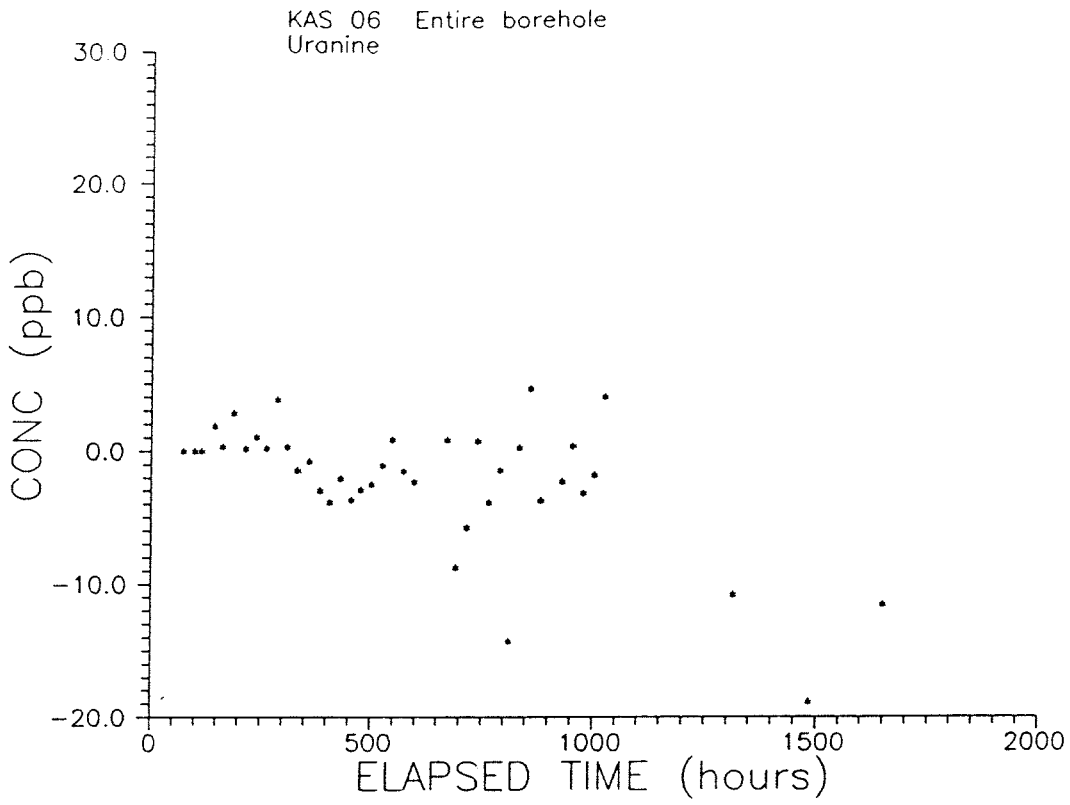
KAS 06 Entire borehole
Uranine
30.0
20.0
10.0
0.0
-10.0
-20.0
CONC (ppb)
0
500
1000
1500
2000
ELAPSED TIME (hours)

APPENDIX F

1-D MODELLING

1-D Modelling of breakthrouth in KAS06

Figure		Page
F- 1: Total discharge, one flow path.	Uranine	F:1
F- 2: Total discharge, two flow paths		
F- 3: level 8 190m, one flow path		F:2
F- 4: level 8 190m, two flow paths		
F- 5: level 5 360m, one flow path		F:3
F- 6: level 5 360m, two flow paths		
F- 7: level 4 390m, one flow path		F:4
F- 8: level 4 390m, two flow paths		
F- 9: level 3 430m, one flow path		F:5
F-10: level 3 430m, two flow paths		
F-11: level 5 360m, two injection points		F:6
F-12: level 4 390m, two injection points		
F-13: Total discharge, one flow path.	Rhenium	F:7
F-14: Total discharge, two flow paths		
F-15: level 8 190m, one flow path		F:8
F-16: level 8 190m, two flow paths		
F-17: level 4 390m, one flow path		F:9
F-18: level 4 390m, two flow paths		
F-19: level 3 430m, one flow path		F:10
F-20: level 3 430m, two flow paths		

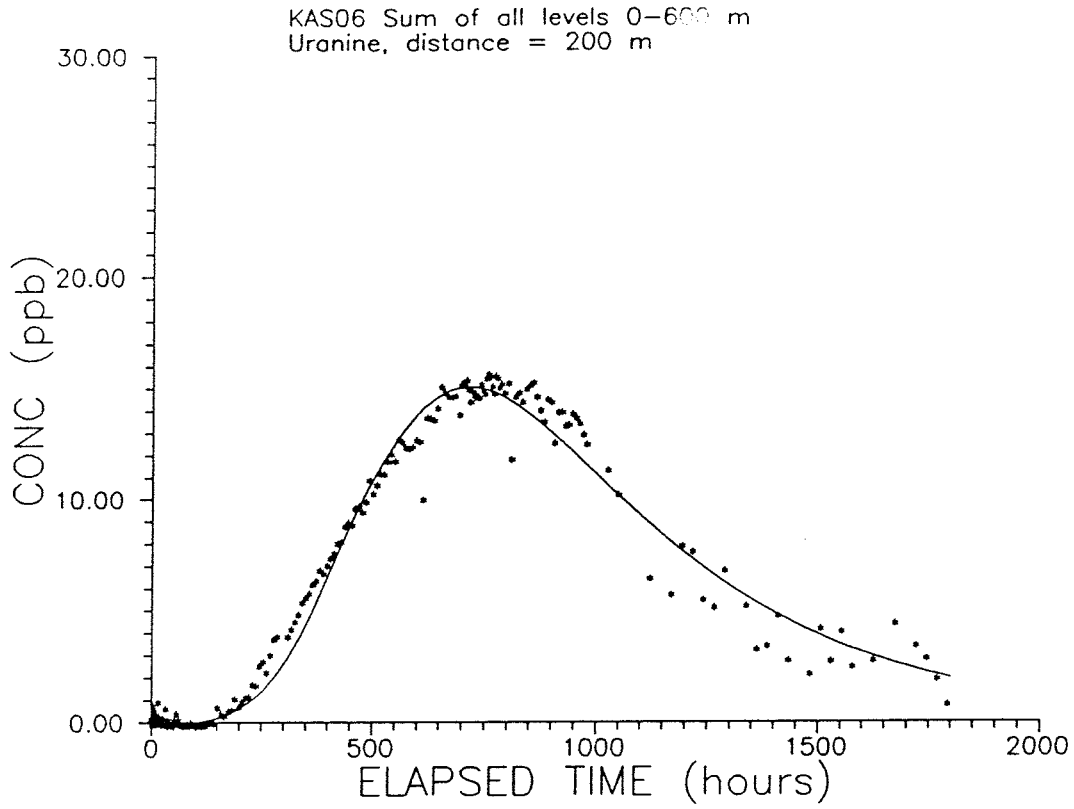
KAS06 Sum of all levels 0–600 m
Uranine, distance = 200 m
30.00
20.00
10.00
0.00
CONC (ppb)
0
500
1000
1500
2000
ELAPSED TIME (hours)

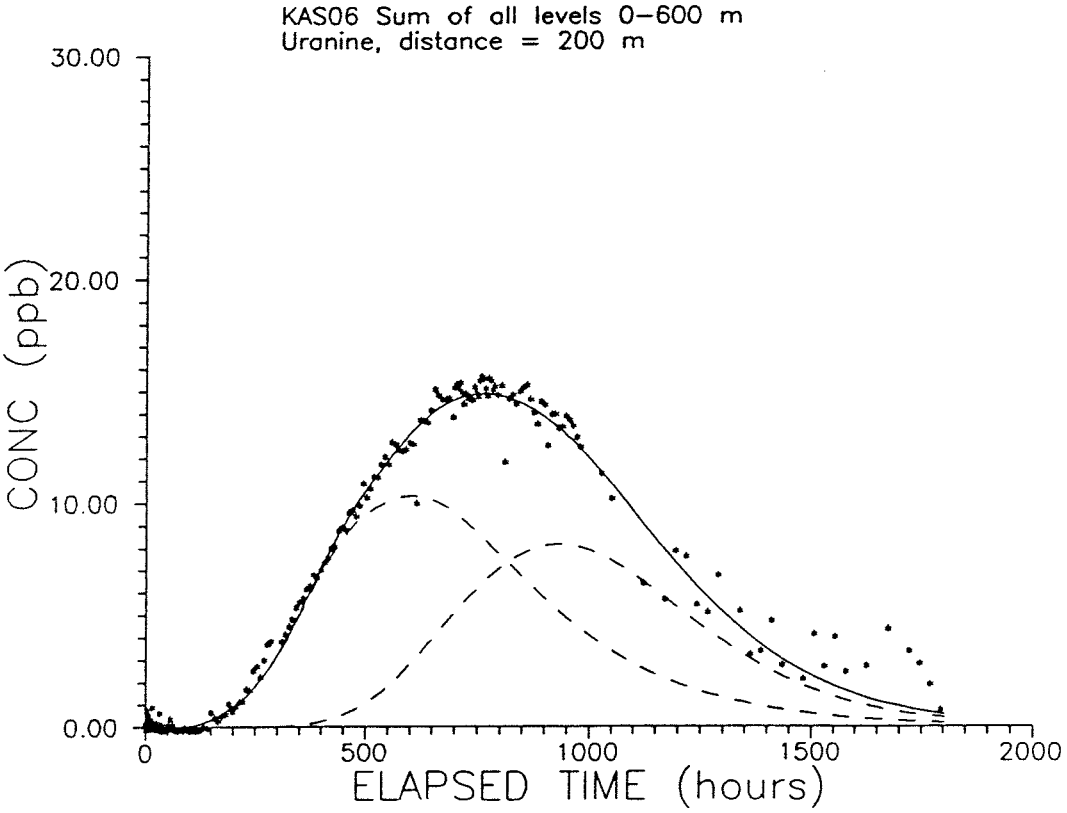
KAS06 Sum of all levels 0–600 m
Uranine, distance = 200 m
30.00
20.00
10.00
0.00
CONC (ppb)
0
500
1000
1500
2000
ELAPSED TIME (hours)

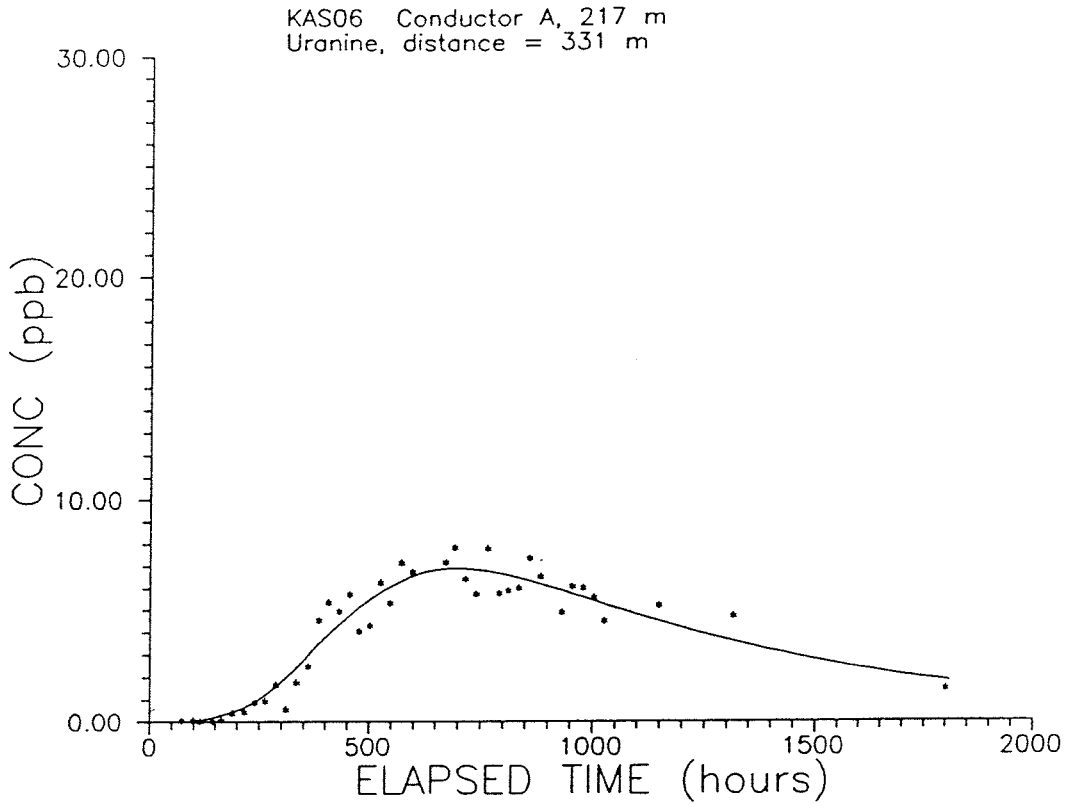
KAS06 Conductor A, 217 m
Uranine, distance = 331 m
30.00
20.00
10.00
0.00
CONC (ppb)
0
500
1000
1500
2000
ELAPSED TIME (hours)

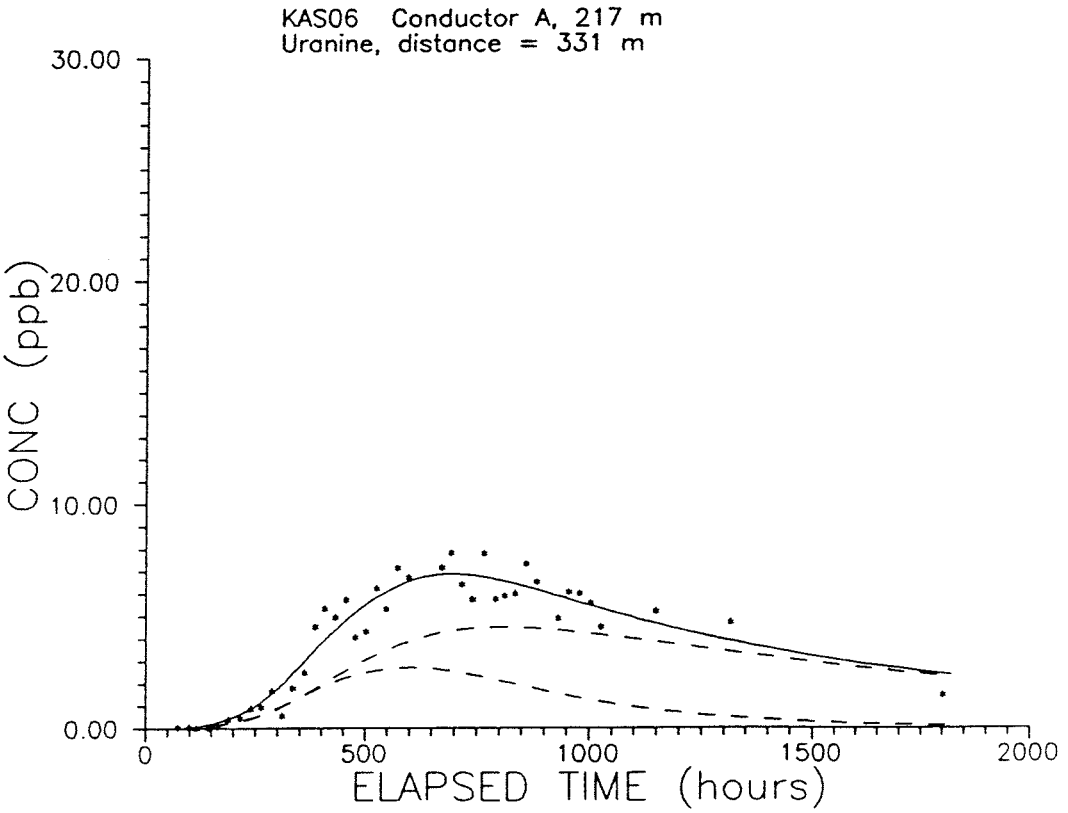
KAS06 Conductor A, 217 m
Uranine, distance = 331 m
30.00
20.00
10.00
0.00
CONC (ppb)
0
500
1000
1500
2000
ELAPSED TIME (hours)

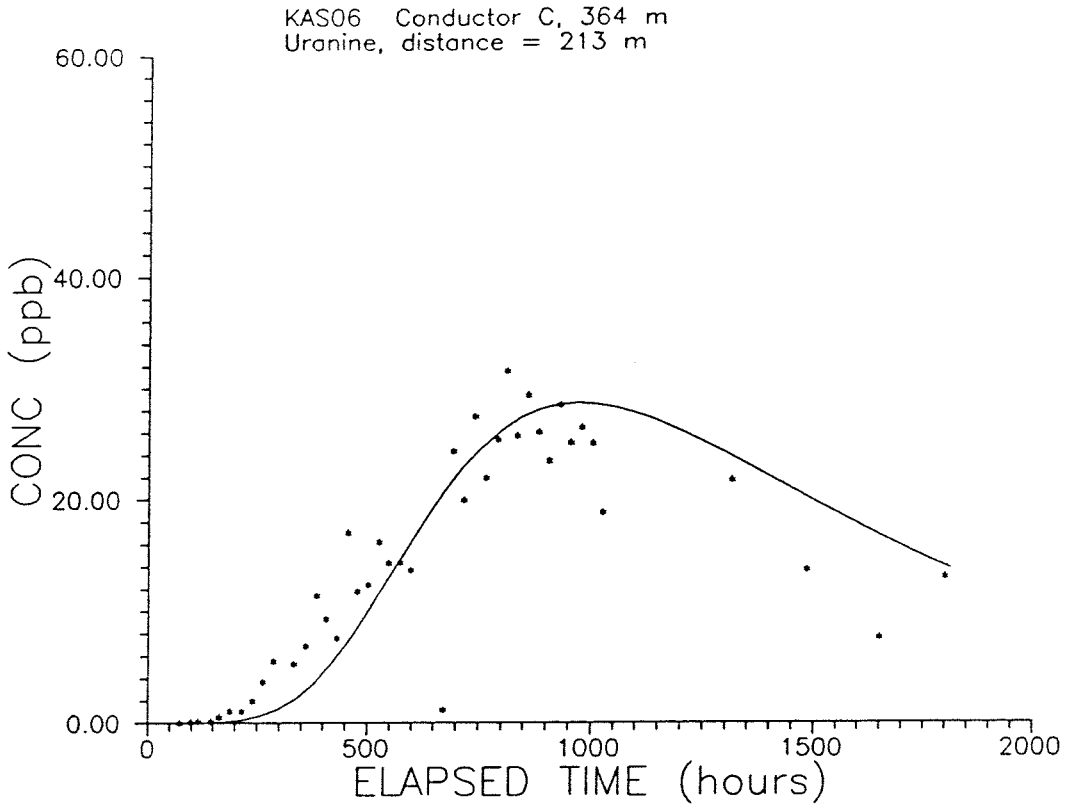
KAS06 Conductor C, 364 m
Uranine, distance = 213 m
60.00
40.00
20.00
0.00
CONC (ppb)
0
500
1000
1500
2000
ELAPSED TIME (hours)

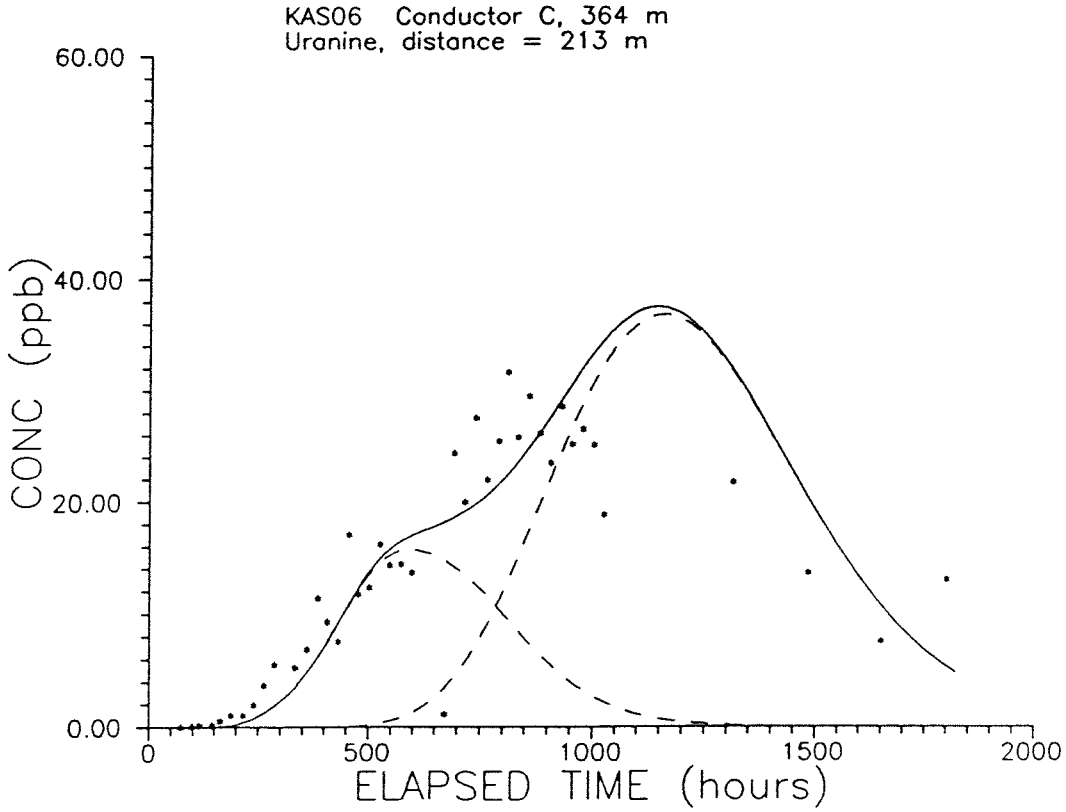
KAS06 Conductor C, 364 m
Uranine, distance = 213 m
60.00
40.00
20.00
0.00
CONC (ppb)
0
500
1000
1500
2000
ELAPSED TIME (hours)

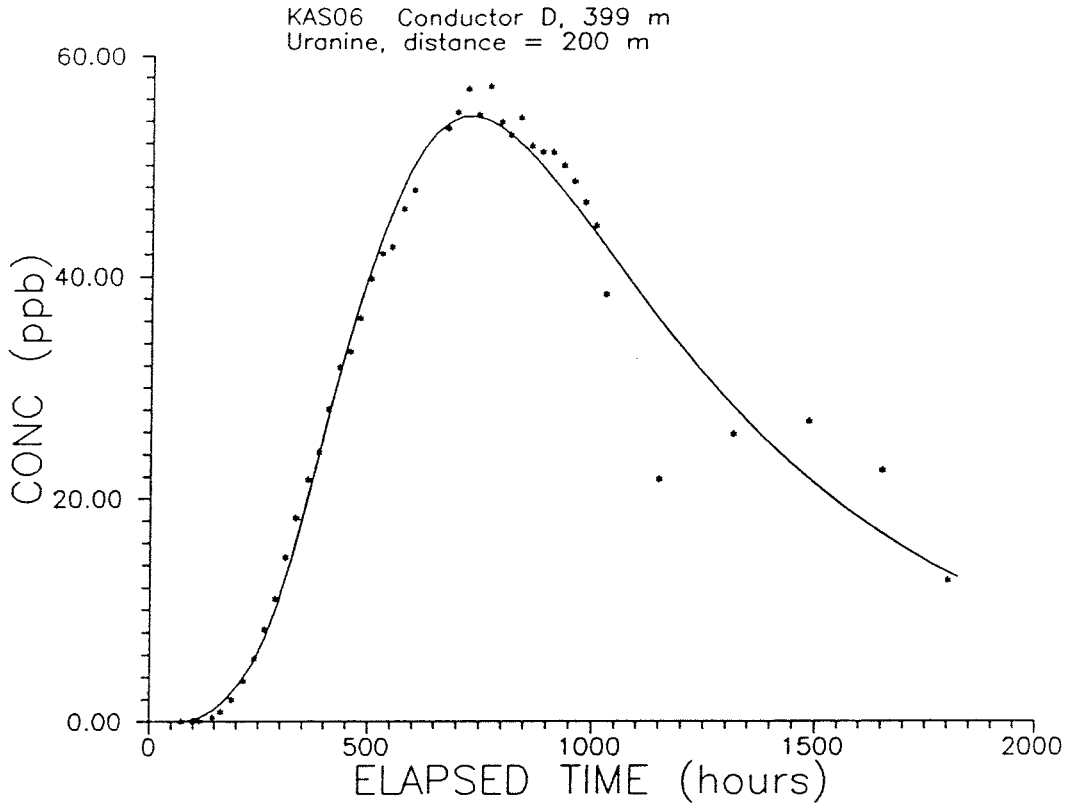
KAS06 Conductor D, 399 m
Uranine, distance = 200 m
60.00
40.00
20.00
0.00
CONC (ppb)
0
500
1000
1500
2000
ELAPSED TIME (hours)

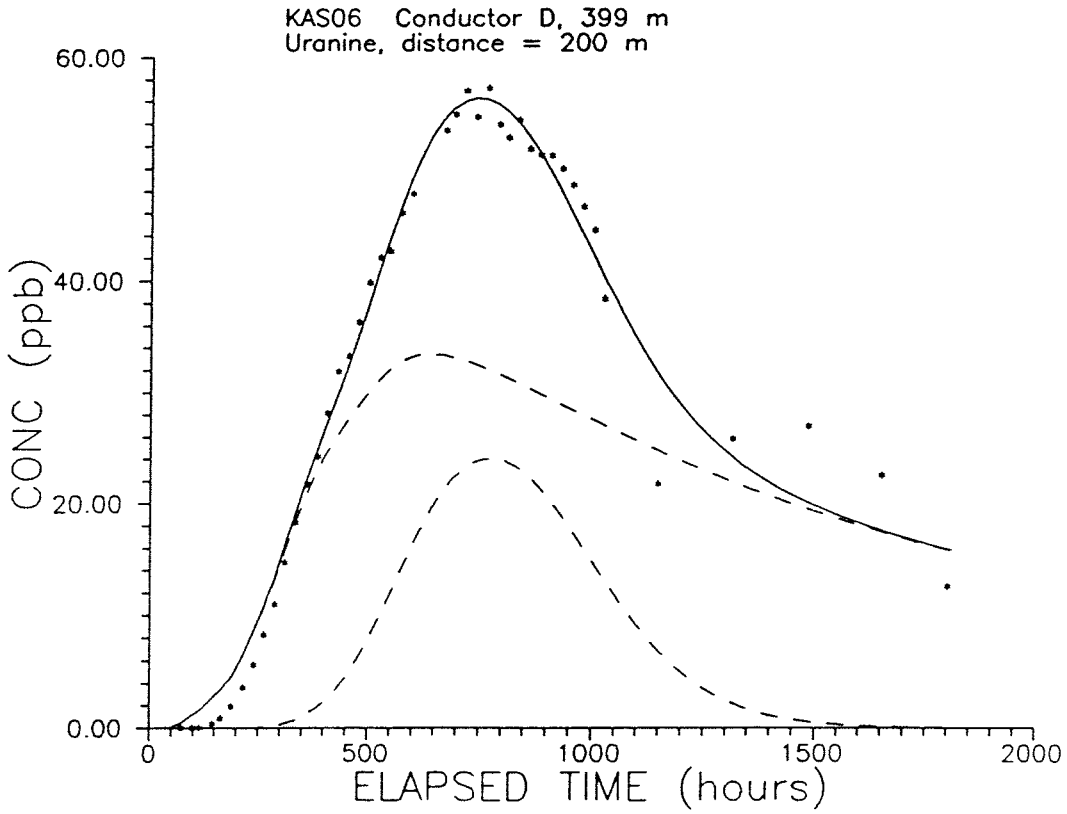
KAS06 Conductor D, 399 m
Uranine, distance = 200 m
60.00
40.00
20.00
0.00
CONC (ppb)
0
500
1000
1500
2000
ELAPSED TIME (hours)

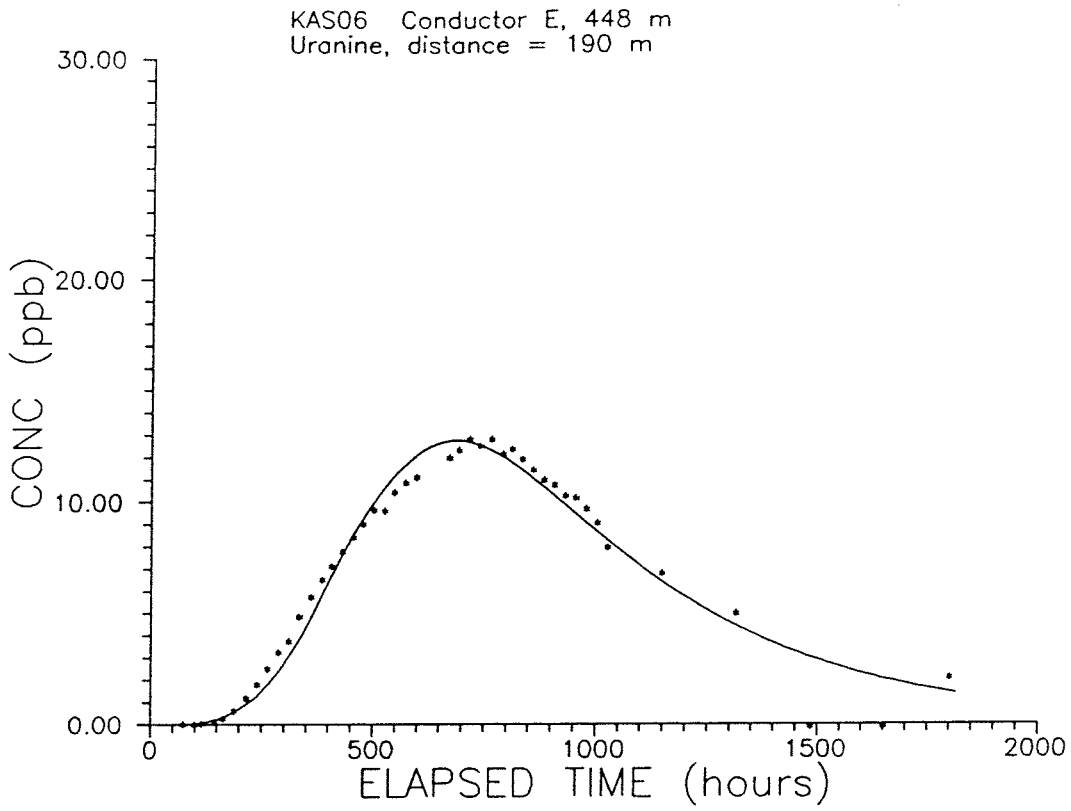
KAS06 Conductor E, 448 m
Uranine, distance = 190 m
30.00
20.00
10.00
0.00
CONC (ppb)
0
500
1000
1500
2000
ELAPSED TIME (hours)

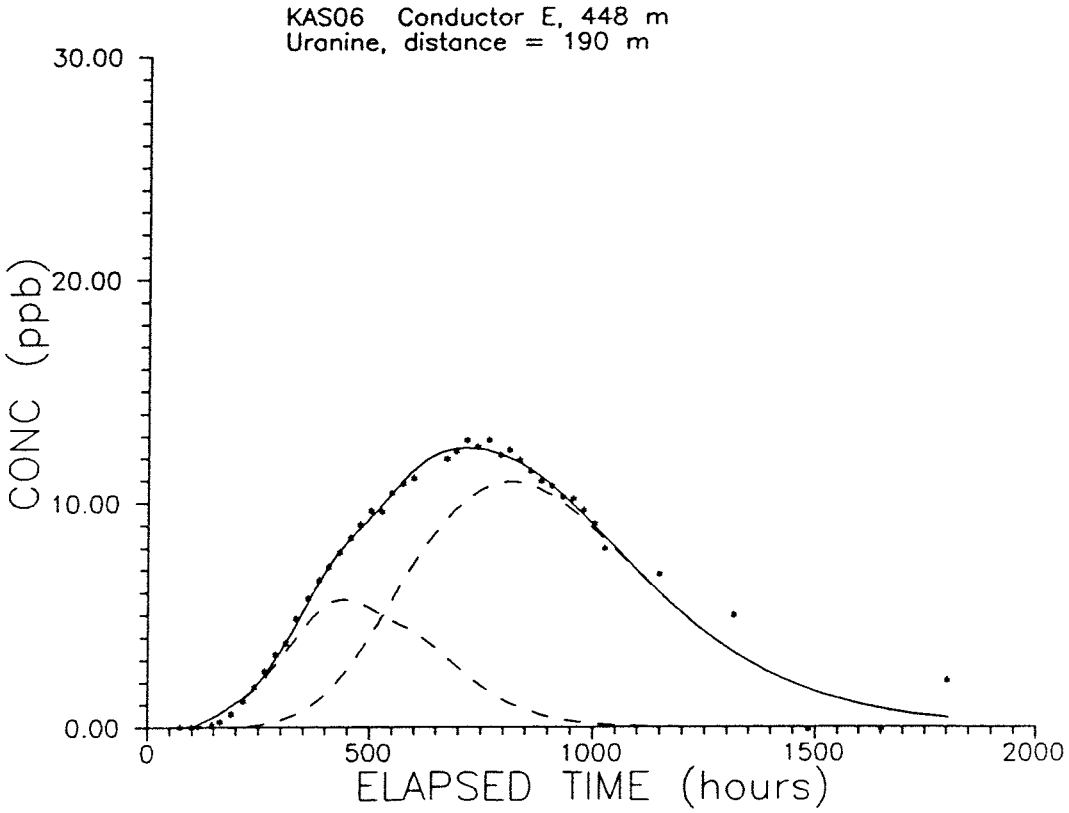
KAS06 Conductor E, 448 m
Uranine, distance = 190 m
30.00
20.00
10.00
0.00
CONC (ppb)
0
500
1000
1500
2000
ELAPSED TIME (hours)

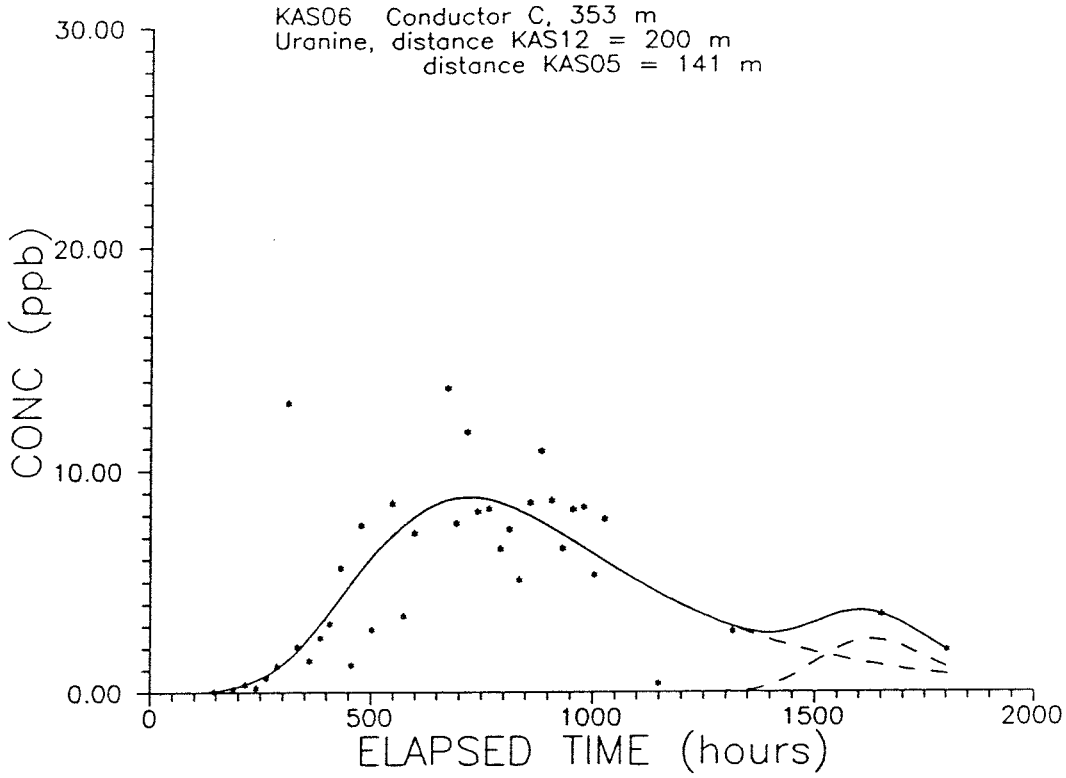
KAS06 Conductor C, 353 m
Uranine, distance KAS12 = 200 m
distance KAS05 = 141 m
CONC (ppb)
30.00
20.00
10.00
0.00
0
500
1000
1500
2000
ELAPSED TIME (hours)

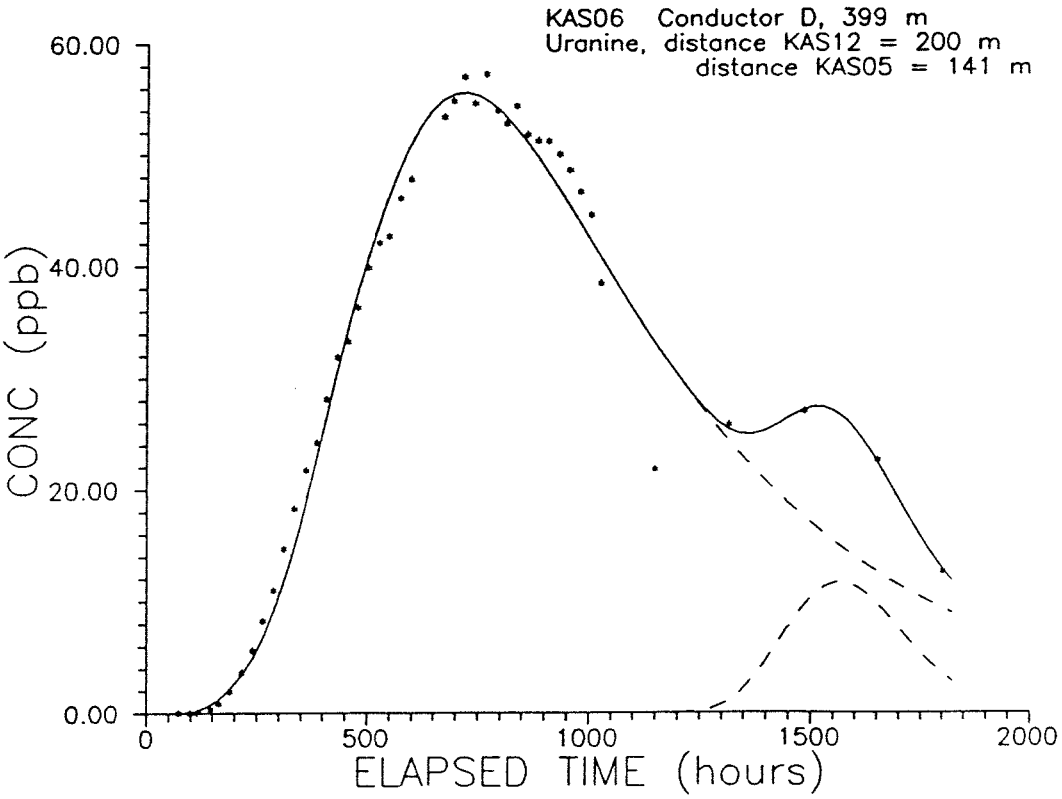
KAS06 Conductor D, 399 m
Uranine, distance KAS12 = 200 m
distance KAS05 = 141 m
CONC (ppb)
60.00
40.00
20.00
0.00
0
500
1000
1500
2000
ELAPSED TIME (hours)

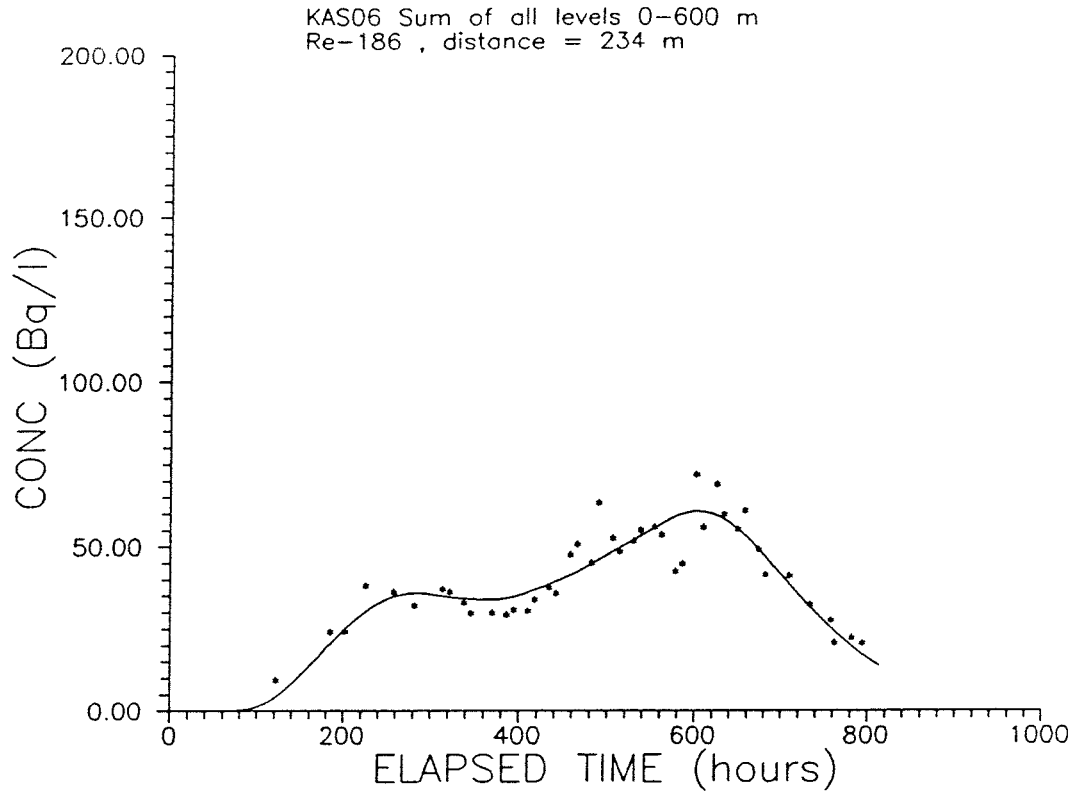
KAS06 Sum of all levels 0-600 m
Re-186 , distance = 234 m
CONC (Bq/l)
200.00
150.00
100.00
50.00
0.00
0
200
400
600
800
1000
ELAPSED TIME (hours)

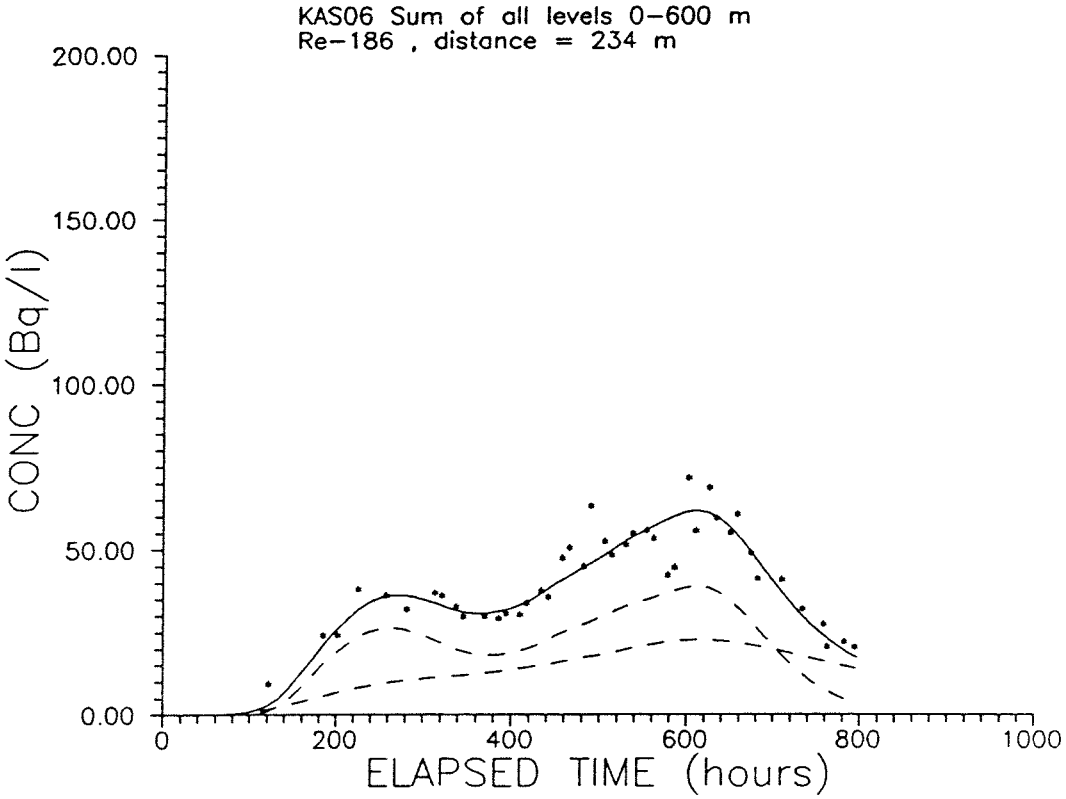
KAS06 Sum of all levels 0-600 m
Re-186 , distance = 234 m
CONC (Bq/l)
200.00
150.00
100.00
50.00
0.00
0
200
400
600
800
1000
ELAPSED TIME (hours)

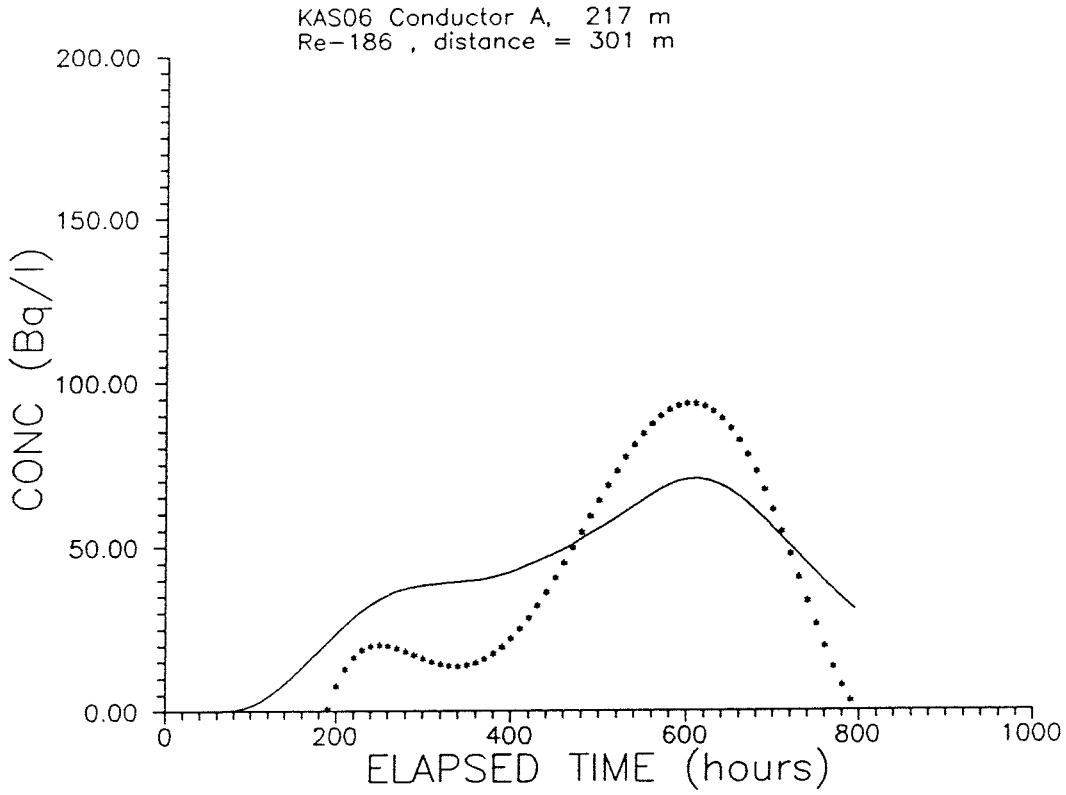
KAS06 Conductor A, 217 m
Re-186 , distance = 301 m
200.00
150.00
100.00
50.00
0.00
CONC (Bq/l)
0
200
400
600
800
1000
ELAPSED TIME (hours)

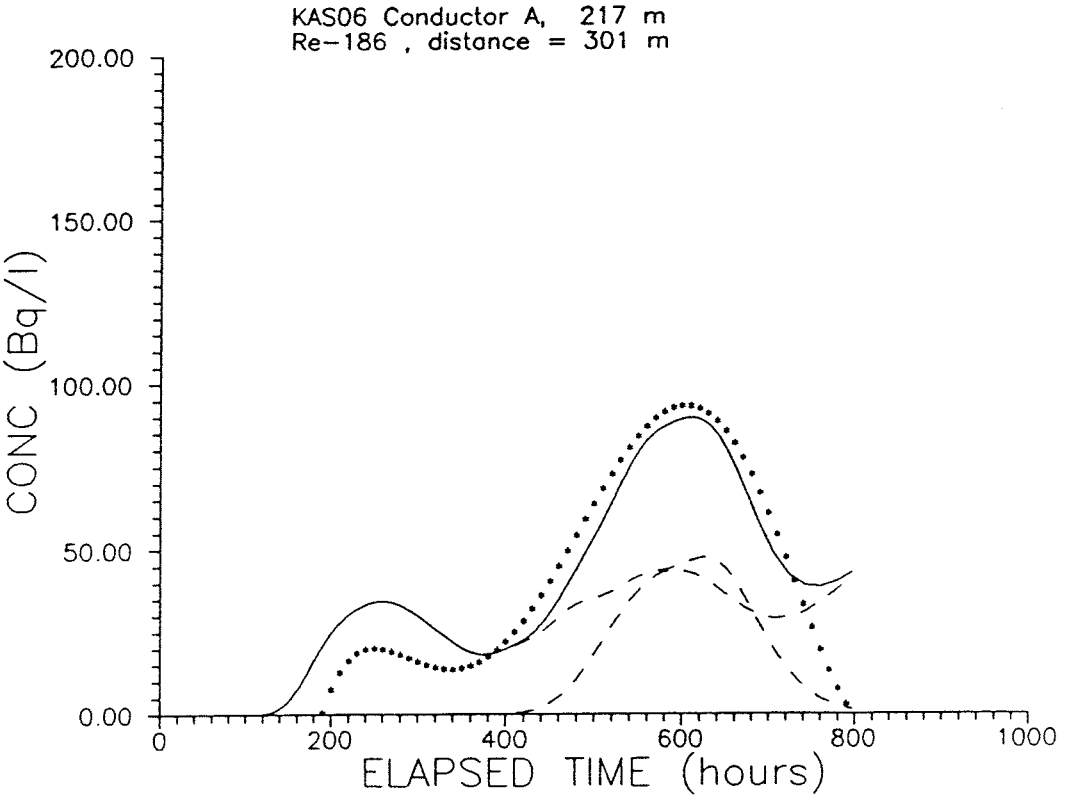
KAS06 Conductor A, 217 m
Re-186 , distance = 301 m
200.00
150.00
100.00
50.00
0.00
CONC (Bq/l)
0
200
400
600
800
1000
ELAPSED TIME (hours)

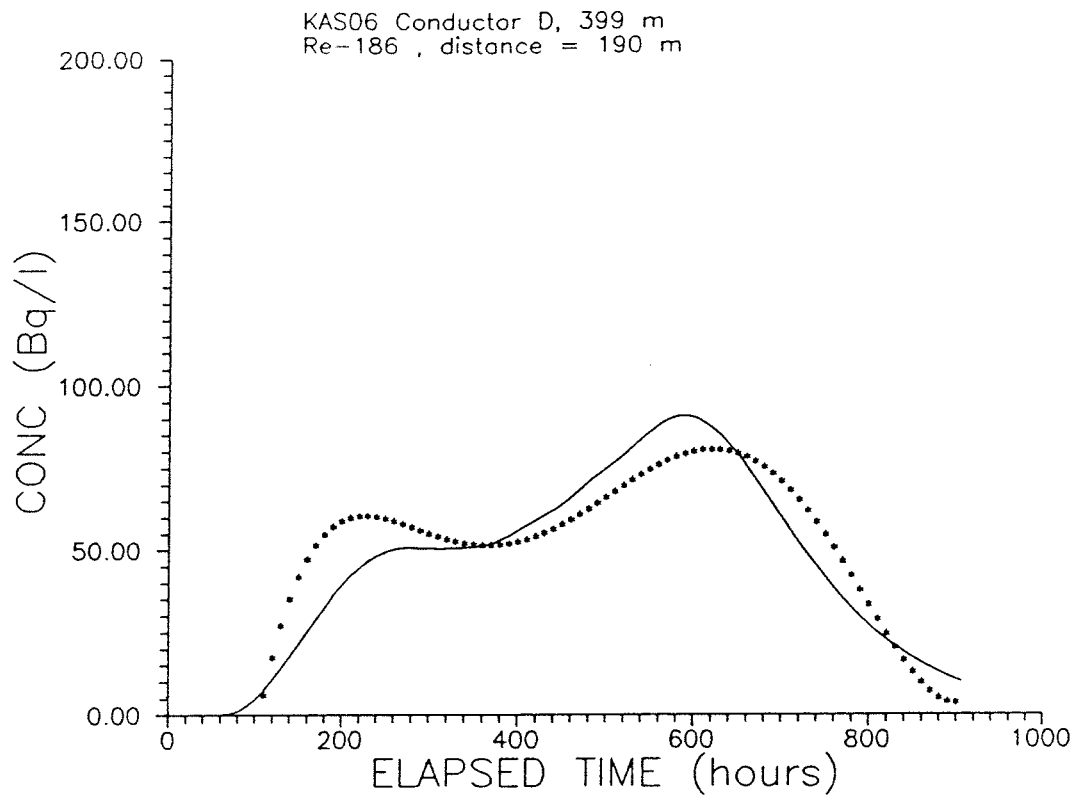
KAS06 Conductor D, 399 m
Re-186 , distance = 190 m
CONC (Bq/l)
200.00
150.00
100.00
50.00
0.00
0
200
400
600
800
1000
ELAPSED TIME (hours)

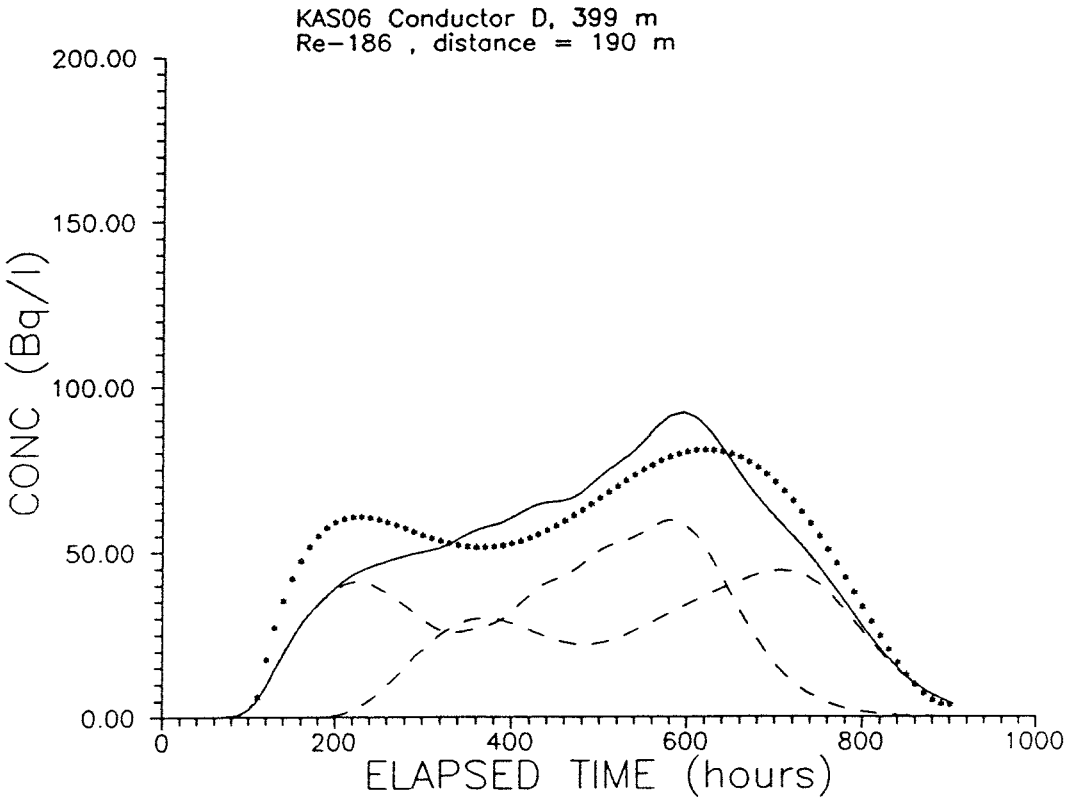
KAS06 Conductor D, 399 m
Re-186 , distance = 190 m
CONC (Bq/l)
200.00
150.00
100.00
50.00
0.00
0
200
400
600
800
1000
ELAPSED TIME (hours)

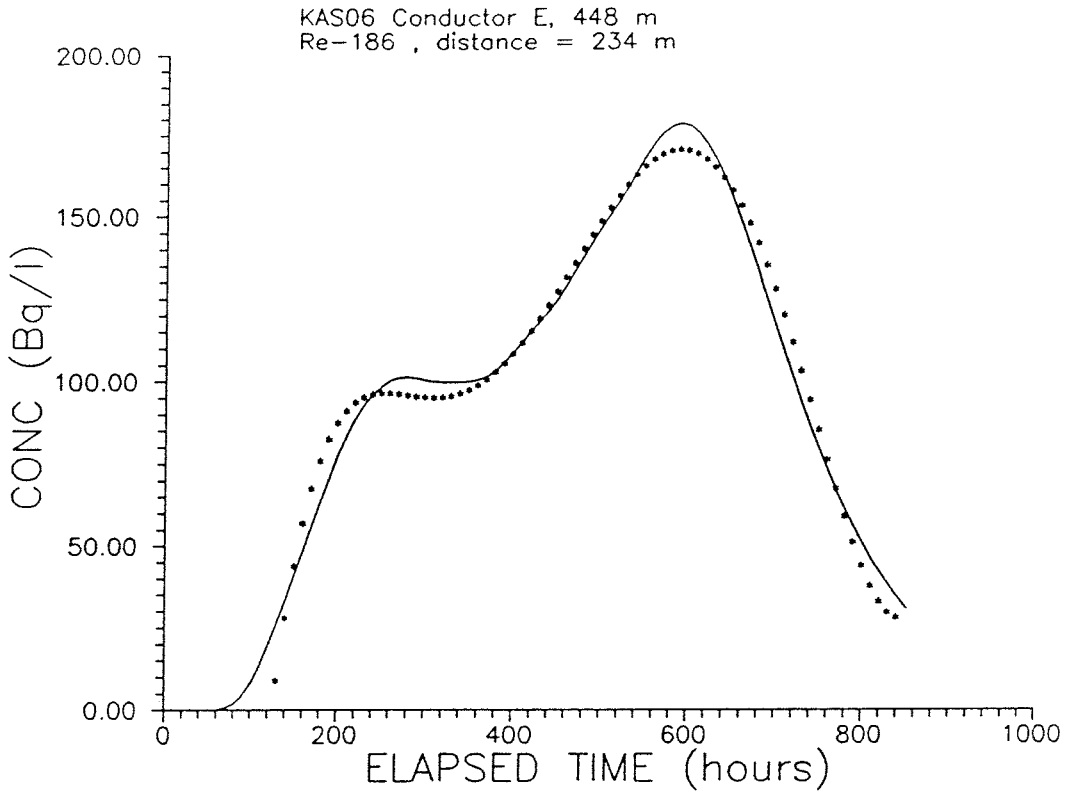
KAS06 Conductor E, 448 m
Re-186 , distance = 234 m
CONC (Bq/l)
200.00
150.00
100.00
50.00
0.00
0
200
400
600
800
1000
ELAPSED TIME (hours)

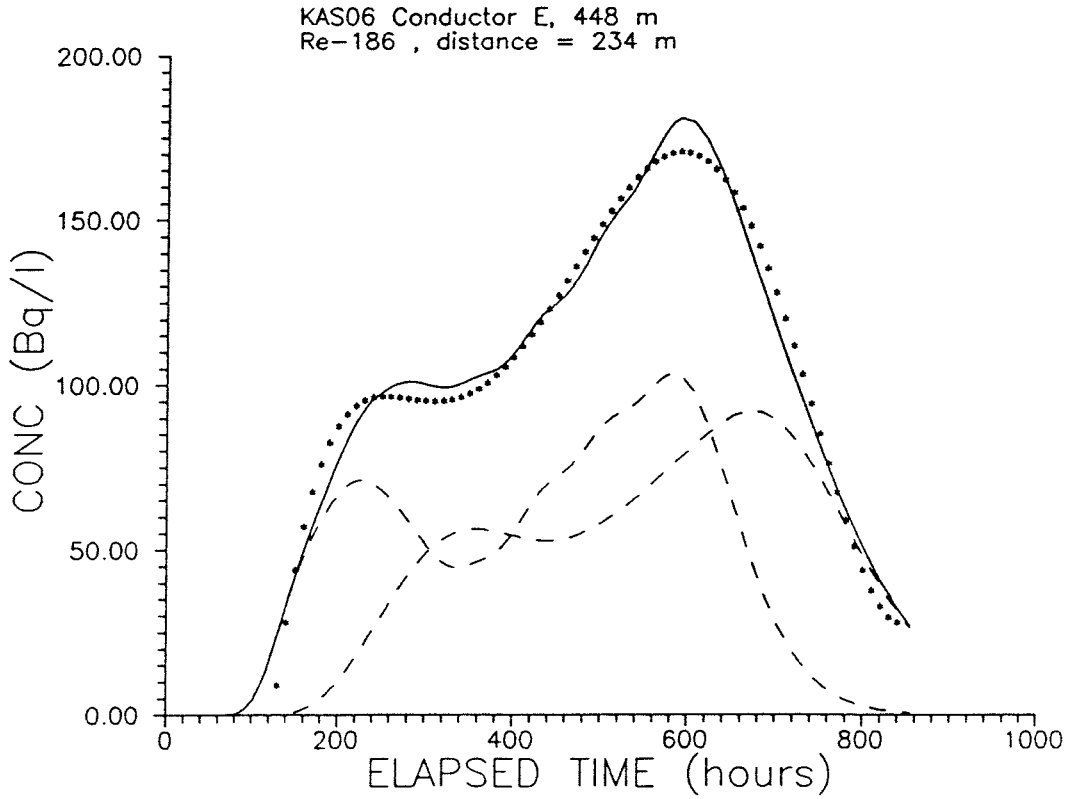
KAS06 Conductor E, 448 m
Re-186 , distance = 234 m
CONC (Bq/l)
200.00
150.00
100.00
50.00
0.00
0
200
400
600
800
1000
ELAPSED TIME (hours)

APPENDIX G

STATISTICS OF THE 1-D MODELING

Legend

Parameter No 1 = velocity, v (m/s) first main flow path
2 = dispersion coefficient, D (m^2/s)
3 = fraction of flow

4 = velocity, v (m/s) second main flow path
5 = dispersion coefficient, D (m^2/s)
6 = fraction of flow

Figure Page

Uranine from KAS12

G-1 : KAS06 217m, distance 292m, one flow path G:1
G-2 : KAS06 217m, distance 292m, two flow paths
G-3 : KAS06 217m, distance 331m, one flow path
G-4 : KAS06 217m, distance 331m, two flow paths

G-5 : KAS06 364m, distance 213m, one flow path G:2
G-6 : KAS06 364m, distance 213m, two flow paths
G-7 : KAS06 399m, distance 200m, one flow path
G-8 : KAS06 399m, distance 200m, two flow paths

G-9 : KAS06 399m, distance 234m, one flow path G:3
G-10 : KAS06 399m, distance 234m, two flow paths
G-11 : KAS06 448m, distance 190m, one flow path
G-12 : KAS06 448m, distance 190m, two flow paths

G-13 : KAS06 448m, distance 220m, one flow path G:4
G-14 : KAS06 448m, distance 220m, two flow paths
G-15 : KAS06 448m, distance 312m, one flow path
G-16 : KAS06 448m, distance 312m, two flow paths

G-17 : KAS06 0 - 600m, distance 200m, one flow path G:5
G-18 : KAS06 0 - 600m, distance 200m, two flow paths

Figure Page

Uranine from KAS12 and KAS05

G-19 : KAS06 353m, distances 200m(KAS12)/141m(KAS05) G:6
G-20 : KAS06 399m, distances 200m(KAS12)/141m(KAS05)

Rhenium from KAS08

G-21 : KAS06 217m, distance 301m, one flow path G:7
G-22 : KAS06 217m, distance 301m, two flow paths
G-23 : KAS06 217m, distance 381m, one flow path
G-24 : KAS06 217m, distance 381m, two flow paths

G-25 : KAS06 399m, distance 190m, one flow path G:8
G-26 : KAS06 399m, distance 190m, two flow paths
G-27 : KAS06 399m, distance 238m, one flow path
G-28 : KAS06 399m, distance 238m, two flow paths

G-29 : KAS06 448m, distance 181m, one flow path G:9
G-30 : KAS06 448m, distance 181m, two flow paths
G-31 : KAS06 448m, distance 234m, one flow path
G-32 : KAS06 448m, distance 234m, two flow paths

G-33 : KAS06 0 - 600m, distance 181m, one flow path G:10
G-34 : KAS06 0 - 600m, distance 181m, two flow paths
G-35 : KAS06 0 - 600m, distance 234m, one flow path
G-36 : KAS06 0 - 600m, distance 234m, two flow paths

********** REGRESSION SUMMARY **********

URANINE FROM KAS12
KAS06, 217 M
DISTANCE: 292 M
NO OF FLOW PATHS: 1

FINAL ESTIMATE FOR PARAMETER 1 = 0.1078E-03
FINAL ESTIMATE FOR PARAMETER 2 = 0.1184E-01
FINAL ESTIMATE FOR PARAMETER 3 = 0.3299E+03

****

REGRESSION STATISTICS

NO. OF OBSERVATIONS: 41

SUM OF SQUARED DIFFERENCES = 0.210E+02

ERROR VARIANCE = 0.552E+00

CORRELATION COEFFICIENT = .96124E+00

STANDARD ERROR FOR PARAMETER 1 = 0.974E-05
STANDARD ERROR FOR PARAMETER 2 = 0.159E-02
STANDARD ERROR FOR PARAMETER 3 = 0.370E+02

CORRELATION BETWEEN PARAMETERS 1 AND 2 = -.7534E+00
CORRELATION BETWEEN PARAMETERS 1 AND 3 = -.9664E+00
CORRELATION BETWEEN PARAMETERS 2 AND 3 = 0.8193E+00

********** REGRESSION SUMMARY **********

URANINE FROM KAS12
KAS06, 217 M
DISTANCE: 331 M
NO OF FLOW PATHS: 1

FINAL ESTIMATE FOR PARAMETER 1 = 0.1240E-03
FINAL ESTIMATE FOR PARAMETER 2 = 0.1497E-01
FINAL ESTIMATE FOR PARAMETER 3 = 0.3238E+03

****

REGRESSION STATISTICS

NO. OF OBSERVATIONS: 41

SUM OF SQUARED DIFFERENCES = 0.210E+02

ERROR VARIANCE = 0.553E+00

CORRELATION COEFFICIENT = .96103E+00

STANDARD ERROR FOR PARAMETER 1 = 0.108E-04
STANDARD ERROR FOR PARAMETER 2 = 0.202E-02
STANDARD ERROR FOR PARAMETER 3 = 0.353E+02

CORRELATION BETWEEN PARAMETERS 1 AND 2 = -.7501E+00
CORRELATION BETWEEN PARAMETERS 1 AND 3 = -.9639E+00
CORRELATION BETWEEN PARAMETERS 2 AND 3 = 0.8191E+00

********** REGRESSION SUMMARY **********

URANINE FROM KAS12
KAS06, 217 M
DISTANCE: 292 M
NO OF FLOW PATHS: 2

FINAL ESTIMATE FOR PARAMETER 1 = 0.1454E-03
FINAL ESTIMATE FOR PARAMETER 2 = 0.1016E-01
FINAL ESTIMATE FOR PARAMETER 3 = 0.7267E+02
FINAL ESTIMATE FOR PARAMETER 4 = 0.8938E-04
FINAL ESTIMATE FOR PARAMETER 5 = 0.1228E-01
FINAL ESTIMATE FOR PARAMETER 6 = 0.2839E+03

****

REGRESSION STATISTICS

NO. OF OBSERVATIONS: 41

SUM OF SQUARED DIFFERENCES = 0.209E+02

ERROR VARIANCE = 0.598E+00

CORRELATION COEFFICIENT = .96130E+00

STANDARD ERROR FOR PARAMETER 1 = 0.151E-02
STANDARD ERROR FOR PARAMETER 2 = 0.152E+00
STANDARD ERROR FOR PARAMETER 3 = 0.613E+04
STANDARD ERROR FOR PARAMETER 4 = 0.999E-03
STANDARD ERROR FOR PARAMETER 5 = 0.400E-01
STANDARD ERROR FOR PARAMETER 6 = 0.545E+04

CORRELATION BETWEEN PARAMETERS 1 AND 2 = -.8916E+00
CORRELATION BETWEEN PARAMETERS 1 AND 3 = -.9830E+00
CORRELATION BETWEEN PARAMETERS 1 AND 4 = 0.9777E+00
CORRELATION BETWEEN PARAMETERS 1 AND 5 = 0.2588E+00
CORRELATION BETWEEN PARAMETERS 1 AND 6 = 0.9793E+00
CORRELATION BETWEEN PARAMETERS 2 AND 3 = 0.9574E+00
CORRELATION BETWEEN PARAMETERS 2 AND 4 = -.9590E+00
CORRELATION BETWEEN PARAMETERS 2 AND 5 = -.6673E+00
CORRELATION BETWEEN PARAMETERS 2 AND 6 = -.9639E+00
CORRELATION BETWEEN PARAMETERS 3 AND 4 = -.9989E+00
CORRELATION BETWEEN PARAMETERS 3 AND 5 = -.4264E+00
CORRELATION BETWEEN PARAMETERS 3 AND 6 = -.9996E+00
CORRELATION BETWEEN PARAMETERS 4 AND 5 = 0.4376E+00
CORRELATION BETWEEN PARAMETERS 4 AND 6 = 0.9980E+00
CORRELATION BETWEEN PARAMETERS 5 AND 6 = 0.4470E+00

********** REGRESSION SUMMARY **********

URANINE FROM KAS12
KAS06, 217 M
DISTANCE: 331 M
NO OF FLOW PATHS: 2

FINAL ESTIMATE FOR PARAMETER 1 = 0.1939E-03
FINAL ESTIMATE FOR PARAMETER 2 = 0.1317E-01
FINAL ESTIMATE FOR PARAMETER 3 = 0.7682E+02
FINAL ESTIMATE FOR PARAMETER 4 = 0.8319E-04
FINAL ESTIMATE FOR PARAMETER 5 = 0.1402E-01
FINAL ESTIMATE FOR PARAMETER 6 = 0.3267E+03

****

REGRESSION STATISTICS

NO. OF OBSERVATIONS: 41

SUM OF SQUARED DIFFERENCES = 0.210E+02

ERROR VARIANCE = 0.599E+00

CORRELATION COEFFICIENT = .96129E+00

STANDARD ERROR FOR PARAMETER 1 = 0.611E-03
STANDARD ERROR FOR PARAMETER 2 = 0.271E+00
STANDARD ERROR FOR PARAMETER 3 = 0.452E+04
STANDARD ERROR FOR PARAMETER 4 = 0.130E-02
STANDARD ERROR FOR PARAMETER 5 = 0.448E+00
STANDARD ERROR FOR PARAMETER 6 = 0.429E+04

CORRELATION BETWEEN PARAMETERS 1 AND 2 = 0.7210E+00
CORRELATION BETWEEN PARAMETERS 1 AND 3 = 0.6573E+00
CORRELATION BETWEEN PARAMETERS 1 AND 4 = -.6421E+00
CORRELATION BETWEEN PARAMETERS 1 AND 5 = -.7572E+00
CORRELATION BETWEEN PARAMETERS 1 AND 6 = -.7165E+00
CORRELATION BETWEEN PARAMETERS 2 AND 3 = 0.9957E+00
CORRELATION BETWEEN PARAMETERS 2 AND 4 = -.9930E+00
CORRELATION BETWEEN PARAMETERS 2 AND 5 = -.9983E+00
CORRELATION BETWEEN PARAMETERS 2 AND 6 = -.9997E+00
CORRELATION BETWEEN PARAMETERS 3 AND 4 = -.9995E+00
CORRELATION BETWEEN PARAMETERS 3 AND 5 = -.9899E+00
CORRELATION BETWEEN PARAMETERS 3 AND 6 = -.9961E+00
CORRELATION BETWEEN PARAMETERS 4 AND 5 = 0.9864E+00
CORRELATION BETWEEN PARAMETERS 4 AND 6 = 0.9932E+00
CORRELATION BETWEEN PARAMETERS 5 AND 6 = 0.9979E+00

********** REGRESSION SUMMARY **********

URANINE FROM KAS12
KAS06, 364 M
DISTANCE: 213 M
NO OF FLOW PATHS: 1

FINAL ESTIMATE FOR PARAMETER 1 = 0.5617E-04
FINAL ESTIMATE FOR PARAMETER 2 = 0.2628E-02
FINAL ESTIMATE FOR PARAMETER 3 = 0.1617E+04

****

REGRESSION STATISTICS

NO. OF OBSERVATIONS: 44

SUM OF SQUARED DIFFERENCES = 0.327E+04

ERROR VARIANCE = 0.796E+02

CORRELATION COEFFICIENT = .78145E+00

STANDARD ERROR FOR PARAMETER 1 = 0.104E-04
STANDARD ERROR FOR PARAMETER 2 = 0.852E-03
STANDARD ERROR FOR PARAMETER 3 = 0.450E+03

CORRELATION BETWEEN PARAMETERS 1 AND 2 = -.6928E+00
CORRELATION BETWEEN PARAMETERS 1 AND 3 = -.9605E+00
CORRELATION BETWEEN PARAMETERS 2 AND 3 = 0.7246E+00

********** REGRESSION SUMMARY **********

URANINE FROM KAS12
KAS06, 399 M
DISTANCE: 200 M
NO OF FLOW PATHS: 1

FINAL ESTIMATE FOR PARAMETER 1 = 0.7558E-04
FINAL ESTIMATE FOR PARAMETER 2 = 0.4516E-02
FINAL ESTIMATE FOR PARAMETER 3 = 0.2419E+04

****

REGRESSION STATISTICS

NO. OF OBSERVATIONS: 44

SUM OF SQUARED DIFFERENCES = 0.374E+03

ERROR VARIANCE = 0.911E+01

CORRELATION COEFFICIENT = .98883E+00

STANDARD ERROR FOR PARAMETER 1 = 0.237E-05
STANDARD ERROR FOR PARAMETER 2 = 0.270E-03
STANDARD ERROR FOR PARAMETER 3 = 0.990E+02

CORRELATION BETWEEN PARAMETERS 1 AND 2 = -.6554E+00
CORRELATION BETWEEN PARAMETERS 1 AND 3 = -.9307E+00
CORRELATION BETWEEN PARAMETERS 2 AND 3 = 0.7671E+00

********** REGRESSION SUMMARY **********

URANINE FROM KAS12
KAS06, 364 M
DISTANCE: 213 M
NO OF FLOW PATHS: 2

FINAL ESTIMATE FOR PARAMETER 1 = 0.1404E-03
FINAL ESTIMATE FOR PARAMETER 2 = 0.1556E-02
FINAL ESTIMATE FOR PARAMETER 3 = 0.2909E+03
FINAL ESTIMATE FOR PARAMETER 4 = 0.5946E-04
FINAL ESTIMATE FOR PARAMETER 5 = 0.4163E-03
FINAL ESTIMATE FOR PARAMETER 6 = 0.1014E+04

****

REGRESSION STATISTICS

NO. OF OBSERVATIONS: 44

SUM OF SQUARED DIFFERENCES = 0.273E+04

ERROR VARIANCE = 0.719E+02

CORRELATION COEFFICIENT = .82033E+00

STANDARD ERROR FOR PARAMETER 1 = 0.599E-04
STANDARD ERROR FOR PARAMETER 2 = 0.330E-02
STANDARD ERROR FOR PARAMETER 3 = 0.288E+03
STANDARD ERROR FOR PARAMETER 4 = 0.514E-05
STANDARD ERROR FOR PARAMETER 5 = 0.367E-03
STANDARD ERROR FOR PARAMETER 6 = 0.337E+03

CORRELATION BETWEEN PARAMETERS 1 AND 2 = -.8389E+00
CORRELATION BETWEEN PARAMETERS 1 AND 3 = -.9651E+00
CORRELATION BETWEEN PARAMETERS 1 AND 4 = 0.8394E+00
CORRELATION BETWEEN PARAMETERS 1 AND 5 = 0.8882E+00
CORRELATION BETWEEN PARAMETERS 1 AND 6 = 0.8921E+00
CORRELATION BETWEEN PARAMETERS 2 AND 3 = 0.8945E+00
CORRELATION BETWEEN PARAMETERS 2 AND 4 = -.7812E+00
CORRELATION BETWEEN PARAMETERS 2 AND 5 = -.6991E+00
CORRELATION BETWEEN PARAMETERS 2 AND 6 = -.7907E+00
CORRELATION BETWEEN PARAMETERS 3 AND 4 = -.8392E+00
CORRELATION BETWEEN PARAMETERS 3 AND 5 = -.8948E+00
CORRELATION BETWEEN PARAMETERS 3 AND 6 = -.8990E+00
CORRELATION BETWEEN PARAMETERS 4 AND 5 = 0.6422E+00
CORRELATION BETWEEN PARAMETERS 4 AND 6 = 0.5911E+00
CORRELATION BETWEEN PARAMETERS 5 AND 6 = 0.8900E+00

********** REGRESSION SUMMARY **********

URANINE FROM KAS12
KAS06, 399 M
DISTANCE: 200 M
NO OF FLOW PATHS: 2

FINAL ESTIMATE FOR PARAMETER 1 = 0.9337E-04
FINAL ESTIMATE FOR PARAMETER 2 = 0.7799E-03
FINAL ESTIMATE FOR PARAMETER 3 = 0.5065E+03
FINAL ESTIMATE FOR PARAMETER 4 = 0.4897E-04
FINAL ESTIMATE FOR PARAMETER 5 = 0.1083E-01
FINAL ESTIMATE FOR PARAMETER 6 = 0.2875E+04

****

REGRESSION STATISTICS

NO. OF OBSERVATIONS: 44

SUM OF SQUARED DIFFERENCES = 0.298E+03

ERROR VARIANCE = 0.785E+01

CORRELATION COEFFICIENT = .99164E+00

STANDARD ERROR FOR PARAMETER 1 = 0.255E-05
STANDARD ERROR FOR PARAMETER 2 = 0.495E-03
STANDARD ERROR FOR PARAMETER 3 = 0.254E+03
STANDARD ERROR FOR PARAMETER 4 = 0.235E-04
STANDARD ERROR FOR PARAMETER 5 = 0.434E-02
STANDARD ERROR FOR PARAMETER 6 = 0.994E+03

CORRELATION BETWEEN PARAMETERS 1 AND 2 = -.1744E-01
CORRELATION BETWEEN PARAMETERS 1 AND 3 = 0.1711E-01
CORRELATION BETWEEN PARAMETERS 1 AND 4 = -.2621E+00
CORRELATION BETWEEN PARAMETERS 1 AND 5 = 0.1004E+00
CORRELATION BETWEEN PARAMETERS 1 AND 6 = 0.3343E+00
CORRELATION BETWEEN PARAMETERS 2 AND 3 = 0.9584E+00
CORRELATION BETWEEN PARAMETERS 2 AND 4 = -.8301E+00
CORRELATION BETWEEN PARAMETERS 2 AND 5 = 0.8377E+00
CORRELATION BETWEEN PARAMETERS 2 AND 6 = 0.7115E+00
CORRELATION BETWEEN PARAMETERS 3 AND 4 = -.9081E+00
CORRELATION BETWEEN PARAMETERS 3 AND 5 = 0.9393E+00
CORRELATION BETWEEN PARAMETERS 3 AND 6 = 0.8024E+00
CORRELATION BETWEEN PARAMETERS 4 AND 5 = -.9616E+00
CORRELATION BETWEEN PARAMETERS 4 AND 6 = -.9770E+00
CORRELATION BETWEEN PARAMETERS 5 AND 6 = 0.9148E+00

********** REGRESSION SUMMARY **********

URANINE FROM KAS12
KAS06, 399 M
DISTANCE: 234 M
NO OF FLOW PATHS: 1

FINAL ESTIMATE FOR PARAMETER 1 = 0.8846E-04
FINAL ESTIMATE FOR PARAMETER 2 = 0.6179E-02
FINAL ESTIMATE FOR PARAMETER 3 = 0.2418E+04

****

REGRESSION STATISTICS

NO. OF OBSERVATIONS: 44

SUM OF SQUARED DIFFERENCES = 0.374E+03

ERROR VARIANCE = 0.911E+01

CORRELATION COEFFICIENT = .98883E+00

STANDARD ERROR FOR PARAMETER 1 = 0.277E-05
STANDARD ERROR FOR PARAMETER 2 = 0.369E-03
STANDARD ERROR FOR PARAMETER 3 = 0.989E+02

CORRELATION BETWEEN PARAMETERS 1 AND 2 = -.6553E+00
CORRELATION BETWEEN PARAMETERS 1 AND 3 = -.9306E+00
CORRELATION BETWEEN PARAMETERS 2 AND 3 = 0.7671E+00

********** REGRESSION SUMMARY **********

URANINE FROM KAS12
KAS06, 448 M
DISTANCE: 190 M
NO OF FLOW PATHS: 1

FINAL ESTIMATE FOR PARAMETER 1 = 0.8724E-04
FINAL ESTIMATE FOR PARAMETER 2 = 0.3547E-02
FINAL ESTIMATE FOR PARAMETER 3 = 0.4409E+03

****

REGRESSION STATISTICS

NO. OF OBSERVATIONS: 44

SUM OF SQUARED DIFFERENCES = 0.268E+02

ERROR VARIANCE = 0.653E+00

CORRELATION COEFFICIENT = .98512E+00

STANDARD ERROR FOR PARAMETER 1 = 0.228E-05
STANDARD ERROR FOR PARAMETER 2 = 0.263E-03
STANDARD ERROR FOR PARAMETER 3 = 0.161E+02

CORRELATION BETWEEN PARAMETERS 1 AND 2 = -.6016E+00
CORRELATION BETWEEN PARAMETERS 1 AND 3 = -.8554E+00
CORRELATION BETWEEN PARAMETERS 2 AND 3 = 0.7757E+00

********** REGRESSION SUMMARY **********

URANINE FROM KAS12
KAS06, 399 M
DISTANCE: 234 M
NO OF FLOW PATHS: 2

FINAL ESTIMATE FOR PARAMETER 1 = 0.1209E-03
FINAL ESTIMATE FOR PARAMETER 2 = 0.2614E-02
FINAL ESTIMATE FOR PARAMETER 3 = 0.5037E+03
FINAL ESTIMATE FOR PARAMETER 4 = 0.6176E-04
FINAL ESTIMATE FOR PARAMETER 5 = 0.8337E-02
FINAL ESTIMATE FOR PARAMETER 6 = 0.2518E+04

****

REGRESSION STATISTICS

NO. OF OBSERVATIONS: 44

SUM OF SQUARED DIFFERENCES = 0.348E+03

ERROR VARIANCE = 0.917E+01

CORRELATION COEFFICIENT = .98960E+00

STANDARD ERROR FOR PARAMETER 1 = 0.296E-04
STANDARD ERROR FOR PARAMETER 2 = 0.407E-02
STANDARD ERROR FOR PARAMETER 3 = 0.134E+04
STANDARD ERROR FOR PARAMETER 4 = 0.651E-04
STANDARD ERROR FOR PARAMETER 5 = 0.520E-02
STANDARD ERROR FOR PARAMETER 6 = 0.554E+03

CORRELATION BETWEEN PARAMETERS 1 AND 2 = -.9006E+00
CORRELATION BETWEEN PARAMETERS 1 AND 3 = -.9567E+00
CORRELATION BETWEEN PARAMETERS 1 AND 4 = 0.9445E+00
CORRELATION BETWEEN PARAMETERS 1 AND 5 = -.9542E+00
CORRELATION BETWEEN PARAMETERS 1 AND 6 = -.6122E+00
CORRELATION BETWEEN PARAMETERS 2 AND 3 = 0.9726E+00
CORRELATION BETWEEN PARAMETERS 2 AND 4 = -.9375E+00
CORRELATION BETWEEN PARAMETERS 2 AND 5 = 0.8165E+00
CORRELATION BETWEEN PARAMETERS 2 AND 6 = 0.4643E+00
CORRELATION BETWEEN PARAMETERS 3 AND 4 = -.9886E+00
CORRELATION BETWEEN PARAMETERS 3 AND 5 = 0.9212E+00
CORRELATION BETWEEN PARAMETERS 3 AND 6 = 0.6127E+00
CORRELATION BETWEEN PARAMETERS 4 AND 5 = -.9504E+00
CORRELATION BETWEEN PARAMETERS 4 AND 6 = -.7224E+00
CORRELATION BETWEEN PARAMETERS 5 AND 6 = 0.7993E+00

********** REGRESSION SUMMARY **********

URANINE FROM KAS12
KAS06, 448 M
DISTANCE: 190 M
NO OF FLOW PATHS: 2

FINAL ESTIMATE FOR PARAMETER 1 = 0.1920E-03
FINAL ESTIMATE FOR PARAMETER 2 = 0.3132E-02
FINAL ESTIMATE FOR PARAMETER 3 = 0.9447E+02
FINAL ESTIMATE FOR PARAMETER 4 = 0.7919E-04
FINAL ESTIMATE FOR PARAMETER 5 = 0.1191E-02
FINAL ESTIMATE FOR PARAMETER 6 = 0.3005E+03

****

REGRESSION STATISTICS

NO. OF OBSERVATIONS: 44

SUM OF SQUARED DIFFERENCES = 0.122E+02

ERROR VARIANCE = 0.321E+00

CORRELATION COEFFICIENT = .99325E+00

STANDARD ERROR FOR PARAMETER 1 = 0.813E-04
STANDARD ERROR FOR PARAMETER 2 = 0.239E-02
STANDARD ERROR FOR PARAMETER 3 = 0.918E+02
STANDARD ERROR FOR PARAMETER 4 = 0.975E-05
STANDARD ERROR FOR PARAMETER 5 = 0.617E-03
STANDARD ERROR FOR PARAMETER 6 = 0.963E+02

CORRELATION BETWEEN PARAMETERS 1 AND 2 = -.9207E+00
CORRELATION BETWEEN PARAMETERS 1 AND 3 = -.9971E+00
CORRELATION BETWEEN PARAMETERS 1 AND 4 = 0.9924E+00
CORRELATION BETWEEN PARAMETERS 1 AND 5 = 0.9664E+00
CORRELATION BETWEEN PARAMETERS 1 AND 6 = 0.9915E+00
CORRELATION BETWEEN PARAMETERS 2 AND 3 = 0.9220E+00
CORRELATION BETWEEN PARAMETERS 2 AND 4 = -.9093E+00
CORRELATION BETWEEN PARAMETERS 2 AND 5 = -.8379E+00
CORRELATION BETWEEN PARAMETERS 2 AND 6 = -.9039E+00
CORRELATION BETWEEN PARAMETERS 3 AND 4 = -.9928E+00
CORRELATION BETWEEN PARAMETERS 3 AND 5 = -.9757E+00
CORRELATION BETWEEN PARAMETERS 3 AND 6 = -.9955E+00
CORRELATION BETWEEN PARAMETERS 4 AND 5 = 0.9605E+00
CORRELATION BETWEEN PARAMETERS 4 AND 6 = 0.9808E+00
CORRELATION BETWEEN PARAMETERS 5 AND 6 = 0.9868E+00

********** REGRESSION SUMMARY **********

URANINE FROM KAS12
KAS06, 448 M
DISTANCE: 220 M
NO OF FLOW PATHS: 1

FINAL ESTIMATE FOR PARAMETER 1 = 0.1011E-03
FINAL ESTIMATE FOR PARAMETER 2 = 0.4734E-02
FINAL ESTIMATE FOR PARAMETER 3 = 0.4400E+03

****

REGRESSION STATISTICS

NO. OF OBSERVATIONS: 44

SUM OF SQUARED DIFFERENCES = 0.268E+02

ERROR VARIANCE = 0.653E+00

CORRELATION COEFFICIENT = .98514E+00

STANDARD ERROR FOR PARAMETER 1 = 0.263E-05
STANDARD ERROR FOR PARAMETER 2 = 0.351E-03
STANDARD ERROR FOR PARAMETER 3 = 0.161E+02

CORRELATION BETWEEN PARAMETERS 1 AND 2 = -.6010E+00
CORRELATION BETWEEN PARAMETERS 1 AND 3 = -.8543E+00
CORRELATION BETWEEN PARAMETERS 2 AND 3 = 0.7757E+00

********** REGRESSION SUMMARY **********

URANINE FROM KAS12
KAS06, 448 M
DISTANCE: 312 M
NO OF FLOW PATHS: 1

FINAL ESTIMATE FOR PARAMETER 1 = 0.1434E-03
FINAL ESTIMATE FOR PARAMETER 2 = 0.9525E-02
FINAL ESTIMATE FOR PARAMETER 3 = 0.4401E+03

****

REGRESSION STATISTICS

NO. OF OBSERVATIONS: 44

SUM OF SQUARED DIFFERENCES = 0.268E+02

ERROR VARIANCE = 0.653E+00

CORRELATION COEFFICIENT = .98514E+00

STANDARD ERROR FOR PARAMETER 1 = 0.373E-05
STANDARD ERROR FOR PARAMETER 2 = 0.707E-03
STANDARD ERROR FOR PARAMETER 3 = 0.161E+02

CORRELATION BETWEEN PARAMETERS 1 AND 2 = -.6010E+00
CORRELATION BETWEEN PARAMETERS 1 AND 3 = -.8544E+00
CORRELATION BETWEEN PARAMETERS 2 AND 3 = 0.7757E+00

********** REGRESSION SUMMARY **********

URANINE FROM KAS12
KAS06, 448 M
DISTANCE: 220 M
NO OF FLOW PATHS: 2

FINAL ESTIMATE FOR PARAMETER 1 = 0.2252E-03
FINAL ESTIMATE FOR PARAMETER 2 = 0.2766E-02
FINAL ESTIMATE FOR PARAMETER 3 = 0.9923E+02
FINAL ESTIMATE FOR PARAMETER 4 = 0.9514E-04
FINAL ESTIMATE FOR PARAMETER 5 = 0.1039E-02
FINAL ESTIMATE FOR PARAMETER 6 = 0.2631E+03

****

REGRESSION STATISTICS

NO. OF OBSERVATIONS: 44

SUM OF SQUARED DIFFERENCES = 0.193E+02

ERROR VARIANCE = 0.509E+00

CORRELATION COEFFICIENT = .99004E+00

STANDARD ERROR FOR PARAMETER 1 = 0.393E-04
STANDARD ERROR FOR PARAMETER 2 = 0.166E-02
STANDARD ERROR FOR PARAMETER 3 = 0.406E+02
STANDARD ERROR FOR PARAMETER 4 = 0.529E-05
STANDARD ERROR FOR PARAMETER 5 = 0.398E-03
STANDARD ERROR FOR PARAMETER 6 = 0.461E+02

CORRELATION BETWEEN PARAMETERS 1 AND 2 = -.8273E+00
CORRELATION BETWEEN PARAMETERS 1 AND 3 = -.9832E+00
CORRELATION BETWEEN PARAMETERS 1 AND 4 = 0.9656E+00
CORRELATION BETWEEN PARAMETERS 1 AND 5 = 0.9169E+00
CORRELATION BETWEEN PARAMETERS 1 AND 6 = 0.9665E+00
CORRELATION BETWEEN PARAMETERS 2 AND 3 = 0.8568E+00
CORRELATION BETWEEN PARAMETERS 2 AND 4 = -.8197E+00
CORRELATION BETWEEN PARAMETERS 2 AND 5 = -.6968E+00
CORRELATION BETWEEN PARAMETERS 2 AND 6 = -.8051E+00
CORRELATION BETWEEN PARAMETERS 3 AND 4 = -.9669E+00
CORRELATION BETWEEN PARAMETERS 3 AND 5 = -.9411E+00
CORRELATION BETWEEN PARAMETERS 3 AND 6 = -.9810E+00
CORRELATION BETWEEN PARAMETERS 4 AND 5 = 0.8779E+00
CORRELATION BETWEEN PARAMETERS 4 AND 6 = 0.9212E+00
CORRELATION BETWEEN PARAMETERS 5 AND 6 = 0.9740E+00

********** REGRESSION SUMMARY **********

URANINE FROM KAS12
KAS06, 448 M
DISTANCE: 312 M
NO OF FLOW PATHS: 2

FINAL ESTIMATE FOR PARAMETER 1 = 0.2506E-03
FINAL ESTIMATE FOR PARAMETER 2 = 0.1093E-01
FINAL ESTIMATE FOR PARAMETER 3 = 0.1585E+03
FINAL ESTIMATE FOR PARAMETER 4 = 0.1255E-03
FINAL ESTIMATE FOR PARAMETER 5 = 0.2056E-02
FINAL ESTIMATE FOR PARAMETER 6 = 0.2189E+03

****

REGRESSION STATISTICS

NO. OF OBSERVATIONS: 44

SUM OF SQUARED DIFFERENCES = 0.141E+02

ERROR VARIANCE = 0.371E+00

CORRELATION COEFFICIENT = .99229E+00

STANDARD ERROR FOR PARAMETER 1 = 0.164E-03
STANDARD ERROR FOR PARAMETER 2 = 0.820E-02
STANDARD ERROR FOR PARAMETER 3 = 0.189E+03
STANDARD ERROR FOR PARAMETER 4 = 0.113E-04
STANDARD ERROR FOR PARAMETER 5 = 0.117E-02
STANDARD ERROR FOR PARAMETER 6 = 0.192E+03

CORRELATION BETWEEN PARAMETERS 1 AND 2 = -.9536E+00
CORRELATION BETWEEN PARAMETERS 1 AND 3 = -.9990E+00
CORRELATION BETWEEN PARAMETERS 1 AND 4 = 0.9631E+00
CORRELATION BETWEEN PARAMETERS 1 AND 5 = 0.9315E+00
CORRELATION BETWEEN PARAMETERS 1 AND 6 = 0.9974E+00
CORRELATION BETWEEN PARAMETERS 2 AND 3 = 0.9489E+00
CORRELATION BETWEEN PARAMETERS 2 AND 4 = -.8617E+00
CORRELATION BETWEEN PARAMETERS 2 AND 5 = -.8150E+00
CORRELATION BETWEEN PARAMETERS 2 AND 6 = -.9421E+00
CORRELATION BETWEEN PARAMETERS 3 AND 4 = -.9676E+00
CORRELATION BETWEEN PARAMETERS 3 AND 5 = -.9425E+00
CORRELATION BETWEEN PARAMETERS 3 AND 6 = -.9989E+00
CORRELATION BETWEEN PARAMETERS 4 AND 5 = 0.9417E+00
CORRELATION BETWEEN PARAMETERS 4 AND 6 = 0.9642E+00
CORRELATION BETWEEN PARAMETERS 5 AND 6 = 0.9526E+00

********** REGRESSION SUMMARY **********

URANINE FROM KAS12
KAS06, SUM OF ALL LEVELS 0–600 M
DISTANCE: 200 M
NO OF FLOW PATHS: 1

FINAL ESTIMATE FOR PARAMETER 1 = 0.8645E–04
FINAL ESTIMATE FOR PARAMETER 2 = 0.3498E–02
FINAL ESTIMATE FOR PARAMETER 3 = 0.5377E+03

****

REGRESSION STATISTICS

NO. OF OBSERVATIONS: 201

SUM OF SQUARED DIFFERENCES = 0.135E+03

ERROR VARIANCE = 0.683E+00

CORRELATION COEFFICIENT = .99105E+00

STANDARD ERROR FOR PARAMETER 1 = 0.963E–06
STANDARD ERROR FOR PARAMETER 2 = 0.113E–03
STANDARD ERROR FOR PARAMETER 3 = 0.887E+01

CORRELATION BETWEEN PARAMETERS 1 AND 2 = –.4788E+00
CORRELATION BETWEEN PARAMETERS 1 AND 3 = –.8448E+00
CORRELATION BETWEEN PARAMETERS 2 AND 3 = 0.7207E+00

********** REGRESSION SUMMARY **********

URANINE FROM KAS12
KAS06, SUM OF ALL LEVELS 0–600 M
DISTANCE: 200 M
NO OF FLOW PATHS: 2

FINAL ESTIMATE FOR PARAMETER 1 = 0.1245E–03
FINAL ESTIMATE FOR PARAMETER 2 = 0.3963E–02
FINAL ESTIMATE FOR PARAMETER 3 = 0.2644E+03
FINAL ESTIMATE FOR PARAMETER 4 = 0.7186E–04
FINAL ESTIMATE FOR PARAMETER 5 = 0.7656E–03
FINAL ESTIMATE FOR PARAMETER 6 = 0.2197E+03

****

REGRESSION STATISTICS

NO. OF OBSERVATIONS: 201

SUM OF SQUARED DIFFERENCES = 0.101E+03

ERROR VARIANCE = 0.519E+00

CORRELATION COEFFICIENT = .99350E+00

STANDARD ERROR FOR PARAMETER 1 = 0.694E–04
STANDARD ERROR FOR PARAMETER 2 = 0.155E–02
STANDARD ERROR FOR PARAMETER 3 = 0.281E+03
STANDARD ERROR FOR PARAMETER 4 = 0.185E–05
STANDARD ERROR FOR PARAMETER 5 = 0.513E–03
STANDARD ERROR FOR PARAMETER 6 = 0.276E+03

CORRELATION BETWEEN PARAMETERS 1 AND 2 = –.9625E+00
CORRELATION BETWEEN PARAMETERS 1 AND 3 = –.9995E+00
CORRELATION BETWEEN PARAMETERS 1 AND 4 = 0.5296E+00
CORRELATION BETWEEN PARAMETERS 1 AND 5 = 0.9796E+00
CORRELATION BETWEEN PARAMETERS 1 AND 6 = 0.9992E+00
CORRELATION BETWEEN PARAMETERS 2 AND 3 = 0.9574E+00
CORRELATION BETWEEN PARAMETERS 2 AND 4 = –.3121E+00
CORRELATION BETWEEN PARAMETERS 2 AND 5 = –.9036E+00
CORRELATION BETWEEN PARAMETERS 2 AND 6 = –.9553E+00
CORRELATION BETWEEN PARAMETERS 3 AND 4 = –.5473E+00
CORRELATION BETWEEN PARAMETERS 3 AND 5 = –.9843E+00
CORRELATION BETWEEN PARAMETERS 3 AND 6 = –.9998E+00
CORRELATION BETWEEN PARAMETERS 4 AND 5 = 0.6348E+00
CORRELATION BETWEEN PARAMETERS 4 AND 6 = 0.5464E+00
CORRELATION BETWEEN PARAMETERS 5 AND 6 = 0.9859E+00

********** REGRESSION SUMMARY **********

URANINE FROM KAS12 AND KAS05
KAS06, 353 M
DISTANCE: 200 M (KAS12), 141 M (KAS05)
NO OF FLOW PATHS: 2

FINAL ESTIMATE FOR PARAMETER 1 = 0.8991E-04
FINAL ESTIMATE FOR PARAMETER 2 = 0.2951E-02
FINAL ESTIMATE FOR PARAMETER 3 = 0.2863E+03
FINAL ESTIMATE FOR PARAMETER 4 = 0.4080E-04
FINAL ESTIMATE FOR PARAMETER 5 = 0.5382E-04
FINAL ESTIMATE FOR PARAMETER 6 = 0.5119E+02

****

REGRESSION STATISTICS

NO. OF OBSERVATIONS: 42

SUM OF SQUARED DIFFERENCES = 0.276E+03

ERROR VARIANCE = 0.766E+01

CORRELATION COEFFICIENT = .76309E+00

STANDARD ERROR FOR PARAMETER 1 = 0.142E-04
STANDARD ERROR FOR PARAMETER 2 = 0.138E-02
STANDARD ERROR FOR PARAMETER 3 = 0.681E+02
STANDARD ERROR FOR PARAMETER 4 = 0.537E-04
STANDARD ERROR FOR PARAMETER 5 = 0.987E-03
STANDARD ERROR FOR PARAMETER 6 = 0.467E+03

CORRELATION BETWEEN PARAMETERS 1 AND 2 = -.7505E+00
CORRELATION BETWEEN PARAMETERS 1 AND 3 = -.9034E+00
CORRELATION BETWEEN PARAMETERS 1 AND 4 = 0.4585E+00
CORRELATION BETWEEN PARAMETERS 1 AND 5 = 0.4917E+00
CORRELATION BETWEEN PARAMETERS 1 AND 6 = 0.5323E+00
CORRELATION BETWEEN PARAMETERS 2 AND 3 = 0.8666E+00
CORRELATION BETWEEN PARAMETERS 2 AND 4 = -.3904E+00
CORRELATION BETWEEN PARAMETERS 2 AND 5 = -.4227E+00
CORRELATION BETWEEN PARAMETERS 2 AND 6 = -.4618E+00
CORRELATION BETWEEN PARAMETERS 3 AND 4 = -.4563E+00
CORRELATION BETWEEN PARAMETERS 3 AND 5 = -.4899E+00
CORRELATION BETWEEN PARAMETERS 3 AND 6 = -.5309E+00
CORRELATION BETWEEN PARAMETERS 4 AND 5 = 0.9677E+00
CORRELATION BETWEEN PARAMETERS 4 AND 6 = 0.9692E+00
CORRELATION BETWEEN PARAMETERS 5 AND 6 = 0.9904E+00

********** REGRESSION SUMMARY **********

URANINE FROM KAS12 AND KAS05
KAS06, 399 M
DISTANCE: 200 M (KAS12), 141 M (KAS05)
NO OF FLOW PATHS: 2

FINAL ESTIMATE FOR PARAMETER 1 = 0.8289E-04
FINAL ESTIMATE FOR PARAMETER 2 = 0.3881E-02
FINAL ESTIMATE FOR PARAMETER 3 = 0.2136E+04
FINAL ESTIMATE FOR PARAMETER 4 = 0.4351E-04
FINAL ESTIMATE FOR PARAMETER 5 = 0.7235E-04
FINAL ESTIMATE FOR PARAMETER 6 = 0.2662E+03

****

REGRESSION STATISTICS

NO. OF OBSERVATIONS: 44

SUM OF SQUARED DIFFERENCES = 0.275E+03

ERROR VARIANCE = 0.725E+01

CORRELATION COEFFICIENT = .99188E+00

STANDARD ERROR FOR PARAMETER 1 = 0.288E-05
STANDARD ERROR FOR PARAMETER 2 = 0.281E-03
STANDARD ERROR FOR PARAMETER 3 = 0.103E+03
STANDARD ERROR FOR PARAMETER 4 = 0.176E-05
STANDARD ERROR FOR PARAMETER 5 = 0.573E-04
STANDARD ERROR FOR PARAMETER 6 = 0.103E+03

CORRELATION BETWEEN PARAMETERS 1 AND 2 = -.8117E+00
CORRELATION BETWEEN PARAMETERS 1 AND 3 = -.9559E+00
CORRELATION BETWEEN PARAMETERS 1 AND 4 = -.6636E-01
CORRELATION BETWEEN PARAMETERS 1 AND 5 = 0.5056E+00
CORRELATION BETWEEN PARAMETERS 1 AND 6 = 0.7580E+00
CORRELATION BETWEEN PARAMETERS 2 AND 3 = 0.8810E+00
CORRELATION BETWEEN PARAMETERS 2 AND 4 = 0.8137E-01
CORRELATION BETWEEN PARAMETERS 2 AND 5 = -.4342E+00
CORRELATION BETWEEN PARAMETERS 2 AND 6 = -.6660E+00
CORRELATION BETWEEN PARAMETERS 3 AND 4 = 0.6748E-01
CORRELATION BETWEEN PARAMETERS 3 AND 5 = -.5060E+00
CORRELATION BETWEEN PARAMETERS 3 AND 6 = -.7587E+00
CORRELATION BETWEEN PARAMETERS 4 AND 5 = -.6726E-01
CORRELATION BETWEEN PARAMETERS 4 AND 6 = -.1415E+00
CORRELATION BETWEEN PARAMETERS 5 AND 6 = 0.7425E+00

********** REGRESSION SUMMARY **********

RHENIUM FROM KAS08
KAS06, 217 M
DISTANCE: 301 M
NO OF FLOW PATHS: 1

FINAL ESTIMATE FOR PARAMETER 1 = 0.2946E-03
FINAL ESTIMATE FOR PARAMETER 2 = 0.8296E-02
FINAL ESTIMATE FOR PARAMETER 3 = 0.9634E+03

****

REGRESSION STATISTICS

NO. OF OBSERVATIONS: 61

SUM OF SQUARED DIFFERENCES = 0.201E+05

ERROR VARIANCE = 0.347E+03

CORRELATION COEFFICIENT = .97262E+00

STANDARD ERROR FOR PARAMETER 1 = 0.191E-04
STANDARD ERROR FOR PARAMETER 2 = 0.400E-02
STANDARD ERROR FOR PARAMETER 3 = 0.809E+02

CORRELATION BETWEEN PARAMETERS 1 AND 2 = -.3292E+00
CORRELATION BETWEEN PARAMETERS 1 AND 3 = -.5313E+00
CORRELATION BETWEEN PARAMETERS 2 AND 3 = 0.7694E+00

********** REGRESSION SUMMARY **********

RHENIUM FROM KAS08
KAS06, 217 M
DISTANCE: 381 M
NO OF FLOW PATHS: 1

FINAL ESTIMATE FOR PARAMETER 1 = 0.3727E-03
FINAL ESTIMATE FOR PARAMETER 2 = 0.1333E-01
FINAL ESTIMATE FOR PARAMETER 3 = 0.9639E+03

****

REGRESSION STATISTICS

NO. OF OBSERVATIONS: 61

SUM OF SQUARED DIFFERENCES = 0.201E+05

ERROR VARIANCE = 0.347E+03

CORRELATION COEFFICIENT = .97258E+00

STANDARD ERROR FOR PARAMETER 1 = 0.243E-04
STANDARD ERROR FOR PARAMETER 2 = 0.644E-02
STANDARD ERROR FOR PARAMETER 3 = 0.812E+02

CORRELATION BETWEEN PARAMETERS 1 AND 2 = -.3312E+00
CORRELATION BETWEEN PARAMETERS 1 AND 3 = -.5334E+00
CORRELATION BETWEEN PARAMETERS 2 AND 3 = 0.7706E+00

********** REGRESSION SUMMARY **********

RHENIUM FROM KAS08
KAS06, 217 M
DISTANCE: 301 M
NO OF FLOW PATHS: 2

FINAL ESTIMATE FOR PARAMETER 1 = 0.3694E-03
FINAL ESTIMATE FOR PARAMETER 2 = 0.2310E-02
FINAL ESTIMATE FOR PARAMETER 3 = 0.5074E+03
FINAL ESTIMATE FOR PARAMETER 4 = 0.1495E-03
FINAL ESTIMATE FOR PARAMETER 5 = 0.2401E-03
FINAL ESTIMATE FOR PARAMETER 6 = 0.7071E+03

****

REGRESSION STATISTICS

NO. OF OBSERVATIONS: 61

SUM OF SQUARED DIFFERENCES = 0.894E+04

ERROR VARIANCE = 0.163E+03

CORRELATION COEFFICIENT = .93588E+00

STANDARD ERROR FOR PARAMETER 1 = 0.182E-04
STANDARD ERROR FOR PARAMETER 2 = 0.109E-02
STANDARD ERROR FOR PARAMETER 3 = 0.492E+02
STANDARD ERROR FOR PARAMETER 4 = 0.368E-05
STANDARD ERROR FOR PARAMETER 5 = 0.891E-04
STANDARD ERROR FOR PARAMETER 6 = 0.909E+02

CORRELATION BETWEEN PARAMETERS 1 AND 2 = 0.2495E+00
CORRELATION BETWEEN PARAMETERS 1 AND 3 = -.2262E+00
CORRELATION BETWEEN PARAMETERS 1 AND 4 = -.5860E+00
CORRELATION BETWEEN PARAMETERS 1 AND 5 = 0.4895E+00
CORRELATION BETWEEN PARAMETERS 1 AND 6 = 0.5886E+00
CORRELATION BETWEEN PARAMETERS 2 AND 3 = 0.4927E+00
CORRELATION BETWEEN PARAMETERS 2 AND 4 = -.4067E+00
CORRELATION BETWEEN PARAMETERS 2 AND 5 = -.6228E-01
CORRELATION BETWEEN PARAMETERS 2 AND 6 = -.1250E+00
CORRELATION BETWEEN PARAMETERS 3 AND 4 = -.1003E+00
CORRELATION BETWEEN PARAMETERS 3 AND 5 = -.1853E+00
CORRELATION BETWEEN PARAMETERS 3 AND 6 = -.6931E+00
CORRELATION BETWEEN PARAMETERS 4 AND 5 = -.3159E+00
CORRELATION BETWEEN PARAMETERS 4 AND 6 = -.3816E+00
CORRELATION BETWEEN PARAMETERS 5 AND 6 = 0.4322E+00

********** REGRESSION SUMMARY **********

RHENIUM FROM KAS08
KAS06, 217 M
DISTANCE: 381 M
NO OF FLOW PATHS: 2

FINAL ESTIMATE FOR PARAMETER 1 = 0.4661E-03
FINAL ESTIMATE FOR PARAMETER 2 = 0.3506E-02
FINAL ESTIMATE FOR PARAMETER 3 = 0.5051E+03
FINAL ESTIMATE FOR PARAMETER 4 = 0.1896E-03
FINAL ESTIMATE FOR PARAMETER 5 = 0.3896E-03
FINAL ESTIMATE FOR PARAMETER 6 = 0.7077E+03

****

REGRESSION STATISTICS

NO. OF OBSERVATIONS: 61

SUM OF SQUARED DIFFERENCES = 0.894E+04

ERROR VARIANCE = 0.163E+03

CORRELATION COEFFICIENT = .93569E+00

STANDARD ERROR FOR PARAMETER 1 = 0.220E-04
STANDARD ERROR FOR PARAMETER 2 = 0.163E-02
STANDARD ERROR FOR PARAMETER 3 = 0.489E+02
STANDARD ERROR FOR PARAMETER 4 = 0.461E-05
STANDARD ERROR FOR PARAMETER 5 = 0.143E-03
STANDARD ERROR FOR PARAMETER 6 = 0.899E+02

CORRELATION BETWEEN PARAMETERS 1 AND 2 = 0.2353E+00
CORRELATION BETWEEN PARAMETERS 1 AND 3 = -.2269E+00
CORRELATION BETWEEN PARAMETERS 1 AND 4 = -.5685E+00
CORRELATION BETWEEN PARAMETERS 1 AND 5 = 0.4863E+00
CORRELATION BETWEEN PARAMETERS 1 AND 6 = 0.5750E+00
CORRELATION BETWEEN PARAMETERS 2 AND 3 = 0.4936E+00
CORRELATION BETWEEN PARAMETERS 2 AND 4 = -.3918E+00
CORRELATION BETWEEN PARAMETERS 2 AND 5 = -.5366E-01
CORRELATION BETWEEN PARAMETERS 2 AND 6 = -.1405E+00
CORRELATION BETWEEN PARAMETERS 3 AND 4 = -.9591E-01
CORRELATION BETWEEN PARAMETERS 3 AND 5 = -.1749E+00
CORRELATION BETWEEN PARAMETERS 3 AND 6 = -.6977E+00
CORRELATION BETWEEN PARAMETERS 4 AND 5 = -.3129E+00
CORRELATION BETWEEN PARAMETERS 4 AND 6 = -.3731E+00
CORRELATION BETWEEN PARAMETERS 5 AND 6 = 0.4212E+00

********** REGRESSION SUMMARY **********

RHENIUM FROM KAS08
KAS06, 399 M
DISTANCE: 190 M
NO OF FLOW PATHS: 1

FINAL ESTIMATE FOR PARAMETER 1 = 0.2097E-03
FINAL ESTIMATE FOR PARAMETER 2 = 0.3852E-02
FINAL ESTIMATE FOR PARAMETER 3 = 0.1192E+04

****

REGRESSION STATISTICS

NO. OF OBSERVATIONS: 80

SUM OF SQUARED DIFFERENCES = 0.831E+04

ERROR VARIANCE = 0.108E+03

CORRELATION COEFFICIENT = .90788E+00

STANDARD ERROR FOR PARAMETER 1 = 0.443E-05
STANDARD ERROR FOR PARAMETER 2 = 0.548E-03
STANDARD ERROR FOR PARAMETER 3 = 0.294E+02

CORRELATION BETWEEN PARAMETERS 1 AND 2 = 0.1109E+00
CORRELATION BETWEEN PARAMETERS 1 AND 3 = -.1803E+00
CORRELATION BETWEEN PARAMETERS 2 AND 3 = 0.4958E+00

********** REGRESSION SUMMARY **********

RHENIUM FROM KAS08
KAS06, 399 M
DISTANCE: 238 M
NO OF FLOW PATHS: 1

FINAL ESTIMATE FOR PARAMETER 1 = 0.2627E-03
FINAL ESTIMATE FOR PARAMETER 2 = 0.6044E-02
FINAL ESTIMATE FOR PARAMETER 3 = 0.1192E+04

****

REGRESSION STATISTICS

NO. OF OBSERVATIONS: 80

SUM OF SQUARED DIFFERENCES = 0.831E+04

ERROR VARIANCE = 0.108E+03

CORRELATION COEFFICIENT = .90788E+00

STANDARD ERROR FOR PARAMETER 1 = 0.555E-05
STANDARD ERROR FOR PARAMETER 2 = 0.860E-03
STANDARD ERROR FOR PARAMETER 3 = 0.294E+02

CORRELATION BETWEEN PARAMETERS 1 AND 2 = 0.1109E+00
CORRELATION BETWEEN PARAMETERS 1 AND 3 = -.1803E+00
CORRELATION BETWEEN PARAMETERS 2 AND 3 = 0.4958E+00

********** REGRESSION SUMMARY **********

RHENIUM FROM KAS08
KAS06, 399 M
DISTANCE: 190 M
NO OF FLOW PATHS: 2

FINAL ESTIMATE FOR PARAMETER 1 = 0.2732E-03
FINAL ESTIMATE FOR PARAMETER 2 = 0.2143E-02
FINAL ESTIMATE FOR PARAMETER 3 = 0.6497E+03
FINAL ESTIMATE FOR PARAMETER 4 = 0.1575E-03
FINAL ESTIMATE FOR PARAMETER 5 = 0.5503E-03
FINAL ESTIMATE FOR PARAMETER 6 = 0.5133E+03

****

REGRESSION STATISTICS

NO. OF OBSERVATIONS: 80

SUM OF SQUARED DIFFERENCES = 0.769E+04

ERROR VARIANCE = 0.104E+03

CORRELATION COEFFICIENT = .92173E+00

STANDARD ERROR FOR PARAMETER 1 = 0.419E-04
STANDARD ERROR FOR PARAMETER 2 = 0.121E-02
STANDARD ERROR FOR PARAMETER 3 = 0.276E+03
STANDARD ERROR FOR PARAMETER 4 = 0.137E-04
STANDARD ERROR FOR PARAMETER 5 = 0.387E-03
STANDARD ERROR FOR PARAMETER 6 = 0.277E+03

CORRELATION BETWEEN PARAMETERS 1 AND 2 = -.8489E+00
CORRELATION BETWEEN PARAMETERS 1 AND 3 = -.9819E+00
CORRELATION BETWEEN PARAMETERS 1 AND 4 = 0.9460E+00
CORRELATION BETWEEN PARAMETERS 1 AND 5 = 0.8303E+00
CORRELATION BETWEEN PARAMETERS 1 AND 6 = 0.9825E+00
CORRELATION BETWEEN PARAMETERS 2 AND 3 = 0.8709E+00
CORRELATION BETWEEN PARAMETERS 2 AND 4 = -.7660E+00
CORRELATION BETWEEN PARAMETERS 2 AND 5 = -.6018E+00
CORRELATION BETWEEN PARAMETERS 2 AND 6 = -.8605E+00
CORRELATION BETWEEN PARAMETERS 3 AND 4 = -.9566E+00
CORRELATION BETWEEN PARAMETERS 3 AND 5 = -.8615E+00
CORRELATION BETWEEN PARAMETERS 3 AND 6 = -.9957E+00
CORRELATION BETWEEN PARAMETERS 4 AND 5 = 0.8661E+00
CORRELATION BETWEEN PARAMETERS 4 AND 6 = 0.9530E+00
CORRELATION BETWEEN PARAMETERS 5 AND 6 = 0.8733E+00

********** REGRESSION SUMMARY **********

RHENIUM FROM KAS08
KAS06, 399 M
DISTANCE: 238 M
NO OF FLOW PATHS: 2

FINAL ESTIMATE FOR PARAMETER 1 = 0.3422E-03
FINAL ESTIMATE FOR PARAMETER 2 = 0.3365E-02
FINAL ESTIMATE FOR PARAMETER 3 = 0.6497E+03
FINAL ESTIMATE FOR PARAMETER 4 = 0.1974E-03
FINAL ESTIMATE FOR PARAMETER 5 = 0.8635E-03
FINAL ESTIMATE FOR PARAMETER 6 = 0.5134E+03

****

REGRESSION STATISTICS

NO. OF OBSERVATIONS: 80

SUM OF SQUARED DIFFERENCES = 0.769E+04

ERROR VARIANCE = 0.104E+03

CORRELATION COEFFICIENT = .92173E+00

STANDARD ERROR FOR PARAMETER 1 = 0.526E-04
STANDARD ERROR FOR PARAMETER 2 = 0.190E-02
STANDARD ERROR FOR PARAMETER 3 = 0.276E+03
STANDARD ERROR FOR PARAMETER 4 = 0.172E-04
STANDARD ERROR FOR PARAMETER 5 = 0.607E-03
STANDARD ERROR FOR PARAMETER 6 = 0.278E+03

CORRELATION BETWEEN PARAMETERS 1 AND 2 = -.8490E+00
CORRELATION BETWEEN PARAMETERS 1 AND 3 = -.9820E+00
CORRELATION BETWEEN PARAMETERS 1 AND 4 = 0.9460E+00
CORRELATION BETWEEN PARAMETERS 1 AND 5 = 0.8302E+00
CORRELATION BETWEEN PARAMETERS 1 AND 6 = 0.9826E+00
CORRELATION BETWEEN PARAMETERS 2 AND 3 = 0.8710E+00
CORRELATION BETWEEN PARAMETERS 2 AND 4 = -.7660E+00
CORRELATION BETWEEN PARAMETERS 2 AND 5 = -.6018E+00
CORRELATION BETWEEN PARAMETERS 2 AND 6 = -.8606E+00
CORRELATION BETWEEN PARAMETERS 3 AND 4 = -.9565E+00
CORRELATION BETWEEN PARAMETERS 3 AND 5 = -.8615E+00
CORRELATION BETWEEN PARAMETERS 3 AND 6 = -.9957E+00
CORRELATION BETWEEN PARAMETERS 4 AND 5 = 0.8661E+00
CORRELATION BETWEEN PARAMETERS 4 AND 6 = 0.9530E+00
CORRELATION BETWEEN PARAMETERS 5 AND 6 = 0.8733E+00

********** REGRESSION SUMMARY **********

RHENIUM FROM KAS08
KAS06, 448 M
DISTANCE: 181 M
NO OF FLOW PATHS: 1

FINAL ESTIMATE FOR PARAMETER 1 = 0.2005E-03
FINAL ESTIMATE FOR PARAMETER 2 = 0.3243E-02
FINAL ESTIMATE FOR PARAMETER 3 = 0.2316E+04

****

REGRESSION STATISTICS

NO. OF OBSERVATIONS: 72

SUM OF SQUARED DIFFERENCES = 0.275E+04

ERROR VARIANCE = 0.398E+02

CORRELATION COEFFICIENT = .98906E+00

STANDARD ERROR FOR PARAMETER 1 = 0.134E-05
STANDARD ERROR FOR PARAMETER 2 = 0.156E-03
STANDARD ERROR FOR PARAMETER 3 = 0.185E+02

CORRELATION BETWEEN PARAMETERS 1 AND 2 = 0.1852E-01
CORRELATION BETWEEN PARAMETERS 1 AND 3 = -.2291E+00
CORRELATION BETWEEN PARAMETERS 2 AND 3 = 0.5479E+00

********** REGRESSION SUMMARY **********

RHENIUM FROM KAS08
KAS06, 448 M
DISTANCE: 234 M
NO OF FLOW PATHS: 1

FINAL ESTIMATE FOR PARAMETER 1 = 0.2592E-03
FINAL ESTIMATE FOR PARAMETER 2 = 0.5421E-02
FINAL ESTIMATE FOR PARAMETER 3 = 0.2316E+04

****

REGRESSION STATISTICS

NO. OF OBSERVATIONS: 72

SUM OF SQUARED DIFFERENCES = 0.275E+04

ERROR VARIANCE = 0.398E+02

CORRELATION COEFFICIENT = .98906E+00

STANDARD ERROR FOR PARAMETER 1 = 0.173E-05
STANDARD ERROR FOR PARAMETER 2 = 0.261E-03
STANDARD ERROR FOR PARAMETER 3 = 0.185E+02

CORRELATION BETWEEN PARAMETERS 1 AND 2 = 0.1852E-01
CORRELATION BETWEEN PARAMETERS 1 AND 3 = -.2291E+00
CORRELATION BETWEEN PARAMETERS 2 AND 3 = 0.5479E+00

********** REGRESSION SUMMARY **********

RHENIUM FROM KAS08
KAS06, 448 M
DISTANCE: 181 M
NO OF FLOW PATHS: 2

FINAL ESTIMATE FOR PARAMETER 1 = 0.2099E-03
FINAL ESTIMATE FOR PARAMETER 2 = 0.4559E-02
FINAL ESTIMATE FOR PARAMETER 3 = 0.1334E+04
FINAL ESTIMATE FOR PARAMETER 4 = 0.1920E-03
FINAL ESTIMATE FOR PARAMETER 5 = 0.2115E-02
FINAL ESTIMATE FOR PARAMETER 6 = 0.9882E+03

****

REGRESSION STATISTICS

NO. OF OBSERVATIONS: 72

SUM OF SQUARED DIFFERENCES = 0.271E+04

ERROR VARIANCE = 0.410E+02

CORRELATION COEFFICIENT = .98921E+00

STANDARD ERROR FOR PARAMETER 1 = 0.372E-04
STANDARD ERROR FOR PARAMETER 2 = 0.157E-02
STANDARD ERROR FOR PARAMETER 3 = 0.196E+04
STANDARD ERROR FOR PARAMETER 4 = 0.156E-04
STANDARD ERROR FOR PARAMETER 5 = 0.205E-02
STANDARD ERROR FOR PARAMETER 6 = 0.193E+04

CORRELATION BETWEEN PARAMETERS 1 AND 2 = 0.4213E+00
CORRELATION BETWEEN PARAMETERS 1 AND 3 = -.9101E+00
CORRELATION BETWEEN PARAMETERS 1 AND 4 = -.6726E+00
CORRELATION BETWEEN PARAMETERS 1 AND 5 = 0.8978E+00
CORRELATION BETWEEN PARAMETERS 1 AND 6 = 0.9055E+00
CORRELATION BETWEEN PARAMETERS 2 AND 3 = -.6652E+00
CORRELATION BETWEEN PARAMETERS 2 AND 4 = 0.2614E+00
CORRELATION BETWEEN PARAMETERS 2 AND 5 = 0.5295E+00
CORRELATION BETWEEN PARAMETERS 2 AND 6 = 0.6735E+00
CORRELATION BETWEEN PARAMETERS 3 AND 4 = 0.3157E+00
CORRELATION BETWEEN PARAMETERS 3 AND 5 = -.9769E+00
CORRELATION BETWEEN PARAMETERS 3 AND 6 = -.9999E+00
CORRELATION BETWEEN PARAMETERS 4 AND 5 = -.3460E+00
CORRELATION BETWEEN PARAMETERS 4 AND 6 = -.3054E+00
CORRELATION BETWEEN PARAMETERS 5 AND 6 = 0.9759E+00

********** REGRESSION SUMMARY **********

RHENIUM FROM KAS08
KAS06, 448 M
DISTANCE: 234 M
NO OF FLOW PATHS: 2

FINAL ESTIMATE FOR PARAMETER 1 = 0.3347E-03
FINAL ESTIMATE FOR PARAMETER 2 = 0.3213E-02
FINAL ESTIMATE FOR PARAMETER 3 = 0.1130E+04
FINAL ESTIMATE FOR PARAMETER 4 = 0.2028E-03
FINAL ESTIMATE FOR PARAMETER 5 = 0.1783E-02
FINAL ESTIMATE FOR PARAMETER 6 = 0.1155E+04

****

REGRESSION STATISTICS

NO. OF OBSERVATIONS: 72

SUM OF SQUARED DIFFERENCES = 0.273E+04

ERROR VARIANCE = 0.414E+02

CORRELATION COEFFICIENT = .98913E+00

STANDARD ERROR FOR PARAMETER 1 = 0.702E-04
STANDARD ERROR FOR PARAMETER 2 = 0.119E-02
STANDARD ERROR FOR PARAMETER 3 = 0.922E+03
STANDARD ERROR FOR PARAMETER 4 = 0.377E-04
STANDARD ERROR FOR PARAMETER 5 = 0.141E-02
STANDARD ERROR FOR PARAMETER 6 = 0.930E+03

CORRELATION BETWEEN PARAMETERS 1 AND 2 = -.9080E+00
CORRELATION BETWEEN PARAMETERS 1 AND 3 = -.9975E+00
CORRELATION BETWEEN PARAMETERS 1 AND 4 = 0.9924E+00
CORRELATION BETWEEN PARAMETERS 1 AND 5 = 0.9515E+00
CORRELATION BETWEEN PARAMETERS 1 AND 6 = 0.9969E+00
CORRELATION BETWEEN PARAMETERS 2 AND 3 = 0.8939E+00
CORRELATION BETWEEN PARAMETERS 2 AND 4 = -.8669E+00
CORRELATION BETWEEN PARAMETERS 2 AND 5 = -.7714E+00
CORRELATION BETWEEN PARAMETERS 2 AND 6 = -.8894E+00
CORRELATION BETWEEN PARAMETERS 3 AND 4 = -.9970E+00
CORRELATION BETWEEN PARAMETERS 3 AND 5 = -.9671E+00
CORRELATION BETWEEN PARAMETERS 3 AND 6 = -.9998E+00
CORRELATION BETWEEN PARAMETERS 4 AND 5 = 0.9743E+00
CORRELATION BETWEEN PARAMETERS 4 AND 6 = 0.9970E+00
CORRELATION BETWEEN PARAMETERS 5 AND 6 = 0.9700E+00

********** REGRESSION SUMMARY **********

RHENIUM FROM KAS08
KAS06, SUM OF ALL LEVELS, 0–600 M
DISTANCE: 181 M
NO OF FLOW PATHS: 1

FINAL ESTIMATE FOR PARAMETER 1 = 0.1979E-03
FINAL ESTIMATE FOR PARAMETER 2 = 0.2481E-02
FINAL ESTIMATE FOR PARAMETER 3 = 0.7642E+03

****

REGRESSION STATISTICS

NO. OF OBSERVATIONS: 43

SUM OF SQUARED DIFFERENCES = 0.156E+04

ERROR VARIANCE = 0.389E+02

CORRELATION COEFFICIENT = .90466E+00

STANDARD ERROR FOR PARAMETER 1 = 0.515E-05
STANDARD ERROR FOR PARAMETER 2 = 0.453E-03
STANDARD ERROR FOR PARAMETER 3 = 0.214E+02

CORRELATION BETWEEN PARAMETERS 1 AND 2 = -.9914E-01
CORRELATION BETWEEN PARAMETERS 1 AND 3 = -.3181E+00
CORRELATION BETWEEN PARAMETERS 2 AND 3 = 0.5533E+00

********** REGRESSION SUMMARY **********

RHENIUM FROM KAS08
KAS06, SUM OF ALL LEVELS, 0–600 M
DISTANCE: 234 M
NO OF FLOW PATHS: 1

FINAL ESTIMATE FOR PARAMETER 1 = 0.2558E-03
FINAL ESTIMATE FOR PARAMETER 2 = 0.4147E-02
FINAL ESTIMATE FOR PARAMETER 3 = 0.7642E+03

****

REGRESSION STATISTICS

NO. OF OBSERVATIONS: 43

SUM OF SQUARED DIFFERENCES = 0.156E+04

ERROR VARIANCE = 0.389E+02

CORRELATION COEFFICIENT = .90466E+00

STANDARD ERROR FOR PARAMETER 1 = 0.665E-05
STANDARD ERROR FOR PARAMETER 2 = 0.758E-03
STANDARD ERROR FOR PARAMETER 3 = 0.214E+02

CORRELATION BETWEEN PARAMETERS 1 AND 2 = -.9921E-01
CORRELATION BETWEEN PARAMETERS 1 AND 3 = -.3182E+00
CORRELATION BETWEEN PARAMETERS 2 AND 3 = 0.5534E+00

********** REGRESSION SUMMARY **********

RHENIUM FROM KAS08
KAS06, SUM OF ALL LEVELS, 0–600 M
DISTANCE: 181 M
NO OF FLOW PATHS: 2

FINAL ESTIMATE FOR PARAMETER 1 = 0.2143E-03
FINAL ESTIMATE FOR PARAMETER 2 = 0.9075E-03
FINAL ESTIMATE FOR PARAMETER 3 = 0.3917E+03
FINAL ESTIMATE FOR PARAMETER 4 = 0.1301E-03
FINAL ESTIMATE FOR PARAMETER 5 = 0.1522E-01
FINAL ESTIMATE FOR PARAMETER 6 = 0.5883E+03

****

REGRESSION STATISTICS

NO. OF OBSERVATIONS: 43

SUM OF SQUARED DIFFERENCES = 0.128E+04

ERROR VARIANCE = 0.346E+02

CORRELATION COEFFICIENT = .92219E+00

STANDARD ERROR FOR PARAMETER 1 = 0.817E-05
STANDARD ERROR FOR PARAMETER 2 = 0.587E-03
STANDARD ERROR FOR PARAMETER 3 = 0.187E+03
STANDARD ERROR FOR PARAMETER 4 = 0.150E-03
STANDARD ERROR FOR PARAMETER 5 = 0.252E-01
STANDARD ERROR FOR PARAMETER 6 = 0.493E+03

CORRELATION BETWEEN PARAMETERS 1 AND 2 = 0.3799E-01
CORRELATION BETWEEN PARAMETERS 1 AND 3 = 0.9964E-01
CORRELATION BETWEEN PARAMETERS 1 AND 4 = -.3775E+00
CORRELATION BETWEEN PARAMETERS 1 AND 5 = 0.2370E+00
CORRELATION BETWEEN PARAMETERS 1 AND 6 = 0.4483E+00
CORRELATION BETWEEN PARAMETERS 2 AND 3 = 0.8646E+00
CORRELATION BETWEEN PARAMETERS 2 AND 4 = -.6168E+00
CORRELATION BETWEEN PARAMETERS 2 AND 5 = 0.5752E+00
CORRELATION BETWEEN PARAMETERS 2 AND 6 = 0.3621E+00
CORRELATION BETWEEN PARAMETERS 3 AND 4 = -.8589E+00
CORRELATION BETWEEN PARAMETERS 3 AND 5 = 0.8407E+00
CORRELATION BETWEEN PARAMETERS 3 AND 6 = 0.6458E+00
CORRELATION BETWEEN PARAMETERS 4 AND 5 = -.9630E+00
CORRELATION BETWEEN PARAMETERS 4 AND 6 = -.9409E+00
CORRELATION BETWEEN PARAMETERS 5 AND 6 = 0.9261E+00

********** REGRESSION SUMMARY **********

RHENIUM FROM KAS08
KAS06, SUM OF ALL LEVELS, 0–600 M
DISTANCE: 234 M
NO OF FLOW PATHS: 2

FINAL ESTIMATE FOR PARAMETER 1 = 0.1959E-03
FINAL ESTIMATE FOR PARAMETER 2 = 0.7035E-02
FINAL ESTIMATE FOR PARAMETER 3 = 0.3626E+03
FINAL ESTIMATE FOR PARAMETER 4 = 0.2826E-03
FINAL ESTIMATE FOR PARAMETER 5 = 0.2304E-02
FINAL ESTIMATE FOR PARAMETER 6 = 0.4385E+03

****

REGRESSION STATISTICS

NO. OF OBSERVATIONS: 43

SUM OF SQUARED DIFFERENCES = 0.143E+04

ERROR VARIANCE = 0.388E+02

CORRELATION COEFFICIENT = .91601E+00

STANDARD ERROR FOR PARAMETER 1 = 0.170E-03
STANDARD ERROR FOR PARAMETER 2 = 0.157E-01
STANDARD ERROR FOR PARAMETER 3 = 0.494E+03
STANDARD ERROR FOR PARAMETER 4 = 0.393E-04
STANDARD ERROR FOR PARAMETER 5 = 0.252E-02
STANDARD ERROR FOR PARAMETER 6 = 0.627E+03

CORRELATION BETWEEN PARAMETERS 1 AND 2 = -.6952E+00
CORRELATION BETWEEN PARAMETERS 1 AND 3 = 0.9054E+00
CORRELATION BETWEEN PARAMETERS 1 AND 4 = 0.7452E+00
CORRELATION BETWEEN PARAMETERS 1 AND 5 = -.8454E+00
CORRELATION BETWEEN PARAMETERS 1 AND 6 = -.9711E+00
CORRELATION BETWEEN PARAMETERS 2 AND 3 = -.4576E+00
CORRELATION BETWEEN PARAMETERS 2 AND 4 = -.8968E+00
CORRELATION BETWEEN PARAMETERS 2 AND 5 = 0.3530E+00
CORRELATION BETWEEN PARAMETERS 2 AND 6 = 0.6340E+00
CORRELATION BETWEEN PARAMETERS 3 AND 4 = 0.6701E+00
CORRELATION BETWEEN PARAMETERS 3 AND 5 = -.9624E+00
CORRELATION BETWEEN PARAMETERS 3 AND 6 = -.9736E+00
CORRELATION BETWEEN PARAMETERS 4 AND 5 = -.5705E+00
CORRELATION BETWEEN PARAMETERS 4 AND 6 = -.7738E+00
CORRELATION BETWEEN PARAMETERS 5 AND 6 = 0.9206E+00

APPENDIX D Groundwater flow measurements at Äspö with the dilution method

GEOSIGMA AB

Client: SKB

REPORT
ID-no: GRAP 91003
Date: 1991-11-25

GROUNDWATER FLOW MEASUREMENTS AT ÄSPÖ WITH THE DILUTION METHOD

Thomas Ittner
Erik Gustafsson
Peter Andersson
Carl-Olof Eriksson

GEOSIGMA AB
UPPSALA, SWEDEN

November 1991

ABSTRACT

Tracer dilution measurements were performed to determine the groundwater flow in packed–off borehole sections during the pre–investigation phase of the Äspö Hard Rock Laboratory. The measurements were performed in 12 boreholes at depths varying from 40 m down to 800 m. The groundwater flow measurements were made within 22 different packed–off sections in fixed borehole installations.

The measurements were made during four periods in 1989 and 1990 both under natural and induced pump gradient. Pump gradient was established during two occasions in different boreholes. The results show that ground–water flow in fractured rock usually is enhanced by pumping, but the overall flow picture is complex. The hydraulic contact between fracture zones are discussed and compared to the conceptual model of the area.

SUMMARY AND CONCLUSIONS

In summary, the flow measurements performed during different hydraulic conditions such as pumping in different boreholes and natural gradient conditions give information not only about the actual flow rates but also about the inter-connections between different zones. The measurements described in this report have been used to verify or refute the conceptual model of the conductive structures at Äspö given by Wikberg et al., 1991.

The conclusion that can be drawn from the measurements performed during natural gradient conditions (NG1 and NG2) is that the values are consistent when comparing the two sets of data although there were only four measurements made during NG1. The only exception is section KAS06-1 (F1) where the measured flow rates differ by a factor 2. One possible explanation for this is that NG1 was performed very shortly after the finish of the long term pumping test LPT-1 and therefore still might be in a transient stage.

The flow measurements performed during pumping in KAS07 (LPT-1) and KAS06 (LPT-2) indicate that the conceptual model of the fracture zones at Äspö, suggested by Wikberg et al., 1991, is correct. However, there are still a few unresolved questions to be answered. There are some sections not responding to the pumping as expected and the reasons for this may be clarified with a combined analysis of the flow responses, the tracer tests and the pressure responses. The main conclusions from the flow measurements during pumping are:

1. Zones NNW-1, NNW-2, and NE-1 are dominating hydraulic structures with high flow rates. Zone NE-2 is well connected to zones NNW-1 and NNW-2.

2. Zone EW-5 also responds well to the pumping but the responses are not as good as in the above mentioned zones.

3. Zone EW-3 seem to isolate the southern part of Äspö from the central parts when pumping in EW-3 during LPT-2. This interpretation is based on the responses in Zone NE-1 which are low during LPT-2.

4. The possibly existing Zone EW-X may not be confirmed or refuted based on the flow measurements as only one section that is interpreted to intersect EW-X has been measured.

5. The structures NW-1 and EW-1 on the northern part of Äspö have relatively high natural flow rates. However, these structures have not been measured during pumping so nothing can be concluded about interconnections with the southern part of Äspö.

CONTENTS

ABSTRACT i

SUMMARY AND CONCLUSIONS ii

CONTENTS iii

1. INTRODUCTION 1

1.1 BACKGROUND AND PURPOSE 1

1.2 SITE CHARACTERIZATION 1

2. EXPERIMENTAL SETUP 4

2.1 GROUNDWATER FLOW MEASUREMENTS 4

2.2 TECHNICAL DESIGN 4

2.3 INJECTION AND MONITORING OF TRACERS 9

3. THEORY 11

3.1 THEORETICAL BACKGROUND 11

3.2 ERROR ESTIMATES 11

4. MEASUREMENTS PERFORMED 13

4.1 DILUTION MEASUREMENTS 13

4.2 SUPPORTING MEASUREMENTS 19

5. RESULTS 20

6. DISCUSSION AND CONCLUSIONS 28

6.1 FLOW IN RELATION TO THE CONDUCTIVE STRUCTURES AT ÄSPÖ 28

6.2 FLOW IN RELATION TO TRANSMISSIVITY AND DEPTH 32

7. REFERENCES 36

1. INTRODUCTION

1.1 BACKGROUND AND PURPOSE

The construction of an underground research facility for storage of spent nuclear fuel in Sweden has started. The underground rock laboratory will be placed at 500 m depth below the island of Äspö situated at the Baltic coast about 20 km north of the city of Oskarshamn in southern Sweden (Gustafson et al., 1989). Within the rather extensive pre-investigations, measurements of groundwater flow have been carried out. The flow measurements were made during four occasions from summer 1989 to autumn 1990 both during natural flow conditions and during pumping.

The main purpose of measuring groundwater flow within the boreholes was to use the data to interpret the flow path distribution in the bedrock at Äspö and use the data to improve the conceptual model of the fracture zones. The two first performed measurements also had the purpose to select borehole sections suitable for injection during the planned tracer test (LPT-2).

1.2 SITE CHARACTERIZATION

The bedrock at the study site consists of precambrian crystalline rocks such as granite, aplite and dolerite. There are several fracture zones intersecting the study site, most of them are steeply dipping but there are also some sub-horizontal fractures intersecting the area, see Figure 1.1. The predominant fracture zones intersecting the core boreholes with their fixed packed-off sections for dilution measurements at southern Äspö are discussed in Wikberg et al., 1991.

The Äspö site was, in spring 1989, provided with four extra core boreholes so during the first two sets of measurements (LPT-1 and NG1) boreholes KAS02 - KAS08 were available for measurements. During spring 1990 six additional boreholes were drilled and equipped so that during NG2 and LPT-2 the boreholes KAS02 - KAS14 were available for measurements. Borehole KAS03 is situated more periphery to the target area but is hydraulically connected with the boreholes within the target area on southern Äspö. Boreholes KAS01 and KAS10 are both shallow observation wells and therefore not used for the dilution measurements. A summary of the boreholes and borehole sections used for the groundwater flow measurements is presented in Table 1.1.

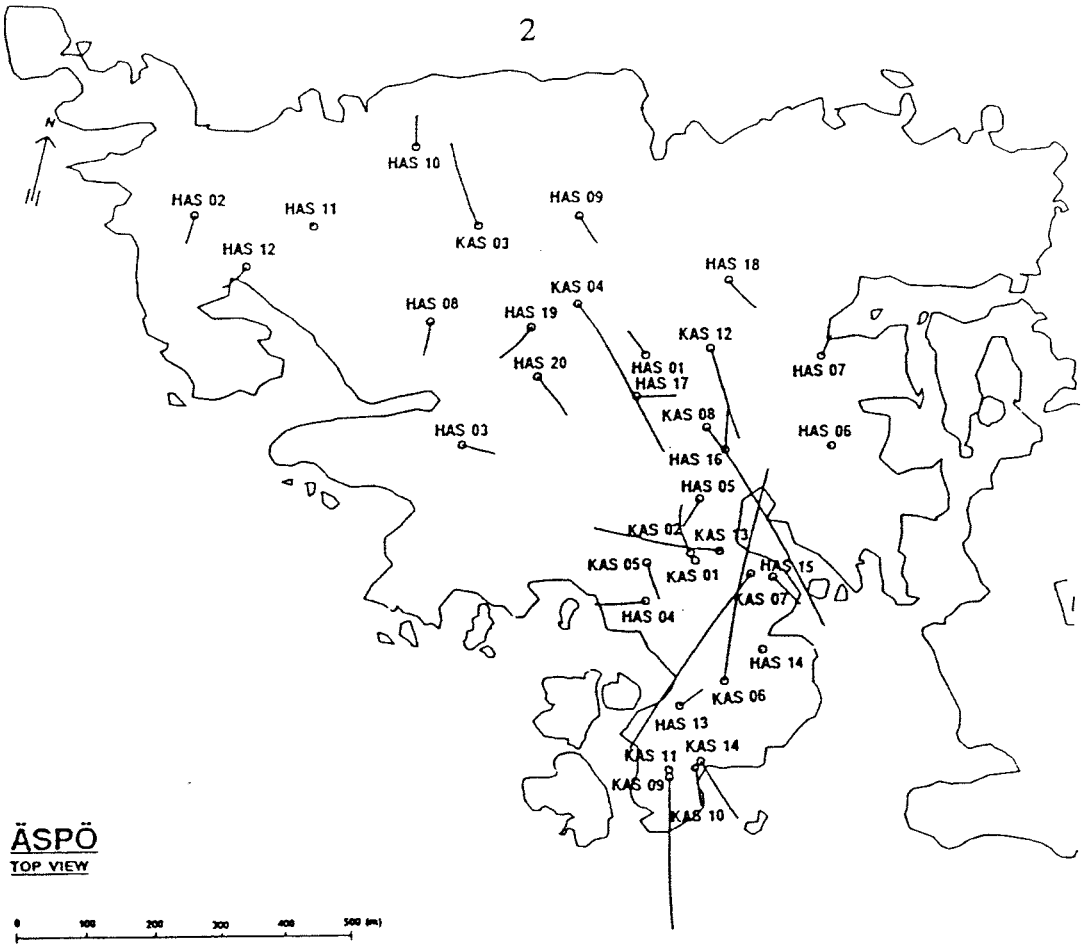

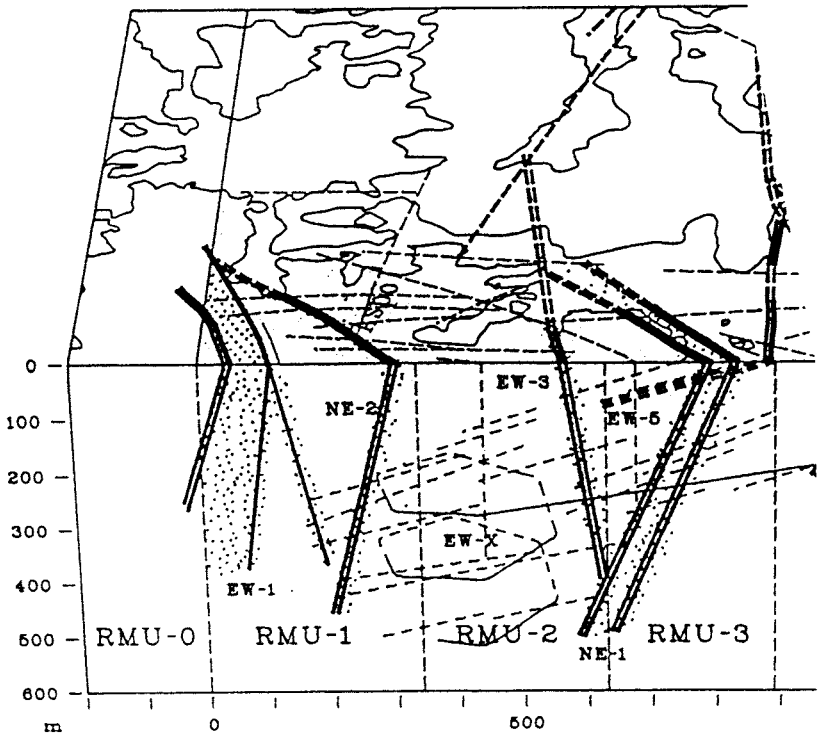

Figure 1.1 Borehole locations and major fracture zones on Äspö. Lines pointing out from boreholes (top) indicate the projection at ground surface. (Wikberg et al., 1991)

Table 1.1 Configuration of boreholes and sections on Äspö equipped for dilution measurements.

Borehole-Section	Code	Depth[1] (m)	Section length (m)	Borehole diameter (m)	Borehole length (m)	inc[2]
KAS02-4*	B4	309 - 345	36	0.056	924	84
KAS02-2	B2	800 - 854	54			
KAS03-3	C5	107 - 152	45	0.056	1002	83
KAS03-2*	C2	533 - 626	93			
KAS04-2	D2	332 - 392	60	0.056	481	60
KAS05-3*	E3	320 - 380	60	0.076	549	85
KAS05-1*	E1	440 - 549	109			
KAS06-5*	F5	191 - 249	58	0.056	602	60
KAS06-1*	F1	431 - 500	69			
KAS07-4*	J4	191 - 290	99	0.056	604	59
KAS07-1*	J1	501 - 604	103			
KAS08-3*	M3	140 - 200	60	0.056	601	59
KAS08-1*	M1	503 - 601	98			
KAS09-4*	AD	116 - 150	34	0.056	450	60
KAS11-5	CE	47 - 64	17	0.056	249	89
KAS11-2	CB	153 - 183	30			
KAS12-3	DC	235 - 378	43	0.056	380	70
KAS12-2*	DB	279 - 330	51			
KAS13-4	ED	151 - 190	39	0.056	407	62
KAS13-3	EC	191 - 220	29			
KAS14-4	FD	131 - 138	7	0.056	212	61
KAS14-2	FB	147 - 175	28			

[1] Borehole distance from casing top, section isolated by packers.

[2] Inclination in degrees to the horizontal plane. Borehole orientation is shown in Figure 1.1.

* Chemical analysis of section water available, sampled in May and June 1990. (Nilsson, 1991)

2. EXPERIMENTAL SETUP

2.1 GROUNDWATER FLOW MEASUREMENTS

Measurements of groundwater flow in packed-off borehole sections down to about 800 m depth below the ground surface were performed. A measurement of groundwater flow in a borehole section is based on the dilution of an added chemical substance that is mixed in the groundwater and thereafter its amount in the water is determined at regular intervals. The decrease of tracer concentration as a function of time is proportional to the groundwater flow through the section (Figure 2.1). This way of measuring groundwater flow is termed dilution technique. The borehole section lengths are chosen from the estimated widths of the water conducting fracture zones intersecting the borehole and varies from 7 to 145 m. The major part of the flow measurements were performed within the equipped boreholes in the southern part of Äspö.

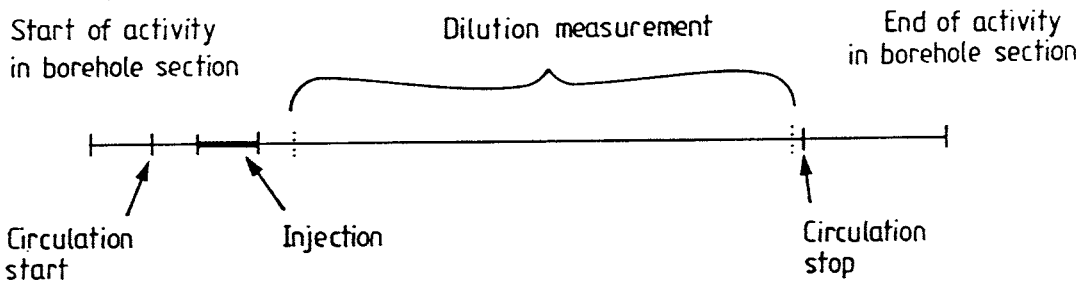

Figure 2.1 General working routine (time sequence) for dilution measurements.

2.2 TECHNICAL DESIGN

The Äspö core boreholes, with prefix KAS, are all of telescope type. The uppermost part, the top 100 m, is enlarged to a diameter of 165 mm. Below the enlarged part the boreholes have a diameter of 56 mm, except for borehole KAS05 which has a diameter of 76 mm (Table 1.1). This type of dilution measurement demands a special type of borehole equipment. Therefore, the existing borehole equipment on Äspö was slightly modified to allow the performance of dilution measurements (Gustafsson, 1988). The borehole equipment was complemented with extra tubing, two tubes emerging in each section chosen for measurement, to enable circulation of the section water and to get the tracer thoroughly mixed.

The circulation pumps, usually two or three pumps connected in series, are placed below the groundwater table within a PEM tube (with an inner diameter of 54 mm) in the enlarged upper part of the borehole, see Figure 2.2. The PEM tube is connected to the borehole section through a thin Nylon tube (inner diameter 6 mm). In connection with starting the circulation in the borehole section, section water is initially brought up to the ground surface

with a vacuum pump in the return/downward tube. This is made so that no air will be injected into the section during start of circulation. In some of the boreholes the distance between the groundwater level and the ground surface is too large for pumping. When this situation occurs, a special by–pass tube is used. This by–pass tube (Figure 2.3) is connected to the circulation tube system well below the groundwater table and when water is injected, the level will rise up to the ground surface. When the section water is circulating it will pass the trace element unit on the ground surface where the circulation flow rate and pressure is registered, see Figures 2.2 and 2.4. Sampling and injection of tracers are also made here. The downward circulation flow outlet is situated in the bottom of the borehole section and the inlet, to the circulation pumps is situated in the uppermost part of the section. This construction is made in order to achieve good mixing of the tracer in the section water.

Due to the relatively low circulation flow rate and small amounts of tracer solution (4–5 liters) the hydraulic head in the borehole section will remain constant during circulation. A high circulation flow rate would cause frictional losses. The pressure registration, however, will register an underpressure during circulation due to the position of the pressure transducer in the PEM–tube just below the circulation pumps.

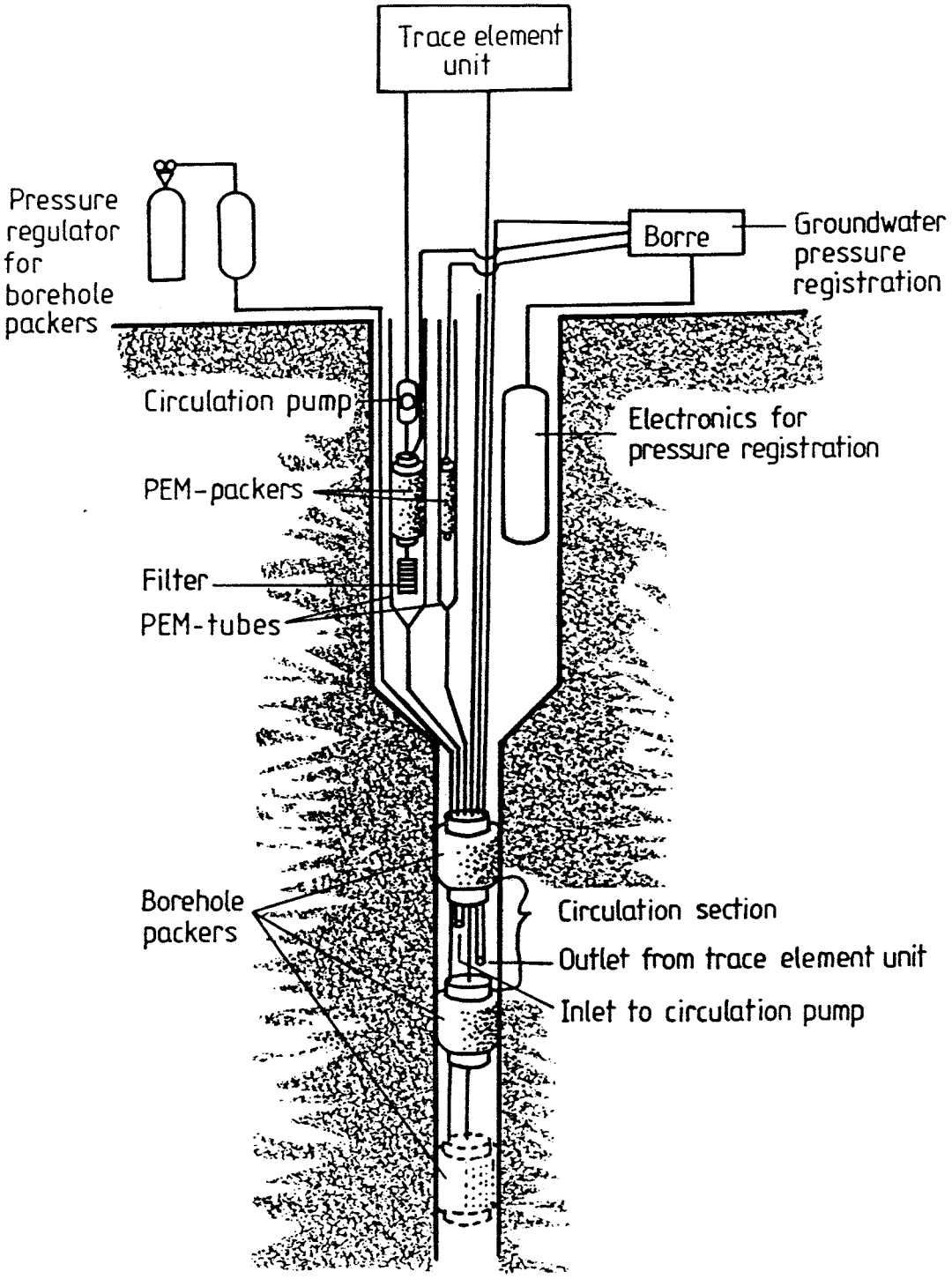

Figure 2.2 Schematic of borehole instrumentation during the dilution measurements. Details are shown in Figure 2.4.

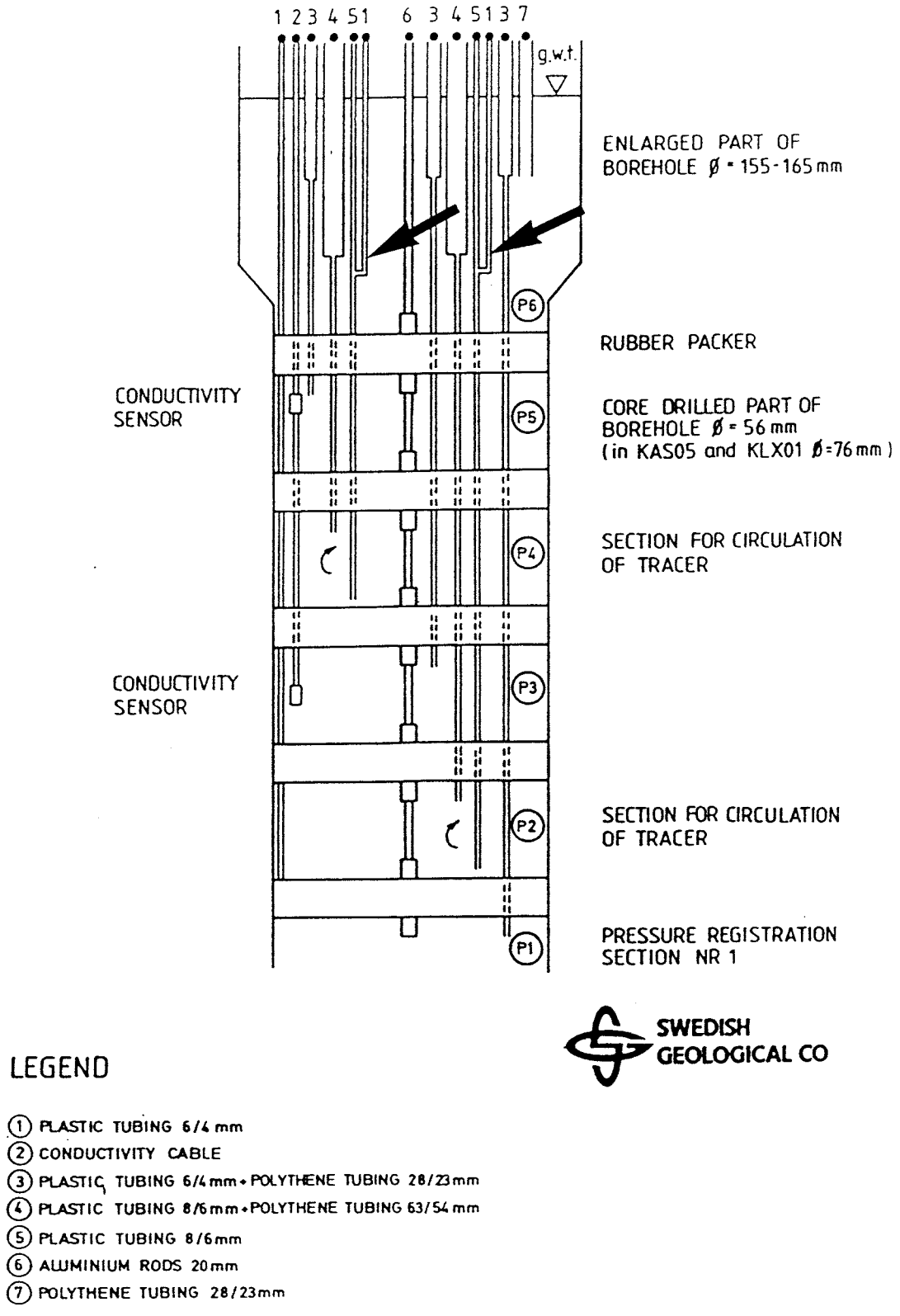

Figure 2.3 Principal instrumentation of core boreholes at Äspö. The arrows indicate the by-pass tubes, cf. Section 2.2.

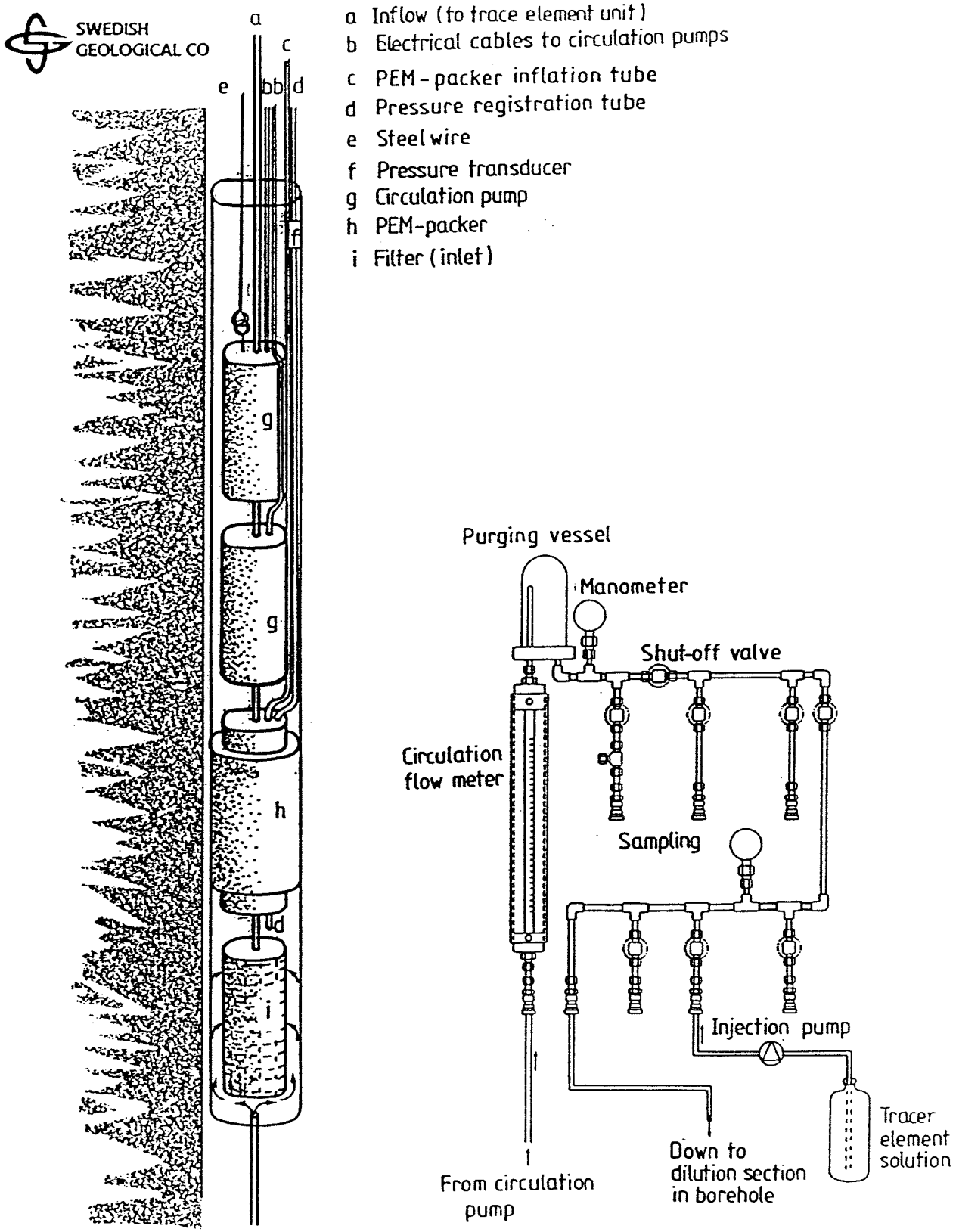

Figure 2.4 Details of borehole equipment (left) and tracer unit (right) for dilution measurements, cf. Figure 2.2.

2.3 INJECTION AND MONITORING OF TRACERS

A small amount of a tracer is injected into the circulating system. The injection is made during one circulation cycle e.g. the time necessary for the water volume in the section to pass through the tracer unit on ground surface. The circulation time is determined by dividing the volume of the borehole section with the reading of the circulation flow rate on the flow meter. The injection of tracer during one circulation cycle is important in order to achieve an even dilution sequence of the tracer in the borehole section.

In order to get a sufficient number of samples evenly distributed over the measurement period, automatic samplers were installed. Samples were taken every second hour during the first 48 hours and then one sample every 4 hours up to six days after start of measurement and thereafter one sample every 8 hour. The measurement period varied from 5–6 days up to 10–12 days depending on how fast the tracer was diluted.

Large sample volumes may introduce errors in the flow calculation if the groundwater flow is small. Therefore, the sample volumes were limited to about 10 – 15 ml. This "extra" discharge of water from the borehole section was measured and corrected for in all dilution measurements.

In the first set of measurements (LPT–1) short nylon tubes (0.1 m) were used between sampler and sampling tubes. In these tubes, remnants from the previous sample was remaining until next sample was taken, so the next sample was "diluted/concentrated" with a few ml of the previous sample. The results had to be corrected for this afterwards. This problem was eliminated during the following measurements by reconstruction of the sampling equipment.

The tracer used in all the dilution measurements on Äspö, was Uranine (Sodium Fluorescein). Before tracer injection a preliminary determination of the Uranine content in the borehole section water was made. In most of the borehole sections the background content was in the order of 1–10 ppb but in some sections the content of Uranine was as high as 1–2 ppm. This background content of Uranine originates from the drilling of the borehole, as Uranine is used as a marker of the drilling fluid, and also from earlier dilution tests. Therefore, in some of the dilution measurements during LPT–2 no extra tracer was injected due to the high background concentrations, cf. Ittner et al., 1991a,b,c,d and Figure 5.1, plot F.

The sorption and desorption behavior of Uranine depending on concentration in the water–rock systems has been documented both in field and laboratory investigations (Gustafsson and Klockars, 1984; Klockars, 1989).

The intention was to increase the content of Uranine in the circulating section water up to about 1 ppm. Usually 50 – 100 mg of Uranine was enough to achieve this. The injection fluid used was mostly pumped up section water or, in a few cases, ordinary tap water.

During LPT–2, each tracer injection was used as a dilution measurement Gustafsson et al., 1991). The Uranine concentration in the sections was then much higher, 600–900 ppm. Also other non–sorbing, radioactive tracers, such as Indium (In–114), Iodine (I–131) and Rhenium (Re–186) was used during LPT–2. The radiotracers were injected with distilled water.

3. THEORY

3.1 THEORETICAL BACKGROUND

The dilution method relies upon the use of a tracer which is introduced as a homogeneous pulse into a borehole section sealed off by rubber packers. The tracer will be diluted due to the native groundwater from the fracture zone flowing through the borehole. The dilution of the tracer introduced is proportional to the water flow through the borehole section and thus to the groundwater flow in the fracture zone.

Within the borehole section, the tracer must be completely mixed at every moment and the concentration is measured as a function of time.

The groundwater flow rate through the borehole section is calculated from the water volume of the section and the dilution as a function of time according to Equation (1) which is the solution of the equation of continuity for the dilution of a homogeneously distributed tracer solution in a constant volume, V, at steady state groundwater flow.

$$Q = -V \ln(C/C_0)/t \qquad (1)$$

where
Q = groundwater flow rate (m^3/s)
V = volume of water in the borehole section (m^3)
C = tracer concentration at time t
C_0= initial tracer concentration
t = time (s)

The dilution as a function of time is obtained from a semi-logarithmic diagram of normalized tracer concentration versus time. In the ideal case the relation is linear. (Gustafsson, 1986)

It is important to notice that the values given by Equation (1) only represents the flow through the borehole section which may differ significantly from the flow through the undisturbed rock. The relation between the flow through the borehole section and the flow in the rock has been investigated by several authors (Gustafsson, 1986; Rhén et al., 1991a). There are two factors which must be taken into account, namely the contraction factor, α, and the angle between borehole and flow direction. For further details see above mentioned authors.

3.2 ERROR ESTIMATES

The errors involved in the determination of groundwater flow with the dilution method may be divided into two categories, instrumental errors and "hydrologic" errors. The instrumental errors, which in this case is errors in the analyses of Uranine content are estimated to be less than 5%. Larger errors may occur when precipitations or other solids, e.g. drilling debris, are

present in the samples or if the samples are exposed to direct sunlight. Drilling debris or precipitations may cause some of the tracer to sorb onto the particles. However, at Äspö most of the borehole sections have water with low particle content. There are only a few sections where dark precipitations occur. The exposure of the samples to sunlight, which may cause a significant decrease of concentration, was avoided by storing the samples in dark boxes.

The samples taken to determine the decrease of tracer concentration, will also contribute to the total flow through the section since the volume removed from the borehole section contains tracer. Therefore, the removed amounts of tracer is measured in each dilution measurement and, if necessary, taken into account when the flow is calculated. In most cases, the error introduced by neglecting the sample volumes is less than 1%. Corrections for the sample volumes has therefore only been made in 2 of the 68 dilution measurements described in this report.

A very important factor for the calculation of the flow through the packed-off section is to determine the section volume correctly (see Equation 1). Since the total section volume, including volumes in the tubing and equipment, is directly proportional to the groundwater flow, special efforts have been assigned to make the determination of the section volumes as exact as possible.

The "hydrologic" error is more difficult to estimate. The presence of the borehole itself causes a disturbance of the flow distribution. The presence of several water conducting fractures within the measured borehole section may cause short-circuits between fractures with different hydraulic heads resulting in enhanced flow rates. At Äspö, the boreholes have been sectionized based on the concept that each section should represent one hydraulic unit (fracture zone) and therefore the hydraulic heads in different fractures within the sections should be approximately the same. The flow in the fractures also has spatial differences due to the uneven distribution of fracture minerals and other heterogeneities. Consequently, if a borehole penetrates a highly conductive fracture in a location where the fracture minerals have high abundance it will show lower values of groundwater flow than if the borehole had penetrated a "flow channel" in the fracture.

4. MEASUREMENTS PERFORMED

4.1 DILUTION MEASUREMENTS

The measurements were performed during four different occasions. The first set of measurements were made during pump gradient in August 1989 (LPT-1). The second and third set of measurements were made in September 1989 and during June - August 1990 both during natural gradient (NG1 and NG2). The last set of measurements were made in October 1990 during pump gradient (LPT-2). The measurements are summarized in Tables 4.1 and 4.2 below.

All 22 borehole sections available for dilution measurements have been measured at least once. In total, 68 dilution measurements have been performed.

Table 4.1 Flow measurements performed at Äspö.

Event	Pump capacity (l/s)	Time	No of meas. sections	No of measurements
LPT-1	125	890807-890901	9	9
NG1	N	890925-891008	4	4
NG2	N	900626-900816	22	22
LPT-2	135	900925-901218	10	33

N = Measurement during natural groundwater gradient

During the first long term pump test (LPT-1) pumping was performed in borehole KAS07 and during the second long term pump test (LPT-2) borehole KAS06 was chosen for pumping.

Table 4.2 Summary of flow measurements performed in each borehole section at Äspö.

Borehole-section	Code	Section depth/length (m)		Measurements
KAS02-4	B4	309-345	36	A - C D
KAS02-2	B2	800-854	54	A - C D
KAS03-5	C5	107-252	145	- - C -
KAS03-2	C2	533-626	93	- - C -
KAS04-2	D2	332-392	60	A - C -
KAS05-3	E3	320-380	60	A - C D
KAS05-1	E1	440-549	109	A B C D
KAS06-5	F5	191-249	58	A B C d
KAS06-1	F1	431-500	69	A B C d
KAS07-4	J4	191-290	99	a - C D
KAS07-1	J1	501-604	103	a - C -
KAS08-3	M3	140-200	60	A - C D
KAS08-1	M1	503-601	98	A B C D
KAS09-4*	AD	116-150	34	C -
KAS11-5*	CE	47-64	17	C -
KAS11-2*	CB	153-183	30	C -
KAS12-3*	DC	235-278	43	C -
KAS12-2*	DB	279-330	51	C D
KAS13-4*	ED	151-190	39	C -
KAS13-3*	EC	191-220	29	C D
KAS14-4*	FD	131-138	7	C -
KAS14-2*	FB	147-175	28	C D

A = (LPT-1) August 1989, B = (NG1) September 1989
C = (NG2) June-August 1990, D = (LPT-2) October 1990.
* = Drilled during spring 1990
a = Pump hole during LPT-1, d = pump hole during LPT-2.

The first set of measurements was performed during the long term pumping in borehole KAS07. The pumping was started on July 10th and lasted for about 8 weeks. Dilution measurements were performed with the purpose to select borehole sections suitable for injection during the planned tracer test (LPT–2).

The dilution measurements were performed in 9 sections starting about 4 weeks after start of pumping when near steady state conditions had been obtained. The measurements were performed during 3 – 14 days depending on the dilution rate. A summary of the measurements performed during LPT–1 is presented in Table 4.3.

Table 4.3 Measurement specifics during LPT–1.

Borehole –section	Code	Start – Stop measurement	Dur[1] (h)	D.p.[2]	Start – Stop circulation
KAS02–4	B4	890811 – 890818	167	26	890807 – 890818
KAS02–2	B2	890810 – 890818	180	34	890807 – 890818
KAS03–5	C5	n m			
KAS03–2	C2	n m			
KAS04–2	D2	890826 – 890901	127	23	890825 – 890901
KAS05–3	E3	890808 – 890816	188	34	890803 – 890816
KAS05–1	E1	890818 – 890831	312	47	890816 – 890831
KAS06–5	F5	890821 – 890824	57	21	890820 – 890824
KAS06–1	F1	890821 – 890824	61	24	890820 – 890824
KAS07		pump hole during LPT–1			
KAS08–3	M3	890818 – 890901	321	58	890817 – 890901
KAS08–1	M1	890807 – 890817	224	52	890806 – 890817

1 = Duration of dilution measurement
2 = Number of data points
n m = no measurement

The second set of measurements was made about 4 weeks after the finish of the pumping during LPT–1 with the purpose to study the possible changes of groundwater flow rates compared to LPT–1 and to serve as basis for the design of the planned tracer test (LPT–2). The measurements were made in 4 of the sections which also were measured during LPT–1. The hydraulic heads in these sections and most of the other sections in the area were the same or almost the same as before start of LPT–1. Therefore, natural gradient conditions were assumed during this flow measurement. The duration of the tests were in the range 22 – 61 hours, see Table 4.4.

Table 4.4 Measurement specifics during NG1.

Borehole -section	Code	Start - Stop measurement	Dur[1] (h)	D.p.[2]	Start - stop circulation
KAS02-4	B4	n m			
KAS02-2	B2	n m			
KAS03-5	C5	n m			
KAS03-2	C2	n m			
KAS04-2	D2	n m			
KAS05-3	E3	n m			
KAS05-1	E1	891001 - 891010	239	22	890926 - 891010
KAS06-5	F5	890927 - 891010	318	53	890926 - 891010
KAS06-1	F1	890928 - 891010	313	49	890926 - 891010
KAS07-4	J4	n m			
KAS07-1	J1	n m			
KAS08-3	M3	n m			
KAS08-1	M1	890927 - 891010	326	61	890926 - 891010

1 = Duration of dilution measurement
2 = Number of data points
n m = no measurement

In the third round of measurements, all 22 sections available were measured with the purpose of improving the conceptual model of the fracture zones at Äspö and to determine the natural flow distribution within the zones. The measurements lasted for 2–10 days, see Table 4.5. Note that boreholes KAS09 – KAS14 were drilled during spring 1990, cf. section 1.2.

Table 4.5 Measurement specifics during NG2.

Borehole -section	Code	Start - Stop measurement	Dur[1] (h)	D.p.[2]	Start - Stop circulation
KAS02-4	B4	900627 - 900701	100	25	900626 - 900705
KAS02-2	B2	900628 - 900702	100	15	900626 - 900705
KAS03-5	C5	900719 - 900722	90	27	900718 - 900730
KAS03-2	C2	900720 - 900723	80	14	900718 - 900726
KAS04-2	D2	900731 - 900806	150	13	900728 - 900808
KAS05-3	E3	900629 - 900706	200	28	900626 - 900706
KAS05-1	E1	900629 - 900706	200	31	900626 - 900706
KAS06-5	F5	900709 - 900715	160	20	900707 - 900715
KAS06-1	F1	900709 - 900715	160	19	900707 - 900715
KAS07-4	J4	900709 - 900717	199	25	900706 - 900717
KAS07-1	J1	900708 - 900717	180	26	900706 - 900717
KAS08-3	M3	900629 - 900707	210	36	900628 - 900707
KAS08-1	M1	900628 - 900707	200	37	900628 - 900707
KAS09-4	AD	900727 - 900808	300	51	900727 - 900808
KAS11-5	CE	900718 - 900726	190	35	900716 - 900726
KAS11-2	CB	900717 - 900719	55	22	900716 - 900726
KAS12-3	DC	900708 - 900716	198	23	900705 - 900716
KAS12-2	DB	900708 - 900716	180	18	900705 - 900716
KAS13-4	ED	900806 - 900816	240	38	900805 - 900816
KAS13-3	EC	900808 - 900816	200	28	900806 - 900816
KAS14-4	FD	900719 - 900725	150	31	900717 - 900727
KAS14-2	FB	900718 - 900727	210	41	900717 - 900727

1 = Duration of dilution measurement
2 = Number of data points

The last set of measurements were made during the pumping for the radially converging tracer test (LPT-2). The purpose of these measurements was to use them to determine the mass release versus time during the injection of tracers. Some of the measurements were also made in order to select injection sections for LPT-2. Totally 10 sections were measured and the 6 sections used as injection sections during LPT-2 were measured several times, see Table 4.6.

Table 4.6 Measurement specifics during LPT-2.

Borehole -section	Code	Start - Stop measurement	Dur[1] (h)	D.p.[2]	Start - Stop circulation
KAS02-4	B4	900927 - 900928	55	6	900924 - 900928
		901003 - 901110	900	65	901002 - 901110
		- 910111	2400	82	901114 - 910121
KAS02-2	B2	901023 - 901026	110	10	901020 - 901027
KAS03-5	C5	n m			
KAS03-2	C2	n m			
KAS04-2	D2	n m			
KAS05-3	E3	901009 - 901018	80	13	901009 - 901015
		901025 - 901029	80	13	901023 - 901212
		901031 - 901228	1400	25	901217 - 910121
					910130 - 910211
KAS05-1	E1	900925 - 900928	80	9	900924 - 900928
KAS06		pump hole during LPT-2			
KAS07-4	J4	900927 - 900928	55	6	900924 - 900928
		901003 - 901009	144	11	901002 - 901110
		901009 - 901015	144	11	
		901015 - 901021	143	11	
		901021 - 901123	369	28	901114 - 901121
KAS07-1	J1	n m			
KAS08-3	M3	901011 - 901019	200	17	901010 - 901020
		901029 - 901031	55	5	901027 - 901121
		901102 - 901114	300	18	
KAS08-1	M1	900926 - 890928	65	7	900924 - 900928
		901003 - 901006	72	5	901002 - 901110
		901006 - 901009	68	5	
		901009 - 901012	75	5	
		901012 - 901015	68	5	
		901015 - 901018	75	5	
		901018 - 901021	71	5	
		901021 - 901029	189	20	
KAS09-4	AD	n m			
KAS11-5	CE	n m			
KAS11-2	CB	n m			
KAS12-3	DC	n m			
KAS12-2	DB	900926 - 900928	60	7	900925 - 900928
		901003 - 901006	73	6	901002 - 901110
		901006 - 901009	71	5	
		901009 - 901012	78	7	
		901012 - 901015	65	5	
		901015 - 901018	78	5	
		901018 - 901021	66	5	
		901021 - 901026	139	23	
KAS13-4	ED	n m			
KAS13-3	EC	900925 - 900928	76	10	900924 - 900928
KAS14-4	FD	n m			
KAS14-2	FB	901022 - 901025	90	8	901017 - 901023

1 = Duration of dilution measurement
2 = Number of data points
n m = no measurement

4.2 SUPPORTING MEASUREMENTS

Long term registration of the hydraulic head in the various packed-off sections have been made in the whole Simpevarp area since the start of the investigations in 1987. The number of boreholes and registration sections has increased every year, so that during the summer 1991 Äspö had altogether about 100 sections in both shallow percussion and deep core boreholes.

The hydraulic head data is recorded with the "BORRE" computer based data collecting system. Data from the boreholes are manually dumped from every borehole with a portable PC. The results of hydraulic head recordings (see Figure 4.1) are presented in Nyberg et al., 1990, Jönsson and Nyberg 1991 and in Gentzschein and Nyberg, 1989.

During the Long term Pump Test (LPT-2) in autumn 1990 electrical conductivity, redox potential and groundwater temperature were registered in the withdrawal water from borehole KAS06 (Jönsson and Nyberg, 1991).

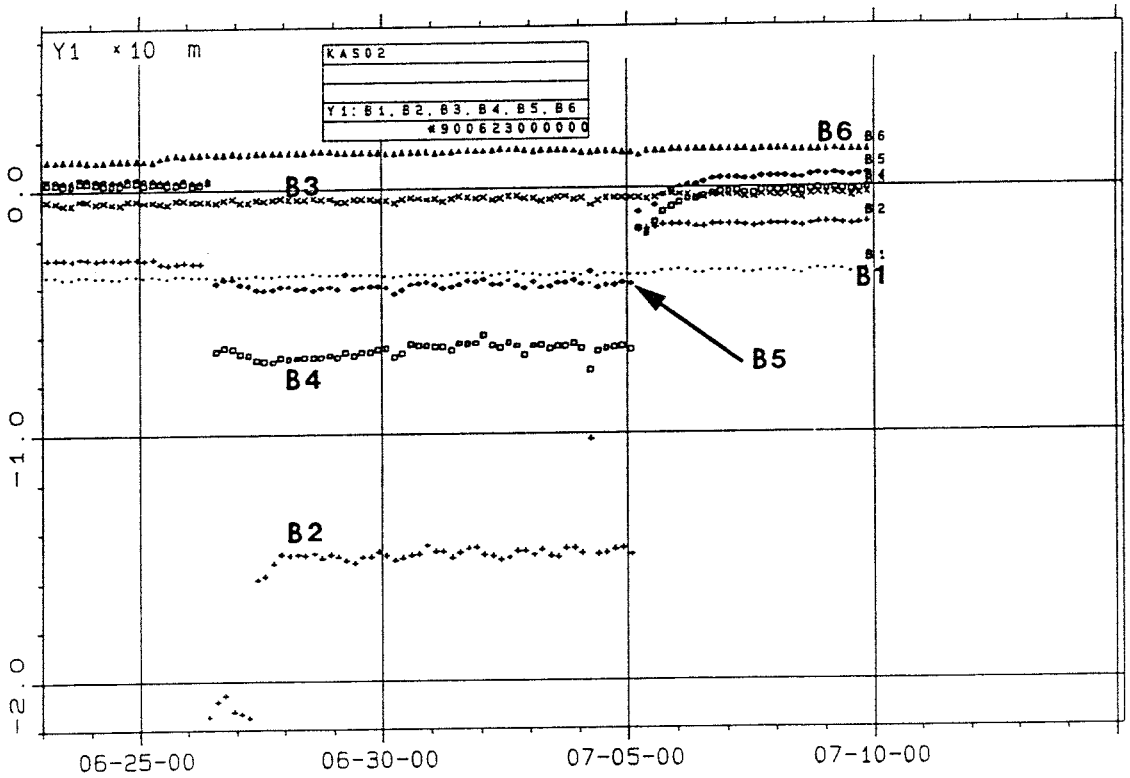

Figure 4.1 Example of long term hydraulic head registration during NG2 in borehole KAS02 at Äspö. This plot clearly shows that section B5 is interfering with the dilution test circulation performed in sections B2 and B4.

5. RESULTS

The results of all dilution measurements presented in this report are summarized in Table 5.1. Comments regarding each measurement such as possible errors, uncertainties, etc. are given below and the values interpreted on the basis of uncertainties etc, are given in Table 5.2. The transmissivity values given for boreholes KAS02–08 are values calculated from packer tests (SKB database GEOTAB), while the values given for KAS09–14 are calculated from spinner measurements (Rhén et al., 1991b). Examples of some typical dilution curves are shown in Figure 5.1. Plot A shows an uneven dilution sequence caused by instrumental errors and/or changes of the hydraulic gradient. Plot C shows an uneven injection of tracer and plot E shows the dilution of "old" Uranine. Plots B,D and F are examples of normal injections and dilution sequences. Detailed information about each dilution measurement made during LPT–1 is documented in Ittner et al., 1991a, NG1 is documented in Ittner et al., 1991b, NG2 is documented in Ittner et al., 1991c and LPT–2 is documented in Ittner et al., 1991d.

Table 5.1 Summary of all results from dilution measurements performed at Äspö 1989–1990. The interpreted results are presented in Table 5.2.

Borehole	Code	Section (m)	Flow (ml/min) LPT–1	NG1	NG2	LPT–2	T [1] (m^2/s)
KAS02–4	B4	309–345	1.1	–	(89)	14, 2	2.0E–5
KAS02–2	B2	800–854	(127)	–	(127)	4	4.0E–5
KAS03–5	C5	107–252	–	–	6.9	–	3.0E–6
KAS03–2	C2	533–626	–	–	164	–	4.0E–6
KAS04–2	D2	332–392	28	–	12	–	4.0E–5
KAS05–3	E3	320–380	6.5	–	0.4	12,10,9	2.4E–6
KAS05–1	E1	440–549	40	1.8	1.3	11	7.8E–6
KAS06–5	F5	191–249	197	25	27	ph	1.7E–4
KAS06–1	F1	431–500	79	52	25	ph	3.1E–5
KAS07–4	J4	191–290	ph	–	1.0	33,20,17,18,18	4.9E–6
KAS07–1	J1	501–604	ph	–	5.3	–	>1.3E–5
KAS08–3	M3	140–200	4.3	–	4.0	16,5,21	3.9E–5
KAS08–1	M1	503–601	20	5.5	7.6	54,51,50,48, 46,47,45,44	3.2E–4
KAS09–4	AD	116–150			11	–	6.4E–4
KAS11–5	CE	47–64			0.3	–	3.3E–5
KAS11–2	CB	153–183			33	–	2.5E–4
KAS12–3	DC	235–278			0	–	2.3E–6
KAS12–2	DB	279–330			12	111,99,94,122, 116,115,100,97	2.7E–5
KAS13–4	ED	151–190			1.1	–	3.7E–6
KAS13–3	EC	191–220			4.7	3.3	2.7E–5
KAS14–4	FD	131–138			3.1	–	2.2E–4
KAS14–2	FB	147–175			18	11	1.0E–4

– = No measurement, ph = pumphole

1 = KAS02–08, transient 3m packer test, evaluated with Jacobs method (SKB database GEOTAB)
KAS09–14, spinner measurements (Rhén et al., 1991b)

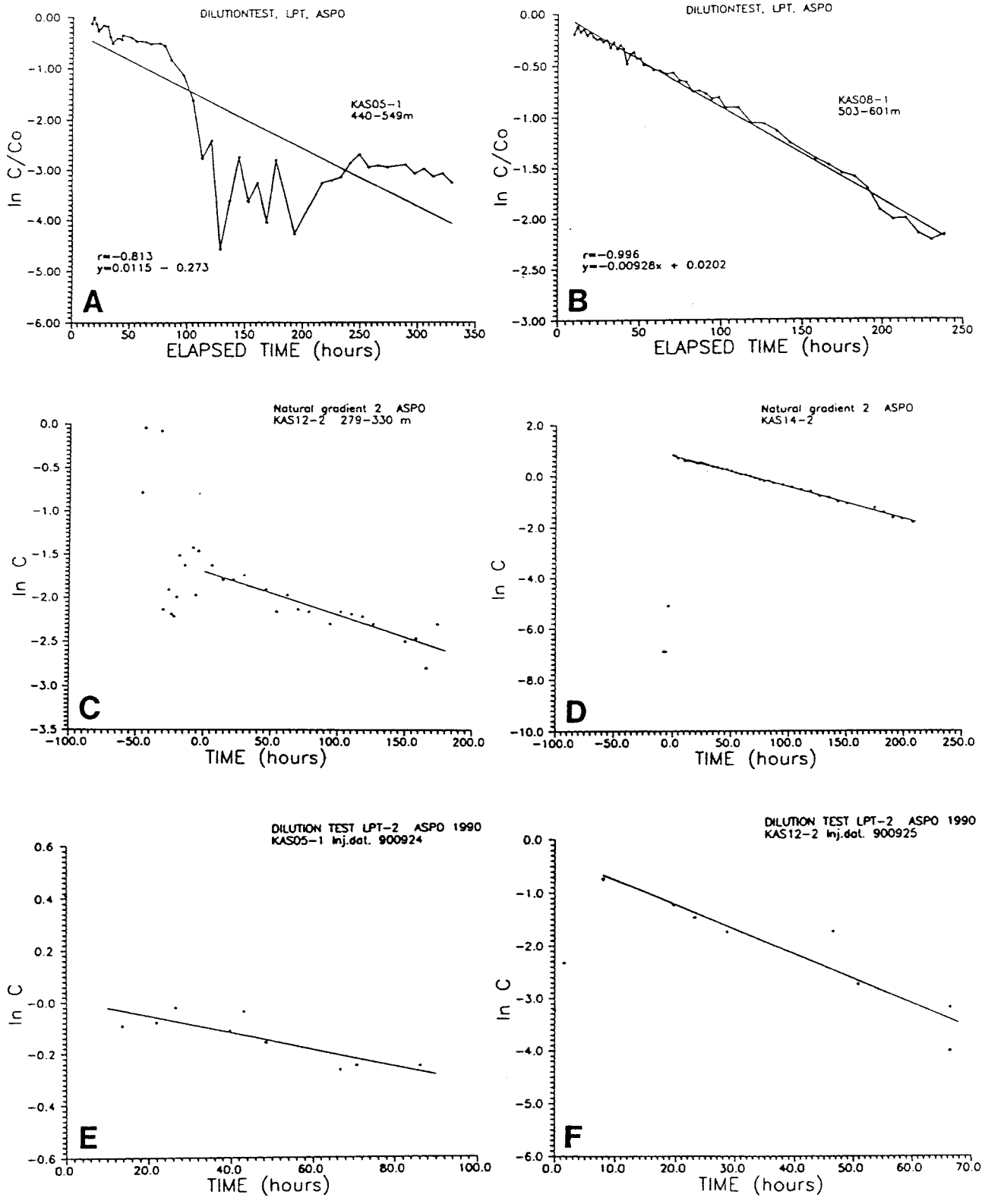

Figure 5.1 Examples of different types of dilution curves. A – uneven dilution, C – uneven dilution and injection. B,D and F – smooth dilution, E – dilution of "old" Uranine (no injection) cf. Section 2.3.

Comments regarding the results of the dilution measurements in each packed off section are given below;

KAS02-4 (B4)

In this section four measurements have been made. The first measurement during LPT-1 shows a very smooth and fine dilution curve except for some initial disturbances caused by a too fast injection procedure. The second measurement, made during NG2 shows a smooth dilution curve but also a very high dilution rate. This is caused by a leakage in the tube fitting within section B5. This is clearly seen by studying the hydraulic head registrations in B4 and B5 during NG2, cf. Figure 4.1 (Nyberg et al., 1990). The value from this measurement should therefore be disregarded. The third and fourth measurement were both made during LPT-2, and shows a relatively large difference, 14 respectively 2 ml/min. The reason for this is probably that the magnitude and/or the direction of the gradient is in a transient stage during the third measurement which was made only one week after start of pumping in KAS06. This is also supported by a decreasing slope in the dilution curve towards the end of the measurement. The value 2 ml/min from the fourth measurement must be seen as an extremely well established value as the measurement was performed during a period of 100 days and with a very smooth dilution curve (Gustafsson et al., 1991).

KAS02-2 (B2)

Three measurements have been made in this section. During LPT-1, a leakage was found between sections B2 and B3 (Gentzschein and Nyberg, 1989) which caused an increased dilution. The value given in Table 5.1, 127 ml/min, is therefore incorrect and should be disregarded. The second measurement, made during natural gradient (NG2), also shows a very high flow rate, 127 ml/min. Also in this case a leakage, which also caused the high dilution in section B4, is the reason and the value must be disregarded. The measurement made during LPT-2 is most likely the only value that can be judged as correct, 4 ml/min.

KAS03-5 (C5)

This borehole section is very long, 145 m, and has a low transmissivity (T=3E-6 m^2/s). It also contains a large volume of water which means that a relatively long measurement period was needed in order to achieve any significant dilution. The measurement performed (NG2) shows a very slow but steady dilution rate and the calculated flow rate of 6.9 ml/min is judged to be accurate. No measurements were performed during pump gradients.

KAS03-2 (C2)

This section has a relatively low transmissivity (T=4E-6m^2/s). The flow measurement show a very high value, 164 ml/min, which was much higher than could be expected. However, the data points are quite scattered due to a high content of particles or precipitations in the samples which may have

caused sorption of the tracer and consequently a too high dilution rate. The scattered data implies that it is possible to vary the flow within the range 70–170 ml/min, or even lower, without changing the correlation coefficient for the regression estimate in any significant way. The value given in Table 5.1 should therefore be regarded as very approximative.

KAS04–2 (D2)

The section was measured at two occasions, LPT–1 and NG2. Both measurements show a steady and smooth dilution curve and the flow rates given in Table 5.1 are considered to be correct.

KAS05–3 (E3)

Five measurements have been made in this section which also was used as injection section during the tracer test (LPT–2). The values determined during pump gradient (LPT–1 and LPT–2) show smooth and fine dilution curves and the measurements were performed without any disturbances. The three measurements performed during LPT–2 differ somewhat (9–12 ml/min) mostly due to the few data points in two of the measurements. The third measurement, which also was the injection of tracer during the tracer test, was sampled during a period of about 60 days and is therefore considered to be the most accurate value (9 ml/min). The measurement performed during natural gradient (NG2) gives a very low flow rate. Given the uncertainty in the analyses, the error is estimated to be ± 100%, i.e 0–0.8 ml/min.

KAS05–1 (E1)

This section was measured at all four different occasions. The first measurement during LPT–1 was clearly affected by a change of the gradient occurring towards the end of the pumping period, see also Figure 4.1 (plot A). This can also be seen in the head measurements (Gentzschein and Nyberg, 1989). The flow rate given in Table 5.1 should be seen as mean value over the measurement period. The flow at the beginning of the measurement, before the changes of the gradient, was about 25 ml/h. The two measurements made during natural gradient show very low flow rates, 1.5–1.8 ml/min. Both these measurements show somewhat scattered dilution curves but the flow rates determined are judged to be accurate. The last measurement was made during LPT–2 by using the Uranine remaining in the borehole and tubing from the previous measurement (NG2), see Figure 4.1 (plot E). The dilution curve is relatively smooth and the flow rate is considered to be correct.

KAS06–5 (F5)

This section has a high transmissivity (T=1.7E–4 m^2/s) and also high flow rates both during LPT–1 and during natural gradient. The two measurements during natural gradient show very consistent results and all three measurements are considered to be correct.

KAS06-1 (F1)

This section was measured three times and all three measurements give quite high flow rates. The measurements were performed without any problems and the dilution curves are smooth. The values given in Table 5.1 are judged to be correct.

KAS07-4 (J4)

This section was used as injection section for the tracer test and was measured 5 times during the tracer test. The flow rates determined are within the range 17–33 ml/min, however the highest value of 33 ml/min is more uncertain than the others as the measurement time was very short, 10 hours, while the last measurement, which gave 18 ml/min, lasted for 39 hours. The latter value is therefore considered to be the most correct one. The measurement made during natural gradient (NG2) gives a very low flow rate, 1 ml/min. This figure is somewhat uncertain due to the very slow dilution and somewhat scattered data points. There are also a comparatively high amount of particles present in the water which to some degree may explain the scatter of the data points. The flow may vary at least within 50%, i.e in the range 0.5–1.5 ml/min.

KAS07-1 (J1)

This section has only been measured once (NG2). The dilution curve is smooth and the value given in Table 5.1 is considered as correct.

KAS08-3 (M3)

This section has been measured four times and the measurements have been performed without disturbances. The section was also used as injection section for the tracer test during LPT–2 and therefore three measurements were made during LPT–2. The flow rate given in Table 5.1, 21 ml/min, was determined from the dilution of Re–186 during the tracer injection and shows an extremely linear dilution curve. The other two values determined during LPT–2 were determined from short time measurements with few data points and are therefore considered as more uncertain.

KAS08-1 (M1)

This is also a section used as injection section during LPT–2 with 7 measurements performed during the tracer injection of Re–186. The dilution curves are very consistent and indicate a slowly decreasing flow rate, from 51 ml/min down to 44 ml/min during the last tracer injection. The section was also measured at the three other occasions and the dilution curves are all smooth and linear, see Figure 5.1 (plot B).

KAS09-4 (AD)

The only measurement performed in section AD was made during natural gradient (NG2). The resulting dilution curve is very smooth and linear and the value given in Table 5.1 is judged to be correct.

KAS11-5 (CE)

This section has also been measured only once during NG2. The data points are quite scattered due to precipitations in the samples but the dilution is very low and the flow rate determined, 0.3 ml/min, is considered to be correct within ± 100%.

KAS11-2 (CB)

The only measurement performed, during NG2, shows a fast dilution and a smooth, linear curve. The flow rate was calculated to 33 ml/min which is one of the highest measured during natural gradient.

KAS12-3 (DC)

This section was measured during natural gradient (NG2). The data points are somewhat scattered due to precipitations in some of the samples but the dilution is lower than the measurement limit, which in this measurement is estimated to about 0.5 ml/min.

KAS12-2 (DB)

This section was measured both during NG2 and at 8 occasions during LPT-2. The values calculated from LPT-2 are all determined from 5-7 data points over relatively short periods (3 days each) except for the last measurement which lasted for 6 days, see Figure 5.1 (plot F). The values varies within 94-122 ml/min with a mean flow rate of 107 ml/min. All dilution curves are smooth and linear with a small exception for the curve from NG2 which is somewhat irregular, possibly due to precipitations in some of the samples, see Figure 5.1 (plot C).

KAS13-4 (ED)

The only measurement performed (NG2) give a very smooth dilution curve and a value of 1.1 ml/min which is considered to be correct.

KAS13-3 (EC)

Two measurements have been performed in this section, during natural gradient (NG2) and during pumping (LPT-2). The dilution curves are smooth and linear and the values given in Table 5.1 are judged to be correct.

KAS14–4 (FD)

This section was measured during natural gradient (NG2). The dilution curve shows a smooth and linear dilution except for the last two days where a decreasing flow rate is indicated. The reason for this decrease may be a changing large scale gradient. This interpretation is also supported by the head measurements (Nyberg et al., 1990) where a rapid change of the head can be seen towards the end of the dilution measurement period.

KAS14–2 (FB)

Both measurements performed in this section (NG2 and LPT–2) show smooth and linear dilution curves. The values determined are of the same magnitude, 18 and 11 ml/min, respectively and are both considered as being correct, see Figure 5.1 (plot D).

Table 5.2 Concluded results of dilution measurements

Borehole	Code	Section (m)	Flow (ml/min) LPT-1	NG1	NG2	LPT-2	T [1] (m^2/s)
KAS02-4	B4	309-345	1.1	-	(*)	2	2.0E-5
KAS02-2	B2	800-854	(*)	-	(*)	4	4.0E-5
KAS03-5	C5	107-252	-	-	6.9	-	3.0E-6
KAS03-2	C2	533-626	-	-	(120)	-	4.0E-6
KAS04-2	D2	332-392	28	-	12	-	4.0E-5
KAS05-3	E3	320-380	6.5	-	0.4	9	2.4E-6
KAS05-1	E1	440-549	40	1.8	1.3	11	7.8E-6
KAS06-5	F5	191-249	197	25	27	ph	1.7E-4
KAS06-1	F1	431-500	79	52	25	ph	3.1E-5
KAS07-4	J4	191-290	ph	-	1.0	18	4.9E-6
KAS07-1	J1	501-604	ph	-	5.3	-	>1.3E-5
KAS08-3	M3	140-200	4.3	-	4.0	21	3.9E-5
KAS08-1	M1	503-601	20	5.5	7.6	48	3.2E-4
KAS09-4	AD	116-150			11	-	6.4E-4
KAS11-5	CE	47-64			0.3	-	3.3E-5
KAS11-2	CB	153-183			33	-	2.5E-4
KAS12-3	DC	235-278			0	-	2.3E-6
KAS12-2	DB	279-330			12	107	2.7E-5
KAS13-4	ED	151-190			1.1	-	3.7E-6
KAS13-3	EC	191-220			4.7	3.3	2.7E-5
KAS14-4	FD	131-138			3.1	-	2.2E-4
KAS14-2	FB	147-175			18	11	1.0E-4

- = No measurement, ph = pumphole

* = Failed measurement (see text)

1 = KAS02-08, transient 3m packer test, evaluated with Jacobs method (SKB database GEOTAB). KAS09-14, spinner measurements (Rhén et al., 1991b)

6. DISCUSSION AND CONCLUSIONS

6.1 FLOW IN RELATION TO THE CONDUCTIVE STRUCTURES AT ÄSPÖ

The dilution measurement at Äspö have been performed in 22 different sections corresponding to eight fracture zones according to the conceptual model given by Wikberg et al., 1991. The discussion below concerns the responses of the different sections to the pumping during LPT-1 and LPT-2 and comparison with the flow during natural gradient. The fracture zones discussed are corresponding to the nomenclature and interpretations given by Wikberg et al., 1991, cf. Figure 1.1.

Zone NE-1

Zone NE-1 is a steeply dipping (72°) NE tending zone and also the most well represented zone among the sections chosen for dilution measurements. The zone is also the most highly transmissive structure at Äspö (T=2E-4 m^2/s). The flow rate was determined in 7 different sections according to Table 6.1. The measurements give values that are consistent with the interpretation of Zone NE-1. Pumping in KAS07 during LPT-1 increases the flow rates in sections B2 and M1, although the value given for section B2 is somewhat uncertain due to leakage as discussed in Section 5. Natural flow rates varies between 3 and 33 ml/min and the high values during natural gradient are all determined on the southern part of Äspö. The pumping in borehole KAS06 (LPT-2), which does not intersect Zone NE-1, indicates that Zone NE-1 has a good hydraulic connection with Zones NNW-1 and/or NNW-2. This conclusion is also supported by the high flow rates determined in KAS06 (sections F1 and F5) during LPT-1. Pumping during LPT-2 seems to give no response on the southern part of Äspö as indicated by the flow rate measured in section FB. This fact may suggest that the structure EW-3 acts as a hydraulic boundary and "cuts off" the southern part of NE-1.

The conclusion of the flow measurements in Zone NE-1 is that the results are consistent with the conceptual model presented by Wikberg et al., 1991. The measurements also suggests that the southern, shallow, parts of NE-1 which has high natural flow rates, is hydraulically "cut off" possibly by the intersecting Zone EW-3.

Table 6.1 Summary of flow measurements in Zone NE-1.

Borehole/ section	Code	Groundwater flow rate (ml/min) LPT-1	NG1	NG2	LPT-2
KAS02-2	B2	(*)	-	(*)	4
KAS07-1	J1	ph	-	5.3	-
KAS08-1	M1	20	5.5	7.6	48
KAS09-4	AD	-	-	11	-
KAS11-2	CB	-	-	33	-
KAS14-4	FD	-	-	3.1	-
KAS14-2	FB	-	-	18	11

(*) Failed measurement

Zone EW-5

Zone EW-5, which is a low angle (37°) zone with a relatively high transmissivity (T=2E-5 m^2/s), is represented in 4 sections according to Table 6.2. The flow rates during natural gradient are consistently low in all sections. The pumping in KAS07 during LPT-1 causes an increased flow rate in section E3 and the pumping in KAS06 (LPT-2) causes an even higher increase in E3 but also an increased flow rate in section J4. This is also consistent with the interpretation of Zone EW-5 which is interpreted to intersect KAS06 as well. Section B4 (KAS02-4) does not respond to the pumping in KAS06 and KAS07 which is not quite consistent with the interpretation, especially as the distance from the pump holes to section B4 is relatively short (about 100 m).

The conclusion of the flow measurements within Zone EW-5 is that the zone has a low groundwater flow during natural gradient conditions. However, during pumping it seems to be a relatively good hydraulic conductor. The only inconsistency in the interpretation is the poor hydraulic response in section B4.

Table 6.2 Summary of flow measurements in Zone EW-5.

Borehole/ section	Code	Groundwater flow rate (ml/min) LPT-1	NG1	NG2	LPT-2
KAS02-4	B4	1.1	-	(*)	2
KAS05-3	E3	6.5	-	0.4	9
KAS07-4	J4	ph	-	1.0	18
KAS11-5	CE	-	-	0.3	-

(*) Failed measurement

NE-2

Zone NE-2, which is a steeply dipping structure with a relatively low transmissivity (T=4E-6 m^2/s), is represented in 3 borehole sections of which sections D2 (KAS04-2) and DB (KAS12-2) shows high flow rates during natural gradient and also a strong influence from the pumping in KAS06 and KAS07, see Table 6.3. As there is no direct hydraulic connection to the pump holes, according to the present conceptual model, this influence indicates that Zone NE-2 has a good hydraulic connection with the steeply dipping structures NNW-1 and NNW-2. Section DC shows a very low or even no dilution of tracer during NG2. The section seem to have a very poor hydraulic connection to Zone NE-2 compared to section DB in the same borehole (KAS12).

Based on the few flow measurements performed within Zone NE-2, it seems as Zone NE-2 is a good hydraulic leader despite the relatively low transmissivity of the zone. It is also possible that the short distance between the good hydraulic conductors NNW-1 and NNW-2 locally gives a high flow rate around section DB during pumping in these structures.

Table 6.3 Summary of flow measurements in Zone NE-2.

Borehole/ section	Code	Groundwater flow rate (ml/min)			
		LPT-1	NG1	NG2	LPT-2
KAS04-2	D2	28	-	12	-
KAS12-2	DB	-	-	12	107
KAS12-3	DC	-	-	0	-

NNW-1 and NNW-2

These two vertical structures are both highly conductive (T=2-4E-5 m^2/s) and seem to be in good hydraulic contact with fracture zones NE-1 and NE-2, as earlier discussed. Both zones are present in borehole KAS06, sections F1 (NNW-2) and F5 (NNW-1), see Table 6.4. NNW-2 is also interpreted to intersect section M3 and this is also supported by the increase of the flow in M3 during pumping in KAS06 (LPT-2). The natural gradient flow rates are also high in both zones in KAS06 while somewhat lower in section M3. The only inconsistency among the measurements performed in zones NNW-1 and NNW-2 is the low flow rate determined in section M3 during LPT-1 which contradicts the interpretation that Zones NNW-2 and NE-1 are well connected.

Sections EC in borehole KAS13 which is interpreted to intersect a NNW structure does not seem to be hydraulically connected to the system NNW-1, NNW-2, NE-1, and NE-2 as the flow not increases in this section during pumping in KAS06 (LPT-2).

Table 6.4 Summary of flow measurements in Zones NNW–1, NNW–2, and a NNW structure, not in the conceptual model.

Borehole/ section	Code	Structure	Groundwater flow rate (ml/min) LPT–1	NG1	NG2	LPT–2
KAS06–5	F5	NNW–1	197	25	27	ph
KAS06–1	F1	NNW–2	79	52	25	ph
KAS08–3	M3	NNW–2	4.3	–	4.0	21
KAS13–4	ED	NNW	–	–	1.1	–
KAS13–3	EC	NNW	–	–	4.7	3.3

ph = pump hole during LPT–2.

EW–X

This low angle structure, which is judged as being "possible" (Wikberg et al., 1991) is only measured in one section in the central parts of Äspö, section E1 (KAS05), see Table 6.5. The natural flow rate is low and pumping in KAS07 during LPT–1 and in KAS06 during LPT–2 both seem to increase the flow in section E1 considerably which supports the conceptual model of a gently dipping structure which may intersect borehole KAS06 close to the bottom of the borehole.

The conclusion is that the groundwater flow data does not contradict the existence of a gently dipping structure, EW–X, in the central part of Äspö although there are only a few data.

Table 6.5 Summary of flow measurements in Zone EW–X.

Borehole/ section	Code	Groundwater flow rate (ml/min) LPT–1	NG1	NG2	LPT–2
KAS05–1	E1	40	1.8	1.3	11

EW-1 and NW-1

In both these structures, located on the northern part of Äspö, only one measurement has been performed during natural gradient (NG2). Section C2 (KAS03) has a very high natural flow, 120 ml/min, which suggests that Zone EW-1 has a high transmissivity. The section may be intersected by one of the single open fractures which are discussed by Wikberg et al., 1991. It should also be noted that the flow measurement showed a very scattered and uneven dilution curve and it is therefore possible that the flow is overestimated, cf Section 5.

The flow in Zone NW-1, section C5 (KAS03), judged as being "probable" by Wikberg et al. (1991), was measured to 6.9 ml/min during natural gradient, which implies a relatively transmissive structure consistent with the hydraulic measurements (T=0.7E-5 m^2/s).

6.2 FLOW IN RELATION TO TRANSMISSIVITY AND DEPTH

In Figure 6.1 the flow rates measured during natural gradient (NG2) are plotted versus the transmissivity of each section. The graph indicates that there is some relation between measured flow rates and transmissivity, as might be expected. The relation is quite weak and it is important to bear in mind that the data represent point measurements and therefore not necessary the flow in the fracture zones. The same also applies for the transmissivity values given, which in some of the borehole sections differ significantly from the "mean" transmissivities of the fracture zones given by Wikberg et al., (1991). There are some measurements which seem to fall outside this relation, namely sections AD, M1 and FD. Notably is that all three sections are interpreted to belong to the fracture zone NE-1 but so is also section CB which has the highest flow rate.

One possible reason for the low flow rates measured in NE-1 might be that the gradient is low. This is also indicated by the modelling presented by Rhén et al., 1991a.

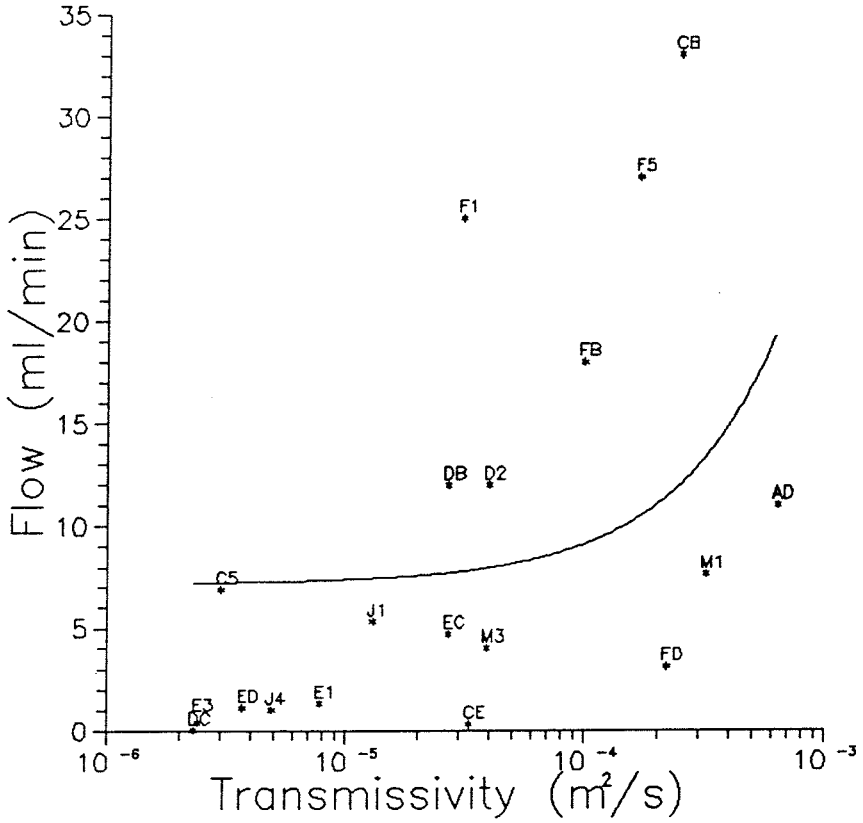

Figure 6.1 Flow versus transmissivity (m^2/s) during natural gradient (NG2). Solid line represents linear regression estimate.

The flow during stressed conditions such as the pumpings during LPT–1 and LPT–2 was used to verify or refute the hydraulic connections between different zones as given by the conceptual model.

In Figure 6.2 the flow during LPT–1 is compared to the natural gradient flow for all sections measured at both occasions. The pumping was made in borehole KAS07 in which the structures EW–5, NNW–1, and NE–1 are the most dominating. The results clearly shows the good response in NNW–1, (section F5) and also the good response in NNW–2 (section F1) probably reacting through Zone NE–1 which is in good contact with NNW–2. Also Zone EW–5 is responding as expected whereas the response in the highly transmissive Zone NE–1 (section M1) is surprisingly low.

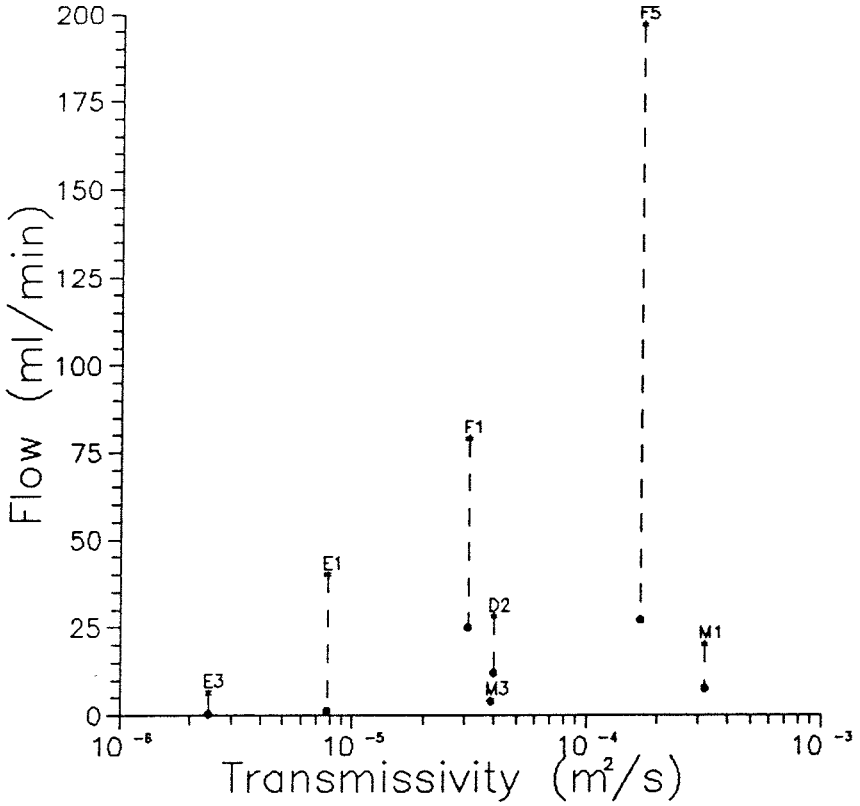

Figure 6.2 Flow versus transmissivity (m^2/s) during LPT–1 compared to natural gradient conditions (lower value).

The same plot was made for the measurements performed during LPT–2 (Figure 6.3). During LPT–2 the pumping was made in KAS06 and the structures directly pumped were NNW–1, NNW–2, EW–5, and EW–3. The results show good responses in zones NE–1 (section M1) and NE–2 (section DB). The latter probably reacting through zones NNW–1 and NNW–2.

It is often argued that the flow and transmissivity should be decreasing with depth below ground surface. Therefore, the measurements during natural gradient was plotted versus depth (Figure 6.4). The graph shows that no such correlation seem to exist based on the flow measurements performed in this investigation.

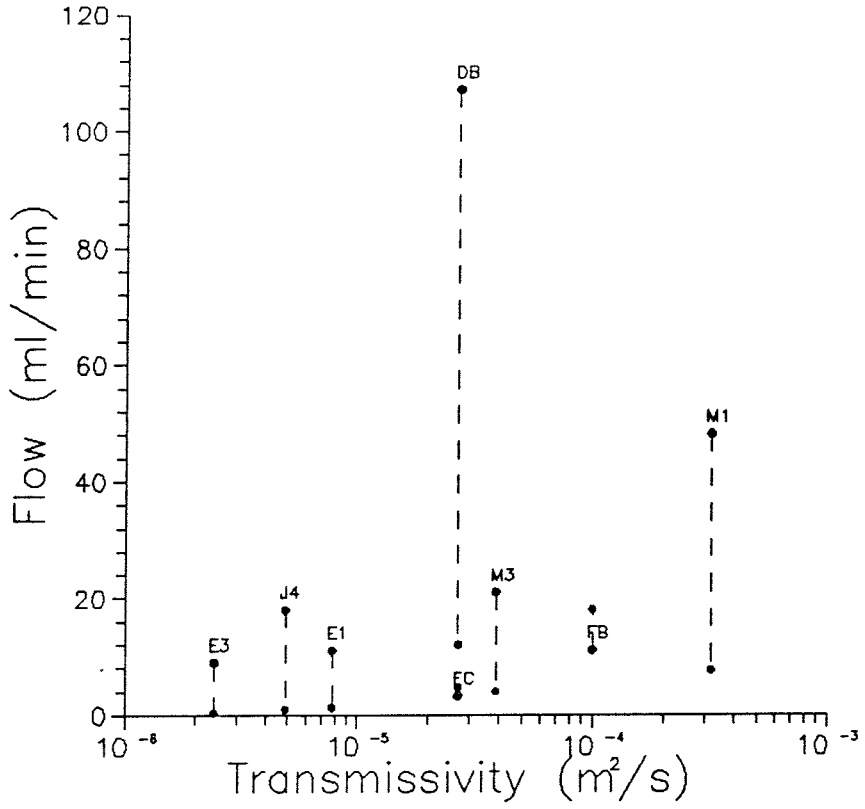

Figure 6.3 Flow versus transmissivity (m^2/s) during LPT–2 compared to natural gradient conditions (lower value).

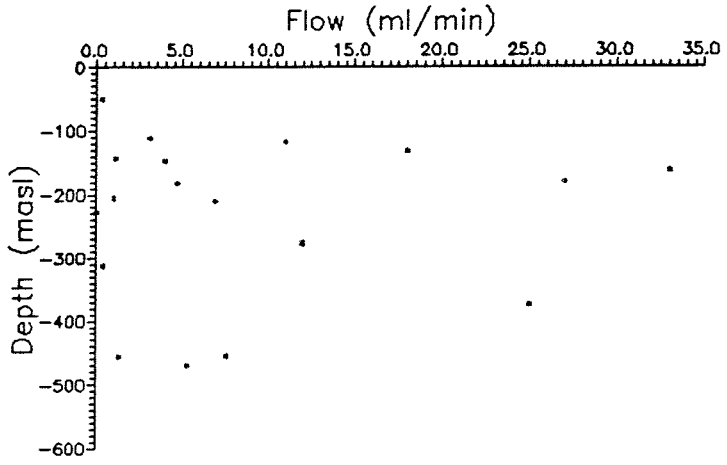

Figure 6.4 Flow versus depth below ground surface during natural gradient (NG2).

7. REFERENCES

Gentzschein B. 1986. Description of hydrogeological data in SKB`s database GEOTAB. SKB TR 86-22.

Gentzschein B., Nyberg G. 1989. Data från långtidspumptest i borrhål KAS07. SGAB IRAP 89236.

Gustafsson E., Andersson, P., Ittner T, Nordqvist R. 1991. Large scale three dimensional tracer test at Äspö. GEOSIGMA GRAP 91001.

Gustafsson E. 1988. Förstudie omfattande möjligheten att utföra utspädning-smätningar i 56mm diameter borrhål. SGAB IRAP 88291.

Gustafsson E. 1986. Bestämmning av grundvattenflödet med utspädnings-teknik. Modifiering av utrustning och kompletterande fältmätningar. SKB AR 86-21.

Gustafsson E., Klockars C-E. 1984. Study of strontium and cesium migration in fractured rock. SKBF/KBS TR 84-07.

Gustafson G., Stanfors R., Wikberg P. 1989. Swedish hard rock laboratory. Evaluation of 1988 Year Pre-investigations and Description of the Target Area, the Island of Äspö. SKB TR 89-16.

Ittner T., Gustafsson E., Andersson P., Eriksson C-O. 1991a. Mätningar av grundvattenflöde med utspädningsteknik under LPT-1, Augusti 1989 på Äspö. Sammanställning av fältdata. GEOSIGMA GRAP 91006

Ittner T., Gustafsson E., Andersson P., Eriksson C-O. 1991b. Mätningar av grundvattenflöde med utspädningsteknik under NG1, Oktober 1989 på Äspö. Sammanställning av fältdata. GEOSIGMA GRAP 91007

Ittner T., Gustafsson E., Andersson P., Eriksson C-O. 1991c. Mätningar av grundvattenflöde med utspädningsteknik under NG2, Sommaren 1990 på Äspö. Sammanställning av fältdata. GEOSIGMA GRAP 91008

Ittner T., Gustafsson E., Andersson P., Eriksson C-O. 1991d. Mätningar av grundvattenflöde med utspädningsteknik under LPT-2. Hösten 1990 på Äspö. Sammanställning av fältdata. GEOSIGMA GRAP 91009

Jönsson S., Nyberg G. 1991. Data från långtidspumptest i borrhål KAS06. SGAB IRAP 91223.

Klockars C-E. 1989. Diffusionsprocesser i borrhål. SGAB IRAP 89247.

Nilsson A-C. 1991. Groundwater chemistry monitoring at Äspö during 1990. Äspö Hard Rock Laboratory. SKB PR 25-91-04.

Nyberg G., Jönsson S., Ekman L. 1990. Äspö Hard Rock Laboratory: Groundwater level program, report for the period 1987 - 1989. SKB PR 25-90-18.

Rhén I., Forsmark T., Gustafson G. 1991a. Conceptual modelling of Äspö. Technical note 30. In: Liedholm M.(Ed.) Conceptual modelling of Äspö. Technical notes 18-32. Äspö Hard Rock Laboratory. SKB PR 25-90-16b.

Rhén I., Forsmark T., Nilsson L. 1991b. Hydraulic tests on Äspö, Bockholmen and Laxemar 1990 in KAS09, KAS11-14, HAS18-20, KBH01-02 and KLX01. Evaluation. Äspö Hard Rock Laboratory. SKB PR 25-91-01.

Wikberg P. (ed), Gustafson G., Rhén I., Stanfors R. 1991. Äspö Hard Rock Laboratory. Evaluation and conceptual modelling based on the pre-investigations 1986-1990. SKB TR 91-22.

APPENDIX E Comparison between calculated and measured drawdown

Table E1 Measured and predicted drawdowns for pumping test LPT2

Name: Borehole name and borehole section name

DIST: Spherical distance from midpoint of KAS06 to the midpoint of the borehole section (m)

DEPTH: Vertical distance below Z=0 (Äspö system) (approximately the sealevel) (m)

PMEAS: Maximum measured drawdown (m)

PCALC: Calculated drawdown - steady state (m)

ERROR: PMEAS - PCALC (m)

NAME	PNATUR	DIST	DEPTH	PMEAS	PCALC	ERROR
KO1-A1	11438.300	223.000	52.000	6.200	8.113	-1.913
KO2-B6	14038.900	222.000	52.000	6.300	7.420	-1.120
KO2-B5	10929.200	114.000	189.000	5.790	7.842	-2.052
KO2-B4	19397.400	131.000	309.000	6.300	5.382	0.918
KO2-B3	40360.500	338.000	537.000	5.400	4.097	1.303
KO2-B2	71440.203	584.000	824.000	2.410	3.794	-1.384
KO2-B1	76235.203	645.000	873.000	2.300	3.667	-1.367
KO3-C6	15145.200	710.000	51.000	0.000	0.138	-0.138
KO3-C5	11442.000	698.000	210.000	0.000	0.251	-0.251
KO3-C4	22012.301	711.000	346.000	0.550	0.563	-0.013
KO3-C3	38551.102	751.000	514.000	0.800	0.678	0.122
KO3-C2	46474.398	806.000	604.000	0.830	0.818	0.012
KO3-C1	54820.102	948.000	677.000	0.820	0.906	-0.086
KO4-D6	8528.160	479.000	139.000	0.000	5.164	-5.164
KO4-D5	10711.900	397.000	149.000	3.270	3.097	0.173
KO4-D4	11230.000	362.000	188.000	3.110	3.258	-0.148
KO4-D3	13432.100	327.000	235.000	3.420	5.151	-1.731
KO4-D2	17815.000	301.000	276.000	3.580	5.176	-1.596
KO4-D1	22428.600	277.000	340.000	3.330	5.110	-1.780
KO5-E5	8318.720	223.000	81.000	5.580	4.047	1.533
KO5-E4	16473.100	133.000	263.000	4.970	4.060	0.910
KO5-E3	19444.400	156.000	312.000	5.450	3.652	1.798
KO5-E2	30457.301	195.000	426.000	3.300	3.411	-0.111
KO5-E1	31997.699	264.000	456.000	3.060	3.418	-0.358
KO7-J6	7932.400	208.000	47.000	15.640	4.180	11.460
KO7-J5	7931.940	137.000	104.000	16.530	10.060	6.470
KO7-J4	15179.900	112.000	206.000	5.610	3.163	2.447
KO7-J3	19489.301	165.000	295.000	1.690	2.540	-0.850
KO7-J2	24059.600	253.000	363.000	1.880	2.173	-0.293
KO7-J1	36584.898	343.000	470.000	2.540	2.234	0.306
KO8-M4	3171.050	290.000	52.000	4.730	3.115	1.615
KO8-M3	8123.610	200.000	147.000	6.580	3.482	3.098
KO8-M2	20959.100	97.000	314.000	4.700	6.330	-1.630
KO8-M1	31980.900	226.000	455.000	3.740	3.730	0.010
KO9-AE	4795.390	392.000	88.000	0.250	0.255	-0.005
KO9-AD	5985.200	396.000	117.000	0.380	0.269	0.111
KO9-AC	8536.090	411.000	151.000	0.450	0.334	0.116
KO9-AB	12641.000	431.000	209.000	0.440	0.459	-0.019
KO9-AA	24163.900	484.000	350.000	0.250	0.653	-0.403
K10-BA	2452.510	365.000	50.000	0.630	0.288	0.342
K11-CF	7796.060	375.000	40.000	0.490	0.208	0.282
K11-CE	4927.860	356.000	50.000	0.570	0.333	0.237
K11-CD	4771.890	338.000	88.000	0.580	0.436	0.144
K11-CC	7169.410	318.000	134.000	0.690	0.599	0.091
K11-CB	9773.580	306.000	162.000	0.900	0.742	0.158
K11-CA	12543.600	295.000	214.000	0.550	0.878	-0.328
K12-DE	5400.210	400.000	88.000	3.540	3.324	0.216
K12-DD	5926.020	314.000	116.000	3.000	3.269	-0.269
K12-DC	13667.300	265.000	228.000	4.200	4.536	-0.336
K12-DB	17964.900	247.000	279.000	5.870	5.334	0.536
K12-DA	22480.100	237.000	345.000	4.130	5.873	-1.743

Table E2 Table E1 continued

NAME	PNATUR	DIST	DEPTH	PMEAS	PCALC	ERROR
K13-EE	9212.000	207.000	85.000	5.530	7.137	-1.607
K13-ED	8830.180	164.000	143.000	5.030	5.765	-0.735
K13-EC	10756.000	160.000	182.000	5.060	4.617	0.443
K13-EB	14986.700	177.000	243.000	3.430	3.170	0.260
K13-EA	22447.199	232.000	332.000	2.620	3.045	-0.425
K14-FE	3658.730	355.000	75.000	0.640	0.202	0.438
K14-FD	5965.680	352.000	111.000	0.700	0.335	0.365
K14-FC	5965.680	352.000	120.000	0.720	0.335	0.385
K14-FB	7227.060	354.000	132.000	0.610	0.324	0.286
K14-FA	8512.140	359.000	157.000	0.630	0.347	0.283
H01-G1	19342.100	451.000	38.000	0.000	0.790	-0.790
H02-H2	3709.210	1020.000	40.000	0.000	0.017	-0.017
H02-H1	3983.910	1006.000	66.000	0.000	0.029	-0.029
H03-I2	7572.650	513.000	2.000	0.000	0.223	-0.223
H03-I1	9988.270	472.000	66.000	0.000	0.567	-0.567
H04-K2	7997.900	270.000	38.000	4.080	0.988	3.092
H04-K1	6704.380	240.000	129.000	2.720	1.118	1.602
H05-L3	7223.940	287.000	2.000	1.870	6.981	-5.111
H05-L2	7182.050	269.000	19.000	5.680	7.400	-1.720
H05-L1	7126.150	233.000	45.000	5.750	7.882	-2.132
H06-N2	7792.660	343.000	20.000	1.570	1.213	0.357
H06-N1	5014.620	309.000	91.000	2.370	1.209	1.161
H07-O2	5835.290	442.000	12.000	0.960	1.220	-0.260
H07-O1	4569.610	436.000	69.000	0.960	1.009	-0.049
H08-P2	9405.690	649.000	20.000	0.000	0.072	-0.072
H08-P1	5456.750	620.000	92.000	0.000	0.098	-0.098
H09-Q2	20149.100	656.000	2.000	0.000	0.150	-0.150
H09-Q1	17274.699	610.000	56.000	0.000	0.186	-0.186
H10-R2	17969.500	865.000	3.000	0.000	0.104	-0.104
H10-R1	8408.360	873.000	57.000	0.000	0.067	-0.067
H11-S2	9769.210	878.000	5.000	0.000	0.050	-0.050
H11-S1	5450.640	867.000	75.000	0.000	0.056	-0.056
H12-T2	1134.870	922.000	6.000	0.000	0.003	-0.003
H12-T1	3376.000	918.000	79.000	0.000	0.028	-0.028
H13-U2	18501.301	300.000	3.000	0.580	0.547	0.033
H13-U1	4755.200	253.000	86.000	1.100	0.743	0.357
H14-V2	6071.380	249.000	29.000	0.000	9.218	-9.218
H14-V1	6520.460	204.000	79.000	4.670	9.722	-5.052
H15-X2	21641.900	244.000	4.000	0.850	0.934	-0.084
H15-X1	3580.940	202.000	65.000	5.200	0.763	4.437
H16-Y2	2854.250	321.000	21.000	1.110	3.096	-1.986
H16-Y1	5022.770	307.000	85.000	3.120	3.240	-0.120
H17-Z2	8658.390	401.000	9.000	2.160	5.313	-3.153
H17-Z1	7105.440	362.000	79.000	2.990	4.475	-1.485
H18-PB	15016.500	512.000	24.000	2.990	0.228	2.762
H18-PA	14487.200	461.000	60.000	3.410	0.566	2.844

*****Error summary *******
Mean error = -7.37578E-02
Goodness of fit = 2.21459

List of SKB reports

Annual Reports

1977-78
TR 121
KBS Technical Reports 1 – 120
Summaries
Stockholm, May 1979

1979
TR 79-28
The KBS Annual Report 1979
KBS Technical Reports 79-01 – 79-27
Summaries
Stockholm, March 1980

1980
TR 80-26
The KBS Annual Report 1980
KBS Technical Reports 80-01 – 80-25
Summaries
Stockholm, March 1981

1981
TR 81-17
The KBS Annual Report 1981
KBS Technical Reports 81-01 – 81-16
Summaries
Stockholm, April 1982

1982
TR 82-28
The KBS Annual Report 1982
KBS Technical Reports 82-01 – 82-27
Summaries
Stockholm, July 1983

1983
TR 83-77
The KBS Annual Report 1983
KBS Technical Reports 83-01 – 83-76
Summaries
Stockholm, June 1984

1984
TR 85-01
Annual Research and Development Report 1984
Including Summaries of Technical Reports Issued during 1984. (Technical Reports 84-01 – 84-19)
Stockholm, June 1985

1985
TR 85-20
Annual Research and Development Report 1985
Including Summaries of Technical Reports Issued during 1985. (Technical Reports 85-01 – 85-19)
Stockholm, May 1986

1986
TR 86-31
SKB Annual Report 1986
Including Summaries of Technical Reports Issued during 1986
Stockholm, May 1987

1987
TR 87-33
SKB Annual Report 1987
Including Summaries of Technical Reports Issued during 1987
Stockholm, May 1988

1988
TR 88-32
SKB Annual Report 1988
Including Summaries of Technical Reports Issued during 1988
Stockholm, May 1989

1989
TR 89-40
SKB Annual Report 1989
Including Summaries of Technical Reports Issued during 1989
Stockholm, May 1990

1990
TR 90-46
SKB Annual Report 1990
Including Summaries of Technical Reports Issued during 1990
Stockholm, May 1991

1991
TR 91-64
SKB Annual Report 1991
Including Summaries of Technical Reports Issued during 1991
Stockholm, April 1992

Technical Reports

List of SKB Technical Reports 1992

TR 92-01
GEOTAB. Overview
Ebbe Eriksson[1], Bertil Johansson[2], Margareta Gerlach[3], Stefan Magnusson[2], Ann-Chatrin Nilsson[4], Stefan Sehlstedt[3], Tomas Stark[1]
[1]SGAB, [2]ERGODATA AB, [3]MRM Konsult AB
[4]KTH
January 1992

TR 92-02
Sternö study site. Scope of activities and main results
Kaj Ahlbom[1], Jan-Erik Andersson[2], Rune Nordqvist[2], Christer Ljunggren[3], Sven Tirén[2], Clifford Voss[4]
[1]Conterra AB, [2]Geosigma AB, [3]Renco AB,
[4]U.S. Geological Survey
January 1992

TR 92-03
Numerical groundwater flow calculations at the Finnsjön study site – extended regional area
Björn Lindbom, Anders Boghammar
Kemakta Consultants Co, Stockholm
March 1992

TR 92-04
Low temperature creep of copper intended for nuclear waste containers
P J Henderson, J-O Österberg, B Ivarsson
Swedish Institute for Metals Research, Stockholm
March 1992

TR 92-05
Boyancy flow in fractured rock with a salt gradient in the groundwater – An initital study
Johan Claesson
Department of Building Physics, Lund University, Sweden
February 1992

TR 92-06
Characterization of nearfield rock – A basis for comparison of repository concepts
Roland Pusch, Harald Hökmark
Clay Technology AB and Lund University of Technology
December 1991

TR 92-07
Discrete fracture modelling of the Finnsjön rock mass: Phase 2
J E Geier, C-L Axelsson, L Hässler,
A Benabderrahmane
Golden Geosystem AB, Uppsala, Sweden
April 1992

TR 92-08
Statistical inference and comparison of stochastic models for the hydraulic conductivity at the Finnsjön site
Sven Norman
Starprog AB
April 1992

TR 92-09
Description of the transport mechanisms and pathways in the far field of a KBS-3 type repository
Mark Elert[1], Ivars Neretnieks[2], Nils Kjellbert[3], Anders Ström[3]
[1]Kemakta Konsult AB
[2]Royal Institute of Technology
[3]Swedish Nuclear Fuel and Waste Management Co
April 1992

TR 92-10
Description of groundwater chemical data in the SKB database GEOTAB prior to 1990
Sif Laurent[1], Stefan Magnusson[2], Ann-Chatrin Nilsson[3]
[1]IVL, Stockholm
[2]Ergodata AB, Göteborg
[3]Dept. of Inorg. Chemistry, KTH, Stockholm
April 1992

TR 92-11
Numerical groundwter flow calculations at the Finnsjön study site – the influence of the regional gradient
Björn Lindbom, Anders Boghammar
Kemakta Consultants Co., Stockholm, Sweden
April 1992

TR 92-12
HYDRASTAR – a code for stochastic simulation of groundwater flow
Sven Norman
Abraxas Konsult
May 1992

TR 92-13
Radionuclide solubilities to be used in SKB 91
Jordi Bruno[1], Patrik Sellin[2]
[1]MBT, Barcelona Spain
[2]SKB, Stockholm, Sweden
June 1992

TR 92-14
Numerical calculations on heterogeneity of groundwater flow
Sven Follin
Department of Land and Water Resources, Royal Institute of Technology
June 1992

TR 92-15
Kamlunge study site.
Scope of activities and main results
Kaj Ahlbom[1], Jan-Erik Andersson[2],
Peter Andersson[2], Thomas Ittner[2],
Christer Ljunggren[3], Sven Tirén[2]
[1]Conterra AB
[2]Geosigma AB
[3]Renco AB
May 1992

TR 92-16
Equipment for deployment of canisters with spent nuclear fuel and bentonite buffer in horisontal holes
Vesa Henttonen, Miko Suikki
JP-Engineering Oy, Raisio, Finland
June 1992

TR 92-17
The implication of fractal dimension in hydrogeology and rock mechanics Version 1.1
W Dershowitz[1], K Redus[1], P Wallmann[1],
P LaPointe[1], C-L Axelsson[2]
[1]Golder Associates Inc., Seattle, Washington, USA
[2]Golder Associates Geosystem AB, Uppsala, Sweden
February 1992

TR 92-18
Stochastic continuum simulation of mass arrival using a synthetic data set. The effect of hard and soft conditioning
Kung Chen Shan[1], Wen Xian Huan[1], Vladimir Cvetkovic[1], Anders Winberg[2]
[1] Royal Institute of Technology, Stockholm
[2] Conterra AB, Gothenburg
June 1992

TR 92-19
Partitioning and transmutation.
A review of the current state of the art
Mats Skålberg, Jan-Olov Liljenzin
Department of Nuclear Chemistry,
Chalmers University of Technology
October 1992

TR 92-20
SKB 91
Final disposal of spent nuclear fuel. Importance of the bedrock for safety
SKB
May 1992

TR 92-21
The Protogine Zone.
Geology and mobility during the last 1.5 Ga
Per-Gunnar Andréasson, Agnes Rodhe
September 1992

TR 92-22
Klipperås study site.
Scope of activities and main results
Kaj Ahlbom[1], Jan-Erik Andersson[2],
Peter Andersson[2], Tomas Ittner[2],
Christer Ljunggren[3], Sven Tirén[2]
[1]Conterra AB
[2]Geosigma AB
[3]Renco AB
September 1992

TR 92-23
Bedrock stability in Southeastern Sweden. Evidence from fracturing in the Ordovician limestones of Northern Öland
Alan Geoffrey Milnes[1], David G Gee[2]
[1]Geological and Environmental Assessments (GEA), Zürich, Switzerland
[2]Geologiska Institutionen, Lund, Sweden
September 1992

TR 92-24
Plan 92
Costs for management of the radioactive waste from nuclear power production
Swedish Nuclear Fuel and Waste Management Co
June 1992

TR 92-25
Gabbro as a host rock for a nuclear waste repository
Kaj Ahlbom[1], Bengt Leijon[1], Magnus Liedholm[2],
John Smellie[1]
[1]Conterra AB
[2]VBB VIAK
September 1992

TR 92-26
Copper canisters for nuclear high level waste disposal. Corrosion aspects
Lars Werme, Patrik Sellin, Nils Kjellbert
Swedish Nuclear Fuel and Waste Management Co, Stockholm, Sweden
October 1992

TR 92-27

Thermo-mechanical FE-analysis of bu welding of a Cu-Fe canister for spent nuclear fuel

B L Josefson[1], L Karlsson[2], L-E Lindgren[2], M Jonsson[2]
[1]Chalmers University of Technology, Göteborg, Sweden
[2]Division of Computer Aided Design, Luleå University of Technology, Luleå, Sweden
October 1992

TR 92-28

A rock mechanics study of Fracture Zone 2 at the Finnsjön site

Bengt Leijon[1], Christer Ljunggren[2]
[1]Conterra AB
[2]Renco AB
January 1992

TR 92-29

Release calculations in a repository of the very long tunnel type

L Romero, L Moreno, I Neretnieks
Department of Chemical Engineering,
Royal Institute of Technology, Stockholm, Sweden
November 1992

TR 92-30

Interaction between rock, bentonite buffer and canister. FEM calculations of some mechanical effects on the canister in different disposal concepts

Lennart Börgesson
Clay Technology AB, Lund Sweden
July 1992

TR 92-31

The Äspö Hard Rock Laboratory: Final evaluation of the hydro-geochemical pre-investigations in relation to existing geologic and hydraulic conditions

John Smellie[1], Marcus Laaksoharju[2]
[1]Conterra AB, Uppsala, Sweden
[2]GeoPoint AB, Stockholm, Sweden
November 1992